ISSN 0386-5878
Tenhnical Memorandum
of PWRI No.3503

PROCEEDINGS OF THE SECOND ITALY-JAPAN WORKSHOP ON SEISMIC DESIGN AND RETROFIT OF BRIDGES

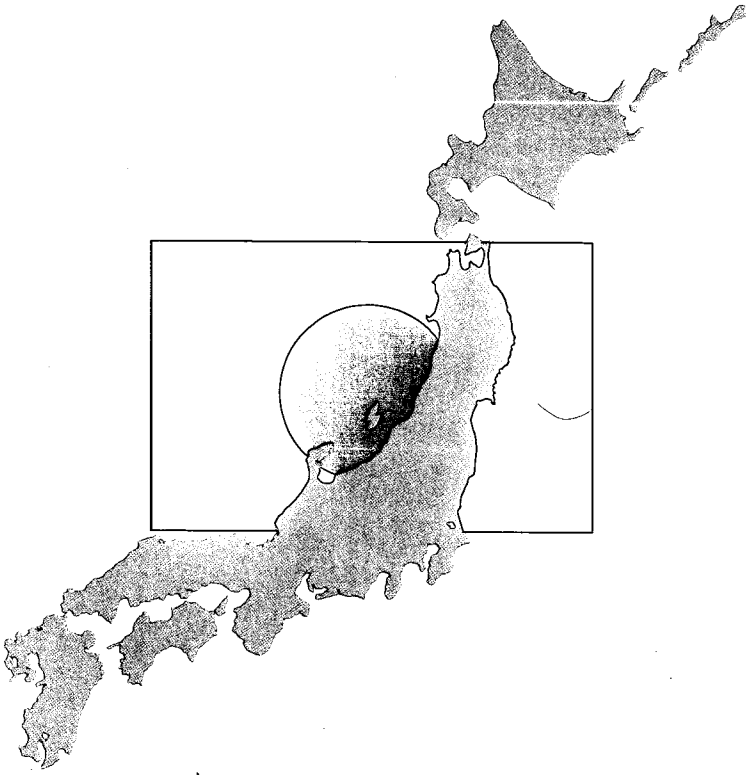

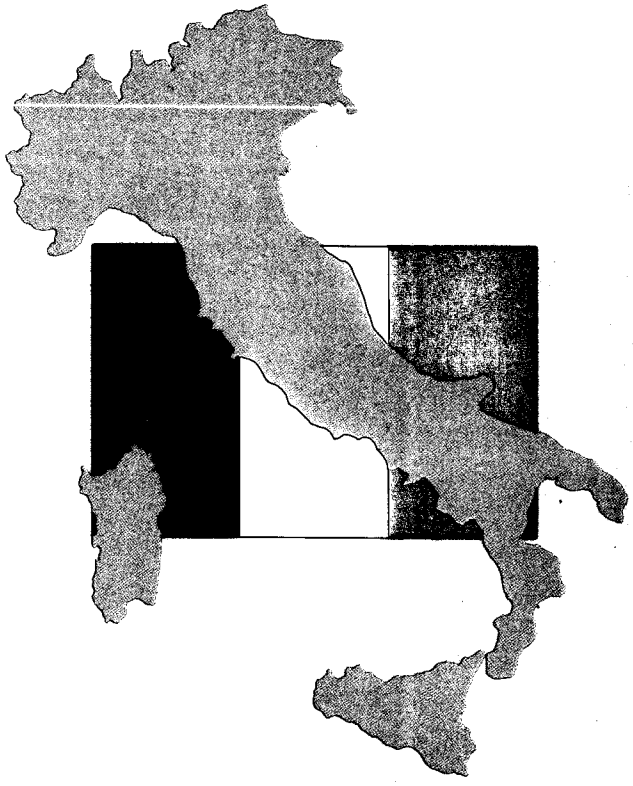

February 27 - 28, 1997
Rome, Italy

Public Works Research Institute
Ministry of Construction

Copyright ©1997 by P.W.R.I.

All rights reserved. No part of this book may be reproduced by any means, nor translated into a machine language without the written permission of the Director General of P.W.R.I.

この報告書は，土木研究所長の承認を得て刊行したものである。したがって，本報告書の全部又は一部の転載，複製は，土木研究所長の文書による承認を得ずしてこれを行ってはならない。

ISSN 0386-5878
Technical Memorandum
of PWRI No. 3503

PROCEEDINGS OF THE SECOND ITALY-JAPAN WORKSHOP ON SEISMIC DESIGN AND RETROFIT OF BRIDGES

February 27-28, 1997
Rome, Italy

by

Earthquake Engineering Division,
Earthquake Disaster Prevention Research Center,
Public Works Research Institute
Ministry of Construction

Synopsis:
This proceedings include the results of the Second Italy-Japan Workshop on Seismic Design and Retrofit of Bridges. The Workshop was held at Rome University in Rome, Italy, on February 27 and 28, 1997.

Key words : Highway Bridge, Seismic Design, Retrofit, Design Specifications, Analysis and Modeling

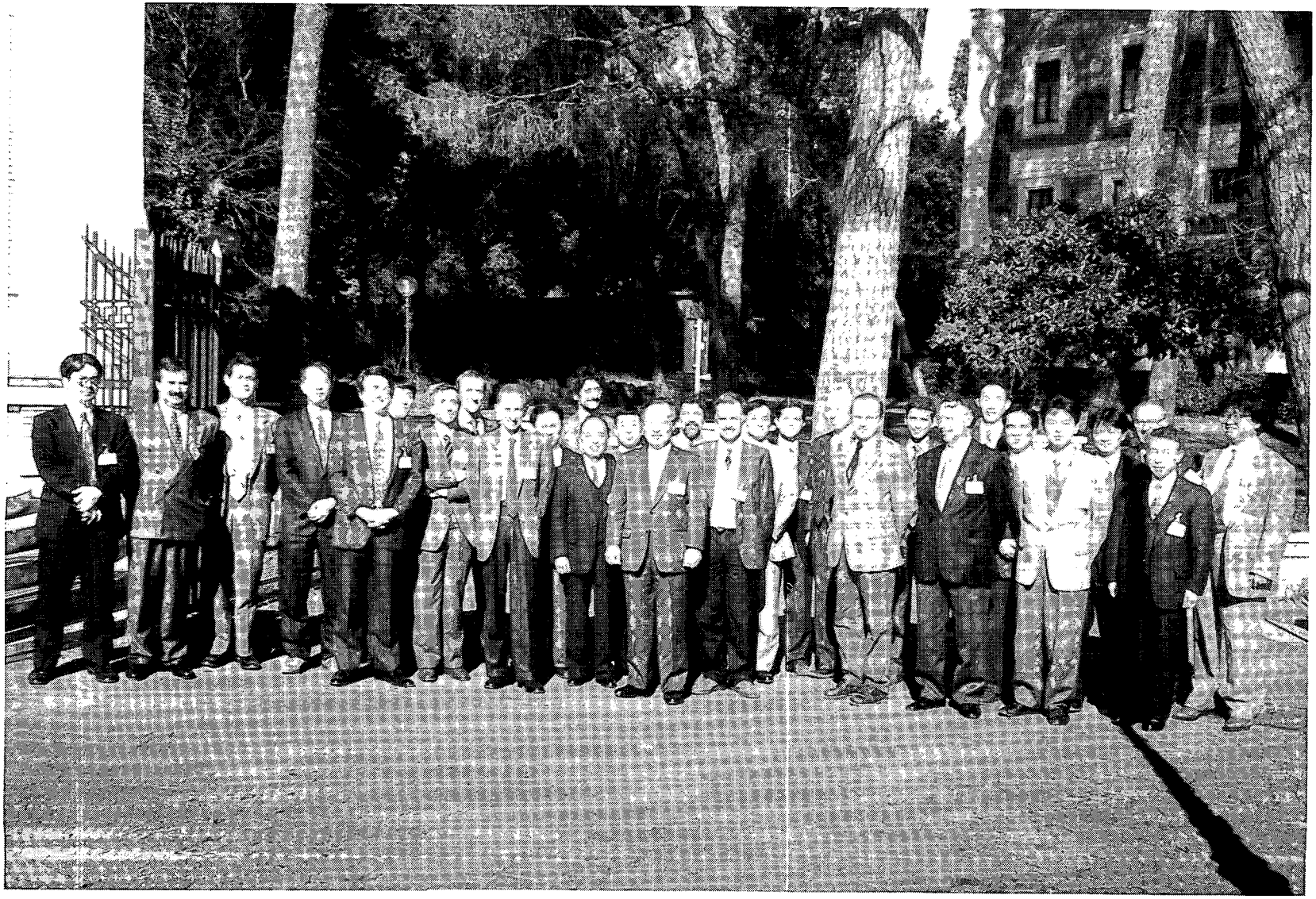

Participants of the Workshop

FOREWORD

The proceedings include the results of the Second Italy-Japan Workshop on Seismic Design and Retrofit of Bridges. The workshop was held at Rome, Italy, on February 27 and 28, 1997, under the "Agreement on Science and Technology Cooperation between Italy and Japan." The workshop was jointly coordinated by Professor Paolo E. Pinto, Professor of the Department of Structural and Geotechnical Engineering of the University of Rome, "La Sapienza," and Dr. Shigeki Unjoh, Head of Earthquake Engineering Division of the Public Works Research Institute (PWRI). The Italy-side financial support was provided by the University of Rome and by the Italian Seismic Survey. The Japan-side financial support was provided by the Japanese Science and Technology Agency and Japan International Science and Technology Center.

The First Japan– Italy Workshop on Seismic Design of Bridges was held at Tsukuba Science City, Japan, on March 13 and 14, 1995, just after the disastrous 1995 Hyogo-ken-nanbu earthquake.

The aims of the workshop were: (1) to bring together experts from both countries to exchange technical information on current research and practical efforts being made in the area of seismic design and retrofit of bridges, and (2) to identify future needs and opportunities between the two countries for cooperative research.

A broad range of technical topics were presented at the workshop. These included:

○ Design Specifications for Bridges
○ Seismic Reliability Evaluation for Highway Networks
○ Seismic Design Input for Bridges
○ Modeling and Analysis for Bridges
○ Design and Case Studies
○ Foundations and Soil Stability
○ Isolation and Retrofit

The workshop was attended by 15 Italian and 18 Japanese participants. In total, 26 papers were presented; 12 papers from Italy, 14 papers from Japan. The proceedings include (1) all technical papers in the order in which they were presented during the workshop, (2) resolutions that were unanimously approved by the participants during the closing session of the workshop, and (3) the workshop program and the list of participants.

A study tour to the ancient bridges in Rome area and visits to the Joint Research Centre, European Commission, and ISMES SPA Research Center had been organized for Japanese participants on the three days after the workshop. The study tour was organized by Professor P. E. Pinto of the University of Rome.

We wish to express our profound gratitude and sincere appreciation to all participants in the workshop for supporting the workshop by active presentations and discussion. Grateful thanks are extended to the Italy-side members. Special appreciation goes to Professor P. E. Pinto of the University of Rome for the coordination of the wonderful workshop. We also would like to thank Dr. F. Sorel, Head of Structural Mechanics Unit, Dr. Artur V. Pinto, Structural Mechanics Unit, JRC-ELSA Laboratory, and Dr. Aldo Castoldi, General Manager, and Dr. Alberto Peano, Director for R & D and New Business, ISMES SPA, for the generous cooperation during the study tour.

Toshinori MIZUTANI
Deputy Director-General

Shigeki UNJOH
Head, Earthquake Engineering Division
Earthquake Disaster Prevention Research Center

Public Works Research Institute
Ministry of Construction

May, 1997

永久保存
9-7.-3
図書館

TABLE OF CONTENTS

PAPERS PRESENTED DURING THE WORKSHOP

Session 1 : Topic 1 General Presentations

1) The 1996 Seismic Design Specifications for Highway Bridges
(K. Kawashima, M. Nakano, S. Unjoh) 1

2) An Automatic Procedure for Analytical Seismic Assessment of the Bridges in Highway System
(P.E. Pinto, R. Giannini, C. Nuti) 25

Session 2 : Topic 2 Seismic Input for Bridges
Topic 3 Modelling and Analysis (1)

3) Ground Motion Characteristics for Seismic Design of Highway Bridges
(K. Tamura, R. Honda, A. Chiba, K. Yamamoto) 45

4) Italian Research Activities for Definition of the Design Seismic Input
(A. Pugliese, T. Sano) 63

5) Ductility Evaluation of Reinforced Concrete Bridge Columns
(J. Hoshikuma, K. Kawashima, S. Unjoh) 81

6) Combined Flexural and Shear Effects on Bridge Piers
(G. Mancini, A. Recupero) 95

Session 3 : Topic 3 Modelling and Analysis (2)

7) Strength and Ductility Characteristics of Two Column – Bents
(T. Terayama, H. Otsuka, K. Nagaya) 115

8) A Numerical Model for Shear – Dominated Bridge Piers
(J. Guedes, A.V. Pinto) 131

9) Shear Strength of Reinforced Concrete Columns – Effect of Specimen Size and Load Reversal –
(H. Kawano, H. Watanabe) 141

10) Seismic Response by Pseudodynamic Tests of RC Bridges Designed to Eurocode 8 and Italian Seismic Code
(A. De Sortis, C. Nuti) 155

Session 4 : Topic 4 Design and Case Studies

11) New Approach for Bearings and Falling – off Prevention Systems of Highway Bridges
(M. Kanda, K. Nishikawa) 171

12) Finite Element Modelling of the Hanshin Viaducts Failure in Kobe
(M. Petrangeli, P.E. Pinto) 189
13) Effects of the Hyogo-ken-nanbu Earthquake on the Akashi Kaikyo Bridge
(S. Saeki, T. Kurihara, R. Toriumi, M. Nishitani) 201
14) Seismic Aspects of the Wadi Dib Cable-Stayed Bridge
(M.P. Petrangeli, M. Petrangeli) 221

Thursday, 27 February 1997
Session 5 : Topic 3 Modelling and Analysis (3)
15) Experimental Assessment of Bridges with Isolation and Non-Synchronous Input Motion
(A.V. Pinto, P. Negro) 233
16) Strength and Ductility Characteristics of Pile Foundations
(J. Fukui, Y. Kimura, M. Okoshi) 255
17) Non Linear Seismic Analysis of Railway Bridges
(M. Dolce, D. Liberatore) 275

Session 6 : Topic 5 Foundations and Soil Stability
Topic 6 Isolation and Retrofit (1)
18) Design Methods of Bridge Foundations against Soil Liquefaction and Liquefaction – Induced Ground Flow
(K. Yokoyama, K. Tamura, O. Matsuo) 297
19) A Study on Measures against Ground Flow Using the Finite Element Method
(M. Ogasawara, H. Tsunoda, T. Makita, S. Gose) 321
20) Menshin Design for Highway Bridges
(K. Kawashima, S. Unjoh) 331
21) Conceptual Design of Isolation Systems for Bridge Structures
(G.M. Calvi, A. Pavese) 351

Session 7 : Topic 6 Isolation and Retrofit (2)
22) Design of the 19 – Span Continuous Rigid Frame Bridge with Seismic Isolator
(H. Hayashi, S. Kawakita, Y. Horie) 375
23) Seismic Retrofitting of a Highway Bridge through Slab Joining and Isolation
(G. Monti, R. Marnetto) 395
24) Seismic Retrofit of Existing Reinforced Concrete Columns by

Steel Jacketing
(J. Hoshikuma, S. Unjoh) 413
25) Analysis of RC Bridge Piers externally Reinforced with Fiber-reinforced Plastics
(G. Monti, M.R. Spoelstra) 429
26) Carbon Fiber Strengthening of Existing High Bridge Piers
(Y. Yasukawa, M. Nakasu, Y. Tamura) 455

RESOLUTION

APPENDICES

1. Schedule of the Workshop
2. Program of the Workshop
3. List of Participants

PAPERS PRESENTED DURING THE WORKSHOP

Session 1

Topic 1 General Presentations

THE 1996 SEISMIC DESIGN SPECIFICATIONS OF HIGHWAY BRIDGES

by

Kazuhiko Kawashima[1)], Masanori Nakano[2)] and Shigeki Unjoh[3)]

1) Professor, Tokyo Institute of Technology, Tokyo, Japan
2) Deputy Director, Information Administration Section, Research and Information Division, Economic Affairs Bureau, Ministry of Construction, Tokyo, Japan
3) Head, Earthquake Engineering Division, Public Works Research Institute, Tsukuba, Japan

Abstract

This paper describes the revised Seismic Design Specifications of Highway Bridges in 1996 as well as the background of the revision. Damage features of bridges in the 1995 Hyogo-ken Nanbu Earthquake is first described with an emphasis on the lessons learned from the earthquake. Seismic performance levels and design method as well as the seismic design force introduced in the 1996 Design Specifications are then described.

Keywords: Seismic Design, Bridge, Design Codes, Hyogo-ken Nanbu Earthquake

INTRODUCTION

Highway bridges in Japan had been considered safe even against extreme earthquakes such as the Great Kanto Earthquake (M7.9) in 1923, because various past bitter experiences have been accumulated to formulate the seismic design method (Kawashima (1995)). Large seismic lateral force ranging from 0.2g to 0.3g has been adopted in the allowable stress design approach. Various provisions for preventing damage due to instability of soils such as soil liquefaction have been adopted. Furthermore, design detailings including the unseating prevention devices have been implemented.

In fact, reflecting those provisions, number of highway bridges which suffered complete collapse of superstructures was only 15 since the 1923 Great Kanto Earthquake. Based on such evidence, it had been regarded that the seismic damage of highway bridges has been decreasing in recent year.

However the Hyogo-ken nanbu earthquake of January 17, 1995, exactly one year after the Northridge, California, USA, earthquake caused destructive damage to highway bridges. Collapse and nearly collapse of superstructures occurred at 9 sites, and other destructive damage occurred at 16

sites (Ministry of Construction, 1995a). The earthquake revealed that there are a number of critical issues to be revised in the seismic design and seismic strengthening of bridges in urban areas.

After the earthquake, the "Committee for Investigation on the Damage of Highway Bridges Caused by the Hyogo-ken Nanbu Earthquake" (chairman: Toshio Iwasaki, Executive Director, Civil Engineering Research Laboratory) was formulated in the Ministry of Construction to survey the damage and clarify the factors which contributed to the damage. On February 27, 1995, the Committee approved the "Guide Specifications for Reconstruction and Repair of Highway Bridges which Suffered Damage due to the Hyogo-ken Nanbu Earthquake," (Ministry of Construction 1995b) and the Ministry of Construction noticed on the same day that the reconstruction and repair of the highway bridges which suffered damage in the Hyogo-ken nanbu earthquake should be made by the Guide Specifications. It was decided by the Ministry of Construction on May 25, 1995 that the Guide Specifications should be tentatively used inall sections of Japan as an emergency measure for seismic design of new highway bridges and seismic strengthening of existing highway bridges until the Design Specifications of Highway Bridges was revised.

In May, 1995, the "Special Sub-Committee for Seismic Countermeasures for Highway Bridges" (chairman: Kazuhiko Kawashima, Tokyo Institute of Technology) was formulated in the "Bridge Committee" (chairman: Nobuyuki Narita, Tokyo Metropolitan University), Japan Road Association to draft the revision of the Design Specifications of Highway Bridges. The Special Sub-Committee drafted the new Design Specifications of Highway Bridges, and after the approval of the Bridge Committee, the Ministry of Construction released it on November 1, 1996.

This paper summarizes the damage feature of highway bridges by the Hyogo-ken nanbu earthquake and the new Design Specifications of Highway Bridges issued in November 1996.

DAMAGE FEATURES OF BRIDGES IN THE HYOGO-KEN NANBU EARTHQUAKE

Hyogo-ken nanbu earthquake was the first earthquake which hit an urban area in Japan since the 1948 Fukui earthquake. Although the magnitude of earthquake was moderate (M7.2), the ground motion was much larger than anticipated in the codes. It occurred very close to the Kobe City with shallow focal depth.

Damage was developed at highway bridges on Routes 2, 43, 171 and 176 of the National Highway, Route 3 (Kobe Line) and Route 5 (Bay Shore Line) of the Hanshin Expressway, and Meishin and Chugoku Expressway. Damage was surveyed for all bridges on National Highways, Hanshin Expressways and Expressways in the area where destructive damage occurred. Total number of piers

surveyed reached 3,396 (Ministry of Construction, 1995a). Fig. 1 shows the Design Specifications referred to in design of the 3,396 piers. Most of piers (bridges) which suffered damage were designed according to the 1964 Design Specifications or older Design Specifications. Although the seismic design methods have been improved and amended several times since 1926 based on damage experience and progress of bridge earthquake engineering, only a requirement for lateral force coefficient was provided in the 1964 Design Specifications or older Specifications.

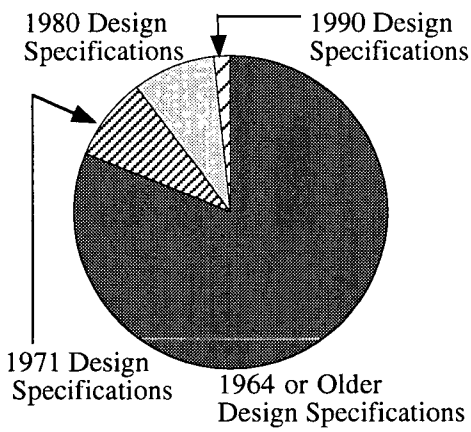

Fig. 1 Design Specifications Referred to in Design of Hanshin Expressway

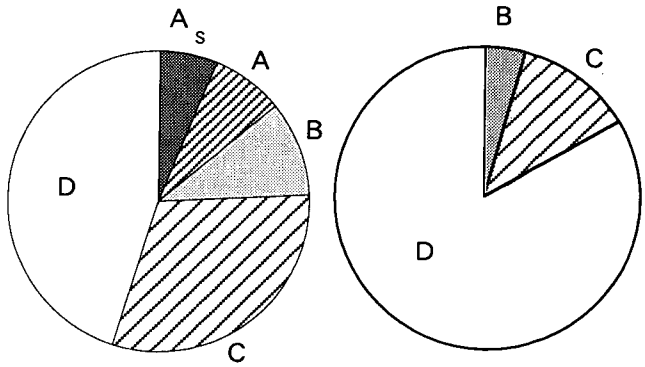

(a) Route 3 (b) Route 5

Fig. 2 Comparison of Damage Degree between Route 3 and Route 5 (As: Collapse, A: Nearly Collapse B: Moderate Damage, C: Damage of Secondary Members, D: Minor or No Damage)

Fig. 2 compares damage of piers on the Route 3, Kobe Line, and Route 5, Bay Shore Line, of the Hanshin Expressway. Damage degree was classified as A_S (collapse), A (nearly collapse), B (moderate damage), C (damage of secondary members) and D (minor or no damage). Substructures of the Route 3 and Route 5 were designed with the 1964 Design Specifications and 1980 Design Specifications, respectively. It should be noted in this comparison that the intensity of ground shaking in terms of response spectra was smaller at the Bay Area than the narrow rectangular area where JMA Seismic Intensity was VII (equivalent to the Modified Mercalli Intensity of X-XI). The Route 3 was located in the narrow rectangular area while the Route 5 was located in the Bay Area. Keeping in mind such difference of ground motion, it is apparent in Fig. 2 that about 14 % of the piers on Route 3 suffered A_S or A damage while no such damage was developed in the piers on the Route 5.

Although damage concentrated on the bridges designed with the older Design Specifications, it was thought that essential revision was required even in the recent Design Specifications to prevent damage against destructive earthquakes such as the Hyogo-ken nanbu earthquake. The main points requiring modifications were;

(1) it was required to increase lateral capacity and ductility of all structural components in which seismic force is predominant so that ductility of a total bridge system be enhanced. For such purpose, it was required to upgrade the "Check of Ductility of Reinforced Concrete Piers," which has been used since 1990, to a "Ductility Design Method," and to apply the Ductility Design Method to all structural components. It should be noted here that "check" and "design" is different; the check is only to verify the safety of a structural member designed by other design method, and is effective only to increase the size or reinforcements if required, while the design is an essential procedure to determine the size and reinforcements,

(2) it was required to include the ground motion developed at Kobe in the earthquake as a design force in the Ductility Design Method,

(3)it was required tospecify input ground motions in terms of acceleration response spectra for dynamic response analysis more actively,

(4) it was required to increase tie reinforcements and to introduce intermediate ties for increasing ductility of piers. It was decided not to terminate main reinforcements at mid-height for preventing premature shear failure, in principle,

(5) it was suggested to adopt multi-span continuous bridge for increasing number of indeterminate of a total bridge system,

(6) it was suggested to adopt rubber bearings for absorbing lateral displacement between a superstructure and substructures. It was important to consider correct mechanism of force transfer from a superstructure to substructures,

(7) it was suggested to include the Menshin design (seismic isolation),

(8) it was required to increase strength, ductility and energy dissipation capacity of unseating prevention devices, and

(9) it was required to consider the effect of lateral spreading associated with soil liquefaction in design of foundations at the site vulnerable to lateral spreading.

BASIC PRINCIPLE OF SEISMIC DESIGN

Table 1 shows the seismic performance level provided in the revised Design Specifications in 1996. The bridges are categorized into two groups depending on their importance; standard bridges (Type-A bridges) and important bridges (Type-B bridges). Seismic performance level depends on the importance of bridges. For moderate ground motions induced in the earthquakes with high probability to occur, both A and B bridges should behave in an elastic manner without essential structural damage. For extreme ground motions induced in the earthquakes with low probability to occur, the Type-A bridges should prevent critical failure, while the Type-B bridges should perform with limited damage.

In the Ductility Design Method, two types of ground motions must be considered. The first is the ground motion which could be induced in the plate boundary-type earthquakes with magnitude of about 8. The ground motion at Tokyo in the 1923 Kanto earthquake is a typical target of this type of ground motion. The second is the ground motion developed in earthquakes with magnitude of about 7-7.2 at very short distance. Obviously the ground motion at Kobe in the Hyogo-ken nanbu earthquake is a typical target of this type of ground motion. The first and the second ground motions are called as Type-I and Type-II ground motions, respectively. The recurrence time of the Type-II ground motion may be longer than that of the Type-I ground motion, although the estimation is very difficult.

Table 1. Seismic Performance Levels

<table>
<tr><td colspan="2" rowspan="2">Type of Design Ground Motions</td><td colspan="2">Importance</td><td colspan="2">Design Methods</td></tr>
<tr><td>Type-A Bridges (Standard Bridges)</td><td>Type-B Bridges (Important Bridges)</td><td>Equivalent Static Lateral Force Methods</td><td>Dynamic Analysis</td></tr>
<tr><td colspan="2">Ground Motions with High Probability to Occur</td><td colspan="2">Prevent damage</td><td>Seismic Coefficient Method</td><td rowspan="3">Step by Step Analysis or Response Spectrum Analysis</td></tr>
<tr><td rowspan="2">Ground Motions with Low Probability to Occur</td><td>Type-I (Plate-boundary type Earthquakes)</td><td rowspan="2">Prevent Critical Failure</td><td rowspan="2">Limited Damage</td><td rowspan="2">Ductility Design Method</td></tr>
<tr><td>Type-II (Inland Earthquakes)</td></tr>
</table>

DESIGN METHODS

Bridges are designed by both the Seismic Coefficient Method and the Ductility Design Method as shown in Fig. 3. In the Seismic Coefficient Method, a lateral force coefficient ranging from 0.2 to 0.3 has been used based on the allowable stress design approach. No change was introduced since the 1990 Specifications in the Seismic Coefficient Method.

In the Ductility Design method, assuming a principal plastic hinge formed at the bottom of pier as shown in Fig. 4 (a) and the equal energy assumption, a bridge is designed so that the following requirement is satisfied.

$$P_a \geq k_{he} W \tag{1}$$

where

$$k_{he} = \frac{k_{hc}}{\sqrt{2\mu_a - 1}} \tag{2}$$

$$W = W_U + c_P W_P \tag{3}$$

in which P_a= lateral capacity of a pier, k_{he}= equivalent lateral force coefficient, W= equivalent weight, k_{hc}= lateral force coefficient, μ_a= allowable displacement ductility factor of a pier, W_U= weight of a part of superstructure supported by the pier, W_P= weight of a pier, and c_P=coefficient depending on the type of failure mode. The c_P is 0.5 for a pier in which either flexural failure or shear failure after flexural cracks are developed, and 1.0 for a pier in which shear failure is developed. The lateral capacity of a pier P_a is defined as a lateral force at the gravity center of a superstructure.

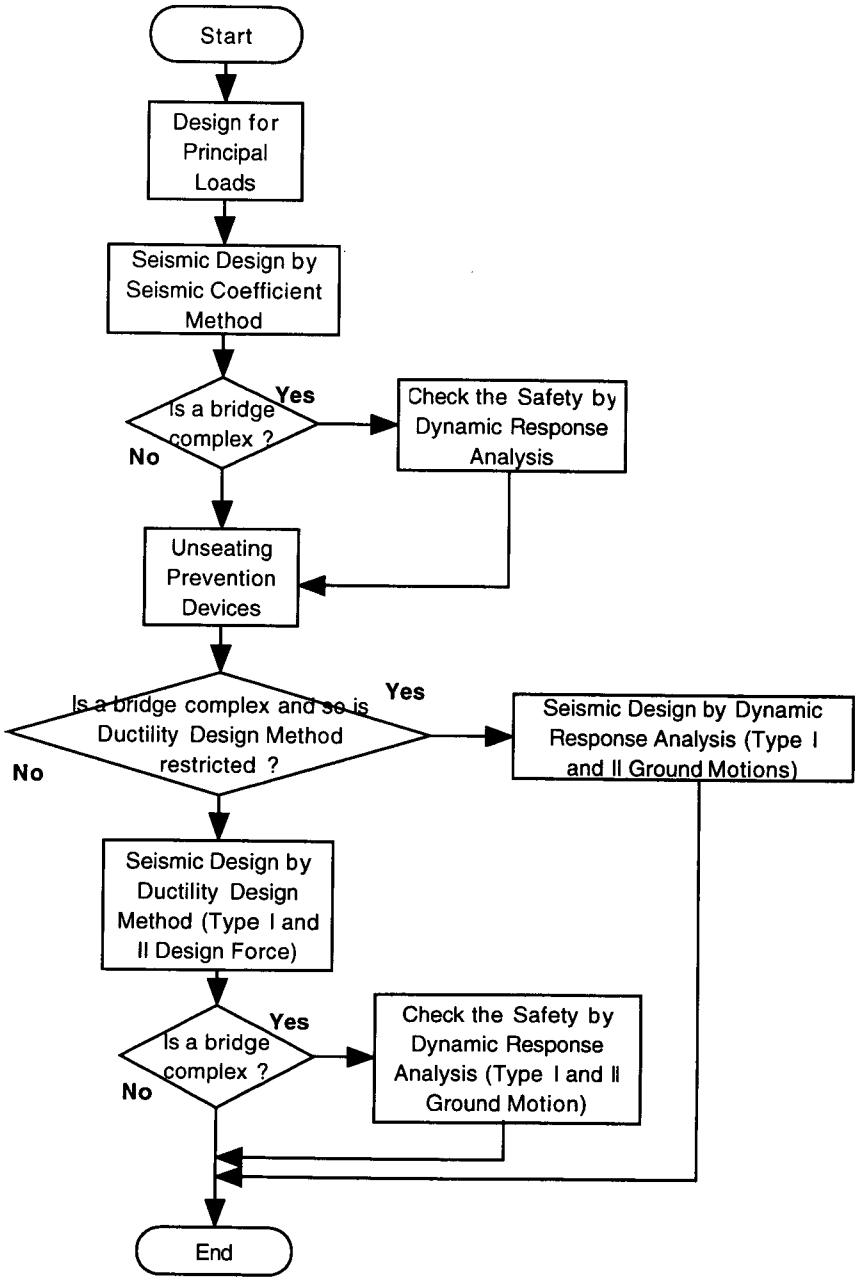

Fig. 3 Flowchart of Seismic Design

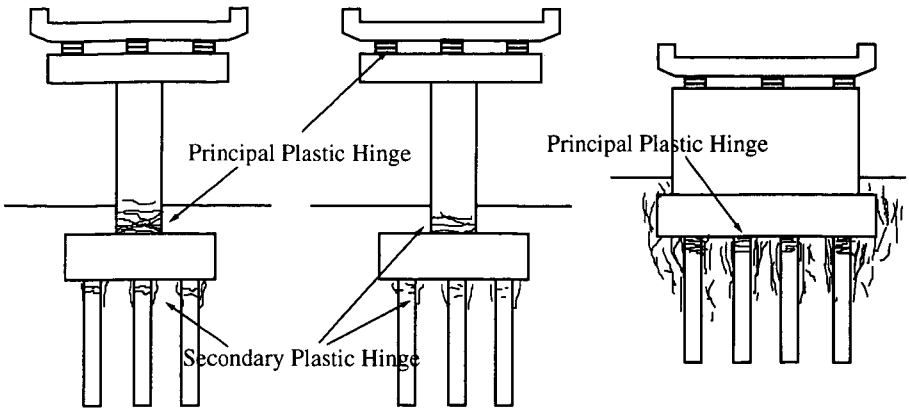

(a) Conventional Design (b) Menshin Design (c) Bridge Supported by a Wall Pier

Fig. 4 Location of Primary Plastic Hinge

In the Type-B bridges, residual displacement developed at a pier after an earthquake must be checked as

$$\delta_R \leq \delta_{Ra} \tag{4}$$

where

$$\delta_R = c_R(\mu_R - 1)(1 - r)\delta_y \tag{5}$$

$$\mu_R = \frac{1}{2}\left\{\left(\frac{k_{hc}W}{P_a}\right)^2 + 1\right\} \tag{6}$$

in which δ_R= residual displacement of a pier after an earthquake, δ_{Ra}= allowable residual displacement of a pier, r= bilinear factor defined as a ratio between the first stiffness (yield stiffness) and the second stiffness (post-yield stiffness) of a pier, c_R= factor depending on the bilinear factor r, μ_R= response ductility factor of a pier, and δ_y= yield displacement of a pier. The δ_{Ra} should be 1/100 of a distance between the bottom of a pier and a gravity center of a superstructure.

In a bridge with complex dynamic response, the dynamic response analysis is required to check the safety of a bridge after it is designed by the Seismic Coefficient Method and the Ductility Design Method. Because this is only for a check of the design, the size and reinforcements of structural members once determined by the Seismic Coefficient Method and the Ductility Design Method can only be increased if necessary. It should be noted however that under the following conditions in which the Ductility Design Method is not directly applied, the size and reinforcements can be determined based on the results of a dynamic response analysis as shown in Fig. 3. The conditions when the Ductility Design Method should not be directly used include

(1) principal mode shapes which contribute to bridge response are different from the ones assumed in the Ductility Design Method,

(2) more than two modes significantly contribute to bridge response,

(3) principal plastic hinges form at more than two locations, or principal plastic hinges are not known where to be formed, and

(4)response modes for which the equal energy assumption are not applied.

In the seismic design of a foundation, a lateral force equivalent to the ultimate lateral capacity of a pier P_u is assumed to be a design force as

$$k_{hp} = c_{df} P_u / W \tag{7}$$

in which k_{hp}= lateral force coefficient for a foundation, c_{df} = modification coefficient (=1.1), and W =equivalent weight by Eq. (3). Because the lateral capacity of a wall-type pier is very large in transverse direction, the lateral seismic force evaluated by Eq. (7) becomes in most cases excessive. Therefore if a foundation has sufficiently large lateral capacity compared with the lateral seismic force, the foundation is designed assuming a plastic hinge at the foundation and the surrounding soils as shown in Fig. 4 (c).

DESIGN SEISMIC FORCE

The lateral force coefficient k_{hc} in Eq. (2) is given as

$$k_{hc} = c_Z \cdot k_{hc0} \tag{8}$$

in which c_Z= modification coefficient for zone, and is 0.7, 0.85 and 1.0 depending on zone, and k_{hc0}= standard modification coefficient. Table 2 and Fig. 5 show the standard lateral force coefficients k_{hc0} for the Type-I and the Type-II ground motions. The Type-I ground motions have been used since 1990 (1990 Specifications), while the Type-II ground motions were introduced in the 1996 Specifications. It should be noted here that the k_{hc0} at stiff site (Group I) has been assumed smaller than the k_{hc0} at moderate (Group II) and soft soil (Group III) sites in the Type-I ground motions as well as the seismic coefficients for the Seismic Coefficient Method. The Type-I ground motions were essentially estimated from an attenuation equation for response spectra that was derived from a statistical analysis of 394 components of strong motion records. Although the response spectral accelerations at short natural period are larger at stiff sites than at soft soil sites, the tendency had not been explicitly included in the past. This was because damage has been more developed at soft sites than at stiff sites. To consider such fact, the design force at stiff sites has been assumed smaller than that at soft sites even at short natural period. However being different from such a traditional consideration, the Type II ground motions were determined by simply taking envelops of response accelerations of major strong motions recorded at Kobe in the Hyogo-ken Nanbu earthquake. It was considered appropriate to set realistic ground motions.

Although the acceleration response spectral intensity at short natural period is higher in the Type-II ground motions than in the Type-I ground motions, the duration of extreme acceleration excursion

is longer in the Type-I ground motions than the Type-II ground motions. As will be described later, such a difference of the duration has been taken into account to evaluate the allowable displacement ductility factor of a pier.

Table 2 Lateral Force Coefficient k_{hc0} in the Ductility Design Method

(a) Type-I Ground Motions

Soil Condition	Lateral Force Coefficient k_{hc0}		
Group I (stiff)	k_{hc0}=0.7 for $T \leqq 1.4$		$k_{hc0}=0.876\ T^{-2/3}$ for $1.4 < T$
Group II (moderate)	$k_{hc0}=1.51\ T^{1/3} \geqq 0.7$ for $T < 0.18$	k_{hc0}=0.85 for $0.18 \leqq T \leqq 1.6$	$k_{hc0}=1.16\ T^{-2/3}$ for $1.6 < T$
Group III (soft)	$k_{hc0}=1.51\ T^{1/3} \geqq 0.7$ for $T < 0.29$	k_{hc0}=1.0 for $0.29 \leqq T \leqq 2.0$	$k_{hc0}=1.59\ T^{-2/3}$ for $2.0 < T$

(b) Type-II Ground d Motions

Soil Condition	Lateral Force Coefficient k_{hc0}		
Group I (stiff)	$k_{hc0}=4.46\ T^{2/3}$ for $T < 0.3$	k_{hc0}=2.0 for $0.3 \leqq T \leqq 0.7$	$k_{hc0}=1.24\ T^{-4/3}$ for $0.7 < T$
Group II (moderate)	$k_{hc0}=3.22\ T^{2/3}$ for $T < 0.4$	k_{hc0}=1.75 for $0.4 \leqq T \leqq 1.2$	$k_{hc0}=2.23\ T^{-4/3}$ for $1.2 < T$
Group III (soft)	$k_{hc0}=2.38\ T^{2/3}$ for $T < 0.5$	k_{hc0}=1.50 for $0.5 \leqq T \leqq 1.5$	$k_{hc0}=2.57\ T^{-4/3}$ for $1.5 < T$

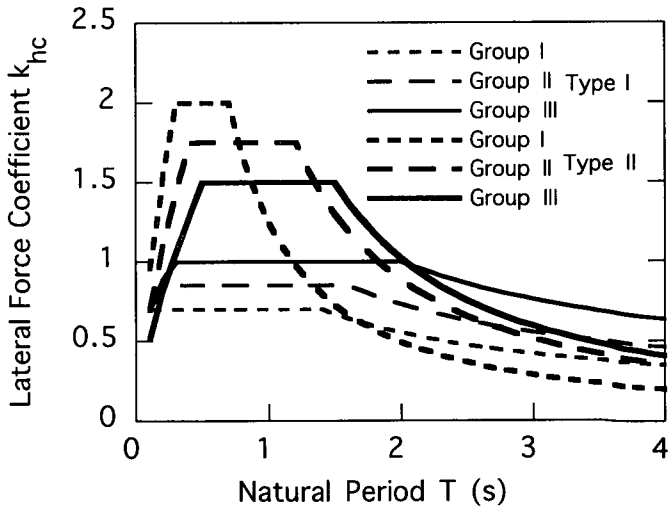

Fig. 5 Type I and Type II Lateral Force Coefficients in the Ductility Design Method

EVALUATION OF DISPLACEMENT DUCTILITY FACTOR OF A PIER

Reinforced concrete pier

The allowable displacement ductility factor of a pier μ_a in Eq. (2) is evaluated as

$$\mu_a = 1 + \frac{\delta_u - \delta_y}{\alpha \cdot \delta_y} \tag{9}$$

in which α = safety factor, δ_y = yield displacement of a pier, and δ_u = ultimate displacement of a pier. As well as the lateral capacity of a pier P_a in Eq. (1), the δ_y and δ_u are defined at the gravity center of a superstructure. In a reinforced concrete single pier as shown in Fig. 4 (a), the ultimate displacement δ_u is evaluated as

$$\delta_u = \delta_y + (\phi_u - \phi_y)(h - L_p/2)L_p \tag{10}$$

in which ϕ_y = yield curvature of a pier at a plastic hinge zone, ϕ_u = ultimate curvature of a pier at a plastic hinge zone, h = height of a pier, and L_p = plastic hinge length of a pier. The plastic hinge length is given as

$$L_p = 0.2h - 0.1D \qquad (0.1D \le L_p \le 0.5D) \tag{11}$$

in which D is a width or a diameter of a pier.

The yield curvature ϕ_y and the ultimate curvature ϕ_u in Eq. (10) are evaluated assuming a stress-strain relation of reinforcements and concrete as shown in Fig. 6. The stress σ_c - strain ε_c relation of concrete with lateral confinement is assumed as

$$\sigma_c = \begin{cases} E_c\varepsilon_c\left\{1 - \frac{1}{n}\left(\frac{\varepsilon_c}{\varepsilon_{cc}}\right)^{n-1}\right\} & (0 \le \varepsilon_c \le \varepsilon_{cc}) \\ \sigma_{cc} - E_{des}(\varepsilon_c - \varepsilon_{cc}) & (\varepsilon_{cc} \le \varepsilon_c \le \varepsilon_{cu}) \end{cases} \tag{12}$$

$$n = \frac{E_c\varepsilon_{cc}}{E_c\varepsilon_{cc} - \sigma_{cc}} \tag{13}$$

in which σ_{cc} = strength of confined concrete, E_c = elastic modulus of concrete, ε_{cc} = strain at maximum strength, and E_{des} = gradient at descending branch. In Eq. (12), the σ_{cc}, ε_{cc} and E_{des} are determined as

$$\sigma_{cc} = \sigma_{ck} + 3.8\alpha\rho_s\sigma_{sy} \tag{14}$$

$$\varepsilon_{cc} = 0.002 + 0.033\beta\frac{\rho_s\sigma_{sy}}{\sigma_{ck}} \tag{15}$$

$$E_{des} = 11.2\frac{\sigma_{ck}^{\ 2}}{\rho_s\sigma_{sy}} \tag{16}$$

in which σ_{ck} = design strength of concrete, σ_{sy} = yield strength of reinforcements, α and β = coefficients depending on the shape of a pier (α=1.0 and β=1.0 for a circular pier, and α=0.2 and β=0.4 for a rectangular pier), and ρ_s = tie reinforcement ratio defined as

$$\rho_s = \frac{4A_h}{s \cdot d} \tag{17}$$

in which A_h= area of tie reinforcements, s= space of tie reinforcements, and d=effect ive width of tie reinforcements.

The ultimate curvature ϕ_u is defined as a curvature when concrete strain at longitudinal reinforcing bars in compression reaches an ultimate strain ε_{cu} defined as

$$\varepsilon_{cu} = \begin{cases} \varepsilon_{cc} & \text{for Type I ground motions} \\ \varepsilon_{cc} + \dfrac{0.2\sigma_{cc}}{E_{des}} & \text{for Type II ground motions} \end{cases} \tag{18}$$

It is important to note here that the ultimate strain ε_{cu} depends on the types of ground motions; the ε_{cu} for the Type-II ground motions is larger than that for the Type-I ground motions. Based on a loading test, it is known that a certain level of failure in a pier such as a sudden decrease of lateral capacity occurs at smaller lateral displacement in a pier subjected to a loading hysteresis with more number of load reversals. To reflect such a fact, it was decidedthat the ultimate strain ε_{cu} should be evaluated by Eq. (18), depending on the type of ground motions.Therefore, the allowable ductility factor μ_a also depends on the type of ground motions; the μ_a is larger in a pier subjected to the Type-II ground motions than a pier subjected to the Type-I ground motions.

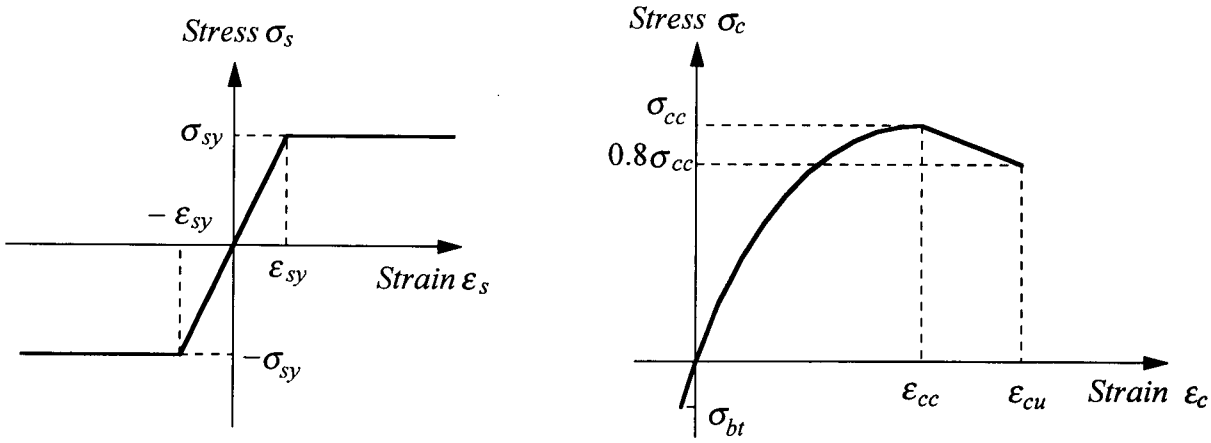

(a) Reinforcing Bars (b) Confined Concrete

Fig. 6 Stress and Strain Relation of Confined Concrete and Reinforcing Bars

It should be noted that the safety factor α in Eq. (9) depends on the type of bridgesas well as the type of ground motions as shown in Table 3. This is to preserve higher seismic safety in the important bridges, and to take account of the difference of recurrent time between the Type-I and the Type-II ground motions.

Table 3 Safety Factor α in Eq. (9)

Type of Bridges	Type-I Ground Motions	Type-II Ground Motions
Type-B	3.0	1.5
Type-A	2.4	1.2

Fig. 7 shows suggested arrangement of tie reinforcement. Tie reinforcement should be deformed bars with a diameter larger than 13 mm, and it should be placed in most bridges at a distance of no longer than 150 mm. In special cases such as the bridges with pier height taller than 30m, the distance of tie reinforcement may be increased as large as 300 mm, but special attention should be paid not to suddenly increase the distance at a height so that pier strength should not be sharply decreased at the section. Intermediate ties should be also provided with the same distance with the ties to confine the concrete. Space of the intermediate ties should be less than 1m.

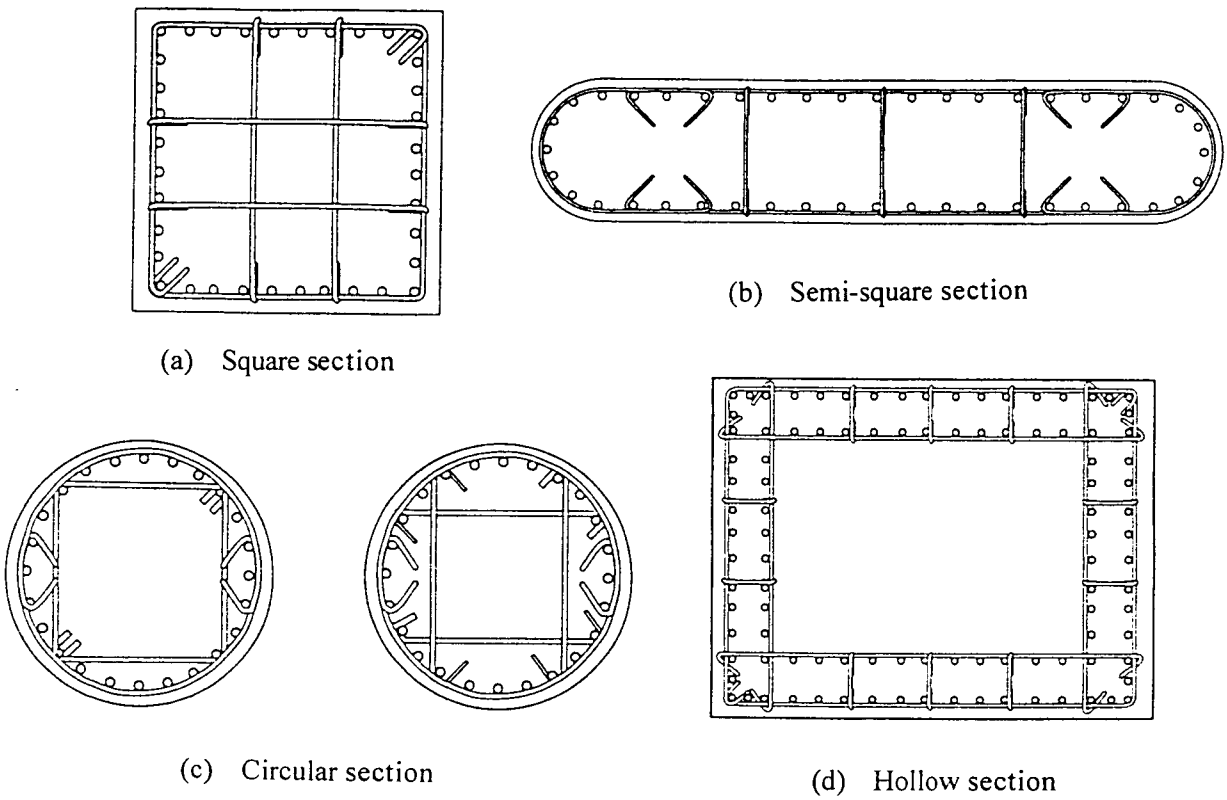

Fig. 7 Confinement of Core-concrete by Tie Reinforcement

Steel pier

In a concrete infilled steel pier, the lateral capacity P_a and the allowable displacement ductility factor μ_a in Eqs. (1) and (2) are evaluated as

$$P_a = P_y + \frac{P_u - P_y}{\alpha} \tag{19}$$

$$\mu_a = \left(1 + \frac{\delta_u - \delta_y}{\alpha \delta_y}\right)\frac{P_y}{P_a} \tag{20}$$

in which P_y and P_u= yield and ultimate lateral capacity of a pier, δ_y and δ_u= yield and ultimate displacement of a pier, and α= safety factor (refer to Table 3). The P_a and the μ_a are evaluated idealizing that a concrete infilled steel pier resists flexural moment and shear force as a reinforced concrete pier. It is assumed in this evaluation that the steel section be idealized as reinforcing bars and that only steel section resists axial force. A stress vs. strain relation of steel and concrete as shown in Fig. 7 is assumed. The height of infilled concrete has to be decided so that buckling is not developed above the infilled concrete.

A steel pier without infilled concrete must be designed with the dynamic response analysis. Properties of the pier need to be decided based on a cyclic loading test. Arrangement of stiffeners and welding at corner must be precisely evaluated so that brittle failure could be avoided.

DYNAMIC RESPONSE ANALYSIS

Dynamic response analysis is required in the bridges with complex dynamic response to check the seismic safety of the static design. Dynamic response analysis is also required as a " design" tool in the bridges for which the Ductility Design Method is not directly applied. In dynamic response analysis, ground motions which are spectral fitted to the following response spectra are used;

$$S_I = c_Z \cdot c_D \cdot S_{I0} \tag{21}$$

$$S_{II} = c_Z \cdot c_D \cdot S_{II0} \tag{22}$$

in which S_I and S_{II}= acceleration response spectrum for Type-I and Type-II ground motions, S_{I0} and S_{II0}= standard acceleration response spectrum for Type-I and Type-II ground motions, respectively, c_Z= modification coefficient for zone (refer to Eq. (5)), and c_D= modification coefficient for damping ratio given as

$$c_D = \frac{1.5}{40h+1} + 0.5 \tag{23}$$

Table 4 and Fig. 8 show the standard acceleration response spectra for the Type-I and Type-II ground motions.

Table 4 Standard Acceleration Response Spectra

(a) Type-I Response Spectra S_{I0}

Soil Condition	Response Acceleration S_{I0} (gal=cm/sec^2)		
Group I	S_{I0}=700 for $T_i \leqq 1.4$		S_{I0}=980/ T_i for $T_i > 1.4$
Group II	S_{I0}=1,505 $T_i^{1/3}$ for $T_i < 0.18$	S_{I0}=850 for $0.18 \leqq T_i \leqq 1.6$	S_{I0}=1,360/ T_i for $T_i > 1.6$
Group III	S_{I0}=1,511 $T_i^{1/3}$ for $T_i < 0.29$	S_{I0}=1,000 for $0.29 \leqq T_i \leqq 2.0$	S_{I0}=2,000/ T_i for $T_i > 2.0$

(b) Type-II Response Spectra S_{II0}

Soil Condition	Response Acceleration S_{II0} (gal=cm/sec^2)		
Group I	S_{II0}=4,463 $T_i^{2/3}$ for $T_i \leqq 0.3$	S_{II0}=2,000 for $0.3 \leqq T_i \leqq 0.7$	S_{II0}=1,104 $T_i^{5/3}$ for $T_i > 0.7$
Group II	S_{II0}=3,224 $T_i^{2/3}$ for $T_i < 0.4$	S_{II0}=1,750 for $0.4 \leqq T_i \leqq 1.2$	S_{II0}=2,371 $T_i^{5/3}$ for $T_i > 1.2$
Group III	S_{II0}=2,381 $T_i^{2/3}$ for $T_i < 0.5$	S_{II0}= 1,500 for $0.5 \leqq T_i \leqq 1.5$	S_{II0}=2,948 $T_i^{5/3}$ for $T_i > 1.5$

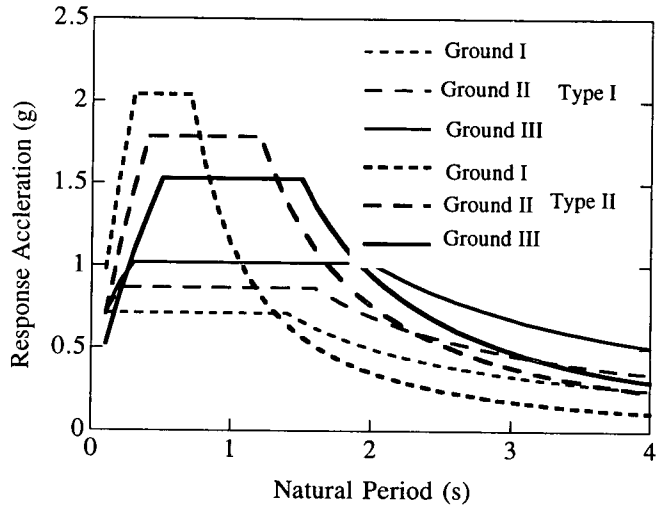

Fig. 8 Type I and Type II Standard Acceleration Response Spectra

It is recommended to use at least three ground motions per analysis, and take an average to evaluate the response.

In the dynamic response analysis, modal damping ratios have to be carefully evaluated. To determine the modal damping ratios, a bridge may be divided into several sub-structures in which energy dissipating mechanism is essentially the same. If one can specify a damping ratio of each sub-structure for a given mode shape, the modal damping ratio for i-th mode h_i may be evaluated as

$$h_i = \frac{\sum \phi_{ij}^T \cdot h_{ij} \cdot k_j \cdot \phi_{ij}}{\Phi_i^T \cdot K \cdot \Phi_i} \tag{24}$$

in which h_{ij}= damping ratio of j-th substructure in i-th mode, ϕ_{ij}=mode vector of j-th substructure in i-th mode, k_j= stiffness matrix of j-th substructure, K= stiffness matrix of a bridge, and Φ_i= mode vector of a bridge in i-th mode, and is given as

$$\Phi_i^T = \left\{\phi_{i1}^T,\ \phi_{i2}^T,\ \cdots\cdots,\ \phi_{in}^T\right\} \tag{25}$$

Table 5 shows recommended damping ratios for major structural components.

Table 5 Recommended Damping Ratios for Major Structural Components

Structural Components	Elastic Response		Nonlinear Response	
	Steel	Concrete	Steel	Concrete
Deck	0.02-0.03	0.03-0.05	0.02-0.03	0.03-0.05
Rubber Bearings	0.02		0.02	
Menshin Bearings	Equivalent damping ratio by Eq. (26)		Equivalent damping ratio by Eq.(26)	
Substructures	0.03-0.05	0.05-0.1	0.1-0.2	0.12-0.2
Foundations	0.1-0.3		0.2-0.4	

MENSHIN DESIGN

Basic principle

Implementation of the menshin bridges should be carefully decided, from not only seismic performance but function for traffic and maintenance point of view, based on the advantage and disadvantage of increasing natural period. The menshin design should not be adopted at the following conditions;

(a) sites vulnerable to lose bearing capacity due to the soil liquefaction and the lateral spreading,
(b) bridges supported by flexible columns,
(c) soft soil sites where potential resonance with surrounding soils could be developed by increasing the fundamental natural period, and
(d) bridges with uplift force at bearings.

It is suggested that the design should be made with an emphasis on an increase of energy dissipating capability and a distribution of lateral force to as many substructures as possible. To concentrate the hysteretic deformation at not piers but bearings, the fundamental natural period of a menshin bridge should be about 2 times or longer than the fundamental natural period of the same bridge supported by the conventional bearings. However, elongation of natural period aiming to decrease the lateral force should not be attempted.

Design procedure

Menshin bridges are designed by both the Seismic Coefficient Method and the Ductility Design Method. In the Seismic Coefficient Method, no reduction of lateral force from the conventional design is made.

In the Ductility Design Method, the equivalent lateral force coefficient k_{hem} in the menshin design is evaluated as

$$k_{hem} = \frac{k_{hcm}}{\sqrt{2\mu_m - 1}} \tag{26}$$

$$k_{hcm} = c_E \cdot k_{hc} \tag{27}$$

in which k_{hcm}= lateral force coefficient in menshin design, μ_m= allowable ductility factor of a pier, c_E= modification coefficient for energy dissipating capability (refer to Table 6), and k_{hc}= lateral force coefficient by Eq. (8). Because the k_{hc} is the lateral force coefficient for a bridge supported by the conventional bearings, Eq. (27) means that the lateral force in the menshin design can be reduced, as large as 30 %, by the modification coefficient c_E depending on the modal damping ratio for the fundamental mode of a bridge.

Table 6 Modification Coefficient for Energy Dissipation Capability

Damping Ratio for 1st Mode h	Coefficient c_E
h<0.1	1.0
0.1≦h<0.12	0.9
0.12≦h<0.15	0.8
h≧0.15	0.7

Modal damping ratio of a menshin bridge h for the fundamental mode is computed as

$$h = \frac{\sum K_{Bi} \cdot u_{Bi}^2 \cdot \left\{ h_{Bi} + \frac{h_{Pi} \cdot K_{Bi}}{K_{Pi}} + \frac{h_{Fui} \cdot K_{Bi}}{K_{Fui}} + \frac{h_{F\theta i} \cdot K_{Bi} \cdot H^2}{K_{F\theta i}} \right\}}{\sum K_{Bi} \cdot u_{Bi}^2 \cdot \left\{ 1 + \frac{K_{Bi}}{K_{Pi}} + \frac{K_{Bi}}{K_{Fui}} + \frac{K_{Bi} \cdot H^2}{K_{F\theta i}} \right\}} \tag{28}$$

in which h_{Bi}= damping ratio of i-th damper, h_{Pi}= damping ratio of i-th pier or abutment, h_{Fui}= damping ratio of i-th foundation associated with translational displacement, $h_{F\theta i}$= damping ratio of i-th foundation associated with rotational displacement, K_{Pi}= equivalent stiffness of i-th pier or abutment, K_{Fui}= translational stiffness of i-th foundation, $K_{F\theta i}$= rotational stiffness of i-th foundation, u_{Bi}= design displacement of i-th menshin device, and H= distance from a bottom of pier to a gravity center of a deck.

In the menshin design, the allowable displacement ductility factor of a pier μ_m in Eq. (26) is evaluated by

$$\mu_m = 1 + \frac{\delta_u - \delta_y}{\alpha_m \cdot \delta_y} \tag{29}$$

in which α_m is a safety factor used in menshin design, and is given as

$$\alpha_m = 2\alpha \tag{30}$$

where α is the safety factor in the conventional design (refer to Table 3). Eq. (30) means that the allowable displacement ductility factor in the menshin design μ_m should be smaller than the allowable displacement ductility factor μ_a by Eq. (2) in the conventional design. The reason for the smaller allowable ductility factor in the menshin design is to limit the hysteretic behavior of a pier at the plastic hinge zone so that principal hysteretic behavior occurs at the menshin device as shown in Fig. 4 (b).

Design of menshin devices

Simple devices stable against extreme earthquakes have to be used. The bearings have to be anchored to a deck and substructures with bolts, and should be replaceable. The clearance has to be provided between a deck and an abutment or between two adjacent decks.

The bearings are classified into two group; the first is the bearings which resist the seismic force of Eq. (2), and the second is the bearings which resist the seismic force in the Seismic Coefficient Method. The first and the second bearings are called as the Type-B bearings and the Type-A bearings, respectively. Seismic performance of the Type-B bearings is, of course, much higher than the Type-A bearings. In the Type-A bearings, a displacement limiting device, which will be described later, has to be co-installed in both longitudinal and transverse directions, while it is not required in the Type-B bearings. Because of the importance of bearings as one of the main structural components, the Type-B bearings should be used in the menshin bridges.

Isolators and dampers must be designed for a desired design displacement u_B. The design displacement u_B is evaluated as

$$u_B = \frac{k_{hem} \cdot W_u}{K_B} \tag{31}$$

in which k_{hem}= equivalent lateral force coefficient by Eq. (27), K_B= equivalent stiffness, and W_u= dead weight of a superstructure. It should be noted that because the equivalent lateral force coefficient k_{hem} depends on the type of ground motions, the design displacement u_B also depends on it.

The equivalent stiffness K_B and equivalent damping ratio h_B of a device are evaluated as

$$K_B = \frac{F(u_{Be}) - F(-u_{Be})}{2u_{Be}} \tag{32}$$

$$h_B = \frac{\Delta W}{2\pi W} \tag{33}$$

$$u_{Be} = c_B \cdot u_B \tag{34}$$

in which $F(u)$= restoring force of a device at a displacement u, u_{Be}= effective design displacement, ΔW= energy dissipaion of a device per cycle, W= elastic strain energy, and c_B= coefficient to evaluate effective displacement (=0.7).

In design of menshin devices, the following requirements have to be satisfied:

1) The displacement computed by Eq. (31) should be within $\pm 10\%$ from the assumed design displacement u_B, and the equivalent damping ratio evaluated by Eq. (33) should not be less than the equivalent damping ratio assumed in design.
2) Shear strain induced in a laminated rubber bearing γ subjected to a lateral force equivalent to the equivalent lateral force coefficient k_{hem} by Eq. (26) are evaluated as

$$\gamma = \frac{u_B}{\sum_{i=1}^{n} t_{ei}} \tag{35}$$

in which u_B= design displacement of a rubber bearing by Eq. (31), t_{ei}=thickness of i-th rubber, and n= number of layers of rubber. The shear strain by Eq. (35) should be less than 250 %.
3) Local shear strain should be less than the rupture strain divided by a safety factor of 1.2. Recommended rupture strains are presented in Table 7.

Table 7 Recommended Rupture Strain of Rubber

Type of Rubbers	Shear Modulus (N/mm^2)	Rupture Strain (%)
Natural Rubbers	80	500
	100	500
	120	400
Chloroplane Rubbers	80	400
	100	400

4) The devices have to be designed and fabricated so that scatter of the equivalent stiffness K_B and the equivalent damping ratio h_B be within $\pm 10\%$ of the design values.
5) The devices have to be stable against at least 50 and 15 load reversals, for the Type-I and Type-II ground motions, respectively, with the design displacement u_B by Eq. (31) under a vertical force equivalent to the dead weight of a superstructure.
6) Tangential stiffness of a device should be positive at any displacement within the design displacement. This is to prevent a possible shake-down of the devices in one side, when they are subjected to large cyclic load reversals.
7) A deck should return to the rest position even after it is subjected to an large earthquake. The residual displacement u_{BR} developed in a device after it is smoothly released from a deformed displacement equivalent to the design displacement u_B by Eq. (31) should be less than 10% of the design displacement u_B.

8) The equivalent stiffness K_B and the equivalent damping ratio h_B of a device shall be stable against a change of load condition and natural environment such as the temperature change.

In addition to the above requirements, a special provision which will be described in the following section should be adopted in the unseating prevention systems.

UNSEATING PREVENTIONSYSTEMS

Unseating prevention measures are required for the highway bridges. The measures required for the highway bridges are as:

1) the unseating prevention systems have to be so designed that unseating of a superstructure from their supports can be prevented even if unpredictable failures of the structural members occur,
2) the unseating prevention systems are consisted of providing enough seat length, a falling-down prevention device, a displacement limiting device, and a device for preventing settlement of a superstructure,
3) enough seat length must be provided and a falling-down prevention device must be installed at the ends of a superstructures against longitudinal response. If the Type-A bearings are to be used, a displacement limiting device has to be further installed at not only the ends of a superstructure but each intermediate support in a continuous bridge, and
4) If the Typr-A bearings are used, a displacement limiting device is requested at each support against transverse response. The displacement limiting device is not generally required if the Type-B bearings are used. But, even if the Type-B bearing is adopted, it is required in skewed bridges, curved bridges, bridges supported by columns with narrow crest, bridges supported by few bearings per piers, and bridges constructed at the sites vulnerable to lateral spreading associated with soil liquefaction.

The seat length S_E is evaluated as

$$S_E = u_R + u_G \geq S_{EM} \tag{36}$$

$$S_{EM} = 0.7 + 0.005l \tag{37}$$

$$u_G = \varepsilon_G \cdot L \tag{38}$$

in which u_R= relative displacement (m) developed between a superstructure and a substructure subjected to a seismic force equivalent to the equivalent lateral force coefficient k_{hem} by Eq. (26), u_G= relative displacement of ground along the bridge axis, S_{EM}= minimum seat length (m), ε_G= ground strain induced during an earthquake along the bridge axis, and is 0.0025, 0.00375, and 0.005 for Group-I, II and III sites, respectively, L= distance which contributes to the relative displacement of ground (m), and l= span length (m). If two adjacent decks are supported by a pier, the lager span length should be l in evaluating the seat length in Eq. (37).

In the menshin design, in addition to the above requirements, following considerations have to be made.

1) To prevent collisions between a deck and an abutment or between two adjacent decks, enough clearance must be provided. The clearance between those structural components S_B shall be evaluated as

$$S_B = \begin{cases} u_B + L_A & \text{between a deck and an abutment} \\ c_B \cdot u_B + L_A & \text{between two adjacent decks} \end{cases} \tag{39}$$

in which u_B= design displacement of a device in Eq. (31), L_A=redundancy of a clearance (generally $\pm$15mm), and c_B= modification coefficient for clearance (refer to Table 8). The modification coefficient c_B was determined based on an analysis of the relative displacement response spectra. It depends on a difference of natural periods $\Delta T = T_2 - T_1$ ($T_1 \geq T_2$), in which T_1 and T_2 represent the natural period of the two adjacent bridge systems.

Table 8 Modification Coefficient for Clearance c_B

$\Delta T / T_1$	c_B
$0 \leqq \Delta T / T_1 < 0.1$	1
$0.1 \leqq \Delta T / T_1 < 0.8$	$\sqrt{2}$
$0.8 \leqq \Delta T / T_1 \leqq 1.0$	1

2) The clearance at an expansion joint L_E is evaluated as

$$L_E = u_B + L_A \tag{40}$$

in which u_B= design displacement of a device in Eq. (31), and L_A= redundancy of a clearance (generally $\pm$15mm).

CONCLUDING REMARKS

The preceding pages presented an outline of the new Seismic Design Specifications of Highway Bridges issued in 1996 as well as the damage features of highway bridges in the 1995 Hyogo-ken nanbu earthquake. The Hyogo-ken nanbu earthquake was the first earthquake which developed destructive damage in an urban area since the 1948 Fukui earthquake. Because it had been considered that such destructive damage could be prevented due to the progress of construction technology in recent years, it provided a large impact on the earthquake disaster prevention measures in various fields. The "Part V Seismic Design" of the "Design Specifications of Highway Bridges" (JRA) was totally revised in 1996, and the design procedure moved from the traditional Seismic Coefficient Method to

the Ductility Design Method. The revision was so comprehensive that the past revisions in the last 30 years look minor.

Major point of the revision was the introduction of explicit two-level seismic design consisting of the Seismic Coefficient Method and the Ductility Design Method. Because the Type-I and the Type-II ground motions are considered in the Ductility Design Method, three design seismic forces are totally used in design. Seismic performance for each design force was clearly stated in the Specifications.

The fact that lack of near-field strong motion records prevented to seriously evaluate the validity of recent seismic design codes is important. The Hyogo-ken nanbu earthquake revealed that history of strong motion recording is very short, and that no near-field records have yet been measured by an earthquake with magnitude on the order of 8. It is therefore essential to have enough redundancy and ductility in a total bridge system. It is hoped that the revised Seismic Design Specifications of Highway Bridges contributes to enhance seismic safety of highway bridges.

REFERENCES

Japan Road Association (1996) Design Specifications of Highway Bridges, Part I Common Part, Part II Steel Bridges, Part III Concrete Bridges, Part IV Foundations, and Part V Seismic Design.

Kawashima, K. (1996) Impact of Hanshin/Awaji Earthquake on Seismic Design and Seismic Strengthening of Highway Bridges, Report No. TIT/EERG 95-2, Tokyo Institute of Technology.

Ministry of Construction (1995a) Report on the Damage of Highway Bridges by the Hyogo-ken Nanbu Earthquake, Committee for Investigation on the Damage of Highway Bridges Caused by the Hyogo-ken Nanbu Earthquake.

Ministry of Construction (1995b) Guide Specifications for Reconstruction and Repair of Highway Bridges Which Suffered Damage due to the Hyogo-ken Nanbu Earthquake.

APPENDIX TABLE OF CONTENTS OF "PART V SEISMIC DESIGN" OF "DESIGN SPECIFICATIONS OF HIGHWAY BRIDGES," JAPAN ROAD ASSOCIATION, 1996

1. General
   1.1 Scope
   1.2 Definition of Terms
2. Basic Principle of Seismic Design
3. Loads and Design Conditions Considered in Seismic Design
   3.1 Loads and Combinations
   3.2 Effects of an Earthquake

3.3 Inertia Force
3.4 Importance
3.5 Modification Factor for Zone
3.6 Modification Factor for Ground Condition
3.7 Ground Surface Assumed in Seismic Design
4. Seismic Design by Seismic Coefficient Method
4.1 Lateral Force Coefficient
4.2 Dynamic Earth Pressure
4.3 Dynamic Hydraulic Pressure
5. Seismic Design by Ductility Design Method
5.1 General
5.2 Evaluation of Safety
5.3 Lateral Force Coefficient
6. Check of Safety by Dynamic Response Analysis
6.1 General
6.2 Analytical Models and Analytical Procedures
6.3 Ground Motions
6.4 Evaluation of Safety
7. Seismic Design of Foundations at the Soils Vulnerable to Unstability
7.1 General
7.2 Seismic Design of Foundations at the Sites Vulnerable to Failure of Clayey Materials or Soil Liquefaction
7.3 Seismic Design of Foundations at the Sites Vulnerable to Lateral Spreading
7.4 Evaluation of Soft Clay or Silty Clay with Potential Failure
7.5 Evaluation of Sandy Soils with Potential to Develop Soil Liquefaction
7.6 Soil Layers Whose Bearing Capacity Should be Decreased
8. Menshin Design
8.1 General
8.2 Menshin Design
8.3 Seismic Force in Menshin Design
8.4 Design of Devices
8.5 Evaluatio n of Natural Period of a menshin Bridge
8.6 Evaluation of Damping Ratio of a Menshin Bridge
8.7 Design Detailings in Menshin Design
9. Capacity and Ductility of Reinforced Concrete Piers
9.1 General
9.2 Lateral Capacity and Ductility

9.3 Lateral Force and Lateral Displacement at Yield and Ultimate
9.4 Stress-Strain Relation Assumed in Concrete
9.5 Shear Capacity
9.6 Design Detailings to Enhance Ductility
9.7 Termination of Main Reinforcements at Mid-height
9.8 Lateral Capacity and Ductility of Frame Piers
9.9 Effect of Eccentricity of Vertical Load in Inverted L-shaped Piers
10. Lateral Capacity and Ductility of Steel Piers
10.1 General
10.2 Steel Piers with Infilled Concrete
10.3 Steel Piers without Infilled Concrete
10.4 Seismic Design of Anchor
10.5 Effect of Eccentricity of Vertical Load in Inverted L-shaped Steel Piers with Infilled Concrete
11. Lateral Capacity of Foundations
11.1 General
11.2 Evaluation of Seismic Force, Reaction Force and Displacement of Foundations
11.3 Yield of Foundations
11.4 Evaluation of Response of Foundations when Principal Plastic Hinge Occurs at Foundations, and Allowable Maximum Response Displacement
11.5 Check of Safety
12. Bearings and Their Surrounding Structures
12.1 General
12.2 Seismic Design Force for Bearings and Their Surroundings
12.3 Evaluation of Safety
12.4 Structures of Bearings and Their Surroundings
13. Unseating Prevention Systems
13.1 General
13. 2 Seat Length
13.3 Unseating Prevention Devices
13.4 Excessive Displacement Limiting Devices
13.5 Devices for Preventing Settlement of a Superstructure
13.6 Joint Protectors
13.7 Strengthening of Portion of Superstructure where Unseating Prevention Device is Connected
13.8 Unseating Prevention Systems in Transverse Direction
14. Structures to Reduce Bridge Response

AN AUTOMATIC PROCEDURE FOR ANALYTICAL SEISMIC ASSESSMENT OF THE BRIDGES IN A HIGHWAY SYSTEM

P.E. Pinto[1] **R. Giannini**[2] **C. Nuti**[3]

[1]Dipartimento di Ingegneria Strutturale e Geotecnica, Univ. di Roma "La Sapienza", Italy
[2]Dipartimento di Progettazione e Scienze dell'Architettura, Univ. di Roma 3, Italy
[3]Dipartimento di Scienze, Storia e Restauro dell'Architettura, Univ. di Pescara, Italy

ABSTRACT

A procedure for rapid analytical seismic assessment of the bridges in a highway system is presented and demonstrated with reference to the northern and central part of the italian network.

The procedure works through the following steps. In order to decide which bridges are worth to be assessed, the 500 years return period intensity at the site of each bridge is compared with the lateral resistance that bridges of the considered type (simply supported) automatically possess due to design requirements other then the seismic one.

The bridges remained after the preliminary screening are examined by having recourse to a data bank (set up by the owner essentially for maintenance purpose) allowing the geometry of the bridge to be reconstructed. On the basis of the geometry, a simulated design of the bridge is carried out using the codes applicable at the time of its construction. On these "virtual" bridges (spot checks have shown close correspondence with the real ones) a probabilistic safety analysis is performed, and the probability of collapse, given the occurrence of the local hazard, is determined.

The adequacy of the calculated safety is judged by comparing it with the one provided by the Eurocode 8 to bridges of new design. This latter is in turn estimated by designing some bridges according to EC8, and performing on these designs the same type of safety analysis made previously. The end result is a list of substandard bridges, ordered for decreasing level of risk, which will enter with a weight proportional to its value in the decision process of a rehabilitation program.

1 INTRODUCTION

After the San Ferdinando earthquake in 1971 and, with accelerating pace, after the more recent destructive events in the USA (Loma Prieta, 1985; Northridge, 1994) and in Japan (Kobe, 1995) a large amount of retrofit work on bridges is taking place all over the developed seismic countries of the world. The deficiencies that make existing bridges,

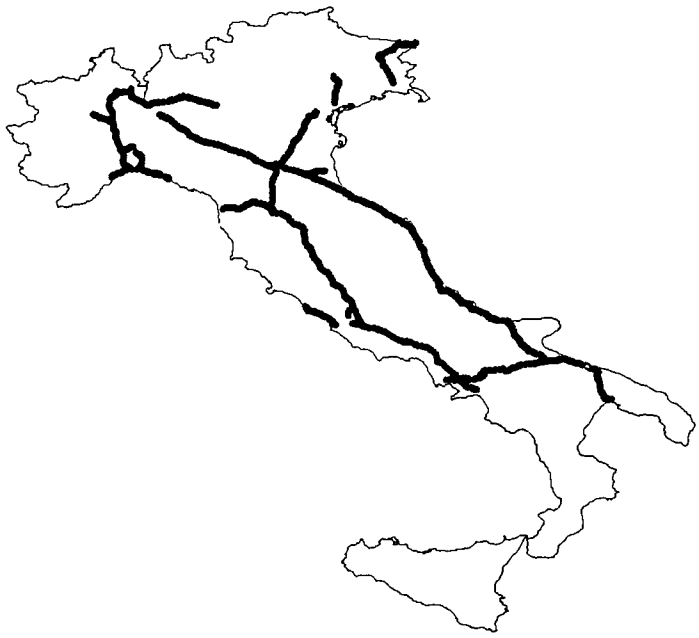

Figure 1: The italian highway network of *Autostrade*

even those built until the very last few years, vulnerable to seismic action are too well known to be repeated once more, (see Priestley et al., [4]) they all have a single common cause: the conventionality of the seismic design approach used in the former codes (and still in some of present ones).

The structural types adopted internationally for urban viaducts and highway bridges are mostly similar; this situation has been of help in arriving at a unified view on the appropriate diagnosis methods and on the remedial measures to be adopted, be these necessary for enhancing strength and/or ductility of the piers, for eliminating excessive mobility of the deck, for ensuring safe transmission of the forces through bearings, etc. This amounts to saying that in seismic retrofit of bridges the focus is not so much on theoretical developments, although technological advances are needed for ex. on materials and techniques for strengthening, as it is on an efficient management of the resources available.

Basic prerequisite is clearly a knowledge of the state of the bridges which is adequate for the stated purpose, and this includes in principle assessment of the present risk, ranking the bridges in order of importance (value of the bridges and its role in ensuring continued communication), rehabilitation cost, simultaneous necessity of interventions for non seismic maintenance and repair, etc.

In Italy, the largest part ($\sim$ 90%) of the existing highway system is owned and operated by a single Company: *Autostrade*. Its network, shown in Fig. 1, has roughly 5500 km of highways, comprising a total of 2826 bridges. The highways were built essentially in the 60's and in the 70's, with only minor additions going on until presently. Seismic design regulations of the time were almost nominal: horizontal forces equal to 10% of the permanent weights in the zones of highest seismicity (7% in the other seismic zones),

with no attention paid to ensure ductile behavior, to check compatibility of displacements between adjacent decks, the strength and admissible displacements of the bearings, etc.; In a large percentage of cases, the reinforcement of the piers is not dictated by the seismic forces, but from wind and braking forces, or more simply by minimum percentage requirements. Fortunately, tradition has in Italy that bridge piers should be (and look) rather rigid, as compared to those of similar bridges elsewhere, and this provides in many cases a much appreciated extra strength. Also for the foundations, italian practice is rather conservative, in order to ensure satisfactory performances under service loads, and this leads in many cases to foundations which are stronger than the superstructure, a desirable property under seismic action.

The seismicity in Italy is certainly less than that for ex. in California or in parts of Japan, but events of Magnitude of the order of 6.5 are rather frequent (the last $M = 6.5$ event did occur in Southern Italy in 1981, and the previous $M = 6.5$ in Northern Italy in 1976), and events of magnitude larger than 7 have also occurred, at a rate of about twice every century starting from the year 1000. Although the seismicity of Italy is well known to geophysicists, and plenty of hazard studies have been produced and are available, no officially approved hazard map exists, while the zoning of the country for the purposes of seismic design reflects more the information from (recent) past events than the input from geophysical studies. Additionally, the seismic zones have been substantially enlarged after the 70's, i.e. after the completion of the highway system, so that in the end a random relation exists between the location of the bridges, the actual hazard at the sites, the present definition of the seismic zones, and the way the bridges have been designed (earthquake resistant or not).

The last strong earthquakes in Italy have not produced significant damages to bridge structures (by chance, due to the fact that the highways were far from epicentral areas). In spite of the lack of this, usually potent, incentive to assessment and rehabilitation programs, *Autostrade* has resolved to undertake a systematic scrutiny of its entire bridge stock in terms of seismic performance. Given the unusually large scale of the problem, particular attention has been devoted to the setting up of an appropriate assessment method, with the constraints that it should not be based on qualitative typological vulnerability forms on one hand, nor it should require detailed analyses based on drawings, at the other extreme. A number of alternatives were initially considered; the one receiving more credit at an early stage was to try to categorize the whole stock into a discrete number of types, then to select a representative bridge within each type and to analyze it in detail. All bridges belonging to the same type would have then been assigned the vulnerability found for the representative structure.

A much more accurate and efficient procedure has been finally set up, which relies upon an existing data bank created by *Autostrade* for maintenance purposes, allowing a complete reconstruction of the geometry of all bridges. Details and limitations of the procedure are described in the following.

The outcome of this part of the study is one number for each bridge, expressing the probability of failure of the bridge, given that the peak ground acceleration having a selected (the same for the whole network) annual probability of exceedance occurs at the bridge site. To evaluate this set of numbers, a reference is needed. The criterion adopted has been to consider as acceptable (i.e. no intervention on the bridge is required) all values which are equal or below the probability of failure of representative bridges designed in

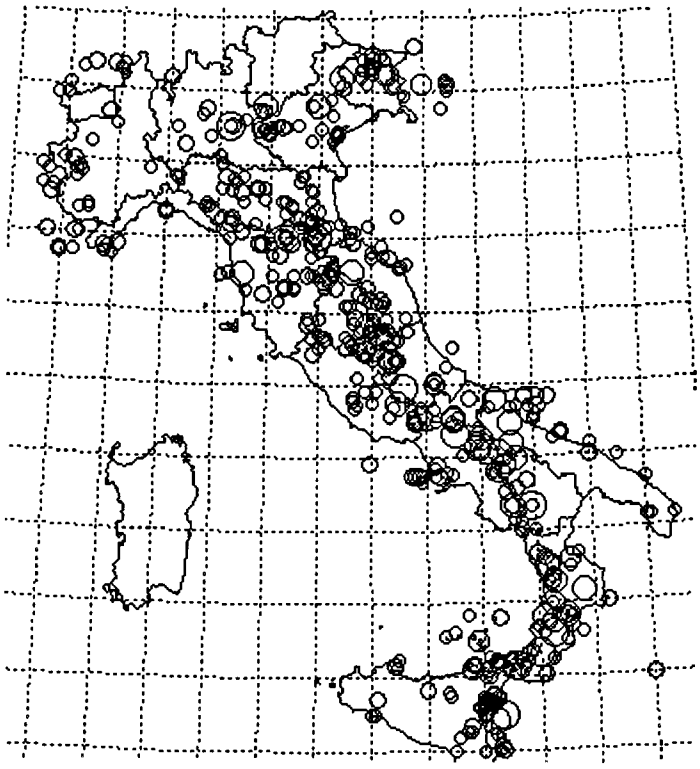

Figure 2: Historical events in Italy with $I_{MM} > 7$

accordance with Eurocode 8/2 [1], given the occurrence of the design acceleration. Of course no such value can be found in EC8/2. This has required a side study, consisting in designing a number of bridge structures, similar to those of interest, in full accordance with the provisions of the EC8/2 and, subsequently, in performing on them a probabilistic risk analysis, conditional to the occurrence of the acceleration used in the design. The values obtained had clearly a certain scatter, and a reasonable upper bound was therefore selected.

The end result of the whole study, as reported in the paper, is a list of bridges, ordered for decreasing values of risk, which do not fulfil the safety requirements for new designs according to a modern code. This is considered to be the point of departure for developing cost-benefit strategies necessary for providing guidance for the amount of strengthening to be provided.

2 SCREENING OF THE BRIDGES TO BE EXAMINED

About three quarters of the italian territory is considered as seismically active, and earthquake resistant design is compulsory. Seismicity is not uniform, however, the southern regions having the heaviest record of destructive events. A plot of all the events occurred since the year 1000 with intensity larger than 7 is shown in Fig. 2. The *Autostrade* network is definitely more dense in the north, with only portions of it running across the more dangerous areas of the north, the center and the Appennine region in the south.

The first necessary step in the study to be undertaken is clearly to determine the seismic hazard along the route of the various highways. This is just one side of the

problem, however, the other one being the level of seismic intensity for which a risk evaluation of bridges is warranted.

Whether designed for earthquakes or not, all bridges posses a certain resistance to lateral loads, which comes from requirements of stiffness and from design for wind and other horizontal forces. If this "natural" resistance, expressed in terms of ground acceleration causing failure, is larger than the ground acceleration at the site having an appropriately chosen (large) return period, any seismic verification becomes unnecessary.

The two steps described above have been carried out according to the following criteria.

2.1 Hazard analysis

The combined historical-geophysical information available allows to subdivide the italian territory into 45 homogeneous regions, for each of which the catalogue data are sufficient for determining a separate Gutemberg-Richter law for the intensity, including upper and lower bounds. Using a single attenuation law for the whole range of intensities and for all regions (alternatives are available, bat they are not adequately supported), a Cornell type of analysis has been carried out to determine the value of I_{MM} having specified values of the return period, T_R, along the highway route. Values of $T_R = 500$ years and 50 years have been considered, the former one to be used for ultimate limit states (ULS) verifications. Selected results for two highways, the N-S Milano–Napoli and the W-E Napoli–Canosa are shown in Fig. 3. The latter highway crosses one of the major seismic regions of the country.

2.2 Natural seismic resistance

Out of the total of 2826 bridges, more than one third: 1151, are made up of decks which are simply supported on different piers systems. Other 1363 bridges are single span structures directly supported on the abutments, and the remaining 312 bridges are variously distributed among Gerber, arch, continuous deck, cantilever construction and frame-like types.

Leaving out bridges of unique characteristics, like for ex. some large arch bridges built in the sixties, as well as other important bridges with large spans (in excess of 100 m), for which specific vulnerability studies are unavoidable, the category of the simply supported bridges has been considered as the one with the largest risk and, inside this category, the piers made up of single bents as the more vulnerable.

Searching in the data base of *Autostrade*, the characteristics of which will be presented later, the whole range of cross-section properties of the piers, the corresponding range of heights for each section geometry, and the span lengths have been examined. Span length is not a strong parameter, since most spans are around 30 m, only the more recent ones reaching 40 m. The key parameter is the ratio between the cross section dimension and the height of the pier. The choice has finally been made of two cross section shapes, each one associated with a range of heights, as shown in Table 1, for a total of 10 cases.

CROSS SECTIONS	(m)	HEIGHTS (m)
Rectangular hollow	6.60×3.80	10, 15, 25, 35, 45
Circular hollow	3.80	8, 12, 16, 20, 24

Table 1: Representative piers examined

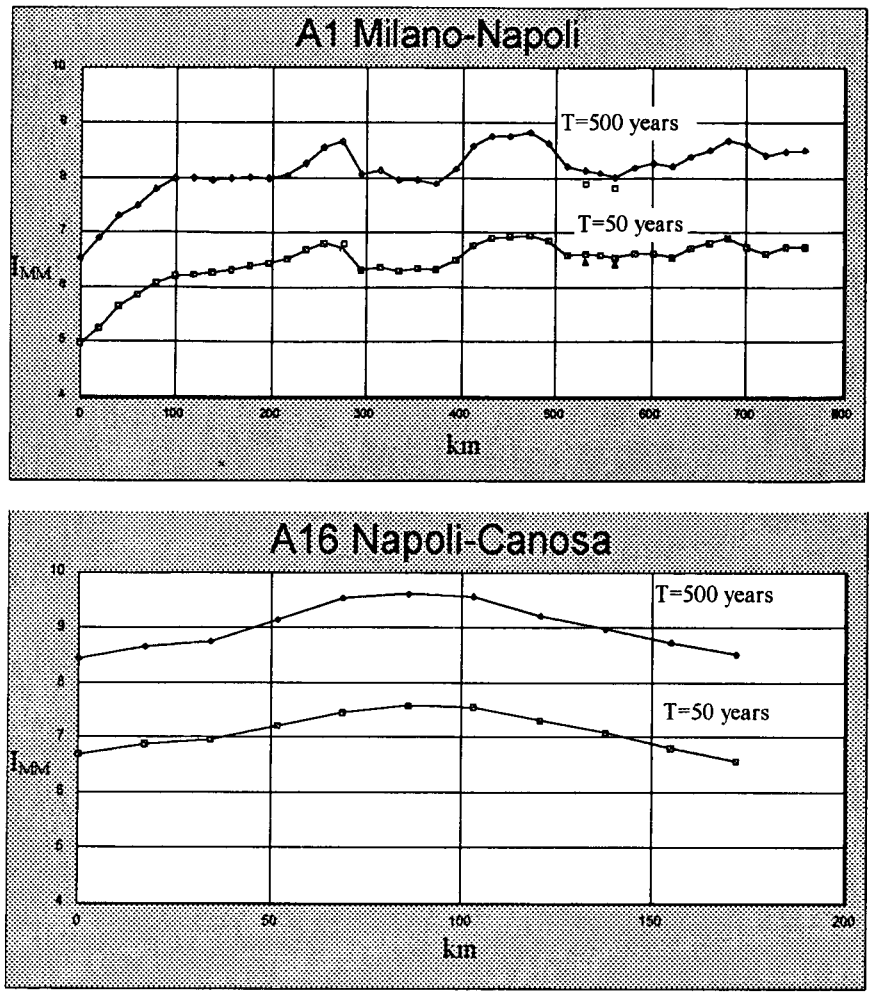

Figure 3: Hazard curves for two italian highways

Although they are representative of the actual population, the cases examined do not correspond to existing bridges: they are believed to be an hypothetical sample lying on the more vulnerable side of the whole set. The virtual bridges have been subsequently designed using the loading and material codes applicable in the period 1960–1970, considering traffic and wind loading, but excluding seismic forces. With the longitudinal and transverse reinforcement known, a numerical model of the bridge can then be constructed.

Flexural behavior is described by means of a bi-linear force-displacement relationship at the top of the pier. The details of this derivation are given later; for the purpose at hand the characteristics that are used are: the yield force F_y, the stiffness $K = F_y/\Delta_y$, where Δ_y is the top displacement at yield, the period $T = 2\pi\sqrt{M/K}$, where M is the mass of the deck inclusive of the pier cap and of the part of the pier, and the ultimate ductility $\mu = \Delta_u/\Delta_y$, where Δ_u is based on the ultimate curvature of the base section, evaluated by assuming conservative values of the compressive strain of the concrete.

If $\overline{S}_a(T)$ denote an appropriate elastic response spectrum normalized to a unit peak

ground acceleration: $A = 1$, the value of A causing flexural collapse can be evaluated as:

$$A_c = \frac{F_y \mu}{M \overline{S}_a(T)} \tag{1}$$

provided $V_u \geq F_y$, where V_u is the ultimate shear capacity of the pier. When the above condition is not satisfied, shear failure precedes flexural failure, and the corresponding acceleration is:

$$A_c = \frac{V_u}{M \overline{S}_a(T)} \tag{2}$$

In the analyses, $\overline{S}_a(T)$ has been taken as the normalized elastic spectrum suggested in the Eurocode 8 for intermediate soil conditions, while shear capacity has been evaluated in accordance with Eurocode 2. The values of A_c obtained for the ten cases of piers, in the transverse direction, are reported in Table 2.

	RECTANGULAR					CIRCULAR				
H (m)	10	15	25	35	45	8	12	16	20	24
A_c (g)	0.25	2.6	1.7	1.4	1.4	0.47	0.37	0.31	0.28	0.34

Table 2: Values of acceleration causing collapse

Shear failure occurs only for the shorter ($H = 10$ m) rectangular pier; in all other piers collapse is governed by exhaustion of ductility. Circular piers have consistently lower values of A_c, due to lower available ductility with respect to the rectangular ones: this in turn is due to the shape of the section and to the higher average vertical stress.

It is observed however, that all values obtained are rather high, perhaps higher than expected, given the total absence of design provisions for seismic resistance. This is principally a consequence of the relatively large dimensions adopted for the piers, for reasons of minimum stiffness and/or aesthetics.

The same piers have been combined in various ways to form longitudinal bridge configurations: the analyses made assuming equal longitudinal displacements have yielded values of A_c of the same order of magnitude than for single piers in the transverse direction.

In addition to the structural failure mechanisms considered up to now, the possibility of collapse due to loss of support of the deck has also been considered. This type of failure has been frequently observed in recent earthquakes even for bridges of the last generation.

The modeling assumptions for this phenomenon have been rather simple: two identical adjacent piers have been considered to move in the opposite direction, with a maximum relative displacement evaluated as: $u_{max} = \sqrt{2u_i^2} = \sqrt{2}u_i$, where u_i is the maximum displacement at the top of each pier. A seating length of 50 cm has been considered; the most unfavorable situation occurred for the tallest rectangular pier ($H = 45$ m) for which the value of $A_c(50\,\text{cm}) = 0.13\,g$ was found.

2.3 Conclusions

For failures of structural types, the lowest value of A_c within the population considered has been: $A_c = 0.25\,g$, related to a shear type of failure. According to the relationship adopted

Figure 4: Highways for which the risk analysis has been performed

between A and I: $A = 10^{-2.3356+0.1908\,I}$, the corresponding value of I is ~ 9. Considering the variability inherent in the relationship on one hand, and the possible existence in the whole network of bridges more vulnerable than those examined, the threshold below which no seismic evaluation is required has been set to $I_{MM} = 8\,(\Rightarrow 0.15\,g)$. Analogous considerations of prudence led to adopt a value of $I = 7$ for the threshold below which no intervention preventing decks from failing needs to be considered.

Comparing the values of the two thresholds with the 500 years return period hazard, it has been found that for what concerns structural failure only 6 of the 15 highways, and not all for their entire length, remain: they are shown in Fig. 4. For the problem of unseating the risk is larger, and 12 out of the 15 highways need to be checked under this respect.

3 EVALUATION OF THE BRIDGES

3.1 Outline of the procedure

Information on all bridges of the network *Autostrade* is contained in a data-bank, to be described in the following section. The procedure for seismic evaluation reads sequentially, for each of the six highways left from the preliminary screening, the location of each bridge: if the calculated local hazard is less than $I = 8$, it passes directly to the next one, until one is found for which $I \geq 8$. The corresponding value of the peak ground acceleration is calculated.

Entering into the data-base, the procedure selects the information required to reconstruct the geometry of the bridge, and all available elements required for the purposes of

the evaluation. Given the geometry, and using the loading and material codes in force at the time of the construction, the longitudinal and transverse reinforcement of the piers is determined in turn. The available data allow this simulated design to be carried out for the majority of existing pier types. When data are not sufficient the bridge in question is tagged for a separate ad hoc treatment.

A mechanical model of the pier is then set up. Evaluation consists in determining the probability of collapse of each pier: P_{fi} for a combined mechanism of flexure and shear, given the value of the site peak ground acceleration characterized by an average return period of 500 years. In obtaining P_{fi}, flexural and shear strength, ultimate ductility, elastic spectral ordinates and inelastic force reduction factors are assumed as random variables. Next, the probability of collapse for the entire bridge is evaluated with the assumption of independent collapses of all piers:

$$P_f = 1 - \prod_i (1 - P_{fi}) \tag{3}$$

3.2 The data bank *SAMOA*

SAMOA has been elaborated by *Autostrade* for several purposes, the main ones being the possibility of keeping up-dated the state of each bridge in terms of deterioration phenomena affecting materials (carbonation of concrete, oxidation of steel, etc.) and elements (loss of concrete, cracking, degradation of joints, bearings, movements in the foundations, etc.), as well as for keeping track of all the interventions made, which may range from ordinary maintenance to structural restoration, with or without upgrading.

Bridges in *SAMOA* are decomposed into the following structural elements: foundations, piers, abutments, arches, decks, bearings, joints. One form is filled for each element, e.g. one form for each of the piers, etc. The case of a simply supported bridge is illustrated in Fig. 5.

For what concerns the piers, that are the elements to be known in more detail for the purpose of evaluation, the following classification is adopted. The structural systems can be: Single bent, Wall, Portal frame and Multi-bay frame, both with or without intermediate transverse beams, plane or spatial. The cross sections of the vertical elements can be: rectangular, circular, polygonal, elliptic and "other", either solid or hollow, in the latter case simply or multiply connected.

The data as described are not in all cases sufficient for reconstructing the geometry of the piers, while in other cases they may be redundant, which is useful for a double checking. The case of sufficient or redundant data refer to: single bents, simple (plane, no intermediate transverse beams) portal and multiple frames. These categories, however, include about 80% of all actual structures. Other data to be read from *SAMOA* are the width of the deck (which is practically constant for a given highway) the span lengths and details concerning the piers caps.

3.3 Simulated design of the piers

Actions considered in the design include permanent loads, traffic, braking, wind loads and, if at the time of construction the site was classified as seismic, static equivalent seismic forces (to be combined with the permanent loads only).

The action effects are of immediate determination in the case of simple cantilevers. For frames, the assumption has been made of a stiff top transverse beam, so as to allow

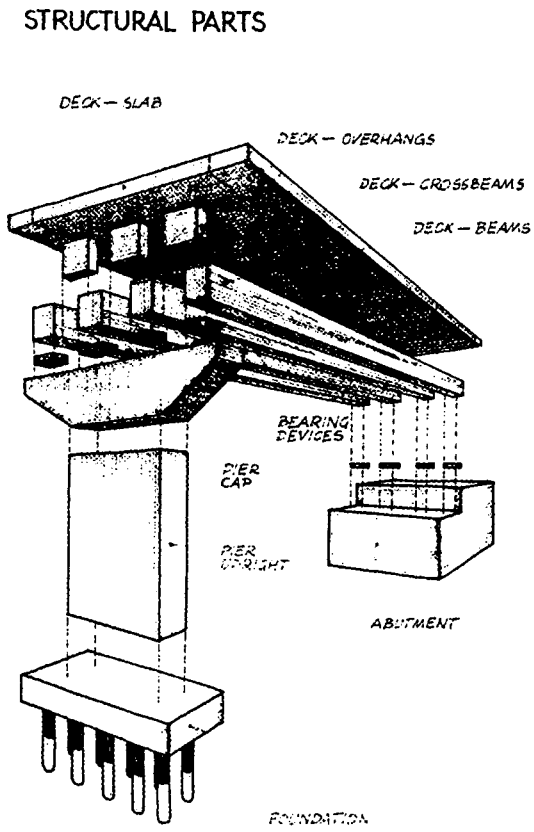

Figure 5: Sketch of bridge elements considered in *SAMOA*.

for the approximation of treating the columns as built in at both ends.

The most unfavorable combination of action effects has been used for the design of the base section of the piers (all piers have uniform dimensions along their height), for bending and for shear. Admissible stress criteria have been adopted, with values consistent with the presumed strength characteristics of concrete and steel. In many cases, the amount of reinforcement (longitudinal as well as transverse) has been found to be governed by minimum requirements. Spot comparisons of the calculated amount of reinforcement with that indicated in the design drawings have shown good agreement between the two.

3.4 Evaluation procedure

The mechanical model of the pier consists in all cases of a cantilever carrying a mass at the top. If the original structure is a frame, with two or more columns, the force-displacement relationship is evaluated considering the columns as built in at one end and with a height equal to half of the clear height between foundation mat and pier cap. The moment-curvature relationship of the end section, calculated using the amount of reinforcement obtained from the simulated design, is sufficient for obtaining the yield (F_y, u_y) and the ultimate (F_u, u_u) points in the F-u curve. As shown in Fig. 6, the variation of the curvature along the height is assumed to be parabolic between yield and decompression sections, and then linear up to the top. The expressions for the two points are:

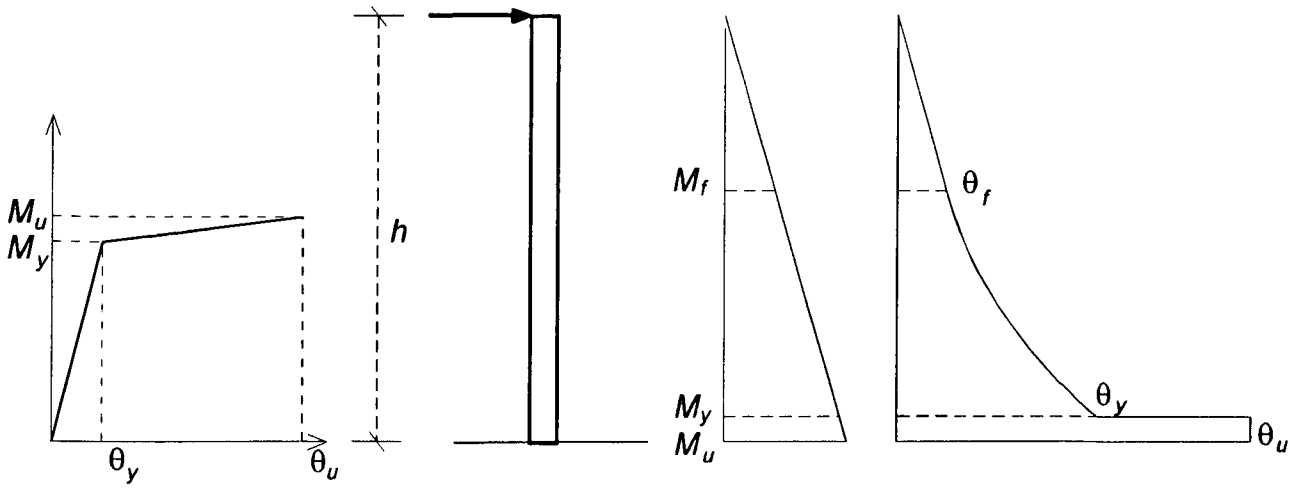

Figure 6: Variation of the curvature along the height of pier

$$u_y = \frac{h^2}{12}\left[\theta_f\left(1+\frac{M_d}{M_y}\right)^2\frac{M_y}{M_d}+\theta_y\left(3+\frac{M_d}{M_y}\right)\left(1-\frac{M_d}{M_y}\right)\right]$$
$$F_y = \frac{M_y - Pu_y}{h} \tag{4}$$

$$u_u = u_y\left(1-\frac{l_p}{h}\right)^2+\theta_u l_p\left(h-\frac{l_p}{2}\right)$$
$$F_u = \frac{M_u - Pu_u}{h} \tag{5}$$

with obvious meaning of the symbols. The length of the plastic hinge has been taken as half of the height of the section. The ultimate compression strain of concrete as been assigned a value of 0.5%.

The F-u diagram defines flexural strength and ductility of the pier.

For the assessment of shear capacity, use has been made of the expressions proposed by Priestley at al. [3]. Shear strength is assumed to be contributed by three terms:

$$V_u = V_c + V_s + V_p \tag{6}$$

where V_c is the contribution of concrete, V_s is the shear carried by transverse steel and V_p is is the horizontal component of the inclined thrust of the vertical load P, which is equilibrated at the base section by the compressive resultant displaced from the axis of the column (see Fig. 7). The expression of V_c is:

$$V_c = 0.29\,k\sqrt{f_c}A \tag{7}$$

with f_c equal to the concrete compressive strength (MPa), $A = 0.8A_g$, where A_g is the gross concrete section and k is a function of the amount of ductility used: is equal to 1 for $\mu \leq 2$, decreases linearly from 1 to 0.3 for $\mu = 4$, and remains constant thereafter. V_s is the usual expression for the truss model and $V_p = P\tan\beta$, where β is defined in Fig. 7.

As indicated previously, the evaluation has been carried out taking into account the uncertain nature of the variables involved, on the action side, on the response side and on the capacity side.

On the action side, the starting point has been the elastic response spectrum contained in EC8. The spectral ordinates of EC8 have been assumed as representing the 50% fractile value of the response, and they have been transformed into random variables (r.v.) by multiplying the median $S(T)$ by a r.v.: $\exp(\alpha_S)$, lognormally distributed and with unit median.

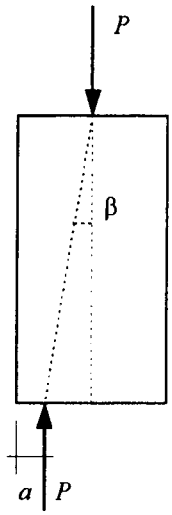

Figure 7: Truss model for the shear force equilibrated by vertical load

Non-linear response behavior has been described through what is commonly called strength reduction factor, representing the ratio between the strength needed in case of elastic response and the minimum strength a structure must have still compatible with its ultimate deformation capacities. The expression adopted for $r(\mu, T)$ is the one proposed by Hidalgo and Arias [2]:

$$r(\mu, T) = 1 + \frac{T}{kT_0 + \dfrac{T}{\mu - 1}} \tag{8}$$

where T is the period of the structure and kT_0 is a parameter depending on the expected frequency content of the motion. The previous expression has been assumed to give the median value of $r(\cdot)$, which is then randomized by multiplication for a r.v. $\exp(\alpha_r)$, log-normally distributed and having unit median.

On the side of the capacity, the three quantities: flexural strength F, ultimate ductility μ_u and shear strength V_u, have also been treated as r.v.'s in the same way as the previous ones, i.e., by multiplying their median values by the three r.v.'s $\exp(\alpha_F)$, $\exp(\alpha_\mu)$ and $\exp(\alpha_V)$, all having unit median and log-normal distribution.

3.5 Quantification of risk

If the response remains within the elastic range, the maximum force acting on the pier is:

$$F_{max} = MA_g\overline{S}_a(T) \tag{9}$$

where A_g is the local value of the peak ground acceleration, and failure can only occur if F_{max} exceeds the shear strength V_u. In the inelastic range, the following equation applies:

$$F(\mu) = \frac{MA_g\overline{S}_a(t)}{r(\mu, T)} \tag{10}$$

where the dependence of F on the ductility actually required has been made explicit. Failure in this case can occur due to two different mechanisms: a flexural failure, if to satisfy eq. (10) μ must be larger than μ_u; a shear failure if $F(\mu)$ is larger than V_u.

The failure domain can in both cases be expressed as the union of the two domains:

$$\mathcal{F} = [\mu \geq \mu_u] \cup [F(\mu) \geq V_u(\mu)] \tag{11}$$

In order to calculate the probability content of $\mathcal{F}$ it is convenient to separate it into the union of two non-overlapping domains:

$$\mathcal{F} = \{[\mu \geq \mu_u] \cap [F(\mu) < V_u(\mu)]\} \cup \{F(\mu) \geq V_u(\mu)\} \tag{12}$$

in which the first domain represents a flexural failure excluding shear failure and the second one a pure shear failure. The probability contents of the two domains are directly summable, while the total probability of failure includes a third contribution, i.e., the probability of a shear failure for $\mu < 1$.

Introducing the notations:

$$m(\mu) = \log\left(\frac{\mu}{\mu_0}\right) \qquad v(\mu) = \log\left(\frac{V_u(\mu)}{F(\mu)}\right) \tag{13}$$

$$X = \alpha_F + \alpha_r - \alpha_S \qquad Y = \alpha_F - \alpha_V \tag{14}$$

$$g(\mu) = \log\left(\frac{MA_g\overline{S}_a(T)}{F(\mu)r(\mu,T)}\right) \tag{15}$$

it can be shown that the probability for flexural failure conditioned to survival in shear is given by the expression:

$$P_{f1} = \frac{1}{\sqrt{2\pi}\sigma_X}\int_1^\infty \Phi\left(\frac{m(\overline{\mu})}{\sigma_u}\right)\Phi\left(\frac{v(\overline{\mu})/\sigma_Y - \rho g(\overline{\mu})/\sigma_X}{\sqrt{1-\rho^2}}\right)e^{-g(\overline{\mu})^2/2\sigma_X^2}\left|\frac{dg(\overline{\mu})}{d\overline{\mu}}\right|d\overline{\mu} \tag{16}$$

while that for shear failure in the inelastic range is:

$$P_{f2} = \frac{1}{\sqrt{2\pi}\sigma_X}\int_1^\infty \Phi\left(\frac{-v(\overline{\mu})/\sigma_Y + \rho g(\overline{\mu})/\sigma_X}{\sqrt{1-\rho^2}}\right)e^{-g(\overline{\mu})^2/2\sigma_X^2}\left|\frac{dg(\overline{\mu})}{d\overline{\mu}}\right|d\overline{\mu} \tag{17}$$

and that for elastic shear failure:

$$P_{f3} = \frac{1}{\sqrt{2\pi}}\int_{(v_0-g_0)/\sigma_X}^\infty \Phi\left(\frac{(\sigma_Y\rho' - \sigma_{X'})u_1 - g_0}{\sigma_Y\sqrt{1-\rho^2}}\right)e^{-u_1^2/2}du_1 \tag{18}$$

where in eq. (18) the new symbols stand for:

$$v_0 = \log\left(\frac{V_u(1)}{F(1)}\right); \qquad g_0 = \log\left(\frac{MA_g\overline{S}_a(T)}{F(1)}\right); \qquad X' = \alpha_S - \alpha_V \tag{19}$$

In the previous equations, $\Phi(\cdot)$ is the Gauss normal distribution function and ρ is the coefficient of correlation between the r.v.'s X and Y; it may be expressed in terms of variances of α_F, α_V, α_r and α_S:

$$\rho = \frac{\sigma_F^2}{\sqrt{\sigma_F^2 + \sigma_s^2 + \sigma_r^2}\sqrt{\sigma_F^2 + \sigma_V^2}} \tag{20}$$

similarly, ρ' is the coefficient of correlation between X' and Y.

The integrals in eq. (16), (17) and (18) are rapidly performed numerically.

3.6 Selected results

The procedure computes automatically P_f in sequence for all bridges belonging to each of 6 highways for which seismic evaluation is warranted, according to the screening procedure illustrated previously. A sample of the results is presented graphically in the Figs. 8 and

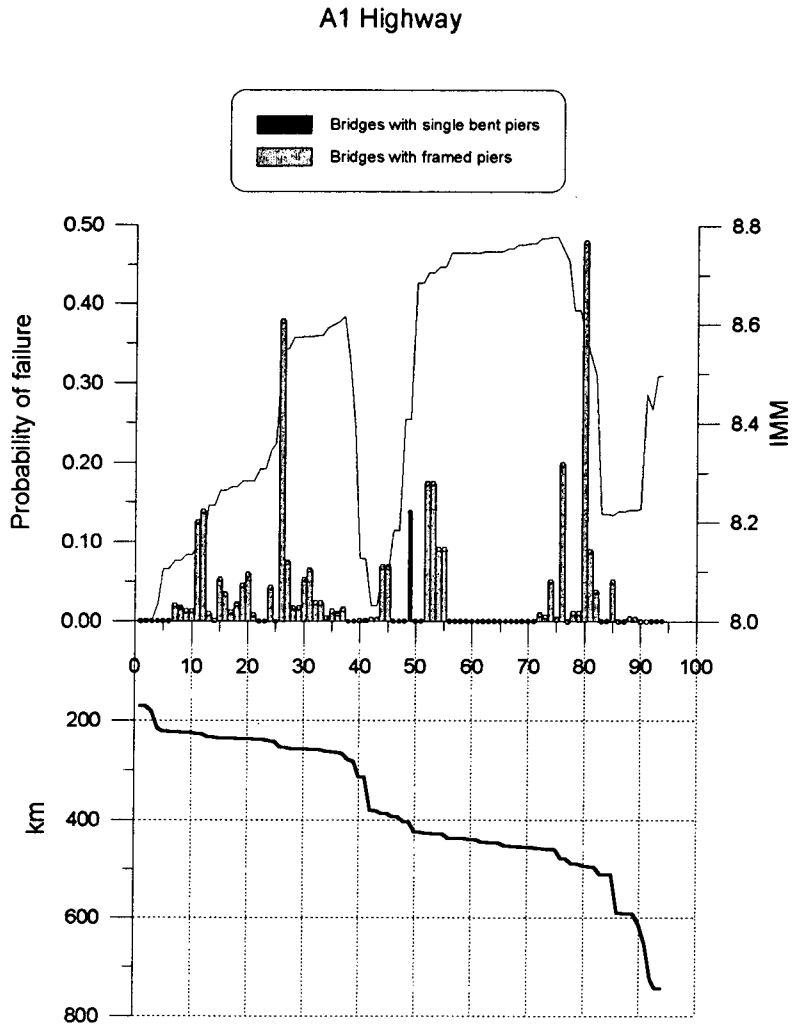

Figure 8: Risk of bridges in the A1 highway

9, which refer to the longest highway (A1 MILANO–NAPOLI), and to the most hazardous one (A16 NAPOLI–CANOSA), respectively.

In the horizontal axis the bridges examined are numbered in progression, their distance from the origin appearing in the lower part of the figure. The vertical axis at left gives the values of P_f corresponding to the spikes in the figure, while in the background the variation of the hazard is also given, with the values to be read in the right vertical scale. A distinction is made between single bent and frame-like type of piers.

One can immediately note that while in the A1 only a few isolated bridges have values of P_f larger then, say, 0.10, in the A16 the risk is much more diffused, with a good number of bridges having a P_f close to 1, given the occurrence of the 500 years event.

Results for the six highways are summarized in Fig. 10, which gives for the total population of bridges examined the distribution of the probabilities of failure. A systematic difference appears between the bridges of the two categories, with framed piers clearly more vulnerable than those with a single bent. For example, about 75% of the latter have a $P_f \leq 10^{-2}$, against 30% of the former. The difference becomes smaller, however, with increasing value of risk, and for $P_f > 0.5$ the situation is inverted.

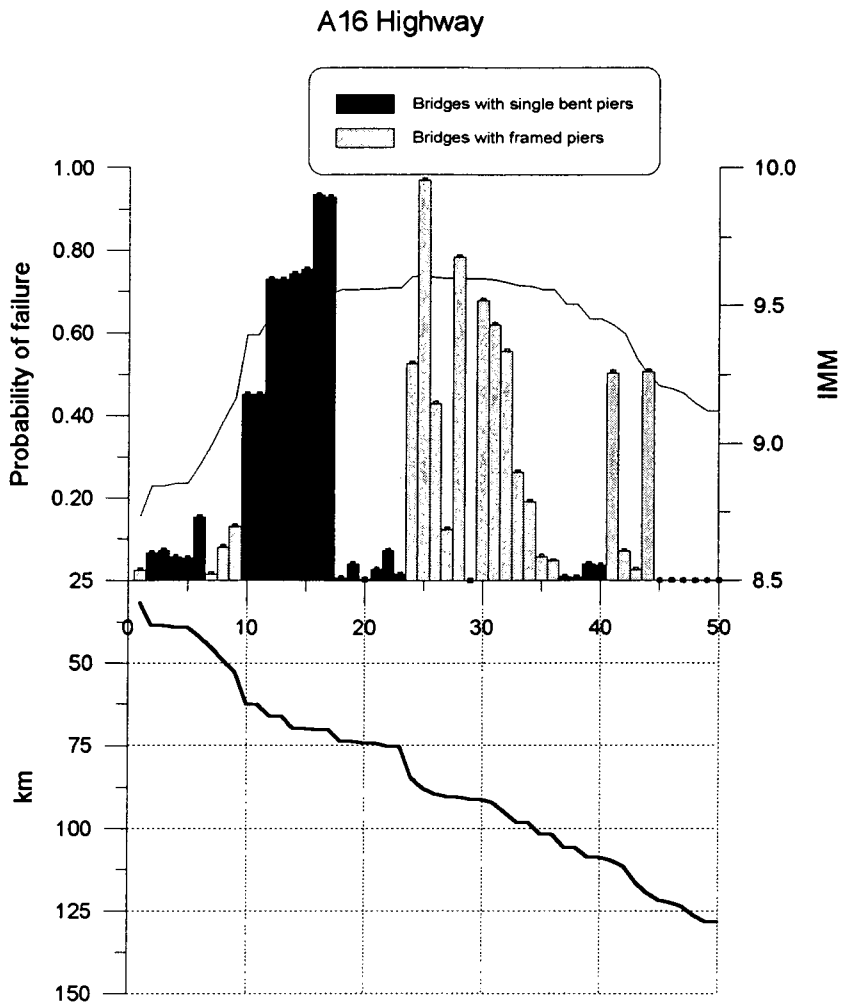

Figure 9: Risk of bridges in the A16 highway

4 ACCEPTANCE CRITERION

The values of P_f obtained with the procedure described in the previous paragraph represent a measure of the risk of the bridges: to judge whether they are acceptable or not an homogeneous reference measure is necessary. Among various alternative possibilities the choice has been made to use as acceptance threshold the safety provided by the modern codes for new structures. This choice might in principle be considered as overly conservative and uneconomical, as it is widely accepted that for existing structures the amount of retrofit can be somewhat less than "complete", i.e., a lower safety level than for new ones can be accepted.

But for the type of bridges under consideration, in which the vulnerable elements are essentially the piers, the economical arguments play differently than, for ex., in the case of substandard reinforced concrete or masonry buildings. In the case of bridges, the total cost of the intervention is made up principally by fixed costs, which do no depend on the amount of strengthening to be provided, while the extra cost due to extra strength is an unsignificant fraction of the total cost. Under these terms, the attainment of a safety level

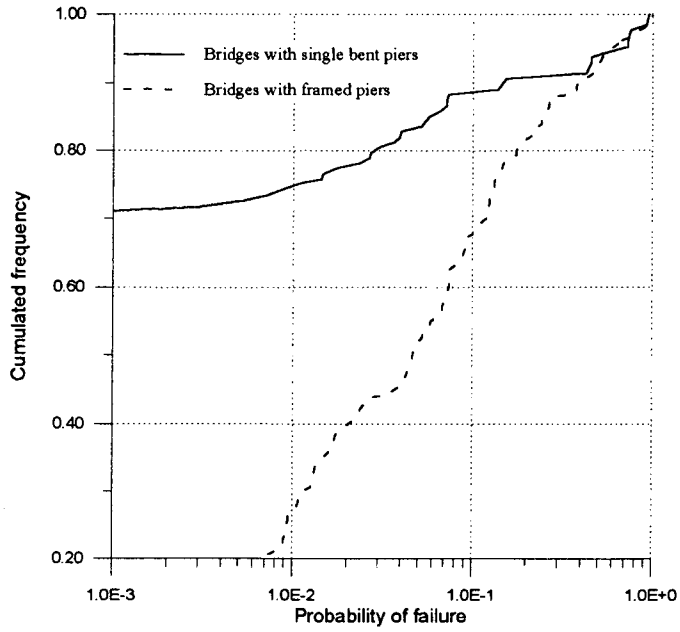

Figure 10: Cumulated frequency of probability of collapse of examinated bridges. Continuous line: bridges with single bent piers; dashed line: bridges with framed piers.

equal to that for new structures is a logical target.

Modern codes, however, are not explicit on the level of protection they provide, which requires it to be inferred from the logic inherent in these documents. Eurocode 8, for example, after stating its objective as that of ensuring, "with an adequate level of reliability", that communications should not be disrupted as a consequence of seismic events, implements the concept in practice in the following way.

The first and main step consists in selecting, according to the importance of the bridge, the return period (T_R) of the design seismic event for the USL. Given T_R (for example 500 years) the corresponding seismic intensity is found and the design made accordingly.

The design rules (analysis, dimensioning and detailing) are deemed to be such as to guarantee, with an adequate level of reliability, that, given the occurrence of the design event, bridges maintain their integrity and a limited capacity for traffic load, though they may need substantial repair work. The idea is therefore clearly expressed of the existence of a non-zero probability that a bridge, designed following the code and for an action of given return period, may collapse at the occurrence of this action.

How high is this conditional probability is not to be found in the code, however, for reasons that are obvious. If, as in the present case, the order of magnitude of the probability inherent for ex. in EC8 is desired, it must be estimated by means of ad hoc analyses on representative designs. This is what has been actually done, by first selecting a number of possible candidate structures and finally by identifying one specific pier type and a single geometry. In detail, the pier is a single bent, with circular hollow cross section having an external diameter $D = 2.60\,\mathrm{m}$ and thickness of $0.30\,\mathrm{m}$. The height is $H = 10\,\mathrm{m}$ and the mass at the top is $10,000\,\mathrm{kN}$, corresponding to a deck length of $40\,\mathrm{m}$.

The criterion adopted for the choice has been that pier dimensions should be related to actual strength requirements and not, as it is often the case, to extraneous reasons as uniformity, aesthetic, etc. Regarding the height, it can be shown that an increase of it within reasonable limits would reduce the response and the necessary amount of reinforcement.

The material properties have been chosen as follows.

Concrete Average strength: $f_c = 30\,\text{MPa}$ (design value $f_{cd} = 20\,\text{MPa}$).
Average tensile strength: $f_{ct} = 0.3\,f_c^{2/3} = 2.9\,\text{MPa}$.
Average ultimate compressive strain: $\epsilon_{cu} = 0.012$.

Steel Average strength: $f_y = 500\,\text{MPa}$ (design value: $f_{yd} = 380\,\text{MPa}$).

The design peak acceleration has been set at $A_g = 0.35\,g$, and the value of behavior factor given in EC8: $q = 3.5$ has been adopted. The design spectrum is that of EC8 for intermediate soil sites.

4.1 Calculation of P_f for $A_g = 0.35\,g$

The rules in EC8 are such as to make shear failure practically a zero probability event. Hence failure can only occur due to exceedance of the available ductility. The mechanical model of the pier is the same used for the seismic assessment of existing piers, and is represented by a bilinear force-displacement relationship. Using mean values of the mechanical properties of the materials, the displacement ductility results to be: $\mu_u = 9.08$.

The failure condition, expressed as balance between capacity in strength and demand, writes as usual:

$$F(\mu) = \frac{M A_g \overline{S}_a(T)}{r(\mu, T)} \tag{21}$$

with the known meaning of the symbols.

The quantities assumed as random are: F, μ_u, $\overline{S}_a(T)$ and $r(\mu, T)$. Each random variable is obtained multiplying the median values by a random variable e^{α_i}, lognormally distributed with unit median. For the parameters of the distributions of the normal variables α_i, the following values have been adopted:

Strength	$\sigma_{\alpha_F} \simeq \text{CoV}(F) = 0.15$
Ductility	$\sigma_{\alpha_\mu} \simeq \text{CoV}(\mu_u) = 0.20$
Spectrum	$\sigma_{\alpha_S} \simeq \text{CoV}(\overline{S}_a) = 0.20$
Reduction factor	$\sigma_{\alpha_r} \simeq \text{CoV}(r) = 0.25$

With:

$$g(\mu) = \log\left(\frac{M A_g \overline{S}_a(T)}{F(\mu) r(\mu, T)}\right) \qquad \sigma_{\alpha_Y}^2 = \sigma_{\alpha_F}^2 + \sigma_{\alpha_S}^2 + \sigma_{\alpha_r}^2 \tag{22}$$

the probability of failure can be expressed in closed form as:

$$P_f = \int_1^\infty \Phi\left(\frac{\log(\mu/\mu_u)}{\sigma_{\alpha_\mu}}\right) \frac{1}{\sigma_{\alpha_Y}} \Phi\left(\frac{g(\mu)}{\sigma_{\alpha_Y}}\right) \left|\frac{dg(\mu)}{d\mu}\right| d\mu \tag{23}$$

and the integral evaluated numerically.

The value of P_f obtained for the pier under consideration is:

$$P_f \simeq 2 \times 10^{-2} \tag{24}$$

This value is in general agreement with the results of other studies on the subject. It is clear that it should not be considered as a "rigid" reference: with different geometries and dimensions, different estimates of the parameters defining the randomnesses, possible inclusion of other parameters, refinements in the mechanical models, etc., the range of values could expand of one order of magnitude in both senses.

If not in absolute terms, however, the result obtained is significant as a relative measure. The same mechanical models have in fact been used in the assessment of the existing and of the new bridges: the possible bias and deficiencies of the models should disappear in the comparison. The values of the parameters defining the randomness are either the same, or are reasonably differentiated for taking into account of the differences between the two situations. The arguments above support the conclusion that the values of P_f attached to each bridge provide a correct ordering criterion in terms of risk, and that the threshold separating the categories of acceptable and non acceptable risk is placed in a defensible position.

5 RESULTS AND CONCLUSIONS

Starting from 1151 bridges with simply supported decks belonging to the *Autostrade* network, the screening procedure based on the comparison between the 500 years return period hazard and their "natural" seismic resistance has reduced the number of those to be evaluated to 425; 307 of these bridges (i.e., those for which the data bank *SAMOA* allowed a reconstruction of their geometry to be made) have been evaluated quantitatively following the criterion of designing them according to the code of the time and then performing on them a reliability analysis.

The measure of the risk adopted has been the probability of collapse conditioned to the local 500 years return period hazard. The values of P_f obtained for the 307 bridges have then been compared with a reference value: $P_f = 10^{-2}$, considered to be representative of the safety provided by a modern code (EC8/2) to bridges of new construction. The result is that 155 bridges have a risk larger than or equal to the acceptable one. Only for about half of them, however, the difference with the target is really significant, while the rest has a risk within a narrow range around the target (values of P_f down to 5×10^{-3} are included in the count of 155). While for the former half an intervention of seismic retrofit is warranted per se, for the second half the decision of intervening should be based on a combination of factors, rather than just on seismic risk.

As far as the procedure in itself is concerned, a few aspects are worth to be mentioned in concluding. The idea of utilizing the geometric data from a data bank to reconstruct the characteristics of the bridges by means of a simulated design has proven to be both accurate and very fast. Few minutes of a 486 Pc are sufficient for processing hundreds of bridges, with an accuracy which is close to that one would get by having recourse to the design drawings. A detailed approach of this type would require, however, overall times which are orders of magnitude longer.

The limits of the procedure are equally obvious as it advantages. Firs of all it presupposes the existence of a data bank of the type described in the paper, where the necessary data can be easily extracted from, which is other thing than to have the full design of the

bridges informatically stored. Secondly, the procedure works reliably for bridge of simple structural types. Hyperstatic bridges, or even hyperstatic piers of simply supported bridges, cannot be designed automatically on the basis of the geometry alone, due to the multiplicity of the design options. These bridges, however, represent a small portion of the existing stock, so small that their seismic evaluation can be realistically carried out on an individual basis.

Aknowledgements

The writers would like to acknowledge the financial support and the cooperation of the Società Autostrade. The research has been also partially supported by a grant of the italian Consiglio Nazionale delle Ricerche.

References

[1] Eurocode 8 – Design Provisions for Earthquake Resistance of Structures ENV 1998-2 - Bridges. Brussels, October 1994. CEN.

[2] P. A. Hidalgo and A. Arias. New chilean code for earthquake resistant design of buildings. In *Proc. of 4th Nat. Conf. Earthquake Engrs*, volume 2, pages 927–936, Palm Springs, California, 1990.

[3] M. J. N. Priesteley, R. Verna, and Y. Xiao. Seismic shear strength of reinforced concrete columns. *Journal of Structural Engineering ASCE*, 120, 1994.

[4] M. J. N. Priestley, F. Seible, and Y. H. Chai. Design guidelines for assessment, retrofit and repair of bridges for seismic performance. Technical Report SSRP 92/01, Dept. of Applied Mechanics and Engineering Sciences – University of California, San Diego, August 1992.

Session 2

Topic 2 Seismic Input for Bridges
Topic 3 Modelling and Analysis (1)

Ground Motion Characteristics for Seismic Design of Highway Bridges

Keiichi Tamura [1], Riki Honda [2], Akira Chiba [2] and Koichi Yamamoto [3]

ABSTRACT

Strength of the ground motions generated by the 1995 Hyogoken Nanbu Earthquake caused serious damage to various structures including the highway bridges. Through the investigation of the damage, it was realized that highway bridges should be designed with the seismic design load that is as large as that of the ground motions of the Hyogoken Nanbu Earthquake. It was also noticed that the seismic design of highway bridges should be conducted considering their real performance during earthquakes, that is inelastic behavior.

In the first part of this paper, the basic concept of revision of the seismic design of the highway bridges after the Hyogoken Nanbu Earthquake is briefly introduced, in which the role of the input ground motions is also mentioned. Secondly, ground motion characteristics of the Hyogoken Nanbu Earthquake and several past earthquakes are compared to study differences in their ground motion characteristics including their effect on the behavior of inelastic structures. The comparison results are reflected on the requirements for the input motions for seismic design, which is discussed in the following part. Examples of the input motion for dynamic analysis of highway bridges are also shown and their characteristics are briefly discussed.

INTRODUCTION

In the early morning of January 17th, 1995, the Hyogoken Nanbu Earthquake occurred causing serious damage to many kinds of structures including highway viaducts, buildings, railroads etc. Its magnitude was M_J=7.2. (M_J is a Japan Meteorological Agency (JMA) Magnitude.) Although its epicenter was located in the ocean area, its causative faults reached inland areas : the Awaji Island in the south and the densely inhabited area of Kobe City in the north, which was unusual for Japan where most of the past large earthquakes were inter-plate

1) Head, Ground Motion Vibration Division, Public Works Research Institute, Ministry of Construction, Japan
2) Research Engineer, ditto.
3) Visiting Researcher, ditto.

earthquakes and therefore occurred in the ocean area. Because of various reasons including such geographical condition, quite strong quake occurred in the densely populated and highly developed area, causing the casualty of more than 6,000, the largest figure since the World War II and the total loss estimated to reach 10 trillion yen. Highway bridges were not exceptional. Many bridges were damaged and some of them were fatally destroyed and fell down.

The destructiveness of the Hyogoken Nanbu Earthquake is obviously attributed to its extremely strong ground motion, and many strong motion records from the earthquake proved it. Many records showed quite large peak acceleration and large response spectra. One of such records was obtained at the Kobe Maritime Observatory of JMA, whose peak ground acceleration was larger than 800 cm/sec^2 and the peak of the acceleration response spectra (damping ratio h=0.05) of the horizontal components was no less than 2g. (Time histories and response spectra are shown in Figs-1 and 2.)

After the earthquake, it was strongly requested to revise the seismic design code and, in response to such request, the Bridge Committee of the Japan Road Association revised the "Specifications for Highway Bridges, Part V : Seismic Design"[1] (hereafter referred to as "Design Specifications") based on the discussion by the Special Sub-committee for Seismic Countermeasures for Highway Bridges, and the seismic design ground motion with the strength of the records from the Hyogoken Nanbu Earthquake were employed. Employment of such strong input motion requires change in the basic idea of seismic design because it is not reasonable to design structures so that they resist such strong input motion elastically, and design method based on the ultimate strength, which was applied only to single-column reinforced concrete piers in the former version of the Design Specifications[2], is adopted as the basic design method of seismic design for most highway bridges. Because of such change in the basic idea of seismic design, inelastic response characteristics of structures, in addition to their elastic response characteristics, gained its importance. It means that inelstic response characteristics of the input motions should be considered and investigated before their application to practical seismic design. In this paper, the characteristics of the ground motion for seismic design are described considering the points mentioned above.

DIFFERENCE IN BASIC IDEA OF SEISMIC DESIGN

In this section, changes in the basic idea of seismic design adopted in the revised Design Specifications are introduced.

One of the most significant modifications was, as is mentioned in the former section, made in the seismic design force. The former version of the Design Specifications had two kinds of seismic coefficients. One had the peak value of 0.2g

- 0.3g (value varies depending on the ground condition) and the other had the peak value of 0.7g - 1.0g. In the revised version, seismic coefficient with the peak value of 1.5g - 2.0g was additionally employed. It is assumed to represent the ground motion caused by intra-plate earthquakes with their epicenters in the inland area, while the seismic coefficient with 0.7g - 1.0g given in the former Design Specifications is to represent the ground motion by inter-plate earthquakes in the ocean area.

Accompanying the modification in seismic design is the employment of the seismic design based mainly on the inelastic response of the structure. In the former version of the Design Specifications, employed was "*check* for design ultimate horizontal strength during an earthquake", and it was not requirements but just recommendation, and it was only for single column reinforced concrete piers. In the revised Design Specifications, however, it is indicated that bridges *must be designed*, in general, based on the ultimate horizontal strength during an earthquake. The revised Design Specifications also show that various highway bridges including steel piers filled with concrete, rigid-framed reinforced concrete piers are also to be designed using their ultimate horizontal strength.

Such modification in the design with static force leads to the change in the role of dynamic response analysis. In the former version, the dynamic analysis is mainly for those bridges whose behavior during an earthquake would be complex and its purpose was to check whether the structures would be able to resist elastically the input motion whose peak acceleration response with damping factor 5% was about 200-300 cm/sec^2. Therefore it was enough to consider the elastic response of the structure. In the revised Design Specifications, however, dynamic response analysis should be conducted with input motions which corresponds to the seismic coefficients of 0.7g -1.0g and 1.5g -2.0g, *i.e.* 5% damped acceleration responses of 700-1,000 cm/sec^2 and 1,500-2,000 cm/sec^2 respectively, and it is inevitable to consider the inelastic response of the structures. It is also indicated that if the structure is complex in its shape and therefore its behavior during an earthquake would be complicated, it must be designed based on the dynamic response analysis with these input motions.

CHARACTERISTICS OF GROUND MOTIONS OF HYOGOKEN NANBU EARTHQUAKE

– difference from the ground motions of past earthquakes –

In this section, the characteristics of the ground motion of the Hyogoken Nanbu Earthquake are compared with those of the past earthquakes in Japan.

As the strong motion records to represent ground motion of the Hyogoken Nanbu Earthquake, three records from the earthquake are used. The employed records are strong motion records obtained at the Kobe Maritime Observatory

(JMA, referred to as "JMA Kobe record" hereafter), at the JR Takatori Station[1] (JR West, "Takatori record") and near the Higashi Kobe Bridge (Hanshin Expressway Public Corporation, "Higashi Kobe Bridge record"). These records are regarded as the representative records observed on the ground corresponding to type I, II and III. Ground type is defined in the Design Specifications [1),2)] and the types I and III indicate the stiff and the soft ground respectively and the II means the ground between them.

The records to represent the ground motion of the past earthquakes were recorded near the Kaihoku Bridge in the 1978 Miyagiken-oki Earthquake (whose magnitude was M_J=7.4 and this record will be referred to as "Kaihoku record" hereafter), near the Itajima Bridge in the 1968 Hyuganada-oki Earthquake (M_J=7.5, "Itajima record"), and near the Tsugaru Ohashi Bridge in the 1983 Nihon-Kai-Chubu Earthquake (M_J=7.7, "Tsugaru record"). They also represent the records at the sites whose ground types are I, II and III, respectively, and they were employed as the original strong motions of input motions in the former version of the Design Specifications.

For the purpose of simplification, one component with the larger acceleration of the two horizontal components of each set of strong motion records is used. Time histories and 5% damped response acceleration spectra of these six records are shown in Figs-1 and 2.

These figures show several points unique to the Hyogoken Nanbu Earthquake, such as :

1) peak acceleration and elastic response spectra are large.

Although it is meaningless to simply compare peak accelerations or response spectra among above-mentioned records, because various conditions such as epicentral distance and magnitude are different, it is true that their peak accelerations and response spectra are among the largest in those of the strong motion records that have ever been observed in Japan.

2) ground motion is larger on the stiff ground.

It should be noticed that the ground motion at the relatively stiff ground is larger than that at the soft ground. According to the records of the past earthquakes, usually the ground motion becomes large on the soft ground. In the Hyogoken Nanbu Earthquake, however, the ground motion on the relatively stiff ground, such as the Kobe Maritime Observatory, was larger in peak acceleration than those recorded on the soft grounds such as the Higashi Kobe Bridge that is a reclaimed land.

It can be attributed to the effect of the inelastic behavior of the ground which was induced by the quite strong input motion, because when inelasticity dominates, damping of the ground becomes large and the rigidity becomes weak, with the result that ground fails to transmit seismic waves, especially high frequency components.

3) Their wave forms are different from those of the past earthquakes.

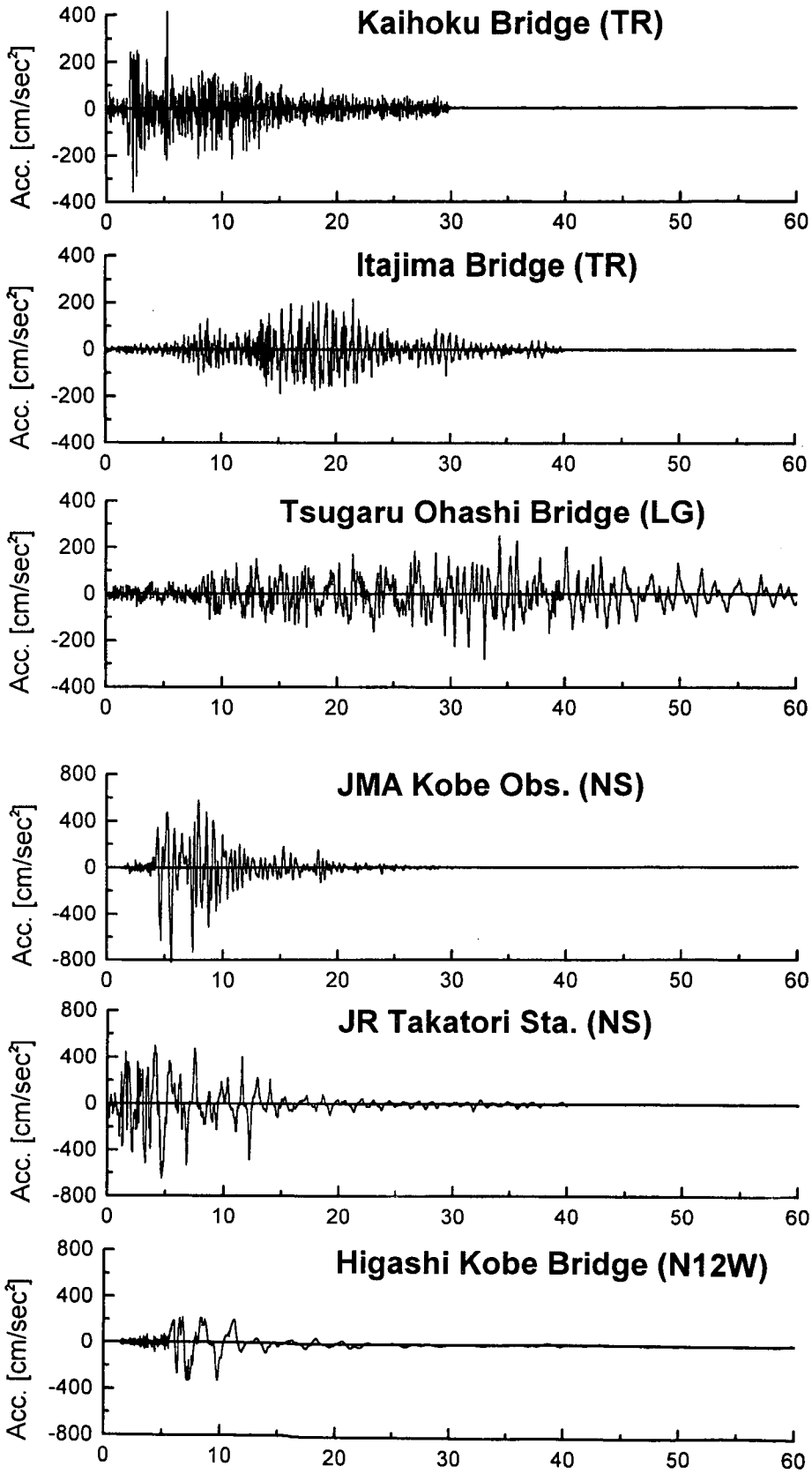

Fig-1 Time Histories of the Strong Motion Records

Comparison of the wave forms of the records from the Hyogoken Nanbu Earthquake and those of the past earthquakes shows that ground motions of the Hyogoken Nanbu Earthquake are unique in that they are small in cyclic number, that they are short in duration time, and that they contain a few relatively-long-period spike-shaped waves.

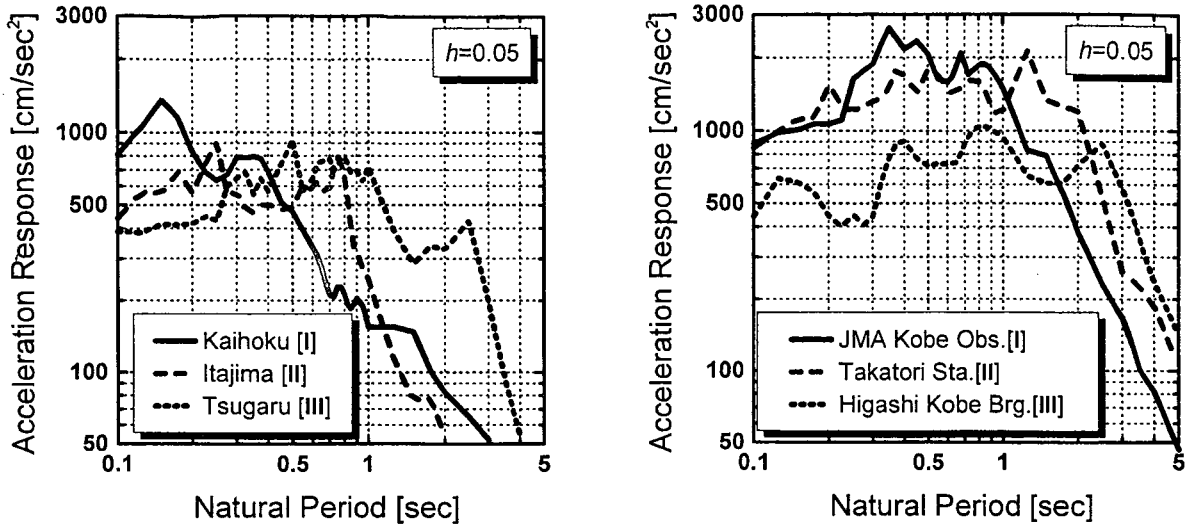

Fig-2 Acceleration Response Spectra of the Strong Motion Records

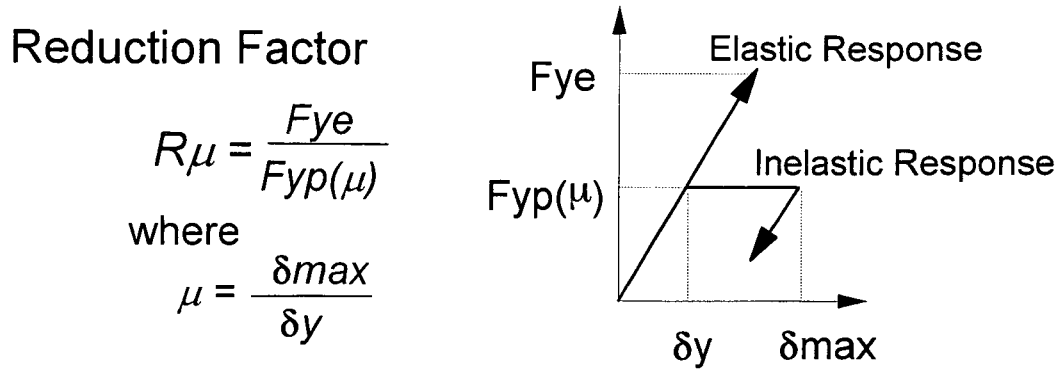

Fig-3 Definition of Strength Reduction Factor $R\mu$

In order to see quantitatively the difference due to the inelastic behavior of structures, strength reduction factor $R\mu$ was calculated. $R\mu$ indicates the possible reduction of the strength of a structure when a certain displacement ductility is allowed, and it is defined as :

$$R\mu = \frac{Fye}{Fyp(\mu)} \tag{1}$$

where

μ: Pre-determined allowable displacement ductility, defined as $\mu = \delta max / \delta y$.

δmax: Peak response displacement of the inelastic system exposed to an input motion.

δy: Yielding displacement of the inelastic system.

Fye: Strength required to prevent the SDOF system from yielding. It corresponds to the force applied to the system when it behaves elastically.

$Fyp(\mu)$: Strength required to maintain the displacement ductility smaller or equal to the pre-determined allowable ductility μ.

The idea of $R\mu$ is shown in Fig-3 and for ordinary cases it is approximately estimated by the following equation which is adopted in the Design Specifications :

$$R_\mu = \sqrt{2\mu - 1}. \tag{2}$$

In this paper, a bi-linear system with damping ratio h=5% ,whose strength after the yield is assumed to be the same as the yielding strength, is adopted for an inelastic single-degree-of-freedom (SDOF) system, and its natural period is evaluated from the initial stiffness. $R\mu$ can be calculated for any natural period and therefore it makes a spectrum. $R\mu$ spectra of the previously mentioned six strong motion records are shown in Fig-4.

Comparison of $R\mu$ spectra reveals that $R\mu$ of the ground motions from the Hyogoken Nanbu Earthquake is small and independent of the allowable ductility μ in the relatively short period range and becomes quite large in the long period range especially for large μ. As for the ground motions from the past earthquakes, $R\mu$ spectra show large dependence on allowable ductility μ in the wide natural period range including long natural period range, and therefore in that range their values are stable independent of the natural period. It is especially clear when $R\mu$ spectra of the ground motions for the ground type I (JMA Kobe record and Kaihoku record) are considered. Reduction factor $R\mu$ of the JMA Kobe record is almost independent of μ for the natural period shorter than 0.5 sec, and it becomes drastically large in the range of longer natural period, while reduction factor $R\mu$ of the Kaihoku record varies depending on μ for the whole natural period range shown here. The same tendency is also seen for other records although it is not so

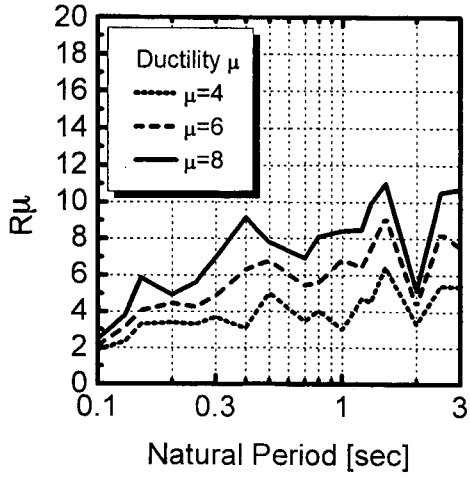

Kaihoku Bridge Record (TR)

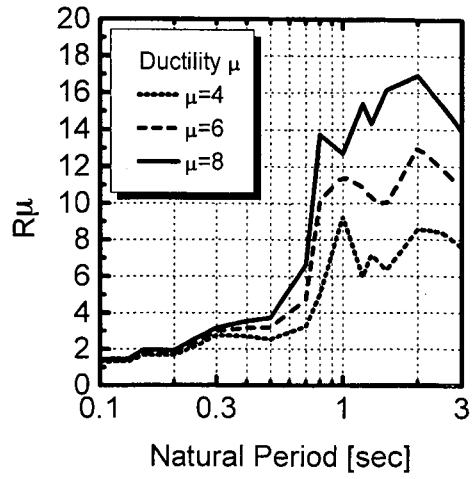

JMA Kobe Record (NS)

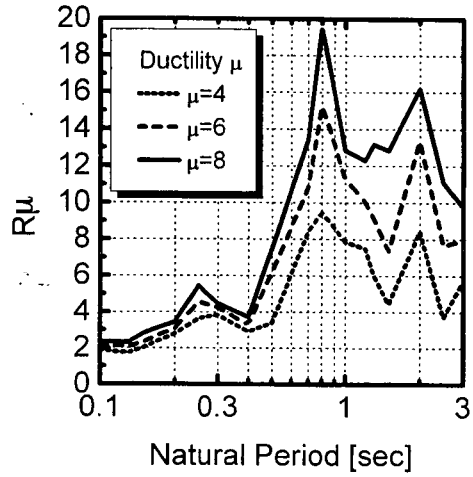

Itajima Bridge Record (TR)

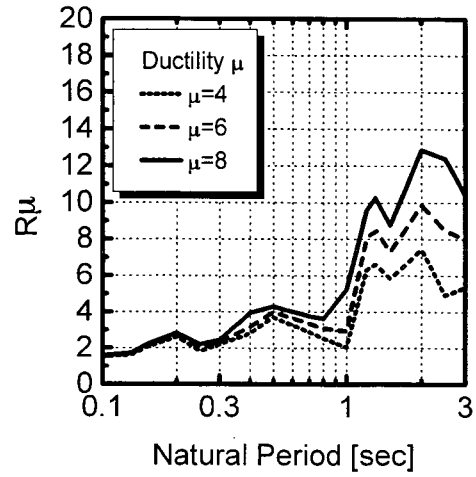

JR Takatori Sta. Record (NS)

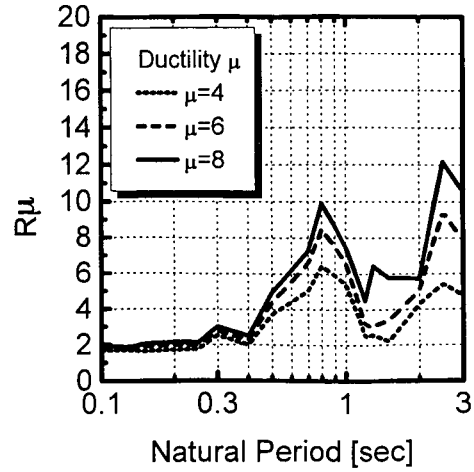

Tsugaru Ohashi Bridge Record (LG)

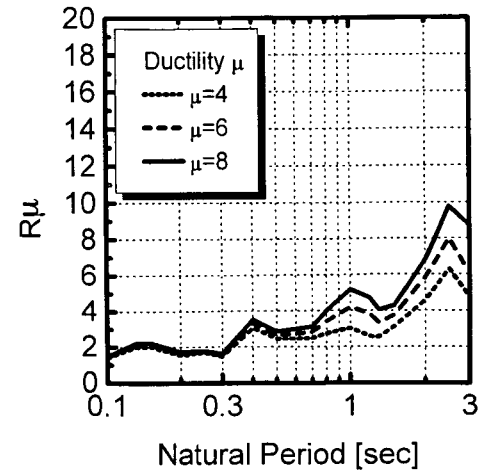

Higashi Kobe Bridge Record (TR)

Fig-4 $R\mu$ Spectra of the Strong Motion Records

clear as it is for the JMA Kobe and Kaihoku records.

Such characteristics of $R\mu$ spectra may be attributed to what was previously mentioned to as the third point of the uniqueness of the Hyogoken Nanbu Earthquake, that is a few relatively-long-period spike-shaped waves, because similar tendency is observed for the $R\mu$ spectra of a sinusoidal wave. $R\mu$ spectra for a single cycle of sinusoidal wave with period of 1.0 sec are shown in Fig-5. They are independent of allowable ductility μ in the short period range and converge to $R\mu = \mu$ in the long period range.

Although further research is required about the mechanism of their similarity, as such difference in $R\mu$ spectra exists between the Hyogoken Nanbu Earthquake records and other records, it should be taken into consideration, as one of the characteristics of the Hyogoken Nanbu Earthquake, when input motions for seismic design are discussed.

In addition to the difference in the ground motion characteristics, difference in the types of earthquakes was also noticed in determination of the seismic design force. The Hyogoken Nanbu Earthquake is an intra-plate earthquake, which was caused by the active faults lying in the inland area, and occurrence frequency of such earthquakes is small compared to that of the inter-plate earthquakes that usually occur in the ocean area. It is also proved by the fact that most earthquakes that caused damage in Japan such as the 1978 Miyagiken Oki Earthquake were intra-plate earthquakes.

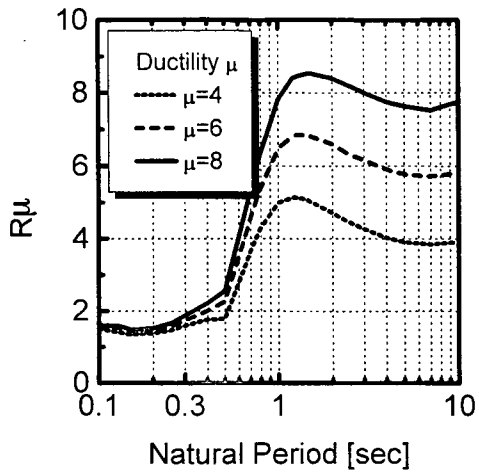

Fig-5 $R\mu$ Spectra of a Single Cycle of a Sinusoidal Wave

GROUND MOTION CHARACTERISTICS FOR SEISMIC DESIGN

Seismic Coefficient and Response Acceleration Spectra

In the Design Specifications, seismic coefficients and response

acceleration spectra of the ground motions are provided and they are slightly different. Seismic coefficient is to be used in the static analysis to evaluate a static seismic design force by multiplying a mass of structure, while the response acceleration spectrum is to be used in the dynamic response analysis to make an input motion. The reason for the difference between the two is that there are several factors whose effect can not be evaluated by static analysis and the effect of such factors must be taken into consideration in advance. One of the most influential factors is the effect of damping ratio. Detail of the process to adjust the seismic design force considering the effect of the damping ratio is not mentioned here because it is mentioned to in other papers[1)4)]. The process can be summarized as : because the damping ratio is likely to be small for highway bridges with long natural period [5)], the seismic design force for them is to be raised. Although seismic coefficients and the response spectra are different in the long natural period range because of this adjustment, they essentially stand for the same ground motion.

Seismic Design Force in the Revised Design Specifications

In the revised Design Specifications, two different seismic design forces are employed. They are referred to as type I and type II. Type I represents the ground motion caused by inter-plate earthquakes that usually occur in the ocean area, and type II represents that by intra-plate earthquakes in the inland area.

Seismic design force of type I is the same as that used in the former version of the Design Specifications for "*check* for design ultimate horizontal strength during an earthquake". It was determined based on the analysis of a number of strong motion records from the past earthquakes, the attenuation characteristics of the ground motion and other various analysis results. It therefore can be regarded to represent the general characteristics of the ground motions. Seismic design force of type II is, on the other hand, determined considering almost solely the strong motion records from the Hyogoken Nanbu Earthquake. The original strong motion should be the one recorded in an earthquake that caused severe damage to some structures. The Hyogoken Nanbu Earthquake was an unprecedented case in Japan and no other earthquakes that had their causative fault in the inland area and inflicted serious damage, left strong motion records.

Seismic coefficient is given as shown in Table-1 and Fig-6, and the response acceleration spectra are as shown in Table-2 and Fig-7. They are set for each of the ground motions types I and II, and for each of ground types I to III.

Response spectra for type I input motions have the peak values of 0.7g, 0.85g, 1.0g for the ground types I, II and III respectively, and those of the type II input motions are 2.0g, 1.75g, and 1.5g. It should be noted that in case of the type II ground motions, peak value for a stiff ground is larger than that for a soft ground. As was described before, in the Hyogoken Nanbu Earthquake, ground

Table-1 Seismic Coefficients

(a) Type I Seismic Design Force

Ground Type	Seismic Coefficient k_h for Natural Period T [sec]		
Type I	$T \leq 1.4$ $k_h = 0.7$		$1.4 < T$ $k_h = 0.876/T^{2/3}$
Type II	$T < 0.18$ $k_h = 1{,}51\ T^{1/3}$ $(k_h \geq 0.7)$	$0.18 \leq T \leq 1.6$ $k_h = 0.85$	$1.6 < T$ $k_h = 1.16/T^{2/3}$
Type III	$T < 0.29$ $k_h = 1{,}511\ T^{1/3}$ $(k_h \geq 0.7)$	$0.29 \leq T \leq 2.0$ $k_h = 1.0$	$2.0 < T$ $k_h = 1.59/T^{2/3}$

(b) Type II Seismic Design Force

Ground Type	Seismic Coefficient k_h for Natural Period T [sec]		
Type I	$T < 0.3$ $k_h = 4.46\ T^{2/3}$	$0.3 \leq T \leq 0.7$ $k_h = 2.0$	$0.7 < T$ $k_h = 1.24/T^{5/3}$
Type II	$T < 0.4$ $k_h = 3{,}22\ T^{2/3}$	$0.4 \leq T \leq 1.2$ $k_h = 1.75$	$1.2 < T$ $k_h = 2.23/T$
Type III	$T < 0.5$ $k_h = 2.38\ T^{2/3}$	$0.5 \leq T \leq 1.5$ $k_h = 1.5$	$1.5 < T$ $k_h = 2.57/T$

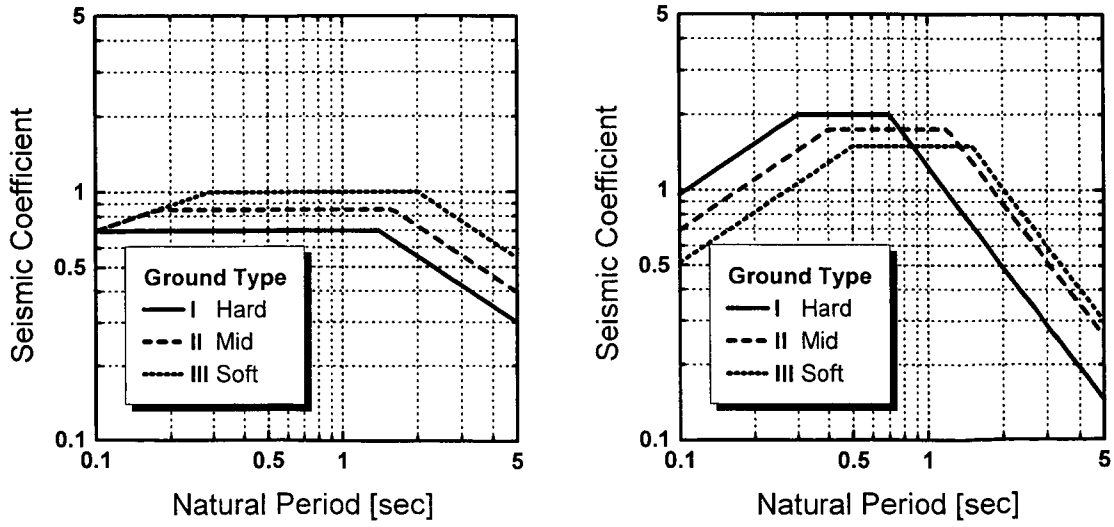

(Type I Seismic Design Force) (Type II Seismic Design Force)

Fig-6 Seismic Coefficients

Table-2 Acceleration Response Spectra of Input Motions for Dynamic Analysis

(a) Type I Seismic Design Force

Ground Type	Spectral Value S[gal] for Natural Period T [sec]		
Type I	$T \leq 1.4$ $S = 700$		$1.4 < T$ $S=980/T$
Type II	$T < 0.18$ $S = 1{,}505\ T^{1/3}$ $(S \geq 700)$	$0.18 \leq T \leq 1.6$ $S = 850$	$1.6 < T$ $S = 1{,}360/T$
Type III	$T < 0.29$ $S = 1{,}511\ T^{1/3}$ $(S \geq 700)$	$0.29 \leq T \leq 2.0$ $S = 1{,}000$	$2.0 < T$ $S = 2{,}000/T$

(b) Type II Seismic Design Force

Ground Type	Spectral Value S[gal] for Natural Period T [sec]		
Type I	$T < 0.3$ $S = 4{,}463\ T^{2/3}$	$0.3 \leq T \leq 0.7$ $S = 2{,}000$	$0.7 < T$ $S = 1{,}104/T^{5/3}$
Type II	$T < 0.4$ $S = 3{,}224\ T^{2/3}$	$0.4 \leq T \leq 1.2$ $S = 1{,}750$	$1.2 < T$ $S = 2{,}371/T$
Type III	$T < 0.5$ $S = 2{,}381\ T^{2/3}$	$0.5 \leq T \leq 1.5$ $S = 1{,}500$	$1.5 < T$ $S = 2{,}948/T$

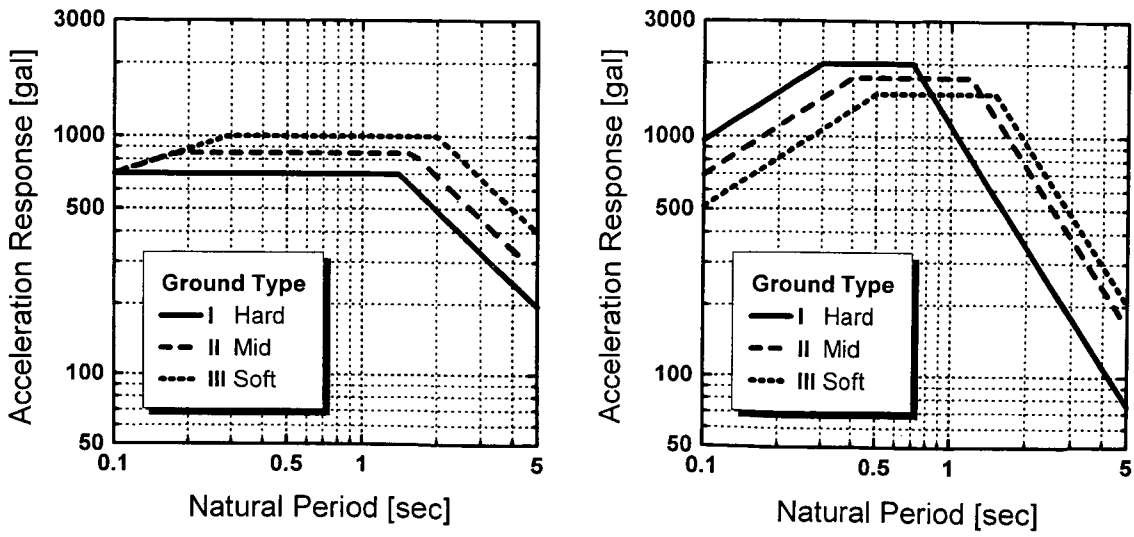

(Type I Seismic Design Force) (Type II Seismic Design Force)

Fig-7 Acceleration Response Spectra of the Input Motions for Dynamic Analysis

motions on the stiff ground such as the JMA Kobe record were stronger than that on the soft ground such as Higashi Kobe Bridge record. It also should be noticed that the seismic design force for a ground type III is much larger than the response acceleration spectrum of the Higashi Kobe Bridge record. This is because the Higashi Kobe Bridge record was obtained on the relatively new reclaimed land which was considerably soft and suffered liquefaction in the Hyogoken Nanbu Earthquake. The ground of the site, therefore, may have failed to transmit the ground motion because of its inelastic behavior. On the ground which is, although classified as the ground type III, harder than the site of the Higashi Kobe Bridge, the ground motion might have been stronger.

Input Motions for Dynamic Analysis

In this section, examples of the input motions for dynamic analysis are demonstrated. The input motions are made by adjusting the amplitudes of various frequency components of the original strong motion records so that their 5% damped acceleration response spectra would be close to the spectra of the input motions for seismic design[6], which are shown in Fig-7. The process is shown in Fig-8. In this process, phase characteristics of the original strong motion records are not changed. As is indicated in the revised Design Specifications, three input motions are made for each combination of an earthquake type and a ground type, because the response of an inelastic structure is affected by various factors and therefore their response vary depending on the input motions even their elastic response spectra are almost identical.

Arakawa and Kawashima[6] suggested that the original strong motion record should be obtained on the ground whose ground type is the same as the targeted ground condition, and also that it was obtained in an earthquake which is similar to the earthquake assumed as the causative earthquake for the targeted type of seismic design force. The input motions for the type I seismic design force and the ground type III, for example, should be made from strong motions which were obtained on a soft ground in inter-plate earthquakes. Considering this, 12 sets of strong motion records listed in Table-3 were selected as the original strong motion records. From 24 horizontal components of these 12 sets of records, 18 records were selected as the original records.

In Fig-9, time histories of the processed input motions are shown : one of the three input motions for each seismic design force type and each ground type is plotted. The original strong ground motions for them were previously shown in Fig-1. Strength reduction factor $R\mu$ spectra for these input motions are shown in Fig-10. In case of type II ground motions, $R\mu$ spectra are relatively small in the short natural period range and they become large in the long natural period range, and their dependence on allowable ductility μ is also small for short natural period and becomes large in the long period range. $R\mu$ spectra for the type I ground

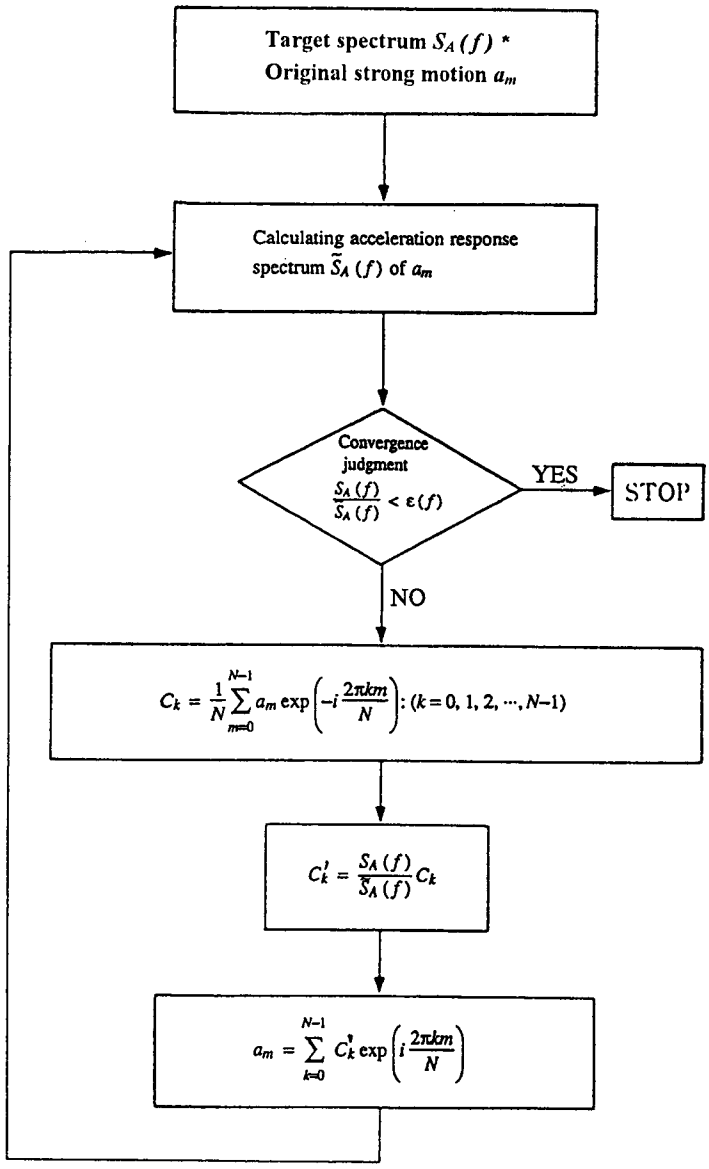

*Expressed by frequency f, not by period

Fig-8 Flow of the Process to Adjust Amplitude of the Original Strong Motion to Fit its Acceleration Response to Design Spectra[6)]

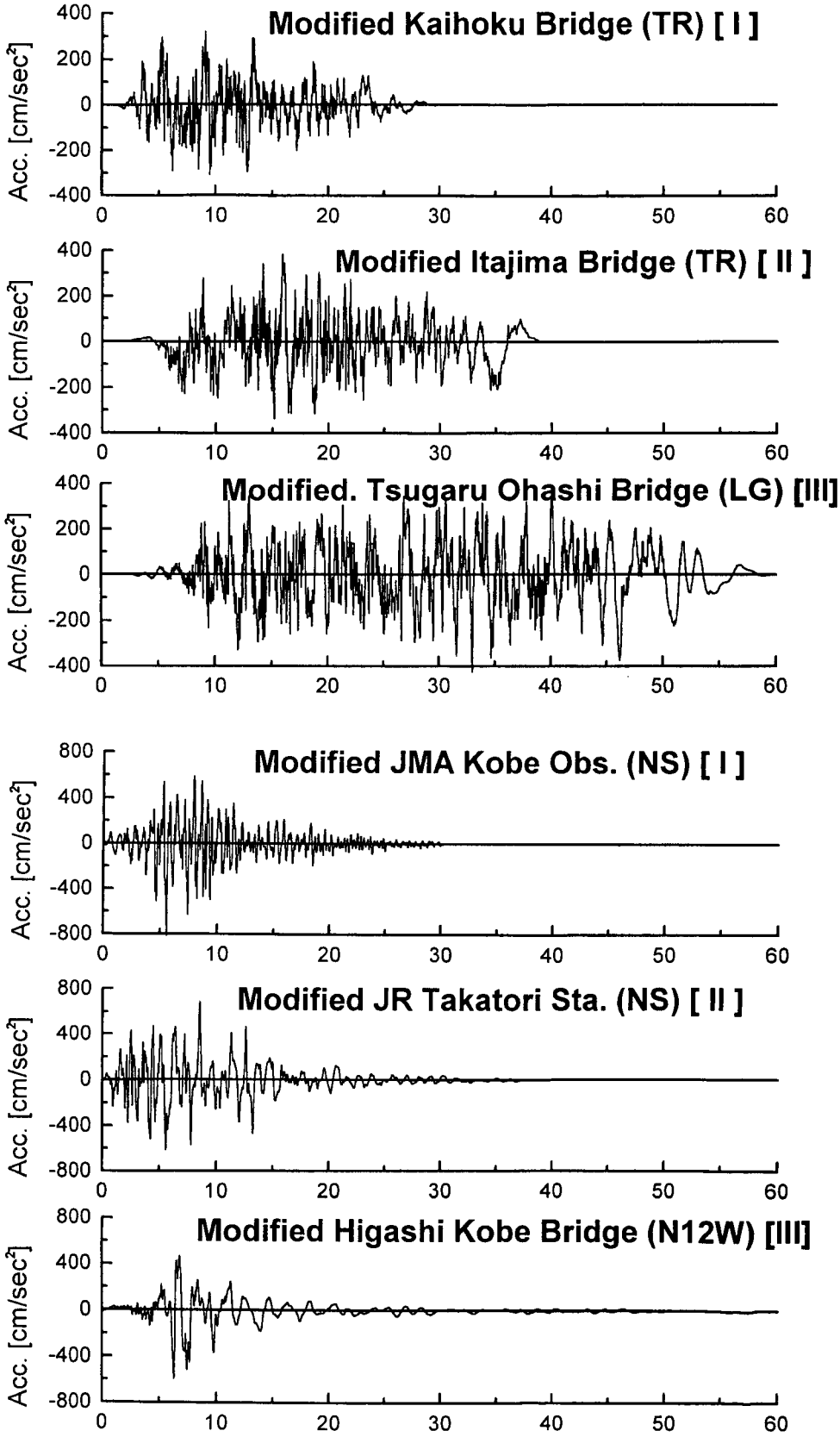

Fig-9 Time Histories of the Examples of Input Motions
Roman figure in the brackets denotes the ground condition for which each input motions should be applied.

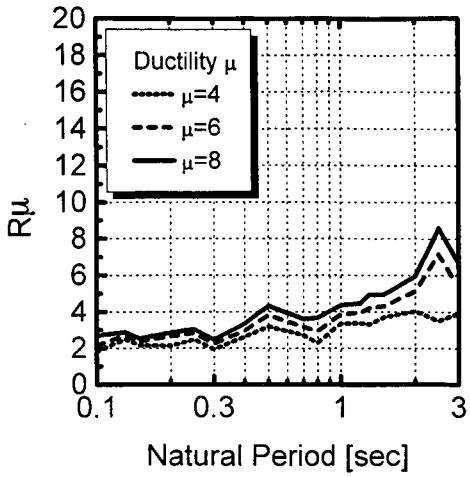

Modified Kaihoku Bridge Record (TR)

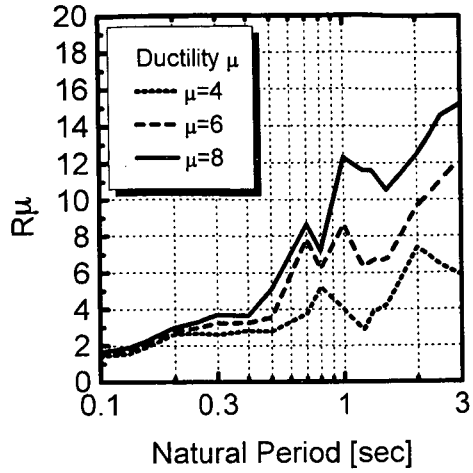

Modified JMA Kobe Record (NS)

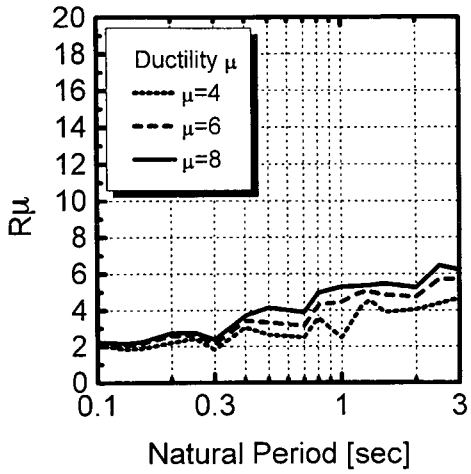

Modified Itajima Bridge Record (TR)

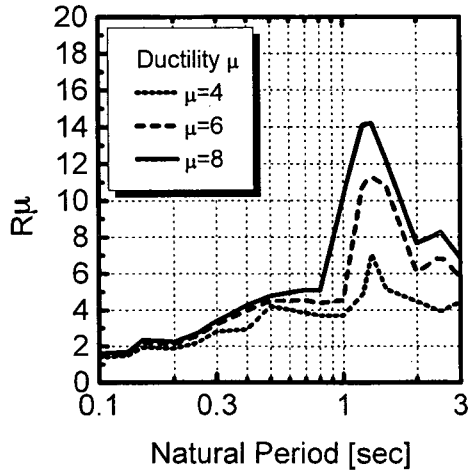

Modified JR Takatori Sta. Record (NS)

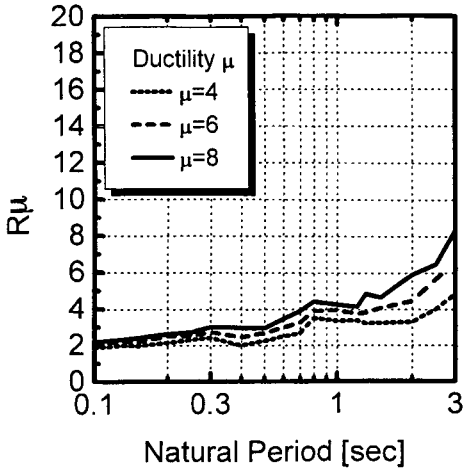

Modified Tsugaru Ohashi Bridge Record (LG)

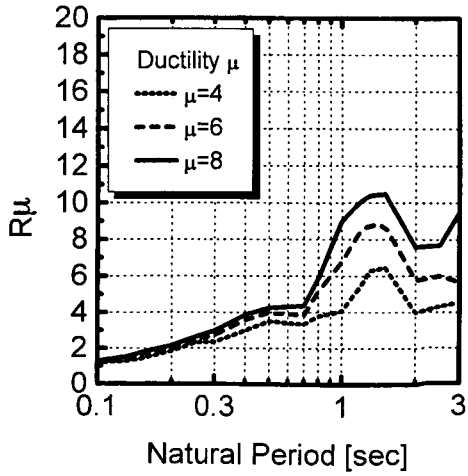

Modified Higashi Kobe Bridge Record (N12W)

Fig-10 $R\mu$ Spectra of the Examples of Input Motions

motions do not vary much over the whole period range and they also shows almost constant dependence on the allowable ductility μ. This trend is in relatively good agreement with the characteristics of the original strong motion records and it can be considered that the process of amplitude adjustment affected but did not spoil the original ground motion characteristics.

Other examples of input motions are not shown here, but their time histories and $R\mu$ spectra showed the similar characteristics described above, and therefore it can be said that they are also reasonably adequate input motions.

There remains a problem, however, because reduction factor $R\mu$ of the type I ground motions is considerably smaller than that of the original strong motions, and $R\mu$ of the type II ground motions shows dependence on μ in the short period range. It is not clear how such difference of the strength reduction factors affect on the behavior of the inelastic structures, and it remains to be studied.

Table-3 Original Strong Motion Records of the Input Motions for Seismic Design.

Type of Seismic Design Force	Ground Type	Earthquake	Magnitude (M_J)	Observation Site (on the ground near :)
Type I	Type I	1978 Miyagiken Oki Eq.	7.4	Kaihoku Bridge
		1993 Hokkaido Nansei Oki Eq.	7.8	Shichiho Bridge
	Type II	1968 Hyuganada Oki Eq.	7.5	Itajima Bridge
		1994 Hokkaido Toho Oki Eq.	8.1	Onnneto Ohashi Bridge
	Type III	1983 Nihonkai Chubu Eq.	7.7	Tsugaru Ohashi Bridge
		1994 Hokkaido Toho Oki Eq.	8.1	Kushirogawa Embankment
Type II	Type I	1995 Hyogoken Nanbu Eq.	7.2	Kobe Maritime Observatory (JMA)
				Inagawa Bridge (HEPC*)
	Type II			JR Takatori Station (JR West)
				Fukiai (Osaka Gas)
	Type III			Higashi Kobe Bridge (HEPC*)
				Port Island (Kobe City)

* HEPC : Hanshin Expressway Public Corporation.

CONCLUSIONS

The 1995 Hyogoken Nanbu Earthquake inflicted serious damage on various structures including highway bridges, and it triggered a revision of the Design Specifications for Highway Bridges. One of the most significant changes is employment of the new seismic design force. The new seismic design force is determined based mainly on the strong motion records from the Hyogoken Nanbu Earthquake, and it has the peak value of 1.5 - 2.0g. Because of its large value, the revised Design Specifications indicates that inelastic behavior of structures must be considered in seismic design.

Dynamic response analysis also should be conducted with the inelastic model, and therefore the input motions also should be proposed considering their

effects on the response of inelastic structures. Comparison of the strong motion records from the Hyogoken Nanbu Earthquake and past several earthquakes, reveals some difference in ground motion characteristics, including their effects on the response of inelastic structures.

Examples of the input motions demonstrated in this paper has an inelastic response characteristics that show reasonable agreement with the difference revealed by the comparison of the strong motion records.

Further research is required because there was slight inconsistency in the inelastic response characteristics of the processed input motions and the original strong motion records.

ACKNOWLEDGMENT

Authors would like to express their gratitude to various organizations including the Japan Meteorological Agency, Railway Technical Research Institute, Osaka Gas Corporation and Hanshin Expressway Public Corporation, for making their precious strong motion records available to public soon after the Hyogoken Nanbu Earthquake.

REFERENCES

1) "Specifications for Highway Bridges, Part V : Seismic Design", Japan Road Association, Feb.1996 (in Japanese)
2) "Specifications for Highway Bridges, Part V : Seismic Design", Japan Road Association, Dec.1990
3) Yutaka Nakamura : Waveform and its analysis of the 1995 Hyogoken Nanbu Earthquake, JR Earthquake Information No.23c, Railway Technical Research Institute, March 1995.
4)Keiichi Tamura *et al.*: Strong Motion Records of the 1995 Hyogoken Nanbu Earthquake and Seismic Design Force Based on These Records, Proc. of 12th US-Japan Bridge Engineering Workshop, UJNR, October 1996.
5)Eiichi Kuribayashi and Toshio Iwasaki : Study on Seismic Designs for Bridges(III) - Experiment Results Concerning Vibration Damping of Bridges, Report of PWRI, No.139,1970.(in Japanese)
6)Tadashi Arakawa and Kazuhiko Kawashima : Determination of Input Ground Motions for Dynamic Analysis, Technical Memorandum of PWRI, No.2120, 1984. (in Japanese)

ITALIAN RESEARCH ACTIVITIES FOR DEFINITION OF THE DESIGN SEISMIC INPUT

Antonio Pugliese and Tito Sanò
Servizio Sismico Nazionale
Roma, Italy

ABSTRACT

Recent Italian research activities dealing with characterisation of ground motion, simulation of accelerograms compatible with seismological parameters and effect of geological and topographic conditions on the ground motion are described in this paper.
Italian strong-motion data were used to characterize the ground motion parameters and to simulate artificial accelerograms as a function of magnitude, distance, and site geology. The data base consists of 95 accelerograms from 17 earthquakes of magnitudes 4.6 to 6.8. Using multiple regressions, empirical predictive equations were developed for the vertical and horizontal components of response spectra corresponding to 14 frequencies ranging from 0.25 to 25 Hz.
The simulation of nonstationary strong ground motions is achieved through an empirical method where time and frequency features of the motion are represented through the Physical Spectrum, extending the spectral moments theory to the nonstationary case. The simulated time-histories fit the recorded accelerograms in terms of several ground motion amplitude measures such as peak acceleration, peak velocity, Fourier spectra, and response spectra.
The effect of geological and topographic condition on ground motion have been studied using a simplified 1D and a 2D boundary element method. The results of two examples show large spatial variations of seismic ground motion, focusing of waves and large amplification of response on the surface. They confirm the great importance of local amplification and the dramatic effects produced in various recent earthquakes.

1. INTRODUCTION

In the field of seismic risk assessment the prediction of shaking intensity in future earthquakes plays a key role. Reliable estimates of the ground motions that structures must be designed to withstand are obtained mainly through empirical predictive relationships developed after statistical analysis of data recorded during strong earthquakes.
The ground motion attenuation relations show that the shape of the response spectra depends strongly on earthquake location, magnitude, and local site conditions. Therefore the engineering practice of using peak acceleration to scale constant spectral shapes, is likely to lead to erroneous estimation of the frequency content of ground motion.
Some engineering methodologies require artificial accelerograms to be used as input in nonlinear dynamic analyses. In recent years many seismological and engineering methods have been proposed for simulating ground motions. While both seismologists and engineers

recognize the stochastic nature of high-frequency ground motions, they estimate the ground motion in fundamentally different ways. The stochastic and empirical models utilized in the engineering approach [1,2] range from filtering and windowing Gaussian noise, to generating accelerograms by linear difference equations; these models do not need to make use of specific geophysical parameters but the resulting time histories are in general poorly correlated with earthquake scaling parameters such as magnitude and distance from the source.

The stochastic and deterministic models used in the seismological approach [3,4,5] rely on the estimation of the motion from the rupture process of a fault of specified dimensions and orientation or from a point source. These models that usually require the knowledge of many parameters, such as the source rupture process and the travel path of the seismic waves, allow a more detailed analysis of the effect of local geology on the ground motion.

The results of statistical analysis performed by Italian researchers [6,7,8,9] on a set of Italian strong motion records are presented in term of predictive equations for the estimation of horizontal and vertical peak ground motions and response spectra using both epicentral and fault distance. Predictive relationships are also provided for other ground motion parameters, such as central frequency, duration, and Arias intensity, used in the simulation of the acceleration time histories. The simulation of nonstationary strong ground motions is achieved through a simple empirical method: summing Fourier series with time dependent coefficients. The simulation method only requires, as input parameters, the magnitude of the reference earthquake, the distance source to site, and the local site geology, producing therefore accelerograms strictly correlated with the generating earthquake and the recording site.

In the last part of this paper we describe the research activities carried out at National Seismic Survey on the simulation of local geological effects on the definition of ground motion. Experimental and numerical approaches have been undertaken. A valley has been selected in the center of Italy as a seismic field laboratory and has been monitored and a computer code [10], based on boundary element method, has been implemented in order to interpret the signals. The analytical approach through numerical computations, in which usually ground irregularities are assumed, shows that the seismic ground motion can be modified point by point on the ground surface. Two examples, reported in this paper, show that modeling of the ground motion for realistic heterogeneous media is nowadays a low-cost but very powerful tool since it allows us to simulate realistic geological conditions of sites.

2. CHARACTERIZATION OF GROUND MOTION IN ITALY

The data base used for the study of characterization of ground motion parameters consists of 190 horizontal components and 95 vertical components of strong motion records from 17 Italian earthquakes recorded at distance less than 100 km with magnitude between 4.6 and 6.8. A detailed analysis of the selection criteria applied to the data are presented in [11].

Acceleration time histories, automatically digitized at 400 samples/s, were baseline- and instrument-corrected with a frequency domain routine [11]. The cut-off frequencies for the high-pass filtering ranged from 0.2 to 0.7 Hz with typical values of 0.3 Hz; the cut-off frequencies for the low-pass filtering ranged from 20 to 35 Hz with typical values of 25 Hz.

A short description of the dependent and independent variables used to develop the regression analysis is given below.

Magnitude. The magnitude scale, which we will refer to as M in this paper, corresponds to the surface-wave magnitude (M_S) when both local magnitude (M_L) and M_S are greater than or equal to 5.5 and corresponds to M_L when magnitude is lower than this value.

Distance. The regression analysis was performed using both "epicentral" and "fault distance"; the last is defined as the shortest distance between the recording station and the surface projection of the fault rupture [12].

Site geology. According to geological and geotechnical information [11] and to the thickness H of the soil layer, the recording sites were classified into three categories: stiff, shallow alluvium (H < 20 m) and deep alluvium (H > 20 m). Stiff sites are characterized by an average shear wave velocity greater than 800 m/sec and alluvium sites by a shear wave velocity between 400 and 800 m/sec.

Response spectra and peak values The regression analysis of peak ground acceleration (PGA), peak ground velocity (PGV), and response spectra was performed using both the vertical and the larger of the two horizontal components of the motion. Pseudo-velocity response spectra (PSV) were calculated at 5 percent of critical damping for 14 frequencies opportunely distributed from 0.25 to 25 Hz.

Arias Intensity and Duration . For the Arias intensity I_A [13], was used the horizontal component of the motion having the larger value of I_A. To specify the duration of the ground motion, DV, was selected the definition given by [14] that is proportional to the quantity I_A/PGA^2 and well correlated to the strong phase of the motion corresponding to the arrival of S waves. For DV was used the horizontal component corresponding to the larger value of I_A.

The general functional form adopted for modeling the attenuation of the ground motion is represented by the expression

$$f(Y) = \mathbf{a} + f_1(M) + f_2(R) + f_3(S) + e \qquad (1)$$

where Y is the ground motion parameter to be predicted; $f_1(M)$ is a function of magnitude; $f_2(R)$ is a function of distance; $f_3(S)$ is a function taking into consideration the site geology and e is a variable representing the uncertainty in y.

Forms of the functions f(Y), $f_1(M)$, $f_2(R)$, and $f_3(S)$ were determined according to the statistical procedure "Alternating Conditional Expectation" (ACE) [11,15] and resulted as follows:

$$f(Y) = \log Y\,; \qquad f_1(M) = \mathbf{b}\,M\,; \qquad f_2(R) \propto \log R. \qquad (2)$$

The final functional form adopted for modeling the attenuation is represented by the following equation:

$$\log_{10}(Y) = \mathbf{a} + \mathbf{b}\,M + \mathbf{c}\log_{10}(R^2 + \mathbf{h}^2)^{1/2} + \mathbf{e_1}\,S_1 + \mathbf{e_2}\,S_2 \pm \mathbf{s} \qquad (3)$$

where M is magnitude, R is distance (fault or epicentral) in km, and s is the standard deviation of the logarithm of Y. The dummy variables S_1 and S_2 refer to the site classification and take the value of 1 for shallow and deep alluvium sites, respectively, and zero otherwise.

The coefficients in equation (3) were estimated through nonlinear multiple regression analyses and the hypothesis that the coefficients were zero was accepted at the 10 per cent significance level using Student's test statistics.
Table 1,2 summarize the results obtained for the coefficients in equation (3) in case of the larger of the two horizontal components of the motion (NS and WE) respectively for epicentral and fault distance. Tables 3,4 provide the same results in case of the vertical component of the motion. The coefficients obtained for peak ground acceleration (PGA) and velocity (PGV) are reported in the same tables.
The values shown in Tables 1-4 are derived from an interpolation aimed to reduce the statistical fluctuation of the coefficients due to the frequency discretization of the spectra. Such interpolation allows to obtain smoothed spectra without significantly modifying the results of the regression.

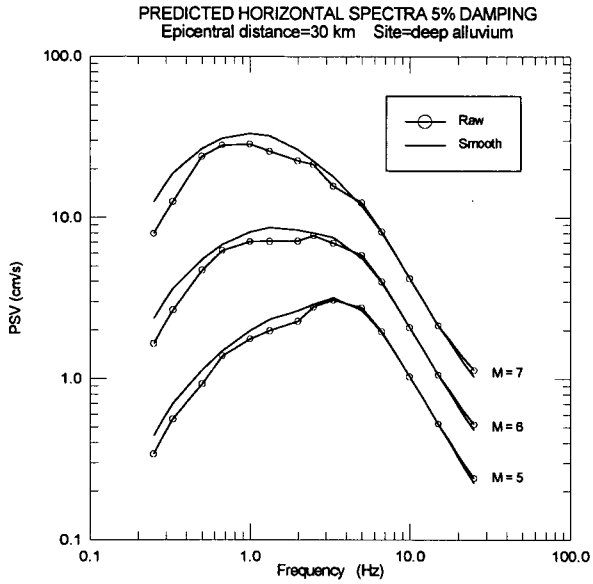

Figure 1. Dependence of the predicted horizontal spectra on magnitude and comparison between spectra calculated with raw and smooth coefficient.

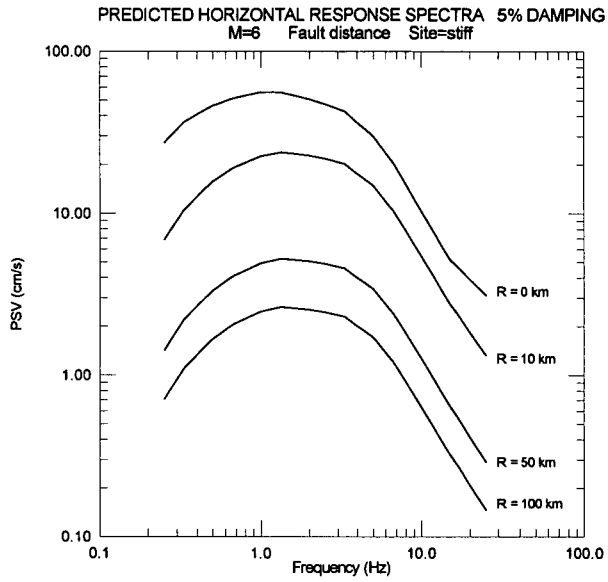

Figure 2. Dependence of the predicted horizontal spectra on distance

Figure 1 shows the dependence on magnitude of the predicted horizontal spectra: higher magnitudes are associated to a proportionally greater spectral content at low frequencies according to the seismological relationship between corner frequency and seismic moment [16]. The spectra labeled as "raw" are those obtained from the regression analysis; the ones labeled as "smooth" are derived from interpolation.
The dependence on distance of the predicted horizontal spectra is given in figure 2: except for distances less than 10 km, where the influence of the parameter **h** is greater, the spectra attenuate with distance maintaining the same shape consistent with the findings of other authors [17,18,19]
The effect of the site geology on the spectral shape is depicted in figure 3. The amplification effects of shallow and deep alluvium sites respect to stiff sites are of the same order of magnitude (40 - 60 %) but act in different frequency ranges (0.25 - 2 Hz for deep alluvium

and 1 - 25 Hz for shallow alluvium) illustrating that alluvium sites should not be classified together in a single category neglecting the depth of the soil deposit.
The spectra for the larger of the two horizontal components are compared in figure 4 with the spectra obtained for the vertical component of the motion. In the same figure the curves corresponding to 50 and 84 percentile are reported. The vertical spectra show lower values with respect to the horizontal ones: the difference is of the same order of magnitude as the standard deviation and decreases with increasing frequency because of the larger high frequency content associated with the vertical component.

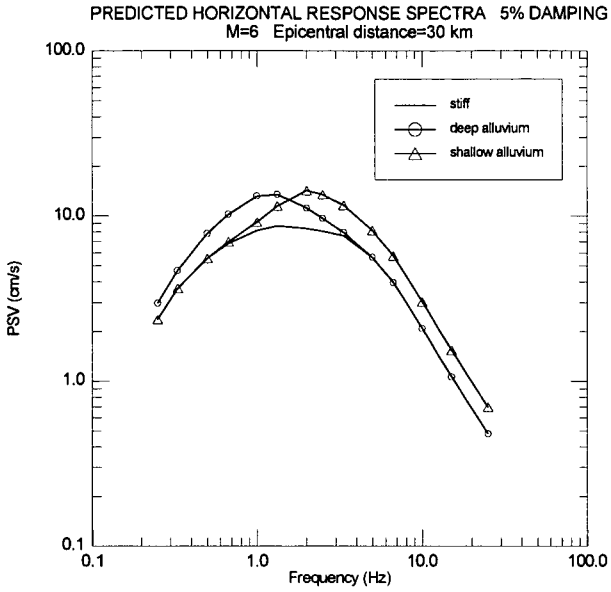

Figure 3. Dependence of predicted horizontal spectra on site geology

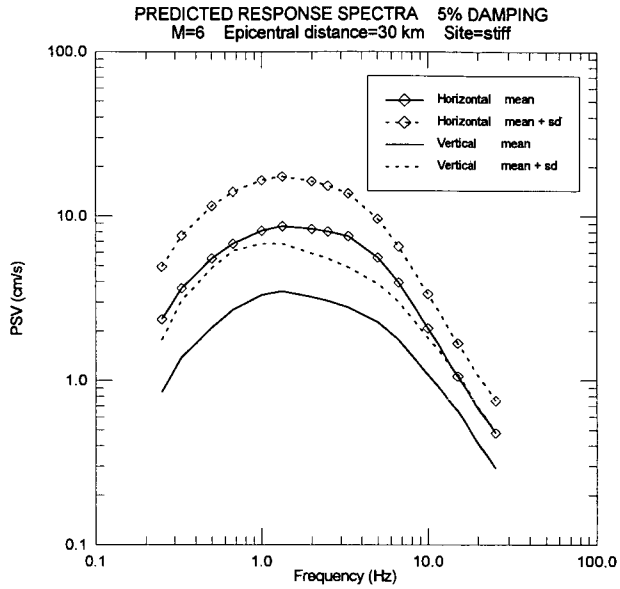

Figure 4. Comparison between horizontal and vertical response spectra

Figure 5 shows, for an epicentral distance of 30 km and a stiff site, the ratio of the vertical/horizontal spectral values with varying frequency and magnitude. For low magnitude values (M=5) the ratio is fairly constant with frequency and fluctuates around the value of 0.4. For high magnitudes (M=7) the ratio varies from a minimum of 0.35 at low frequencies to a maximum of 0.85 at high frequencies. The comparison, given in the same figure, with the vertical/horizontal ratios normally adopted in the engineering practice as suggested by the Regulatory Guide 1.60 [20] or by the eurocode EC8 [21] shows that our ratios are comparable to those proposed by EC8 but much lower than the RG-1.60 ratios. As far as the peak values are concerned, the vertical/horizontal ratio ranges from 0.4 (M=5) to 0.6 (M=7) for PGA and from 0.5 (M=5) to 0.7 (M=7) for PGV. Such values, particularly in case of high magnitudes, are in basic agreement with the suggestions of the literature [22] and regulations [21] .
In figure 6 the comparison with the relationship by [23], developed with up-to-date data bases of recordings of western north American earthquakes, is made using the multiplying coefficient of 1.09, suggested by the author to take into account the amplification effect of oblique faults respect to strike-slip faults. The predicted spectral values, for M=5,6,7 and R=30 km, are in good agreement except for frequencies lower than 0.5 Hz where our results could be underestimated by the high pass filtering.

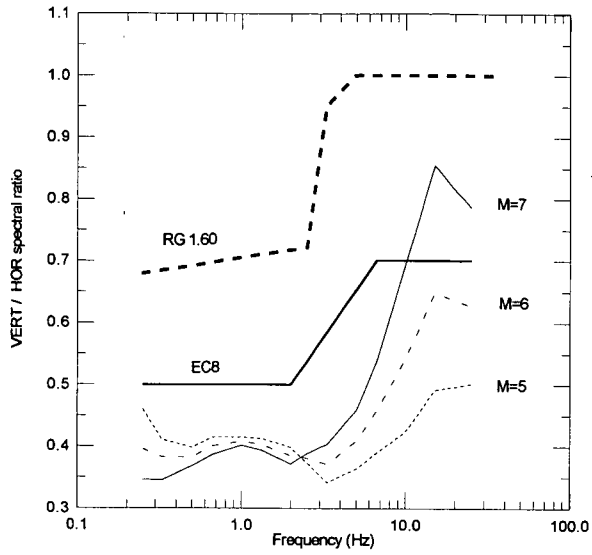

Figure 5. Spectral ratio between the vertical and the horizontal component of the ground motion (R=30 km, stiff site), as a function of frequency and magnitude, compared with the ratios proposed bu eurocode EC8 and R.G. 1.60.

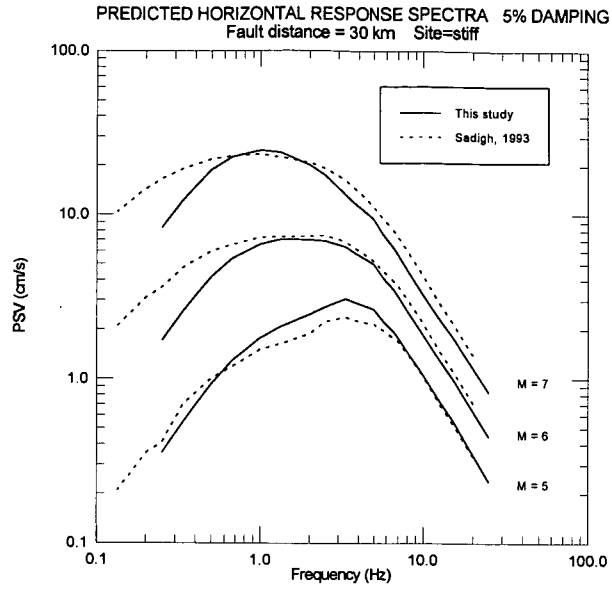

Figure 6. Comparison of median horizontal spectra, for a stiff site, with Sadigh, 1993 attenuation relationship.

3. SIMULATION OF NONSTATIONARY ACCELEROGRAMS

To simulate nonstationary strong ground motions correlated with parameters such as magnitude of the reference earthquake, distance source to site, and local site geology, an empirical methodology has been developed by the SSN based on a statistical analysis of the Italian accelerogram data base.

The simulation of artificial accelerograms is performed summing Fourier series with time dependent coefficients derived as follows:

$$a(t) = 2\sum_{n=1}^{N} C_n(t)\cos(n2\pi f_0 t + \varphi_n) \tag{4}$$

$$C_n(t) = \sqrt{2\pi f_0 PS(f_n,t)} \tag{5}$$

where a(t) is the acceleration, f_0 is the fundamental frequency (reciprocal of the total duration), and the phases φ_n are random numbers uniformly distributed in the range $0 - 2\pi$, and PS is the Physical Spectrum. The PS is a frequency-time decomposition of the expected energy of a process, a natural extension of the power spectrum to the nonstationary case. If we consider the acceleration component x(t), its PS is defined as:

$$PS(t,f) = \left| \int_{-\infty}^{+\infty} w(t-u)x(u)e^{-i2\pi fu}\,du \right|^2 \tag{6}$$

where t and f represent time and frequency, u is a dummy variable and w(t-u) is a running time window function whose characteristics have been described in a previous paper [24].

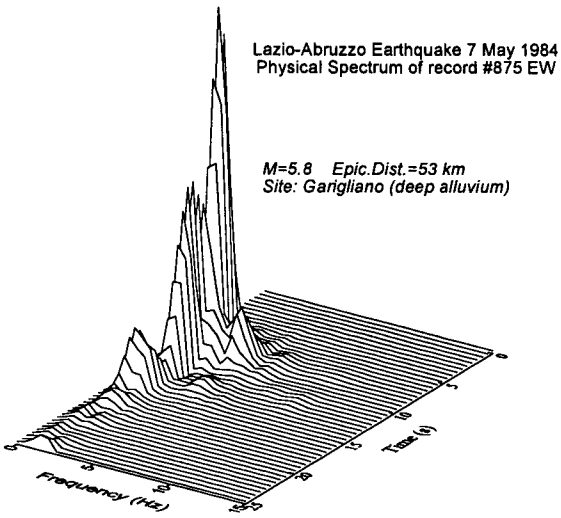

Figure 7. Physical spectrum calculated for the M=5.8 Lazio-Abruzzo earthquake of May 1984 recorded at the "Garigliano station.

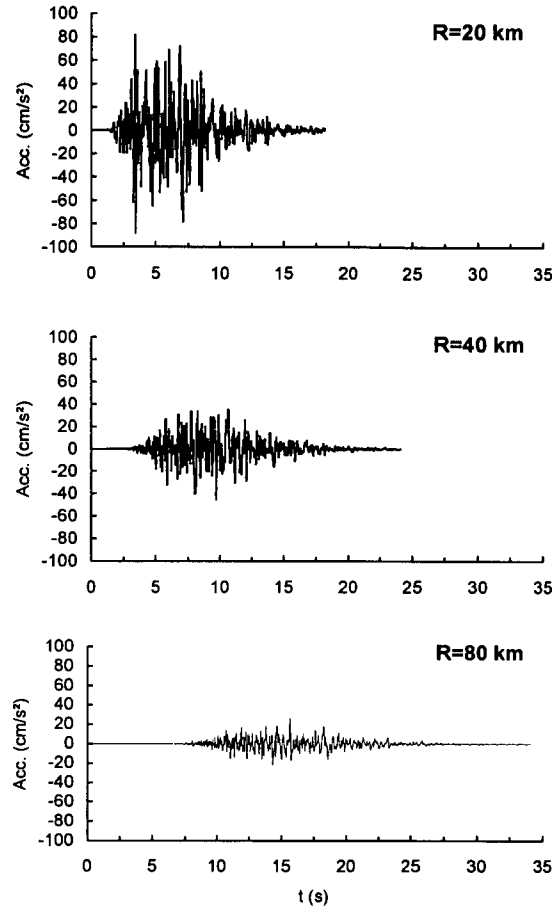

Figure 8. Simulated accelerograms in case of a stiff site, M=6, and R=20, 40, and 80 km

Figure 7 shows an example of PS calculated, with a Gaussian moving window of 2.5 sec width, for an accelerogram recorded in 1984 at the "Garigliano" station.
The PS(t,f) has been fitted with a lognormal function [25] as following :

$$PS_{approx}(t,f) = \frac{Pa(t)}{f\sqrt{2\pi}\,\delta} e^{-\left[(\ln f - \ln \beta(t))^2/2\delta^2\right]} \tag{7}$$

Pa(t), instantaneous average power, is the time envelope function describing the amplitude variation of ground motion and its integral in the time domain is equal to the integral of PS in

the time-frequency plane and correspond to the Arias intensity. It can be also approximated with a lognormal function :

$$Pa(t) = \frac{I_A}{t\sqrt{2\pi\sigma}} e^{-\left[(\ln(t)-\mu)^2/2\sigma^2\right]} \tag{8}$$

$\beta(t)$,δ, I_A, σ, μ, are correlated with magnitude, distance and site geology.
A complete description of the methodology and the predictive equation coefficients are reported in [9] .
The attenuation of the ground motion with epicentral distance is represented in figure 8. As expected larger distances correspond to smaller accelerations and higher durations.

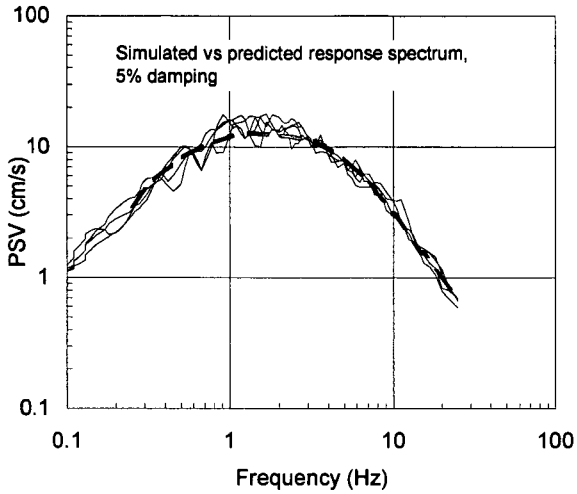

Figure 9. Response spectra of four simulated accelerograms compared with the spectrum predicted by attenuation relationship in case of M=6, R=20 km, for a stiff site

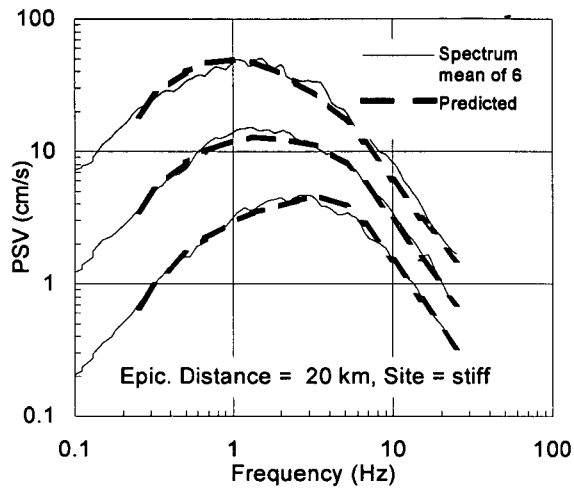

Figure 10. Comparison of the mean response spectra derived from six simulated accelerograms, with spectra predicted by attenuation relationship for magnitude 5, 6 and 7.

Figure 9 compares the pseudo-velocity response spectra of 4 simulated accelerograms with the 50 percentile spectrum predicted by the attenuation relationships illustrated in the previous section. The level of fit is satisfactory even for single simulations also because the variability of the simulated spectra is only due to the different phases of the corresponding time histories and does not include the uncertainty in the prediction of the ground motion parameters used for the simulation.
The comparison of the mean response spectra, derived each from six simulations, with the predicted ones is presented in figure 10 for different magnitudes showing a very good fit in all the considered cases.

4. EFFECTS OF GEOLOGICAL IRREGULARITIES ON GROUND MOTION

The definition of the design ground motion for sites, without topographic irregularities, is nowadays a routine task.
Usually the soil underlying a site is idealized as horizontal layers overlying rock, and the seismic incident waves, generating the reference motion, are assumed to be plane waves propagating in vertical direction through the rock half-space (SHAKE [26]). Such reference motion can be determined knowing the source parameters or the characteristics of the seismogenetic areas and the attenuation laws of the motion to the site. There are many different ways to determine such motion, but it is out of our scope to make a survey of all the methodologies. The main uncertainties are related to the knowledge of mechanical characteristics of soils and to the randomness of the motion. The approximation due to the assumed hypothesis of vertically propagating shear waves is often masked by the larger previous uncertainties. Nevertheless for horizontally layered sites such hypothesis has been shown to be acceptable from the design point of view.
For sites located in relatively narrow valley, edges and mountains, the effect of the complex landscape morphology need to be consider too. In fact it involves a heterogeneity of soil motion from point to point as the hypotheses of plane horizontal strata are not more valid.
A vast amount of theoretical works has been done in the last 20 years on the effect of complex topography and heterogeneity of soils using different methodologies. Keiti Aki [27] has given a complete survey of such methodologies and their results and he has emphasized the successful comparisons of observations and theory. Such methods have been used for long time by seismologists to study the wave propagation, but nowadays they are becoming inexpensive and easy to be used also by larger number of technicians to solve microzoning problems. They allow to avoid the hypothesis of horizontally layered strata and only vertically propagating waves. So it is possible to consider both volume and surface waves and any kind of soil layer and surface shape. The Boundary Element Method, BEM, [28] seems to be the most promising method and the easiest to be used by engineers. One of the authors has developed a computer code, BESOIL [10], based on the boundary element indirect method [29]. In it the reference motion can be a time history or either a response or a power density spectrum. In the last case the random vibration theory is used to consider the uncertainties of the reference motion [30,31]. Moreover the response or power density spectrum represents a family of time histories characteristic of the reference ground motion and then suitable for design. The method allows to obtain, in simple way, in every point of the soil surface, the time histories, the upper, medium and lower bound of a family of possible vibration ground motions.
With the massive accumulation of seismic records, the effect of heterogeneous underground interface and topographic irregularities on seismic waves has become one of the major experimental research subjects in the last ten years. Among the others we refer mainly to two international experiments, that is the Turkey flat [32] and Ashigara valley [33]. In both sites, one in California USA and the other in Japan, a valley has been monitored to provide a data base for comparing and testing methods developed to predict the effects of local geology on ground motion. The scientific community has been called to foresee the present and future experimental results. Also, in Italy we have planned a similar project. The National Seismic Survey has selected a valley in central Italy (Aterno, L'Aquila) as a seismic field laboratory [34], The valley (figure 11), about 700 m over the sea level, is surrounded by relieves over 2,000 m. high and shows olocenic alluvial sediments and lacustrine Pleistocenic soils. Large historical earthquakes are reported for this area with epicentral intensities up to X MCS scale. Recent seismicity shows

the largest shocks having magnitude less than 4. Unfortunately the characterization of the soil properties has not been completed yet.

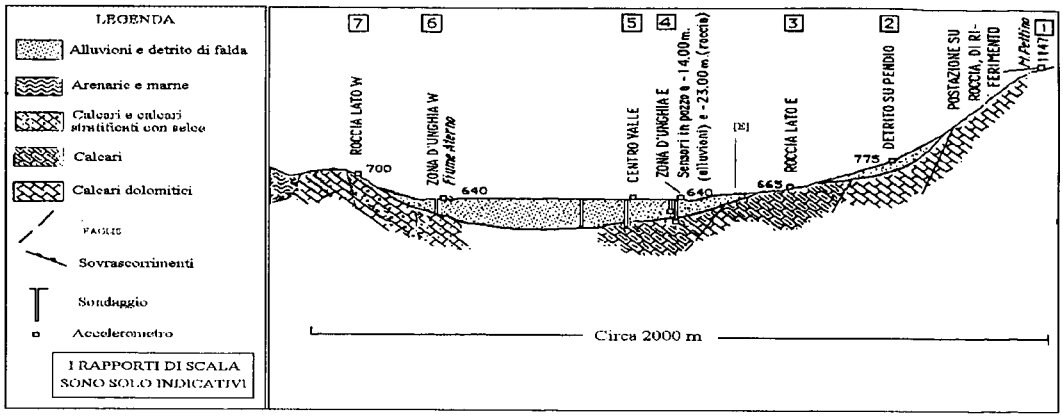

Figure 11. Scheme of Aterno Valley

A demonstration of the capability of the BESOIL methodology, two examples are shown. The first regards the Aterno valley [34]. In figure 11 the scheme of the valley is shown. The reference motion, that is the undisturbed motion on a hypothetical rocky half space, is a time history recorded on the rock at the side of the valley during a swarm of weak shocks on June 1994. The figures 12 and 13 show the results of the analyses in term of accelerograms and response spectra on equally spaced stations on the surface of the valley. The upper time history shown in figure 12 represents the reference input motion.

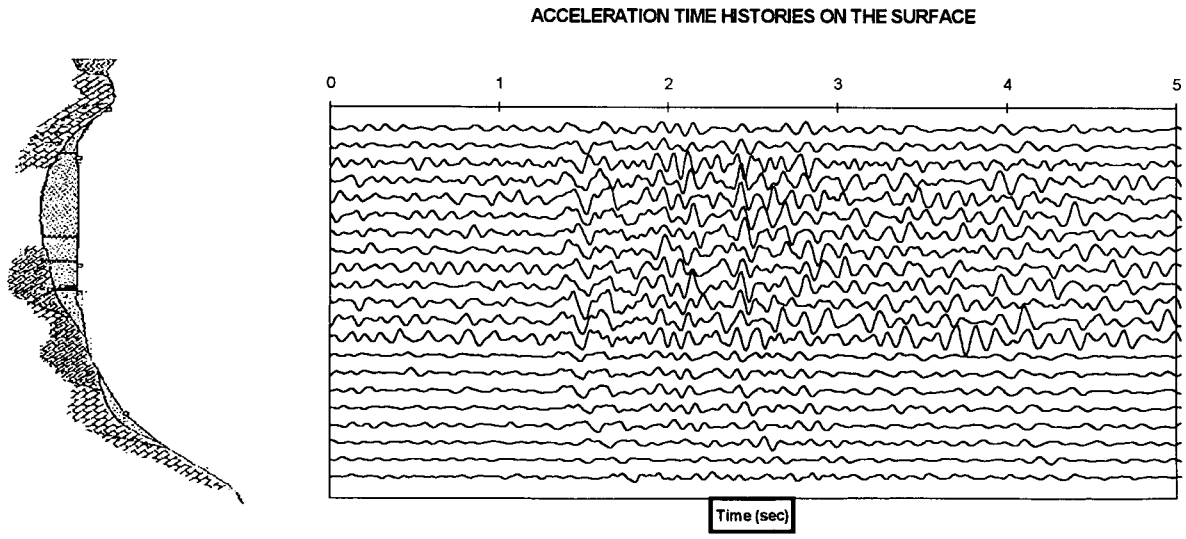

Figure 12. Aterno Valley. Computed time histories

We have assumed that such time history is set up by SV plane waves vertically incident to a horizontal plane. It is clear the effect of amplification of the soft soil and the heterogeneity of the surface motion due to the topography. The incident SV waves are reflected and diffracted producing P, SV and Rayleigh waves. They are combined in such a way that is difficult to

distinguish each other. Their amplitude ratio is strongly dependent on the shape of the soil interfaces and of the free surface.

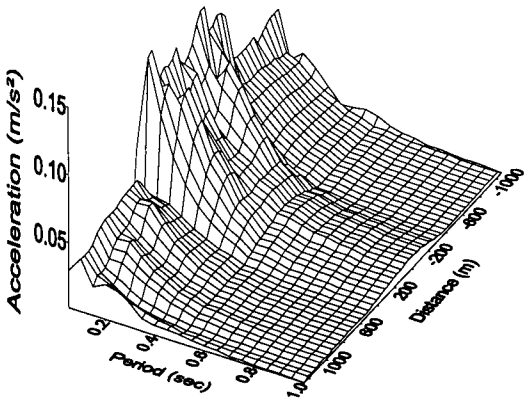

Figure 13. Aterno valley. Horizontal response spectra

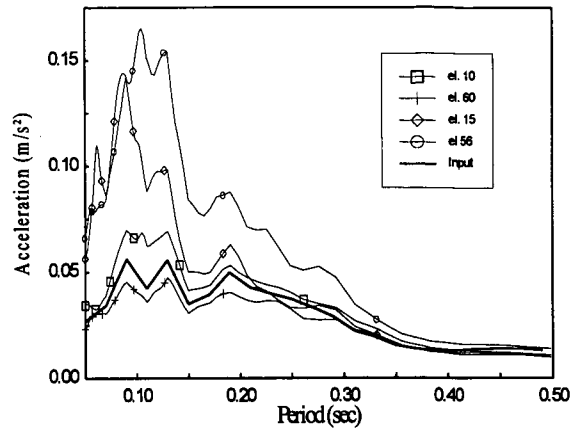

Figure 14. Spectra at the edges of Aterno valley

The same conclusions can be drawn from figure 13 that shows in a 3D diagram the distribution of the response spectra. In the vertical axis is reported the acceleration spectra, in the horizontal axes are respectively the distance of the stations from the center of the valley and the periods of the response spectra. Figure 14 shows the spectra referring to the stations at the edges of the valley (labels 15 and 56), and to the stations on the rock (labels 10 and 60 corresponding to the stations 3 and 7 of figure 11) immediately near the valley edges. The largest amplifications, observed at the stations labeled 15 and 56, are probably due to the basin effect induced by the Rayleigh waves traveling on the free surface and reflected from both edges. The curves concerning the rock sites, where likely the bridge piers would be founded, show evident differences each other of about 40% due mainly to the topographic effect.

The second example regards the Angitola site, in southern Italy. The reference input motion, in a hypothetical homogeneous rocky half space at the site, after seismological studies, has been chosen to be described by the artificial accelerogram scaling at 0.6 PGA the record obtained at Brienza during the 1980 Irpinia earthquake. Its response spectrum has been chosen to be representative of a family of events that can occur at the site. In figure 15 the scheme of the site is shown. The computer code, BESOIL, considers in this case that the incident waves are set up of only SH ones coming from the infinity. The results, as acceleration response spectra, are synthetically shown in fig 16 in a 3D diagram. The heterogeneity of the response and the great amplification at the center of the valley is evident. Figure 17 shows the response spectra at the center of the valley; the thick line represents the mean value. The other curves refer to the upper and lower bounds corresponding respectively to the 90% and 10% probabilities to be exceeded and take into account the randomness of motion. In figure 18 we have compared the response spectrum at the center of the valley with that obtained from PSHAKE computer code [31] that consider horizontally layered soil in a 1D analysis. The large amplification obtained with BESOIL is due to the effect of focusing of the waves because the shape of the interface between rock and soil and the constructive interference of waves from both edges.

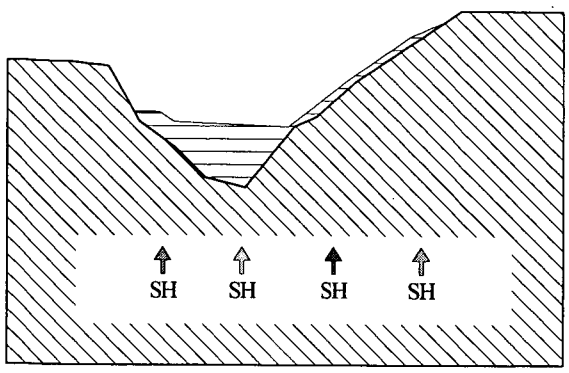

Figure 15. Scheme of Angitola site.

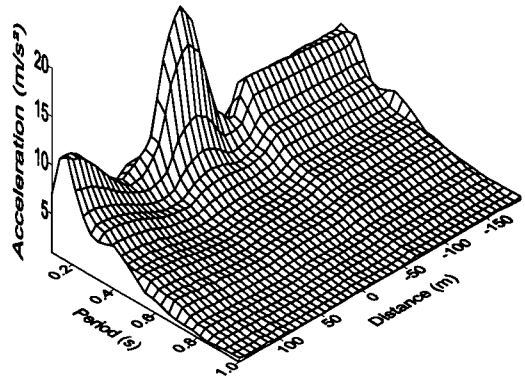

Figure 16. Angitola site. Horizontal acceleration spectra.

The selected examples suggest the great utility of the BEM in treating the wave propagation problem and its flexibility in term of geometry, materials and direction of incident waves.

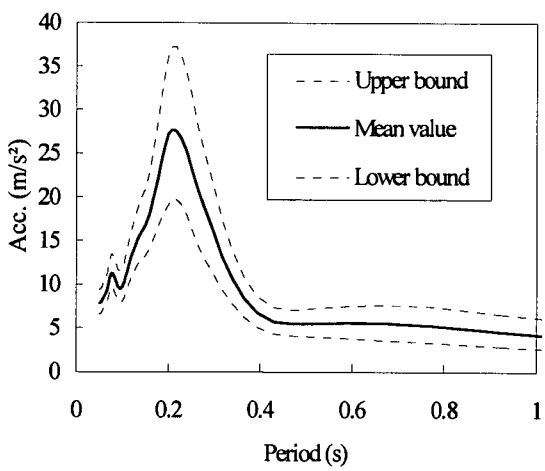

Figure 17. Spectra at the centre of Angitola site.

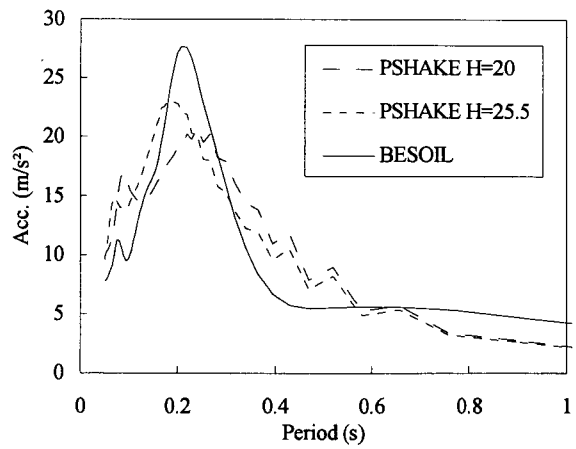

Figure 18. Mean values acceleration spectra at the centre of Angitola valley. Comparison between PSHAKE and BESOIL.

The above described examples do not consider the effect of the soil non-linearities. Seismologists tend to find a good correlation between weak and strong motions at a given site, namely, similar amplification factors for both, implying that non-linearities are not important as the first order effect in most cases. As a matter of fact, it is usually not easy to clearly recognize the non-linear effect on observed strong motion records as the influence of non-linearities is often masked by other effects due to the complexity of source and propagation path [35]. Then

for a given site using the weak motion could be used to predict the first order effect on strong ground motion at the site. This is true except the obvious case of liquefaction. Such phenomenon can have dramatic effects on the soil motion.

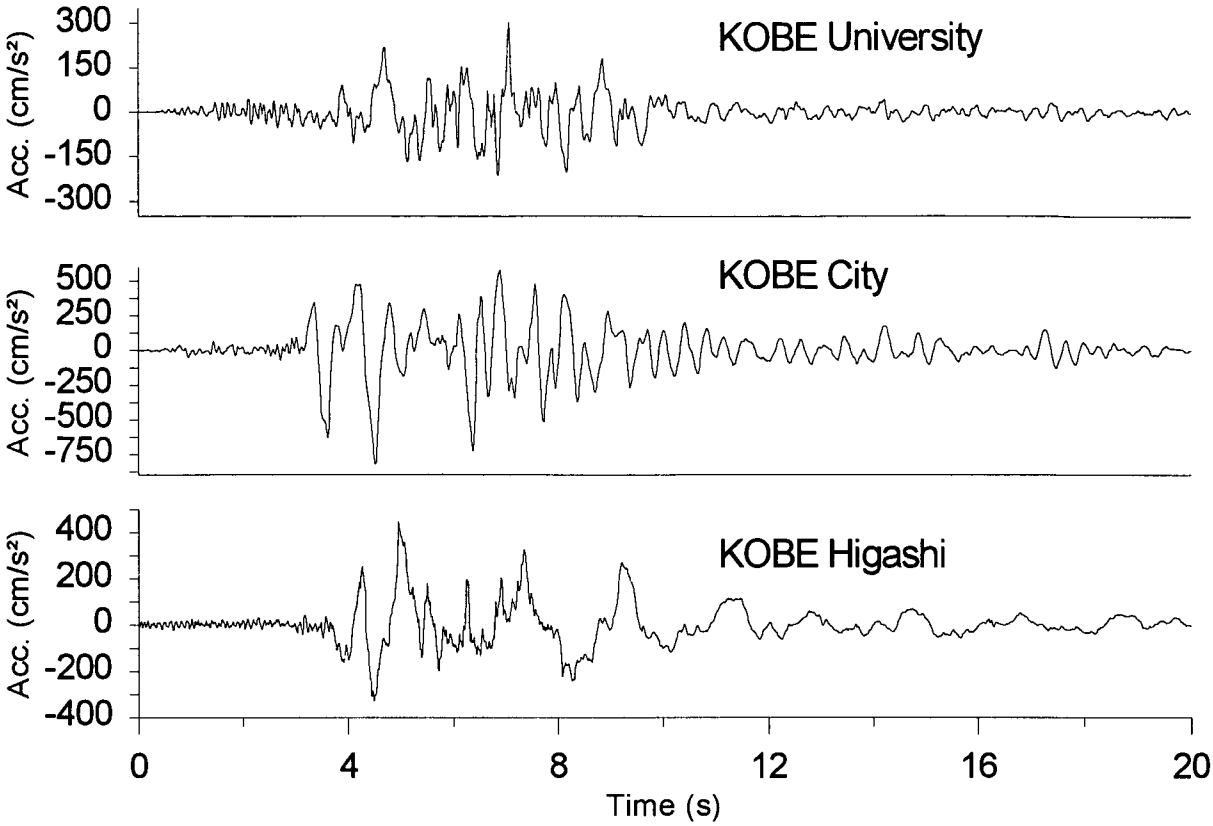

Figure 19. Time histories recorded in Kobe.

As an example in figure 19 the time histories recorded in Kobe during the main shock of the 1995 Hyogo-ken Nambu earthquake are shown. The recording stations were distant about 1-2 km each other and from the causative fault; the first on rock, the second on soft soil and the third where liquefaction happened. The second time history shows the great amplification due to the soft soil. The third time history shows the effect of soil liquefaction that consists in a reduction of the peak acceleration and a lengthening of the dominant period to about 3 sec. An attempt has been made [36] to reproduce such effect using conventional computer codes. The conclusions are that in conditions of large soil deformations the conventional methodologies are not applicable and further researches are needed.

5. CONCLUSIONS

The prediction of 5% damped response spectra on the basis of the vertical and the larger of the two horizontal components of 95 strong motions recorded in Italy lead to the following conclusions:

- the alluvium sites show an amplification effect of about 50% with respect to the stiff sites, acting at low frequencies for deep alluvium sites and at high frequencies for shallow alluvium sites;

The empirical method proposed for the simulation of artificial accelerograms has features that make it particularly interesting:
- it reproduces the nonstationarity, in amplitude and frequency, of the real ground motions, playing an important role in nonlinear structural analysis;
- it allows the simulation of a family of time-histories, similar in general appearance but different in details, requiring only the magnitude of the reference earthquake, the distance source to site, and the local site geology as input parameters.
- the simulated time-histories fit the recorded accelerograms in terms of several ground motion amplitude measures such as peak acceleration, peak velocity, Fourier spectra, and response spectra.

Finally the successful comparisons of observation and results of theoretical methodologies, reported by literature, suggest that we may have an adequate state-of-art in predicting the site effect on ground as far as we know the soil mechanic properties and geometry. Methods based on BEM seem to be the most powerful and low-cost ones to solve practical problems related to geological irregularities. The application of the method to two examples shows the heterogeneity of motion on sites characterized by complex morphology and soil mechanical proprieties.
The effect of nonlinearity is likely to be less important on site effects except the obvious case of liquefaction. In such cases the conventional methodologies are not applicable and further researches are necessary.

REFERENCES

[1] Saragoni, G.R. and G.C. Hart. Simulation of artificial earthquakes, *Earthquake Eng. Structural Dyn.*, **2**, 249-267, 1974.

[2] Nau, R.F, R.M. Oliver and K. S. Pister. Simulating and analyzing artificial nonstationary earthquake ground motions, *Bull. Seism. Soc. Am.* **72**, 615-636,1982.

[3] Boore, M.D. Stochastic simulation of high-frequency ground motions based on seismological models of the radiated spectra. *Bull. Seism. Soc. Am.* **73**, 1865-1894. 1983.

[4] Bolt, B.A. ed. Seismic strong motion synthetics, *Academic Press, Inc.*, Orlando, Florida, 1987.

[5] Atkinson, G.M. and P.G. Somerville. Calibration of time history simulation methods. *Bull. Seism. Soc. Am.* **84**, 400-414, 1994.

[6] Pugliese, A. and F. Sabetta. Stima di spettri di risposta da registrazioni di forti terremoti italiani, *Ingegneria Sismica*, **2**, 3-14, 1989.

[7] Pugliese, A. and F. Sabetta. Attenuazione della componente verticale del moto del terreno, *Proc. 6th Nat. Conf. on Earthq. Eng.*, Perugia, Italy, **1**, 75-84, 1993

[8] Pugliese, A. and F. Sabetta, Simulation of nonstationary time histories scaled for magnitude, distance and soil conditions, *Proc. 10th Europ. Conf. on Earthq. Eng.*, Vienna, Austria, **1**, 247-252,1994.

[9] Sabetta, F. and A. Pugliese. Estimation of Response Spectra and Simulation of Nonstationary Earthquake Ground Motions. *Bull. Seism. Soc. Am.* **86**, 337-352, 1996.

[10] Sanò T. BESOIL-Un programma per il calcolo della propagazione delle onde sismiche. *Rapporto Tecnico SSN/RT/96/9 1996,*.

[11] Sabetta, F. and A. Pugliese, Attenuation of peak horizontal acceleration and velocity from Italian strong-motion records, *Bull. Seism. Soc. Am.* **77**, 1491-1513, 1987.

[12] Joyner, W. B. and D. M. Boore, Peak horizontal acceleration and velocity from strong-motion records including records from the 1979 Imperial Valley, California, earthquake, *Bull. Seism. Soc. Am.* **71**, 2011-2038, 1981.

[13] Arias, A., A measure of earthquake intensity, in *Seismic Design of Nuclear Power Plants, R. Hansen editor, M.I.T. Press*, Cambridge, 1970.

[14] Vanmarcke, E.H. Parameters of the spectral density function, their significance in the time and frequency domain, *MIT Civil Engineering and Design*, **60**-1, 1980.

[15] Breiman, L. and J.H. Friedman, Estimating optimal transformations for multiple regression and correlation, *J. Am. Statist. Assoc.* **80**, 580-619, 1985.

[16] Boore, D.M., W.B. Joyner and T.E. Fumal, Estimation of response spectra and peak accelerations from western North American earthquakes: an interim report-part 2, *U.S. Geol. Surv.Open File Rept.,* 94-127, 1994.

[17] Console, R. and A. Rovelli, Attenuation parameters for Friuli region from strong-motion accelerogram spectra, *Bull. Seism. Soc. Am.* **71**, 1981-1991, 1981.

[18] Joyner W.B. and D.M. Boore, Prediction of earthquake response spectra, *U.S. Geol. Surv.Open File Rept.*, 82-977, 1982.

[19] Boore, D.M., W.B. Joyner and T.E. Fumal, Estimation of response spectra and peak accelerations from western North American earthquakes: an interim report, *U.S. Geol. Surv.Open File Rept.,* 93-509, 1993.

[20] Atomic Energy Commission, Regulatory Guide 1.60, Design response spectra of nuclear power plants. 1973

[21] Commission of the European Communities, Eurocode 8: Earthquake resistant design of structures, *CEN / TC250 / SC8* - Part 1-1: Seismic actions and general requirements for structures. 1993.

[22] Newmark, N.M. and W.J. Hall, Development of criteria for seismic review of selected nuclear power spectra, *NUREG-CR-* 0098. 1978.

[23] Sadigh, K.R., A review of attenuation relationships for rock site conditions from shallow crustal earthquakes in an interplate environment, *Proc. International Workshop on Strong Motion Data*, II, 179-236. 1993.

[24] Sabetta, F., R. Masiani and A. Giuffrè, Frequency nonstationarity in Italian strong motion accelerograms, *Proc. 8th Europ. Conf. on Earthq. Eng.*, Lisbon, Portugal, 3.2, 25-32. 1986.

[25] Hammoutene, M., B.Tiliouine and P.Y. Bard, A two dimensional nonstationary optimized accelerogram scaled for magnitude, distance and soil conditions, *Proc. 10th World Conf. on Earthq. Eng.*, 817-821. 1992.

[26] Schnabel B, J.Lysmer, H.B.Seed SHAKE, a computer program for the non-linear analysis of vertically propagating shear waves in horizontally layered deposits, *EERC Report No. 78/23*, October 1978.

[27] Keiti Aki, Recent Advances in Ground Motion Evaluation, Geotechnical *Special Publication* No 20, ASCE, 1988.

[28] Brebbia, C. A., The boundary element method for engineers, Pentech Press, London, 1978.

[29] Sanchez-Sesma F.J., Campillo M., Diffraction of P,SV, and Rayleigh waves by topographic feature: a boundary integral formulation. *Bull. Seis. Soc. Am.* **81**, 2234-2253, 1991.

[30] Romo-Organista M.P., Jen-Hwa Chen, Lysmer J., Seed H.B., PLUSH-A computer program for probabilistic finite element analysis of seismic soil-structure interaction. *UBC EERC* report No 77/01, 1977.

[31] Sanò T., Pugliese A,. PSHAKE, Analisi probabilistica della propagazione delle onde sismiche, ENEA, RT/DISP/91/03, 1991,.

[32] Real C.R. and C.H.Cramer, Turkey Flat, USA, Site Effects Test Area; Calfornia *Department of Conservation, Div. of Mines and Geology, Report NO 89-1*, 1989.

[33] Ashiagara Valley Blind Prediction Test : The Effects of Surface Geology on Seismic Motion; *Japaneese National Working Group on the Effects of surface Geology on Seismic motion (JESG),* 1991.

[34] Bongiovanni G., Marsan P., Romeo W.R., Combined Geological and Geophysical Investigations for Site Effects Analyses in Seismic Zoning Perspective, *Proceedings of the Fifth International Conference of Seismic Zonation, Nice October 17-18, Vol. III, 903-910,* 1995.

[35] Esteva, L. Microzoning: models and reality, Proc of 6th WCEE, New Delhli, 1977.

[36] Sanò T., A.Pugliese, R.Romeo Amplificazione locale in condizione di alta non linearità, Atti del VII Convegno Nazionale *" L'Ingegneria Sismica in Italia", Vol. 3, Siena-Italy, 25-28 Sett.* 1995.

Table 1 - Regression coefficients of equation (3) for PSV, PGA, and PGV, for the larger horizontal component and epicentral distance

	Const. Term	Mag. Coeff.	Dist. Coeff.	Site Coeff.	Site Coeff.		
Freq (Hz)	**a**	**b**	**c**	**e_1**	**e_2**	**h**	**s**
0.25	-2.500	0.725	-1	0.000	0.100	2.6	0.319
0.33	-2.250	0.715	-1	0.000	0.108	3.0	0.319
0.50	-1.900	0.687	-1	0.000	0.150	3.6	0.319
0.67	-1.647	0.660	-1	0.010	0.175	4.0	0.315
1.00	-1.280	0.612	-1	0.050	0.208	4.4	0.308
1.33	-1.000	0.570	-1	0.120	0.190	4.7	0.303
2.00	-0.595	0.500	-1	0.230	0.124	5.0	0.290
2.50	-0.281	0.445	-1	0.222	0.078	5.2	0.280
3.33	0.100	0.377	-1	0.185	0.020	5.4	0.260
5.00	0.296	0.323	-1	0.161	0.000	5.7	0.234
6.67	0.222	0.310	-1	0.161	0.000	5.9	0.220
10.00	-0.019	0.304	-1	0.161	0.000	6.2	0.208
15.00	-0.312	0.304	-1	0.161	0.000	6.3	0.200
25.00	-0.817	0.330	-1	0.161	0.000	4.7	0.195
PGA (g)	-1.845	0.363	-1	0.195	0.000	5.0	0.190
PGV (cm/s)	-0.828	0.489	-1	0.116	0.116	3.9	0.249

Table 2 - Regression coefficients of equation (3) for PSV, PGA, and PGV, for the larger horizontal component and fault distance

	Const. Term	Mag. Coeff.	Dist. Coeff.	Site Coeff.	Site Coeff.		
Freq (Hz)	**a**	**b**	**c**	**e_1**	**e_2**	**h**	**s**
0.25	-2.400	0.685	-1	0.000	0.130	2.1	0.297
0.33	-2.170	0.675	-1	0.000	0.151	2.5	0.297
0.50	-1.800	0.650	-1	0.000	0.184	3.1	0.297
0.67	-1.510	0.620	-1	0.010	0.210	3.5	0.295
1.00	-1.120	0.570	-1	0.050	0.242	4.0	0.290
1.33	-0.850	0.530	-1	0.120	0.232	4.4	0.283
2.00	-0.400	0.455	-1	0.220	0.156	5.0	0.271
2.50	-0.077	0.400	-1	0.210	0.115	5.3	0.264
3.33	0.400	0.315	-1	0.165	0.065	5.7	0.245
5.00	0.550	0.273	-1	0.130	0.000	6.3	0.215
6.67	0.500	0.255	-1	0.130	0.000	6.7	0.200
10.00	0.290	0.245	-1	0.130	0.000	7.3	0.190
15.00	-0.035	0.255	-1	0.130	0.000	7.2	0.182
25.00	-0.505	0.273	-1	0.130	0.000	5.8	0.182
PGA (g)	-1.562	0.306	-1	0.169	0.000	5.8	0.173
PGV (cm/s)	-0.710	0.455	-1	0.133	0.133	3.6	0.215

Table 3 - Regression coefficients of equation (3) for PSV, PGA, and PGV, for the vertical component and epicentral distance

	Const. Term	Mag. Coeff.	Dist. Coeff.	Site Coeff.	Site Coeff.		
Freq (Hz)	**a**	**b**	**c**	**e_1**	**e_2**	**h**	**s**
0.25	-2.507	0.660	-1	0.000	0.	2.2	0.320
0.33	-2.400	0.670	-1	0.000	0.	2.5	0.346
0.50	-2.280	0.670	-1	0.000	0.	2.8	0.362
0.67	-1.960	0.645	-1	0.000	0.	3.2	0.358
1.00	-1.630	0.605	-1	0.010	0.	4.1	0.313
1.33	-1.336	0.560	-1	0.030	0.	4.6	0.289
2.00	-0.920	0.485	-1	0.090	0.	5.0	0.267
2.50	-0.750	0.453	-1	0.120	0.	5.0	0.258
3.33	-0.550	0.413	-1	0.155	0.	5.0	0.245
5.00	-0.400	0.373	-1	0.190	0.	5.0	0.235
6.67	-0.550	0.380	-1	0.210	0.	4.5	0.230
10.00	-0.950	0.411	-1	0.235	0.	3.5	0.225
15.00	-1.250	0.424	-1	0.252	0.	2.5	0.221
25.00	-1.626	0.428	-1	0.258	0.	1.5	0.219
PGA (g)	-2.637	0.443	-1	0.209	0.	4.1	0.195
PGV (cm/s)	-1.499	0.561	-1	0.000	0.	5.2	0.228

Table 4 - Regression coefficients of equation (3) for PSV, PGA, and PGV, for the vertical component and fault distance

	Const. Term	Mag. Coeff.	Dist. Coeff.	Site Coeff.	Site Coeff.		
Freq (Hz)	**a**	**b**	**c**	**e_1**	**e_2**	**h**	**s**
0.25	-2.395	0.629	-1	0.000	0.	2.4	0.300
0.33	-2.292	0.636	-1	0.000	0.	2.4	0.328
0.50	-2.154	0.639	-1	0.000	0.	2.5	0.351
0.67	-1.900	0.615	-1	0.000	0.	2.9	0.345
1.00	-1.547	0.574	-1	0.010	0.	3.9	0.305
1.33	-1.155	0.515	-1	0.018	0.	4.9	0.280
2.00	-0.712	0.441	-1	0.040	0.	5.1	0.254
2.50	-0.480	0.399	-1	0.080	0.	5.1	0.240
3.33	-0.350	0.370	-1	0.137	0.	5.1	0.232
5.00	-0.130	0.320	-1	0.173	0.	5.1	0.225
6.67	-0.323	0.337	-1	0.185	0.	4.7	0.221
10.00	-0.700	0.370	-1	0.205	0.	3.8	0.215
15.00	-1.000	0.380	-1	0.220	0.	3.0	0.210
25.00	-1.411	0.385	-1	0.230	0.	2.2	0.212
PGA (g)	-2.365	0.387	-1	0.182	0.	4.9	0.181
PGV (cm/s)	-1.359	0.525	-1	0.000	0.	4.9	0.212

DUCTILITY EVALUATION OF REINFORCED CONCRETE BRIDGE COLUMNS

Jun-ichi Hoshikuma[1], Dr. Kazuhiko Kawashima[2] and Dr. Shigeki Unjoh[3]

1) Research Engineer, Earthquake Engineering Division, Public Works Research Institute
2) Professor, Department of Civil Engineering, Tokyo Institute of Technology
3) Head, Earthquake Engineering Division, Public Works Research Institute

ABSTRACT

A controlled cyclic lateral displacement pattern with gradually increasing amplitude has been classically applied to test specimens. In such cyclic loading test, a definition of cyclic number is very important, because it affects the ductility of reinforced concrete columns significantly. In this paper, a series of four identical reinforced concrete bridge columns were loaded with various cyclic number, and the differences in observed damage were studied. The skeleton model of strength-displacement relation for reinforced concrete bridge columns was idealized, and the ultimate point was determined to be applicable to seismic design. Furthermore, the evaluation method of the ultimate curvature/displacement taking account into effect of cyclic number was proposed. It is found from a comparison with test results that calculated ultimate displacements correspond well to observed ultimate displacements when cover concrete initiates spalling-off.

INTRODUCTION

A design specifications for highway bridges was revised in 1996, in which a strength-ductility design method was introduced to every component of bridge structures. The seismic design of reinforced concrete columns was improved in the ductility evaluation process. At first, the ultimate displacement at the center of mass of superstructure is calculated based on plastic rotational capacity at potential plastic hinge region. Secondary, a stress-strain model of confined concrete is newly introduced for a moment-curvature analysis. In most of earthquake engineering studies, the estimated ductility factor have been compared with many cyclic loading test results. However, it should be noted that a loading hysteresis path has greatly influenced on the ductility factor of reinforced concrete columns. Consequently, the loading hysteresis path given to test columns in laboratory should be controversial for the ductility evaluation.

The Hyogo-ken Nanbu Earthquake occurred in the early morning of January 17, 1995, and reinforced concrete bridge columns were severely damaged. Characteristics of ground motion during the Hyogo-ken Nanbu Earthquake were significantly different from one in past earthquakes. In the Hyogo-ken Nanbu Earthquake, the elastic acceleration response spectrum was recorded as approximately 2.0G, although the current design elastic acceleration

response spectrum is 0.7G to 1.0G. On the other hand, the duration time of the ground motion is so short that cyclic number of seismic response in columns is small as compared with response during past recorded ground motions in Japan.
In studies of the ductility evaluation of reinforced concrete columns, a controlled 10-cyclic lateral displacement pattern with gradually increasing amplitude has been classically applied to test specimens. This is because the ductility factor is used for the seismic design supposing an earthquake with long duration time so that large cyclic number of response will be expected. On the other hand, it has been found that the effect of loading hysteresis on the ductility of reinforced concrete columns is significant. Consequently, in the seismic design for the ground motion such as the record observed in the Hyogo-ken Nanbu Earthquake, the ductility factor should be evaluated based on the loading test by small cyclic number.
In this paper, four identical reinforced concrete column specimens were loaded with various cyclic number, and the effect of loading hysteresis was examined. A skeleton of lateral force-displacement relation was idealized, and evaluation method of the ductility was proposed to be applicable to the seismic design based on the test results.

CYCLIC LOADING TESTS OF REINFORCED CONCRETE BRIDGE COLUMNS WITH VARIOUS CYCLIC NUMBER

Test Specimens

To examine the effect of cyclic number on response, four identical specimens shown in Fig. 1 were constructed. A cross section is square with 60cm dimension, and a column height is 3.01m so that an aspect ratio is 5.0. There are forty-eight longitudinal reinforcing bars of SD295/D10 in the section, and square hoops of SD295/D6 with 75mm spacing. The ratio of longitudinal reinforcing bar to cross sectional area is 0.95%, and the volumetric ratio of hoops is 0.3%. Curvature of sections were measured through the section from the base to 520mm column height by LVDTs as shown in Fig. 1.

Test Setup and Loading History

The footing of test specimens were fixed to the reaction wall as shown in Photo 1, and a controlled lateral displacement was supplied to the column top by a dynamic actuator. A static axial loading of 353kN was also given, which corresponded to 0.98MPa in a uniaxial stress.
A first-yield displacement 1 δ_{yo} was determined here as a displacement at the top of column when the extreme tensile longitudinal reinforcing bars yielded at the base section. The lateral cyclic displacement was applied with gradually increasing amplitude under the displacement control. Based on observed strain of the extreme tensile longitudinal reinforcing bars at the base section, the first-yield displacement was defined here as 11mm.
The displacement hysteresis histories applied to specimens were shown in Fig. 2. The cyclic numbers in each loading step for P-1, P-2 and P-3 were one, three and ten, respectively. In P-4, the loading pattern ($\pm 1\ \delta_{yo}$, $\pm 3\ \delta_{yo}$, $\pm 5\ \delta_{yo}$, $\pm 15\ \delta_{yo}$) was different from others.

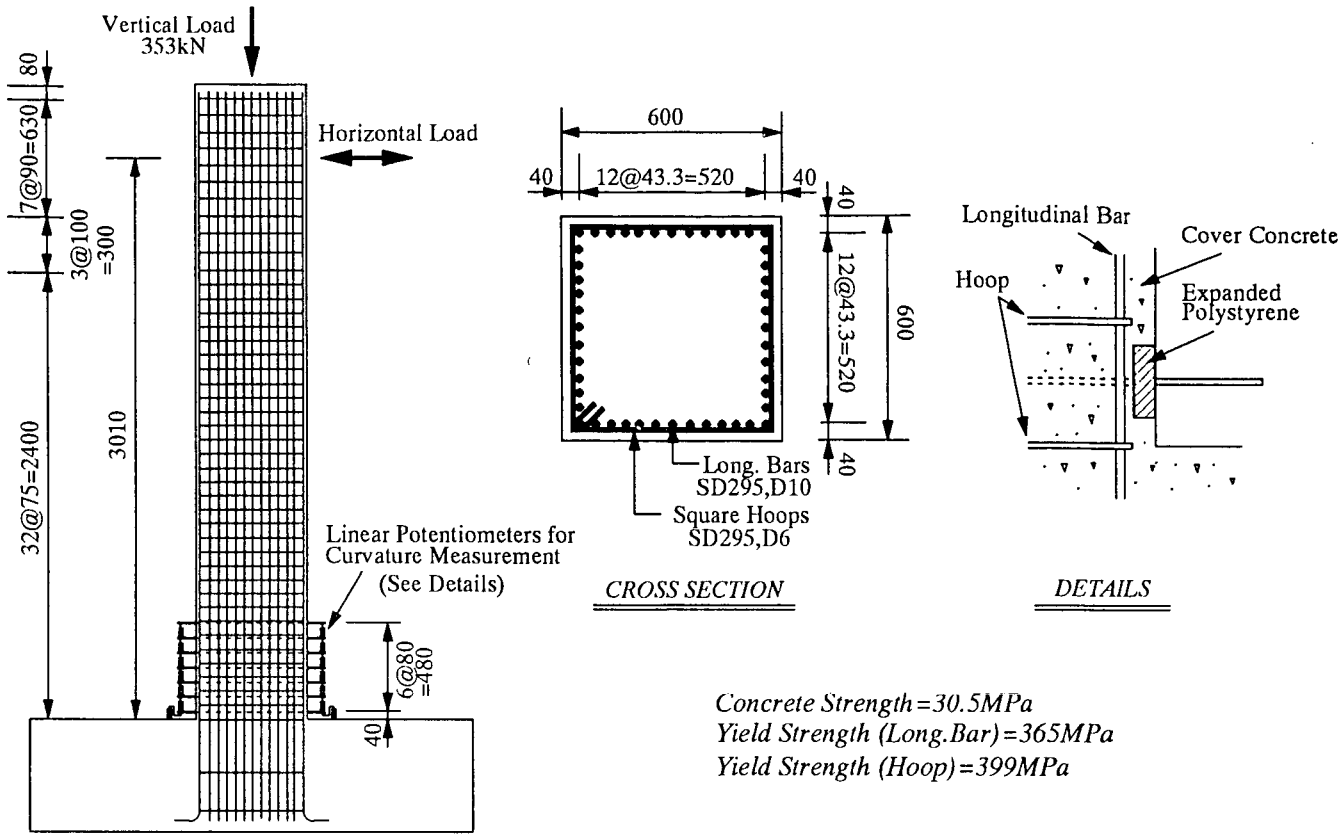

Fig. 1 Test Specimen

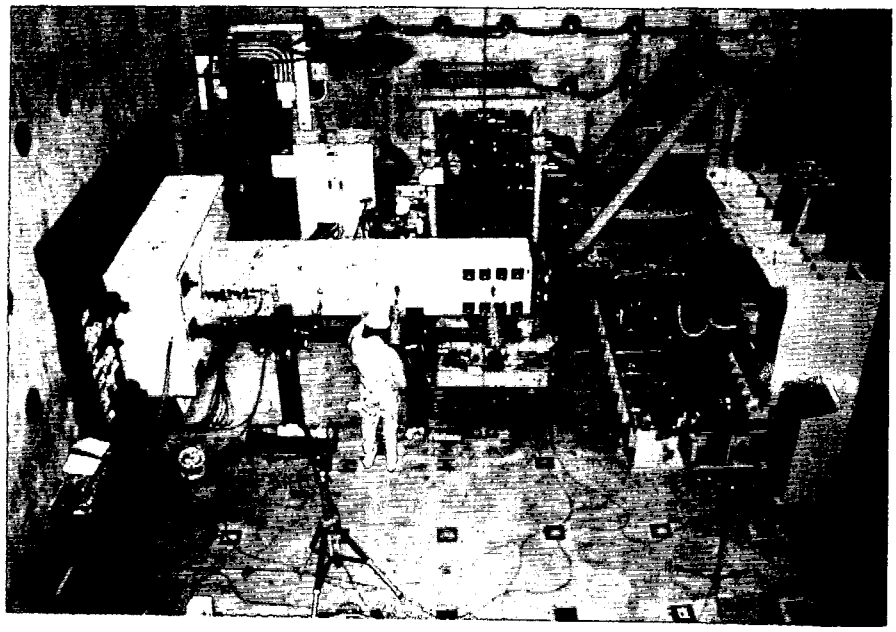

Photo 1 Test Setup for Cyclic Loading

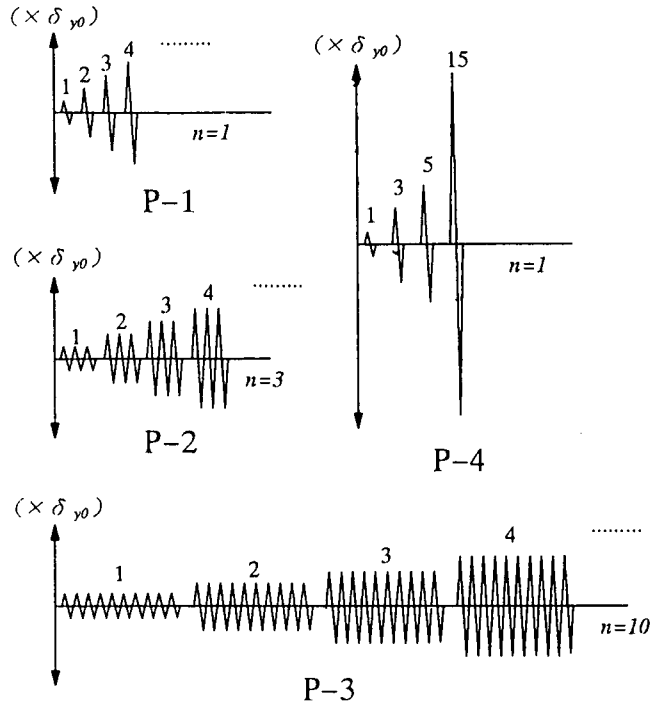

Fig. 2 Loading History

Observed Hysteresis Curves and Damage Mode

Fig. 3 shows the observed lateral force-displacement hysteresis curve. The peak lateral strength of every specimen was approximately 150kN, so that the effect of cyclic number on the lateral strength was less significant. It can be, however, observed that the cyclic number affected the ductility, and a displacement when the lateral force deteriorated was large as the cyclic number was small.

Damages developed on the transversal face of specimens are illustrated in Fig. 4. As compared the damage after 5 δ_{yo} loading step, cover concrete spalled and longitudinal reinforcing bars buckled in P-3, on the other hand, only the horizontal cracks were developed in other specimens. This means that the damage propagation accelerates as the cyclic number becomes large.

DUCTILITY EVALUATION

Skeleton Model for Lateral Force-Displacement Relation of Reinforced Concrete Columns

A lateral response of reinforced concrete column can be approximated by elasto-plastic curve as shown in Fig. 5. A yield curvature and a yield displacement are calculated as

$$\phi_y = (M_u / M_{yo})\,\phi_{yo} \qquad (1)$$

$$\delta_y = (M_u / M_{yo})\,\delta_{yo} \qquad (2)$$

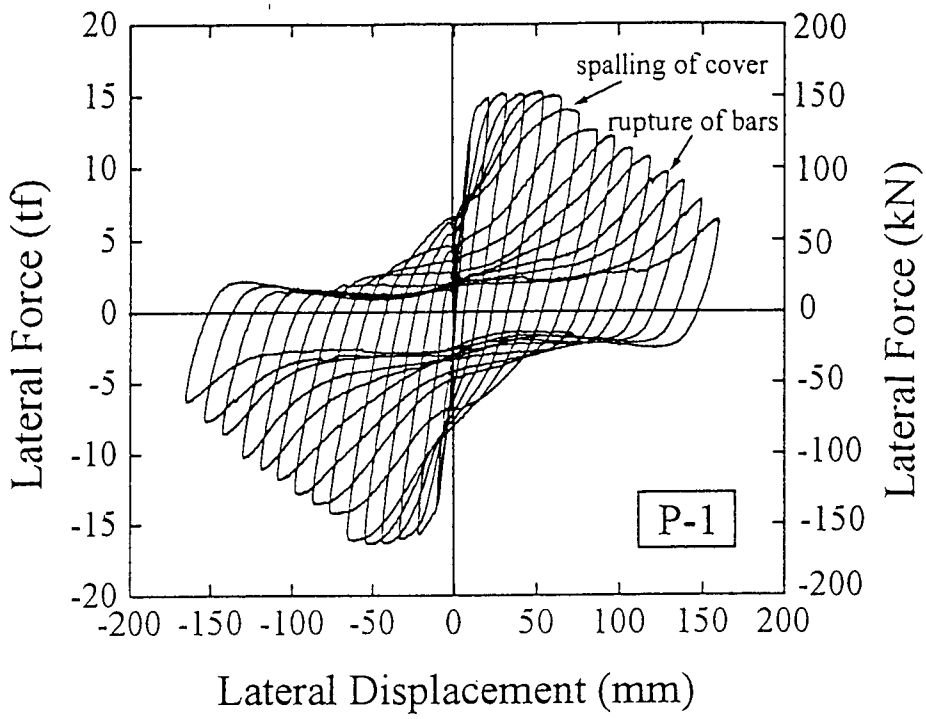

(a) P-1 Specimen (1-Cycle in Each Step)

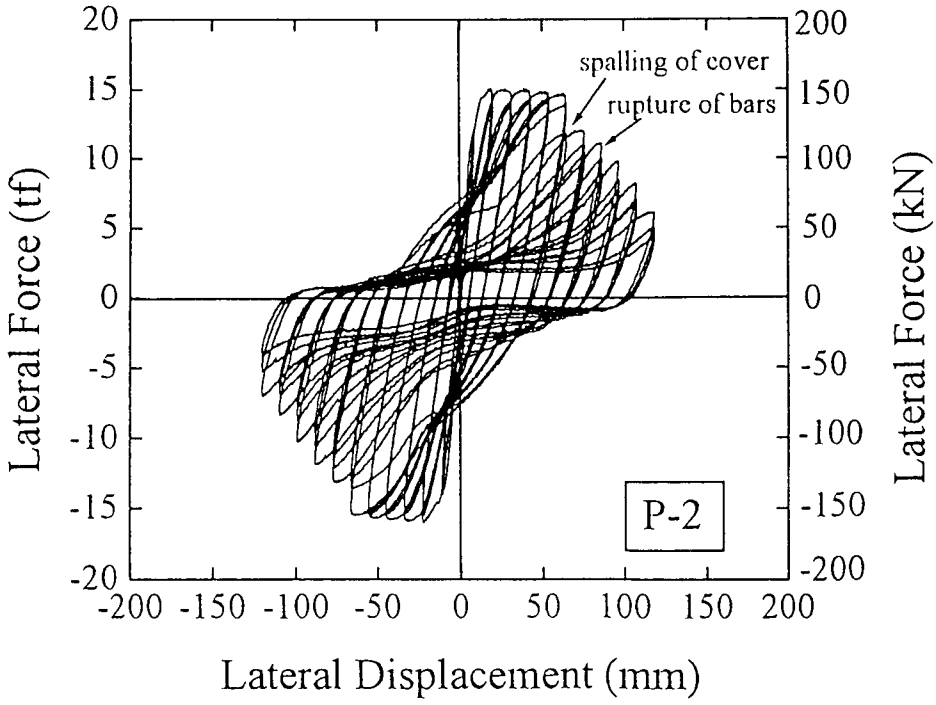

(b) P-2 Specimen (3-Cycle in Each Step)

Fig. 3 Observed Hysteresis Curves

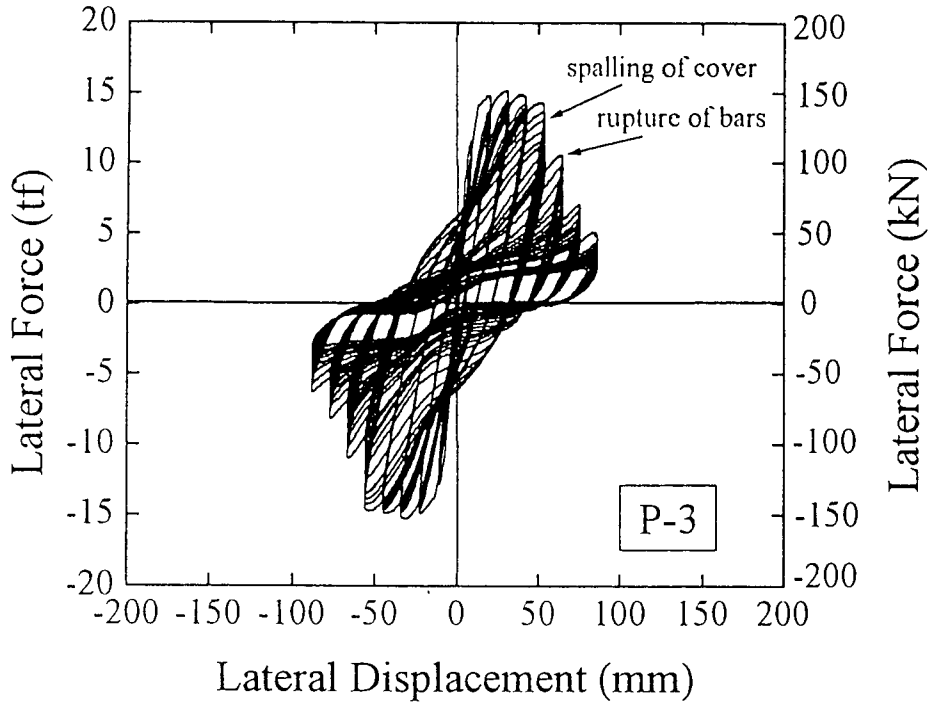

(c) P-3 Specimen (10-Cycle in Each Step)

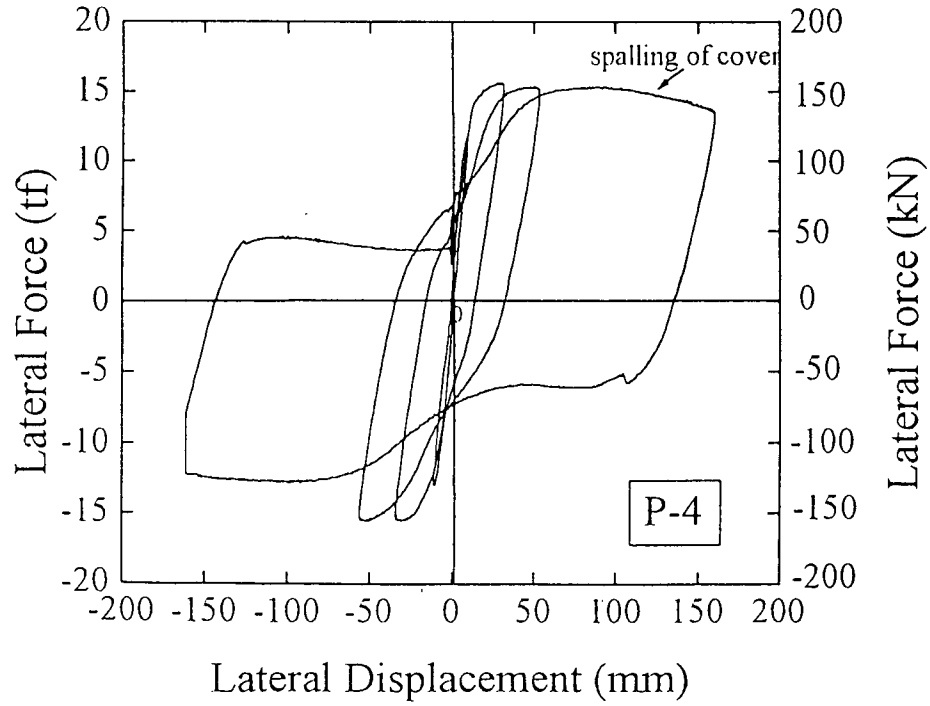

(d) P-4 Specimen (1-Cycle)

Fig. 3 Observed Hysteresis Curves

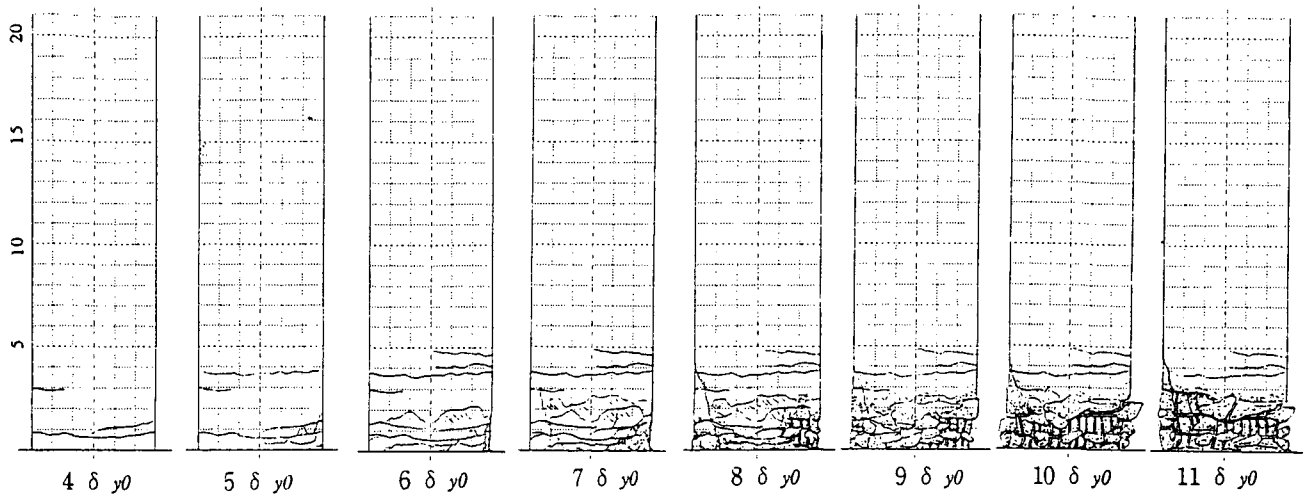

(a) P-1 Specimen

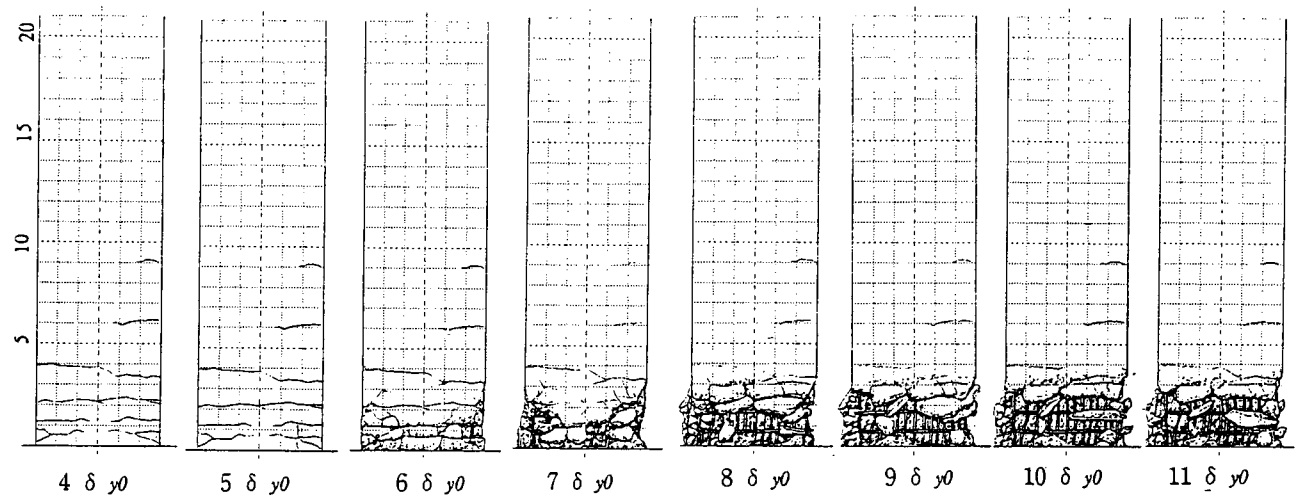

(b) P-2 Specimen

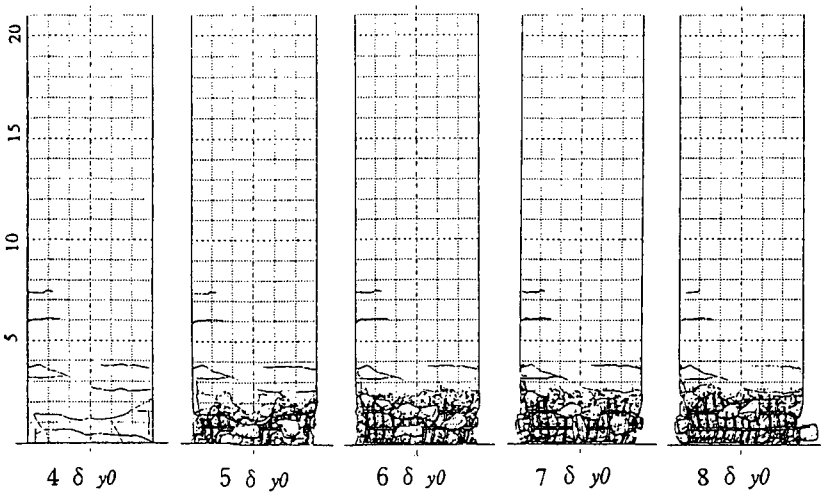

(c) P-3 Specimen

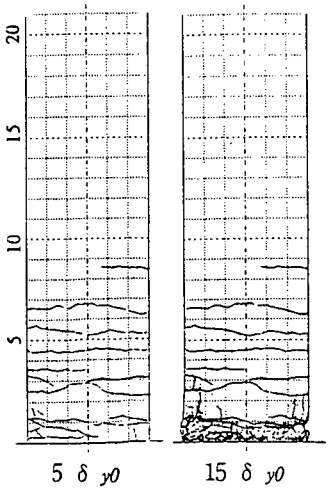

(d) P-4 Specimen

Fig. 4 Damage Propagation

where, ϕ_y, δ_y : yield curvature and yield displacement,

ϕ_{yo}, δ_{yo} : first-yield curvature and first-yield displacement, and

M_{yo}, M_u : first-yield moment and ultimate moment.

In the skeleton curve, an idealization is not made for the lateral force deteriorating branch, in which the lateral force-displacement hysteresis response is unstable due to failure of core concrete section following buckling of longitudinal reinforcing bars as shown in Fig. 3.

Some definitions of the ultimate condition have ever been proposed as the lateral force deteriorates to 80% of the peak lateral strength or to the first-yield strength. However, it should be noted how a displacement ductility factor is applied to the seismic design by an equal-energy approach, in which the lateral design force is reduced according to the displacement ductility factor. Applicability of the equal-energy approach to seismic design of fixed-base cantilever columns has been examined by Kawashima et al. In their studies, it is concluded that equal-energy approach would be applicable to a prediction of inelastic response of reinforced concrete columns as long as hysteresis response curves can be idealized by Mutou model. It can be observed in Fig. 3 that hysteresis response tends to be unstable after cover concrete is spalling-off. The event of spalling-off of cover concrete indicates that longitudinal reinforcing bars buckle and damage has developed to a core section, which results in the unstable response. The ultimate point, therefore, would be theoretically determined as cover concrete spalls-off, for seismic design by the equal-energy approach.

Ultimate Strain of Confined Concrete and Moment-Curvature Analysis

A moment-curvature relation of sections was calculated based on stress-strain curve of the confined concrete. In the analysis, a model of Hoshikuma et al. shown in Fig. 6 was used for the stress-strain model of confined concrete, because their model was developed for reinforced concrete columns with structural details specific in Japanese design codes. To evaluate the effect of cyclic characteristic of response, two ultimate strains of concrete are defined for small cyclic number loading (Loading Type-I) and large one (Loading Type-II) as

$$\varepsilon_{cu} = \begin{cases} \varepsilon_{cc} & \text{for Type-I Loading} \\ \varepsilon_{cc} + 0.8\,\sigma_{cc} / E_{des} & \text{for Type-II Loading} \end{cases} \qquad (3)$$

where, σ_{cc} is a peak stress of confined concrete, ε_{cc} is a strain at peak stress, and E_{des} is a deteriorating rate on the stress descending branch.

The strain distributions at the first-yield and ultimate conditions were assumed here as shown in Fig. 7. It should be noted that the ultimate strain is given at the extreme confined fiber, where longitudinal reinforcing bars are placed on the section. The compressive stress developed at cover concrete is assumed to be zero because cover concrete is expected to crash at the ultimate stage.

Lateral Displacement

The first-yield displacement is calculated by integrating curvature developed in whole section through the column height when the base moment reaches a first-yield moment M_{yo}, and

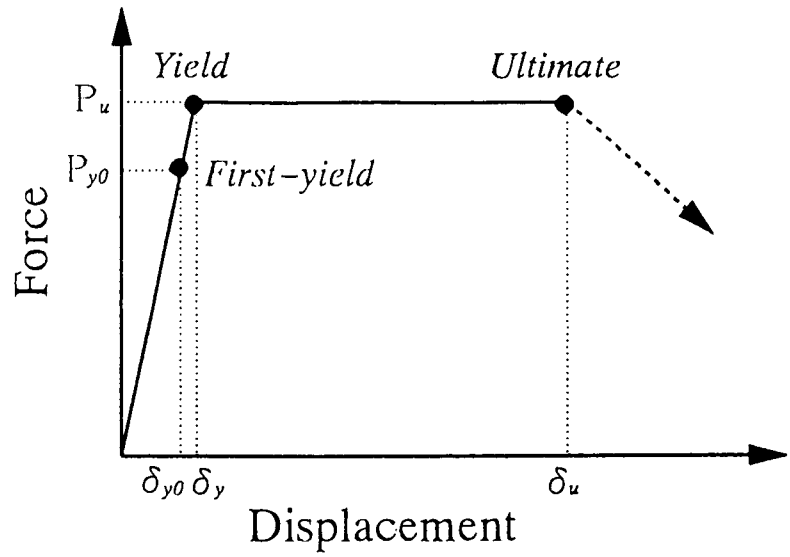

Fig.5 Skeleton Model of Lateral Force-Displacement Relation for Seismic Design

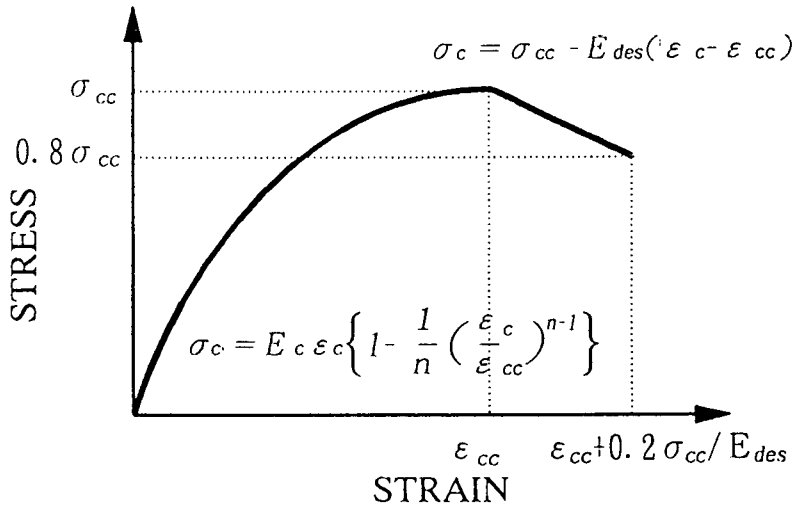

Fig.6 Stress-strain Model of Confined Concrete

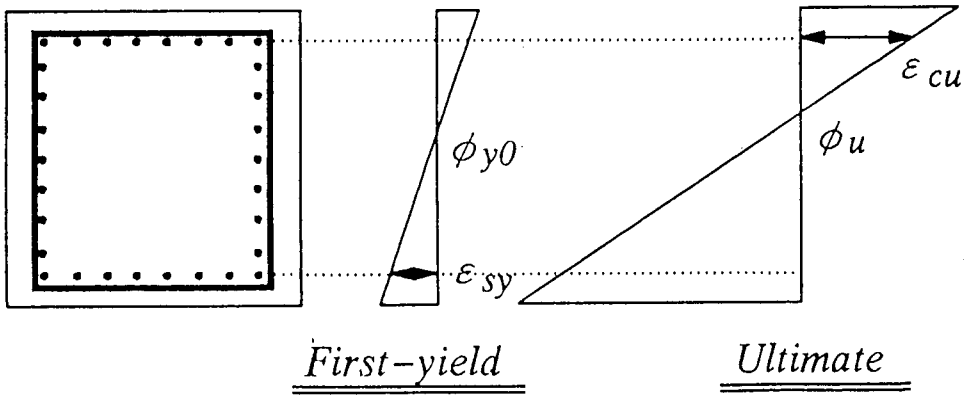

Fig.7 Strain Distributions at First-yield and Ultimate Conditions

written as

$$\delta_{yo} = \frac{H^2}{6}\{(\phi_c + 2\phi_{yo}) - (\phi_{yo} - \phi_c)\frac{M_c}{M_{yo}} - \phi_{yo}\frac{M_c^2}{M_{yo}^2}\} \quad (4)$$

where, M_c and ϕ_c are cracking moment and cracking curvature, respectively. The yield displacement is calculated by substituting Eq. (4) to Eq. (2).
The ultimate displacement is given by the yield curvature of section and the yield displacement defined in Eqs. (1) and (2), and described by

$$\delta_u = \delta_y + (\phi_u - \phi_y) L_p (H - L_p / 2) \quad (5)$$

where, L_p is an equivalent plastic hinge length.

ANALYSIS FOR SPECIMENS AND COMPARISON WITH TEST RESULTS

Curvature Distributions and Equivalent Plastic Hinge Length

Fig. 8 shows measured plastic curvature distributions at the determined ultimate displacements which are 6.5 δ_{yo} for P-1, 6 δ_{yo} for P-2, and 5 δ_{yo} for P-3. The plastic curvature is calculated by subtracting the yield curvature given in Eq. (1) from measured ultimate curvature. Note that the curvature developed at section from base to 40mm height is assumed to be caused by yield penetration of longitudinal reinforcing bars to footing, so that no indicator is drawn in the chart, to distinguish the elasto-plastic column deformation from the rotation due to the yield penetration. The plastic curvature was measured through the section from bottom to 440mm column height in any specimens.
Table 1 shows the moment-curvature relations of test specimens calculated by above analytical model. It was supposed in Eq. (3) that the 10-cyclic loading be Type-I Loading and the 1- or 3-cyclic loading be Type-II Loading. An equivalent plastic hinge length was given by the distribution of measured plastic curvature ϕ_{EXP} and the calculated ultimate plastic curvature ϕ_{CAL}, and written as

$$L_p = (\int \phi_{EXP}\, dh) / \phi_{CAL}$$
$$= (\Sigma \phi_{EXP} \triangle h) / \phi_{CAL} \quad (6)$$

where, $\triangle h$ is a gauge length for curvature measurement, and is 80mm in the test. It can be found that the equivalent plastic hinge length was estimated as 300mm to 330mm in test specimens with 600mm cross sectional dimension.

Lateral Strength and Displacement Ductility

The lateral force-displacement relations of specimens were calculated by Eqs. (4) and (5) based on the moment-curvature analysis, and compared with measured hysteresis envelopes as shown in Fig. 9. The measured rotational displacements due to yield penetration of longitudinal reinforcement were included in calculated displacements. The estimated lateral strength is equivalent to the strength when cover concrete initiates to spall-off, which corresponds well to assumption of the analytical model. On the other hand, the calculated

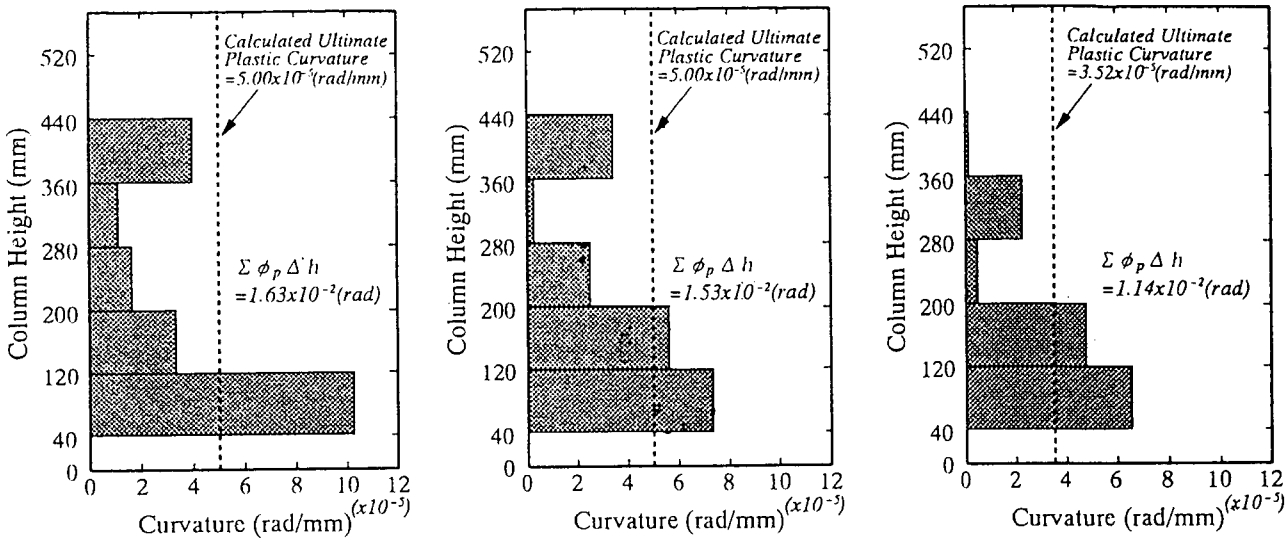

Fig. 8 Plastic Curvature Distributions at Potential Plastic Hinge Region

Table 1 Calculated Moment-Curvature Relation and Equivalent Plastic Hinge Length

Specimen		P-1	P-2	P-3
Loading Type		Type II		Type I
First-yield	Flexural Strength M_{y0} (kJ)	337.8		337.8
	Curvature ϕ_{y0} (rad/mm)	4.44×10^{-6}		4.44×10^{-6}
Yield	Flexural Strength M_y (kJ)	392.3		392.3
	Curvature ϕ_y (rad/mm)	5.16×10^{-6}		5.16×10^{-6}
Ultimate	Flexural Strength M_u (kJ)	392.3		392.3
	Curvature ϕ_u (rad/mm)	5.52×10^{-5}		4.04×10^{-5}
Plastic Curvature ϕ_p (rad/mm)		5.00×10^{-5}		3.52×10^{-5}
$\Sigma \phi_p \Delta h$ (rad)		1.63×10^{-2}	1.53×10^{-2}	1.14×10^{-2}
Equivalent Plastic Hinge Length L_p (mm)		326	306	324

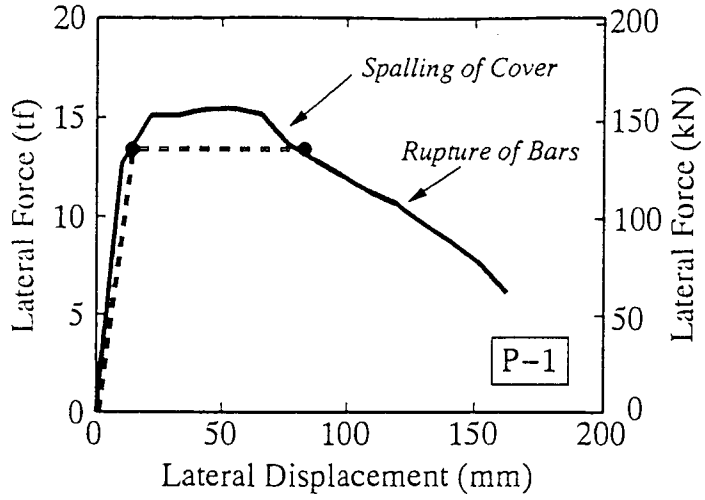

(a) P-1 Specimen

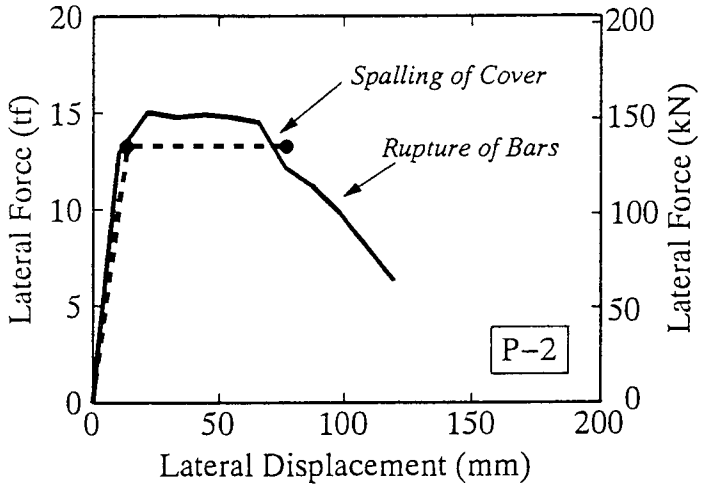

(b) P-2 Specimen

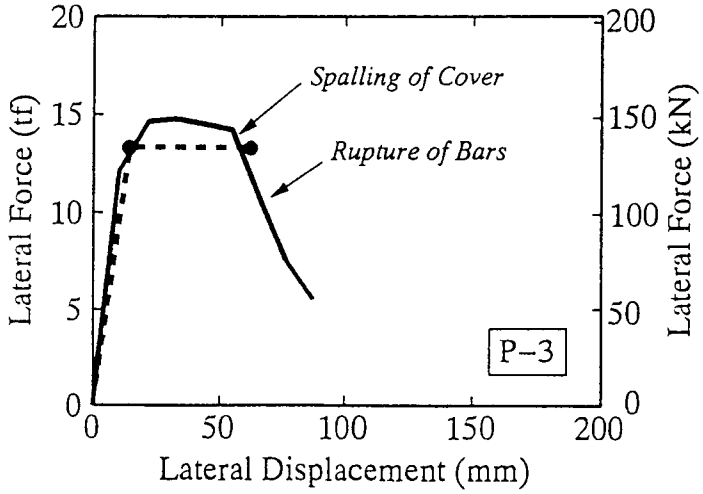

(c) P-3 Specimen

Fig. 9 Observed Envelopes of Lateral Force-Displacement Relation and Calculated Skeleton Curves

ultimate displacements show good agreement with the displacements just after the cover concrete spalls, which is just ultimate condition determined in above section. It can be also found that tentative ultimate strains of confined concrete given in Eq. (3) would be roughly appropriate, because the ultimate displacements are well predicted in both Type-I and II loadings.

CONCLUSIONS

This paper presented the effect of loading hysteresis on ductility of reinforced concrete columns and proposed its evaluation method applicable to seismic design. The identical reinforced concrete columns were loaded with various cyclic number, and test results showed that the controlled displacement history given to top of columns affected the ductility significantly. In case of column with the volumetric ratio of lateral steel bars of 0.3%, it was observed from comparison during the loading step of 5 δ_{yo} that longitudinal reinforcements buckled seriously in P-3 (10-cyclic loading), on the other hand, only horizontal cracks were developed in P-1 (1-cyclic loading). To take account such effect into the ductility evaluation, two ultimate compression strains of confined concrete were determined according to cyclic number, so that two ductility factors would be estimated. At the result of ductility analysis based on moment-curvature relation and the equivalent plastic hinge approach described here, it can be found in any specimens that the calculated ultimate displacement corresponded well to the displacement when cover concrete spalled, and also showed good agreement with the proposed ultimate condition.

ACKNOWLEDGEMENTS

The research presented herein was made under auspices of the Special Sub-Committee for Seismic Countermeasures for Highway Bridges, Japan Road Association (Chair: Prof. K. Kawashima, Tokyo Institute of Technology). The authors extend their sincere appreciation to the strong support of the Special Sub-Committee.

REFERENCES

1) Kawashima, K. and Koyama, T. : Effect of Number of Loading Cycles on Dynamic Characteristics of Reinforced Concrete Bridge Pier Columns, Proceedings of JSCE, No.392/I-9, pp.205-213, 1988.4
2) Hoshikuma, J., Kawashima, K. and Nagaya, K. : A Model of Confinement Effect on Stress- strain Relation of Reinforced Concrete Columns for Seismic Design, 11th WCEE, 1996.6
3) M.J.N. Priestley, F. Seible, G.M. Calvi : Seismic Design and Retrofit of Bridges, Wiley-Interscience, 1996

COMBINED FLEXURAL AND SHEAR EFFECTS ON BRIDGE PIERS

G. Mancini A. Recupero

Department of Structural Engineering, Polytechnic of Turin

10129 Turin (TO), Italy

ABSTRACT

In seismic areas the combination of normal force (N), bending moment (M) and high shear (V) on bridge piers requires the development of design models able to take into account the combined effect of several internal actions. An operational tool to analyse this interaction effect is the stress fields theory application, in agreement with the static theorem of plasticity theory. It may be demonstrated that axial action can have both a favourable or an unfavourable effect on shear ultimate bearing capacity and, consequently, a design method is proposed, for piers subjected to M, N, V combination.

1. INTRODUCTION

In piers of bridges located in seismic areas the interaction between bending moment (M), axial force (N) and shear (V) plays a significant role in the definition of safety conditions. Therefore separate verifications for M, N and V are not enough in the design process and a combined physical model should be used. The M, N, V interaction has been experimentally analysed by several authors[1], [2], [3], [4], [5], [6], [7], [8], [9] who proposed design approaches strictly inspired by the experimental evidence and particularly by the ultimate behaviour.

Analytical empirical and semiempirical models have also been proposed for ultimate design in the presence of high shear combined with M, N [10],[11]. A comparative interpretation of experimental results and proposed models, as described in [12], [13], however, showed that no satisfactory model for the M, N, V, interaction has yet been developed. More recently two further physical models have been presented [14], [15], the first of which was inspired by the interaction model proposed in Model Code 90 [16].

In the paper a new physical model is proposed, based on the stress fields in concrete theory application, as observed in the recent trend to consider interaction effects of internal combined actions in concrete [17], [18], [19], [20], [21]; for the time being this model is able to account only for monotonic actions, but its extension to cyclic actions should be easily reached by the introduction of a graduated limitation of stress field orientation, in relation to the deterioration of materials.

2. MODEL FOR M, N, V, INTERACTION

As mentioned in the introduction, the model proposed for the M, N, V interaction is based on the stress fields approach; consequently the following assumptions should be made:

- the ultimate limit state is reached with a resisting multiple truss in which tensile forces are concentrated in longitudinal and transverse reinforcement, and compressive forces in compressed chord and web stress field in concrete;
- longitudinal and transverse reinforcement may be assumed as uniformly distributed in concrete and are subjected only to axial forces;
- web concrete is subjected to a uniaxial compression stress field, inclined at a θ angle on the longitudinal element direction;
- dowel and interlock effects are included in the deviation between θ and first cracking angle.

With these assumptions, the following non-dimensional parameters may be introduced (fig. 1), as mechanical ratios for transverse and longitudinal reinforcement.

$$\omega_w = \frac{A_{sw} \cdot f_{ywd}}{b_w \cdot s \cdot \sin\alpha \cdot f_{cd2}} \qquad \omega_\ell = \frac{A_{s\ell} \cdot f_{y\ell d}}{b_w \cdot z \cdot f_{cd2}}$$

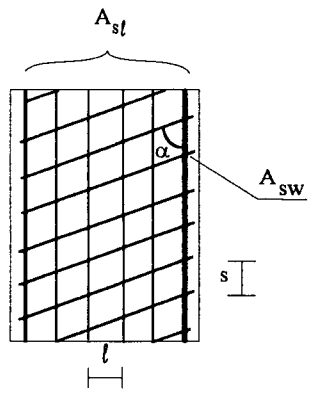

Fig. 1 - Transverse and longitudinal pier reinforcement

where:

- f_{ywd}, $f_{y\ell d}$ stand for the transverse and longitudinal design yield strength;
- f_{cd2} is the concrete strength in presence of shear.

Considering a segment of pier having length x, subjected to actions applied to the extreme sections and transversely uniformly distributed, we may impose the following equilibrium conditions (fig. 2):

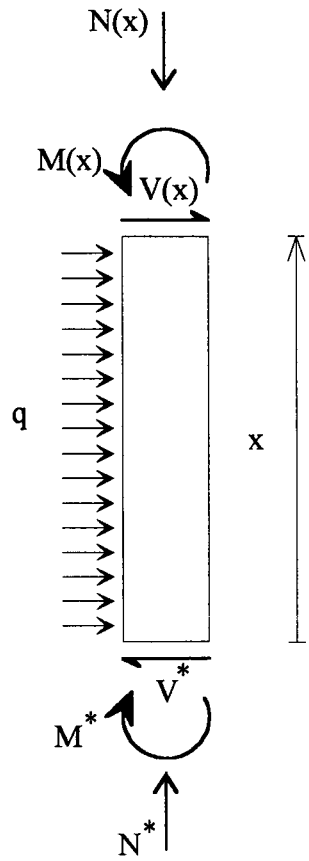

Fig. 2 - Pier segment and related actions

$$M(x) = M^* + V^* \cdot x - \frac{q \cdot x^2}{2} \tag{1}$$

$$V(x) = V^* - q \cdot x \tag{2}$$

$$N(x) = N^* \tag{3}$$

Let us now consider a segment of pier defined by a section orthogonal to its axis and another section parallel to stress field inclination θ on the longitudinal axis (fig. 3).

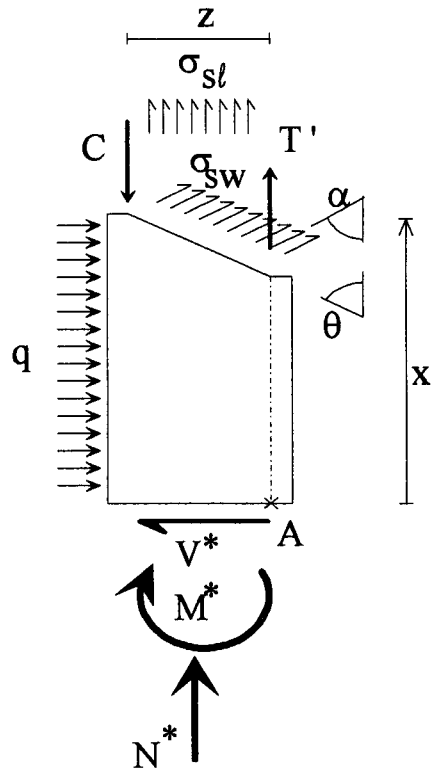

Fig. 3 - Segment with a section parallel to the stress field inclination θ.

Imposing the equilibrium in the longitudinal direction we obtain:

$$T'+N^* + \left(\frac{\sigma_{s\ell}}{f_{yld}}\right)\cdot\omega_\ell\cdot f_{cd2}\cdot z\cdot b_w + \left(\frac{\sigma_{sw}}{f_{ywd}}\right)\cdot\omega_w\cdot f_{cd2}\cdot z\cdot b_w\cdot(\mathrm{ctg}\theta+\mathrm{ctg}\alpha)\cdot\sin\alpha\cdot\cos\alpha - C = 0 \tag{4}$$

where:

- T' is the force in the tensed chord;
- C is the force in the compressed chord;
- $\sigma_{s\ell}$, σ_{sw} are the stresses in the longitudinal and transverse reinforcement respectively;
- z is the internal lever arm;
- b_w is the web width
- α is the angle of inclination of transverse reinforcement on the longitudinal axis ($45° \le \alpha \le 90°$);

By the equilibrium in the transverse direction we get:

$$V^* - q \cdot x - \left(\frac{\sigma_{sw}}{f_{ywd}}\right) \cdot \omega_w \cdot f_{cd2} \cdot z \cdot b_w \cdot (\mathrm{ctg}\theta + \mathrm{ctg}\alpha) \cdot \sin^2\alpha = 0 \tag{5}$$

And by the equilibrium to rotation around point A:

$$M^* + \frac{q \cdot x^2}{2} + \left(\frac{\sigma_{sw}}{f_{ywd}}\right) \cdot \omega_w \cdot f_{cd2} \cdot z \cdot b_w \cdot (\mathrm{ctg}\theta + \mathrm{ctg}\alpha) \cdot \sin^2\alpha \cdot \left(x - \frac{z \cdot \mathrm{ctg}\theta}{2}\right) +$$

$$+N^* \cdot \frac{z}{2} + \left(\frac{\sigma_{s\ell}}{f_{yld}}\right) \cdot \omega_\ell \cdot f_{cd2} \cdot z \cdot b_w \cdot \frac{z}{2} +$$

$$+\left(\frac{\sigma_{sw}}{f_{ywd}}\right) \cdot \omega_w \cdot f_{cd2} \cdot z \cdot b_w \cdot (\mathrm{ctg}\theta + \mathrm{ctg}\alpha) \cdot \sin\alpha \cdot \cos\alpha \cdot \frac{z}{2} - C \cdot z = 0 \tag{6}$$

Substituting now eq. (2) into eq. (5) we find:

$$V(x) = \left(\frac{\sigma_{sw}}{f_{ywd}}\right) \cdot \omega_w \cdot f_{cd2} \cdot z \cdot b_w \cdot (\mathrm{ctg}\theta + \mathrm{ctg}\alpha) \cdot \sin^2\alpha \tag{7}$$

and introducing eq. (7) into eq. (6):

$$M^* + \frac{q \cdot x^2}{2} + V^* \cdot x - q \cdot x^2 + \left(\frac{\sigma_{s\ell}}{f_{yld}}\right) \cdot \omega_\ell \cdot f_{cd2} \cdot z \cdot b_w \cdot \frac{z}{2} +$$

$$+N^* \cdot \frac{z}{2} - C \cdot z = V(x) \cdot \frac{z}{2} \cdot (\mathrm{ctg}\theta - \mathrm{ctg}\alpha) \tag{8}$$

Substituting now eq. (1) into eq. (8):

$$M(x) + \left[\left(\frac{\sigma_{s\ell}}{f_{yld}}\right) \cdot \omega_\ell \cdot f_{cd2} \cdot z \cdot b_w + N(x)\right] \cdot \frac{z}{2} - C \cdot z = V(x) \cdot \frac{z}{2} \cdot (\mathrm{ctg}\theta - \mathrm{ctg}\alpha) \tag{9}$$

The entire axial force in the pier may be now divided between chords and web: $N(x) = N_c(x) + N_w(x)$. Then eq.(9) may be transformed into:

$$M(x) + \left[\left(\frac{\sigma_{s\ell}}{f_{yld}}\right) \cdot \omega_\ell \cdot f_{cd2} \cdot z \cdot b_w + N_c(x) + N_w(x)\right] \cdot \frac{z}{2} +$$

$$-C \cdot z = V(x) \cdot \frac{z}{2} \cdot (\mathrm{ctg}\theta - \mathrm{ctg}\alpha) \tag{10}$$

and substituting the force in the compressed chord with its expression $\left(C = \frac{M(x)}{z} + \frac{N_c(x)}{2}\right)$, we obtains:

$$\left[\left(\frac{\sigma_{s\ell}}{f_{yld}}\right)\cdot\omega_\ell\cdot f_{cd2}\cdot z\cdot b_w + N_w(x)\right]\cdot\frac{z}{2} = V(x)\cdot\frac{z}{2}\cdot(\mathrm{ctg}\theta - \mathrm{ctg}\alpha) \tag{11}$$

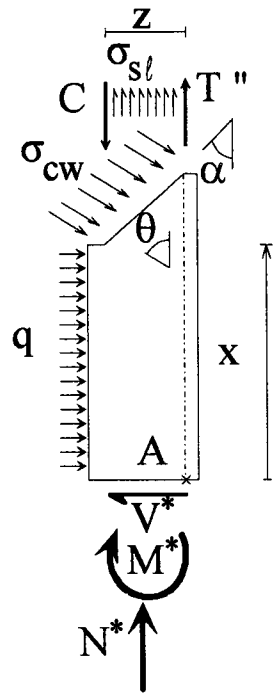

Fig. 4 - Segment with a section parallel to the transverse reinforcement inclination α

Considering now a pier segment defined by a section orthogonal to its axis and another section parallel to the transverse reinforcement inclination α on the longitudinal axis (fig. 4), we may impose the equilibrium in the longitudinal direction:

$$T'' + N^* + \left(\frac{\sigma_{s\ell}}{f_{yld}}\right)\cdot\omega_\ell\cdot f_{cd2}\cdot z\cdot b_w - \sigma_{cw}\cdot z\cdot b_w\cdot(\mathrm{ctg}\theta + \mathrm{ctg}\alpha)\cdot\sin\theta\cdot\cos\theta - C = 0 \tag{12}$$

By the equilibrium in the transverse direction:

$$V^* - q\cdot x - \sigma_{cw}\cdot z\cdot b_w\cdot(\mathrm{ctg}\theta + \mathrm{ctg}\alpha)\cdot\sin^2\theta = 0 \tag{13}$$

and by the equilibrium to the rotation around point A:

$$M^* + \frac{q\cdot x^2}{2} + \sigma_{cw}\cdot z\cdot b_w\cdot(\mathrm{ctg}\theta + \mathrm{ctg}\alpha)\cdot\sin^2\theta\cdot\left(x + \frac{z\cdot\mathrm{ctg}\alpha}{2}\right) +$$

$$+\left(\frac{\sigma_{s\ell}}{f_{yld}}\right)\cdot\omega_{\ell}\cdot f_{cd2}\cdot z\cdot b_w\cdot\frac{z}{2}+N^*\cdot\frac{z}{2}+$$

$$-\sigma_{cw}\cdot z\cdot b_w\cdot(\mathrm{ctg}\theta+\mathrm{ctg}\alpha)\cdot\sin\theta\cdot\cos\theta\cdot\frac{z}{2}-C\cdot z=0 \tag{14}$$

where σ_{cw} is the stress in the web stress field.

Substituting eq. (2) into eq. (13) we obtain:

$$V(x)=\sigma_{cw}\cdot z\cdot b_w\cdot(\mathrm{ctg}\theta+\mathrm{ctg}\alpha)\cdot\sin^2\theta \tag{15}$$

and then introducing eq. (15) into eq. (14) we get:

$$M^*+\frac{q\cdot x^2}{2}+V^*\cdot x-q\cdot x^2+\left(\frac{\sigma_{s\ell}}{f_{yld}}\right)\cdot\omega_{\ell}\cdot f_{cd2}\cdot z\cdot b_w\cdot\frac{z}{2}+$$

$$+N^*\cdot\frac{z}{2}-C\cdot z=V(x)\cdot\frac{z}{2}\cdot(\mathrm{ctg}\theta-\mathrm{ctg}\alpha) \tag{16}$$

which coincides with eq. (8).

From the foregoing equations it is now easy to work out the stresses in longitudinal and transverse reinforcement and in web concrete.

From eq.(7)

$$\sigma_{sw}=f_{ywd}\cdot\frac{V(x)}{\omega_w\cdot b_w\cdot z\cdot f_{cd2}\cdot(\mathrm{ctg}\theta+\mathrm{ctg}\alpha)\cdot\sin^2\alpha} \tag{17}$$

From (11):

$$\sigma_{s\ell}=f_{y\ell d}\cdot\frac{V(x)\cdot(\mathrm{ctg}\theta-\mathrm{ctg}\alpha)-N_w(x)}{\omega_{\ell}\cdot b_w\cdot z\cdot f_{cd2}} \tag{18}$$

From (15):

$$\sigma_{cw}=\frac{V(x)}{b_w\cdot z\cdot(\mathrm{ctg}\theta+\mathrm{ctg}\alpha)\cdot\sin^2\theta} \tag{19}$$

In agreement with the static theorem of theory of plasticity the limit conditions for stresses in different materials should be now introduced:

$$\begin{cases} \sigma_{cw} \le f_{cd2} \\ \sigma_{sw} \le f_{ywd} \\ \sigma_{s\ell} \le f_{y\ell d} \\ \sigma_{s\ell} \ge -f_{yld} \end{cases} \tag{20}$$

in which the last disequation shows that the longitudinal reinforcement may be compressed.

Using positions (20), equations (17), (18), (19) are transformed in the following disequations:

$$V(x) \le b_w \cdot z \cdot f_{cd2} \cdot (\mathrm{ctg}\theta + \mathrm{ctg}\alpha) \cdot \sin^2\theta \tag{21}$$

$$V(x) \le \omega_w \cdot b_w \cdot z \cdot f_{cd2} \cdot (\mathrm{ctg}\theta + \mathrm{ctg}\alpha) \cdot \sin^2\alpha \tag{22}$$

$$V(x) \le \frac{N_w(x) + \omega_\ell \cdot b_w \cdot z \cdot f_{cd2}}{(\mathrm{ctg}\theta - \mathrm{ctg}\alpha)} \tag{23}$$

$$V(x) \ge \frac{N_w(x) - \omega_\ell \cdot b_w \cdot z \cdot f_{cd2}}{(\mathrm{ctg}\theta - \mathrm{ctg}\alpha)} \tag{24}$$

Disequations (21) ÷ (24) may be then presented in non-dimensional form by means of position: $v(x) = \dfrac{V(x)}{b_w \cdot z \cdot f_{cd2}}$ and $n(x) = \dfrac{N_w(x)}{b_w \cdot z \cdot f_{cd2}}$; it turns out:

$$v(x) \le (\mathrm{ctg}\theta + \mathrm{ctg}\alpha) \cdot \sin^2\theta \tag{25}$$

$$v(x) \le \omega_w \cdot (\mathrm{ctg}\theta + \mathrm{ctg}\alpha) \cdot \sin^2\alpha \tag{26}$$

$$v(x) \le \frac{n(x) + \omega_\ell}{(\mathrm{ctg}\theta - \mathrm{ctg}\alpha)} \tag{27}$$

$$v(x) \ge \frac{n(x) - \omega_\ell}{(\mathrm{ctg}\theta - \mathrm{ctg}\alpha)} \tag{28}$$

The solution of the system of disequations (25) ÷(28) may be easily analysed graphically.

3. INTERACTION MODEL WITH $\alpha = 90°$

The solution with $\alpha = 90°$ corresponds to the most frequent case in design practice; disequation (25) ÷(28) transform into:

$$v(x) \leq \cos\theta \cdot \sin\theta \tag{29}$$

$$v(x) \leq \omega_w \cdot \mathrm{ctg}\theta \tag{30}$$

$$\frac{n(x) - \omega_\ell}{\mathrm{ctg}\theta} \leq v(x) \leq \frac{n(x) + \omega_\ell}{\mathrm{ctg}\theta} \tag{31}$$

3.1 No longitudinal shear reinforcement is provided ($\omega_\ell = 0$)

In this case the longitudinal reinforcements is located only in the chords and does not include the reinforcement necessary to the equilibrium of the longitudinal component of the stress field in the web concrete; obviously, the equilibrium condition may be reached only in presence of a compression axial force. Disequations (29) and (30) remain unchanced, but disequation (31) is transformed into equation:

$$v(x) = \frac{n(x)}{\mathrm{ctg}\theta} \tag{32}$$

We consider separately the case in which it is $n(x) > 0.5$ and $n(x) < 0.5$.

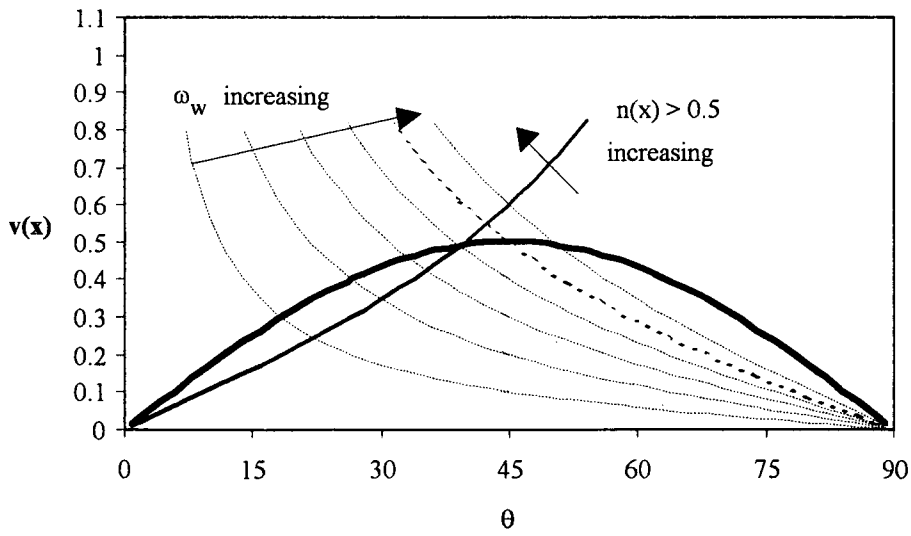

Fig. 5 - Graphic solution of system for n(x) > 0.5

In figure 5 the graphic solution of system for $n(x) > 0.5$ is presented. It may be appreciated that for $n(x) > 0.5$ the axial compression force has an unfavourable effect, because maximum shear capacity $v(x)$ decreases with increasing $n(x)$. In any case the θ angle is determined by equation (32) and equilibrium may be reached only if, for the same θ value, disequations (29) and (30)

are satisfied; that is, the solution of equilibrium corresponds to a point located along function n(x) = constant and identified by the lower of the values obtained from eqs. (29) and (30).

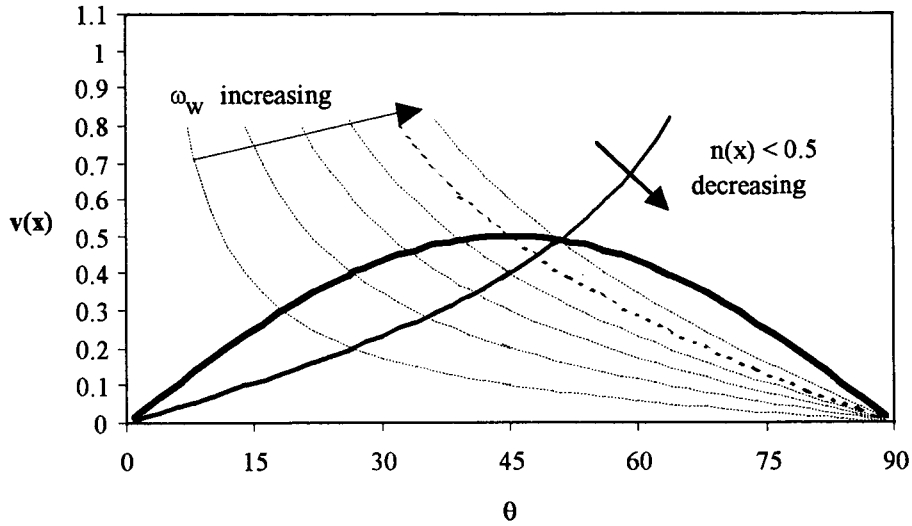

Fig. 6 - Graphic solution of system for n(x) < 0.5

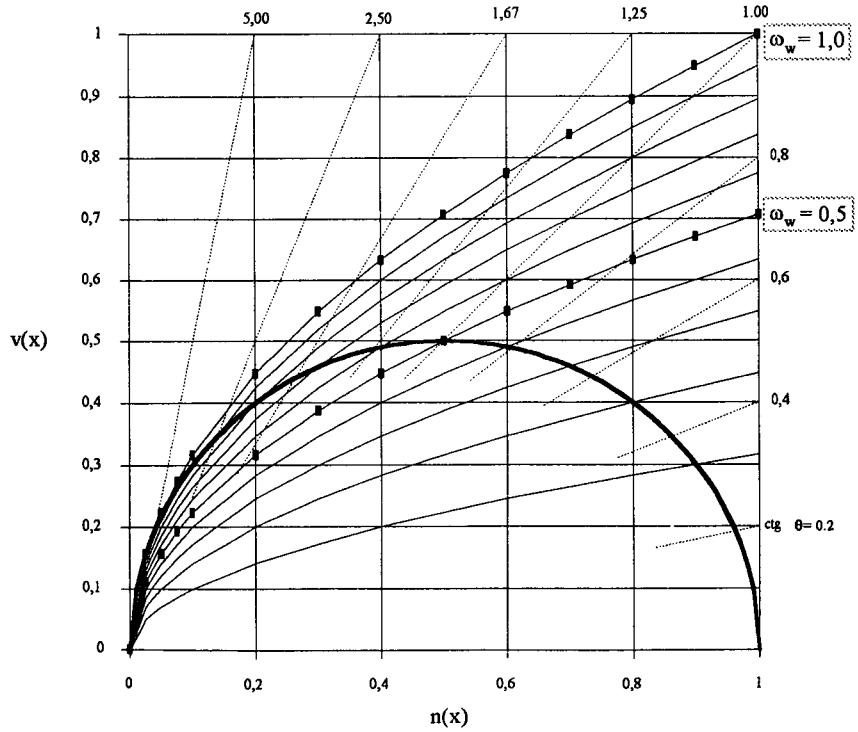

Fig. 7 - Design and verification diagram

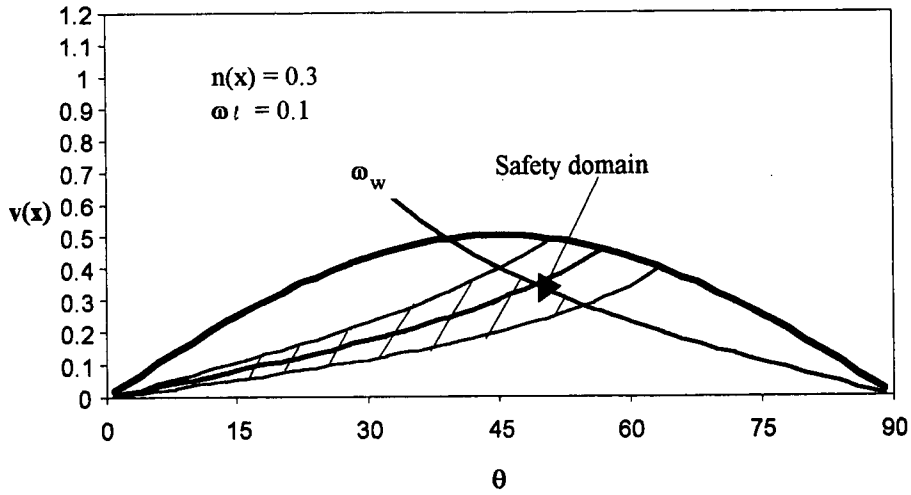

Fig. 8 - Safety domain in case of n(x) < 0.5

Figure 6 presents the case in which n(x) < 0.5; it can be easily appreciated that, in this case, the axial compressive force in the web has a favourable effect, because an increase in axial force corresponds to an increase in maximum shear capacity v(x).

In any case the influence of axial force on shear capacity may be presented in a more comprehensive form by introducing, in equations (29) and (30), $\cos\theta \cdot \sin\theta = \dfrac{\mathrm{tg}\theta}{1+\mathrm{tg}^2\theta}$ and the $\mathrm{ctg}\theta$ value derived from eq.(32) hence:

$$v(x) \le \sqrt{\omega_w \cdot n(x)} \tag{33}$$

$$v(x) \le \sqrt{n(x) \cdot (1 - n(x))} \tag{34}$$

The limiting function of equation (34) represents the analytical equation of a circle; both the disequations (33) and (34) may be plotted on the same diagram (fig. 7), which may be used both in the design and in the verification of piers subjected to a combination of M, N, V internal actions.

In the design process v(x) and n(x) are known and the diagram permits the direct evaluation of ω_w; obviously no equilibrium is possible if the point having co-ordinates v(x), n(x) is located outside the circle region. At the verification stage, ω_w and n(x) are known and the maximum shear capacity corresponds to the higher value of the intersections of n(x) ordinate with the two limiting functions of disequations (33) and (34).

3.2. Longitudinal reinforcement is provided ($\omega_l \neq 0$)

In this case the solution of equilibrium is given by the complete system of disequations (29), (30), (31). Limiting functions (29) and (30) have been described above; in the presence of two limiting functions (31), two different case are possible:

- the upper limit function is monotonically increasing;
- the lower limit function is monotolically increasing for $\omega_\ell \leq n(x)$ and monotonically decreasing for $\omega_\ell > n(x)$.

Figure 8 shows the safety domain plotted for n(x) < 0.5 (n(x) = 0.3); the domain corresponds to the dotted region, having as mean curve the one corresponding to the case of $\omega_\ell = 0$; if the longitudinal reinforcement is increased the safety domain area increases, having as its limit the horizontal axis. Along the vertical axis the limitation is given by the more restrictive condition between eq. (29) (stress field in concrete) and eq. (30) (yelding of transverse reinforcement). In particular in the case shown in figure 8, the limiting condition is given by the ω_w value. In general, it may be easily observed that the presence of longitudinal reinforcement increases the shear capacity and, in case n(x) < 0.5, the upper limiting function make it possible to achieve a greater shear capacity, reaching the equilibrium condition with a smaller θ value.

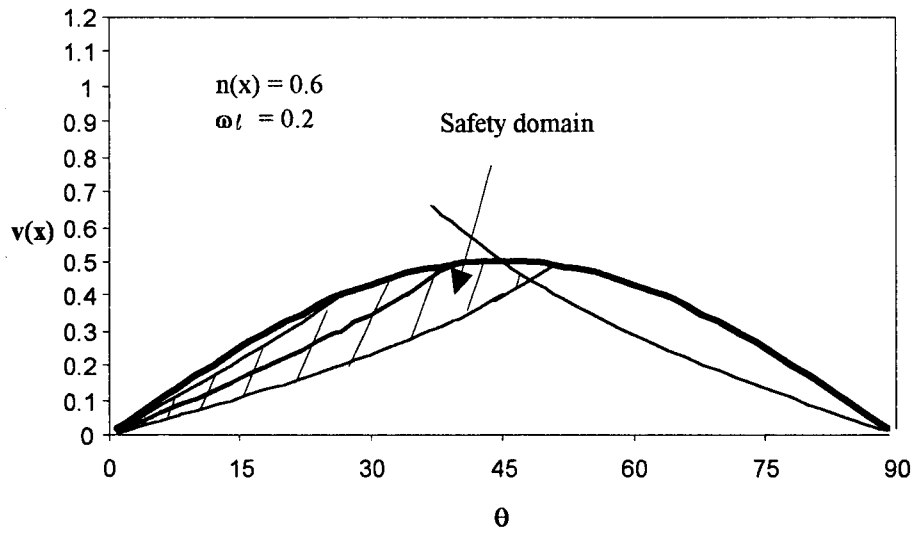

Fig. 9 - Safety domain in case of n(x) > 0.5

Figure 9 shows the case in which n(x) > 0.5 (n(x) = 0.6); even in this case the presence of longitudinal reinforcement in the web leads to an increase in shear capacity; this reinforcement in fact permits the equilibrium of a fraction of the axial force, thereby decreasing the stress level in the web stress field in concrete. The different solution presented above may be generalised in a common diagram (fig. 10) which may be used for both the design and the verification processes; curves relating to the ω_ℓ values are not explicitly plotted because may be derived using the corresponding curves related to the axial force n(x).

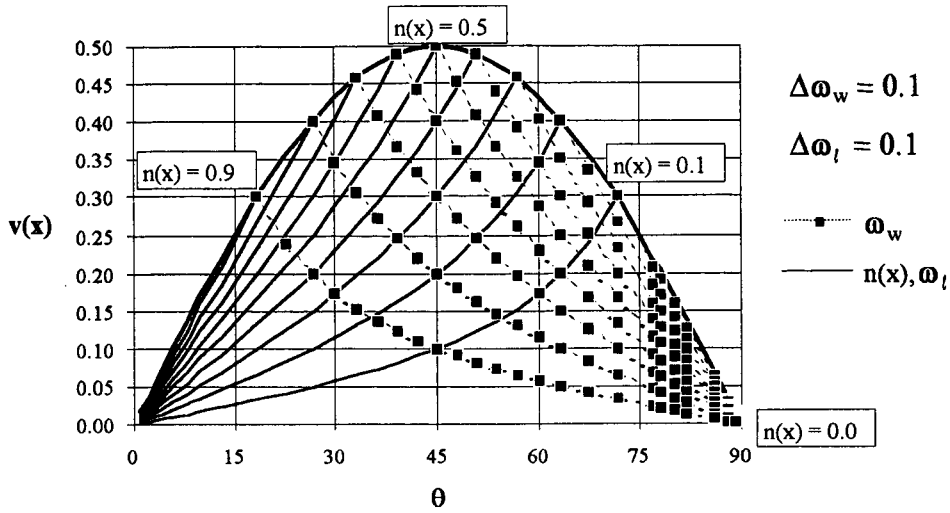

Fig. 10 - Normalised diagram for both design and verification

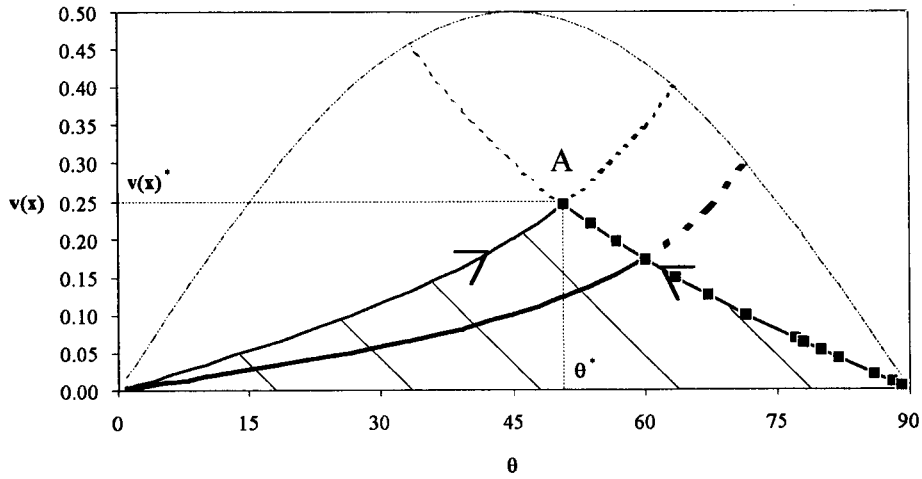

Fig. 11 - Yelding of longitudinal and transverse reinforcement

In case of verification n(x), ω_w and ω_ℓ are known, and the maximum shear capacity may be evaluated, as shown in fig. 11, as the maximum ordinate of the intersection between curve ω_w with one of the limiting functions of the safety domain $n(x) \pm \omega_\ell$; obviously the corresponding point should fall inside the safety domain for concrete strength in the web. In this case the ultimate limit state is reached by yelding of longitudinal and transverse reinforcement.

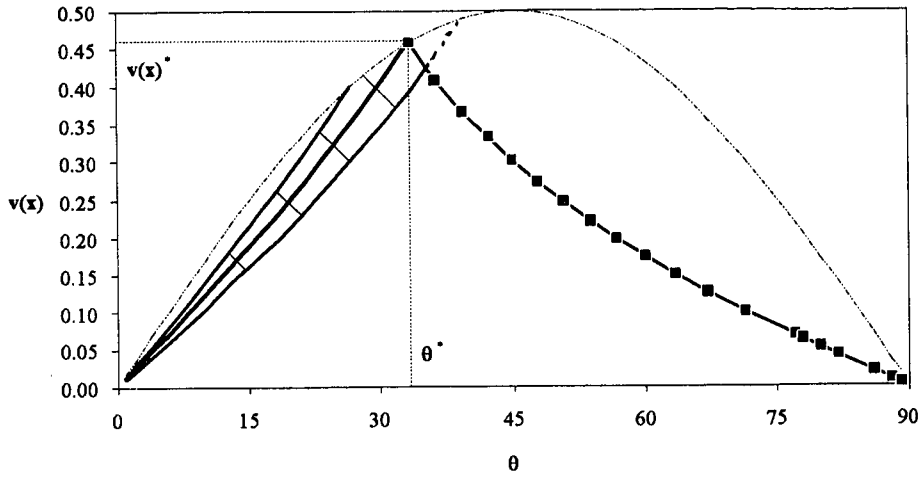

Fig. 12 - Crushing of concrete web and yelding of transverse reinforcement.

Figure 12 illustrates instead a case in which the ultimate limit state is reached by crushing of concrete web and yelding of transverse reinforcement.

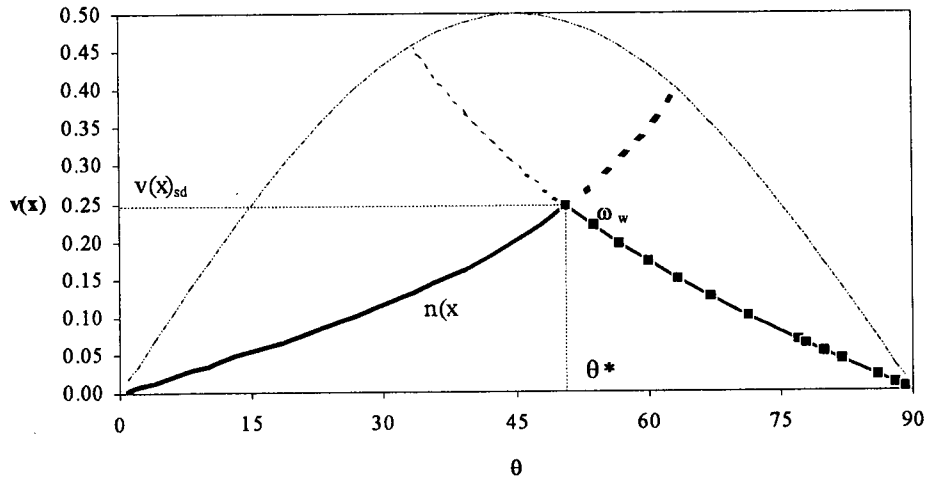

Fig. 13 - Shear design when ω_ℓ in not necessary.

When using the diagram shown in fig. 10 for design purposes, the available strength sources may be optimised. We should distinguish two possible different situations, which may correspond to a given value of v(x):

- the intersection between the abscissa corresponding to v(x) with n(x) curve is located internally to the safety domain for web concrete (eq. (29));
- the intersection between the abscissa corresponding to v(x) with n(x) curve is located outside the safety domain for web concrete.

In the first case, shown in fig. 13, the design may be performed by the identification of the ω_w curve passing through the point above; no longitudinal reinforcement in the web is necessary.

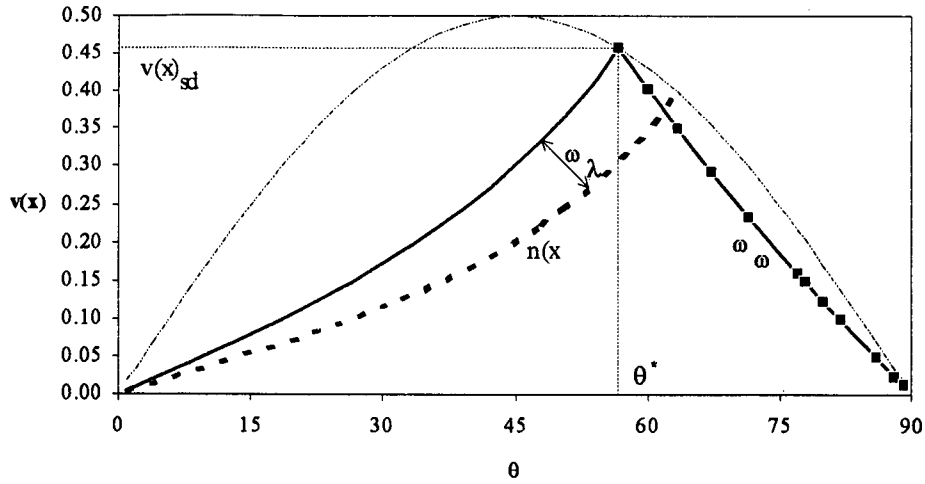

Fig. 14 - Shear design when the axial force value (n(x)) is small.

In the second case, on the contrary, to verify the limit conditions for the web concrete, a longitudinal reinforcement in the web is necessary. When the axial force value is small (fig. 14) an ω_ℓ tensed longitudinal reinforcement is necessary to put the intersection point in the safety domain for concrete; the same point identifies the transverse reinforcement ω_w.

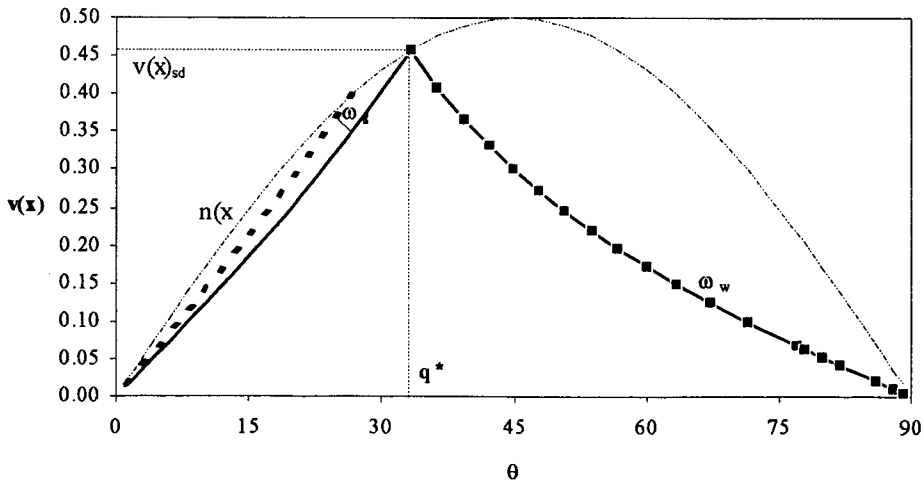

Fig. 15 - Shear design when the axial force value (n(x)) is high.

If the axial force (fig. 15) is high, compressed longitudinal reinforcement should be introduced to position the intersection point on the web concrete limit curve. In both cases the design procedure permits the optimisation of available strength resources, the ultimate limit state being reached by yelding of both reinforcement and by crushing of concrete. It should be underlined that different procedures for reaching of ULS may be chosen in the design; fig. 16

illustrates a case of three different design outputs corresponding to the same v(x) value, in which different ratios between longitudinal and transverse reinforcement may be adopted.

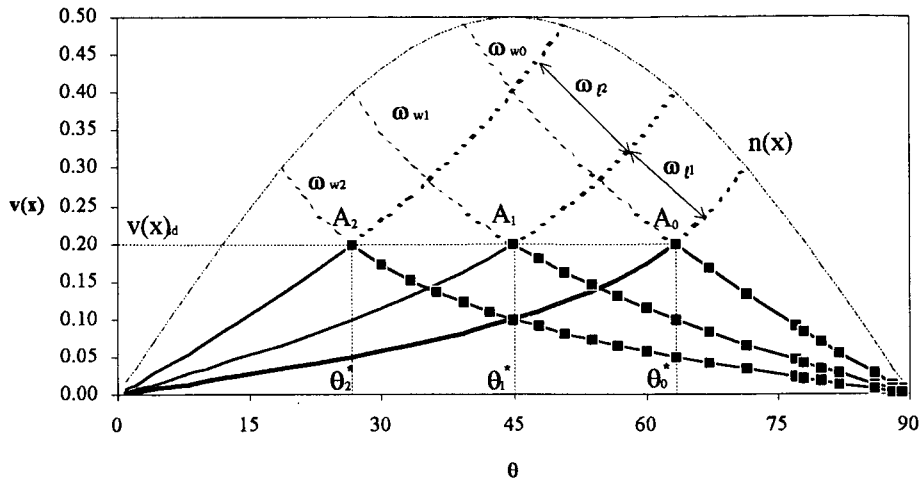

Fig. 16 - Shear design without complete material optimisation

4. DESIGNE EXAMPLE

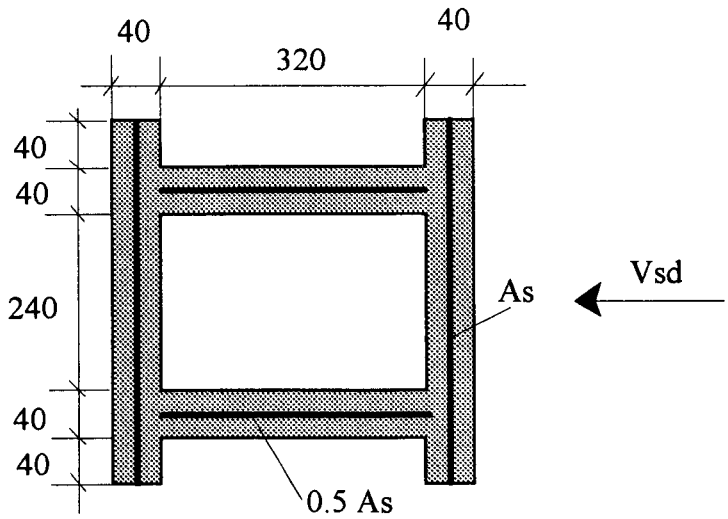

Fig. 17 - Pier transverse section

In the following a design example is presented, related to a boxed pier, having the transverse section drawn in fig. 17. The material mechanical parameters are:

- concrete C30/25, having compression and shear strength respectively f_{cd1} =13.2 MPa and f_{cd2} = 8.9 MPa;

- steel design strength f_{yd} = 374 MPa;

  In table 1 the following parameters are presented:

- N_{sd}: design axial force on the pier;
- σ_m: mean axial stress in the column
- V_{sd}: design shear value;
- M_{sd}: design bending moment value;
- A_s: required reinforcement area in a chord, in relation with the λ value;
- $\lambda = \frac{N_c}{N_{sd}}$: percentage of axial force in the chords;

As shown in table 1 two different chosen λ values (λ = 1.0 and λ = 0.5) have been adopted and, in addition, the λ value corresponding to the minimum required reinforcement area has been calculated.

It can be easily appreciated that the minimum reinforcement corresponds to an optimisation process of shear resources in the web and axial resources in the chord.

N_{sd}	σ_m	V_{sd}	M_{sd}	A_s	λ
kN	MPa	kN	kNm	cmq	[ ]
34560	-6	7200	1.44E+05	965.642	1.0000
34560	-6	7200	1.44E+05	838.503	0.5000
34560	-6	7200	1.44E+05	786.564	0.6124
28800	-5	6048	1.21E+05	717.513	1.0000
28800	-5	6048	1.21E+05	705.882	0.5000
28800	-5	6048	1.21E+05	615.441	0.7349
23040	-4	4896	9.79E+04	469.385	1.0000
23040	-4	4896	9.79E+04	573.262	0.5000
23040	-4	4896	9.79E+04	444.318	0.9186

Tab. 1 Design parameters for different λ values.

5. CONCLUSIONS

In the paper the M, N, V interaction in bridge piers is analysed, by means of a model based on the stress fields theory. Both the favourable and unfavourable effect of axial force on shear have been pointed out and design / verification procedures have been presented.

A numerical example on a bridge pier put in evidence the opportunity to optimise the axial force distribution between webs and chords to minimise the required reinforcement area.

REFERENCES

[1]. M. Yamada, S. Furui (1968) - Shear Resistance and Explosive Cleavage Failure of Reinforced Concrete Members Subjected to Axial Load, Final Report, 8th Congress IABSE, New York, 1968, pp.1091-1102.

[2]. M. Yamada (1974) - Shear Strength Deformation and Explosion of Reinforced Concrete Short RC Columns, ACI SP42, Shear Reinforced Concrete, Detroit, V. 2, 1974, pp.617-638.

[3]. J. O. Jirsa et alt. (1980) - The Influence of Load History on the Shear behaviour of Short RC Columns, Proc. 7th World Conference Earthquake Engineering, Instanbul, 6, 1980.

[4]. R. Shohara, B. Kato (1981) - Ultimate Strength of Reinforced Concrete Members under Combined Loading, IABSE Colloquium on Advanced Mechanics in Reinforced Concrete, Delft, 1981, pp.701-716.

[5]. K. Minami, M. Wakabayashi (1981) - Rational Analysis of Shear in Reinforced Concrete Columns, IABSE Colloquium on Advanced Mechanics in Reinforced Concrete, Delft, 1981, pp.603-614.

[6]. H. Umehara, J.O. Jirsa (1982) - The Shear Strength of Short RC Columns, Proc. of European Conference Earthquake Engineering, Athens, 4, 1982.

[7]. K. Woodward, J. O. Jirsa (1984) - Influence of Reinforcement on RC Short Columns Resistance, Journal of Structural Engineering ASCE, V. 110, 1,1, 1984.

[8]. Y. Tanaka et alt. (1984) - Study on Shear Failure Properties of Reinforced Concrete Short Columns, Proc. 9th World Conference Earthquake Engineering, Tokyo-Kyoto, vol. IV, 1984.

[9]. G. Konig, S. Tang, C. Graham (1993) - Untersuchung zum Nichtlinearen Verhalten von kurzen Stutzen unter Erdbeben-Beanspruchung, Abschlussbericht, Institut fur Bautechnik, Darmstadt, 1993.

[10]. Y. Kaneko, Y. Tanaka (1978) - Shear Failure Mechanism of Reinforced Concrete Short Columns, Proc. 5th Japan Earthquake Engineering Symposium, 1978.

[11]. Y. Kaneko, Y. Tanaka .(1980) - Brittle Failure Criteria of Reinforced Short Columns Caused by Earthquake Loading, Proc. 7th World Conference on Earthquake Engineering, vol. VII, Instanbul, 1980, pp. 565-568.

[12]. C.E.B. (1994) - Bulletin d'Information, No. 220, Behaviour and Analysis of Reinforced Concrete Structures under Alternate Actions Inducing Inelastic Response, v. 2, May 1993, pp.135-177.

[13]. C.E.B. (1996) - Bulletin d'Information, No. 231, RC Frames under Earthquake Loading - State of Art Report, 1996.

[14] . G. Fanti, G. Mancini (1995) -Shear, Normal Force, Bending Moment Interaction in Bridge Piers, Procedings of the First Japan - Italy Workshop on Seismic Design of Bridge, Tsukuba, Japan, 13-14 March 1995.

[15] . M Petrangeli, P. E. Pinto (1995) -A Fiber Model for Elements under Cyclic Bending Shear, Procedings of the First Japan - Italy Workshop on Seismic Design of Bridge, Tsukuba, Japan, 13-14 March 1995.

[16] . C.E.B. - F.I.P. (1993) - Bulletin d'information No.213/214 - Model Code 90, C.E.B., Thomas Jelford Editor.

[17] . F. Bach, M.W. Braestrup, M.P. Nielsen (1978) - Rational Analysis of Shear in Reinforced Concrete Beams, I.A.B.S.E. Proceedings, P 15-78.

[18] . S. Dei Poli, P.G. Gambarova, M. Di Prisco (1990) - Stress Field in Web of Thin-Webbed Beams Failing in Shear,Journal of Structural Division, A.S.C.E. 1990.

[19] . P. Marti, J. Meyboom (1992) - Response of Prestressed Concrete Elements to In-Plane Shear Forces, ACI Structural Journal, Vol. 89, No. 5, September-October 1992, pp. 503,514.

[20] . C.E.B. (1995) - Bulletin d'Information No. 223, Ultimate Limit State Design Models, A State of Art Report, C.E.B., June, 1995.

[21] . G. Mancini, A. Recupero, C.D. Scilipoti (1996) -Taglio nel C.A. in Presenza di armature d'Anima Longitudinali e Trasversali, Studi e Ricerche, Vol. 17, 1996, Milano.

Session 3

Topic 3 Modelling and Analysis (2)

Strength and Ductility Characteristics of Two-Column Bents

Toru Terayama[1], Hisanori Otsuka[2], Kazuhiro Nagaya[3]

1) Senior Research Engineer, Earthquake Engineering Division, Earthquake Disaster Prevention Research Center, Public Works Research Institute, Ministry of Construction, Tsukuba Science City, Ibaraki-ken, Japan, 305

2) Professor, Department of Civil Engineering, Kyushu University, Hakozaki, Higashi-ku, Fukuoka, Japan, 812
(Former, Head of Earthquake Engineering Division, Earthquake Disaster Prevention Research Center, Public Works Research Institute, Ministry of Construction)

3) Research Engineer, Earthquake Engineering Division, Earthquake Disaster Prevention Research Center, Public Works Research Institute, Ministry of Construction, Tsukuba Science City, Ibaraki-ken, Japan, 305

Abstract

This paper describes mainly four topics. The damaged two-column bents during Kobe Earthquake are shown first. Secondly, the history of design codes for the two-column bents for highway bridges in Japan are discussed. Thirdly, the results of the cyclic loading tests of three two-column bents are shown. Lastly, test results are compared with the results of push-over analysis, which is newly introduced in the "Design Specifications for Highway Bridges, 1996".

Introduction

Recently, three large destructive earthquakes have occurred in the United States and Japan. These earthquakes, the Lama Prieta earthquake in 1989, the Northridge earthquake in 1994, and the Kobe earthquake in 1995, have severely damaged a number of highway bridges, and have cost many lives and billions of dollars. In the Kobe earthquake, not only the single-column bents but also the two-column bents are damaged. The major reason of the damage is considered to be insufficient ductility and inadequate shear reinforcement. After 1990, the single-column bents for highway bridges in Japan basically must to be checked by the horizontal dynamic capacity, which is a kind of limited stage design, in the Design Specifications for Highway Bridges Part V. Seismic Design, 1990[1], but two-column bents need not be checked. In other words, the two-column bents had been designed by allowable stress design method until the Kobe earthquake.

In the United States, especially in California, the multi-column bents tends to be integral cap beam/superstructure type rather than bearing supported superstructure type. In order to analyze

these structure, the push-over analysis method has been already developed, such as DRAIN-3D[2]. Taking the fact into the account that some of the two-column bents damaged during the Kobe earthquake and that most of the two-column bents in Japan are bearing supported superstructure type as can be seen in Fig.1, the intensive work has been done in Public Work Research Institute to develop the similar type of analysis method to check the horizontal dynamic capacity for the two-column bents.

In this paper, the damaged multi-column bents during the Kobe earthquake are shown first. Then, the history of design codes for the two-column bents for highway bridges in Japan are discussed. The results of the cyclic loading tests of three two-column bents are shown and the test results are compared with the results of push-over analysis, which is newly introduced in the "Design Specifications for Highway Bridges, 1996"

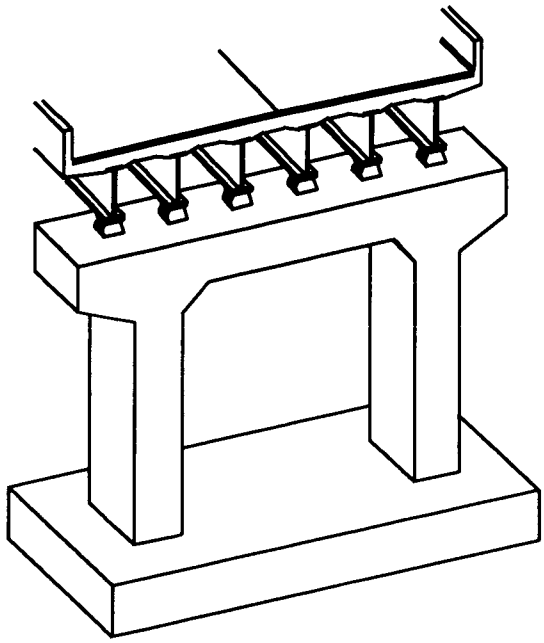

Fig. 1 Typical Multi-Column Bents in Japan

Damages during Kobe Earthquake

Photo 1 and Photo 2 show the damages of two-column bents in the transverse direction caused by the Kobe earthquake. Both are located at Iwaya district where is very close to the area recording an intensity of 7 in the JMA seismic intensity scale. These columns are designed by the Design Specifications for Highway Bridges, 1964[3]. The transverse reinforcement of both columns are D16 with a spacing of 300 mm. The spall-off of cover concrete at the top of the right column can be seen in Photo 1. It is not clear in the photo, but the cover concrete is spalling off at the bottom of the left column and the small cracks are observed at the cap beam. The damages of these parts are mainly caused by the inadequate ductility capacity due to the insufficient

transverse reinforcement. Photo 2 shows the shear failure occurred at the column of another two-column bent. As can be seen, this shear failure is mainly caused by the seismic force of transverse direction. This damage is mainly caused by the insufficient shear reinforcement. It can be said that the sufficient transverse reinforcement and the adequate reinforcement details are needed to design the ductile two-column bents, which is the very same as the single-column bents.

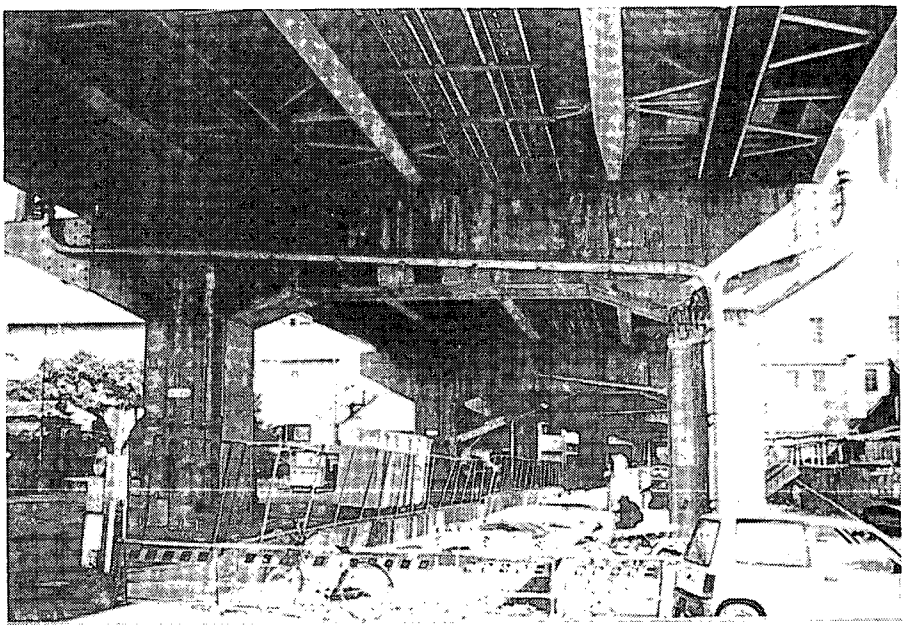

Photo 1 Damages of Two-Column Bents

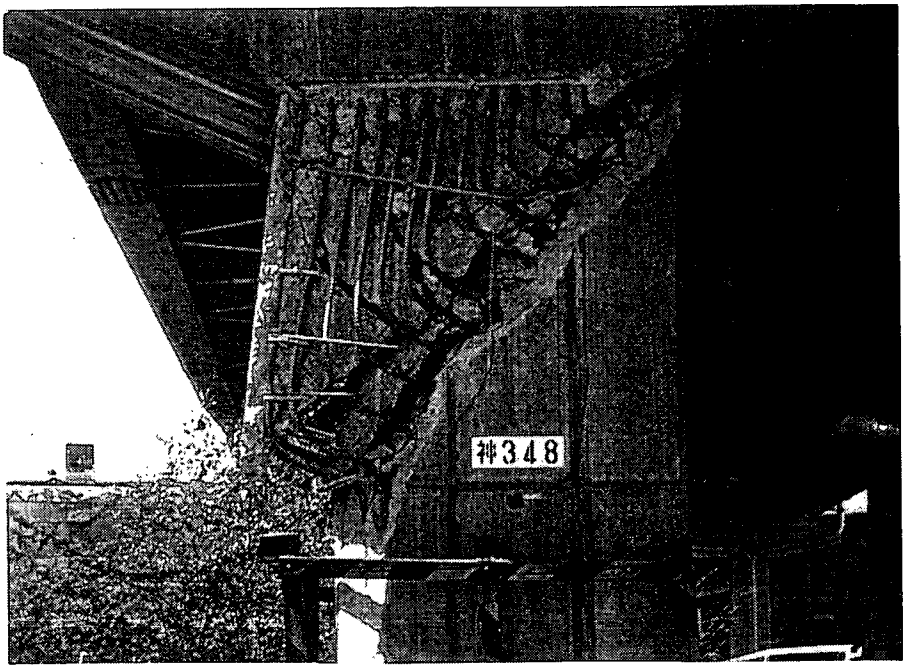

Photo 2 Shear Failure of Two-Column Bents

History of Codes for Two-Column Bents

History of the specifications and the codes for the design of concrete columns in Japan have been already discussed by K. Kawashima, et al. [4][5] Although the checking method of the ductility, namely the check of the horizontal dynamic capacity, was introduced in the specifications of 1990 [1] for the single-column bent, the two-column bent has been designed by the allowable stress design and the seismic coefficient method until the new Design Specification for Highway Brides, 1996 [6] was issued. In the new specifications, the checking method of the horizontal dynamic capacity for the two-column bents was introduced, and using that method, the transverse reinforcement should be arranged adequately preventing from the shear failure or the brittle failure due to the insufficient ductility.

Reinforcement details were specified in the past specifications for highway bridges. In the Design Specifications for Highway Bridges Part IV Substructure, 1980[7], the minimum diameter of transverse reinforcement was specified as 13mm and the spacing should be less than 300mm, less than the twelve times of the diameter of the longitudinal reinforcement and also less than the half of the diameter or the shorter dimension of the column. In the Design Specifications for Highway Bridges Part IV Substructure, 1990[1], the appropriate ratio of the transverse reinforcement was suggested. The ratio of transverse reinforcement should be 0.15% for the column with a longitudinal tensile reinforcement ratio from 0% to 0.5%, 0.2% for the column with a longitudinal tensile reinforcement ratio from 0.5% to 1.0% and 0.25% for the column with a longitudinal tensile reinforcement ratio bigger than 1.0%. The ratio of the transverse reinforcement is calculated by dividing the area of the transverse reinforcement by width of the column and the spacing of the transverse reinforcement. The Design Specifications for Highway Bridges, Part III Concrete Bridges. 1990 [1] specifies the reinforcement details for the frame structure as shown in Fig.2. For the frame structure, the ratio of the transverse reinforcement is specified as 0.2% for the part A and the part B, 0.25% for the part C and 0.15% for the part D.

Cyclic Loading Tests

Test Setup

Cyclic loading tests were carried out to examine the seismic behavior of three kinds of two-column bents. The specimen is set in the horizontal position , as shown in Photo 3. The simulated seismic load was applied using hydraulic actuator acting against the reaction strong wall. To simulate selfweight of superstructure and the column, an additional axial load was applied by means of an axial load apparatus. The axial stress of the simulated deadload was determined as 10kg/cm^2. The test sequence consisted of three cycles of 1δy, 2δy, 3δy and so on in displacement control. The displacement was continued to increase until the test specimen caused the serious damage such as a fracture of the longitudinal reinforcement.

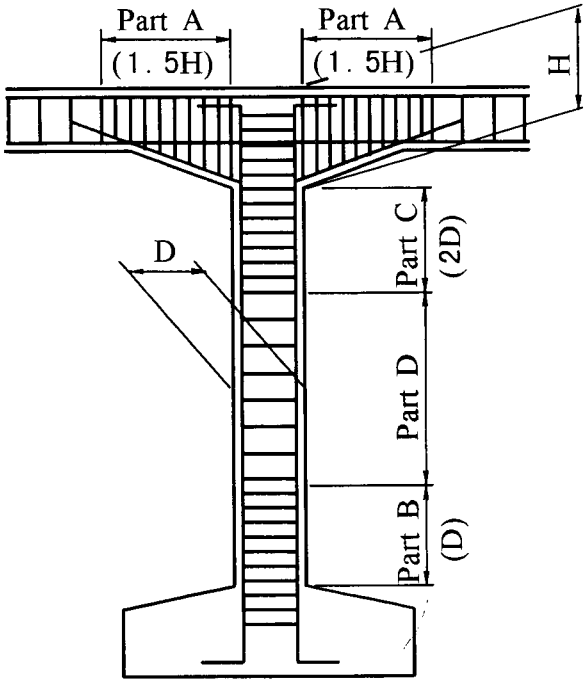

Fig. 2 Reinforcement Details specified in 1990

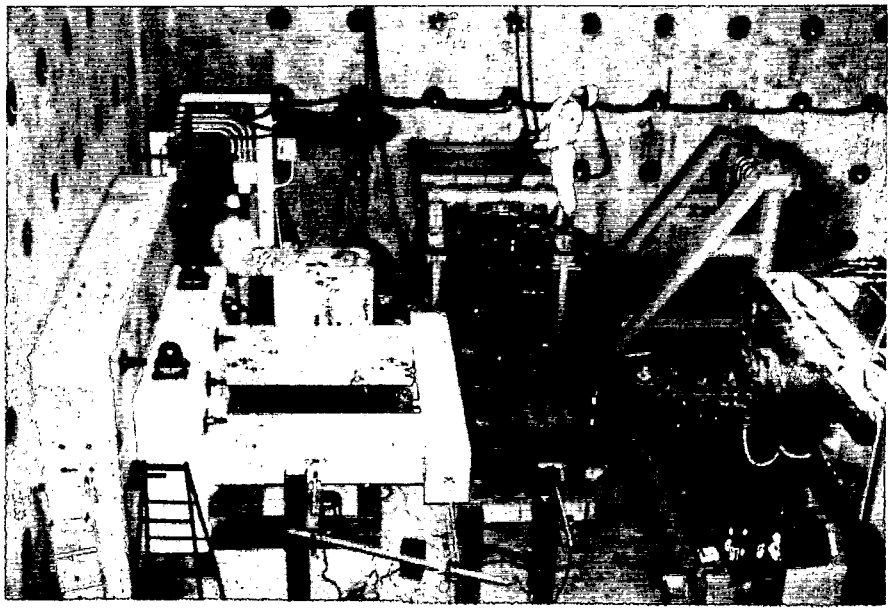

Photo 3 Test Setup

The distance from the bottom of the column to the top of the cap-beam of the specimen No.1 is 1670mm. The column reinforcement of the No.1 specimen, with a rectangular section of 350mm*480mm, consists of 14-D16 bars with a concrete cover of 35mm, resulting in a longitudinal reinforcement ratio of 1.7%. The horizontal confinement is provided by a D6 reinforcement on a 90mm pitch, resulting in a horizontal volumetric ratio of 1.0%. The cap-beam reinforcement of the No.1 specimen with a rectangular section of 370mm*480mm, consists of 18-D13 bars with a concrete cover of 35mm, resulting in a longitudinal reinforcement ratio of 1.3%. The horizontal confinement is provided by a D10 reinforcement on a 60mm pitch, resulting in a horizontal volumetric ratio of 1.2%.

The height and the reinforcement of the column of the No.2 specimen are the same as the No.1 specimen. But the cap-beam reinforcement of the No.2 specimen with a rectangular section of 370mm*480mm, consists of 17-D16 bars with a concrete cover of 35mm, resulting in a longitudinal reinforcement ratio of 1.9%. The horizontal confinement is the same as the No.1 specimen.

The height of the column of the No.3 specimen is determined as 2170mm. The sections and the reinforcement arrangement of the column and the cap-beam is same as the No.2 specimen. Table 1 summarize the sections and the reinforcement details. Reinforcement details are also shown in Fig.3.

Table 1 Test Specimen

	Specimen No.1	Specimen No.2	Specimen No.3
Height	1670mm	1670mm	2170mm
Column Section	350mm*480mm	350mm*480mm	350mm*480mm
Long. Reinforcement of the Column	14-D16	14-D16	14-D16
Trans. Reinforcement of the Column	D6 ctc. 90mm	D6 ctc. 90mm	D6 ctc. 90mm
Cap-Beam Section	370mm*480mm	370mm*480mm	370mm*480mm
Long. Reinforcement of the Cap-Beam	18-D13	17-D16	17-D16
Trans. Reinforcement of the Cap-Beam	D10 ctc. 60mm	D10 ctc. 60mm	D10 ctc. 60mm

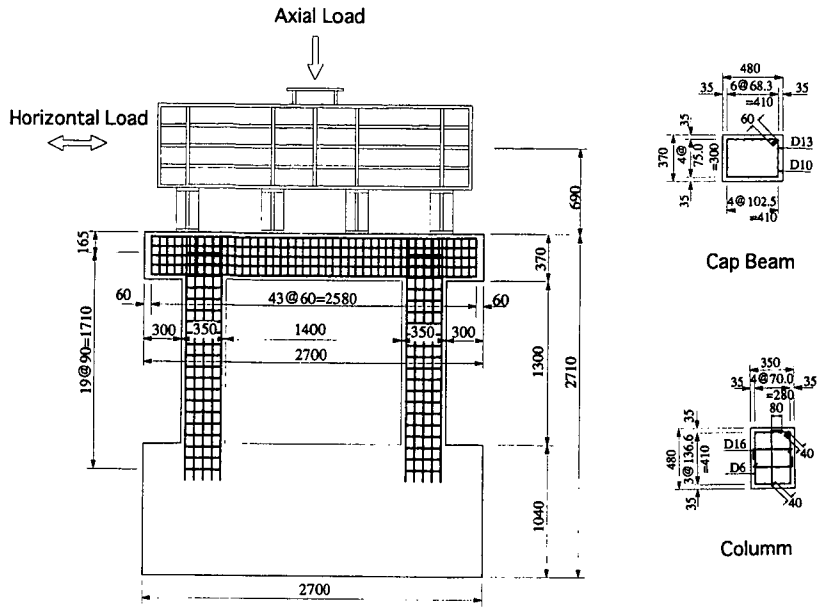

(a) Specimen No.1

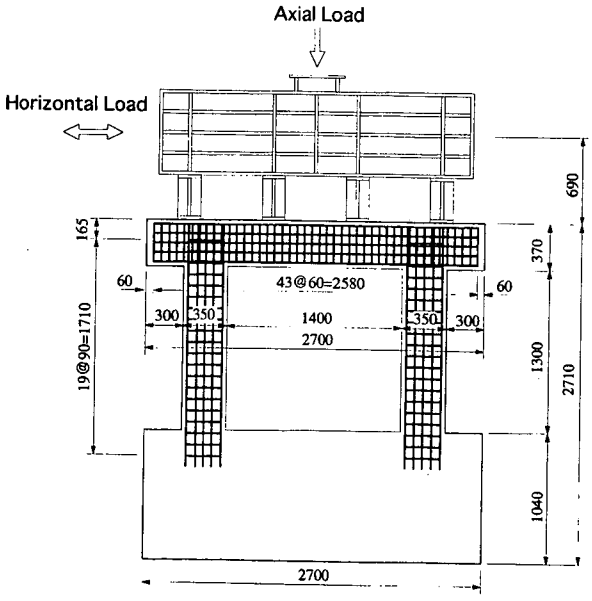

(b) Specimen No.2

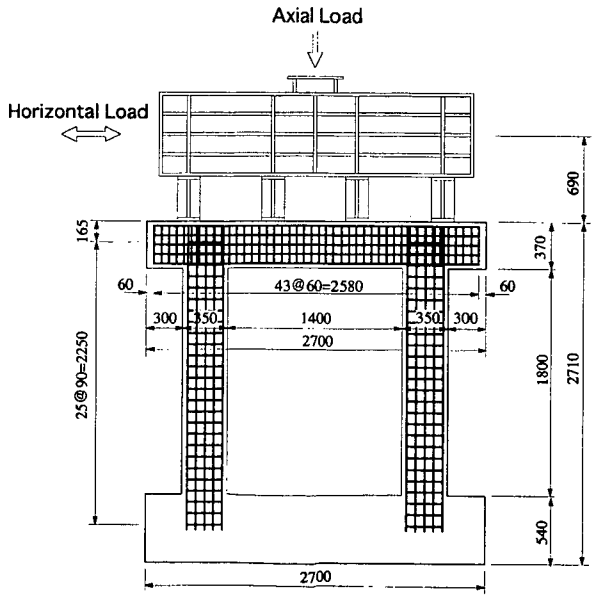

(c) Specimen No.3

Fig. 3 Test Specimen

Test Results

Fig.4 shows the hysteresis loop for the three specimens. Fig.5, Fig.6 and Fig.7 show the crack patterns of each specimen at the stage of the spalling-off of cover concrete and at the stage of the completion of the test, respectively.

Taking a look at the No.1 specimen, the damage was observed in the cap-beam rather than in the column until the displacement of 4 δ y. However, the damage at the bottom of the column developed after the spalling-off of cover concrete after the displacement of 5 δ y. The longitudinal reinforcement fractured at the bottom of the column at the displacement of 11 δ y and the test completed, see Fig.5.

As for the specimen No.2, a spall-off of the cover concrete was noticed at the bottom at the displacement of 4 δ y. After that displacement, the damage was observed at the bottom and the top of the column. The longitudinal reinforcement was fractured at the displacement of 10 δ y and the test was completed, see Fig.6.

With regard to the No.3 specimen, a spall-off of the cover concrete was noticed at the bottom at the displacement of 4 δ y. After that displacement, the damage was observed at the bottom and the top of the column. The longitudinal reinforcement was fractured at the displacement of 13 δ y and the test was completed, see Fig.7.

The damages were observed at the cap-beam and at the bottom of the column in the No.1 specimen, while the damages were seen at the bottom and the top of the column in the No.2 specimen. This differences are considered to be the difference of the longitudinal reinforcement of the cap-beam. The much developed damages were observed at the top of the column of the No.3 specimen compared with the No.2 specimen. The differences are mainly caused by the difference of the column height. The method is needed to evaluate effects of the reinforcement arrangement and the dimension of the two-column bent.

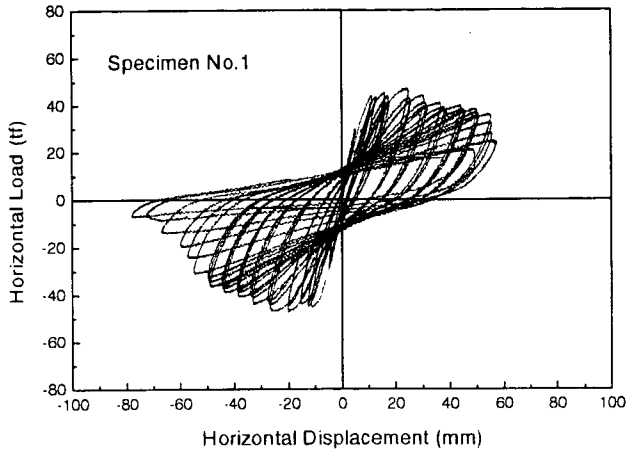

(a) Specimen No.1

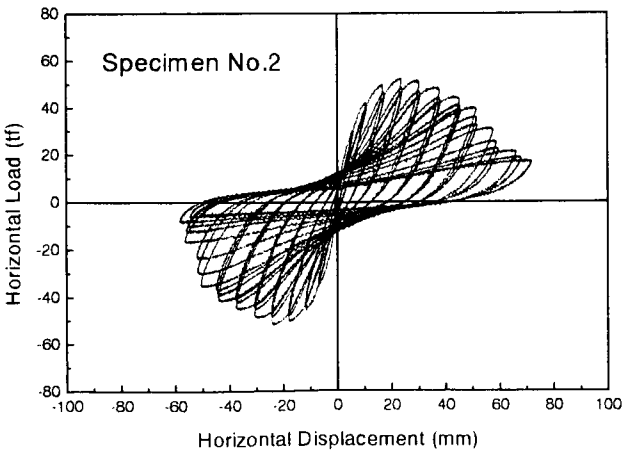

(b) Specimen No.2

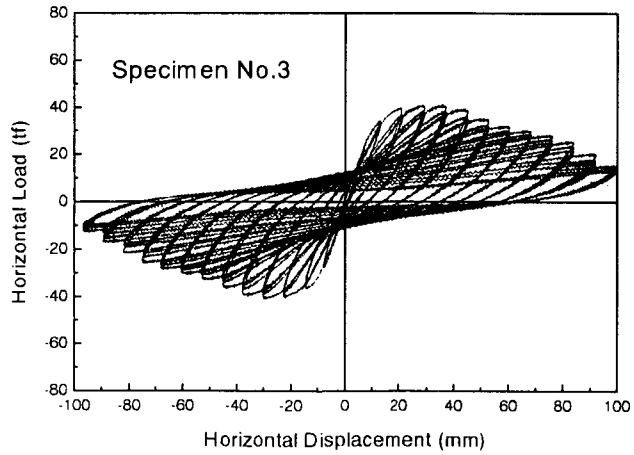

(c) Specimen No.3

Fig. 4 Hysteresis Loop

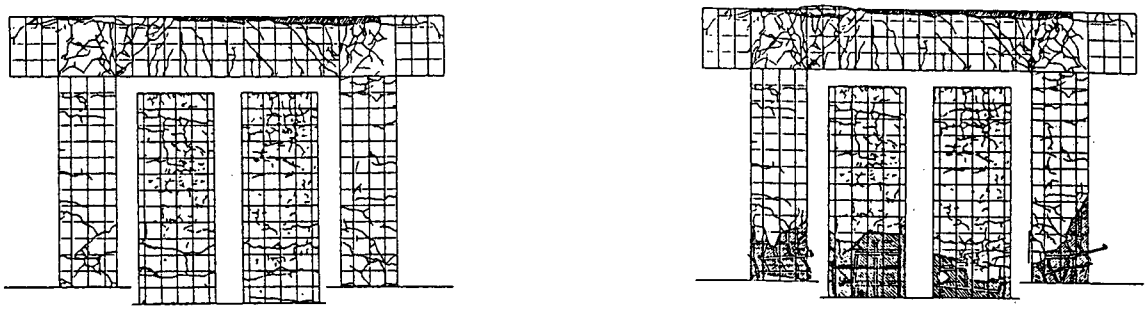

(a) 5 δ y (Spall-off of Cover Concrete) (b) 11 δ y (Completion of Test)

Fig. 5 Crack Patterns of Specimen No.1

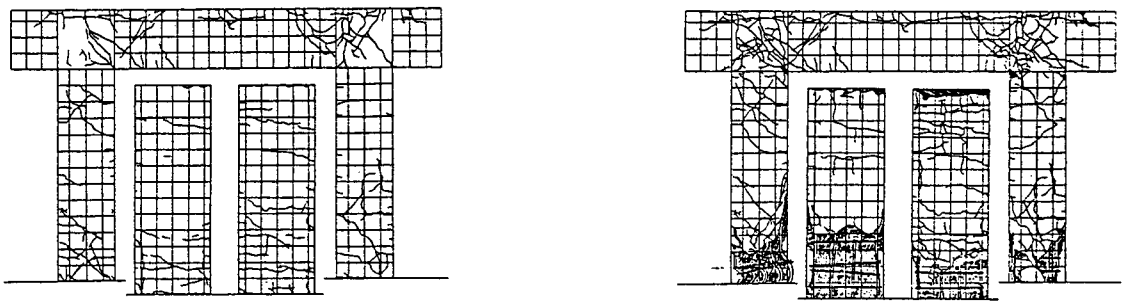

(a) 4 δ y (Spall-off of Cover Concrete) (b) 10 δ y (Completion of Test)

Fig. 6 Crack Patterns of Specimen No.2

(a) 4 δ y (Spall-off of Cover Concrete) (b) 13 δ y (Completion of Test)

Fig. 7 Crack Patterns of Specimen No.3

Analytical Model

To obtain the ultimate flexural strength and the ductility characteristics, the two-column bents are modeled to the frame model with plastic hinges, as can be seen in Fig. 8. Each elastic frame member has the yield stiffness which is based on the axial load by the dead load of the superstructure and the column itself. The plastic hinge is placed at the end part of a cap beam and the top and bottom part of each column. The location of the plastic hinge is a half distance of the plastic hinge length off from the end edge of each member, where plastic hinge length Lp is assumed to be the following equation.

$$Lp = 0.2h - 0.1D \quad and \quad 0.1D \leq Lp \leq 0.5D$$

where h is a half distance of the member and D is the dimension of the column or the cap beam. Fig. 9 shows the moment and curvature diagram, which is based on the stress- strain relationship developed by Hoshikuma et al.[8] Using the model depicted in Fig. 8, the horizontal load is statically increased, which is simulating the inertia force. As the horizontal load increases, the axial load of the column changes. Consequently, the moment-curvature relationship of the column changes, which is considered by N-M interaction curve, see Fig. 10. By increasing the horizontal load statically, the horizontal load-horizontal displacement envelope is obtained, as can be seen in Fig. 11. The ultimate state of each plastic hinge is obtained by the ultimate plastic angle θ pu, which is calculated by the following equation.

$$\theta pu = \left(\frac{\phi u}{\phi y} - 1\right) \times Lp \times \phi y$$

where ϕ u is the ultimate curvature and ϕ y is the yield curvature calculated by the section analysis.

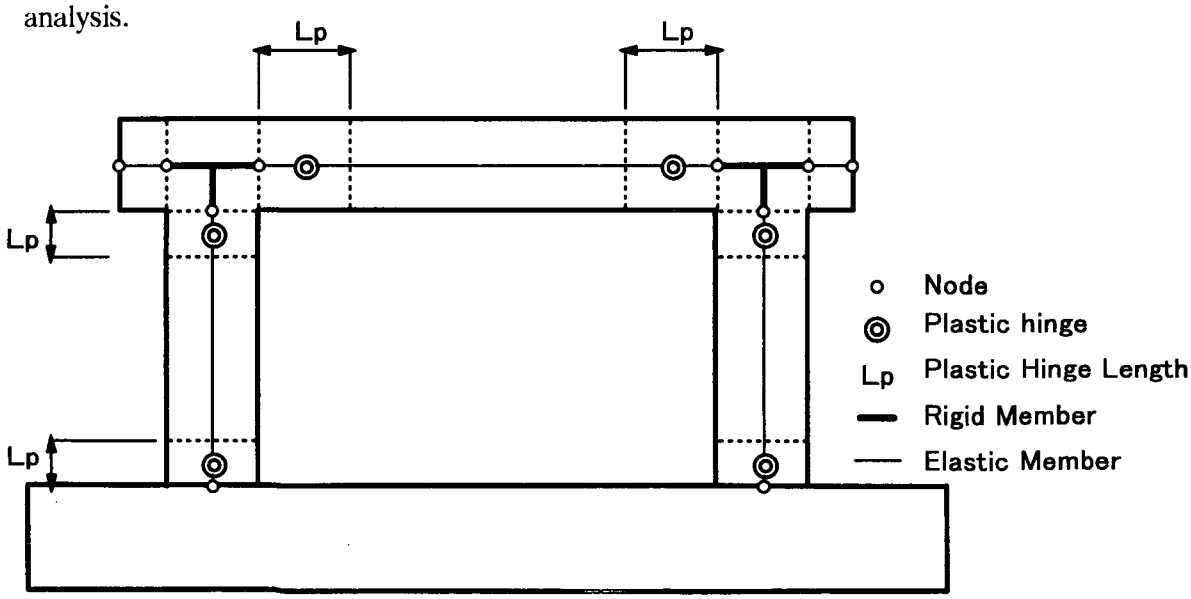

Fig. 8 Model for the Two-Column Bent

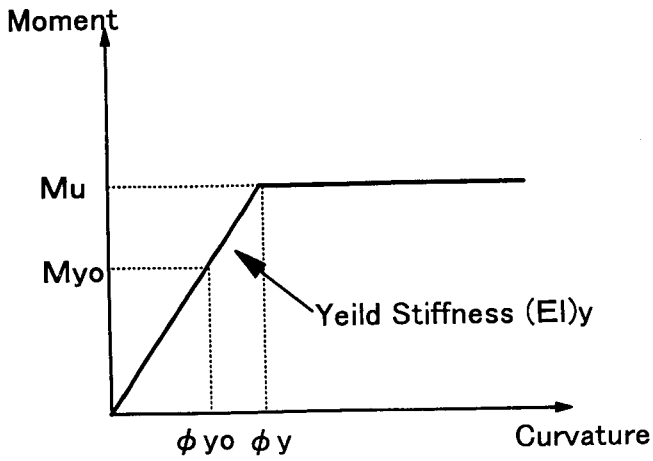

Fig. 9 Moment-Curvature Diagram

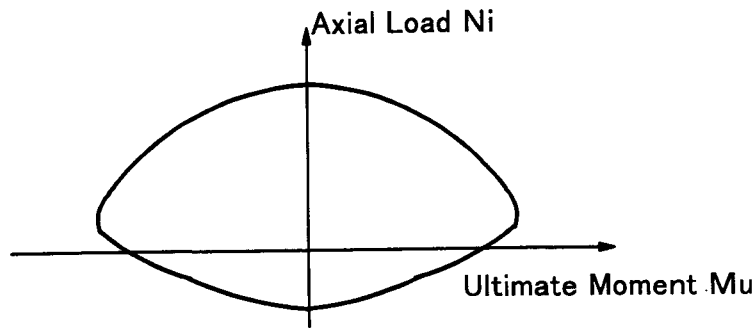

Fig. 10 Axial Load-Moment Interaction

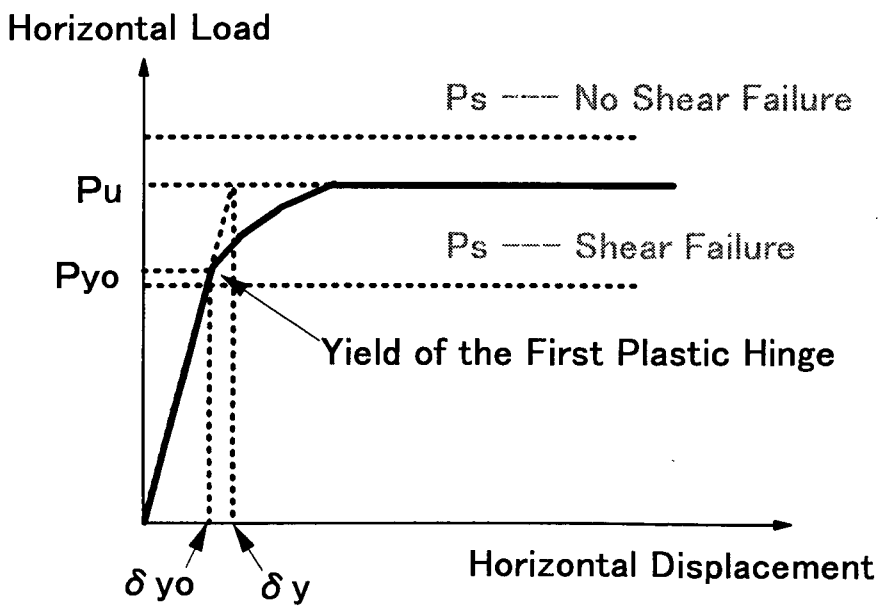

Fig. 11 Horizontal Load-Horizontal Displacement Envelope

Comparison between Test Results and Analysis

The analyses for the test specimen were carried out to verify the above mentioned analysis. Fig.12 shows the comparison between the envelope of horizontal load-horizontal displacement of the test specimen No.3 and the result of the analysis. From the analysis, it can be said that the plastic hinge A, F, B and E will yield at the displacement of around 7mm. F and E are reached to the ultimate stage at the displacement of 30mm, while A and B are reached to the ultimate stage at the displacement of 55mm. To compare the test results with the analytical results, it can be said that the analysis can predict the behavior of the two-column bents pretty well.

But discussion remained that where is the ultimate stage of two-column bents? The ultimate horizontal displacement of 30mm is considered to be too conservative, because the cover concrete just began to spall off at the base of the columns at that displacement. So, with the engineering judgement, the ultimate displacement is taken as the displacement where all plastic hinge reached to the ultimate stage. As a consequence, in Fig. 12, the ultimate horizontal displacement was determined as about 55mm where the plastic hinge B reached to the ultimate stage. This decision is not too bad, because the damage of the cover concrete progressed but the large deformation of the longitudinal reinforcement was not observed at this displacement .

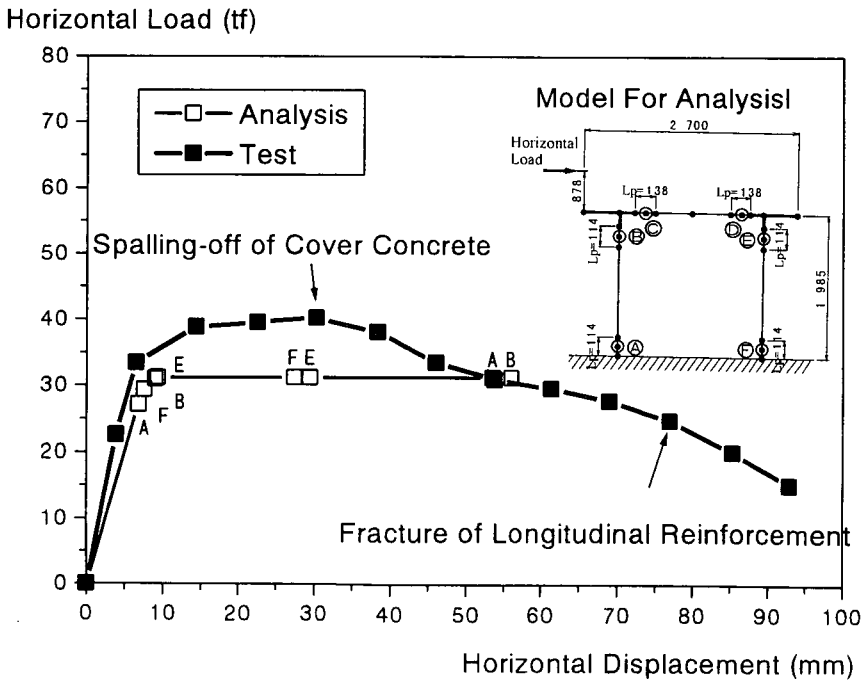

Fig. 12 Comparison between the Test and the Analysis

Concluding Remarks

The purpose of this study was to evaluate the strength and ductility characteristics of the two-column bents in Japan. Based on the field study, experimental observation and preliminary research, the following conclusions were reached.

1. The damages of two-column bents in the transverse direction caused by the Kobe earthquake were observed. Sufficient transverse reinforcement and adequate design details are needed to design the ductile two-column bents.

2. The past seismic design codes for the two-column bents for highway bridges in Japan were reviewed, which are all based on the allowable stress design method. By the lessons learned from the Kobe earthquake, the checking method for the dynamic strength and the ductility are needed for the seismic design of two-column bents.

3. The cyclic loading tests of three specimen were carried out to study the strength and ductility characteristics of the two-column bents. It was found out that the method is needed to evaluate the effects of the reinforcement arrangement and the dimension of the two-column bent.

4. The test results were compared with the results of the analysis. The strength and ductility characteristics of the test results are well predicted by the newly developed push over analysis, which is newly introduced in the "Design Specifications for Highway Bridges, 1996". But discussion remained that where is the ultimate displacement should be taken?

Acknowledgements

Checking method of horizontal dynamic capacity for the two-column bents were developed through the beneficial and fruitful discussions in the "Special Sub-Committee for Seismic Countermeasures for Highway Bridges"chaired by Dr. K. Kawashima.

References

[1] Japan Road Association, Design Specifications for Highway Bridges, Part III Concrete Bridges, Part IV Substructure, Part V Seismic Design, 1990.

[2] V. Prakash, G.H. Powell, S. Campbell, DRAIN-3D, Base Program Description and User Guide, Report No. UCB/SEMM-94/07, University of California, August 1994.

[3] Japan Road Association, Design Specifications for Highway Bridges, 1964.

[4] K. Kawashima, Seismic Design, Seismic Strengthening and Repair of Highway Bridges in Japan, Proceedings of the First U.S.-Japan Workshop on Seismic Retrofit of Bridges, Tsukuba, December 1990.

[5] T. Akimoto, Design Details of Reinforced Concrete Bridges in Japan, Proceedings of the

First U.S.-Japan Workshop on Seismic Retrofit of Bridges, Tsukuba, December 1990.

[6] Japan Road Association, Design Specifications for Highway Bridges, Part V Seismic Design, 1996.

[7] Japan Road Association, Design Specifications for Highway Bridges, Part IV Substructure, 1980.

[8] Hoshikuma, J., Kawashima K., Nagaya K.,"A Stress-Strain Model for Reinforced Concrete Bridge Piers Confined by Hoop Reinforcement," Proceedings of 2nd International Workshop on Seismic Design and Retrofitting of Reinforced Concrete Bridges, 365-385, Edited by R. Park, University of Canterbury, New Zealand, 1994

A NUMERICAL MODEL FOR SHEAR DOMINATED BRIDGE PIERS

J. Guedes[1] and A.V. Pinto[2]

[1] CEEES - National Laboratory for Civil Engineering
Av. do Brasil, 1799, Lisbon, Portugal
(Former Human Capital Mobility Grant-Holder at ELSA)

[2] ELSA Laboratory, Institute for Systems Informatics and Safety
Joint Research Centre, European Commission
21020 Ispra (VA), Italy

ABSTRACT

A model for simulation of squat piers under important transverse forces is presented; a classic fibre model with shear behaviour simulated through the strut-and-tie approach. The model includes an additional fibre working in parallel with the standard longitudinal fibres. The results obtained from numerical are compared with the experimental response of a large-scale bridge pier tested in the ELSA laboratory of the Joint Research Centre (JRC) at Ispra.

1. INTRODUCTION

Earthquakes damage civil engineering structures every year and bridges are no exception. Historically, bridges have proven to be vulnerable to earthquakes, sustaining damage to substructures and foundations and in some cases being totally destroyed as superstructures collapse from their supporting elements. In particular, shear failure due to inadequate detailing and/or poor confinement of core concrete, was observed in several bridge piers emphasizing the importance of shear strength to design; the design should provide sufficient deformation capacity and shear strength to ensure adequate ductile behaviour and to prevent shear failure [1]. It is now generally accepted that the ductile behaviour of a reinforced concrete column can be reached supplying sufficient transverse reinforcement in the plastic hinge regions to provide adequate shear strength and, at the same time, to properly confine the concrete core and prevent premature buckling of the longitudinal reinforcement.

The behaviour of bridge structures subject to important transverse loading is now, more than ever, a matter of great experimental and numerical research interest. The aim of this paper is to describe the non-linear shear model developed at the European Laboratory of Structural Assessment (ELSA) at Ispra, Italy, for bridge piers with low shear span ratio: a strut-and-tie type formulation coupled with the fibre model. The numerical response of a bridge pier using the proposed model is compared with the results from the experimental campaign carried out at the ELSA laboratory.

2. THE FIBRE MODEL

2.1. Standard model

In a fibre model the structure is divided in three-dimensional linear elements which are subdivided in longitudinal fibres defining a mesh in the transverse section. The model described in the paper has been implemented in the computer code CASTEM 2000 [2] in a three-dimensional Timoshenko beam element [3]: plane sections remain plane after being deformed but do not, necessarily, maintain the initial angle with the beam axial axis (see Figure 1).

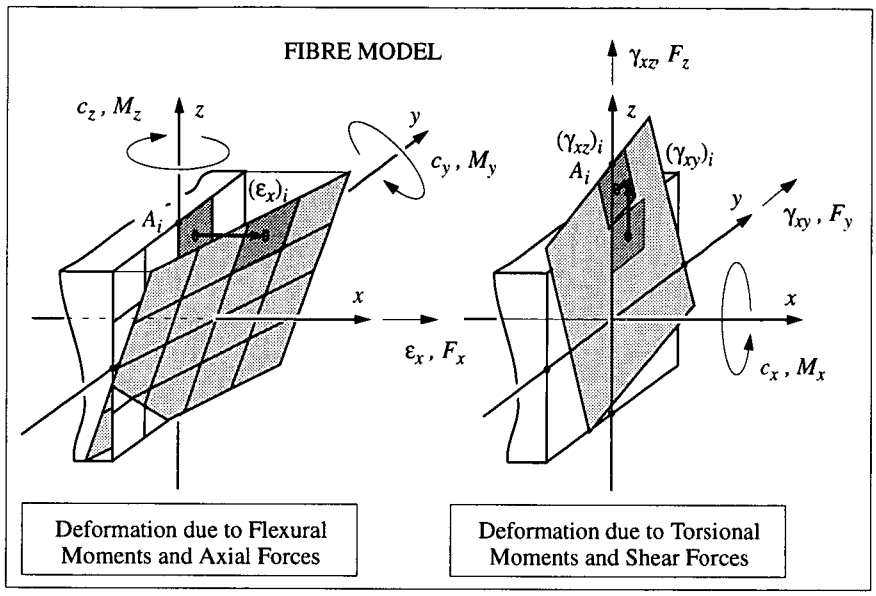

Figure 1. Fibre model: deformation of the transverse section

Thus, as in any three-dimensional (3D) beam model, given a loading history a numerical step-by-step procedure is used to compute the shear and axial strains and the rotations along the three main axis of each Gauss point of each 3D element. Then, making use of the assumptions of the Timoshenko beam element, the program goes deeper in the cross-section and computes the strain at each Gauss point i of each fibre that respects the compatibility of displacements in the transverse section:

$$\begin{aligned} (\varepsilon_x)_i &= \varepsilon_x - y_i c_z + z_i c_y \\ (\gamma_{xy})_i &= \gamma_{xy} - z_i c_x \\ (\gamma_{xz})_i &= \gamma_{xz} + y_i c_x \end{aligned} \tag{1}$$

No warping of the cross-section is considered; a constant unitary function is adopted for the distribution of shear strain in the transverse section. With the strain values and the constitutive laws for the materials, the axial stress σ_i and the shear stresses $(\tau_{xy})_i$ and $(\tau_{xz})_i$ are computed and integrated in the section.

With this element, different interactions between axial and shear forces and bending moments can be considered. The complexity of the model depends on the complexity of the constitutive laws representing the behaviour of the materials. Typically, a fibre model considers axial stress-strain constitutive laws uncoupled with linear elastic shear behaviour laws at each fibre.

2.2. Constitutive laws

2.2.1. Concrete

The model used for the concrete follows a law of Hognestad type with two branches: a hardening branch before the compression peak followed by a softening branch until a residual compression plateau. The model accounts for the confinement effect of transverse steel through a parameter which modifies the strength and post-peak stiffness of the concrete. Tensile stresses are included through a linear model with a post-peak softening behaviour. The equations used in the model and a brief description of the phenomena involved can be found in [3].

For cyclic loading, the model follows empiric based rules. Loading and unloading branches to take into account phenomena like: crack closing, stiffness degradation and tension stiffening, are considered and represented by an exponential equation. Different parameters are prescribed for unloading and reloading cycles. An arbitrary axial stress-strain cyclic history (from point 1 to 11) is illustrated in Figure 2.

2.2.2. Steel constitutive model

The constitutive law used for the cyclic behaviour of the steel bars is the explicit formulation of Menegotto-Pinto [5]. The steel of the longitudinal bars follows first the monotonic curve (elastic branch, plateau and hardening branch) and only when, or if, an important unloading after yielding occurs the hysteretic Menegotto-Pinto model is activated. The model defines a family of transition curves between two asymptotes with slopes E_o and E_h having (ε_o,σ_o) as common point. The shape of the curve depends on the maximum strain ever reached under tensile and compression forces. A stress-strain curve representing a cyclic loading history from point 1 to 4 is illustrated in Figure 2.

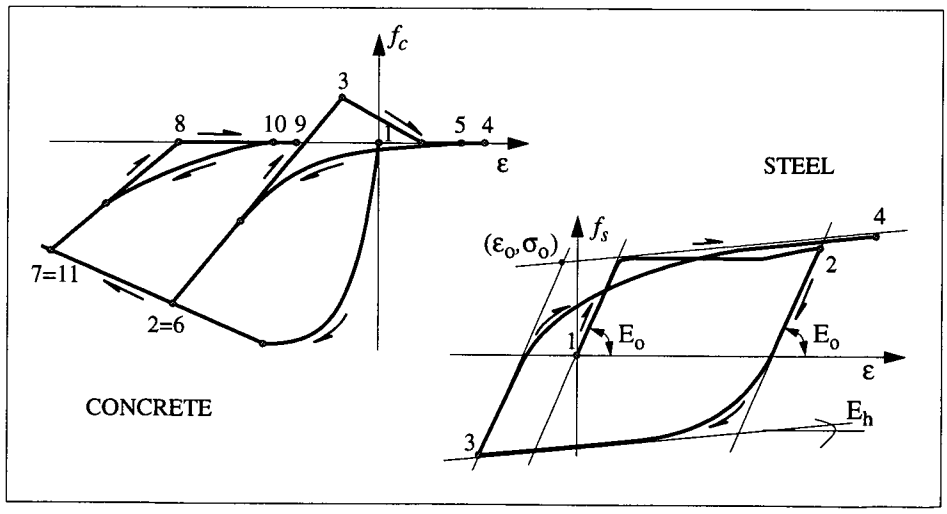

Figure 2. Axial stress-strain constitutive laws: concrete and steel

3. NON-LINEAR SHEAR MODEL

The global behaviour of reinforced concrete piers/columns with low shear span ratio may be strongly influenced by shear forces and this effect must be considered in the response. In fact, the tests on squat reinforced concrete bridge piers carried out at the ELSA Laboratory [7] [8]

confirmed that shear deformation may be as important as the flexural ones. Figure 3 and Figure 4 show some results obtained from those tests. The displacement profiles given in Figure 3 include separately shear and flexural deformations. It is clear that shear deformations for the stronger pier (Bridge-213B) are comparable with the flexural deformations while the later deformations predominate over the shear ones for the 'weak' pier (Bridge-213C). Figure 4 shows the crack patterns for the three squat piers tested in ELSA. Again the predominance of shear cracking is apparent for the stronger pier. Therefore, a general model capable to represent flexural and shear non-linear behaviour under cyclic loading was considered necessary to closely trace out the seismic response of bridges with low shear span ratio piers.

3.1. The strut-and-tie model

Classic fibre models consider a linear elastic behaviour law for shear; the fibres belonging to the same section '*see*' the same shear strain and contribute to the final force proportionally to their area and distortional modulus. The influence of the stirrups is neglected and it only interferes in the axial stress-strain law of the concrete core through the confinement effect.

Figure 5 illustrates the main internal resisting forces in a short cantilever beam damaged by transverse and longitudinal forces applied at the extremity. From this figure, one can observe that a new structure, analogous to a truss made of transverse and longitudinal steel ties and diagonal concrete struts, appears from diagonal cracking. Actually, the non-linear shear model presented in the paper is based on this analogy: a strut-and-tie model for shear forces coupled with a classic fibre model for flexural forces.

3.2. Compatibility equations

Two concrete diagonals are considered in the formulation. For each loading direction there is one strut under compression forces and another under tensile forces. In the case of shear forces in both main transverse directions of the element, the procedure described for one direction is valid for the perpendicular direction and the two responses are superimposed.

The struts are represented by their central axis. The same cracking angle is adopted for both diagonals, i.e., the two struts are symmetric in relation to the axis of the column. The angle is a model parameter; it is imposed by the user and it does not change during the loading history.

The diagonals represent the direction of the pseudo principal stresses. The word pseudo refers to the fact that the principal directions were estimated and not calculated through the Mohr's circle. Moreover, the fibre and the strut-and-tie models interact through the '*average axial strain*' that is computed at each transverse section. Actually, the coupling between the fibre and the strut-and-tie model is ensured by the deformation l_{oe} in Figure 6.

The equations of compatibility of displacements are established in the transverse section through the contribution of: the average axial deformation, ($\varepsilon_{oe} = l_{oe}/l$), the shear deformation γ and the stirrups deformation, ($\varepsilon_{wy} = \Delta_{wy}/h$). Assuming a cracking angle θ, as illustrated in Figure 6, the total deformation of each diagonal is given by

$$\begin{aligned} \varepsilon_1 &= \frac{\Delta_1}{l/(\cos\theta)} = \varepsilon_{oe}\cdot(\cos\theta)^2 + \varepsilon_{wy}\cdot(\sin\theta)^2 - \frac{\tan\gamma}{2}\cdot(\sin(2\theta)) \\ \varepsilon_2 &= \frac{\Delta_2}{l/(\cos\theta)} = \varepsilon_{oe}\cdot(\cos\theta)^2 + \varepsilon_{wy}\cdot(\sin\theta)^2 + \frac{\tan\gamma}{2}\cdot(\sin(2\theta)) \end{aligned} \tag{2}$$

where the strains γ and ε_{oe} are computed within the Timoshenko beam algorithm. Instead, the

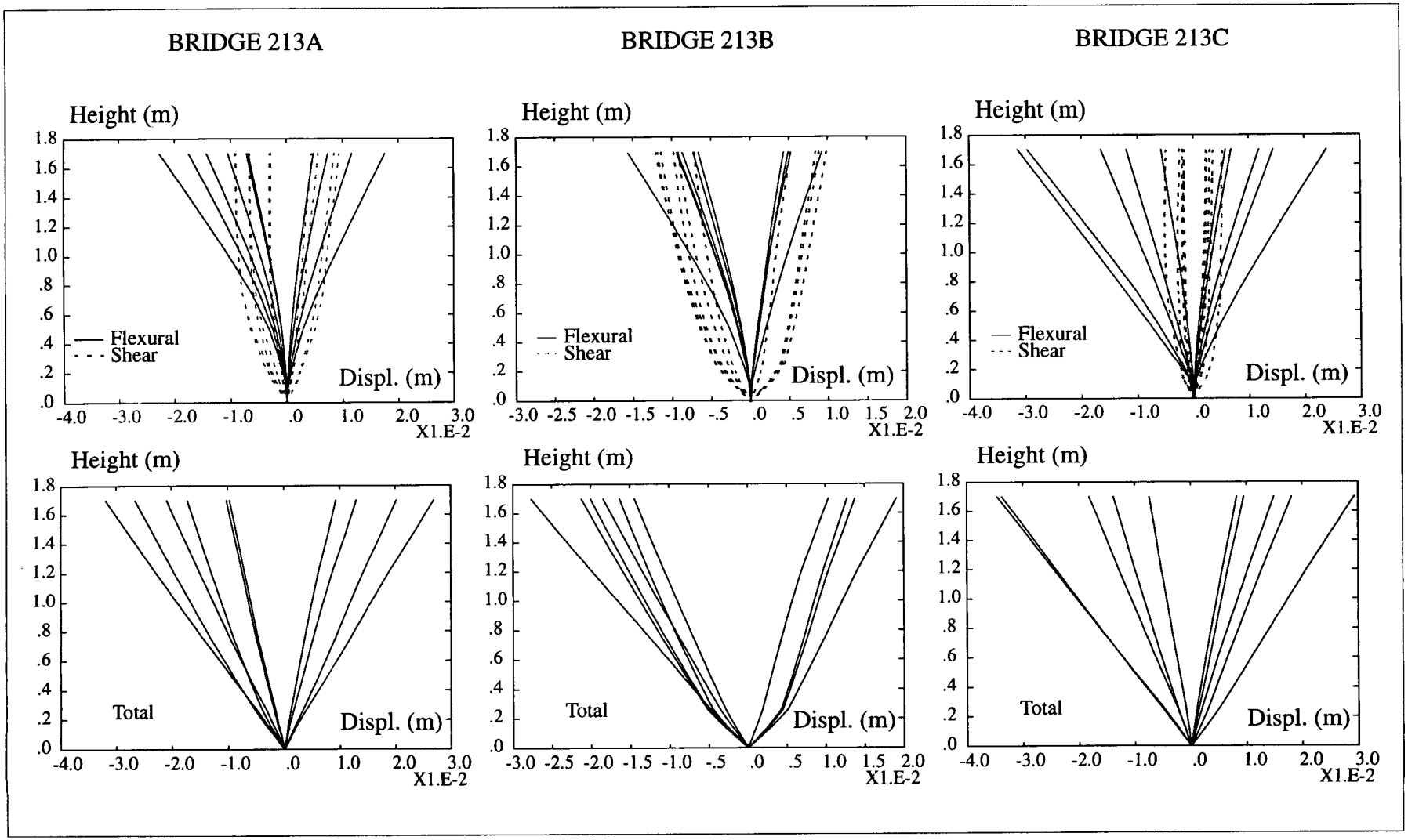

Figure 3. Flexural and shear deformations of the short piers for the HLE (10 peak values)

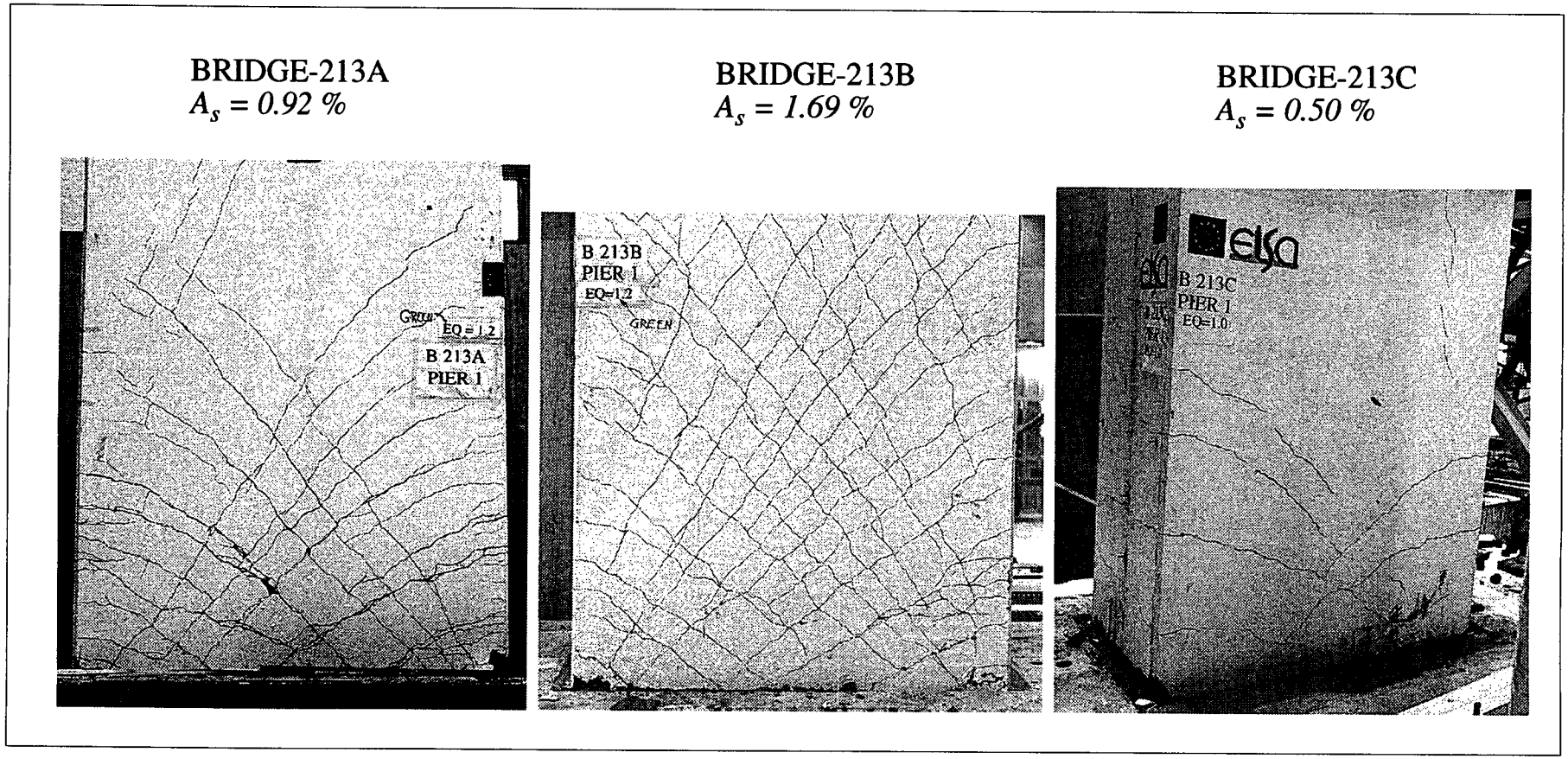

Figure 4. Cracking patterns for the central piers of the irregular bridges with different steel ratios - Lateral view

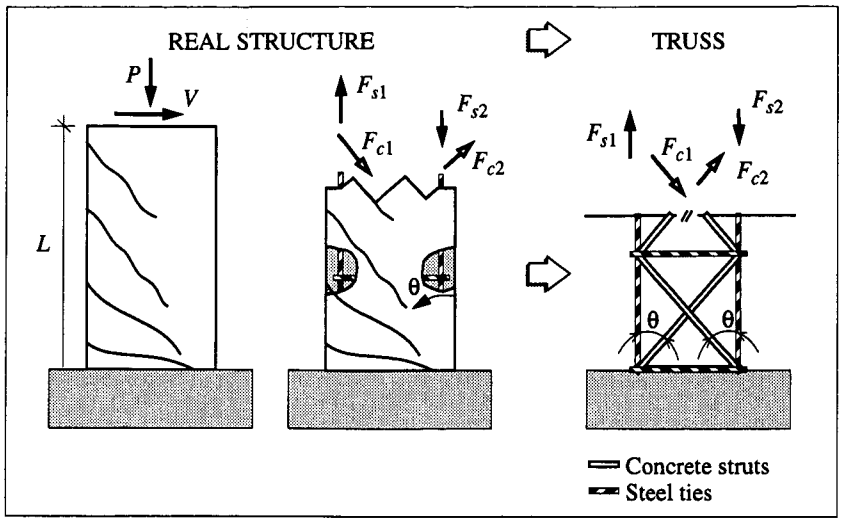

Figure 5. Truss analogy

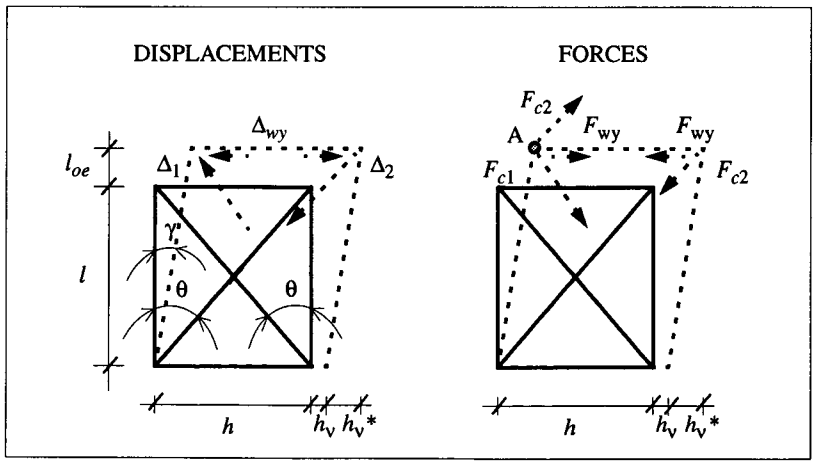

Figure 6. Compatibility of displacements and equilibrium of forces

stirrups strain ε_{wy} is computed internally for each cross-section.

3.3. Equilibrium equations

With the deformation of each diagonal calculated through (2), the forces in the struts, F_{c1} and F_{c2} illustrated in Figure 6, and in the stirrups, F_{wy}, are computed through the constitutive laws of the materials,

$$
\begin{aligned}
F_{c1} &= f_c(\varepsilon_1) \cdot A_{Sturt} = \sigma_c(\varepsilon_1) \cdot b \cdot h \cdot (\cos\theta) \\
F_{c2} &= f_c(\varepsilon_2) \cdot A_{Sturt} = \sigma_c(\varepsilon_2) \cdot b \cdot h \cdot (\cos\theta) \\
F_{wy} &= f_{sw}(\varepsilon_{wy}) \cdot \frac{h/(\tan\theta)}{s} \cdot (2 \cdot A_{sw})
\end{aligned}
\tag{3}
$$

f_c and f_{sw} being the concrete and the stirrups stresses, respectively, A_{sw} the cross-sectional area of the transverse steel, s the stirrups spacing and b the transverse dimension of the column cross-section. The hysteretic curves adopted for the concrete and the stirrups are those presented in section 2.2. However, the parameters that control the crack-closing and the tension-stiffening effects in the concrete model may present different values. Note that the non-linear shear model attempts to reproduce the response of a structure through the behaviour of just two elements made of concrete and one made of steel. Thus, it is not possible for the model to '*disguise*' any singularity present in the axial stress-strain response curve of these three elements. Therefore, the constitutive law of the transverse steel does not consider the monotonic part of the curve.

Referring to Figure 6, the forces in (3) must respect, simultaneously, the equilibrium of internal forces at point A and the equilibrium of external forces in the structure, respectively:

$$
\begin{aligned}
F_{wy} + (F_{c1} + F_{c2}) \cdot (\sin\theta) &= 0 \\
V + (F_{c1} - F_{c2}) \cdot (\sin\theta) &= 0
\end{aligned}
\tag{4}
$$

This system of equations is solved in two stages. Firstly, the top equation is used to calculate the deformation of the stirrups, i.e., the strain at the transverse steel satisfying at the same time the compatibility of displacements and the internal equilibrium in the element. Then, with ε_{wy}, the shear resisting force V in the transverse section is computed through the second equation.

The damage of the concrete elements of the truss is considered in the model through a damage parameter depending on the state of the concrete under flexural and axial forces. In this way, the decrease of the compressive active area of the diagonals can be taken into account, being the degradation of the shear strength of the structure properly taken into account. The damage parameter adopted for the truss is proportional to the maximum strain observed in the compressive concrete core area of the cross section. As for the minimum axial strain, different parameters are considered for each diagonal (two more internal variables and a new component defining the ultimate strain of the concrete in the model, ε_{ult}):

$$
D_i = \frac{(\varepsilon_i)_{max}}{\varepsilon_{ult}} \tag{5}
$$

$$
F_{ci} = \sigma_c(\varepsilon_i) \cdot (1 - D_i) \cdot b_w \cdot h \cdot (\cos\theta) \tag{6}
$$

which means that the concrete stresses $\sigma_c(\varepsilon_i)$ must be substituted by $\sigma_c(\varepsilon_i) \cdot (1 - D_i)$ in all the previous equations. Details on the present shear model and implementation notes can be found elsewhere [4].

4. MODEL VALIDATION

The response of a bridge pier is simulated using the fibre model with the new approach for the shear forces. The cross-section of the pier illustrated in Figure 7 has been represented by a simplified 'I' cross-section with nine fibres for the confined concrete, four for the unconfined concrete and nine for the longitudinal steel. According to the same figure, the 3D structure is

divided into five 0.34*m* high elements plus two 0.55*m* high elements. The main characteristics of the concrete are: the Young modulus (E_c=25.6*GPa*, 20.5*GPa*), the compressive strength (f_{co}=32*MPa*, 40*MPa*) at the peak strain (ε_{co}=0.25%, 0.39%) and an after peak descending branch with a slope ($(f_c-f_{co})/(\varepsilon_c-\varepsilon_{co})$=1.1*GPa*, 3.2*GPa*); the two values correspond to the unconfined and to the confined concrete. The longitudinal and the transverse steel have a yielding strength (f_{sy}=540*MPa* and 700*MPa*), respectively. Both have a Young modulus (E_s=206*GPa*) and a hardening ratio (E_h/E_o=0.55%). The area of the cross-section that contributes to the shear resisting mechanism is (A_{shear}=0.32x1.44m^2).

The history of displacements that has been applied to the top of the numerical structure corresponds to a series of cycles of increasing amplitude: 1, 2, 4, 8, 10*mm*, followed by three cycles at amplitude 18*mm* (ductility=1.5), three cycles at amplitude 36*mm* (ductility=3) and, finally, three cycles at amplitude 72*mm* (ductility=6). The following response curves are illustrated: transverse force versus total transverse displacement at the top of the pier and at a height of 1.70*m*, transverse force versus shear and flexural transverse displacements at a height of 1.70*m*, and, finally, the bridge pier peak displacement profiles. A cracking angle ($\theta = 45°$) has been adopted. The analytical results are compared with the experimental response obtained at the ELSA laboratory [6].

5. CONCLUSIONS

The curves illustrated in Figure 7 show a very good agreement between the numerical and the experimental results. The numerical curves base shear force versus displacement at the top and at 1.70m high fit the experimental results. The behaviour of a structure where the effect of shear forces in the response is not negligible has been well reproduced by the non-linear shear model; the narrowing and lengthening (pinching) of the force versus displacement curves observed in the experimental results due to important shear forces, is well represented. Furthermore, the numerical and the experimental displacement profiles, illustrated in the same figure, are quite similar.

ACKNOWLEDGEMENTS

This work has been developed under the Human Capital and Mobility programme of the European Commission (EC), which financial support is gratefully acknowledged.

REFERENCES

[1] Buckle, I. G. - "Seismic Design and Retrofitting of Reinforced Concrete Bridges" *in proceedings of the International Workshop held in Bormio on April 2-5*. Edited by G. M. Calvi and M. J. Priestley. Bormio, Italy, 1991

[2] CEA - "CASTEM 2000, Guide d'Utilisation". CEA, Saclay, France, 1990

[3] Guedes, J., P. Pegon and A.V. Pinto - "A Fibre/Timoshenko Beam Element in CASTEM 2000" *in Special Publication* Nr. I.94.31. Applied Mechanics Unit, Safety Technology Institute, Commission of the European Communities, Joint Research Centre, Ispra Establishment, 21020 Ispra (VA), Italy, 1994

[4] Guedes, J. and A.V. Pinto - "Non-Linear Shear Model for R/C Piers". *Report EUR,* Safety Technology Institute, Commission of the European Communities, Joint Research Centre, Ispra Establishment, 21020 Ispra (VA), Italy, 1997 *(to appear)*

[5] Menegotto, M. and P.E. Pinto - "Method of Analysis for Cyclically Loaded Reinforced Concrete Plane Frames Including Changes in Geometry and Non-elastic Behaviour of

Elements under Combined Normal Force and Bending". *IABSE Symposium on Resistance and Ultimate Deformability of Structures Acted On by Well-Defined Repeated Loads*, Final Report, Lisbon, 1973

[6] Pinto, A.V., G. Verzeletti, P. Negro and J. Guedes - "Cyclic Testing of a Squat Bridge-Pier". *Report EUR 16247 EN*. Safety Technology Institute, Commission of the European Communities, Joint Research Centre, Ispra Establishment, 21020 Ispra (VA), Italy, 1995

[7] Pinto A.V.; G. Verzeletti; P. Pegon; G. Magonette; P. Negro and J. Guedes. "Pseudo-Dynamic Testing of Large-Scale R/C Bridges". *Report EUR 16378 EN*, EC, JRC, Ispra, Italy, 1996

[8] Pinto, A.V. (Editor). "Pseudo-dynamic and Shaking Table Tests on RC Bridges". *ECOEST/PREC8 Report*. LNEC, Lisbon, 1997

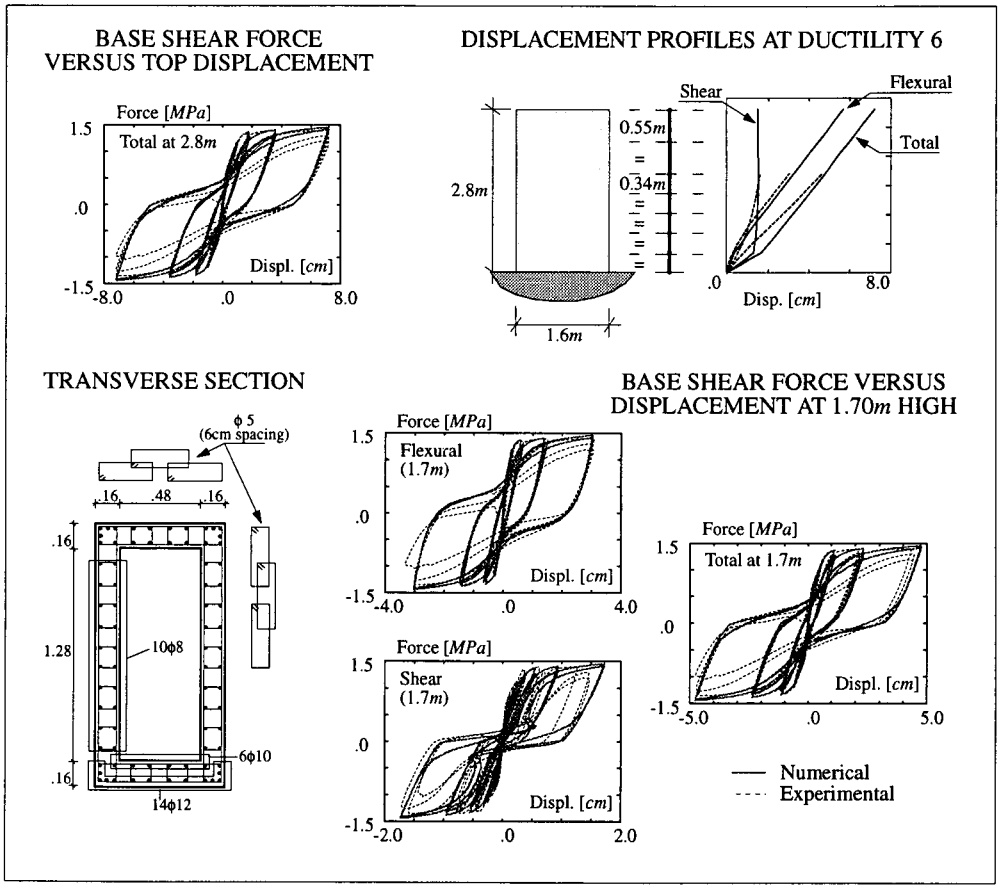

Figure 7. Reinforcement layout. Numerical versus experimental results: displacement profiles and base shear force versus top displacement curves

SHEAR STRENGTH OF REINFORCED CONCRETE COLUMNS - EFFECT OF SPECIMEN SIZE AND LOAD REVERSAL -

Hirotaka Kawano[1], Hiroshi Watanabe[2]

[1]Head of Concrete Division, Public Works Research Institute, Ministry of Construction, Japan
[2]Senior Research Engineer of Concrete Division, ditto

ABSTRACT

Effect of size of depth and load reversals on shear strength carried by concrete of RC piers are discussed in this paper. Large size RC beam specimens whose effective depth is up to 2.0m without any web reinforcement were tested to estimate the degree of scale effect on shear strength of concrete. Nominal shear strength of concrete decreases with effective depth of the member approximately to the power of -0.25 to -0.4.

Cyclic loading test of 6 RC column specimens were also conducted to evaluate the reduction of shear strength of concrete. It is shown that the shear strength of concrete subjected to cyclic load becomes smaller compared to one subjected to monotonic load, but reduction rate is affected the number of load reversals.

INTRODUCTION

It is very important to ensure enough ductility of RC columns in order to improve earthquake resistance. To design RC columns having excellent earthquake-resistance, members must have greater shear strength than flexural strength to avoid brittle shear failure. To ensure preventing shear failure, the flexural and shear strengths of RC columns must be accurately evaluated.

A method to calculate the flexural strength of RC members has already been established; the ultimate flexural strength can be calculated with great accuracy based on Bernoulli's assumption if proper stress-strain curves of the concrete and reinforcing bar are used. Many studies have been also carried out on the method of calculating the shear strength of RC members. In most design specifications, shear resistance of RC members is classified into two component; one is carried by the concrete and the other is carried by web reinforcement such as hoops and stirrups, and these two components are added to obtain the shear strength. The shear strength to be carried by the concrete is determined from loading test data, while the shear strength carried by the web reinforcement is calculated usually based on the truss analogy.

However, there are still many unclear points in the calculation of shear strength of RC members, and this is preventing improvement of the accuracy of shear strength evaluation. In particular, when the shear strength of an RC member with a relatively large cross section such as an RC pier, subjected to load reversals, there may be scale effects on the shear strength of concrete, or the shear strength may be reduced by the effect of repeated loads. To improve the earthquake-resistant design of RC piers, these problems must be solved and the accuracy of the shear strength evaluation improved.

This report outlines the results of a research on the scale effect on nominal shear stress that can be carried by the concrete and the effect of load reversals of an RC pier.

SCALE EFFECT ON NOMINAL SHEAR STRENGTH OF CONCRETE

Outline

When shear occurs in an RC member, the mean shear stress that can be carried by the concrete is affected by the scale effect, and decreases as the effective depth of the member increases. This has been well-known for many years[1)].

Material strength of concrete is generally affected by the scale effect. For example, it has been reported that the compressive strength of concrete decreases by the 1/10th-power of the diameter of cylindrical specimens tested, while the split tensile strength decreases by the 1/3rd-power of the diameter[2)].

All members using concrete material are therefore inevitably affected by the scale effect to varying degrees. Evaluation of the shear strength of RC members in the design specification must clarify how to deal with scale effect. Analytical studies based on fracture mechanics are being conducted to clarify the cause of the scale effect, and it is now possible to predict the scale effect to a certain degree. However, some tasks still remain, such as modeling of the mechanical characteristics of concrete including cracks. Thus, it is very important to accumulate loading test data using large-size test specimens to quantitatively evaluate the extent of the scale effect.

In this study, a shear loading test was conducted on RC beam specimens without any web reinforcement, and the test data including those from previous loading tests were analyzed in order to assess the degree of the scale effect on the nominal shear stress that can be carried by the concrete.

Shear loading test on RC beam specimens

(a) Outline of experiment

In this experiment, a shear loading test was conducted on RC beam specimens of different effective depths and without web reinforcement. The size of the specimens is given in Table 1 and **Fig.** 1. The shear span to effective depth ratio for each specimen was fixed and set to 3. Note that two specimens were tested under the same conditions for each group of specimens. The target slump of the concrete was 8cm, and the target compressive strength was 210kg/cm^2 (20.6MPa) .

(b) Results of loading test

All the specimens developed inclined tension cracks after developing flexural cracks. They then rapidly lost their load bearing capacity, and typical shear failure occurred (Photo 1). Table 2 shows the results of the loading test. The nominal shear stress of concrete at the time of shear failure was obtained from the following expression:

$$\tau_u = \frac{P_u}{bd} \qquad (1)$$

Where

P_u: shear force at the time of shear failure accounting for the effect of dead weight

b : width of cross section of specimens

d : Effective depth of cross section of specimens

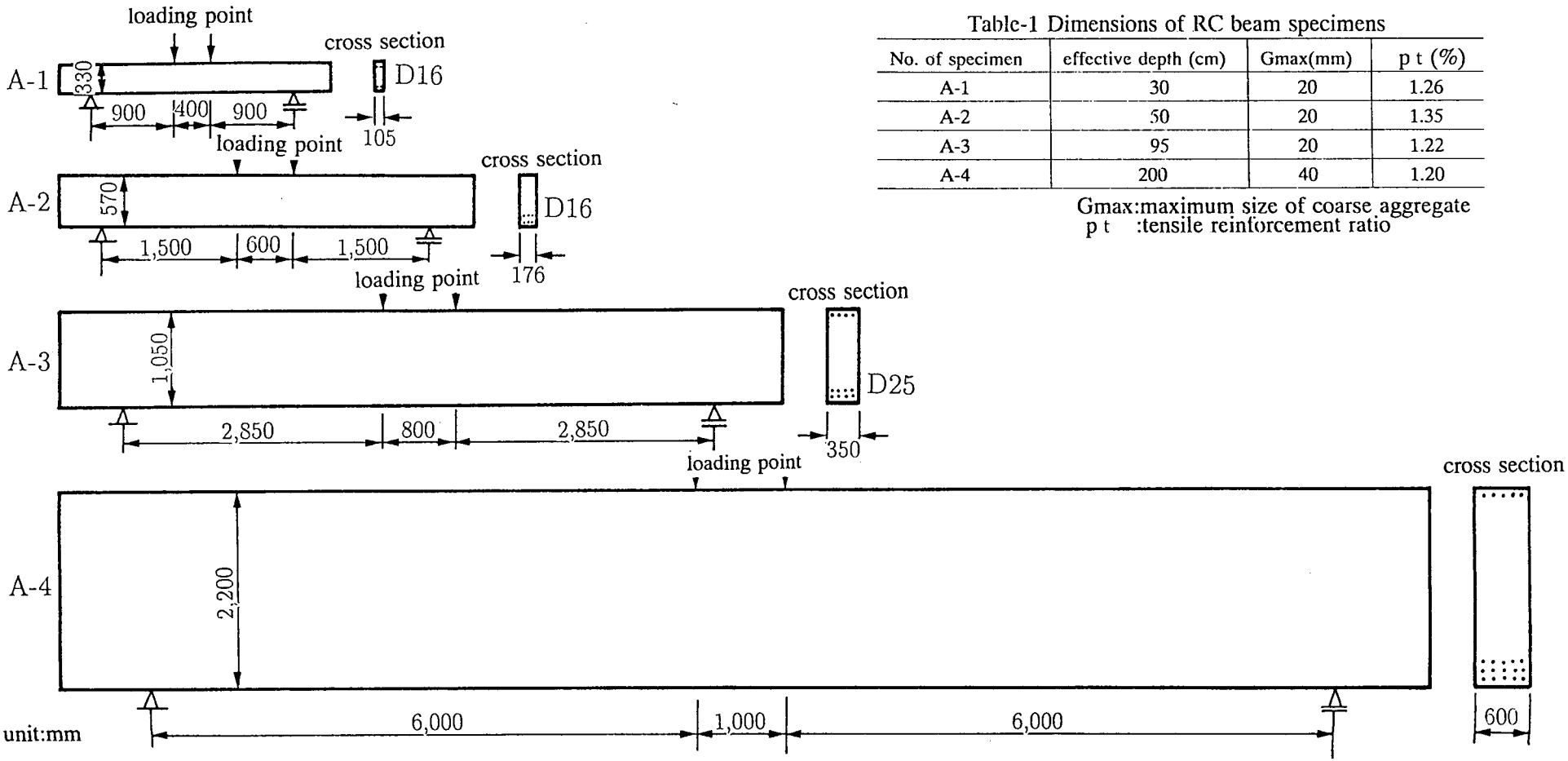

Table-1 Dimensions of RC beam specimens

No. of specimen	effective depth (cm)	Gmax(mm)	p t (%)
A-1	30	20	1.26
A-2	50	20	1.35
A-3	95	20	1.22
A-4	200	40	1.20

Gmax:maximum size of coarse aggregate
p t :tensile reinforcement ratio

Figure 1 Dimensions of RC beam specimens

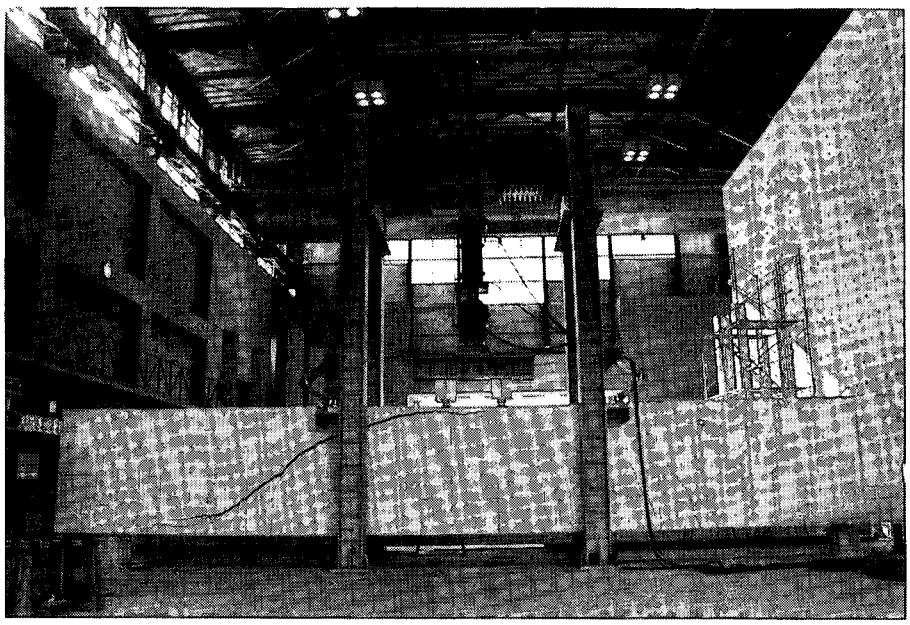

Photo.1 Shear failure of large RC specimens(A-4)

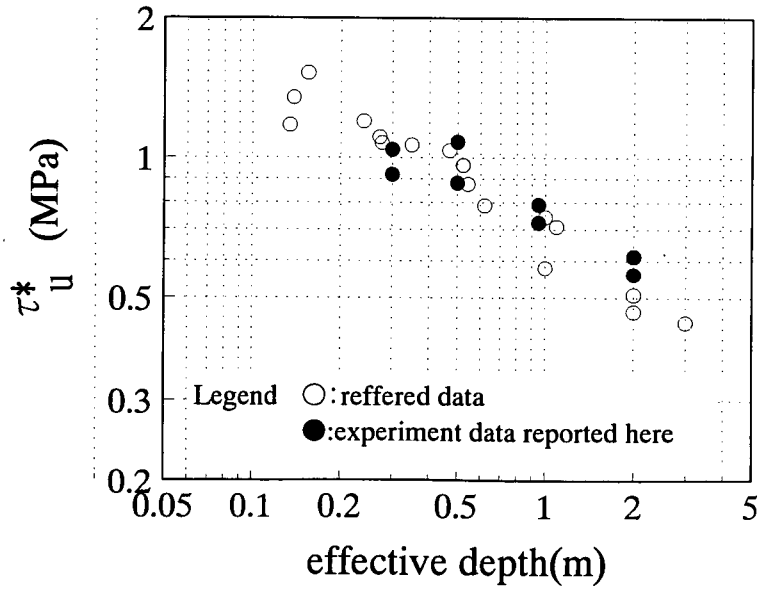

Figure 2 Scale effect of τ_u^*

Table-2 Test results

no of specimens	failure load (kN)	τ_u (MPa)	compressive strength of concrete (MPa)	tensile strength of concrete (MPa)
A-1	67	1.06	24.8	2.29
	59	0.93	24.8	2.29
A-2	165	0.93	27.3	2.27
	203	1.16	27.3	2.27
A-3	432	0.65	20.7	1.87
	475	0.72	20.6	2
A-4	1,221	0.51	22.2	2.05
	1,120	0.47	23.1	2.15

Table-3 Refered test data

no. of ref.	testing condition			No. of refered data	results of analysis		
	effective depth(m)	reinforcement ratio(%)	comp. strength of concrete (MPa)		a_1	a_2	r^2
5	1 ~ 3	0.4	21.5 ~ 27.9	3	0.17	-0.25	0.96
6	1 ~ 3	0.14 ~ 0.28	24.9 ~ 27.5	3	0.2	-0.42	0.75
7	0.16 ~ 0.62	1.23 ~ 1.24	20.3 ~ 25.1	5	0.19	-0.42	0.94
8	0.23 ~ 0.93	1.35	31.2 ~ 35.7	5	0.2	-0.07	0.23
1	0.14 ~ 1.09	2.66 ~ 2.89	25 ~ 27.4	8	0.23	-0.25	0.89
this exp.	0.3 ~ 2	1.19 ~ 1.35	20.6 ~ 27.3	10	0.2	-0.31	0.82

Table-4 Hoop arrangement of column specimens

No. of specimen	diameter of hoop (mm)	spacing of hoop (cm)	cross tie	web reinforcement ratio (%)
B-1	-	-	-	0
B-2	6	12	-	0.07
B-3	6	8	○	0.15
B-4	10	12	-	0.15
B-5	10	8	-	0.22
B-6	10	8	○	0.33

Although efforts were made to ensure that the concrete strength and tensile reinforcement ratio were the same for all the specimens used for the loading test, not all the specimens may have had the same values, and therefore they cannot be directly compared. Thus, assuming that the nominal shear stress that can be carried by the concrete is proportional to the cube root of the compressive strength and tension reinforcement ratio[4)], experimental values were corrected so that all the specimens could be regarded to have a compressive strength of concrete of 240 kg/cm^2 (23.5MPa) and a tensile reinforcement ratio of 1.2%. τ_u^* denotes the nominal shear stress that can be carried by the concrete after the correction, and τ_u^* is used to discuss the scale effect. **Fig.** 2 shows the relationship between the effective depth of each specimen and τ_u^* (experimental values plotted with ●). The figure shows that τ_u^* decreases as the effective depth of the member increases, and thus the scale effect on nominal shear strength of concrete certainly exists.

(c) Evaluation of scale effect including review of previous loading tests

To verify whether the extent of the degree of the scale effect shown by the loading test performed in this experiment is adequate, the results of previous loading tests were also reviewed. Table 3 lists the results of the shear loading tests reviewed. The nominal shear stresses at the time of shear failure reported in those loading tests were converted to the nominal shear stress applicable with a compressive strength of 240 kg/cm^2 (23.5MPa) and a tensile reinforcement ratio of 1.2% to obtain τ_u^*. Figures in columns a_1 and a_2 represent regression coefficients using formula (2) and subjected to regression analysis. r^2 indicates the square of the correlation coefficient.

$$\tau_u^* = a_1 d^{a_2} \qquad (2)$$

Fig. 2 shows the relation between τ_u^* and the effective depth of the member excluding the data of reference8 that indicated relatively low correlation between the two. From the results, it is reasonable to assume that the nominal shear stress that can be carried by the concrete is affected by the scale effect, and decreases with the effective depth of the member by approximately to the power of -0.25 to -0.4.

EFFECT OF REPEATED LOADING ON SHEAR FORCE CARRIED BY CONCRETE

Outline

When +/- cyclic loads are applied to an RC member, an X-shaped crack develops in the member and the ability of the concrete to transfer shear force deteriorates considerably as compared with one-way loading. It has been reported that RC members shift to the shear failure mode after giving in to flexural yield.

However, it is always extremely difficult to obtain the shear force carried by the concrete after the RC member has yielded, and the shear resistance of concrete has never been quantified. In this experiment, a cyclic loading test was conducted on RC columns, and attempts were made to quantify the reduction of shear resistance of concrete.

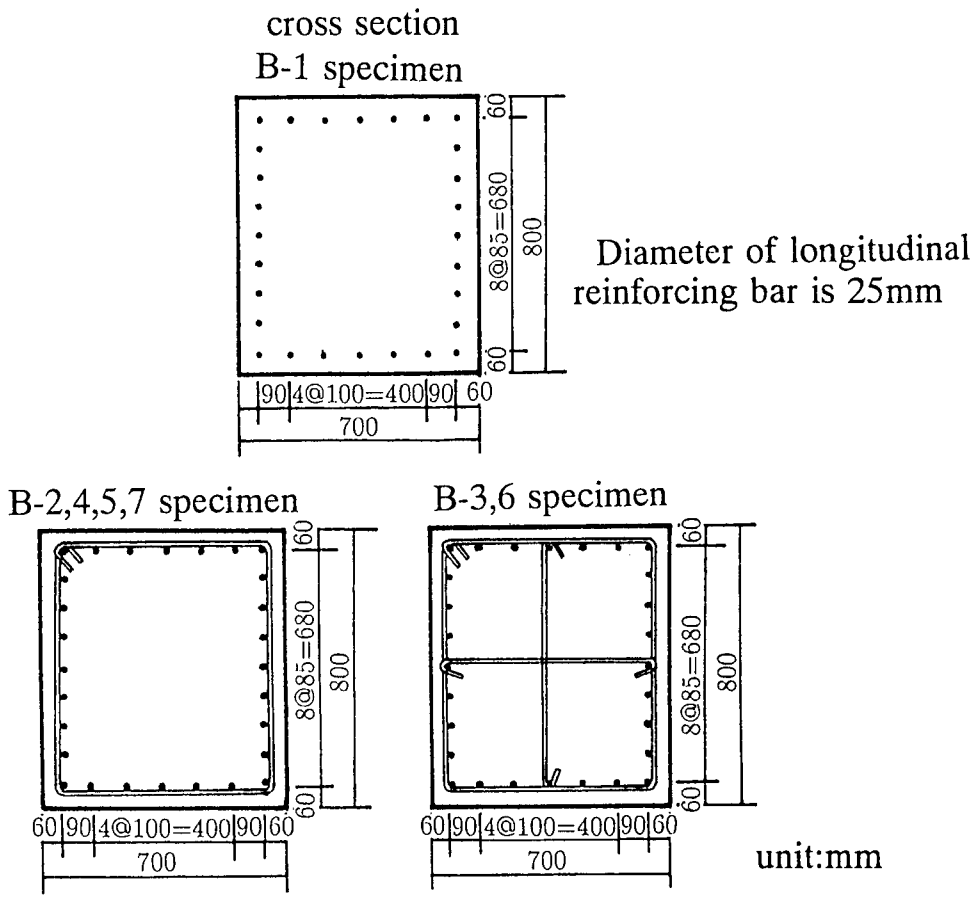

Figure 3 Dimensions of cross section of column specimens

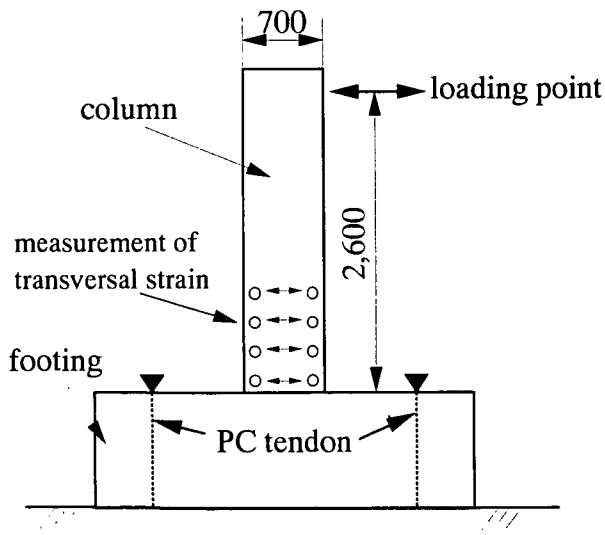

Figure 4 test setup (unit:mm)

Loading test procedure

In this experiment, six RC column specimens were produced, and static cyclic loading tests were performed. The only varying factor in all the specimens was the quantity of hoops, and all the other factors were fixed.

Figure 3 shows the cross-section size and bar arrangement for each specimen. Specimen B-1 was provided to obtain the shear strength carried by the concrete, which did not have any hoop. The hoop arrangement for each specimen is given in Table 4. The concrete used had a target strength of 240 kg/cm^2 (23.5MPa). The loading method was as shown in Table 4; force was applied to the point 2,6m from the column base and displacement controlled loading was employed. Cyclic loads were applied to all the specimens except for specimen B-1, and as shown in **Fig.** 5, repeated number of each displacement amplitude is 3. The definition of yield displacement of the column (δ_y) was at the time when the measured strain of the longitudinal reinforcing bar in the column reached the yield point at the column base.

Method of calculating shear force carried by concrete

The tensile stress acting on the hoop must be accurately measured in order to estimate shear force carried by the concrete with accuracy. The tensile stress acting on the hoop can be determined from the strain measured by a strain gauge attached on the hoop. However, the measurement of strain of hoops is unstable after yielding of the hoops or occurring cracks in the concrete. In this experiment, to determine the tensile strain of hoops in the plastic hinging zone, bolts were anchored in concrete, and the elongation between adjacent bolts was measured to obtain the mean strain of hoops. The stress of the hoop was calculated from the mean tensile strain, and a bilinear model in which the secondary gradient is set to 0 was assumed for the stress-strain relation of the hoops to calculate the tensile stress.

Results of loading test

Test specimen B-1 that did not contain hoops developed inclined tensile cracks just before the longitudinal tensile reinforcement yielded, and failed due to shear force. All of the test specimens from B-2 to B-6 showed post-yield shear failure, i.e. after yielding of the longitudinal tensile reinforcement, X-shaped cracks developed in the plastic hinge section and their strength was lost. **Figure** 6 shows an example of the hysteresis curve of the load-displacement relation. Photos 2 to 4 show the state of cracks of specimens at points (i) to (iii) given in **Fig.** 6.

Fig.7 shows the tensile stress distribution of hoops calculated from measured strain at the peak load of each loading cycle. The tensile stresses acting on the hoops was not uniformly distributed in the direction of the member axis of the RC column specimens tested, and greater stresses tended to appear at the column base. While the hoops that reached the yield point were found in a relatively narrow area of the column base when many hoops were used, the area where hoops yielded tends to relatively extend for specimens with fewer hoops.

When cyclic loads are applied and removed after reaching their peak, the strain of the hoops does not return to zero even if the applied load is reduced to zero, and in some cases residual stress develops. In this study, the shear force to be carried by the hoops was determined by applying the truss analogy to the increment of the hoop stress from load zero to peak load. That is, assuming the shear force carried by the hoop when the load reached its peak in load hysteresis of i-th cycle is V_{si}, then

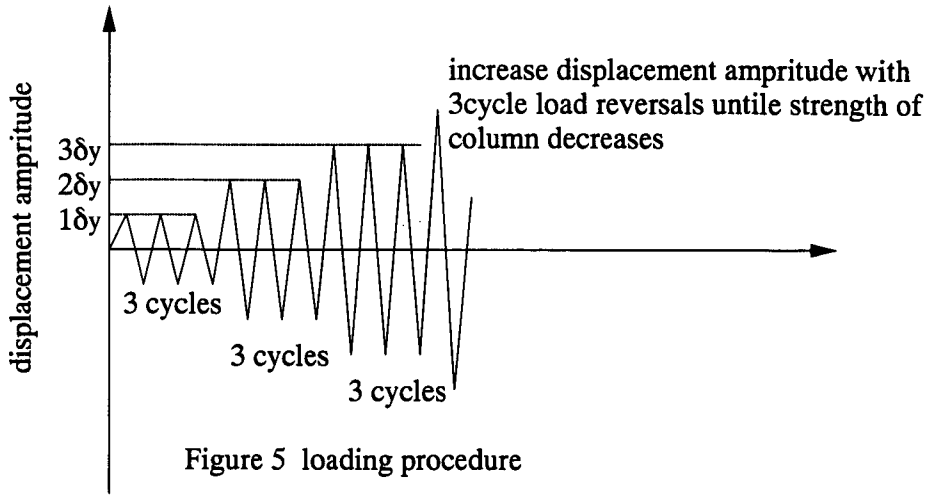

Figure 5 loading procedure

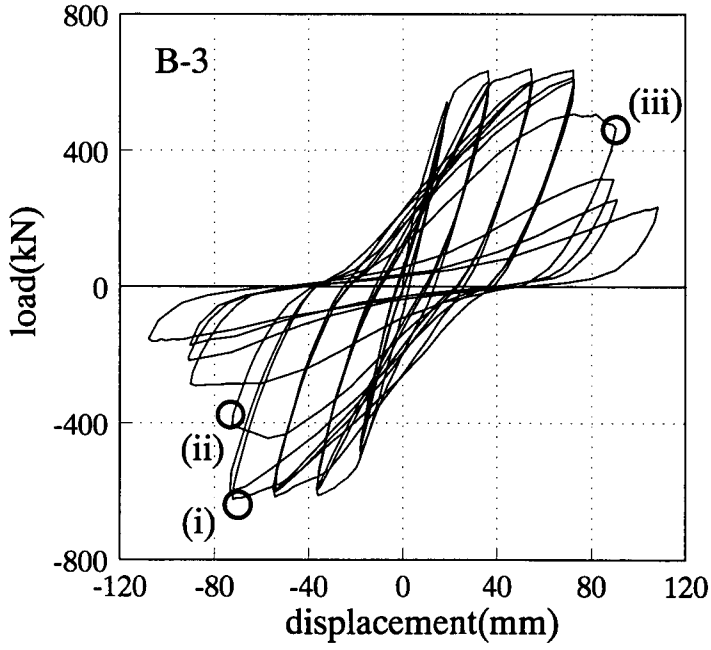

Figure 6 Hysteresis of load displacement relationship (B-3 specimen)

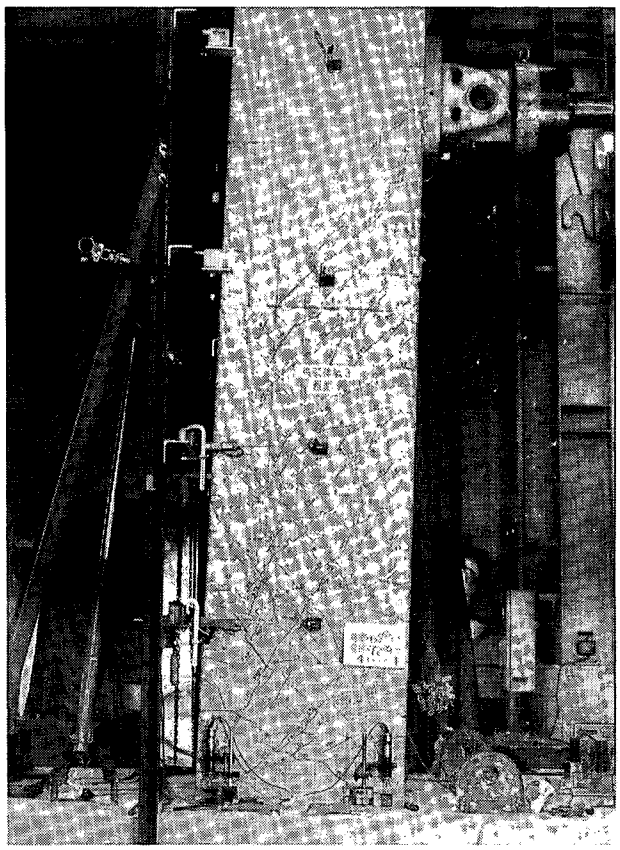

Photo.2 Crack of column specimen(B-3) at the point(i) of Fig.6

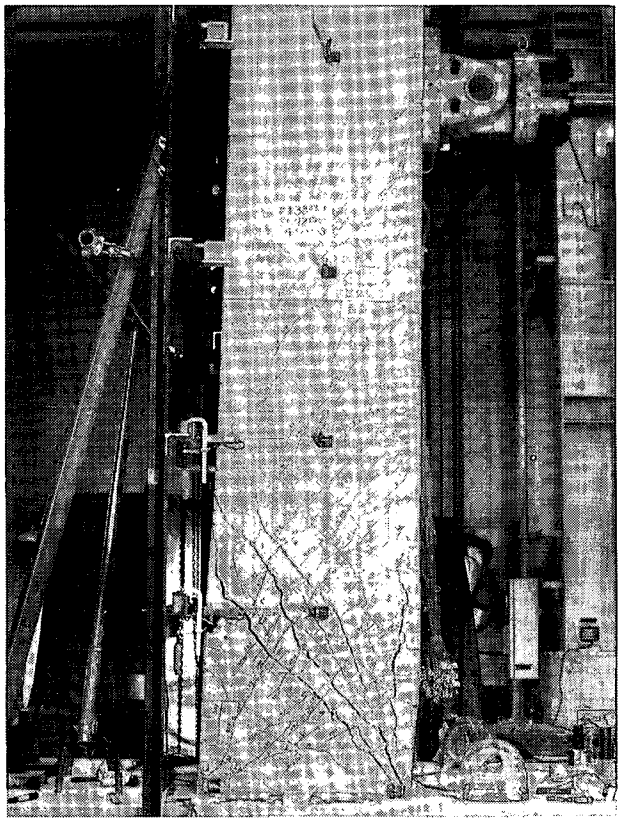

Photo.3 Crack of column specimen(B-3) at the point(ii) of Fig.6

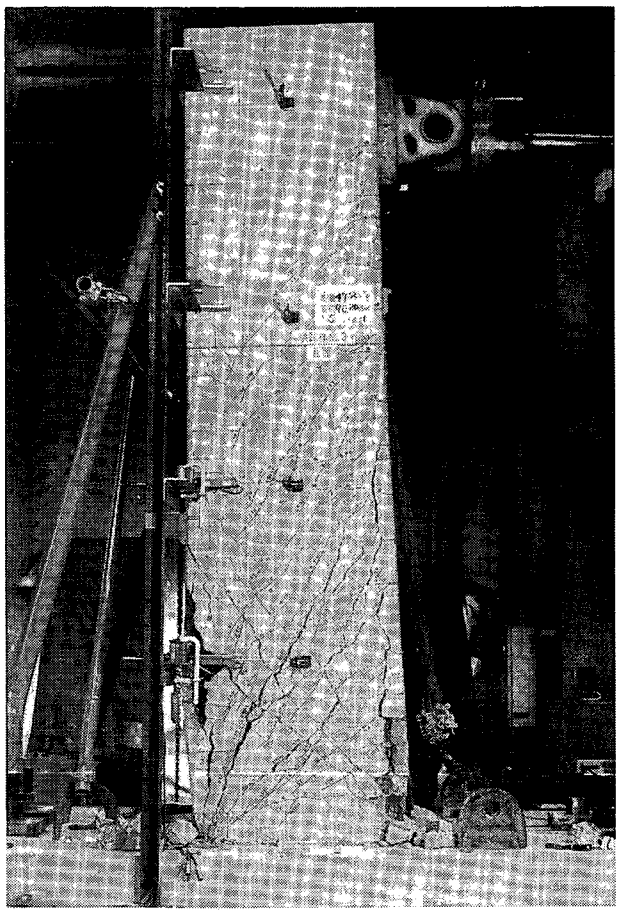

Photo.4 Crack of column specimen(B-3) at the point(iii) of Fig.6

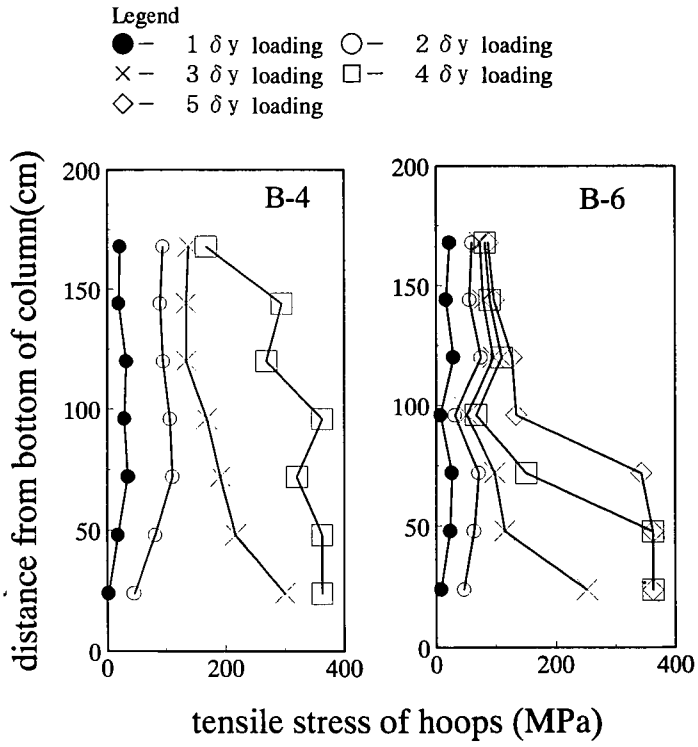

Figure 7 Distribution of tensile stress of hoops

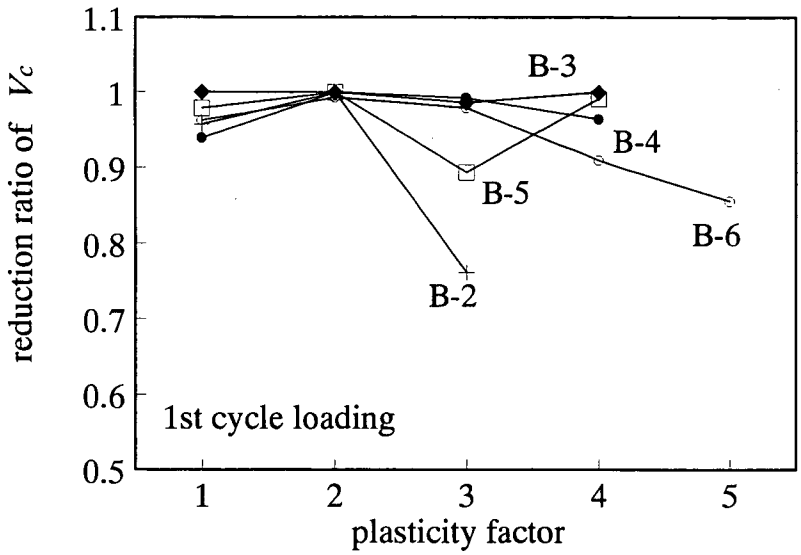

Figure 8 Reduction of V_c with incresing plasticity factor (at 1st cycle loading)

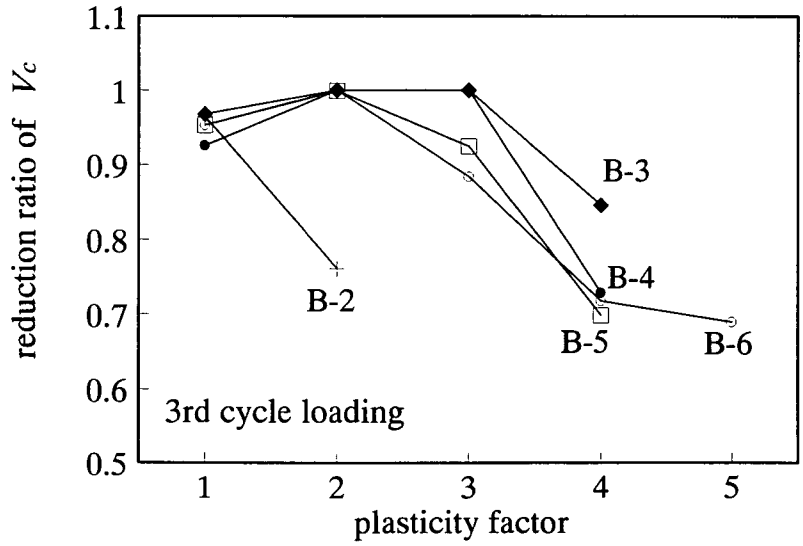

Figure 9 Reduction of Vc with incresing plasticity factor (at 3rd cycle loading)

$$V_{si} = \frac{A_w(\sigma_{wi} - \sigma_{wi0})}{1.15s} \qquad (3)$$

Where,

A_w: Area of cross section of the hoop

σ_{wi}: Tensile stress acting on the hoop at peak load

σ_{wio}: Residual tensile stress acting on the hoop when load is 0

d : Effective depth of cross section

s : spacing of hoops

The shear force carried by the concrete V_c was determined by subtracting V_{si} from the applied shear force. **Figures** 8 and 9 show how the V_c determined in this manner changed as the ductility factor increased. **Fig.** 8 shows the values at peak load in the 1st cycle of $n\delta_y$ loading, while **Fig.** 9 shows the values in the 3rd cycle of $n\delta_y$ loading. Note that the vertical axis shows the shear force carried by the concrete divided by the shear strength carried by the concrete determined in the loading test performed on test specimen B-1. This result indicates that there was not such a marked reduction in the shear strength carried by the concrete during loading of the 1st cycle, but that the shear strength carried by the concrete started to decrease during loading of the 3rd cycle at just about the time when the ductility factor exceeded 3, and decreased to about 70% when the ductility factor was 4-5.

From the above, the fact that the shear strength carried by the concrete will decrease at least to 70% must be taken into consideration in order to prevent post-yield shear failure when repeated loads are applied. When number of repeated load cycles assumed to be small, it is reasonable to estimate the reduction rate of shear strength carried by the concrete is slightly larger than this (about 80%).

CONCLUSIONS

This report assessed the effects of size of effective depth and load reversals that have not been previously fully discussed in connection with the shear strength of RC piers, and outlined the results of a study based on loading test data. The following findings were made:

1) The size effect of nominal shear strength of concrete can be roughly expressed as the function of effective depth to the power of -0.25 to -0.4.

2) When the shear strength of an RC member is to be calculated based on the truss analogy in current design specification, the reduction of shear strength carried by the concrete due to the effect of repeated loads must be considered.

3) However, the extent of the effect of loading repetition varies depending on the number of loading cycles, and the amount of reduction in shear strength carried by the concrete is small during the first cycle loading.

According to these findings, scale effect of nominal shear strength of concrete has been taken into account for the shear design of RC piers in recent earthquake resistant design specification of highway bridges in Japan. In addition, the effect of the number of load cycles is also taken into consideration, and the shear strength carried by the concrete is reduced according to the number of load cycles assumed. However, these results were obtained from limited experimental findings, and therefore further experiment data and theoretical verification are required for wider application of these findings.

References

1) G. N. J. Kani: "How safe are our large reinforced concrete beams?" Journal of ACI, March, 1967

2) Report of study on mechanical characteristics of concrete, Japan Society of Civil Engineering Concrete Library 69, 1991 (in Japanese)

3) J. Niwa, N. Zareen, T. Tanabe: Analysis of scale effect on shear strength concrete beams based on fracture mechanics, Proceedings of Japan Society of Civil Engineering (Proc.of JSCE), No. 508, 1995 (In Japanese)

4) H. Okamura, T. Higai: Proposed Design Equation for Shear Strength of Reinforced Concrete Beams without Web Reinforcement, Proc. of JSCE, No.300, 1980.

5) M. Iguro, T. Shioya, Y. Nojiri, A. Akiyama: Experimental study on shear strength of large RC concrete beams under equally distributed load, Proc. of JSCE No. 348, Aug. 1984 (in Japanese)

6) J. Niwa, K. Yamada, K. Yokozawa, H. Okamura: Re-evaluation of shear strength formula for RC beams without web reinforcement, Proc. of JSCE No. 372, Aug. 1986 (in Japanese)

7) Collection of shear experiment data on RC concrete beams: Public Works Research Institute, Technical Note No.2045, 1984

8) P. J. Taylor: Shear strength of large beams, Proc. of ASCE, ST11, 1972

9) I. Higai, J. Niwa, H. Okamura: Study of failure mechanism of RC members that ended in shear fracture after flexural yield, Concrete Engineering, Collection of Annual Papers No. 9-2, 1987

SEISMIC RESPONSE BY PSEUDODYNAMIC TESTS OF RC BRIDGES DESIGNED TO EUROCODE 8 AND ITALIAN SEISMIC CODE

A. De Sortis[1] **C. Nuti**[2]

[1]Servizio Sismico Nazionale, Via Curtatone 3, 00185 Roma, Italy
[2]Dip. di Scienze, Storia dell'Architettura e Restauro,
Università "G. D'Annunzio", 65127 Pescara, Italy

ABSTRACT

This work is a contribution to the assessment of EC8 capability of providing adequate ductility and low damageability to regular and irregular bridges. Comparison with Italian code is carried out. Results are based on pseudodynamic tests on whole bridges.

Two bridges (one regular and one irregular) have been designed according to EC8 Part 2: design PGA was 0.35 g, the structural behaviour factor was 3. Two companion bridges having the same geometry have been also designed to Italian Seismic Code DM 24.1.1986. For each bridge a 1:6 model of the most stressed pier has been tested in laboratory, while the remaining components: deck and piers, have been simulated numerically by substructuring techniques. Scale problems to prepare RC pier models have been deeply studied. Reinforcement scaling criteria, based on similitude fulfilment of global quantities: flexural and shear strength, confinement effect, post-elastic buckling and pull-out of rebars, are proposed. Two accelerograms have been used: Tolmezzo E-W, from 1976 Friuli Earthquake to test the irregular bridge, and Kobe-Kayou E-W from 1995 Hansin Earthquake, for the regular. Results for EC8 show good performance of the bridge under severe seismic action. Results for Italian code show good performance for the regular structure and substantial damages for the irregular one.

1. INTRODUCTION

The new Eurocode 8 Part 2 (EC8.2) for the design of bridges in seismic areas is an European Prestandard (ENV) since 1994 and will become an operative code in a few time. The Code represents an important step forward, with respect to present regulations, it is in fact a rather comprehensive document which considers many of the complex problems involved in seismic response of bridges subjected to intense seismic shaking. In the last years, many numerical

and experimental studies have been presented on the effectiveness of the provisions contained in EC8 [15]. The authors of the present paper presented first experimental results on EC8 bridges at 11th WCEE [7]: two continuous deck bridges designed to EC8, one regular and the other irregular, have been subjected to pseudodynamic tests on specimen scaled 1:6, with extensive use of substructuring technique. In the present paper those results are presented with a comparisons to results relative to laboratory tests carried out on the same two bridges designed to Italian seismic regulations [13].

Testing apparatus was set up in house and a software for instrumentation control and numerical integration was purposely developed [2, 16]. The pseudodynamic test method allows to perform tests on large structural elements, because the masses involved are numerically simulated and the strong reactions are easily carried by static actuators. Huge dimensions of bridges imply that their scaled model still represent structures of considerable dimensions. Though scale reduction problems are easily handled from a theoretical point of view [1], the crude application of theory can give rise to serious practical problems which complicate the RC specimen fabrication. Moreover, past studies showed that some parameters, such as steel-concrete bond, are hardly controlled and, if not properly scaled, could significantly distort the response. Therefore alternative scaling criteria for large structural elements to be experimentally tested, such as RC bridge piers are proposed. Similitude criteria between model and prototype are developed with respect to global quantities, such as: flexural and shear strength, confinement effect, post-elastic buckling and pull-out of rebars. This approach does not imply the "perfect" geometrical scaling of aggregate granulometry, reinforcing diameters and deformed bar shape and spacing, allowing the use of ordinary concrete mixing and commercial reinforcing bars.

Two bridges (one regular and one irregular) have been designed accordingly to EC8: design peak ground acceleration was 0.35 g, the structural behaviour factor was 3. The irregular bridge was subjected to 1976 Italian Tolmezzo E-W earthquake (PGA = 0.35 g), the regular one to 1995 Japanese Kobe-Kayou Weather Bureau N-S (PGA = 0.82 g). Preliminary numerical simulations showed that shorter piers of both bridges are expected to experience large inelastic deformation, while the remaining elements should remain in the elastic range. Six reduced models were manufactured, varying the number and the diameter of longitudinal bars and the spiral spacing, or adding a anchorage detail to improve bond-slip scaling accuracy.

Bridge performance of the irregular bridge was very satisfactory: significant deformation occurred in the tested pier, which anyway showed enough strength to cope with the imposed seismic action. High shear deformations, that is hardly predictable by analytical models, occurred. Comparison between models with and without special anchorage detail showed that the response was highly influenced by pull-out scaling. Also the regular bridge showed very small damages at the end of the test. In this case numerical models accurately predicted the response, that was mainly influenced by flexural behaviour. Test results suggested that bridges designed to EC8 had enough safety and low damageability. Perhaps less severe design parameters could pursue adequately safe structures at reduced cost.

Pier design was repeated with Italian seismic code. The last version of the code was upgraded in 1996. In this research, the previous version dated 1986 [13] was adopted, due to the interest

in the behaviour of bridges constructed in the 80's. In fact, their reference code was very similar to the 1986 version. Large differences between Italian and Eurocode, in case of irregular bridges, both for longitudinal and transversal reinforcements, were observed. For regular bridges the same longitudinal reinforcement was obtained, with a lower percentage of transverse one.

Italian piers have been tested with the same accelerograms and cyclic load history of the Eurocode ones. The regular bridge essentially had a god behaviour, similar to the EC8 one, while the irregular one had a poorer response with substantial reduction in energy dissipation and larger damages.

2. DESIGN OF THE BRIDGES

2.1 EC8 Bridges

The reference Codes were Eurocode 8 Part 1 [9] and Eurocode 8 Part 2 [10] for the design of bridges in seismic areas, Eurocode 2 [8] for the general rules on concrete structures. Figure 1 shows both regular and irregular bridge geometry, with continuous box deck hinged on the cantilever circular section piers and on the abutments. The elastic response spectrum was assumed to have 0.35 g peak ground acceleration. The behaviour factor was 3 for horizontal and 1 for vertical component of input motion. Materials characteristics were: pier concrete strength 25 N/mm^2, steel yielding stress 500 N/mm^2. Deck self weight and dead load was 200 KN/m. Elastic stiffness of the deck was calculated on the basis of the gross section; for piers the stiffness of the cracked section (one half that of the gross) was assumed. Figure 2 shows the central pier of irregular bridge and the lateral piers of regular one, experimentally tested.

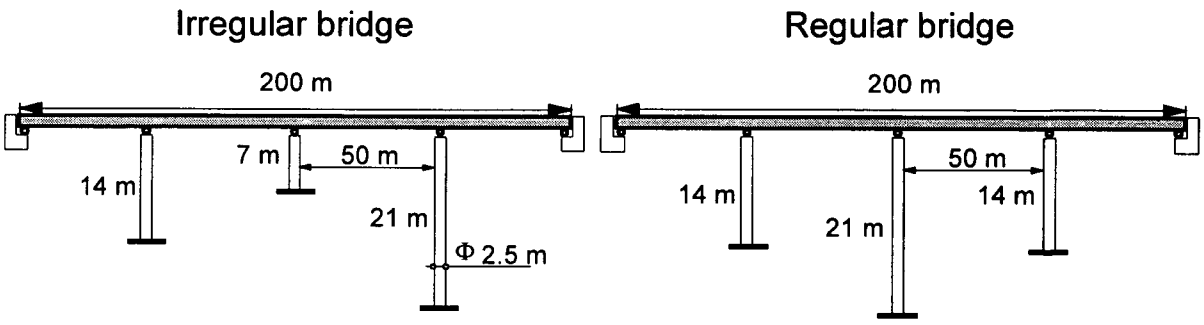

Fig. 1: Layout of designed bridges

2.1.1 Irregular Bridge

First mode of the structure had a period of about 0.7 s. Reinforcing details of the central pier are reported in Fig. 2a. While for lateral piers the minimum longitudinal reinforcement (0.8% of the gross section) was sufficient, for the central 3.5% of the gross section was required. For the latter, capacity design prescribed a dense spiral to avoid shear failure. For construction simplicity such transversal reinforcement was continued in a short part outside the plastic hinge.

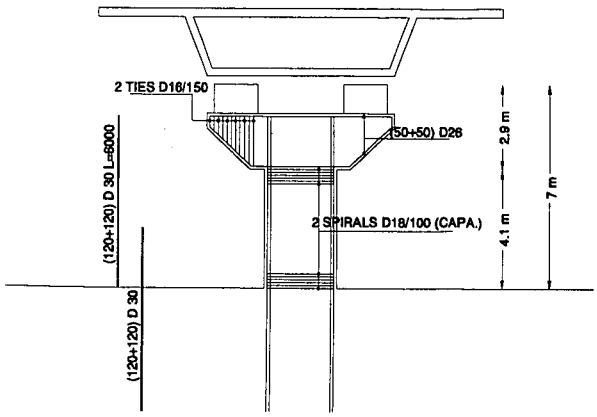

Fig. 2a: EC8 irregular bridge central pier: rebars arrangement (mm)

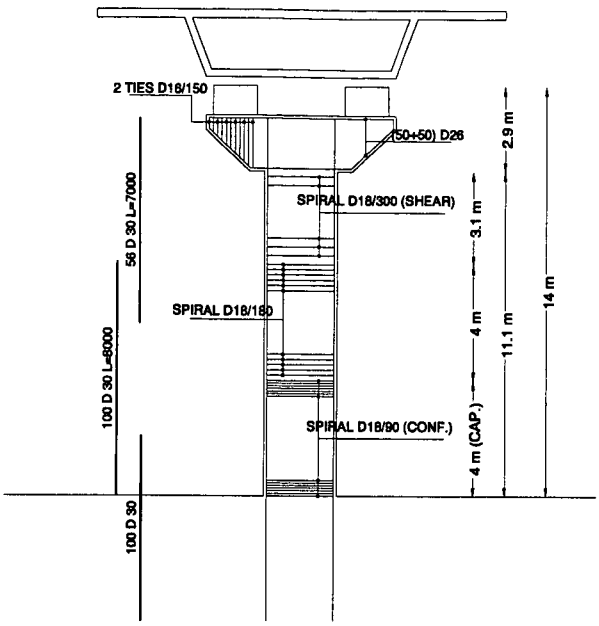

Fig. 2b: EC8 regular bridge lateral pier: rebars arrangement (mm)

2.1.2 Regular Bridge

First mode of the structure, based on cracked section geometrical characteristics as requested by the code, had a period of about 1.3 s. Reinforcing details of the lateral piers are reported in Fig. 2b. Minimum longitudinal reinforcement was sufficient for the central pier; for the lateral one was required a 1.5% of the gross section. In all piers transversal reinforcements at the base were due to confinement effect; outside plastic hinge they were determined by shear verifications.

2.2 Italian Bridges

The reference Code was [13] for the design of bridges in seismic areas, [14] for the general rules on concrete structures. Both regular and irregular bridge geometry are depicted in Fig. 1. The design spectrum which gives forces for the design at allowable stresses has a constant intensity 0.1 g peak from 0.0 to 0.8 s. Allowable stresses in steel is about 1.5 times the ultimate one. Materials characteristics, deck self weight and dead load were the same of EC8 bridges. Elastic stiffness of the deck and of the piers was calculated on the basis of the gross sections, as usually adopted by structural designers.

2.2.1 Irregular Bridge

First mode of the structure, based on gross section characteristics, had a period of about 0.5 s. While for lateral piers the minimum longitudinal reinforcement (0.35% of the gross section) was sufficient, for the central 0.86% of the gross section was required. Minimum transversal

reinforcement was sufficient for all piers. Reinforcing details of the piers, compared with EC8 ones, are reported in the following table. One can note that only 25% of EC8 longitudinal reinforcement is needed, and 8.8% of transverse one.

	Longitudinal reinforcement			Transversal reinforcement		
	Pier H=14	Pier H=7	Pier H=21	Pier H=14	Pier H=7	Pier H=21
Eurocode 8	56 D30	(120+120) D30	56 D30	D18/90-180-300	2 D18/100	D18/90-180-300
Italian code	24 D30	60 D30	24 D30	D12/250	D12/250	D12/250

2.2.2 Regular Bridge

First mode of the structure, based on gross section, had a period of about 0.9 s. For central pier longitudinal reinforcement 0.72% of the gross section was required, for the lateral ones 1.44% of the gross section was required. Minimum transversal reinforcement was sufficient for all piers. Reinforcing details of the piers, compared with EC8 ones, are reported in the following table. One can see that while piers have the same longitudinal reinforcement, transverse reinforcement varies from 10% in the lower part of the pier to 50% in the current section.

	Longitudinal reinforcement		Transversal reinforcement	
	Pier H=14	Pier H=21	Pier H=14	Pier H=21
Eurocode 8	100-56 D30	56 D30	D18/90-180-300	D18/90-180-300
Italian code	100-32 D30	50-24 D30	D12/250	D12/250

3. SCALING CRITERIA (from[7])

Because of the laboratory hardware limitations, piers were scaled 1:6. Classical scaling [11] consists in a rigorous geometrical reduction of both concrete and rebars dimensions. That implies the need of microconcrete and steel wires annealed (for yielding) and threaded (for bond-slip).

However, the behaviour of microconcrete and treated steel was often found to be different from that of original materials. The great number of longitudinal bars and the small spacing between transversal ones (Fig. 2), highlight the difficulties of fabrication arising from that approach.

The alternative scaling criteria here adopted [3, 4] permitted the use of ordinary concrete and commercial rebars. Given the geometrical scale factor (l_r) and the longitudinal bar scale factor (ϕ_r), the similitude of prototype (index p) and model (index m) global quantities leaded to remaining scaling factors. Longitudinal bar number (N) is given from the similitude of the resisting moments (M_u), corresponding to the stress σ_s in the extreme bar:

$$M_u^{(p)} = \frac{\psi D^{(p)} N^{(p)} \pi \phi^{(p)2} \sigma_s}{4} = \frac{M_u^{(m)}}{l_r^3} = \frac{\psi l_r D^{(p)} N^{(m)} \pi \phi_r^2 \phi^{(p)2} \sigma_s}{4 l_r^3} \qquad (1)$$

(where $D^{(p)}$ is the pier section diameter, σ_s is the steel stress and ψ is a non dimensional factor that accounts for section form and longitudinal bar disposition),

$$N^{(m)} = \frac{l_r^2 N^{(p)}}{\phi_r^2} \qquad (2)$$

Spiral spacing (i) is given from similitude of post-elastic buckling of rebars, spiral diameter (ϕ_t) from similitude of shear strength and confinement effect, anchorage length (L) from similitude of concrete-steel bond:

$$i^{(m)} = \phi_r i^{(p)} \qquad \phi_t^{(m)} = \phi_t^{(p)} \sqrt{l_r \phi_r} \qquad L^{(m)} = \frac{L^{(p)} \phi_r u_{1r}^{\alpha}}{\nu n_b q_{1r}^{\alpha} l_r^{\alpha}} \qquad (3,4,5)$$

To fulfil the latter requirement (u_{1r}, q_1 and α are parameters of the Filippu bond-slip model, whose values was obtained on the basis of experimental results published by Eligehausen, see [12]) with limited anchorage length for the longitudinal bar diameters to be used in the models, two bars were added laterally at each rebar through welding in the anchorage zone. In the formula $\nu = (3\ n_b + 1) / (4\ n_b)$ is a factor that takes in account the bond surface reduction due to bar proximity and welding (n_b=3 is the number of bars welded in parallel instead of the single bar).

3.1 EC8 Bridges

For the irregular bridge central pier 4 specimens were manufactured: specimen I71A was arranged with 42 12 mm diameter longitudinal bars and a 6 mm spiral 40 mm spaced with plain anchorage; specimen I72A was arranged with 24 16 mm diameter longitudinal bars and a 8 mm spiral 50 mm spaced with plain anchorage; specimen I71B and I72B had the same reinforcements of A specimen, but with the improved anchorage detail described before. Two specimens were manufactured of the regular bridge lateral piers: specimen R141A was arranged with 24 10 mm diameter longitudinal bars and a 5 mm spiral 30/60/100 mm spaced with plain anchorage (Fig 3a); specimen R141B had the same reinforcement but with improved anchorage (Fig. 3b).

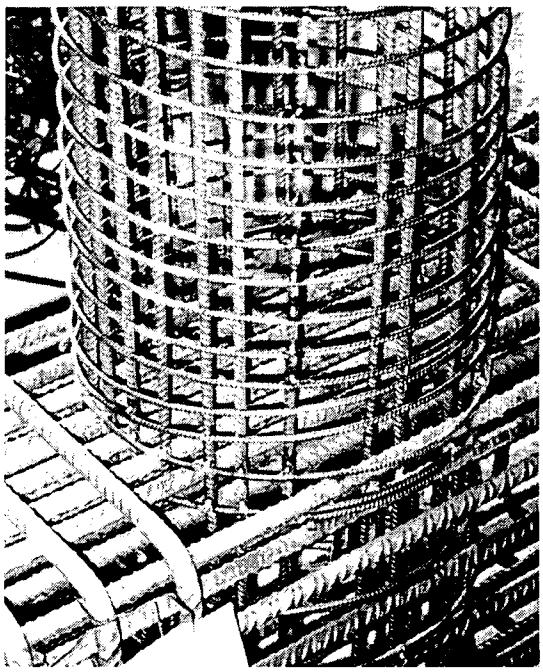

Fig. 3a: EC8 specimen reinforcement detail: plain anchorage

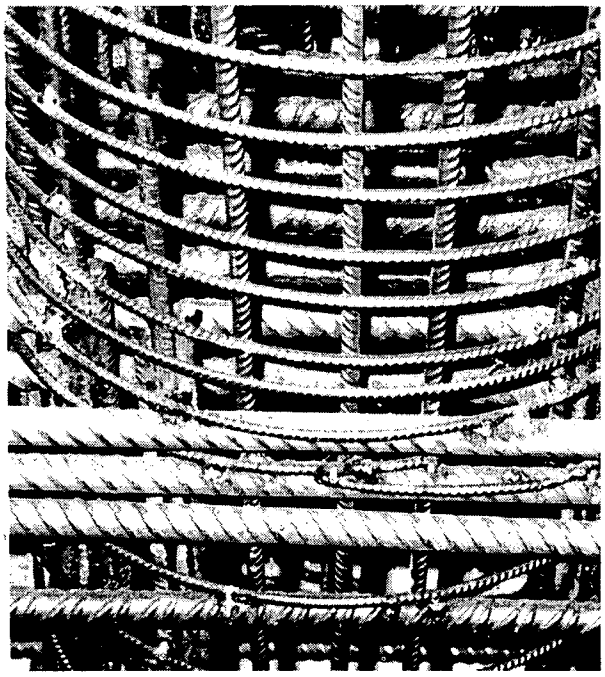

Fig. 3b: EC8 specimen reinforcement detail: improved anchorage

3.2 Italian Bridges

Four specimen of the piers were set up, two for each bridge. All specimen had to be prepared having the improved anchorage in the foundation. For the irregular bridge two specimen having the same reinforcement were prepared. Longitudinal reinforcement was given by 12 12mm bars, transverse reinforcement by circular stirrups, placed each 12 cm. However for an error during the construction phase one of the 7m (irregular bridge central pier) had the plain anchorage. For the regular bridge two specimen were prepared, scaled 1:6. Longitudinal reinforcement was given by 24 12mm diameter bars; in one case (specimen IR14BN2) there was a lap splice at the base of the column, having an overlapping of 40 bar diameters, in one specimen (specimen IR14AN2) there was no lap splice. Transverse reinforcement was given by spiral having 6 mm with a pitch of 12 cm.

4. TEST SEISMIC INPUT

4.1 Irregular Bridge

Elastic response spectra with 5% damping of about 100 Italian accelerograms were compared in the period range (0.5-0.8 s), where the first mode of the structure falls. Tolmezzo (E-W) accelerogram from 1976 earthquake with 0.35 g peak ground acceleration resulted the most severe for the bridge.

4.2 Regular Bridge

Two different registrations: Kobe-Kayou Weather Bureau E-W (PGA=0.82 g) and Amagasaki elevated bridge N-W (PGA=0.35 g), from Great Hansin Earthquake of 1-17-1995, were

suitable. By numerical preliminary simulations (Fig. 5) the latter resulted as the most severe and adopted. The differences between design and test action can be appreciated in Fig. 4. Elastic 5% damping response spectra of Tolmezzo, Kobe-Kayou, Amagasaki and EC8 design spectrum reduced by three behaviour factors: 1, 1.7, 3 are shown. The value 1.7 corresponds to the effective reduction resulting from the following effects: 2% damping adopted instead of 5%; design horizontal components, which acted simultaneously in two directions in the design, while only one transversal component was applied in the test; material's mean strengths, that exceeded design ones.

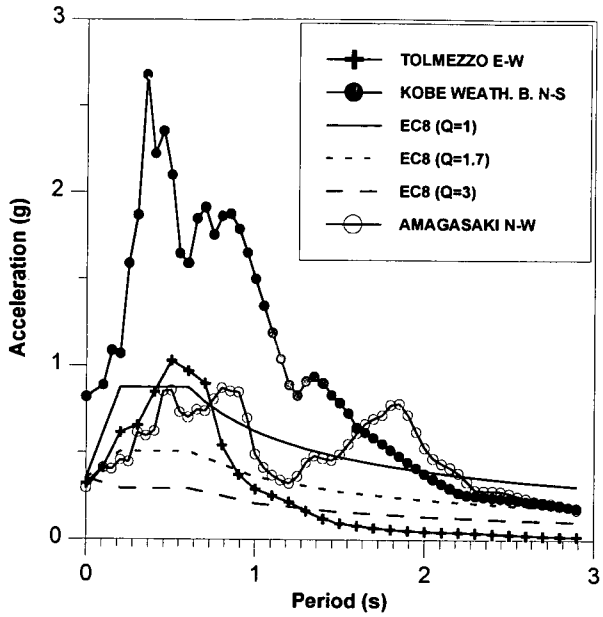

Fig. 4: Natural earthquakes and EC8 spectrum design

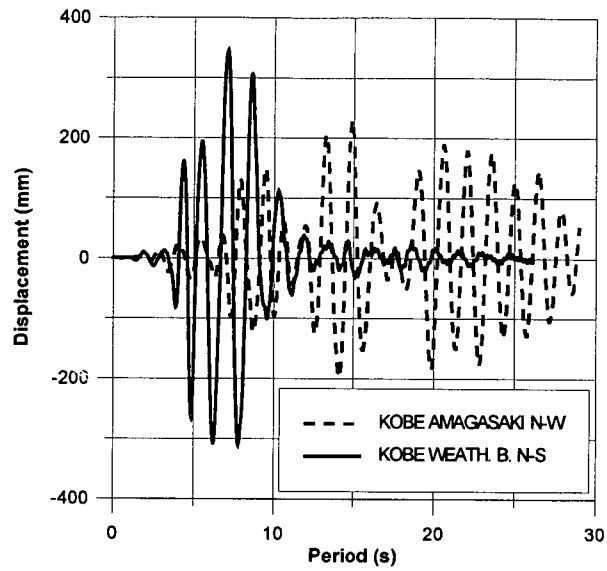

Fig. 5: EC8 regular bridge: numerical simulations response with Kobe earthquake registrations

5. RESULTS

5.1 EC8 Bridges

5.1.1 Irregular Bridge

Four tests were carried for each of the four specimens: preliminary free vibrations, Tolmezzo pseudodynamic, Tolmezzo scaled to 0.7 g pseudodynamic, static cyclic until failure. Results are reported in prototype scale. Tested concrete strength was about the same of the design, steel yielding varied from 500 to 600 MPa, therefore greater than the design one [5, 7].

Specimens having same type of anchorage but different bar diameter: I71A and I72A (plain anchorage), I71B and I72B (special anchorage) behaved in very similar manner. This results validated the reinforcement scaling criteria. Instead specimen I71A versus I71B and I72A versus I72B (same reinf. different anchorage) behaved very differently. Low intensity free vibrations tests in the elastic range showed the same secant stiffness, equal to 70% of that of the gross section, for both plain and special anchorage. Secant stiffness in high intensity elastic free vibrations was respectively 34% for plain anchorage and 50% for special.

In pseudodynamic tests, lateral piers behaved elastically, therefore in the following only central pier response will be described. As shown in Fig. 6, top displacement in A and B piers from 0 to 4 s, was nearly the same and elastic; from 4 to 5 s, 4 high amplitude (more than 80 mm) cycles were obtained; the following semicycles until 6.5 s were still large for special anchorage, while decreasing for plain. In the last 4.5 s, amplitude decreased for special and remained the same for plain. At the end both specimens showed low damages, whit 45° cracking on the whole height, due to intense shear effect. The dissipated energy was higher in special anchorage specimen: at any cycle (Fig 8) and the total (Fig.7), B dissipated twice than A .

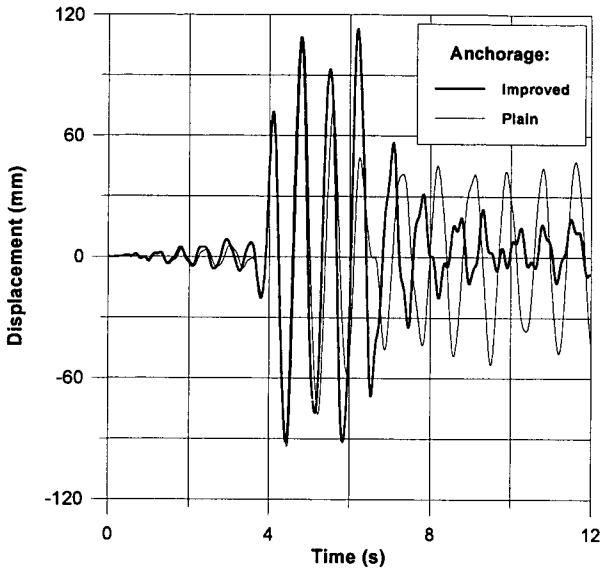

Fig. 6 : EC8 irregular bridge central pier: pseudodynamic test with Tolmezzo - displacement time history

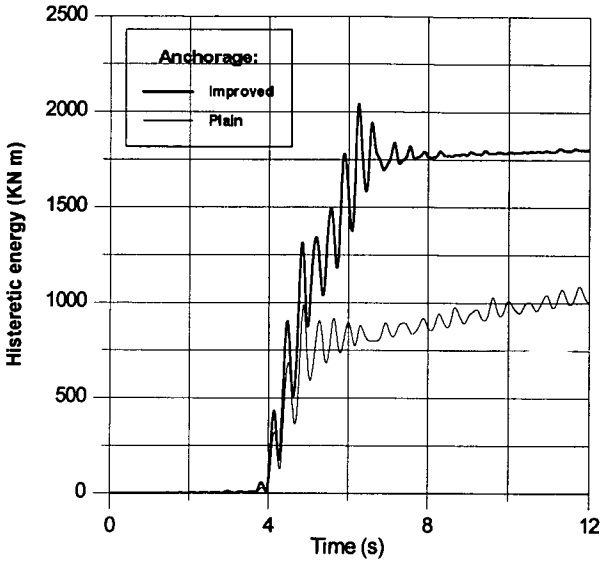

Fig. 7 : EC8 irregular bridge central pier: pseudodynamic test with Tolmezzo - dissipated energy time history

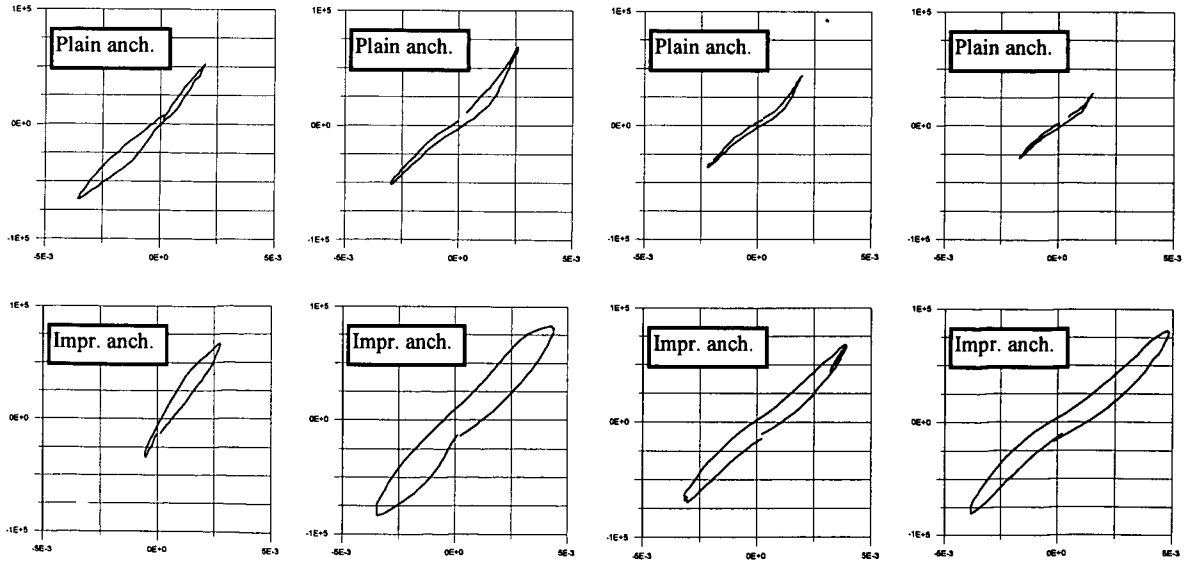

Fig. 8: EC8 irregular bridge central pier - pseudodynamic test with Tolmezzo: Moment (KNm)-Curvature (1/m) cycles from 4 to 6.5 s

Displacements due to flexure only were computed by integrating curvatures on the height, the contribution due to shear was then derived by difference from the total. Displacement due to shear was about 50% of the total (Fig. 9). This explains why preliminary numerical simulations, based on flexural models, leaded to smaller maximum displacements (the abrupt change of slope at zero displacement is due to the fact that in the abscissa the steps of data acquisition are given, which are not constant in time and to some gap in the instrumentation).

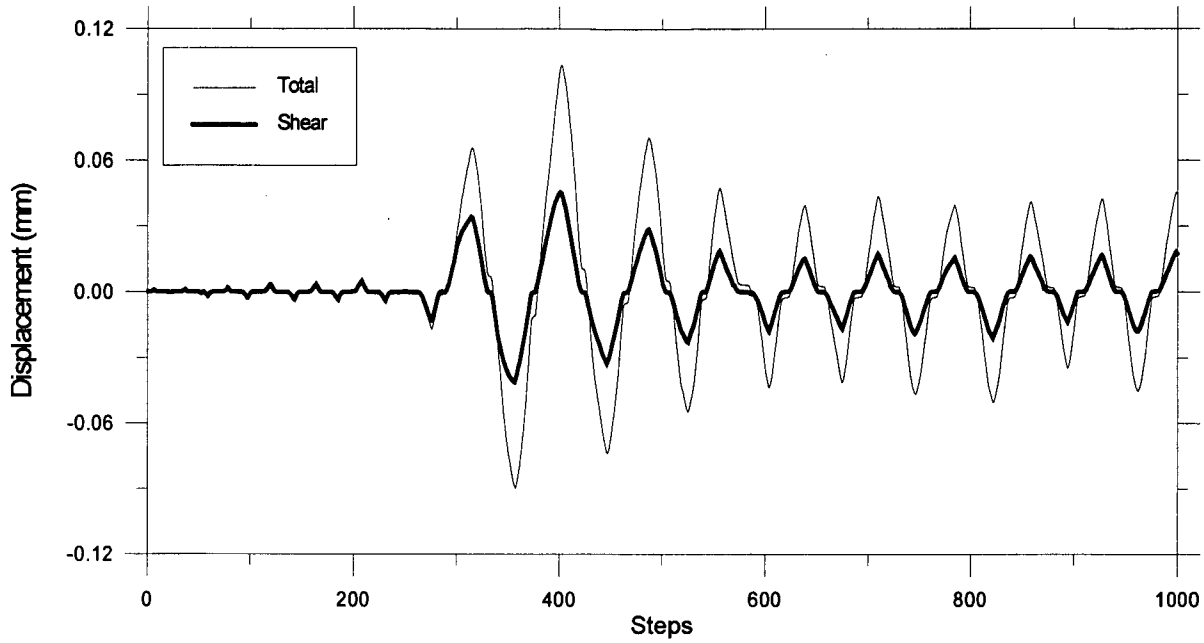

Fig. 9: EC8 irregular bridge central pier with improved anchorage: evaluation of displacements due to shear and flexure.

In the following test, scaled to 0.7 g, smaller differences between A and B specimen have been obtained. Maximum displacement was 0.18 m (at prototype scale) and very limited final damage. In static cyclic tests, collapse was reached due to spiral failure immediately followed by longitudinal rebar buckling and breakage.

5.1.2 Regular Bridge

Two tests were carried for each of the two specimens: preliminary free vibrations and Kobe Kayou pseudodynamic. Results are reported in prototype scale [6]. R141A and R141B (same reinforcement and different anchorage) behaved not very differently. In fact pull-out is less important for slender piers than for squat ones, therefore accurate reproduction is not necessary.

In pseudodynamic tests, central piers remained in the elastic field. Figure 10 shows time history on the top of the lateral pier. Numerical preliminary simulation, shown in Fig. 5, was very similar to experimental results. In fact no shear deformations appeared, and the numerical model which only accounts for bending is therefore accurate. Significant amplitude cycles (150 to 300 mm) were from 4 to 16 s. In Fig. 11 the total force-displacement history is reported. Maximum attained ductility was about 4, greater than the ratio of Kobe and EC8

(q=1.7) spectral ordinate at 1.3 s period which is about 3. At the end both specimens were only slightly damaged, with an incoming crushing of the cover. However, the increase of the bridge period indicated some damage of rebars. The good performance of the pier essentially depended on transversal reinforcement that gave sufficient concrete confinement and avoided buckling of rebars.

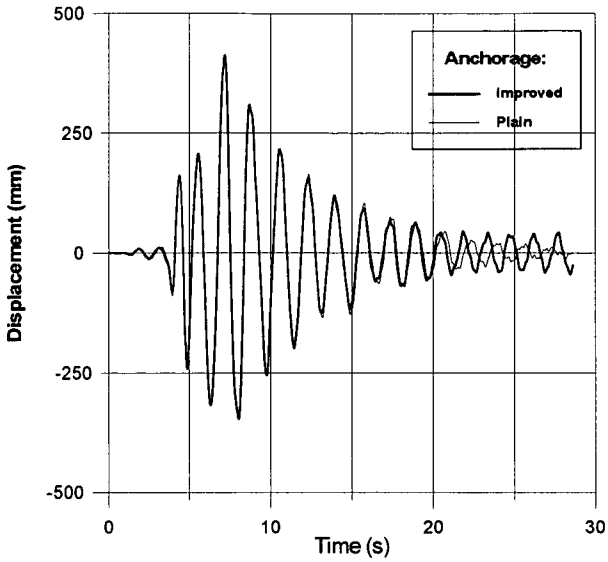

Fig. 10: EC8 regular bridge central pier - pseudodynamic test with Kobe - displ. time history

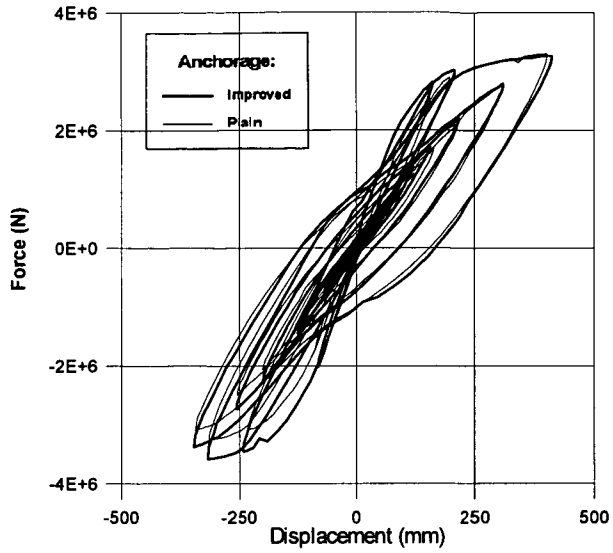

Fig. 11: EC8 regular bridge central pier- pseudodynamic test with Kobe - Force-Displacement cycles

5.2 Italian Bridges

Only preliminary results can be given in the present paper. At the moment results are in fact available only for the irregular bridge with plain anchorage and for the regular without lap splices at the base.

5.2.1 Irregular Bridge

Free vibration response at small amplitude is shown in Fig. 12. The period of vibration of Italian bridge is about 0.8 seconds, while the EC8 has a period of about 0.4 seconds. The long period of the Italian bridge is strongly influenced by the anchorage in the foundation which is not properly scaled. In Fig. 13 force displacement diagrams are given together with the corresponding EC8 piers, in case of plain anchorage. One can see that the ratio between Italian and EC8 stiffness of the column is about 0.4. Part of this difference is due to the inaccurate anchorage scaling, while must be recalled that the Italian bridge has only 25% of the reinforcement of EC8 bridge. Total inertia of the section can be obtained summating the concrete section inertia to that of rebars:

$$J_{tot} = J_c + 2 \cdot \frac{E_r}{E_c} \cdot \rho \cdot J_{gross}$$

being $E_{r,c}$ the moduli of reinforcement and of concrete, ρ geometrical reinforcement ratio, J_c the inertia of the concrete section, J_{gross} the inertia of the gross section; this contribution becomes significant for the EC8 pier where $\rho = 0.035$. For example, if the cracked concrete section inertia has the value $J_c = 0.5\ J_{gross}$, the aforesaid ratio become 0.56.

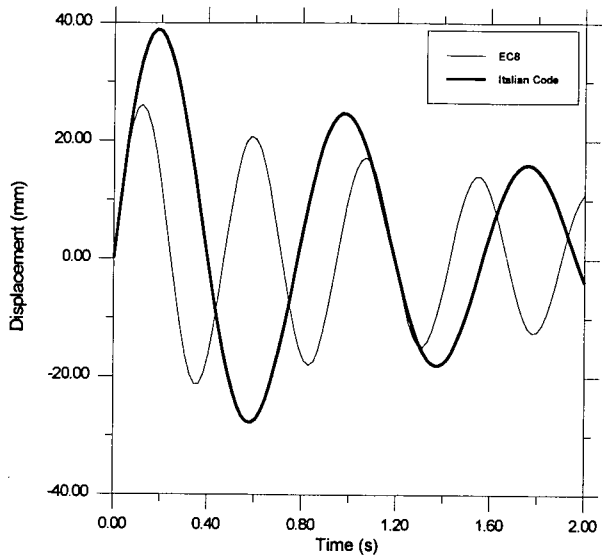

Fig. 12: EC8 and Italian irregular bridge central pier - free oscillations - displ. time history

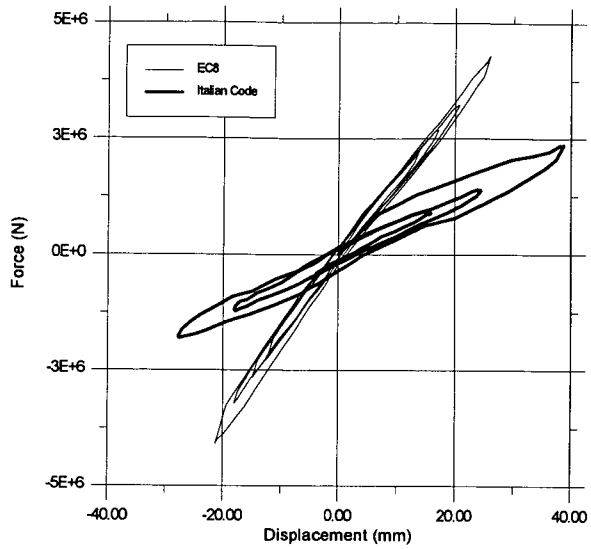

Fig. 13: EC8 and Italian irregular bridge central pier - free oscillations - Force-Displacement cycles

The response history to Tolmezzo accelerogram is shown in Fig 14. In the same the response of the EC8 bridge having plain anchorage is shown. In Fig. 15 the response in terms of Force Displacement is given. One can see that the reduction of the secant stiffness with respect to the EC8 bridge is obviously larger at large displacements with respect to the elastic free oscillations. Dissipation is substantially smaller, as one can see in Fig 16, in fact the only pier which undergo into the plastic range is the central, which has a resistance of approximately 25% of the corresponding EC8 case, while total energy of the bridge is similar, due to the fact that the remaining part of the structure remains elastic. This fact makes the ratio between elastic energy of the bridge and dissipated smaller in the Italian case, therefore at the end of the strong part of seismic shacking the structure still undergoes to large displacements. It is well evident from Fig. 14 that the structure suffers of a greater number large non linear cycles than EC8 one.

With reference to cracking pattern, there is a substantial difference with respect to EC8 structure. In this case in fact, due to smaller flexural strength, the shear force is reduced proportionally to about one fourth of the EC8 column. There is a large diagonal crack at the base of the structure. This originates as soon as concrete section tends to be overcome at the edge of the section due to flexure. The crack has a considerable inclination due to the presence of shear, but no other cracks appear in the column Therefore while in EC8 structure a substantial contribution to total displacement was given by crack opening due to shear along the entire pier, in the Italian Bridge plastic distortion is concentrated in the cracked base section.

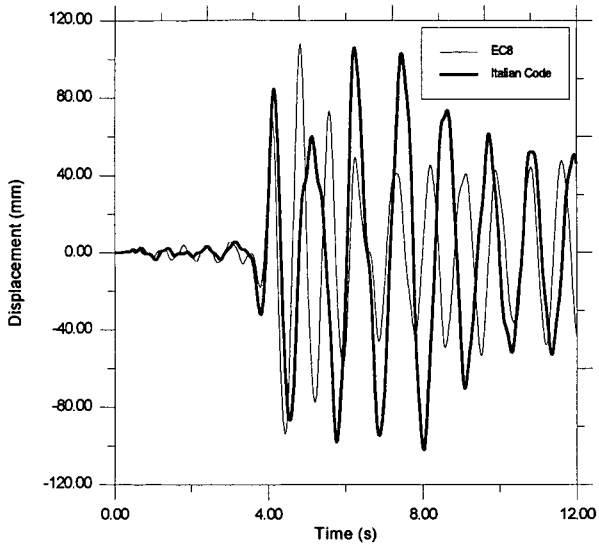

Fig. 14: EC8 and Italian irregular bridge central pier - test with Tolmezzo PGA=0.35g displacements time history

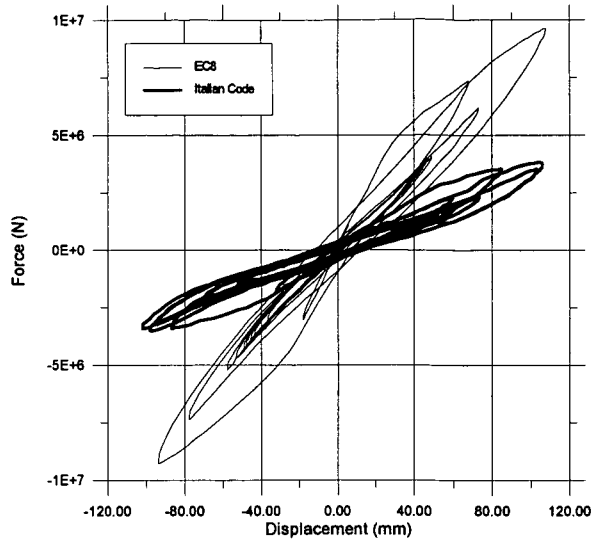

Fig. 15: EC8 and Italian irregular bridge central pier - test with Tolmezzo PGA=0.35g Force-Displacement cycles

The response at 0.7g is shown in fig 17. For this intensity the structure has a larger response than EC8, damages become relevant, while in the EC8 one they were extremely reduced, however the structure survives the earthquake.

Failure of the column has been obtained through a cyclic load history. This is essentially due to buckling of longitudinal bars. Substantial degradation appeared in the high amplitude cycles, due to buckling of rebars not adequately restrained. Instead, no degradation appeared in the EC8 plain anchorage case, where in fact buckling could not happen due to the small stirrup spacing.

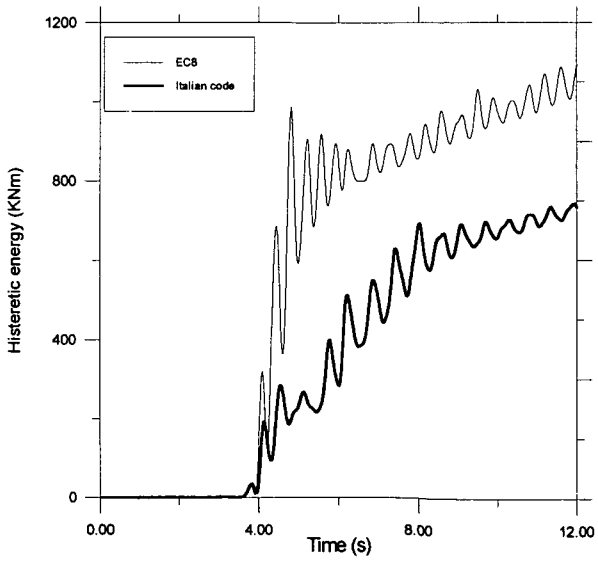

Fig. 16: EC8 and Italian irregular bridge central pier: test with Tolmezzo PGA=0.35g dissipated energy time history

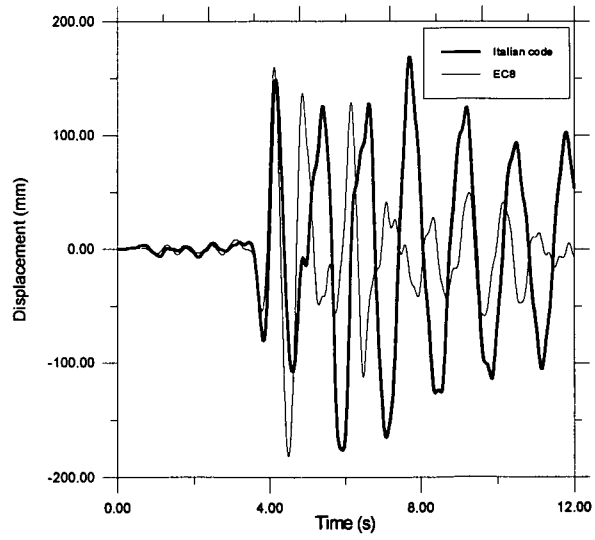

Fig. 17: EC8 and Italian irregular bridge central pier - test with Tolmezzo PGA=0.7g displacements time history

5.2.2 Regular Bridge

Figure 18 shows free oscillation time history of the regular bridge. One can see that curves are quite coincident with EC8 bridge, in fact the two structure have the same longitudinal reinforcement, the only contributing to elastic response. The period of vibration is 1.3 seconds.

In Fig. 19 the pseudodynamic response to Kobe accelerogram is shown, compared to the EC8 case. It is clear that seismic response is quite coincident, though the final stiffness is reduced with respect to EC8. This latter difference may depend from a larger degradation of the Italian specimen, having less transverse reinforcement, but could also depend from the inevitable scatter that specimen can usually exhibit due to manufacture, material characteristics and so on. It should be observed in fact that the quality of the manufacture of this Italian specimen is lower than for the EC8 one. It is therefore difficult to conclude that the difference should depend on smaller transverse reinforcement ratio and larger stirrup spacing. However it has been observed in cyclic loading to failure that at large ductility demand longitudinal bars buckle, and a large spalling of concrete cover happens.

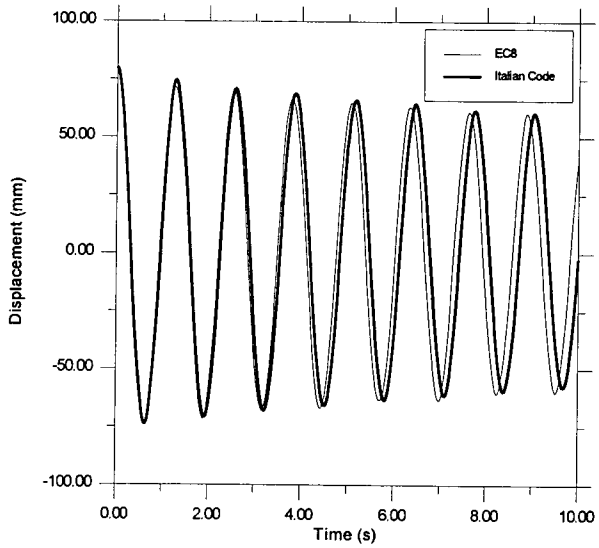

Fig. 18: EC8 and Italian regular bridge lateral pier - free oscillations displacements. time ' 'story

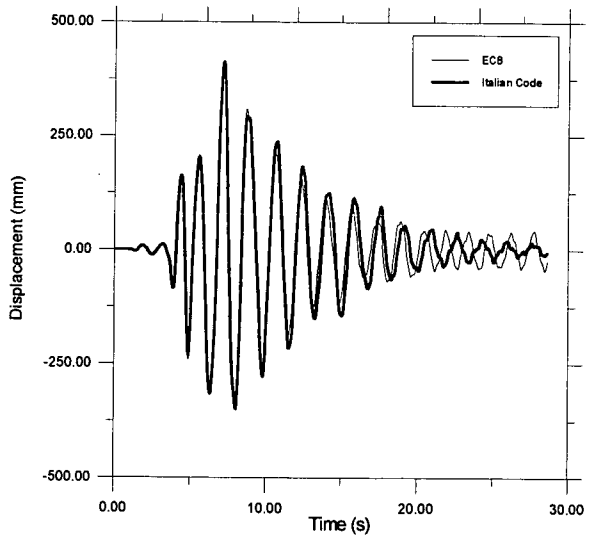

Fig. 19: EC8 and Italian regular bridge lateral pier - pseudodynamic test with Kobe displacements. time history

6. CONCLUSIONS

Results have been presented concerning continuous deck r.c. bridges designed to EC8.2 and preliminary results concerning bridges designed to Italian Seismic Code before 1986.

EC8.2 provides a large capability to undergo inelastic deformations with limited damage. This is essentially due to capacity design and small pitch of confining spiral. However possible simplifications with less stringent requirements could probably lead to adequate performances and should be investigated.

The preliminary results discussed for Italian Code designed bridges showed acceptable performances for regular bridges, similar to the EC8 one. On the contrary in case of strongly irregular ones the behaviour is less satisfactory. Large ductility can be required, and the structure shows a sensible degradation in cyclic response.

Accurate scaling of anchorage in the foundation is of large importance to obtain meaningful results in tests, especially in squat piers.

Shear deformation represents an important contribution to the total and strongly reduces the stiffness of squat piers. This fact can produce positive effects on structural behaviour, in fact it reduces structural irregularity.

One should be aware that continuous deck usually has a positive influence to structural response. The results relative to Italian Bridge represent an upper bound of good behaviour, in fact the quality of r.c. bridges from seismic design point of view is usually lower than the one here realised. For example old bridges do not have continuous deck, but simply supported beams.

Finally, results concerning Italian Code bridges are now under elaboration. Those here presented refer to structures in which longitudinal reinforcement anchorage in the foundation is not properly scaled This fact is not very effective for the slender structure: the lateral pier of the regular bridge, however it can be important for the irregular one. For this latter, as for the companion EC8 case, larger degradation are expected for the squat pier causing possible problems. The problem of lap splicing in the plastic hinge zone will be investigated and presented.

ACKNOWLEDGEMENTS

The pseudodynamic equipment was partially purchased under the grant of the Università "G. D'Annunzio", Pescara.

Special tanks to Mr. V. La Mesa, who carried out pseudodynamic tests at Università "La Sapienza", Roma.

Tests on the Italian Bridge have been funded by European Community (CEE Contract EV5V-CT93-0297, Environment Program, DGXII).

REFERENCES

[1] Buckingham E. (1914). On physically similar systems; illustrations of the use of dimensional equations, *Phys. Review*, **4**, 345-376.

[2] Colangelo, F. and A. De Sortis (1994). *Esperimenti Pseudodinamici: Studio Preliminare e Realizzazione su Sistemi ad un grado di libertà.* Rapporto n. 1/94, Dip. Ing. Str. Acque e Terr., Univ. dell'Aquila, Italia.

[3] De Sortis, A., G. Monti and C. Nuti (1994). Problemi di scala nella sperimentazione pseudodinamica di pile da ponte in c.a. In: *Atti del Worksop su Danneggiamento, Prove Cicliche e Pseudodinamica*, Dip. Analisi e Prog. Str., Università "Federico II", Napoli, Italia.

[4] De Sortis, A. (1995). *Sperimentazione Pseudodinamica e Modellazione in Scala Ridotta del Comportamento dei Ponti in Calcestruzzo Armato Soggetti ad Azioni Sismiche*. Tesi di dottorato di ricerca, Dip. Ing. Str. e Geot., Università "La Sapienza", Roma, Italia.

[5] De Sortis, A., G. Monti and C. Nuti (1995). Comportamento sismico di ponti progettati secondo Eurocodice e sottoposti a prove pseudodinamiche in scala ridotta. In: *Atti del 7° Conv. Naz. Ing. Sismica*, Siena, Italia

[6] De Sortis, A. and C. Nuti (1995). Prova pseudodinamica di un ponte progettato con EC8.2 e sottoposto al terremoto di Kobe del 1995. In: *Atti del 7° Conv. Naz. Ing. Sismica*, Siena, Italia.

[7] De Sortis, A. and C. Nuti (1996). Seismic response by pseudodynamic tests of RC bridges designed to EC8. In: *Proc. 11th World Conf. on Earthq. Eng.*, Acapulco, Mexico.

[8] Eurocode 2, Design of Concrete Structures, Part 1: General Rules and Rules for Buildings (1991).

[9] Eurocode 8, Structures in Seismic Zones, Design, Part 1: General Part and Buildings (1993).

[10] Eurocode 8, Structures in Seismic Zones, Design, Part 2: Bridges (1993).

[11] Krawinkler, H. and P.D. Moncarz, Similitude requirements for dynamic models (1982). In: *Dynamical Modeling of Concrete Structures*, Ch. SP73-1, A.C.I., U.S.A.

[12] Monti, G. (1994). *Modellazione agli Elementi Finiti di Nodi Trave-Pilastro in Cemento Armato con Scorrimento delle Barre di Armatura*. Tesi di dottorato di ricerca, Dip. Ing. Str. e Geot., Università "La Sapienza", Roma, Italia.

[13] Norme tecniche per le costruzioni in zone sismiche (1986), D.Min. LL.PP. 24/1/86

[14] Norme tecniche per l'esecuzione delle opere in cemento armato normale e precompresso e per le strutture metalliche (1992), D.Min. LL.PP. 14/2/92

[15] Nuti, C. and G. Monti (1994). Seismic Analysis of Bridges, a state of the art. In: *Proc. of 10th Eur. Conf. on Earth. Eng.*, Vienna, Austria.

[16] Shing, P.B., M.T. Vannan and E. Cater (1991). Implicit time integration for pseudodynamic tests. *Earth. Eng. Str. Dyn.*, **20**, 551-576.

Session 4

Topic 4 Design and Case Studies

New Approach for Bearings and Falling-off Prevention Systems of Highway Bridges

M.Kanda[1], K.Nishikawa[2]

1)Senior Research Engineer, Bridge Division, Public Works Research Institute, Ministry of Construction, Tsukuba Science City, Ibaraki-ken, Japan, 305

2)Head, Bridge Division, Public Works Research Institute, Ministry of Construction, Tsukuba Science City, Ibaraki-ken, Japan, 305

ABSTRACT

Bearings and falling-off prevention devices have suffered severe damage in the Hyogo-ken Nanbu Earthquake, and great deal of knowledge was gained by the studies on this disaster. Since the damage of bearing supports and falling-off prevention devices was the result of the design method of the former Specifications of Highway Bridges, it was necessary to amend the specifications about them. To develop the new concept on bearing supports and falling-off prevention systems, it was significant to be started from the facts, that is, damage itself. Data is analyzed in detail, and knowledge gained by investigations has been utilized to make up a new concept and new specifications.

INTRODUCTION

In Hyogo-Ken-Nanbu Earthquake which occurred on January 17, 1995, many highway bridges suffered a lot of damage. The Bearings and falling-off prevention devices of the bridges have also suffered various kinds of damage and destruction, which caused not only the possibility of falling-off of superstructures but obstacles against the traffic and the emergency restoration after the Earthquake. Although the guidelines of design methods for these structures had been indicated in "Specifications for Highway Bridges (Japan Road Association)" before, many criteria and methods of design were amended after the Earthquake based on the knowledge gained from the experience of this time, and the new Specifications have been published at the end of 1996.

Right after the Earthquake "Guide Specifications for Reconstruction and Repair of Highway Bridges which Suffered Damage due to the Hyogo-ken Nanbu Earthquake(Draft)" was issued on February 27, 1995, and "Reference for Applying 'Guide Specifications' to New Highway Bridges and Seismic Strengthening of Existing Highway Bridges" was published on June 30. On the other hand, a number of investigations and researches have been conducted about the seismic performance of highway bridges. Referring to the

knowledge and result of these studies, the Specifications were notified by the Ministry of Construction on November 1, 1996. "Specifications for Highway Bridges" consists of five parts, which are Ⅰ:Common Specifications, Ⅱ:Steel Bridges, Ⅲ:Concrete Bridges, Ⅳ:Substructures, Ⅴ:Seismic Design. In this paper, the detail of the investigation and the sequence of amendment of part V, specially about bearings and falling-off prevention systems, are reported here.

1.Damage of Bearings and falling-off prevention devices in the Hyogo-ken Nanbu Earthquake

At the Hyogo-ken Nanbu Earthquake, many bearings and falling-off prevention devices suffered damage more widely than at any earthquake which had occurred in Japan before. Therefore, in amending of the specifications for bearings and falling-off prevention devices, the first thing that should be done was collecting the detail information and the data of damage, destruction and collapse of these structures and analyzing them carefully and with no prejudice. One of the most important things for this case is that the investigation on the specifications we should be started from the recognition of the facts themselves. In other words, problems should be clarified from the point of facts, not from the assumption, for such a site-oriented issue. This is because there were a lot of facts about the actual force functioned to bearings and falling-off prevention devices caused by the Earthquake and damage form of these structures, which were found for the first time from the results of the investigations on the damage caused by the Earthquake.

First, the summary of damage of bearings and falling-off prevention devices are shown, as following.

(1)Damage to Bearings

The number of support lines of highway bridges which could be surveyed along all the damaged route of major highways, the National Highways and Expressways, was 5,741. Among these, 4,773 support lines were metal bearings, 244 were rubber bearings, and others were special bearings such as Mesnager hinges and rigid bearings.

Damage to bearings is classified into four patterns;

- Collapse or damage of connecting parts, such as breaking of set bolts and anchor bolts, deformation of sole plate, breaking away of shear keys, and damage to mortar of bearing seats
- Damage to body of bearings, such as breaking of pins of steel bearings, and breaking away of rollers
- Damage to stoppers for shifting of movable bearings

• Damage to surrounding superstructures and substructures around bearing supports

Table 1 Degree of Damage to Bearing Supports

Degree of Damage	Definition
A	Breaking of set bolts or anchor bolts Damage to sole plate or shear keys Destruction of concrete of bearing seats
B	Breaking of pins Breaking of stopper of upper shoe Breaking away of rollers and anchor bolts Destruction of mortar of bearing seats
C	Deformation of upper shoe or lower shoe Looseness of set bolts Deformation or cracks on stoppers for shifting of movable bearings Cracks of concrete or mortar of bearing seats Slight separation, displacement or deformation of rubber bearings
D	No damage or almost no damage

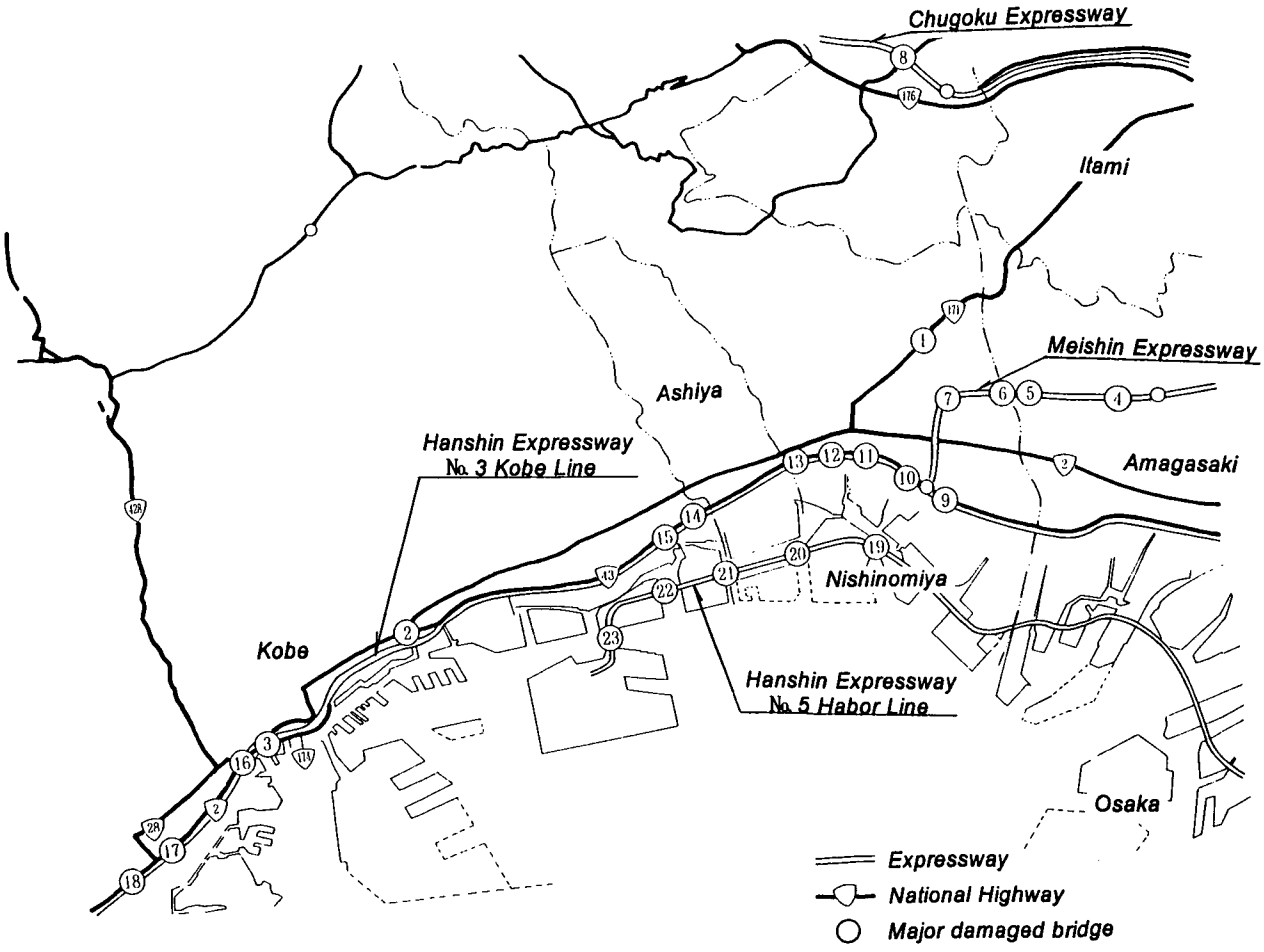

Fig. 1 Location of Major Highways in Kobe area

Table 1 shows the definition of the degree of damage to bearings. Fig.1 is the map of Kobe area, which shows the location of Expressways and major highways. Table 2 shows damage of bearings along each route by using damage degrees, where it is recognized that National Highway No.2, Meishin Expressway, and No.3 Kobe Line suffered remarkable damage. However, each route has it's own characteristics, for instance, ratio of degree B and C of Chugoku Expressway exceeds that of Hanshin Expressway, and, in the case of Hanshin Expressway the ratio of slight damage(degree C) of No.5 Harbor Line exceeds that of No.3 Kobe Line.

Table 2 Damage to Bearings of Major Highways

Unit:suppoort line

Name of Highway		Degree of Damage				
		A	B	C	D	Total
National Highway	No.2	63 (24)	10 (4)	2 (1)	190 (72)	265 (100)
	No.43	8 (3)	13 (4)	13 (4)	272 (89)	306 (100)
	No.171	6 (3)	5 (2)	16 (7)	195 (88)	222 (100)
	No.176	0 (0)	0 (0)	2 (4)	45 (96)	47 (100)
	Total	77 (9)	28 (3)	33 (4)	702 (84)	840 (100)
Japan Highway Corp. Expressway	Meishin	401 (28)	65 (4)	11 (1)	974 (67)	1,451 (100)
	Chugoku	112 (15)	174 (23)	85 (11)	377 (50)	748 (100)
	Total	513 (23)	239 (11)	96 (4)	1,351 (61)	2,199 (100)
Hanshin Expressway	No.3 Kobe Line	371 (17)	274 (13)	383 (18)	1,090 (51)	2,118 (100)
	No.5 Harbor Line	30 (5)	72 (12)	196 (34)	286 (49)	584 (100)
	Total	401 (15)	346 (13)	579 (21)	1,376 (51)	2,702 (100)
TOTAL		991 (17)	613 (11)	708 (12)	3,429 (60)	5,741 (100)

※ The number inside ( ) implies % of the ratio.

Table 3 shows the difference of damage level between metal bearings and rubber bearings, where it is obvious that damage to rubber bearings is notably light compared to metal bearings. As to metal bearings, ratios of degree A, B, and C are 21%, 13%, and 14%, respectively. On the other hand, ratios of degree A,B, and C of rubber bearings are only 0%, 2%, and 8%, respectively. Hence, it is surely rational to conclude that rubber bearings have better seismic performance than metal bearings.

Table 4 shows the situation of damage of various types of metal bearings and difference between fixed bearings and movable bearings. It is understood that, in the case of metal bearings, movable bearings tend to suffered damage more easily than fixed bearings and that the damage of pin bearings and roller bearings are comparatively high.

Table 3 Relationship between Material and Damage level of Bearings

Unit:suppoort line

Material of Bearing	Degree of Damage				Total
	A	B	C	D	
Steel Bearing	986(21)	603(13)	681(14)	2,503(52)	4,773(100)
Rubber Bearing	0(0)	6(2)	19(8)	219(90)	244(100)
Total	986(20)	609(12)	700(14)	2,772(54)	5,017(100)

※ The number inside ( ) implies % of the ratio.

Table 4 Damage of Steel Bearings According to Type of Bearing

(a)Fixed Bearing Support

Unit:suppoort line

Type of Bearing	Degree of Damage				Total
	A	B	C	D	
Base Plate	133(13)	146(14)	126(12)	634(61)	1,039(100)
Pin	86(34)	28(11)	23(9)	116(46)	253(100)
Pivot	12(12)	9(9)	45(44)	36(35)	102(100)
Line	32(9)	17(5)	55(15)	269(72)	373(100)
Total	263(15)	200(11)	249(14)	1,055(60)	1,767(100)

(b)Movable Bearing Support

Unit:suppoort line

Type of Bearing	Degree of Damage				Total
	A	B	C	D	
Base Plate	476(26)	239(13)	224(12)	909(49)	1,851(100)
Roller	238(30)	141(18)	152(19)	257(33)	788(100)
Line	6(2)	23(6)	56(15)	282(77)	367(100)
Total	723(24)	403(13)	432(14)	1,448(48)	3,006(100)

※ The number inside ( ) implies % of the ratio.

(2)Characteristics of Damage to Bearings

Based on data shown above and prudential analysis about individual damaged bearings, the tendency of damage to bearings can be summarized as following3),

1)Menshin Bearings

・No damage. However, there is no Menshin bearing along the most intensively damaged highways.

2)Rubber Bearings

・Little damage.

- There was the only one case that cracks were found at rubber itself(Ring-type Bearing).
- At some multi-layer rubber bearings, separation and displacement between layers was observed, however, the influence of the damage for girders and piers was rather small.

3)Steel Bearings

- Various kinds of damage were observed on every type of steel bearings.
- Breaking away of rollers was widely observed on both one-roller bearings and multi-roller bearings.
- Breaking away of pins was observed at many pin bearings, because of lack of strength of setting bolts and shear keys.
- Damage to bearing plate support bearings with PTFE(Polytetrafluorethylene) plates was light.
- There were some steel bearings which seemed to have lost their own function because of rust before the Earthquake , and this could worsen the performance of the bearings during the Earthquake.

4)Fixed bearings, movable bearings

- The ratio of severely damaged movable bearings was bigger than that of fixed bearings, and the ratio of no-damaged fixed bearings exceeded that of movable bearings.
- Damage to piers with movable bearings tends to be lighter than that to piers with fixed bearings.
- As to fixed bearings, there were some broken bearings which seemed to perform like a "fuse", however, it is not easy to expect such function for bearings under intensive seismic excitation when designed, because it is uncertain whether a broken bearing should become a "fuse" or not.
- Most of all Mesnager hinges worked as fixed supports from the beginning to the end of the Earthquake, and some piers with them suffered severe damage.

(3)Damage to Falling-off Prevention Systems

Falling-off prevention systems usually consisted of seat length and restrainers. According to Specifications for Highway Bridges revised in 1990, either of them should be installed, however, at Kobe area many bridges had both. Connecting devices, side stoppers, anchor bars et al were used for restrainers. There is no report which describes comprehensively about damage to falling-off prevention systems, however, highway bridges with unseated girders were investigated in detail individually and the results are reported[1),2)] . There were many cases that restrainers functioned and prevented unseating of girders after destruction of bearings. Furthermore, there were some cases that seat length contributed to prevent the unseating.

As to restrainers, damage to connecting devices using steel plate was remarkable. Especially, damage was appeared as following,

1.Breaking of web, connecting plate and pin, and so on
2.Damage to restrainers because of lateral shifting
3.Damage to superstructures because of collision between girders

(4)Characteristics of Damage to Restrainers and its Function under Large Earthquake

1) Connecting Devices of Girders

Connecting devices of girders suffered a lot of damage. The damage was observed as breaking of connecting boards, breaking and buckling of web of girders and breaking of pins(see Pic.1 and 2). Though a connecting device seemed to function as a falling-off prevention system longitudinally up to designed level, destruction of the device was typically caused by transverse shifting. Therefore, a connection device has some points which should be improved.

2)Side Stoppers

Bucking of girders was observed at many sites, the reason of which was thought that the side stoppers were stronger than girders.

3)Anchor Bolts

Anchor bolts suffered little damage.

4)Function of Seat Length

There were a lot of cases which seat length worked effectively during the Earthquake. Pic.3 shows a typical example.

(5)Damage to Surroundings of Bearings and Restrainers

1)Steel Superstructures

At a number of supporting points buckling of girders was observed, where bearings shifted transversely after destruction.

2)Concrete Superstructures

There were some cases in which cross beams of a PC girder bridge suffered damage because of the force to be acted through falling-off prevention devices.

3)Top End of Substructures

Damage was observed which was caused by at top ends of piers and abutments with pulling off of anchor bolts. At some concrete piers with narrow top ends suffered severe damage around supporting points(see Pic.4).

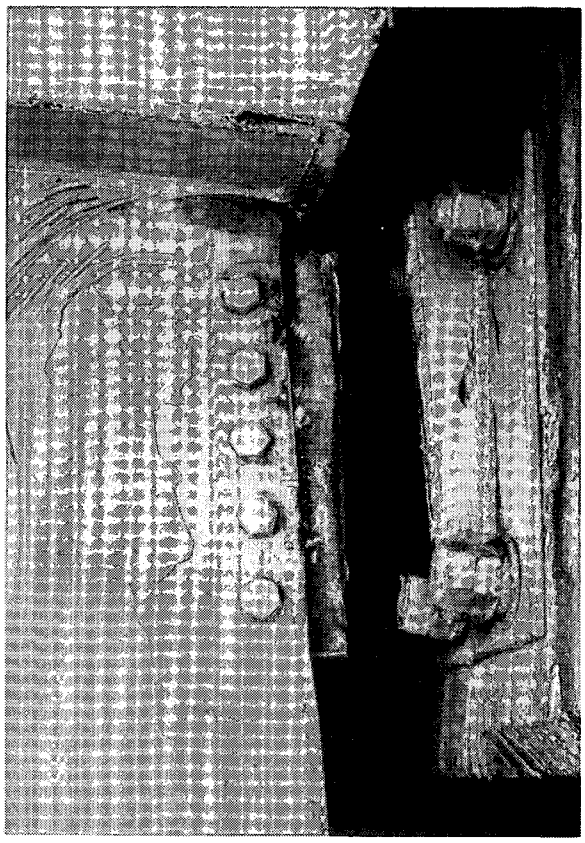

Pic.1 An Example of Falling-off Prevention Device Broken by the Transversal Shifting

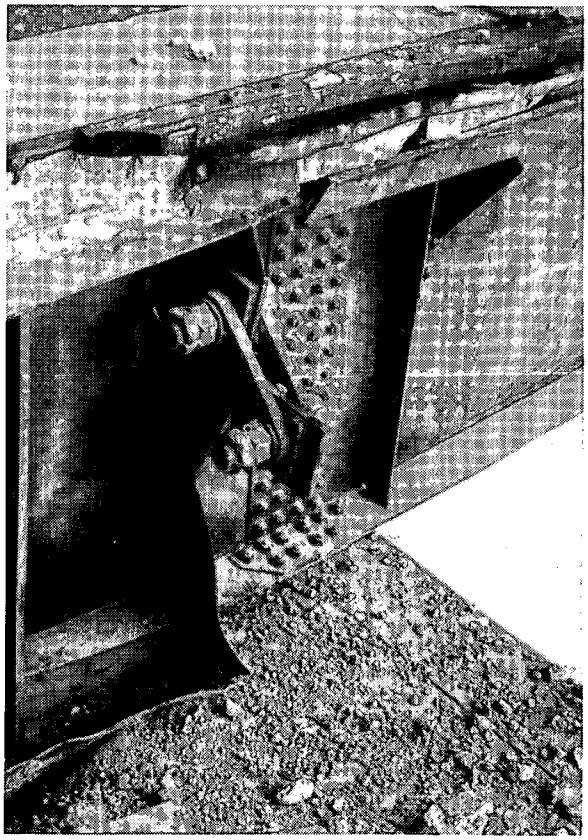

Pic.2 Destruction of a Connecting Device at a Girder End

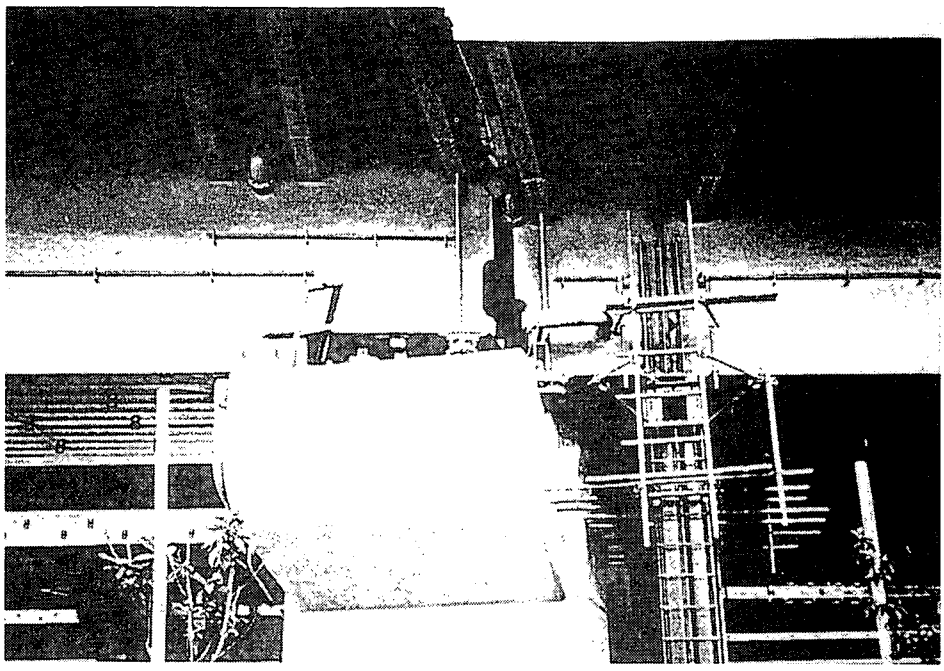

Pic.3 An Example of Function of Seat Length

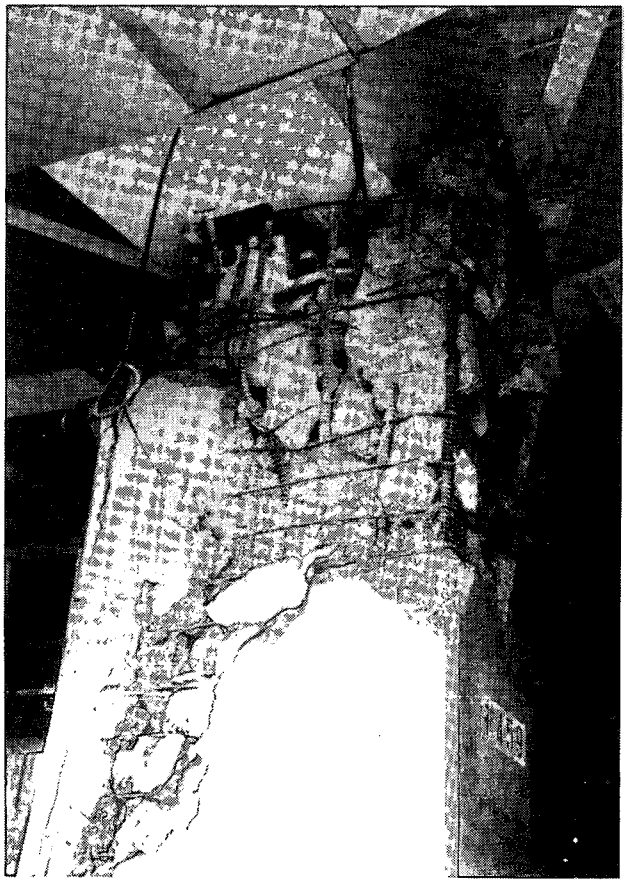

Pic.4 A Damaged Pier with a Narrow Top End

3.Approach for the Basic Concept of Bearings and Falling-off Prevention Systems

In constituting the basic concept concerning to bearings and falling-off prevention systems of highway bridges, recognition of damage caused by the Earthquake of this time, should be always the start line, because it is the positive way to avoid any assumption which had sometimes led to unpredictable damage in previous earthquakes.

In analyzing the damage to highway bridges, it is usual way to classify the damage with damage to structure. However, considering that a highway bridge is a part of a road, it is thought to be important to develop the another index with which passableness of highway bridges after an earthquake can be indicated. The later index is named "functional damage", which is distinguished from the former index named "structural damage". Table 5 shows the correspondence between these two damage level indexes. Here, about functional damage, the levels are represented with using the influence for traffic after an earthquake and for restorative construction. Considering the retaining of function, it is necessary to improve the performance to prevent unseating or settlement of girders, and gap or unevenness of road surface. According to all these things, one direction can be given in carrying out the seismic design of highway bridges; that is, a bridge should be grasped as one whole system and the function of a highway bridge as a road should be retained as much as possible even after an unprecedentedly intense earthquake.

Table 5 Correspondence Between Structural Damage and Functional Damage

Degree of Damage	Structural Damage	Functional Damage
As	・Falling-off of girders ・Collapse or destruction of piers	・The only way to recover the function is reconstruction
A	・No falling-off nor collapse ・Remarkable reduction of strength of piers	・Great deal of repair is necessary for transportation
B	・Damage with reduction of strength of piers, but no fatal damage	・Emergency traffic is passable ・Common traffic is passable with using steel board for bump around expansion joint
C	・Slight damage to bearing supports ・No emergency repair is needed, but repair is necessary for long use	・Private vehicle is passable
D	・No damage	・Usual traffic

4.Basic Concept on Falling-off Prevention and Reduction of Functional Damage

Based on the approaching way mentioned above, basic concept to prevent the falling-off of girders and to reduce the functional damage was made as following;

1)Seat length is the most fundamental structure to keep the safety, when a relative displacement occurs between a superstructure and a substructure.
2)Restrainers should be installed to fail-safe the falling-off prevention function, considering that the seat length works effectively.
3)Bearings should be selected, considering the safety for a bridge in case of an intensive earthquake, the excitation of which exceeds the design level, because difference of performance among types of bearings is typical under such situation as beyond the limit state.
4)Because the height of a steel bearing is sometimes rather large and may cause a big bump on road surface, some other devices should be attached for steel bearings, with which the function of a bridge as a road can be retained.

5.Bearing Supports and Surroundings

'Bearing supports and surroundings' include the body of bearings, connecting members like anchor bolts, and surrounding superstructures and substructures. In the case of bearing supports, as damage of steel bearings was remarkable compared with rubber bearings, rubber bearings and Menshin bearings are recommended since "Guide Specifications for Reconstruction and Repair of Highway Bridges". Furthermore, in designing it is concluded to be desirable to utilize Menshin design method and inertia force distributing design method.

Bearing supports are divided into 2 types;

Type A: Bearings which can stand against seismic force with complementing the falling-off prevention systems.

Type B: Bearings which are designed for inertia force corresponding to equivalent horizontal seismic coefficient to be used for checking ultimate strength during an earthquake.

Type A bearing support is used only for 50m-long or less bridges with continuous girders and unavoidable cases judging from bearing supports structure. Fig.2 shows the flow of basic thinking way on selecting the type of bearings.

The uplift force is given as following;

$$Ru = R_D - \sqrt{R_{heq}^2 + R_{veq}^2} \qquad (1)$$

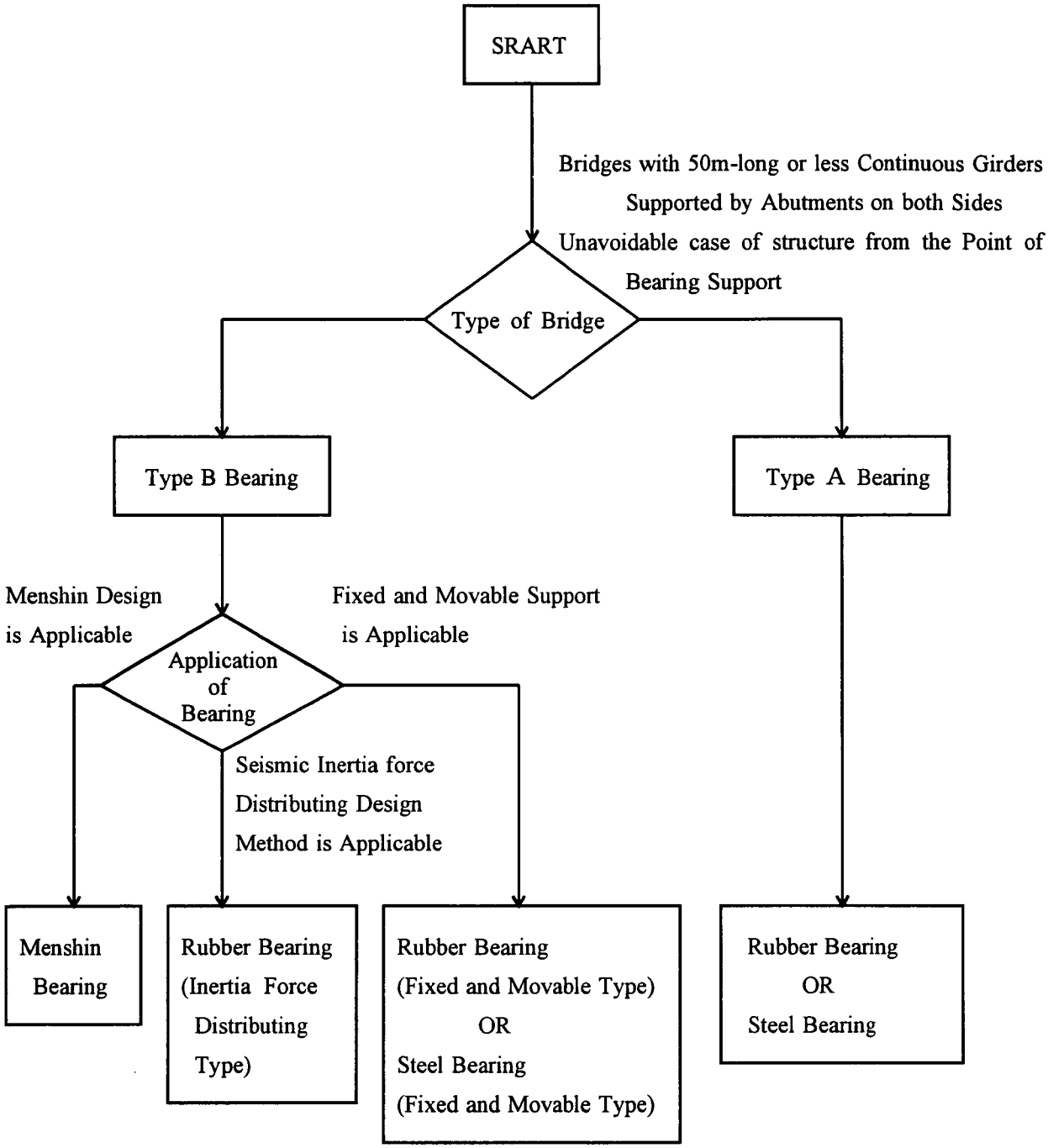

Fig.2 Basic Thinking Way on Selecting the Type of Bearings

where, R_{heq} and R_{veq} are vertical reactions caused by horizontal force and vertical force respectively during an earthquake(see Fig.3).

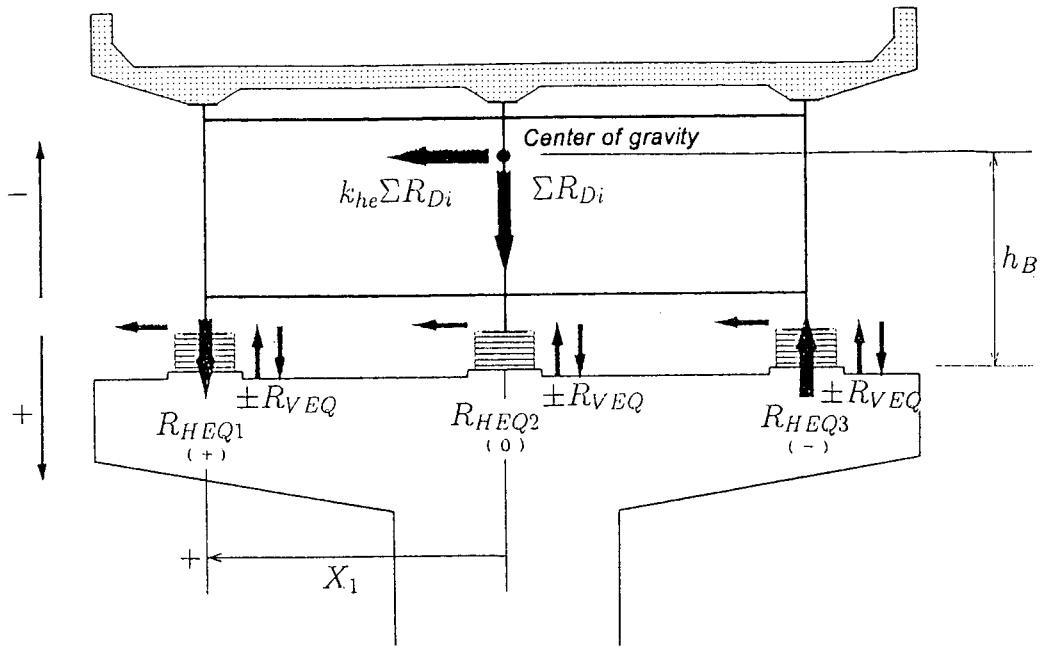

Fig.3 Vertical Reactions on Bearing Supports Caused by an Earthquake

6.Falling-off Prevention Systems

As a countermeasure to prevent falling-off of superstructures, new falling-off prevention systems are constituted, in which the falling-off function is realized systematically.

Composition of falling-off prevention systems for each bridge is different by the type of bearings. The systems are made up with a seat length, falling-off prevention structures, restrainer for shiftings, and road surface retainers. Furthermore, a joint protector is also installed if it is needed, in order to prevent damage caused by slight earthquakes whose possibility of occurrence is rather high during the service life of the bridge.

A seat length(S_E(cm)) is the most important and the most basic structure among the falling-off systems, and in the new Specifications of Highway Bridges it is given as following,

$$\left.\begin{aligned} S_E &= u_R + u_G \leqq S_{EM} \\ S_{EM} &= 70 + 0.5\,l \\ u_R &= 100\,\varepsilon_G L \end{aligned}\right\} \quad (2)$$

where,

u_R : relative displacement between a superstructure and a substructure, caused by inertia force corresponding to equivalent horizontal seismic coefficient to be used for checking ultimate strength during an earthquake(cm)

u_G : relative displacement of the ground caused by ground strain during an earthquake(cm)

S_{EM} : minimum seat length(cm)

ε_G : ground strain during an earthquake

L : length between the two subjected substructures(m)

l : span length of the bridge(m)

A falling-off prevention structure, which corresponds to the former falling-off prevention device, needs higher design level and performance than before.
A restrainer for shifting is the device which can resist the inertia force with a type A bearing and prevent the large relative displacement between a superstructure and a substructure after bearings are broken.
A road surface retainer is the structure which can prevent bump around an expansion joint so as to keep traffic as much as possible even when a tall bearing is broken by an earthquake. And the function of a stopper for shifting of movable bearings is clarified, and the role of which is divided into two parts; a restrainer for shifting and a joint protector.

Fig.4 shows an example of a girder end with a type B rubber bearing, supported by an abutment. The functions of falling-off prevention systems are represented according to the level of earthquake.

Table 6 shows the summary of bearing supports and falling-off prevention systems.

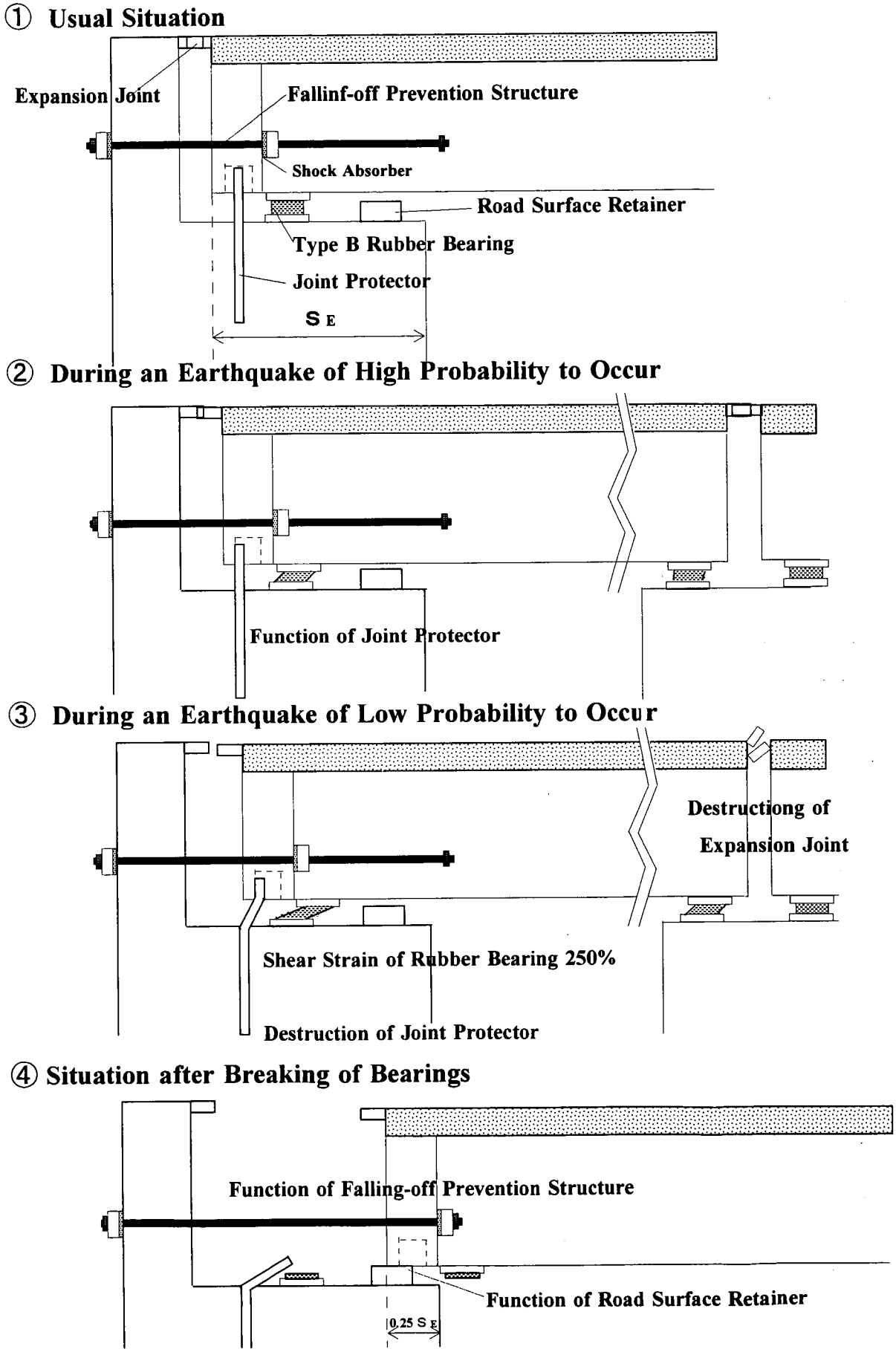

Fig.4 An Example of a Girder End with a Type B Rubber Bearing and Function during Earthquakes

Table 6 The Summary of Falling-off Prevention Systems of "Specifications of Highway Bridges, Part V, Seismic Design,1996"

(a)Longitudinal Direction

Seat length	Calculated with span length, ground strain, displacement of a pier, influence of liquefaction and induced ground flow, and influence of skew and curve
Falling-off prevention structure	Necessary in both case of using type A and B bearings Needless for 50m-long or less girder whose both ends are supported by abutments in case of ground type Ⅰ, and 25m-long or less in case of round type Ⅱ and Ⅲ
Restrainer for shifting	Necessary when using type A bearings Needless when using type B bearings
Joint protector	Combined use with restrainer for shifting is possible
Road surface retainer	For important bridges using tall steel bearings

(b)Transversal Direction

Restrainer for shifting	Necessary in case of skewed bridges, curved bridges, bridges with narrow top end of substructures, bridges with a few bearing supports, and bridges which have the possibility that piers might shift transversally because of ground flow induced by liquefaction.

CONCLUDING REMARKS

Although the 1995 Hyogo-ken Nanbu Earthquake caused huge damage, on the other hand it was a variable event which gave much lesson and knowledge to the world of seismic design. This is also true for bearing supports and falling-off prevention systems. The specifications of highway bridges on these structures and systems have been changed in a great way according to knowledge gained from the studies of this earthquake disaster. It might be delightful if the concept and the basic direction on bridge supports and falling-off prevention systems shown here should be understood widely and applied properly to many bridges of not only Japan but the other earthquake countries.

REFERENCES

1)Ministry of Construction: Report on the Damage of Highway Bridges by the Hyogo-ken Nanbu Earthquake, Committee for Investigation on the Damage of Highway Bridges Caused by the Hyogo-ken Nanbu Earthquake,1995

2)Public Works Research Institute: Report on the Disaster Caused by the 1995 Hyogoken Nanbu Earthquake, Report of Public Works Research Institute Ministry of Construction, Vol.196, March 1996

3)Ministry of Construction: Guide Specifications for Reconstruction and Repair of Highway Bridges which Suffered Damage due to the Hyogo-ken Nanbu Earthquake,1995

4)Japan Road Association: Specifications of Highway Bridges, Part Ⅰ Common Part, Part Ⅴ, Seismic Design, 1996

5)Japan Road Association: Specifications of Highway Bridges, Part Ⅰ Common Part, Part Ⅴ, Seismic Design, 1990

6)Kanda, M.: Damages for Bearing and Falling-off Prevention Structures of Highway Bridges, Bridge and Foundation Engineering, pp156-162, Vol.30, No.8, 1996

7)Nishikawa, K., Kanda, M.: New Direction of Seismic Design Methods for Bearings and Falling-off Prevention Structures of Highway Bridges, Bridge and Foundation Engineering, pp163-164, Vol.30, No.8, 1996

8)Nishikawa, K., Kanda, M.: Bearings and Falling-off Prevention Systems of Highway Bridges, Civil Engineering Journal, Vol. 39, No.2, February, 1997

FINITE ELEMENT MODELLING OF THE HANSHIN VIADUCT'S FAILURE IN KOBE

M.Petrangeli P.E.Pinto

Dipartimento di Ingegneria Strutturale e Geotecnica

Università di Roma "La Sapienza"

ABSTRACT

The paper presents the numerical simulation of the Hanshin pier failure using a fibre beam element with shear modelling. The analyses seem to indicate that a shear failure of the piers has caused the collapse of the viaduct due to the insufficient transverse reinforcement and poor anchorage detailing of it. with respect to available empirical rules for the shear strength evaluation, the proposed model has the advantage of describing the evolution of the various damage mechanisms in r.c. element down to the final structural collapse. The insight gained on the behaviour of these structures is hopefully a first step in view of a future revision of present seismic shear design recommendations which are based on strength criteria only, while energy-based provision should clearly also be introduced.

1. THE NUMERICAL ANALYSES

The analyses presented in the following intend to focus on two construction details of the Hanshin concrete piers which played a determinant role in failure of the viaduct. The first one is the much discussed interruption of the inner rebar layer at 2.5 metres above the foundation plinth. this interruption has immediately come to the research attention since clearly the failure has localised in that section. Not enough attention has been given instead to the obvious consequence that, with the interruption of the inner rebar layer, also the inner hoop layer terminated at the same section.

This interruption has been even more critical as all hoops lacked of proper anchorage in the concrete core and therefore failed with the spalling of the outer concrete layers. The inner layer, although doubly spaced compared to the outer one (the same as for the corresponding longitudinal rebar layer, the two represented 20% of the reinforcing steel), had obviously a better anchorage given its inner position into the section.

The lack of anchorage of the transverse steel, which is the second detail to be analysed, has been included among the causes of failure but no quantitative assessment of its role has been carried out. Using current empirical formulae [1][2] for the calculation of the pier shear strength we can only choose between including this transverse steel or not. If we do include it, the shear strength of the pier comes out to be in excess of the bending one, while if, on the contrary, we do not include it, we should have had immediate shear failure even without yielding of the longitudinal rebars.

The analyses presented in the following, based on a more physical modelling of the behaviour of elements subjected to high shear, will try to provide an insight on the actual evolution of damage which may have taken place in the Hanshin piers.

Four configurations have been analysed at first by combining the two details discussed above:

• CASE A - Pier with rebars and hoop interruption and hoop cut-off strain at 2%.
• CASE B - Pier with rebars and hoop interruption and no hoop cut-off strain
• CASE C - Pier with no rebars and hoop interruption and hoop cut-off strain at 2%.
• CASE D - Pier with no rebars and hoop interruption and no hoop cut-off strain
The hoop cut-off strain is an approximation for the complete loss of anchorage which we may assume to take place after concrete spalls, which for the Hanshin piers could be estimated to occur at strains in the order of 1%. For properly anchored hoops we may assume instead that their cut-off strain does coincide with the steel max. elongation although this may be a bit optimistic.

2. THE FINITE ELEMENT MODEL

A single pier has been modelled using the finite element program FIBER with four 2D fibre beam element with shear modelling developed by the authors [3][4][5] in the last few years. A concentrated mass has been placed on top of the pier with a translational and rotational inertia equivalent to one span of the viaduct (M_t = 1100 kN, M_r = 29000 kNm^2). Full Lagrangian formulation (large displacement) has been used. The structure has been subjected to the Kaiyou Weather Bureau accelerogram with a PGA = 0.81 g.
The reinforced concrete section has been subdivided in 40 concrete fibres and 20 longitudinal steel ones. Each of the concrete fibre is laterally confined by a steel transverse fibre which models the effect of the hoops. During the analyses equilibrium is enforced between the concrete fibre and the transverse steel one. In order to do that, the proposed model while retaining most of the characteristics of a traditional fibre element, makes use of a 2D concrete constitutive model which allows for the description of the 2D stress strain field due to shear and Poisson's effect in the concrete. The following simplifying assumptions are maintained:
- Plane sections remain plane
- Shear strains are constant over the section
- Perfect bond is assumed between concrete and steel in the transverse direction

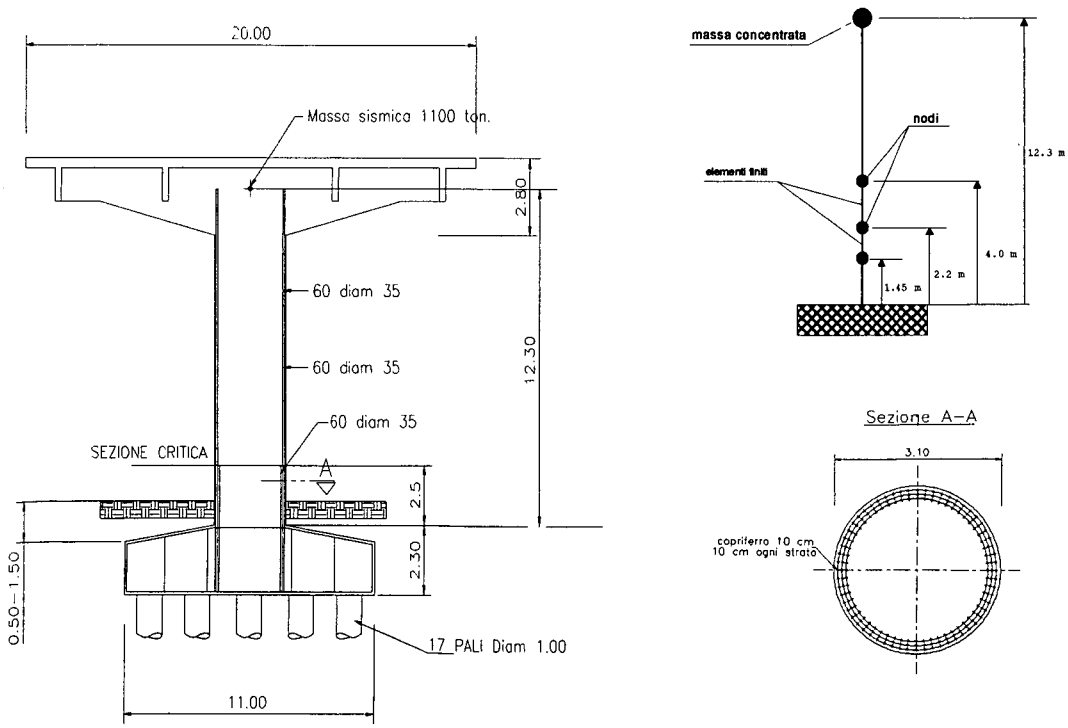

FIG. 1 - Hanshin' s pier geometry and F.E. schematisation

The steel constitutive behaviour used for the longitudinal steel is based on the Menegotto-Pinto curves [6] while for the transverse steel a simplified elasto-plastic formulation with cinematic hardening is used.
The transverse steel area attributed to the concrete core fibres is equal to the corresponding hoop area per unit length (40 to 50 cm^2). Mechanical properties of the steel are the following: yield strength = 350 MPa, ultimate strength = 450 Mpa (380 Mpa for the hoops), Young's modulus = 200000 Mpa, ultimate strain 0.12. Mechanical properties of the concrete are: cubic strength = 30 Mpa, Young's modulus = 30000 Mpa, tensile strength = 25 Mpa, fracture energy 0.1 kN/m.
Since the concrete constitutive model is a microplane based [7][8] 2D model, the base curves used for the microplane behaviour need to be defined according to the out of plane boundary conditions. In other words, the strength and ductility of concrete must be adjusted via a calibration of the base curves used by the model since the latter does not cover automatically the response of concrete due to varying stress/strain states in the third direction. In practice, the input parameters for the concrete fibres have been assigned depending on their effective confinement i.e. fiber position inside the section.

3. THE RESULTS

We shall interpret the results of the analyses with the following plots. From the pier top displacement histories plotted in Fig.2 we can see that only one structure survives, which is the pier with no rebar interruption and proper hoop anchorage (Case D). Failure of the pier with rebar interruption and proper hoop anchorage (case B) does take place later than the two cases with poor hoop anchorage (Case A and C). The shear force-pier displacement histories are plotted in the following Fig.3 (no rebar interruption) and Fig.4 (rebar interruption).

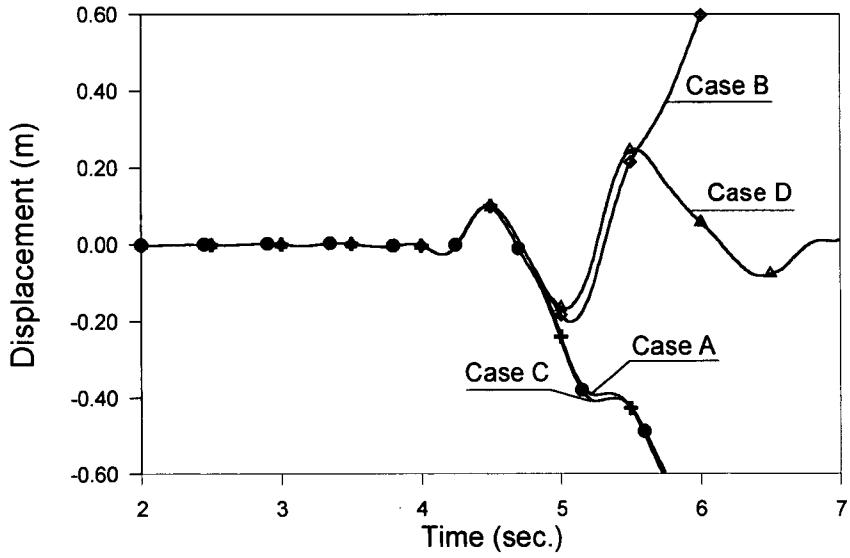

FIG. 2 - Pier Top Displacement History

It does come out immediately how the dissipated energy of the survived pier exceeds that of the other three structures. It must be remembered that the piers do not behave as simple cantilevers since there exists a mass rotational inertia of the deck; this is why Fig. 3 and 4 show sometimes increasing forces associated to decreasing displacement due to the out-of-phase response of the rotational mass. Nonetheless, the bending moments due to this rotational mass are not particularly significant and do not cause an increase of the maximum shear force compared to that which would be obtained by a cantilever type of response. This is caused by the fact that the maximum bending moments at the pier base and pier top, although not in phase, do not happen to be in opposition of phase.

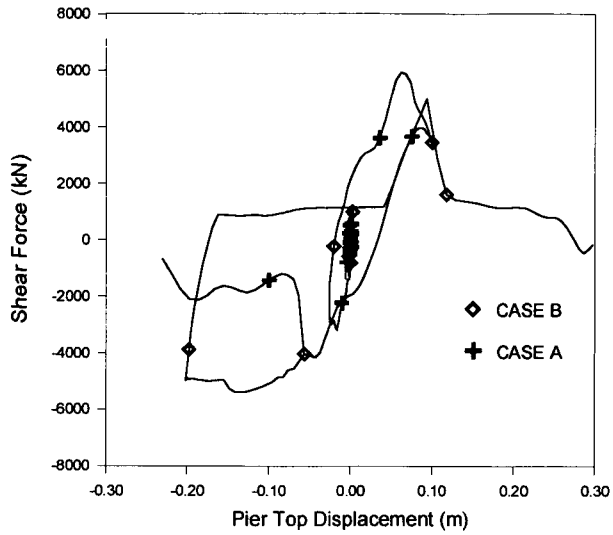

FIG. 3

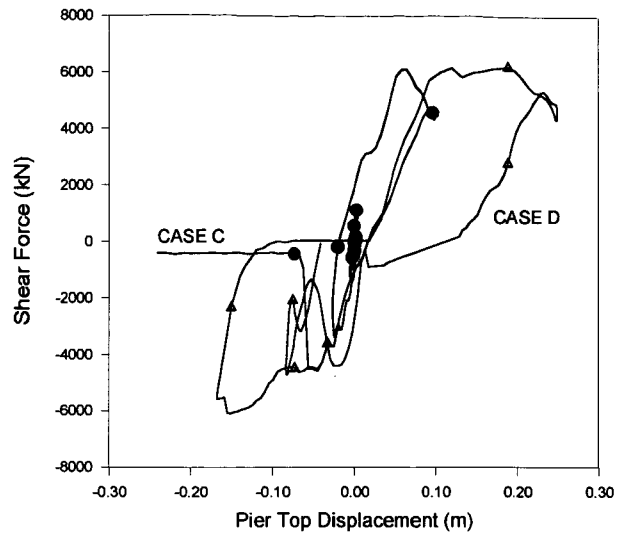

FIG. 4

The most significant plots illustrating the failure of these structures are certainly the shear force and shear deformation time-histories of Fig.5 and Fig.6 respectively. Shear failure is there, brittle as it is expected to be, following previous peak corresponding to diagonal cracking of the section. The numerical simulation shows in fact the development of a diffuse shear crack pattern which drastically reduces the shear strength and stiffness of the section and activates the transverse steel resisting mechanisms: at a certain point the hoops fail, and the section collapses.
The sections where failure takes place are obviously the base ones for the two configurations without bar interruption and that at the rebar interruption in the other cases.

The pier with rebar interruption and proper hoop anchorage (Case B) does fail as well, although later, since more energy is needed to take the hoops to failure. It should be noticed that from a strength point of view the interruption of the transverse reinforcement is more critical than that of the longitudinal one since shear force is constant along the pier while bending moment decreases linearly along the height.

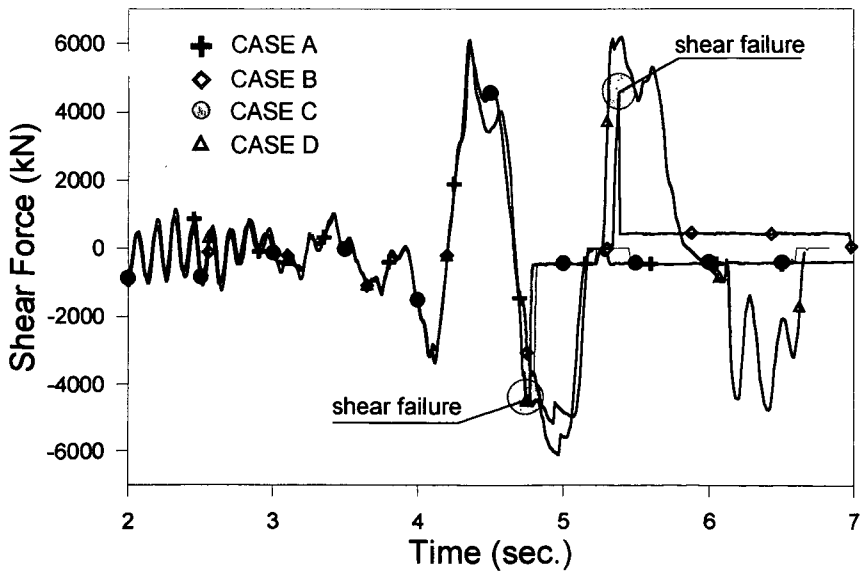

FIG. 5 - Shear force time history

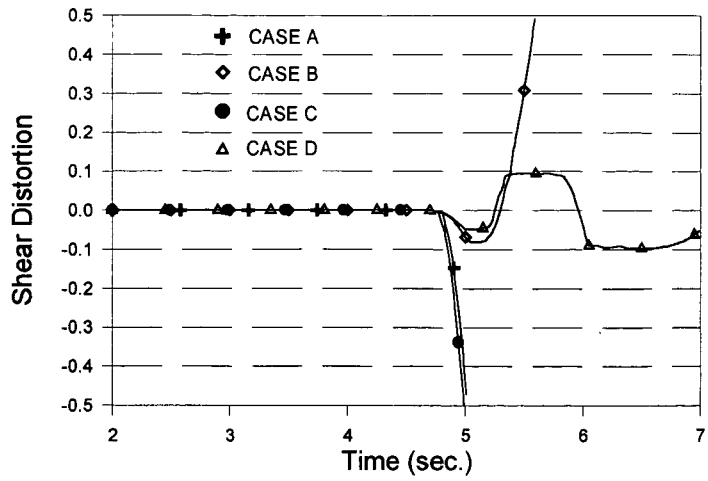

FIG. 6 - Shear deformation time history

Further evidence on the driving role played by the shear failure in the collapse of the viaduct can be seen from the curvature time histories of the collapsed section, Fig. 7 and their bending moment-curvature histories, Fig.8 and Fig.9.

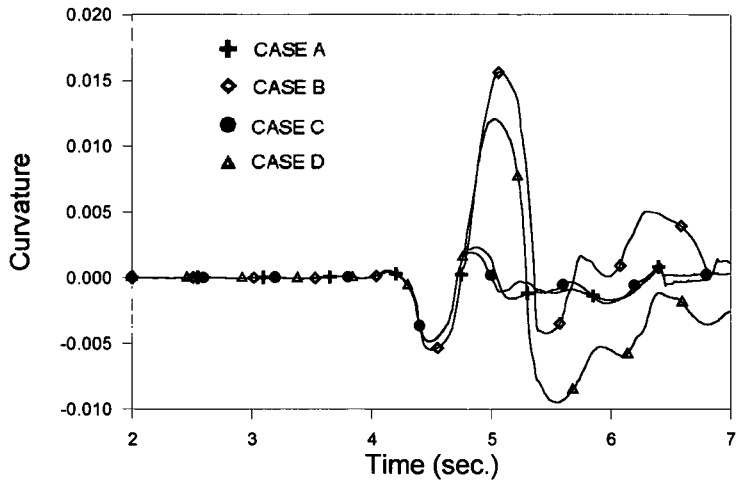

FIG. 7 - curvature time history

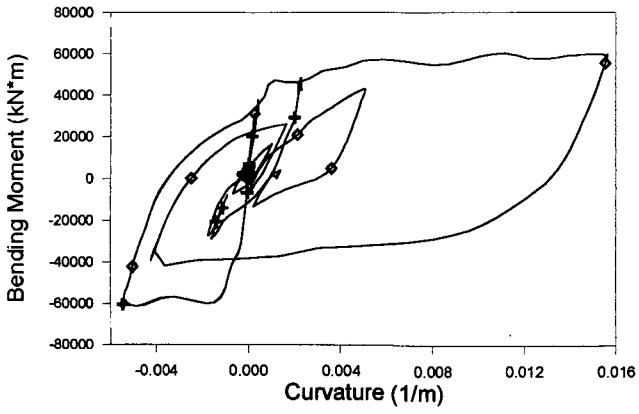

FIG. 8- Moment Curvature (h=2.5m)

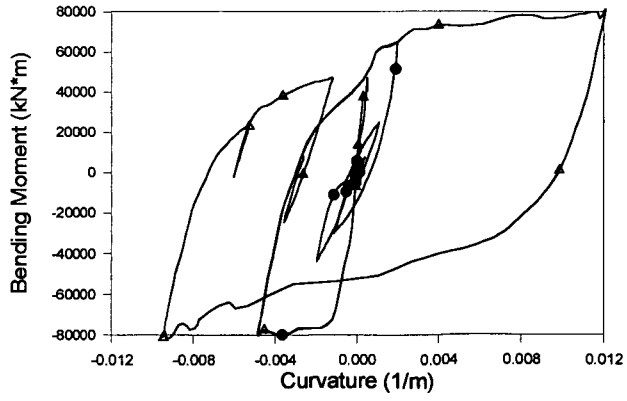

FIG. 9 - Moment-Curvature (h=0)

While the shear distortion of these sections increases dramatically, the flexural response shrinks. Only the pier with no rebar interruption and proper hoop anchorage is capable of resisting the imposed acceleration with a flexural mechanisms and a large amount of dissipated energy.

4. THE FAILURE MECHANISM

An insight on the failure mechanism can be achieved by looking at the fibre stress-strain histories inside the collapsed sections. Before doing that we introduce a fifth type of pier where the longitudinal reinforcement does interrupt as in the real structure but the transverse hoops do not (Case E). In other words we investigate the case where we have a column with varying longitudinal reinforcement but constant transverse reinforcement properly anchored (no cut-off strain).
The pier top displacement history for this structure is plotted in Fig.10 together with the two other previous cases of proper hoop anchorage, with (Case B) and without (Case D) longitudinal rebar interruption.
The structure with longitudinal rebar interruption but constant transverse reinforcement does survive with smaller displacement than the others. This result suggest that the longitudinal rebar interruption has not been a problem as such but only as it came together with the interruption of the inner hoop layer. By keeping the same transverse reinforcement through the weak section at 2.5 metres, the piers behave as well as or even better than the structure without rebar interruption.

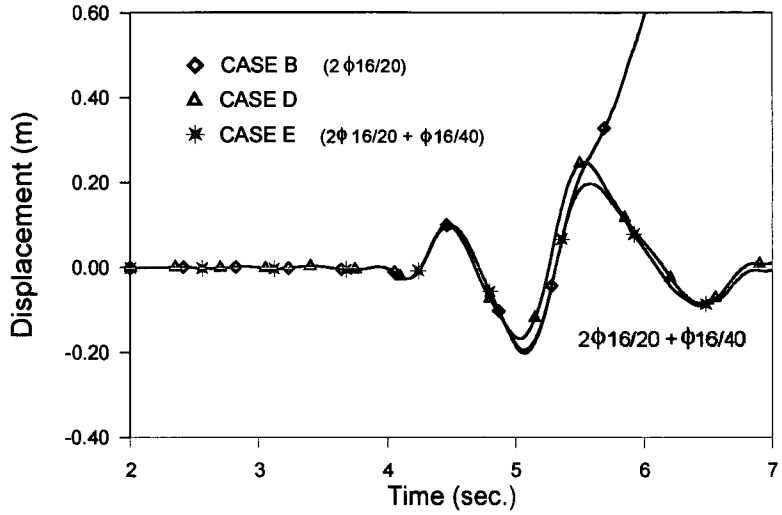

FIG. 10 - Pier Top displacement history

With reference to the notation in Fig.11, we look now at the stress and the strain time-histories of a concrete core fibre located roughly half a metre inside the outer hoop layer.
Fig. 12 shows the time history of the lateral deformation ε_y, while Fig.13 that of the shear stress σ_{xy}. The plots refer to the two structures with longitudinal rebar interruption, proper hoop anchorage, with (Case B) and without (Case E) inner hoop layer interruption. The concrete core does crack in both cases at around 4.5 sec as can be seen from the shear time-history (peak resistance of 4.5 Mpa and sudden drop). After that the concrete fibre dilates and is resisted against shear opening by the transverse steel until the latter collapses: this occurs for the case of transverse hoop interruption only. The corresponding stress-strain histories for the longitudinal, transverse and shear components for the same concrete core fibre are plotted in Fig.14 to Fig.16.

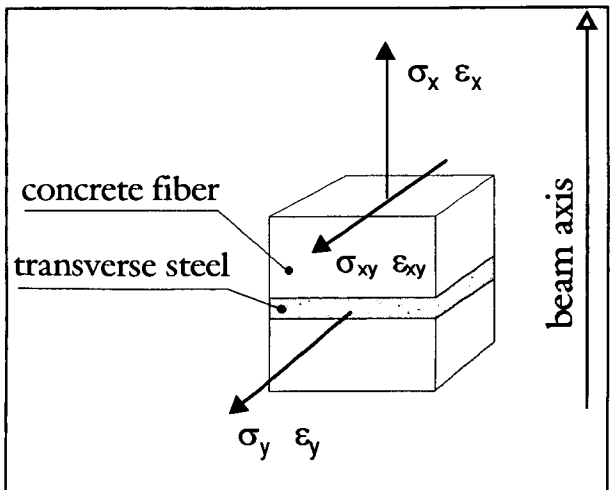

FIG. 11

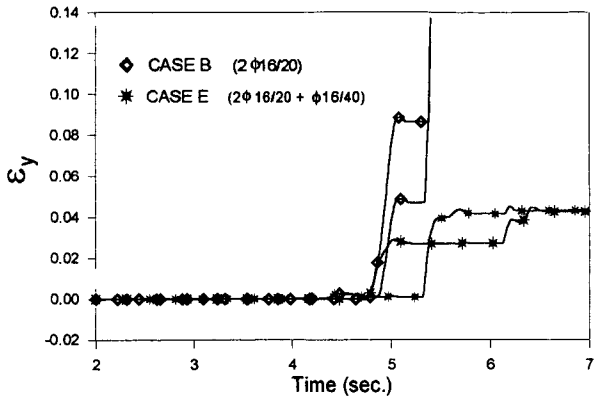

FIG. 12

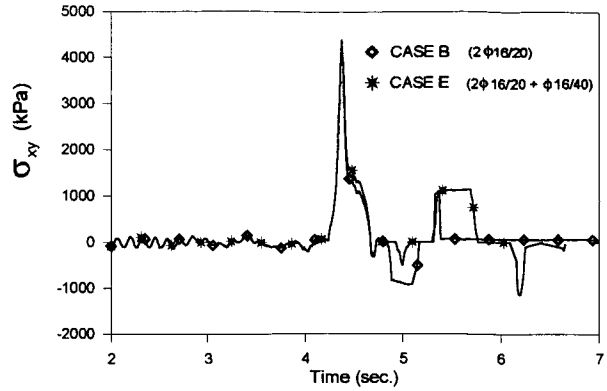

FIG. 13

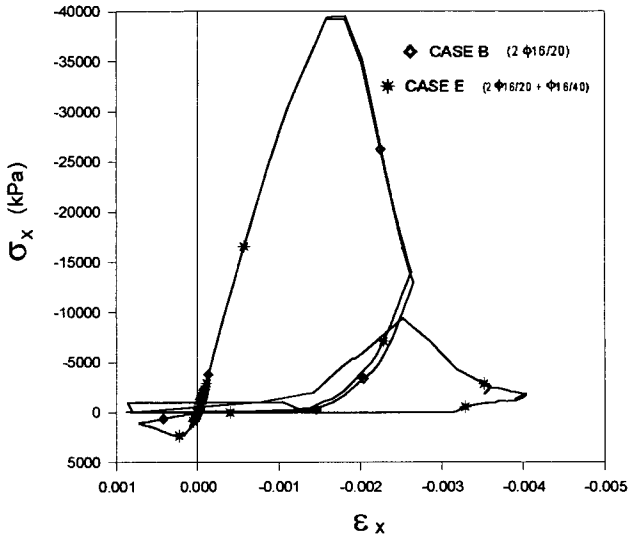

FIG. 14 Longitudinal fibre behaviour

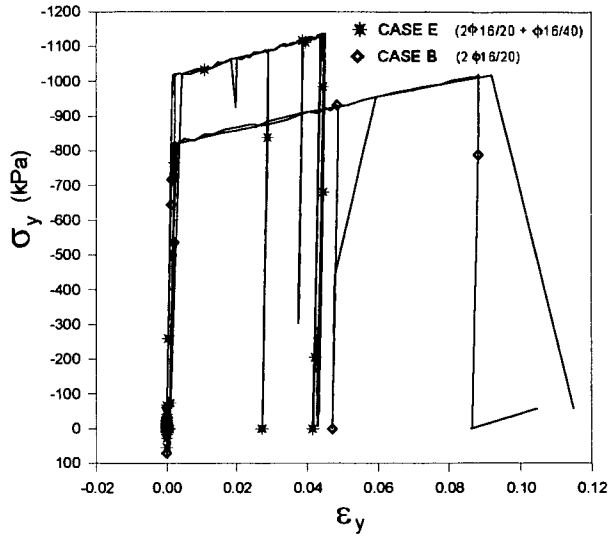

FIG. 15 - Transverse fibre behaviour

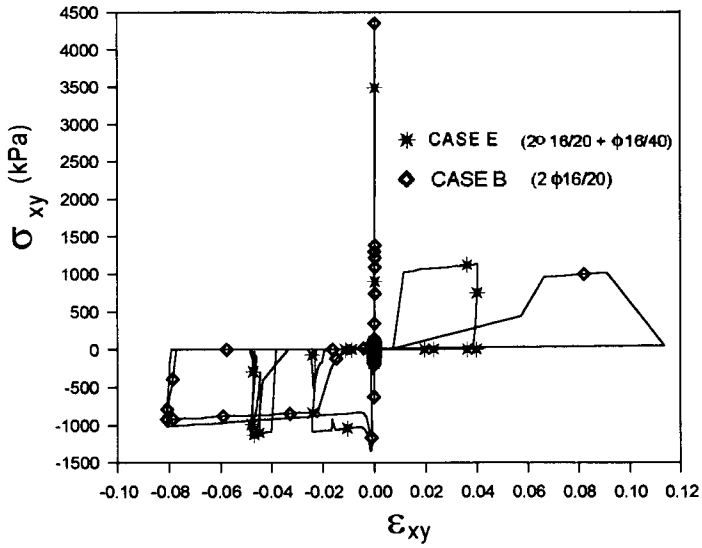

FIG. 16 - Fibre shear behaviour

5. FINAL REMARKS

We do ignore now the poor anchorage of the transverse hoops which caused their premature failure and look at Fig. 17 where the moment-curvature and shear force-shear distortion for the weak section located at the longitudinal rebar interruption under monotonic imposed displacement of the pier top are plotted.

Three configurations are proposed; the actual configuration with two hoop layers at 200mm centre (previous Case B), a configuration with the same transverse reinforcement and an additional shear resistance of 4000 kN, and a configuration with twice the amount of transverse reinforcement (two hoop layers at 100mm centre).

The monotonic pier behaviour with the actual configuration (Case B) is the following: with increasing displacement the section yields at about 60000 kN*m, shortly afterwards the concrete section develops diagonal cracks which cut through the compression zone. This crack pattern activates the truss mechanism based on the transverse steel. Since the amount of transverse steel is only 0.13% of the concrete section, the shear cracking yields a reduction of the shear capacity of the section down to a residual value of 5000 kN. It must be noticed that the shear bearing capacity of the concrete compression zone suffers from the high damage due to the bending stresses associated with poor confinement. With increasing displacements, the deformation localise in the shear mechanisms with yielding of the transverse reinforcement until the cut off strain is reached (5% in the specific case). At this point we have a curvature unloading and a dramatic increase of the shear distortion (left out in the graphic representation).

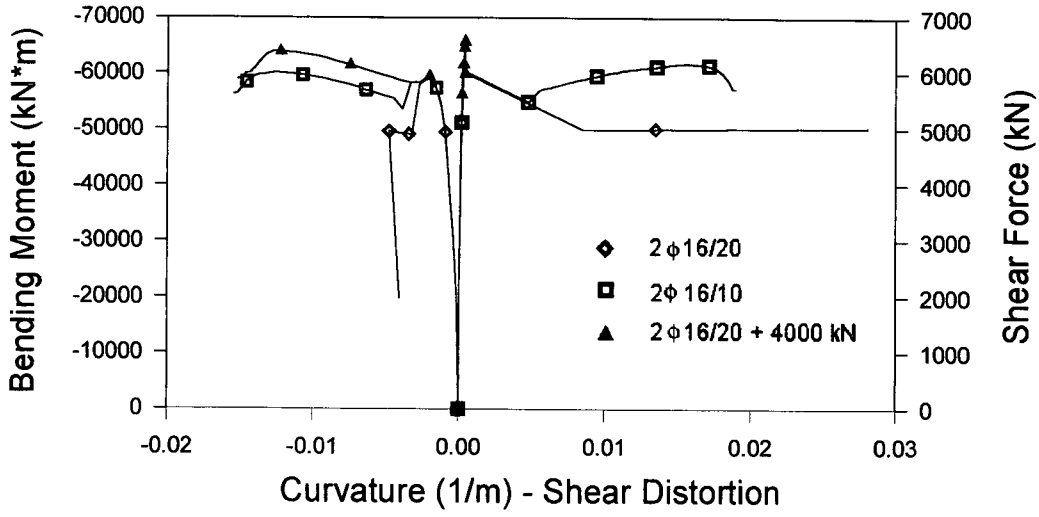

FIG. 17 - Monotonic Section Behaviour

Doubling the transverse reinforcement, the pier behaves similarly to the previous case until the truss mechanism is activated. In this case, however, the pier has enough transverse steel strength, therefore allowing for the development of a ductile flexural response. Still, significant shear deformations are found since the stirrups yield under combined shear and lateral expansion of the compression core.

A final contribution to the shear stiffness of the section which may be relevant and should be taken into account is that of the longitudinal reinforcement behaving as a shear connector across the cracks. In the Hanshin case, the area of the longitudinal rebar at the weak section is equal to 1154 cm^2 (1.5%), which means roughly ten times more than the transverse one. Even though the strength and stiffness of this contribution decrease with increasing bending deformations of the section due to spalling of concrete and buckling of the rebars, still in case of low ductility and for sections with proper transverse reinforcement detailing, this contribution cannot be ignored. The effect of this mechanism can be seen in Fig.17 where the response of the pier section when adding an additional

shear resistance of 4000 kN (only 33 kN per ϕ 35mm longitudinal bar) has been plotted. Participation of this mechanism to the section shear strength may result in the uncoupling of the bending and shear behaviour as shown in Fig. 17. The pier force-displacement response for the three cases is finally reported in Fig.18.

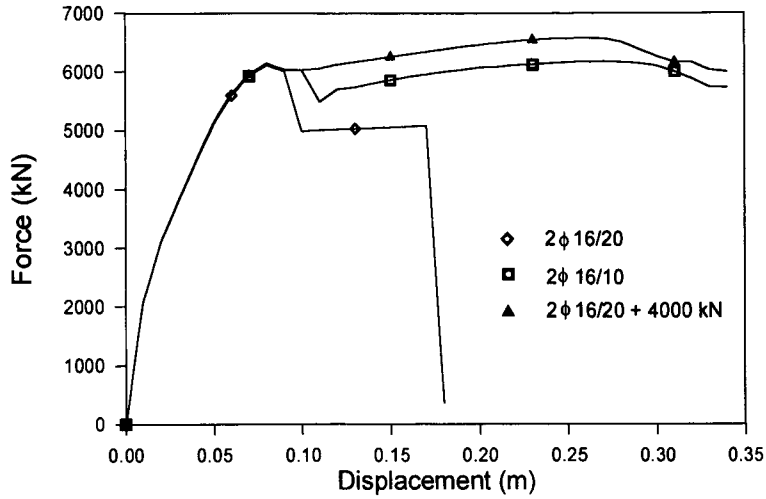

FIG. 18 - Pier monotonic force-displacement response

A final remark is worth making on the response of this type of structures. Fig.19 reports the time history of the pier axial force. Reinforced concrete sections do experience a good deal of rocking, especially for null to moderate axial load, when subjected to alternate bending actions. This rocking, which is a result of the shift of the neutral axis of the section, does bring as a consequence axial pulses and hence axial vibration of the pier. The adequacy of the model in quantifying this vibration intensity may be arguable since damping of these high frequencies may well be underestimated, but the phenomenon exists and we should be careful when using the axial force in our section strength calculations as if we were in a quasi static test.

A curiosity: since a full Lagrangian formulation is used (finite displacement), the axial force in the failed piers goes to zero since the structure looses support and goes almost in free fall although the mechanical models cannot be considered to be fully representative of the real situation for such large deformations.

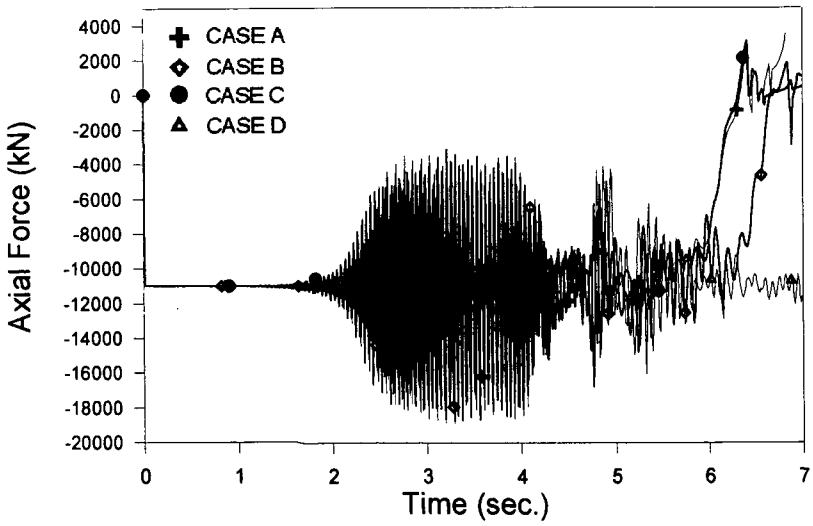

FIG. 19 - Axial Force Time History

6. CONCLUSION

The results of the analyses seem to indicate that the Hanshin's piers have failed because of lack of transverse reinforcement especially as it suddenly changed from one section to the other under an almost constant shear force (cf. [9]). Failure of the section located at the longitudinal and transverse inner rebar layer interruption did yield a localisation of the shear deformation and a curvature unloading along the element: we therefore classify the Hanshin failure as shear failure. With a more slender structure we would have had a localisation of curvature and a P-Δ driven failure which was not the case for the Hanshin pier since the ultimate bending moment of the base section could bear an overturning bending moment due to deck displacement in excess of 5 metres while failure took place at only 20 cm.

Independently of the poor anchorage detail of the transverse hoop, the Hanshin piers represent an example of the problems arising when the transverse reinforcement is only a fraction of the longitudinal one. When ductile behaviour of reinforced concrete members is required, a smeared reinforcement in two orthogonal directions is required to avoid deviatoric driven brittle failures, caused either by compression splitting, shear or a combination of the two.

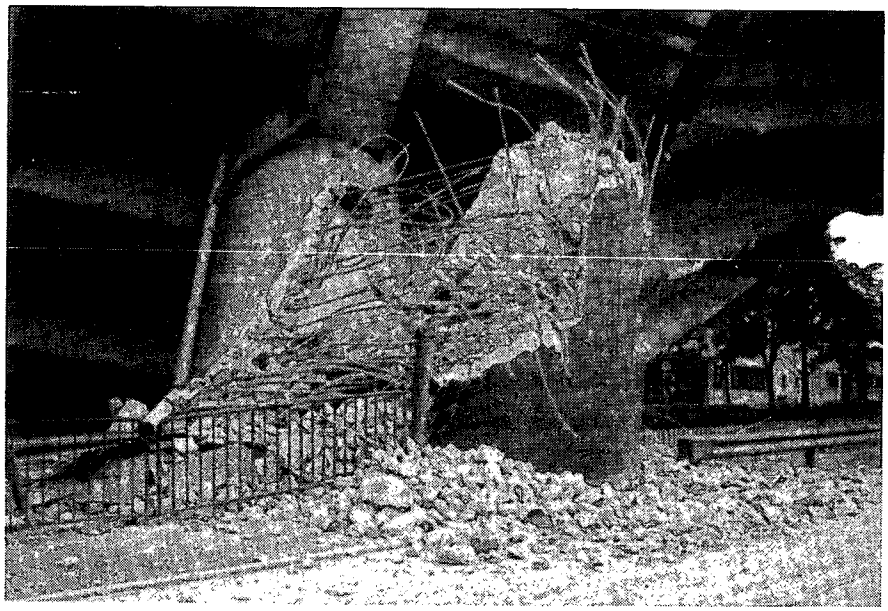

Photo 1 - The Hanshin Viaduct - A collapsed pier.

REFERENCES

[1] CEB (1994). "Behaviour and Analysis of Reinforced Concrete Structures under Alternate Actions Inducing Inelastic Response". Vol.2: Frame Members. *CEB Bull. d'Inf. N. 220.* *Chpt.2 Frame Members in Flexure and Axial Force with High Shear.

[2] Priestley M.J.N., Verma R. and Xiao Y. (1994). "Seismic Shear Strength of Reinforced Concrete Columns", J. Struct. Engrg., ASCE 120(8), 2310-2328.

[3] Petrangeli, M. and Pinto, P.E. (1995). "A Fiber Model for elements under cyclic bending and shear." *Proc. of "The First Italy-Japan Workshop on Seismic Design and Retrofit of Bridges"*, ISSN 0386-5878 Technical Memorandum of PWRI No.3369, Ministry of Construction, Japan.

[4] Petrangeli, M. (1996). "Modelli Numerici per Strutture Monodimensionali in Cemento Armato" *Dissertation*, University of Rome "La Sapienza", Rome, Italy. (in italian).

[5] Petrangeli, M. and Ciampi, V. (1997). "Equilibrium based numerical solutions for the nonlinear beam problem", *Int. Journal for Num. Meth. in Engrg*, 40(3), 423-438.

[6] Menegotto, M. and Pinto, P.E. (1977). "Slender RC Compressed Members in Biaxial Bending."

J. Struct. Engrg, ASCE, 103(3), 587-605.
[7] Bazant, Z.P. and Prat, P.C. (1988). "Microplane model for brittle-plastic material. Parts I and II." *J. Engrg. Mech.*, ASCE 114(10), 1672-1702.
[8] Petrangeli, M., Ozbolt, J., (1996). "Smeared crack approaches - material modelling", *J. Engrg. Mech.*, ASCE, 112(6), 545-554.
[9] Seible F., Priestley M.J.N., MacRae G. (1995). "The Kobe earthquake of January 17, 1995", *Report No. SSRP-95/03*, University of California, San Diego, California, USA..

EFFECTS OF THE HYOGO-KEN-NANBU EARTHQUAKE ON THE AKASHI KAIKYO BRIDGE

S. Saeki[1], T.Kurihara[2], R. Toriumi[3], M. Nishitani[2]

1)Executive Director, Honshu-Shikoku Bridge Authority,45 Mori Bldg.,5-1-5, Toranomon, Minato-ku, Tokyo

2)3rd. Desigh Div., Design Dept, ditto.

3)1st. Design Div., Design Dept., ditto.

ABSTRACT

The Hyogo-ken-Nanbu Earthquake struck Kobe on 17 January 1995, severely damaging the city and vicinity. After the earthquake, the aseismic characteristics of the Akashi Kaikyo Bridge, which was under construction very close to the epicenter, were examined. Through these examinations, it was concluded that the substructures of the bridge remained stable even though the ground was partially close to failure, and that the superstructure did not collapse even though stresses on limited sections of the tower bases momentarily exceeded the allowable stress. This is an intermediate report, and further study on estimation of seismic input at the bridge site, response of bridge is continued.

INTRODUCTION

At 5:46 a.m. on 17 January 1995, the Hyogo-ken-Nanbu Earthquake struck the city of Kobe. The epicenter of the earthquake was longitude 135° 03" E and latitude 34° 36" N. The depth of the hypocenter was 14 km and the magnitude was 7.2 in the Richter scale. The earthquake severely damaged the city of Kobe, as well as buildings and roads in the vicinity.

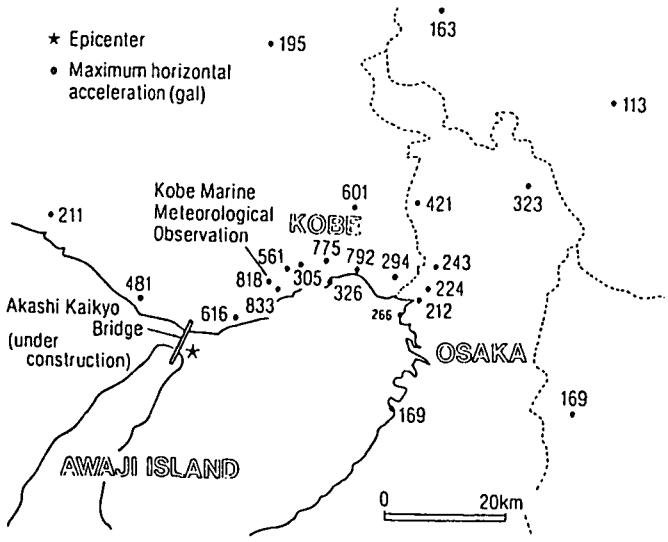

Fig.1 Epicenter of the Hyogo-Ken-Nanbu Earthquake

Figure 1 shows the distribution of the maximum horizontal acceleration of the earthquake recorded. At the Kobe Marine Meteorological Observatory, the maximum acceleration recorded was 818 gal (cm/sec^2) in a south-north direction. This was close to gravitational acceleration (see **Figure 2**).

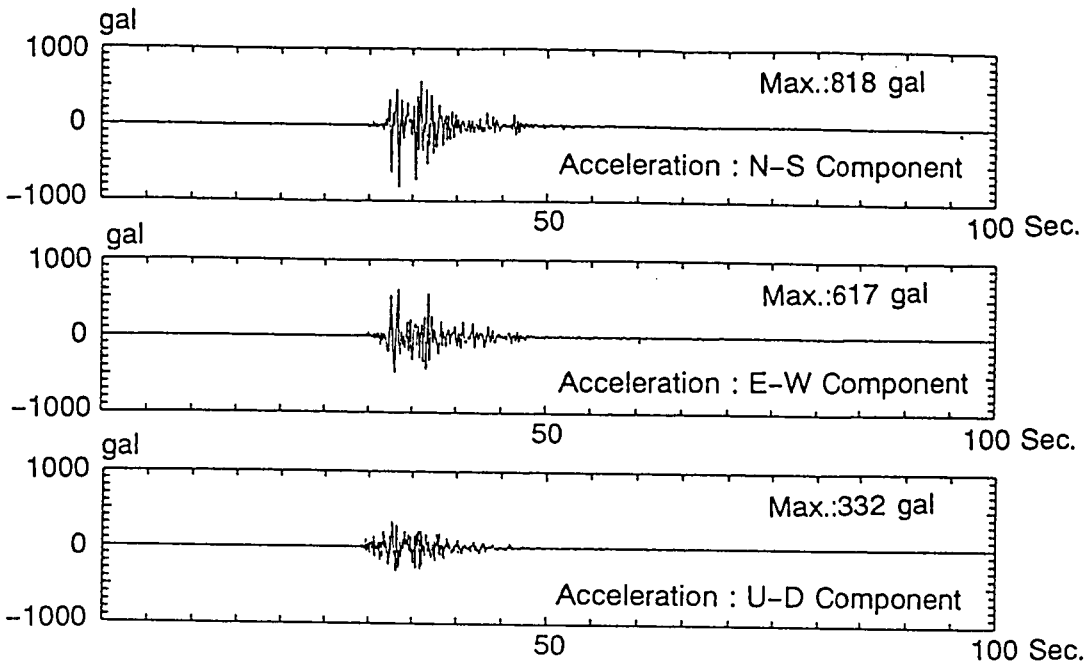

Fig.2 Acceleration Record at the Kobe Marine Observation

Figure 3 shows the distribution of the active faults near the epicenter. Measurements taken after the earthquake revealed a dislocation in the Nojima Fault. The Rokko Fault System also may be related to the the cause of the earthquake.

At the time of the earthquake the Akashi Kaikyo Bridge (see **Figure 4**), a suspension bridge about 4 km long with a 1,990-m center span, was under construction close to the epicenter. The substructures and towers had been completed, the strands of the main cables had all been installed, and cable squeezing work to round the cable cross sections was underway. Although seismometers installed around the bridge site did not record earthquake motions because the input was far above its setting, seismometers (velocity) installed at the top and middle level of the towers for the purpose of measuring wind-induced tower vibration, recorded the response to the earthquake, even though they were partially off the scale.

This report discusses the aseismic characteristics of the Akashi Kaikyo Bridge. The seismic records obtained from the Kobe Marine Meteorological Observatory were used because, as explained above, there are no seismic records from the bridge site. For examinations of the

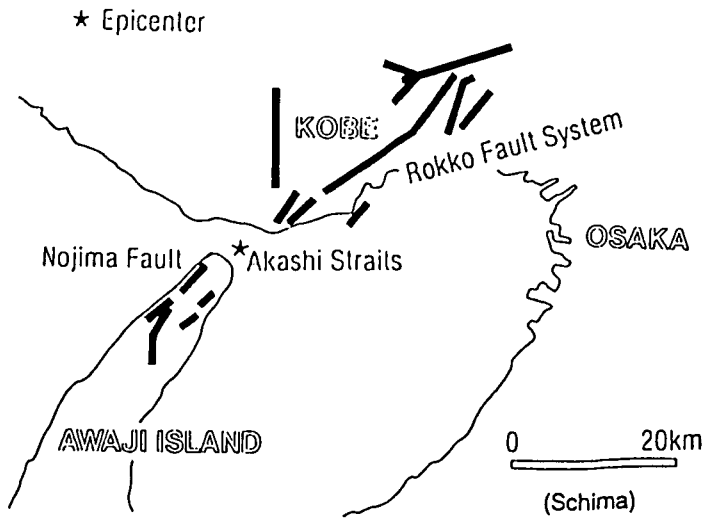

Fig.3 Distribution of Active Faults

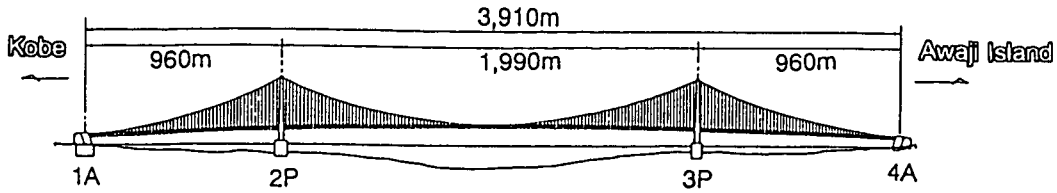

Fig.4 Akashi Kaikyo Bridge

aseismic characteristics of the substructure, seismic waves from the Kobe Marine Meteorological Observatory were adjusted out of consideration for differences in ground conditions. Examinations of the aseismic characteristics of the superstructure were based on records from tower top and middle level as well as seismic records from the Kobe Marine Meteorological Observatory.

DESIGN SEISMIC INPUT OF THE AKASHI KAIKYO BRIDGE

As **Figure 5** shows, only the anchorage on the Awaji Island side of the bridge was on the granite layer; the other substructures were built on the Kobe layer, an alternative of sandstone and mudstone layer, or on the Akashi layer, a Pleistocene sand and gravel layer. The aseismic design of the Akashi Kaikyo Bridge was based on the following two types of earthquake:

1. A epicenter distance of 150 km and a magnitude of 8.5
2. A epicenter distance of 300 km or less and a magnitude of 6.0 or more for return period of 150 years

Figure 6 shows the acceleration response spectrum used in the design of the Akashi Kaikyo Bridge. In the aseismic design calculations, interaction between the ground and the foundations were considered.

RESULTS OF POST-EARTHQUAKE INVESTIGATION

Immediately after the Hyogo-ken-Nanbu Earthquake, an investigation on the damage to the bridge was conducted. Visual inspections revealed no damage to permanent structures. Further inspections with an underwater camera, bathymetric survey, and sonic prospecting revealed no earthquake-induced damage to the ground around the foundations.

Figure 7 shows relative displacement of foundations measured after the earthquake, and it indicates that the center span was lengthened by 0.8 m and the overall bridge was lengthened by 1.1 m. Since there was no evidence of movement of the foundations relative to the ground, relative displacement of foundations was thought to be attributable to ground movement. Due to the changes in span length, the lengths of the main girders, which had not been built when the earthquake occurred, were adjusted by partially changing the lengths of girder members.

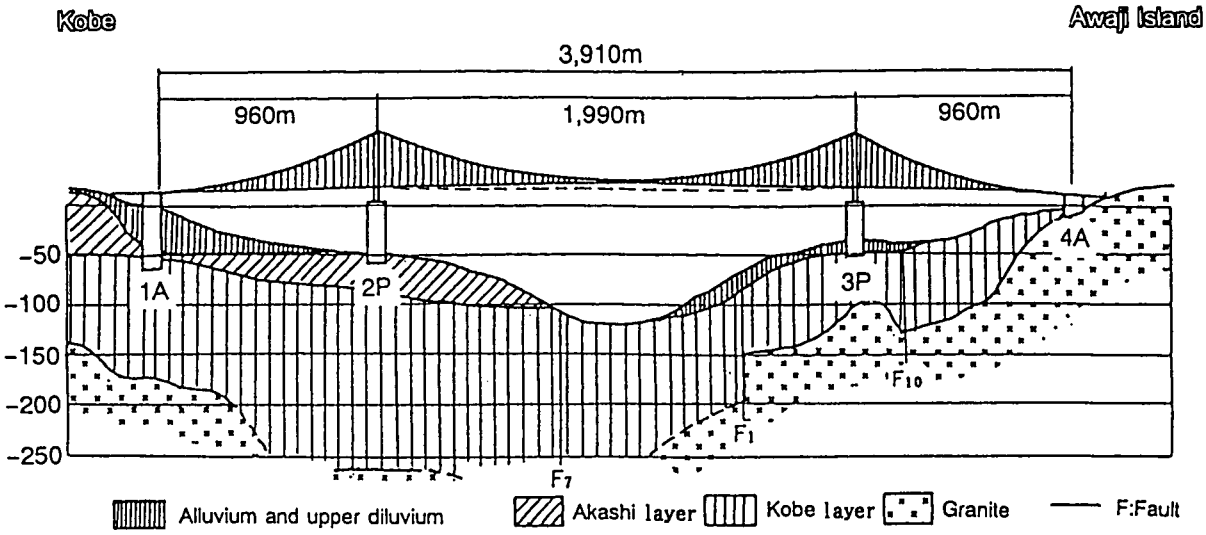

Fig.5 Geological Profile of the Akashi Kaikyo Bridge

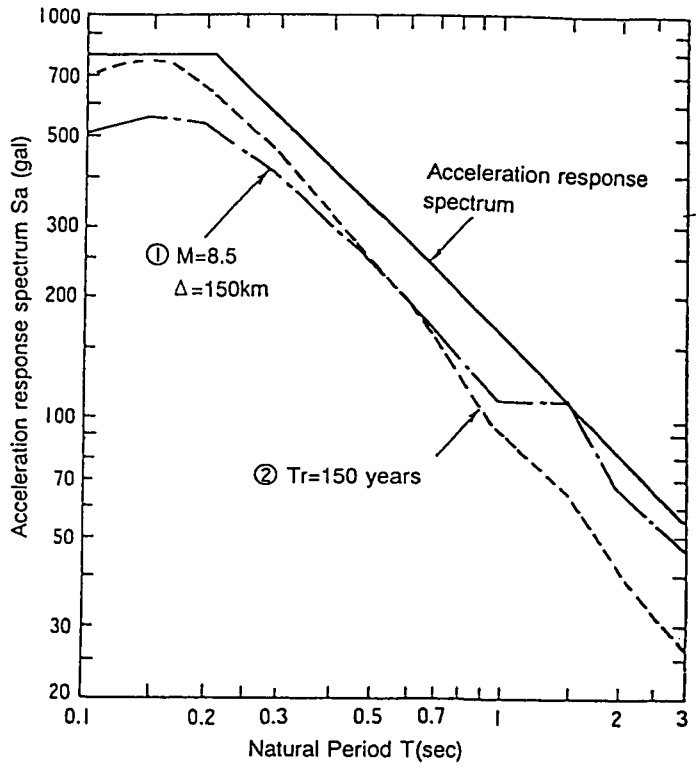

Fig.6 Design Acceleration Response Spectrum

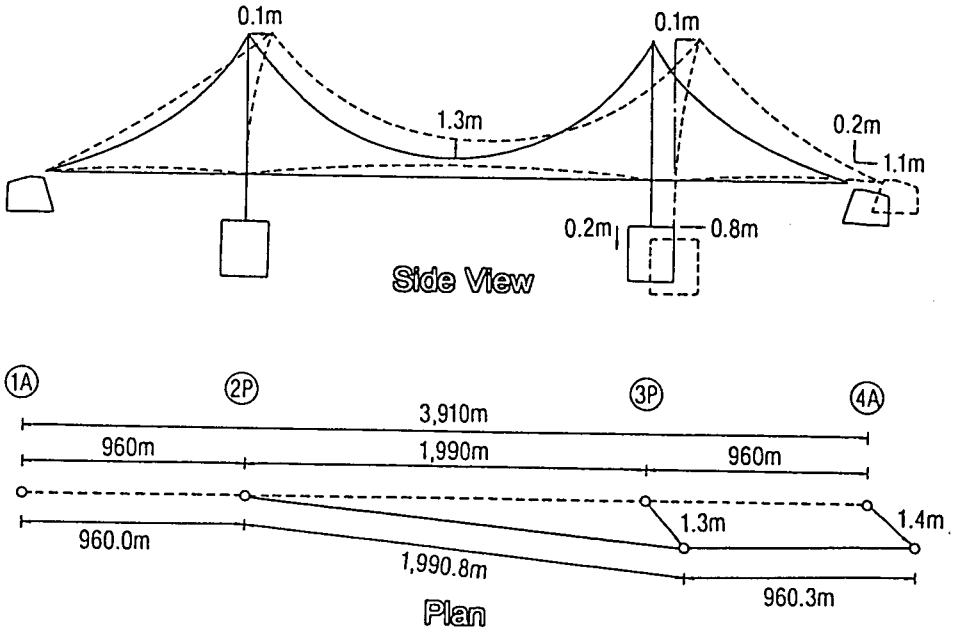

Fig.7 Relative Displacement of the Akashi Kaikyo Bridge

EXAMINATION OF SUBSTRUCTURE RESPONSE

Analysis outline

To evaluate the effects of the Hyogo-ken-Nanbu Earthquake on the substructure, a dynamic analysis and an examination of the stability and response characteristics of the substructure were conducted. This report outlines below the results of analysis of the main tower foundations (2P) on the Kobe side.

The input earthquake motions used in the analysis at the bedrock surface (top of the granite layer) were estimated from earthquake record at the Kobe Marine Meteorological Observatory. In the analysis, the ground was expressed with a two-dimensional, plane-strain FEM model, and the non-linearity of the ground was considered.

In this analysis, research results, which were obtained after the Akashi Kaikyo Bridge Aseismic Design Standard was established by the Honshu-Shikoku Bridge Authority, were incorporated to supplement the design standard. New items incorporated include the non-linearity of the ground, the separation between the foundations and the ground, and residual strain induced by cyclic shear loading.

Estimation of seismic input

The seismic input were estimated from the NS component (maximum 818 gal) and the UD component (maximum 332 gal) of the records of the Hyogo-ken-Nanbu Earthquake at the Kobe Marine Meteorological Observatory. As for the horizontal component, ground vibration at the top of the granite layer was estimated by one-dimensional wave propagating analysis for ground conditions at the Kobe Marine Meteorological Observatory considering the non-linearity of ground. As for the vertical component, the vertical transfer function of the injection points (top of the Akashi layer) for the top of the granite layer was calculated by using the convergence material values of the ground obtained through one-dimensional wave propagation analysis. And then earthquake motions at the top of the granite layer were calculated from observation records using the vertical transfer function.

These estimated waves were injected to the bottom of FEM model explained in the next section. **Figure 8** shows the estimated horizontal seismic input when the top of the granite layer was exposed.

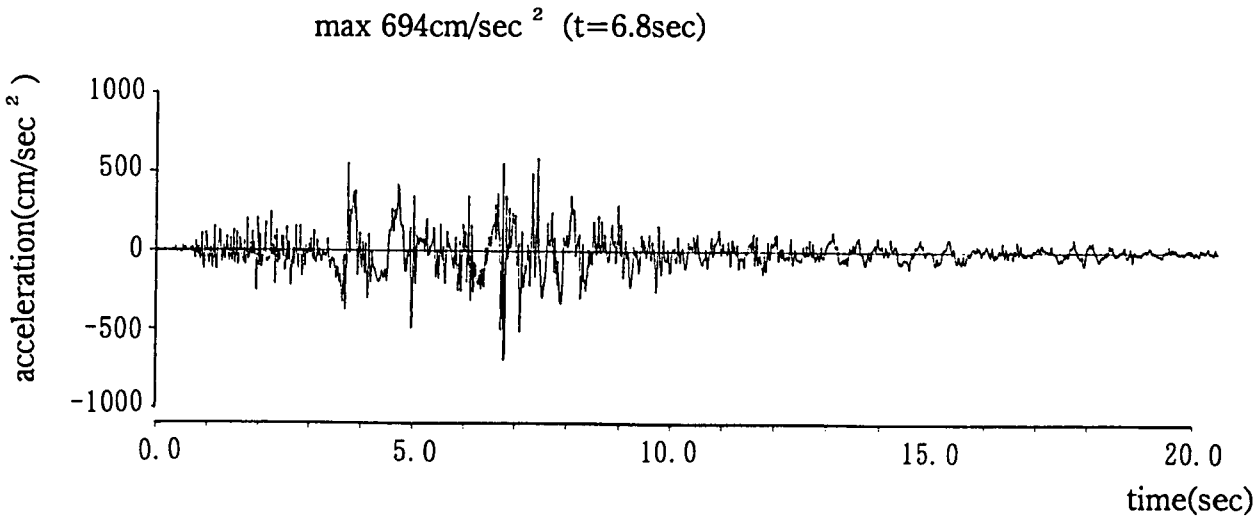

Fig.8 Estimated Horizontal Seismic Input(Top of Granite Layer)

Dynamic elastio-plastic FEM analysis

The non-linearity of the ground was taken into consideration by setting the stress-strain relationship in the modified Ramberg-Osgood model (hereinafter referred to as the "modified R-O model"). The boundary conditions of the bottom of the model (top of the granite layer) were set as fixed boundaries and those of the sides were set as viscous boundaries. The foundation was

assumed to be rigid body and foundation weight was concentrated at the center of gravity of the foundation in the model. To incorporate separation and sliding of the foundation relative to the ground, the joint element was used. **Figure 9** shows the analytic model. The tower was modeled by bar members to calculate the response of the tower.

Equation (1) shows the skeleton curve, which expresses the stress-strain relationship in the ground, and **Figure 10** shows the conceptual diagram of the non-linearity of the ground. In the non-linearity of the ground, the parameters α and β were set in a way that satisfied the relationship between the shear modulus G and the shear strain γ, and the damping constant h and the shear strain γ.

Skeleton curve:

$$\gamma = \frac{\tau}{G_0}\left(1 + \alpha\,|\tau|^{\beta}\right)$$
$$\alpha = \left(\frac{2}{\gamma_{0.5} G_0}\right)^{\beta}, \quad \beta = \frac{2\pi h_{max}}{2 - \pi h_{max}} \tag{1}$$

where: γ : shear strain
τ : shear stress
G_0 : initial shear modulus
α, β : parameter of the modified R-O model

As the modified R-O model is based on the Masing rule, stress-strain curve has a closed form. In this analysis, for the Akashi layer, to incorporate residual strain, non-linear parameter was introduced considering the results of the triaxial compression test on undrained condition. **Figure 11** shows the results of the triaxial compression test on undrained condition on the undisturbed sample of the Akashi layer. The vertical axis shows the stress ratio τ_{max}/σ'_{mc}(maximum shear stress/average principal stress); the horizontal axis shows the number of load repetitions. To reproduce the relationship between the number of repetitions N and axial strain when SRd=0.4 in Figure 11, equation (1) was modified to equation (2). The stress ratio SRd=0.4 was adopted because the preliminary analysis showed this value as the average stress ratio in the Akashi layer during the earthquake.

When loading and unloading:

$$\gamma = \frac{\tau}{G_0}\left(1 + \alpha\,|\tau|^{\beta}\right)$$

When reloading:

$$\gamma = \frac{\tau}{G_0'}\left(1 + \alpha\,|\tau|^{\beta}\right) \quad \text{where } G_0' = \frac{G}{F} \tag{2}$$

As for the F value in equation (2), 1.2 was adopted for the Akashi layer with which cyclic loading analysis with one element showed the relationship of the shear stress τ-shear strain γ approximated test results.

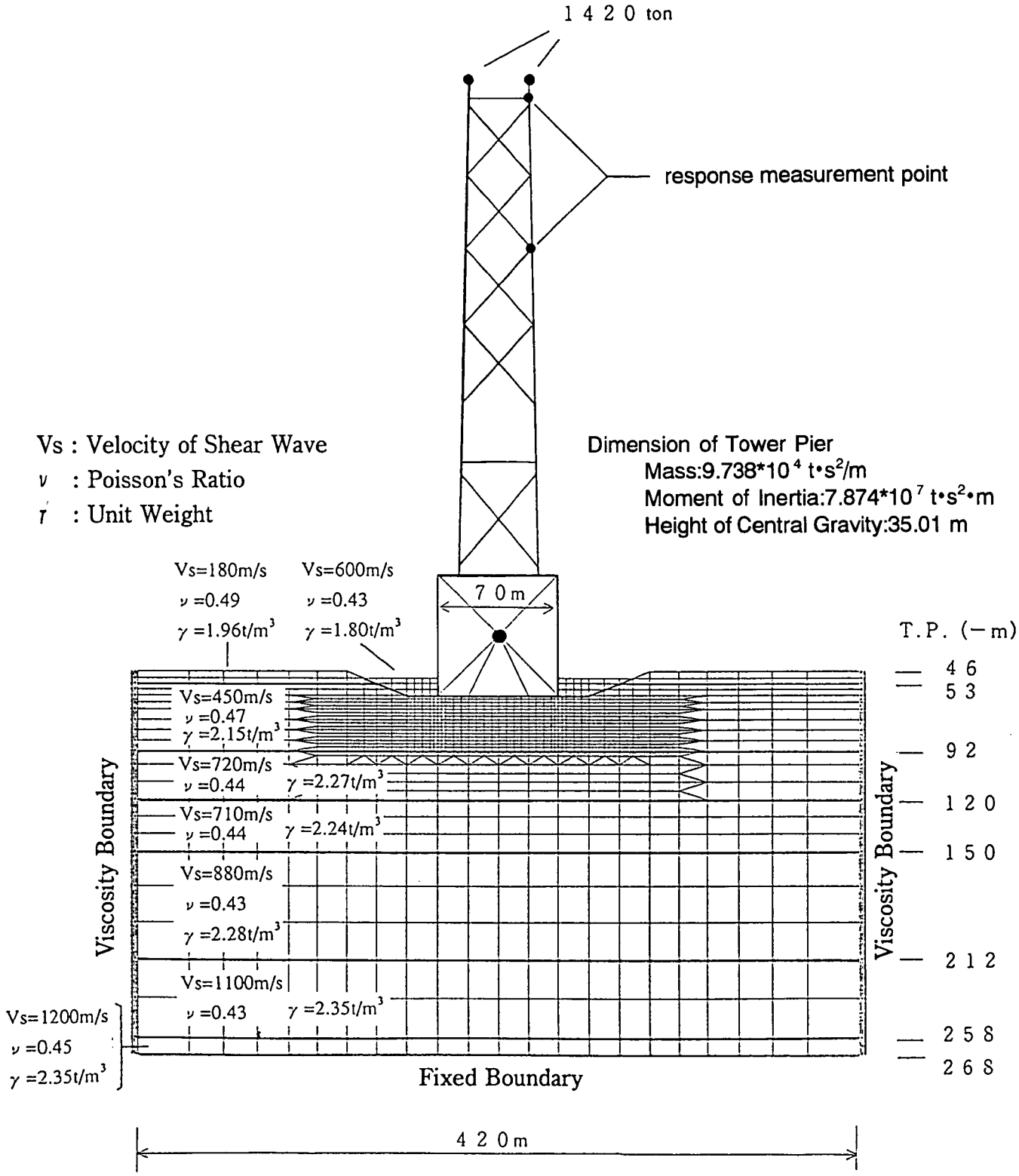

Fig.9 Analysis Model

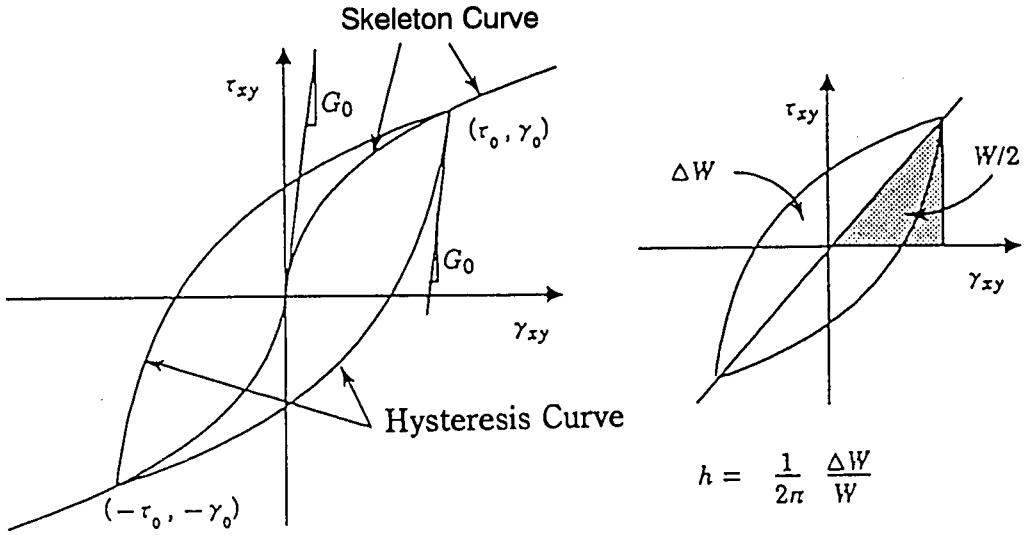

Relation of Shear Stress(τ) and Shear Strain(γ) , and Damping Factor(h)

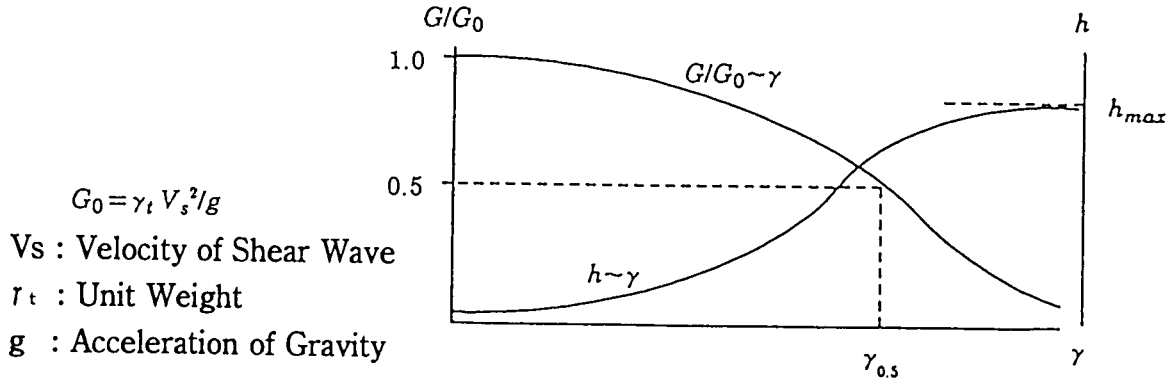

Analytical Model of Nonlinear Characteristics

Fig.10 Modified Ramberg-Osgood Model

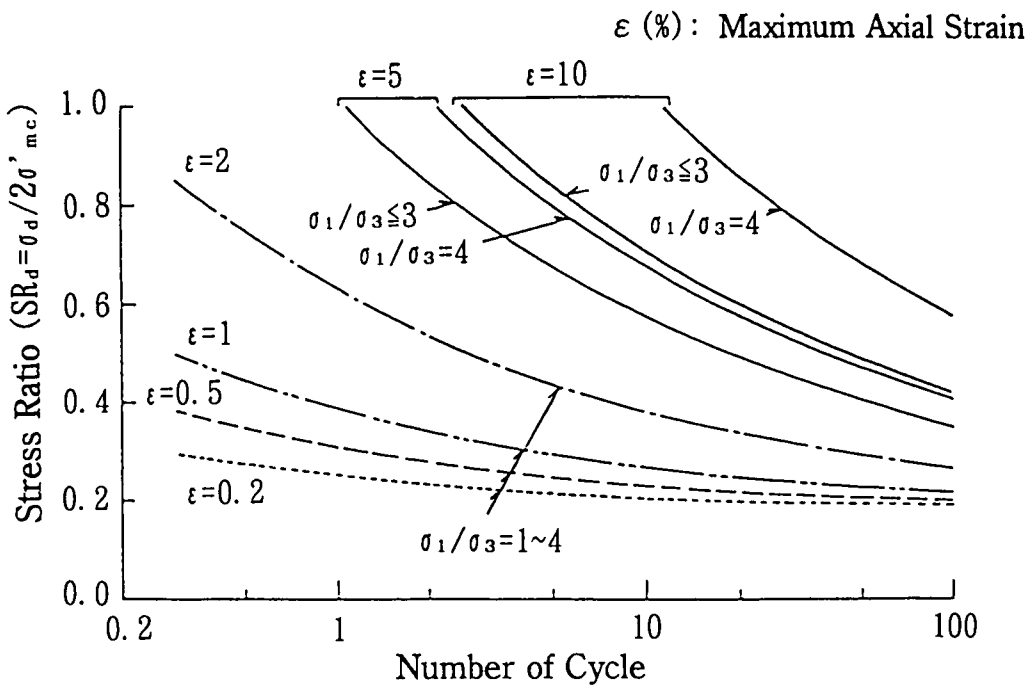

Fig.11 Triaxial Compression Test on Undrained Condition(Akashi Layer)

Analysis results

Table 1 shows the maximum response value at the center of gravity of the foundation and **Table 2** shows the forces at the foundation bases. The results of stable calculations when the moment was at its maximum, the condition at which the foundation was thought to be most likely to be unstable, indicated that the 2P foundations was stable at the time of the Hyogo-ken-Nanbu Earthquake.

Table-1 Estimated Substructure Maximum Response(Gravity Center)

	Horizontal	Vertical	Torsional
Displacement	15.2 cm	3.2 cm	0.0015 rad
Acceleration	363.5 cm/sec^2	264.4 cm/sec^2	0.0819 rad/sec^2

Table-2 Estimated Forces(Foundation Base)

	Horizontal	Overturning Moment	Vertical
Force	272,690 ton	11,579,971 ton•m	-804,420 ton

Figure 12 shows the time history of horizontal response acceleration at the center of gravity of the foundation. The center of gravity of the foundation vibrated as one degree of freedom system, and the natural period was 1.2 seconds. **Figure 13** shows the maximum accumulative shear strain contour. The maximum accumulative shear strain at the ends of the foundation was about 0.5% and it was thought that some parts of the ground were close to failure. **Figures 14 and 15** show time history and fourier spectrum of response at the top and middle level of the tower from the analytical result with measured record. As the analytical result cohere with measured record at the middle level of the tower, estimated seismic input is thought to be acceptable, and maximum acceleration was about 700 gal. However, at the top of the tower, the analysis result did not cohere with the measured record. This difference is thought to be due to effect of cable whose vibration is not considered in the analysis.

In this report, only the foundation of the main tower (2P), which is constructed on the weakest ground in the four foundations of the Akashi Kaikyo Bridge, are discussed. The same examinations have been conducted to the other foundations and their safety was checked.

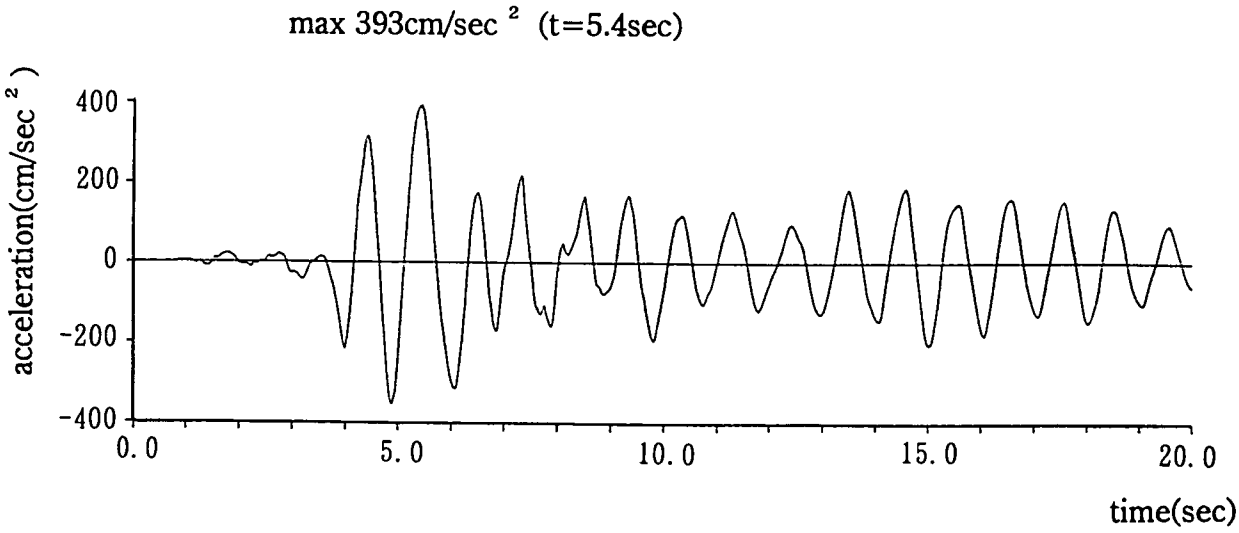

Fig.12 Time History of Response Acceleration at 2P Foundation

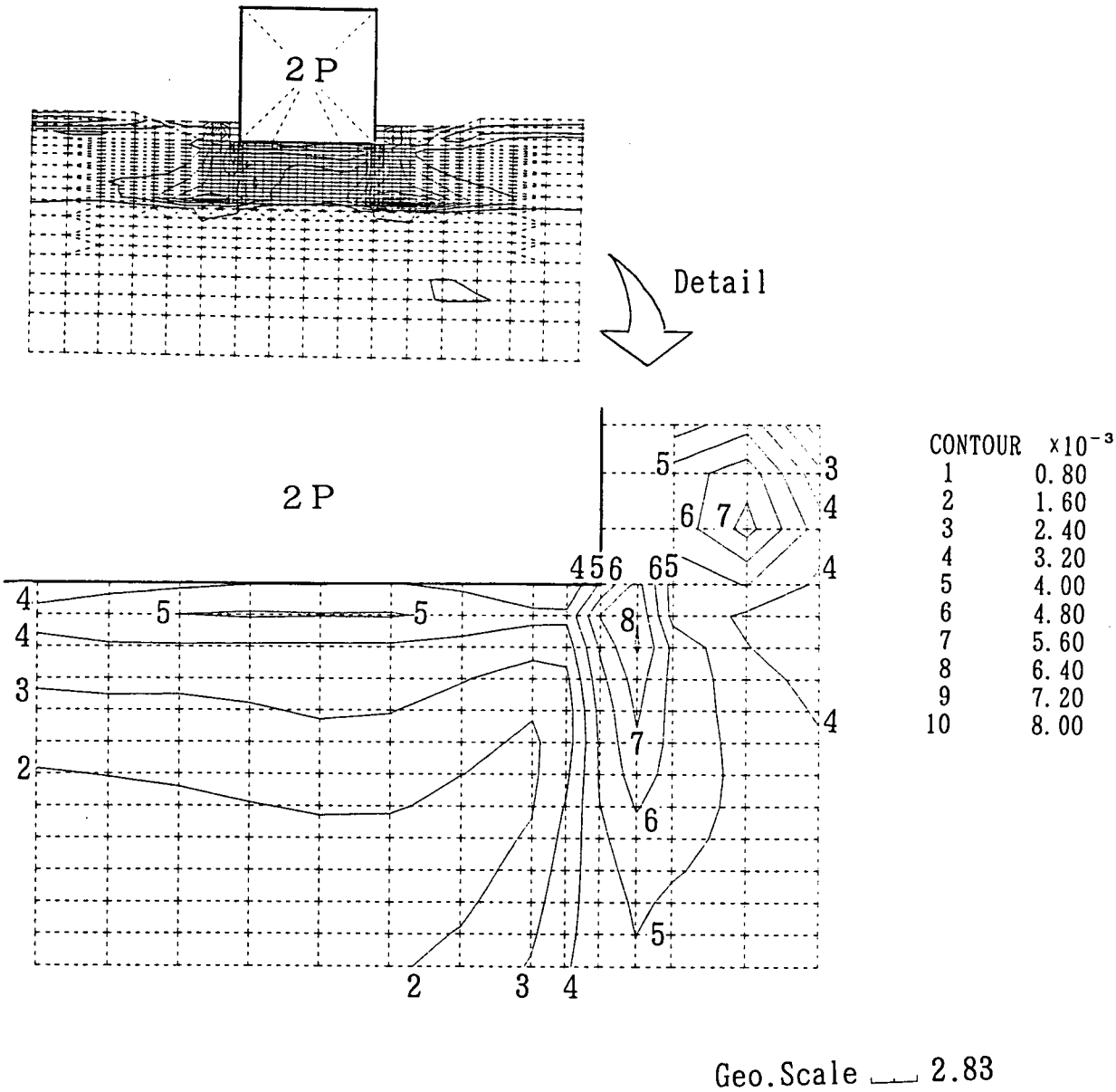

Fig.13 Contour of Cumulative Shear Strain

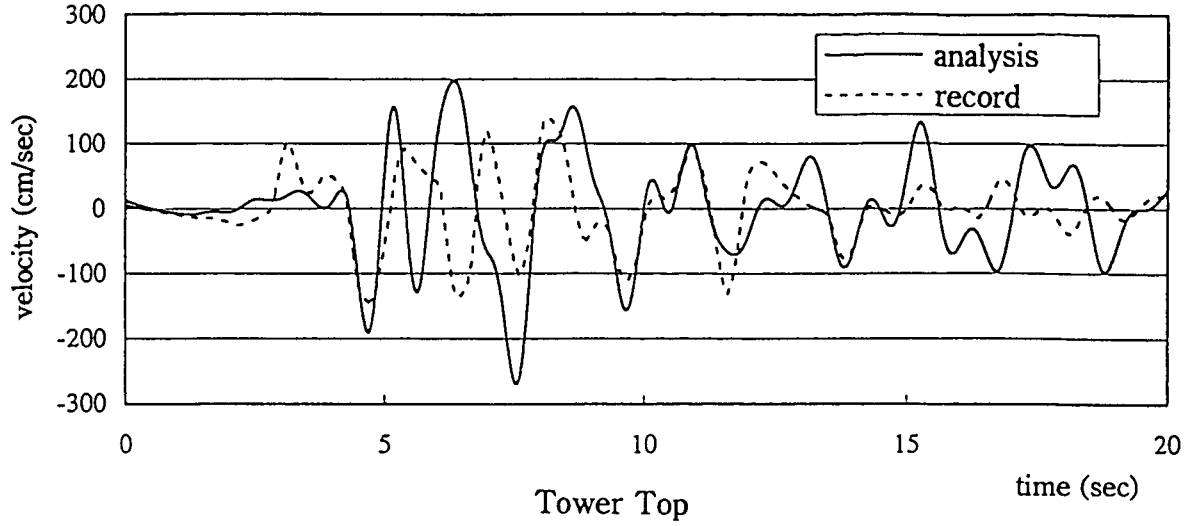

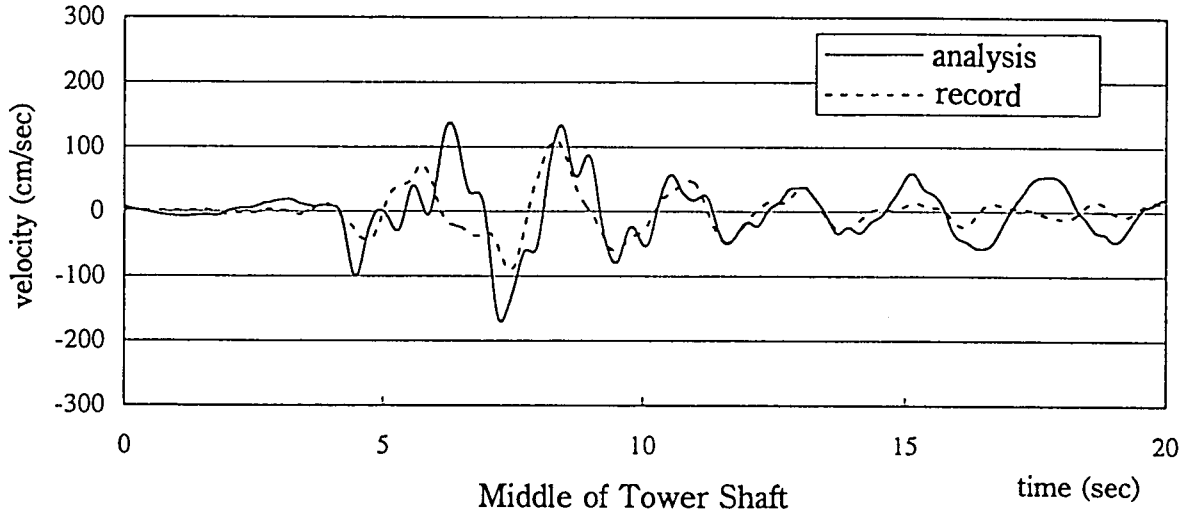

Fig.14 Time History of Response of Tower Shaft

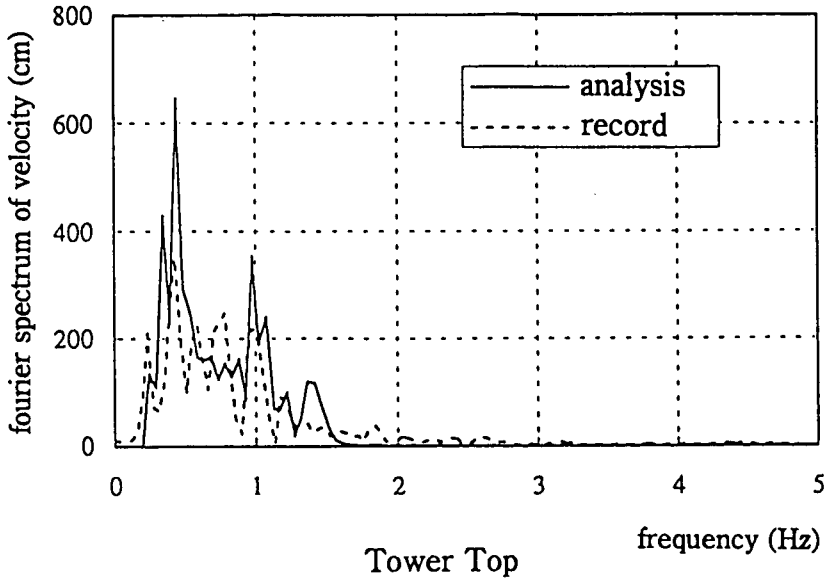

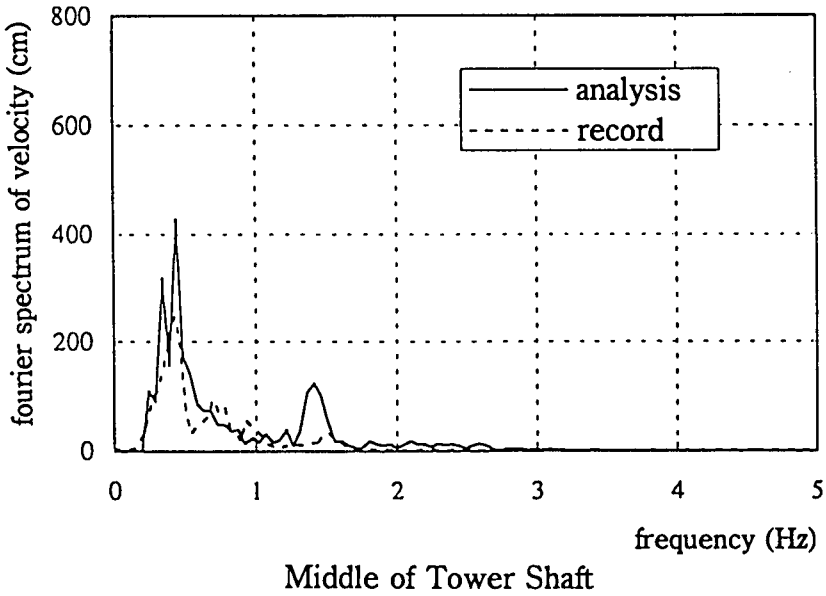

Fig.15 Fourier Spectrum of Response of Tower Shaft

EXAMINATION OF SUPERSTRUCTURE RESPONSE

Analysis outline

The aseismic features of the superstructure were examined based on the response records from the top and middle level of the main towers. This section discusses the feature of the records, the response estimation analysis method for when the Hyogo-ken-Nanbu Earthquake was input to the completed bridge, and the analysis results. As the earthquake motions at the site were unknown, records of the earthquake from the Kobe Marine Meteorological Observatory were used for the input earthquake motions in the response analysis, and the analysis results were adjusted by referring to the response records of the towers to obtain estimation results.

Seismic response records at the main towers

The response records of the main towers were obtained from the top and middle level of the main towers (see **Figure 16**). **Figure 17** shows the time history velocity records from the top of the towers on the 2P and **Figure 18** shows their power spectrum. The peak of the power spectrum was around 0.47 Hz along the bridge axial direction and around 0.40 Hz at transverse to the bridge axial direction. These matched the natural frequencies shown in **Figure 19**. The input of the main earthquake motions was a few seconds long but the response record showed large vibration for more than 30 seconds. This means that damping of the bridge system is very low. Maximum acceleration calculated from velocity records, exceeded 1,000 gal at transverse to the bridge axial direction.

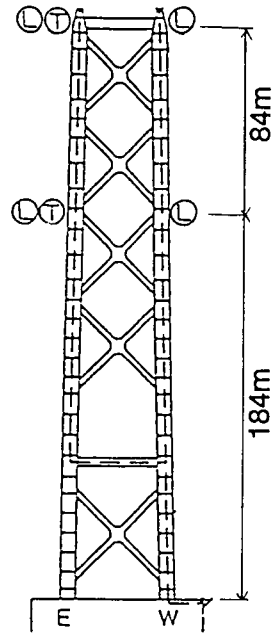

Ⓛ Along Bridge Axis
Ⓣ Transverse to Bridge Axis

Fig.16 Location of Velocity Meters

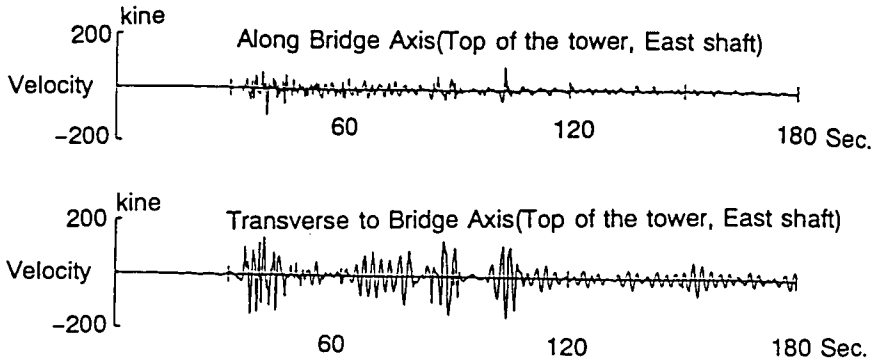

Fig.17 Velocity Record at the top of Kobe Side Tower

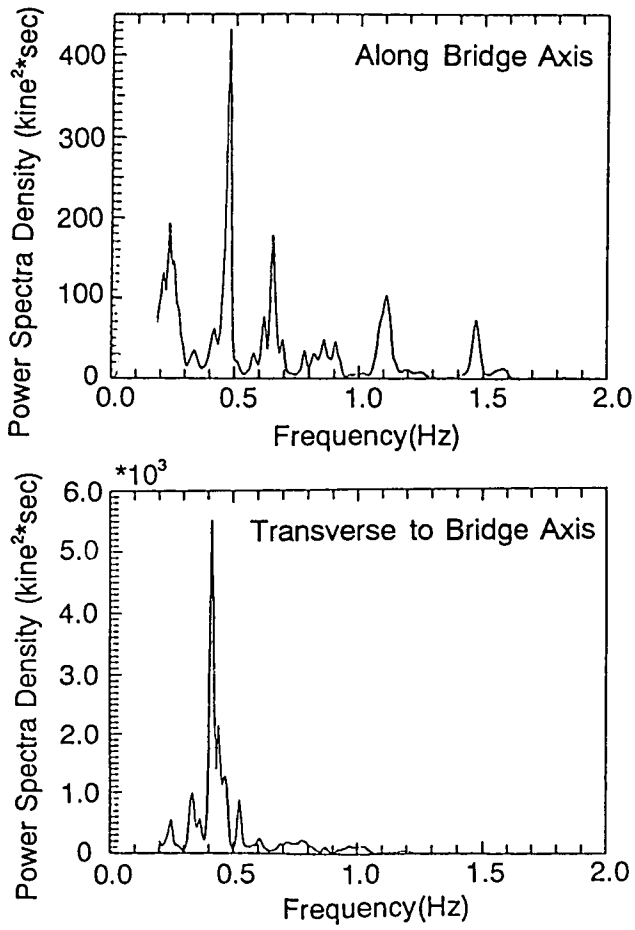

(2P,Tower Top)

Fig.18 Power Spectrum of Measured Velocity Record

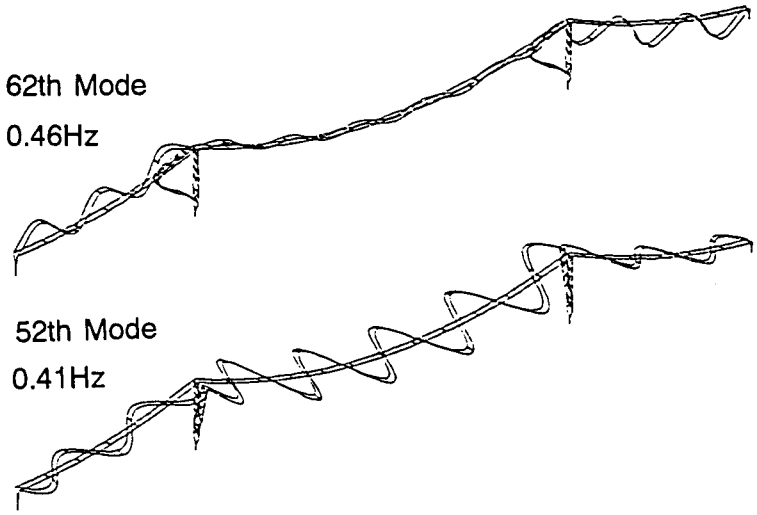

Fig.19 Natural Vibration Mode

Response estimation analysis method

In response estimation for the case at which the Hyogo-ken-Nanbu Earthquake was input to the completed bridge, response calculations for the superstructure were done by inputting records from the Kobe Marine Meteorological Observatory to the bases of the main towers as a hypothetical earthquake for analysis. However, the actual earthquake motions input to the bases of the main towers of the Akashi Kaikyo Bridge were different from those in the records from the Kobe Marine Meteorological Observatory because they were affected by the substructure, the ground, and interactions between the ground and the foundations. To adjust these effects, observation records taken at the top and middle level of the towers were referred to. In other words, the records from the Kobe Marine Meteorological Observatory were input to the tower bases of a model of the Akashi Kaikyo Bridge at the time of the earthquake (uncompleted system), and differences between the analysis results and observation records were expressed as transfer functions. And the transfer functions were used as correction functions. Response displacement were compared to create the correction functions. **Figure 20** shows an example of a created correction function.

Records from the Kobe Marine Meteorological Observatory were then input to the tower bases of a structural model of the completed bridge, and the analysis results were corrected using the above correction functions. **Table 3** shows that application of the correction functions depended on the section examined.

The structural model used in the analysis had only the superstructure above the tower bases; it did not have a substructure. The model was rigidly connected to the ground and ground spring was ignored. Structural damping was set to be h=0.01 for all modes. Earthquake motions were input to the tower bases and phase differences between the foundations were not considered.

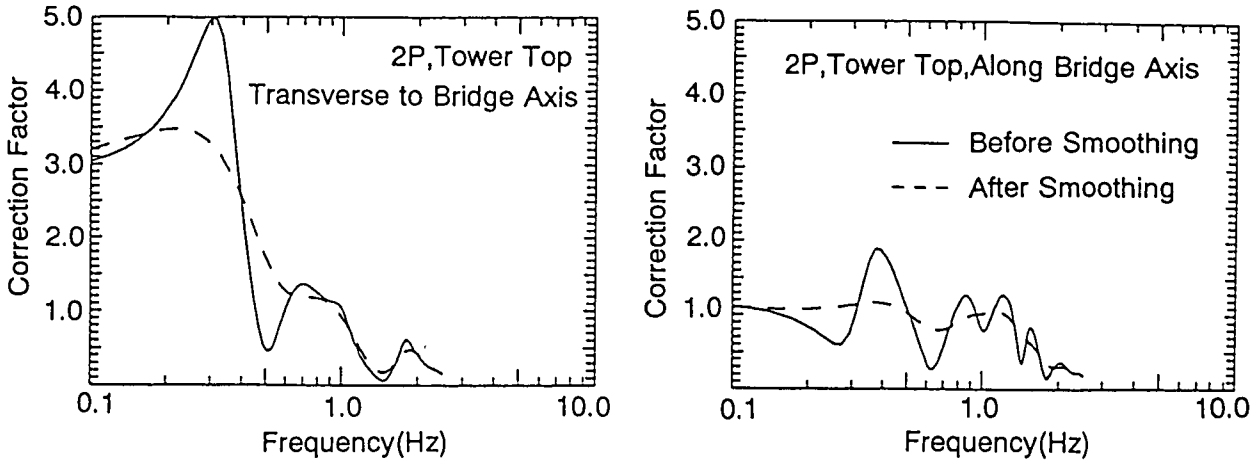

Fig.20 Correction Function

Table-3 Application of Correction Function

Location	Applied Correction Function
Tower Top	Correction Function form Record of Tower Top
Mid height of Tower	Correction Function form Record of Mid Hight of Tower
Tower Bottom	Average of above 2 Correction Functions

Response analysis results of the completed system

Figure 21 shows the response (speed) time history at the 2P tower top and middle level of the completed system after the analysis results were corrected.

Based on the corrected analysis results, the stresses on the tower bases, among the most critical parts of the bridge for the earthquake, were calculated. **Figure 22** shows a time history of the stresses on the corner of a cross-section of a tower bottom where the greatest stresses are generated. As the figure shows, there were brief moments when the stresses on both 2P and 3P exceeded the allowable stress level, but given their brevity the stresses did not reach the yield stress. Further, the area where stress exceed allowable stress was limited to small parts of corner sections. Given the above, it is thought that the entire suspension bridge system is very unlikely to fail.

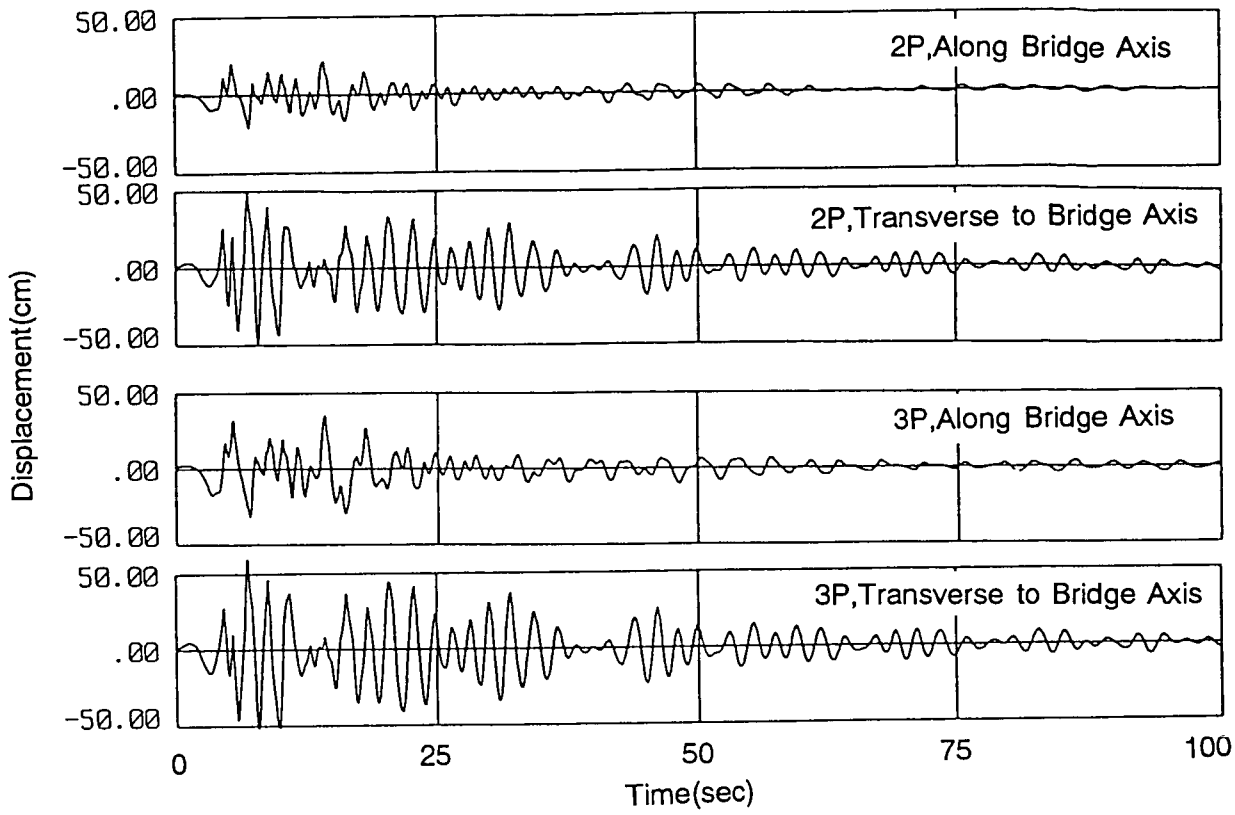

Fig.21 Displacement of Tower Top (Analytical Result)

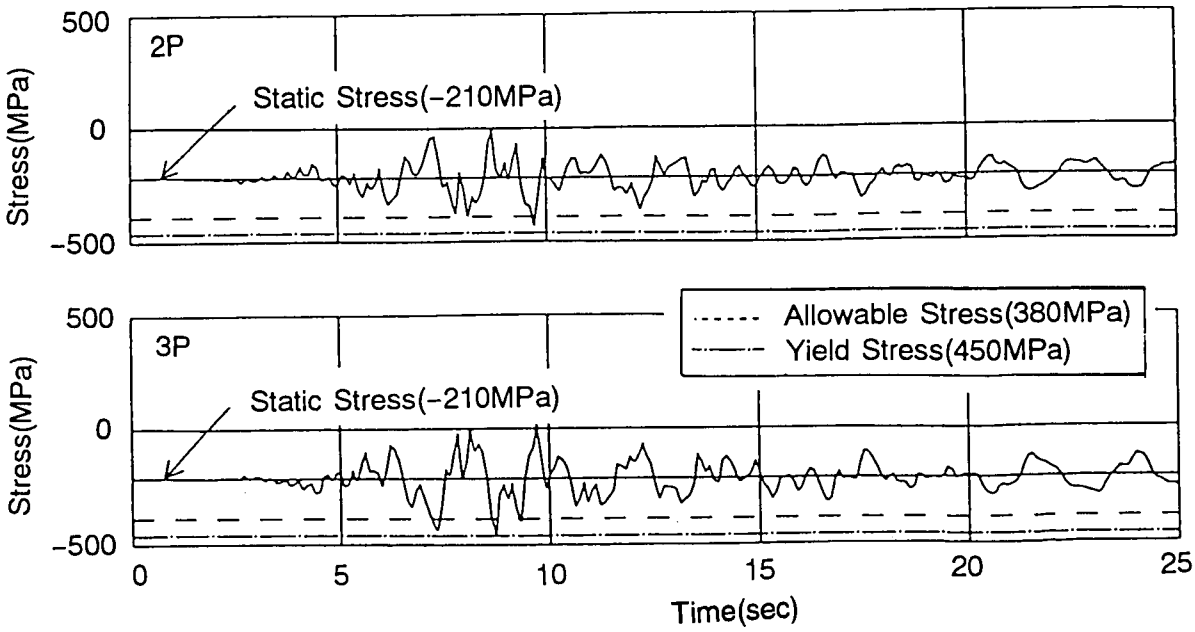

Fig.22 Stress at Corner of Tower Bottom

CONCLUSION

This report has discussed the aseismic features of the Akashi Kaikyo Bridge, particularly the response characteristics of the bridge when it was subjected to the forces of the Hyogo-ken-Nanbu Earthquake. The results of examinations suggest that if the Akashi Kaikyo Bridge had been completed at the time of the Hyogo-ken-Nanbu Earthquake, though at the ends of substructure, ground was close to failure, and with the superstructure, stresses on very limited sections of the tower bases exceeded the allowable stress momentarily, but will not reach the yield stress, the bridge would not have failed.

This is an intermediate report, and further study on estimation of seismic input at the bridge site, response of bridge is continued.

REFERENCES

1)K.Tada, H.Jin, M.Kitagawa, A.Nitta, R.Toriumi:Effect of the Southern Hyogo Earthquake on the Akashi Kaikyo Bridge,Structural Engineering International,Vol. 5, Number 3, August 1995.

2)S.Saeki, K.Tada, M.Kitagawa, A.Nitta, T.Kurihara:EFFECTS OF HANSHIN=AWAJI GREAT QUAKE DAISASTER ON THE AKASHI KAIKYO BRIDGE,11th Confference on Earthquake Engineering 1996

SEISMIC ASPECTS
OF THE WADI DIB CABLE-STAYED BRIDGE

M.P.Petrangeli M.Petrangeli

Dipartimento di Ingegneria Strutturale e Geotecnica

Università di Roma "La Sapienza"

ABSTRACT

The Wadi Dib bridge in Algeria, now in an advanced stage of construction, is a large cable stayed bridge characterised by very tall piers and a central span of 280 metres built using precast concrete deck segments. The bridge is located in a seismic region and therefore has required a careful evaluation of its seismic response, especially since the piers will be submerged by an artificial lake making it very difficult to carry out repair and strengthening in case of damage due to earthquake.
The paper summarise the seismic studies carried out by the designers and discuss some aspects related to the seismic input and seismic behaviour of these special structures, which are not explicitly covered by the codes.

1. THE BRIDGE

The bridge crosses the Wadi Dib along the road connecting Constantine to Jijel in Algeria. The area will be submerged by an artificial lake created by a dam across the Rhumel river downstream the confluence with the Wadi Dib. The bridge will be therefore required to cross this stretch of the lake at roughly 85 metres above the ground level.
The Dib valley around the crossing is deeply excavated into limestone with very steep slopes and heights in excess of 100 metres. The valley bottom is covered with detrital deposits of up to 15 metres thickness.
The bridge is 502 metres long [1], with a 280 metre central span and tower heights of 140 and 110 metres respectively as shown in **Fig.1**. The deck, **Fig.2**, has a multi-cellular concrete box cross-section stiffened by diaphragm at each stay anchorage (12 metres centre). The deck, now under construction, is made of 4 metres long precast segment which are lifted in place and joined together with a mixed type system. The box webs are glued together while a 40 cm wide strip on both top and bottom flange is cast in situ so as to provide continuity of the reinforcing steel and therefore assuring a ductile behaviour in case of catastrophic events. Longitudinal (external) and transverse (inside the diaphragms) prestressing is used.
Boundary conditions are the following: the deck is built in at the Jijel abutment while it rests on sliding supports at the Constantine side though these supports have been arranged so as to constrain rotations in the vertical plane and provide simple support in the horizontal one. Rigid connection is also realised between the deck and the towers in the transverse direction while in the vertical direction the deck rests on elastic bearings having a stiffness comparable to that of the adjacent stays so as to avoid hard points and therefore minimise the deck bending moments in the vertical plane.

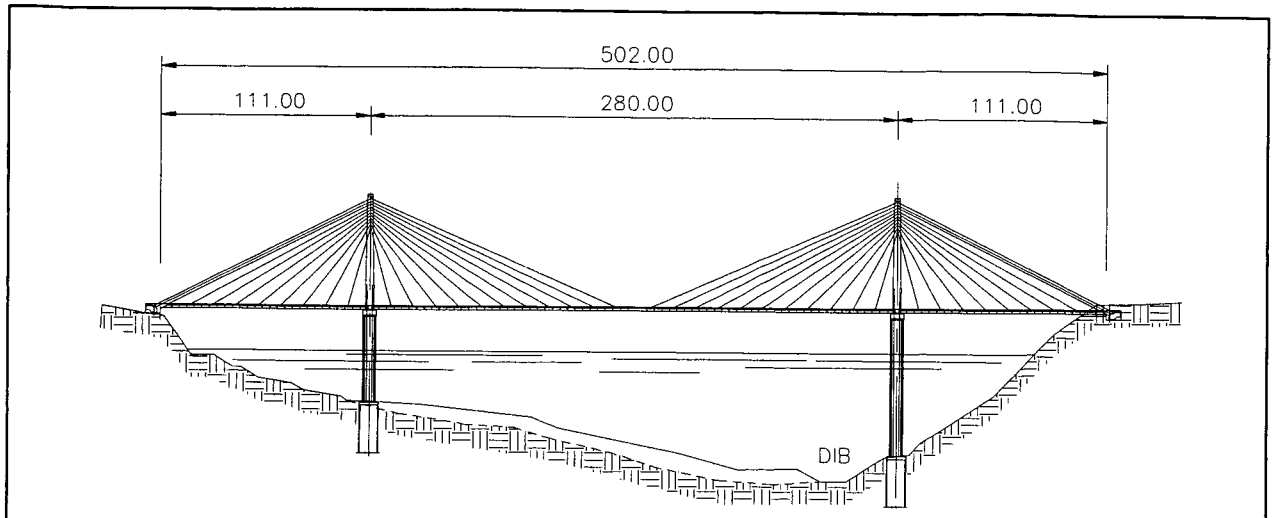

FIG. 1 - The Wadi Dib Bridge layout

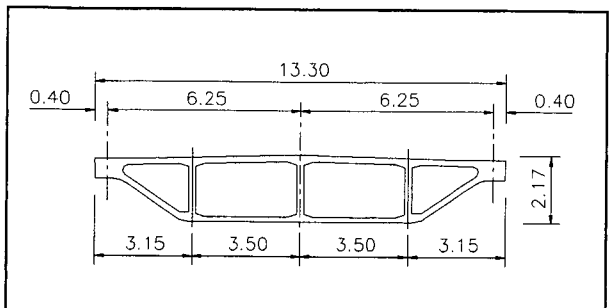

FIG. 2 - The deck cross section

The piers, extending from the foundations up to the deck level, have a reinforced concrete circular hollow section; the towers above instead have a concrete rectangular hollow section. The top segment of the towers, where the stay anchorages are located, is of the mixed type with a steel box, carrying the horizontal stay forces, encased into the concrete section, as shown in **Fig.3**. Stays are made of 19 to 45 galvanised 0.6" strands, singularly sheathed and greased, placed inside a HDPE sheath without grouting.

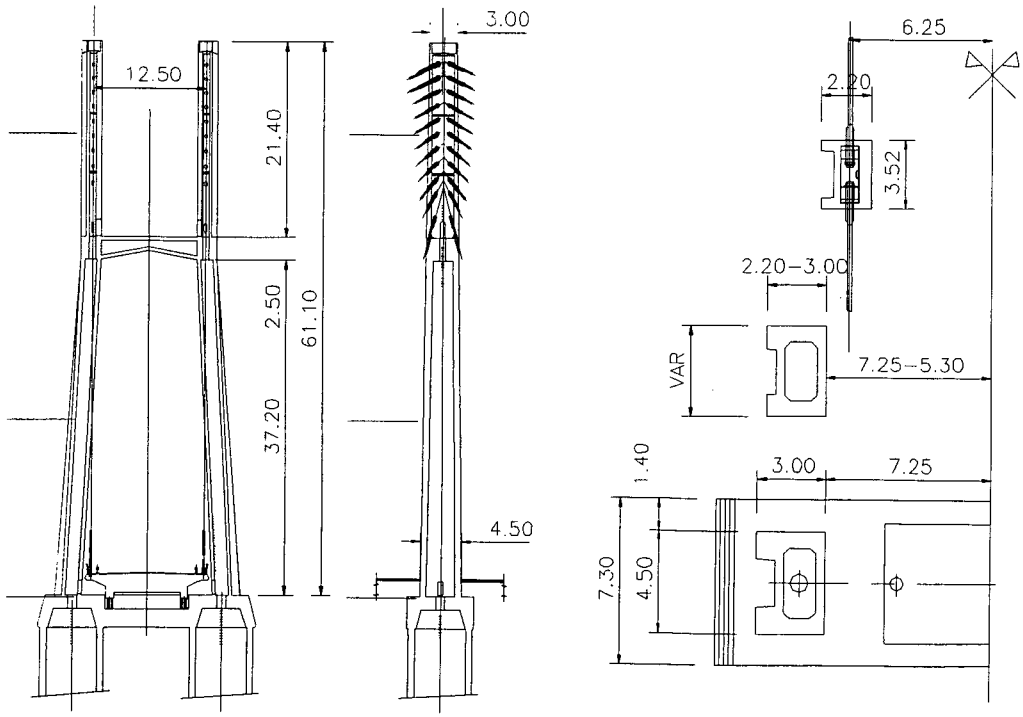

FIG. 3 - The bridge towers

2. THE LINEAR ANALYSIS

The bridge is build in a region of medium seismicity, with an expected GPA equal to 0.25g. Because of the bridge importance and the need to prevent serious damage in the piers given the difficulty to repair them once they will be submerged, a GPA equal to 0.30g has been assumed for the analyses.

Seismic analyses have been initially carried out on a 3D F.E. linear elastic model of the bridge as shown in Fig.4. Two different models have been set up, the first corresponding to dry condition (no water), the second to the maximum water level. In the latter, the mass of the water inside the hollow piers and an additional mass equivalent to the volume of the pier has been added to that of the structure.

The first five mode shapes of the bridge in "dry condition" are plotted in **Fig.4** to **8**, the first ten periods are summarised in the following Tab.1. It can be seen that modal participation factors are low, as a matter of fact in the seismic analysis the first 100 modes had to be considered to excite a sufficient percentage of the bridge mass.

MODE	Period (sec)	Mx %	My %	Mz %
1	2.720	34.76	0.00	0.00
2	2.701	0.00	0.51	9.49
3	1.888	0.00	4.09	0.11
4	1.672	8.01	0.00	0.00
5	1.672	0.00	9.97	0.72
6	1.131	0.00	11.14	0.01
7	0.978	15.57	0.00	0.00
8	0.978	0.00	0.15	3.70
9	0.948	0.00	2.63	17.85
10	0.834	0.00	0.00	0.05

Tab. 1 - Bridge mode shape and modal participation factors

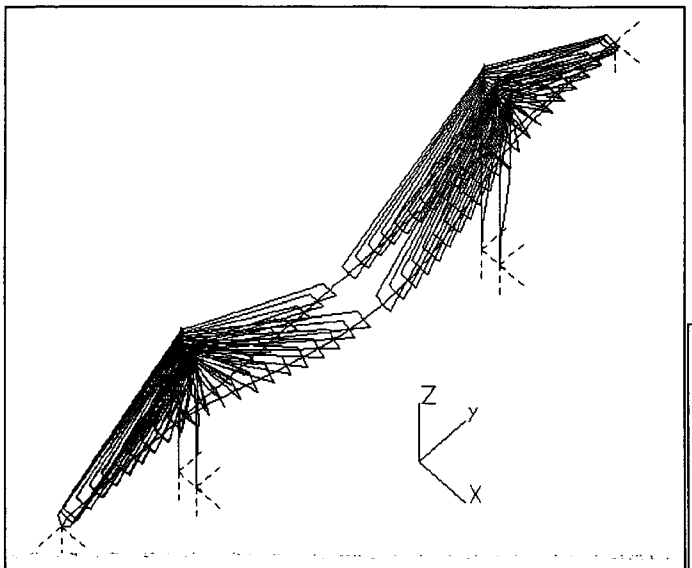

FIG. 5 - Mode Shape 1 (T=2.72sec.)

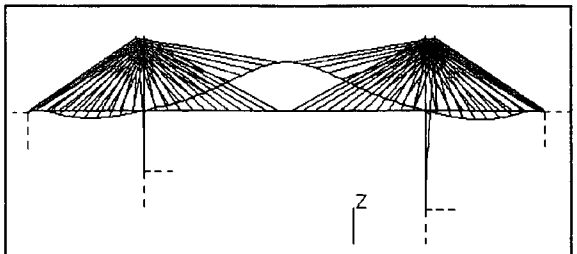

FIG. 6 - Mode Shape 2 (T = 2.70sec)

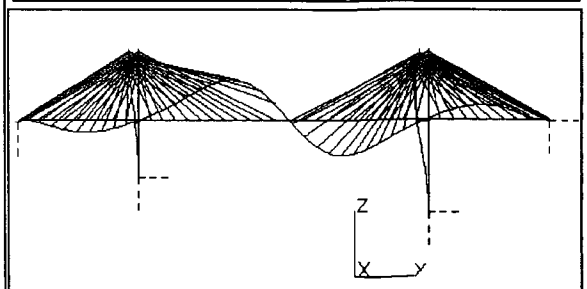

FIG. 4 - Mode Shape 3 (T=1.89sec.)

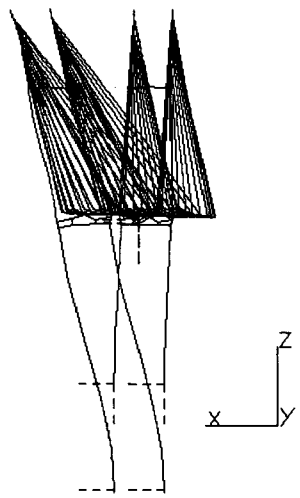

FIG. 7 - Mode shape 4 (T = 1.67 sec.)

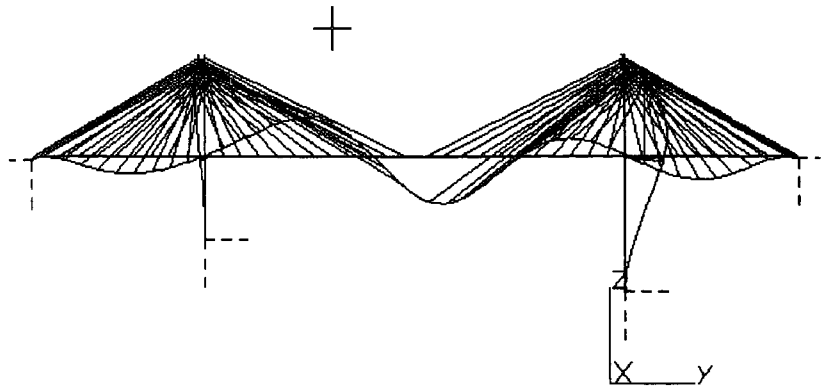

FIG. 8 - Mode shape 5 (T = 1.67 sec.)

The response spectrum analysis using the Algerian spectrum has then been performed along three orthogonal directions (longitudinal and transversally and vertically to the bridge axis). A plot of the Algerian response spectrum and of the Eurocode one is shown in **Fig.9**. It can be noticed that the European response spectrum is more severe then the Algerian one.
A structural ductility factor of 1.5 has been used for the dimensioning of the towers under horizontal seismic input thus obtaining a maximum response acceleration of:

$R_a = 0.3 \;\; 9.81 \;\; 2 \;/\; 1.5 \;\; = 3.94 \text{ m/sec}^2 \;=\; 0.4 \text{ g}$

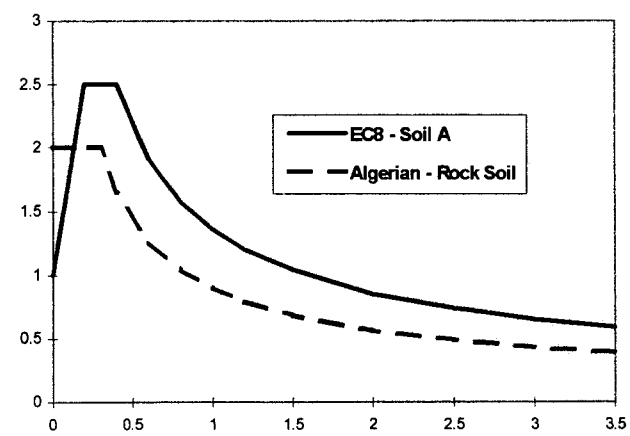

FIG. 9 - The Algerian and European response spectrum

The analyses clearly indicated that the most stressed part of the structure are the piers (below deck) and the towers (above deck). The most critical sections are the pier base sections (above the foundations) and the tower base section (above the deck). The bending moments found with the response spectrum analysis for these sections are reported in Tab.2.

The stresses in the deck due to the seismic input in the transverse direction are typical of a continuos beam on elastic supports (the towers). A structural ductility factor of 2 has been used for the deck which is capable of a more ductile behaviour, especially in the vertical plane where it can relay on the

stay support. Maximum stresses are localised at the Jijel tower (the stiffer one) followed by mid span and at the Constantine tower as shown in **Fig.10**. These bending moments correspond to a maximum stress, for the uncracked section of roughly 10 MPa.

	Longitudinal (kNm)		Transverse (kNm)	
	Dry	Flooded	Dry	Flooded
CONSTANTINE Base Section	96000	152000	197000	240000
JIJEL Base Section	139000	149000	144000	155000
CONSTANTINE Deck Section	/	/	21000	24000
JIJEL Deck Section	/	/	33000	36000

Tab. 2 - Bending moment in the towers

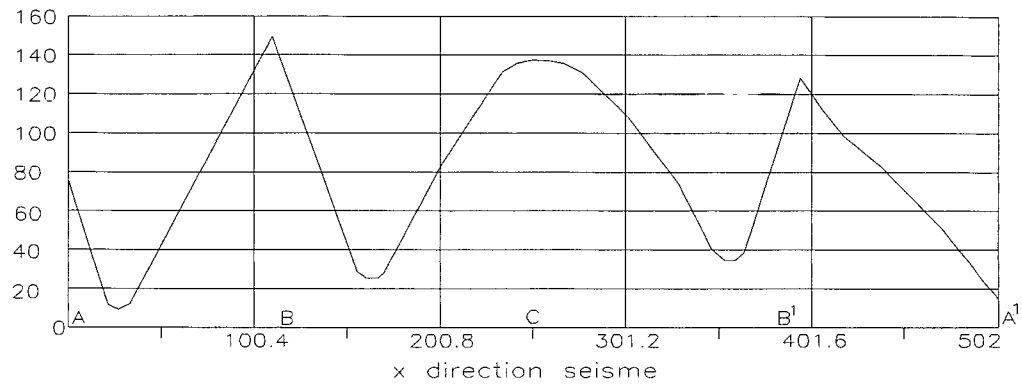

FIG. 10 - Bending moment in the deck - Transverse direction

For the seismic input in the longitudinal direction instead, the axial stiffness of the deck is much bigger than that of the stays and the towers and therefore it basically behaves independently of the rest of the structure. The fundamental axial frequency of the deck, with a cross section area of $7.1m^2$, a length of 502 metre and a mass of 20 kN/m almost uniformly distributed, is found to be equal to:

$$f_{Hz.} = 0.25/l \ \sqrt{E/\gamma} = 1.75 \qquad T = 0.57 \text{ sec.}$$

where $\gamma = 20/7.1 = 2.82$ and $E = 3.5e7$. The response amplification factor corresponding to this period being 1.3. Taking into account a ductility factor of 2, the Jijel abutment has been therefore dimensioned for an horizontal force of:

$$F_h = 502 \ 20 \ 1.3 \ 0.3 \ 9.81 / 2 = 19000 \text{ kN}$$

3. THE NON-LINEAR ANALYSIS

Following the preliminary assessment using the linear elastic response spectrum analysis, a number of non-linear analyses [2] using ground input motion have been carried out on 2D models of the bridge as represented in **Fig.10** and **Fig.11** .

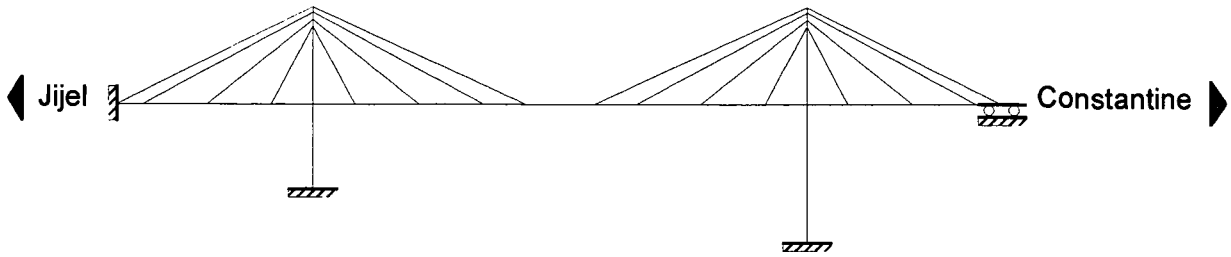

FIG. 11 - Wadi Dib stay Cable Bridge - Longitudinal model for the non-linear analysis

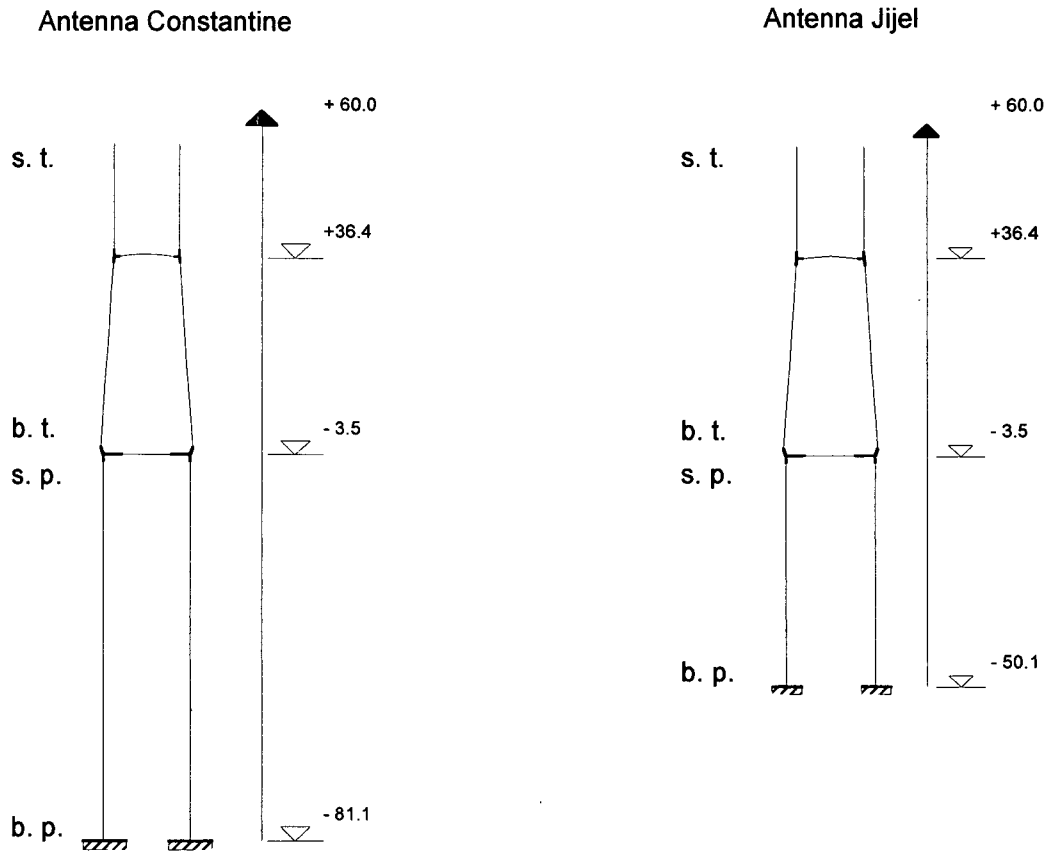

FIG. 12 - Wadi Dib stay Cable Bridge - Transverse model for the non-linear analysis

The longitudinal model is a 2D discretization of the bridge with the towers replaced by a single element having the same mechanical characteristic of the real frame structure and each three pairs of stays lumped in one. The model is therefore made of 35 beam elements for the towers, 18 beam elements for the deck and 18 truss elements for the stays. All the element are linear elastic except for the pier and tower element adjacent to the transverse beam below the deck and the pier base elements placed above the foundation. Details on these 2D non-linear beam element will be discussed in the following.

Two transverse models have been set up for the towers. The two models have been analysed separately therefore ignoring the interaction due to the stiffness of the deck. The mass of the deck has been taken into account instead by adding a nodal mass in the model, equivalent to that found with the modal analysis (i.e. modal mass). All the other geometrical and mechanical characteristics of the tower have been reproduced using linear and non-linear beam element. As for the longitudinal model,

non-linear element have been used for the pier base sections and for the pier and tower sections adjacent to the transverse beam at the deck level.

The non-linear element used in the analysis are smeared type plasticity elements using a hysteretic moment-curvature relation along the element [3][4]. This local behaviour is integrated along the element using an equilibrium based approach [5] which, contrary to the traditional stiffness approach, is capable of satisfying both equilibrium and compatibility.

The moment-curvature relations to be input into the non-linear elements are found before using a sectional program based on the layered approach and realistic uniaxial stress-strain relations for the concrete and steel constitutive behaviours. Mechanical properties of the two materials have been assumed as follows:

MECHANICAL PROPERTIES	CONCRETE	STEEL
ELASTICITY MODULOUS (KN/m^2)	2,3E07	2.0E08
STRENGTH(KN/m^2)	32.500	430.000

Tab. 3 - Mechanical properties of the materials

Although the moment-curvature relations found with the layered approach do take into account the effect of the axial force, once these curves are implemented into the beam model, the effect of the variation of the axial force in the element during the analysis is ignored. Three characteristic points of the monotonic moment curvature relation for the pier base sections and the towers base sections in the transverse direction are reported in Tab.4. These points correspond respectively to: cracking of the section (1), yielding of outer steel reinforcement (2), ultimate bending resistance (3). It must be noticed that the geometrical and mechanical characteristics of the Jijel and Constantine sections are the same and therefore the difference between the two moment-curvature behaviour is only due to their different axial load.

	M_1 (kNm)	χ_1 (1/m)	M_2 (kNm)	χ_2 (1/m)	M_3 (kNm)	χ_3 (1/m)
Constantine Pier Base	1.2079E+05	0.7721E-04	3.0196E+05	0.1801E-03	3.3999E+05	0.2972E-02
Jijel Pier Base	1.0629E+05	0.6618E-04	2.9133E+05	0.1820E-03	2.9919E+05	0.3556E-02
Tower Base Transv. Dir.	3.4213E+04	0.1985E-03	7.9655E+04	0.4963E-03	8.1259E+04	0.8403E-02

Tab. 4 - Tower base sections - Moment-Curvature relation - Characteristic values

Each of the three non-linear F.E. model has been subjected to two different ground input motions corresponding to the accelerogram records of El Centro and Taft scaled to 0.3 PGA. For each of the two accelerograms both dry and flooded configurations have been analysed for a total number of four analyses for each model. The moment-curvature time histories for the two pier base sections are reported. These plots refer to the El Centro analysis in the "dry configuration". It can be seen that the piers only experience cracking but no yielding of the rebars take place. Input motion in the transverse direction, where the towers do not benefit from the stay contribution, provide a slightly more severe condition.

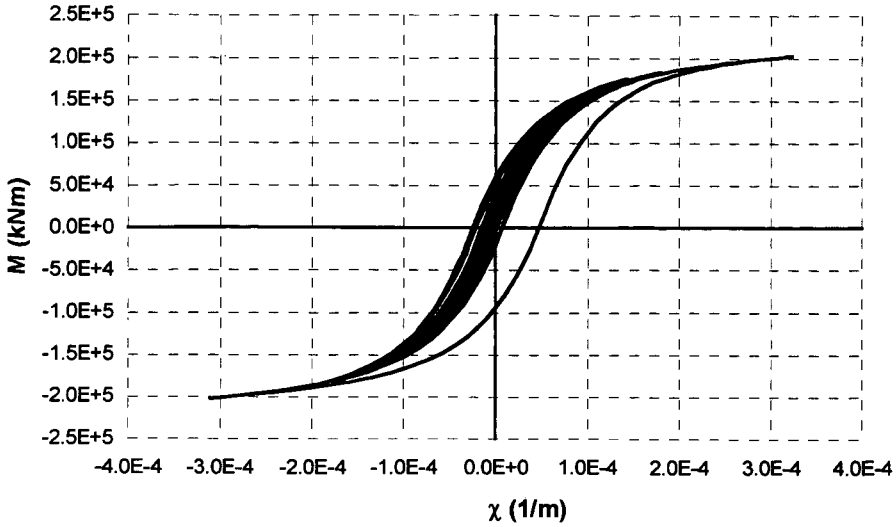

FIG. 13 - Jijel Pier Base section - El Centro - Longitudinal direction

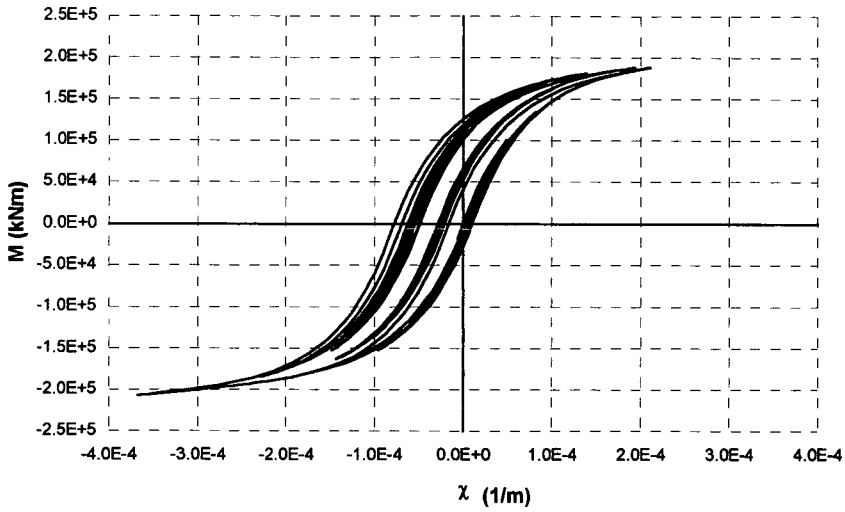

FIG. 14 - Jijel Pier Base Section - El Centro - Transverse direction

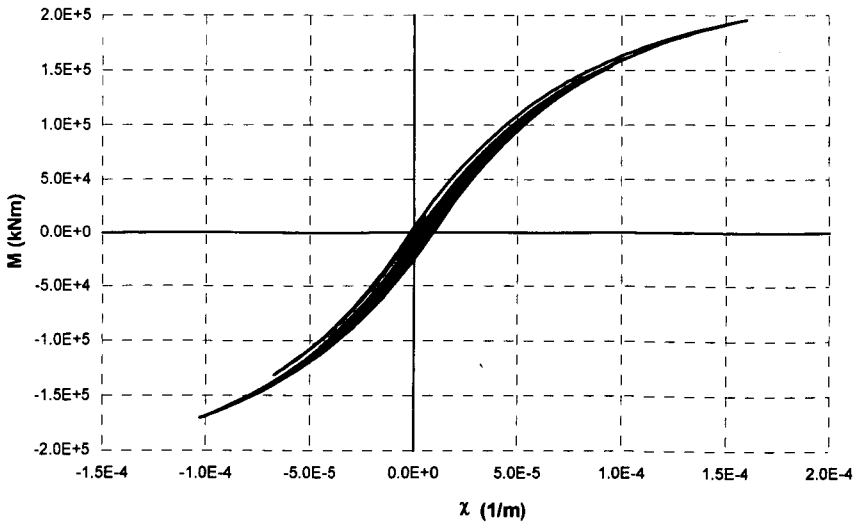

FIG. 15 - Constantine Pier Base Section - El Centro - Longitudinal direction

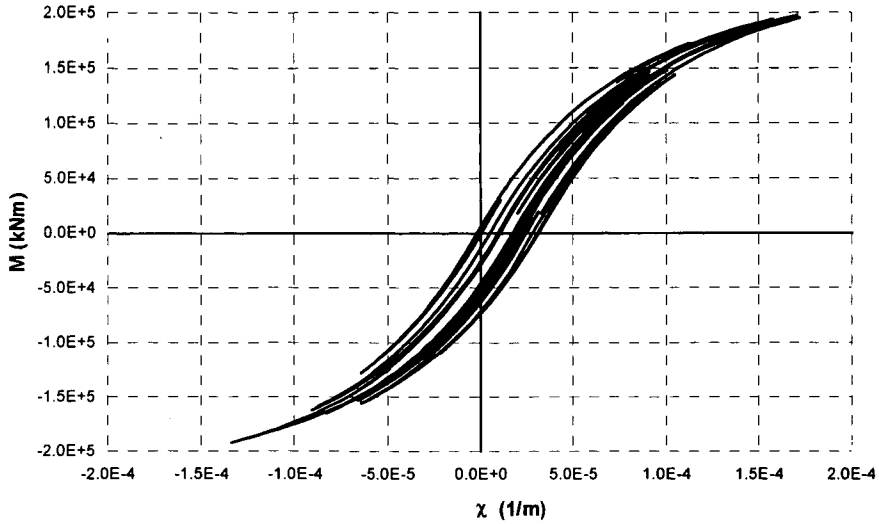

FIG. 16 - Constantine Pier Base Section - El Centro - Transverse direction

The maximum bending moments in the piers and towers found with the non linear analyses are summarised in Tab.5 and compared with the corresponding values found with the elastic analyses. All values in Tab.5 refer to the input motion in the transverse direction.

	Elastic analysis	Non-linear analysis
Constantine Pier Base	240000	233000
Jijel Pier Base	155000	207000
Constantine Tower Base	24000	48000
Jijel Tower Base	36000	56000

Tab. 5 - Bending Moment in the Pier/Tower - Linear versus non-linear analysis

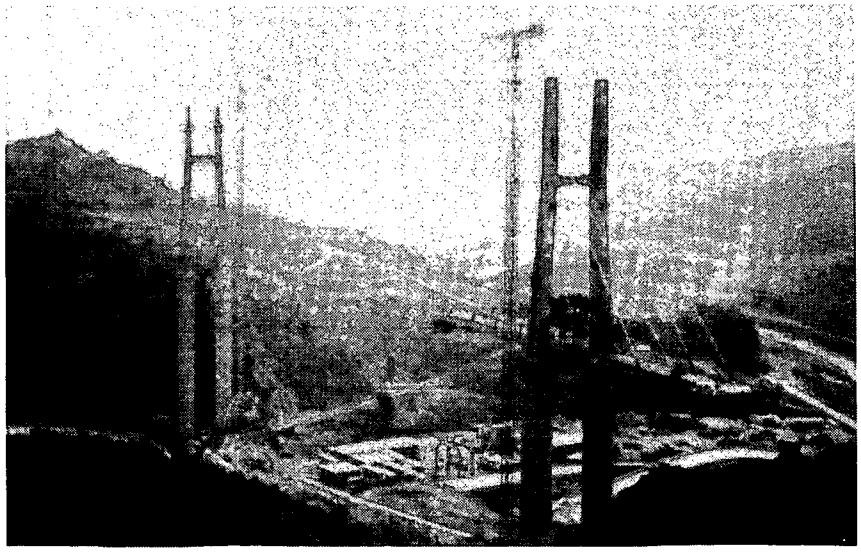

Photo 1 - The bridge under construction

4. THE CONSTRUCTION WORK

At February 1977, both towers and abutment have been completed and the deck cantilevering from the Jijel pier has reached the fourth stay. The segments, 4 metres long, are lifted from the yard by a travelling chariot travelling on the deck, placed in position and postensioned. Every three segments a couple of stays are erected and tensioned.
The construction is expected to be completed by the end of the year.

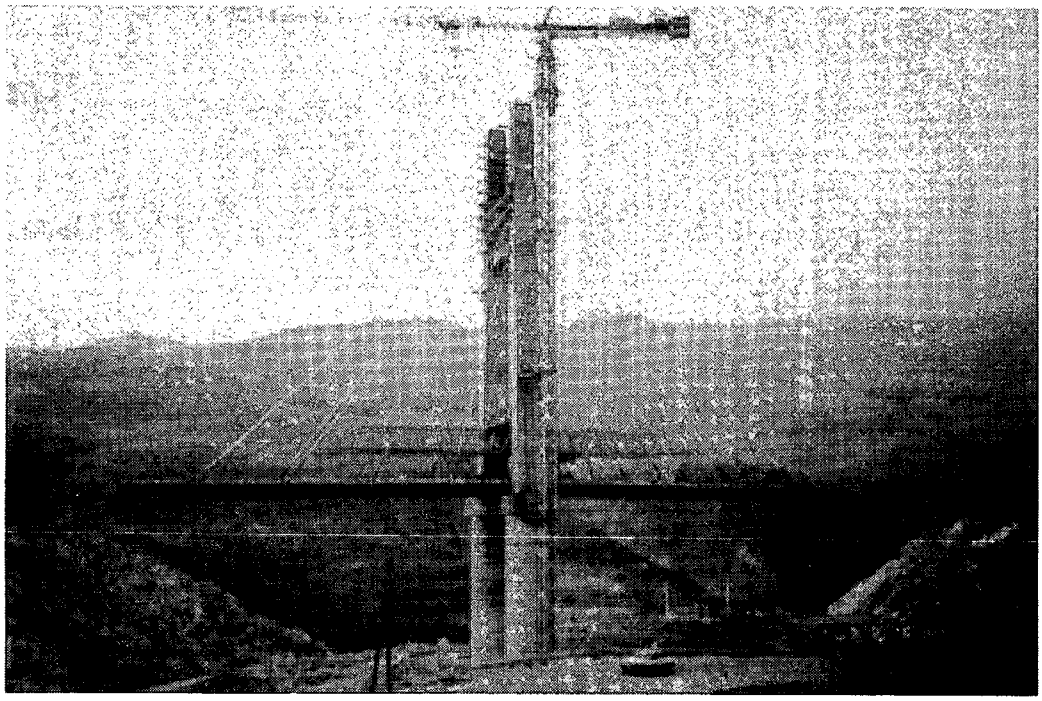

Photo 2 - Cantilevering out from the Jijel pier

5. CONCLUSIONS

Large and relatively flexible structures built in seismic areas as the bridge under consideration require a careful assessment of the their seismic response. There are two main factors distinguishing these structures from ordinary reinforced concrete bridges and frames which should be taken into due consideration when performing their seismic analysis.
Because of the very low frequencies the overall response of these structures normally fall well of the peak of the typical response spectrum. Therefore, very often the additional cost of keeping the global response of these structures due to seismic excitation in the elastic range is minimal compared to the overall cost of construction.
Structural ductility (the behaviour factor of the Eurocode) should be therefore fixed to a value reasonably close to unity. Reduction of the seismic response due to the ductile behaviour of these structures would cause in fact large displacements and localised damage in the piers as the overall behaviour is hardly redundant.
The second aspect which need to be pointed out is the existence of significant modes of the structures with completely different frequencies. This situation, which is a consequence of the structural complexity of these kind of bridges, requires a careful evaluation of the design procedures since there

may the necessity to use different "partial coefficients" (i.e. ductility allowances) for the various sub-components of the bridge.
For all the reasons recalled above, analyses using equivalent static forces or mode superposition may be inadequate for the assessment of the seismic performance of these structures since these methods do not provide a time history of the structural behaviour. To this extent the direct integration in the time domain of the structure response under seismic excitation should be performed, especially as these kind of analyses are today easily performed using finite element techniques.

REFERENCES

[1] Petrangeli, M.P. (1994). "Wadi Dib Bridge", *Proc. World. Conf. on Cable-Stayed and Suspension bridges*, 12-15 October, Deauville, France.
[2] Mondkar, D.P. and Powell, G.H. (1975). "Static and dynamic analysis of nonlinear structures", Earth quake Engineering Research Center University of California *Report No.75/10.*
[3] Ciampi, V. and Brancaleoni, F. (1983). "Modellazione e risposta sismica di strutture con degradazione" (in Italian) *Proc. I Convegno Nazionale di Ingegneria Sismica*, June, Rapallo, Italy.
[4] Ciampi, V. and Carlesimo, L. (1986). "A Nonlinear Beam element for Seismic Analysis of Structure". *8th Europ. Conf. on Earth. Eng.*, September, Lisbon, Portugal.
[5] Petrangeli, M. and Ciampi, V. (1996). "Equilibrium based numerical solutions for the non linear beam problem", *Int. Journal for Num. Meth. in Engrg*, 40(3), 423-438.

Session 5

Topic 3 Modelling and Analysis (3)

ITALY-JAPAN WORKSHOP ON SEISMIC DESIGN AND RETROFIT OF BRIDGES
Rome, February 27-28, 1997.

EXPERIMENTAL ASSESSMENT OF BRIDGES WITH ISOLATION AND NON-SYNCHRONOUS INPUT MOTION

A.V. Pinto and P. Negro

ELSA Laboratory, Institute for Systems Informatics and Safety
Joint Research Centre, European Commission
21020 Ispra (VA), Italy

ABSTRACT

Six large-scale (1:2.5) bridge specimens were constructed and tested pseudodynamically at the European Laboratory for Structural Assessment (ELSA). The tests were conducted in the framework of the activities of the integrated European programme of pre-normative research in support of Eurocode 8 involving eighteen research institutions from the European Union. The experimental programme was intended to provide background and improvement to the analysis and design methods. In particular, calibration and improvement of numerical models were sought. The first part of the programme (testing of four bridges) was devoted to exploring different design solutions aimed at obtaining a more homogeneous ductility demand in irregular bridges. The second part of the ELSA testing campaign was devoted to bridges with seismic isolation and to the non-synchronous input motion issue.

The series of pseudodynamic tests conducted for the bridges are described. Analysis concentrates on the results obtained from the tests with isolation and asynchronous input motion.

1. THE PRE-NORMATIVE RESEARCH PROGRAMME

The Eurocodes --the European provisional standards for constructions-- are being prepared by the European Committee for Standardization (CEN, Technical Committee No 250) under mandate of the European Commission. The Eurocodes are being released by the CEC as provisional norms (ENV). After a period of three years, during which comments are expected, the Eurocodes will be accepted as European norms (EV). The process of approval of each Eurocode has reached different stages. For the case of Eurocode 8 (EC8) [8] [9], the code relevant to the design of structures in seismic areas, priority needs for supporting research have been identified.

A scientific network has been set up to accomplish a Pre-normative Research Programme in support of EuroCode 8 (PREC8), under the Human Capital and Mobility programme of the European Commission. The network groups 18 research organisations in the European Union. The identified priority topics are: *Reinforced concrete frames and walls, Infilled frames, Bridges, Foundations and retaining walls.*

The research programme of the Bridge Group includes the following main tasks [3], [4], [7]: *Definition of regularity, Definition of design procedures for irregular bridges, Seismic isolation devices, Asynchronous base motion* and *Soil-structure interaction and second order effects.*

The experimental part of the programme included shaking table tests and pseudodynamic tests of six bridge models being performed in Ispra (JRC-ELSA). In particular, a series of tests devoted to the regularity issue for bridges were carried out including a test with isolation/dissipation devices. A final test with non-synchronous input motion was also performed. This paper will concentrate on these last tests. Detailed results and corresponding analysis can be found in [16] and [17].

2. THE LARGE-SCALE TESTING PROGRAM

The testing program at ELSA included a preliminary cyclic test of one squat pier, and pseudodynamic tests on six complete bridges. The bridges had three piers with height ranging from 7 to 21 meters and identical cross sections (rectangular hollow section with 400 mm thickness) and a continuous deck (200m long). The scheme of the full-scale bridges is shown in Figure 1. and Table 1 includes the geometric and reinforcement characteristics of the piers.

Table 1: Bridges selected to be tested pseudodynamically

Bridge Identification Label	Pier 1		Pier 2		Pier 3	
	Full-size height [m]	Steel percentage	Full-size height [m]	Steel percentage	Full-size height [m]	Steel percentage
B232	14.0	1.15	21.0	0.62	14.0	1.15
B213A	14.0	0.50	7.0	0.92	21.0	0.50
B213B	14.0	0.50	7.0	1.69	21.0	0.50
B213C	14.0	1.15	7.0	0.50	21.0	1.15
B213A I/D	14.0	0.50	7.0	0.92	21.0	0.50
B213A N/S	14.0	0.50	7.0	0.92	21.0	0.50

Two different schemes were adopted, having in mind to test the structures in the direction orthogonal to the bridge axis. One represented a typical regular bridge. The regularity was intended in the sense that the fundamental deflected configuration of the structure was similar to the one of the deck alone. The other scheme -the one with the shortest pier in the middle-, was regarded as highly irregular, since the stiffness of the deck induces higher forces in the internal stiffer pier.

As shown in Table 1, six bridge specimens were tested. The numbers which appear in the test identification labels represent the height modules in each of the three piers. The height module is 7 metres for the full-scale bridges, thus the bridge 232 had piers respectively 14, 21 and 14 metres high, and is the regular bridge. The other bridges -with 213 in the label- were irregular, with piers 14, 7 and 21 metres high.

The letters A, B and C in the label refer to the different design approaches. The label B213A stands for standard design according to EC8, part 2. The bridge B213B corresponded to the most straightforward design solution to the high ductility demands expected for the central pier, i.e. the central pier has been made stronger. In bridge B213C the taller piers have been made stronger instead, in an attempt to relieve the central pier from high forces.

The other two bridge specimens (B213A I/D and B213A N/S) were identical to the specimen

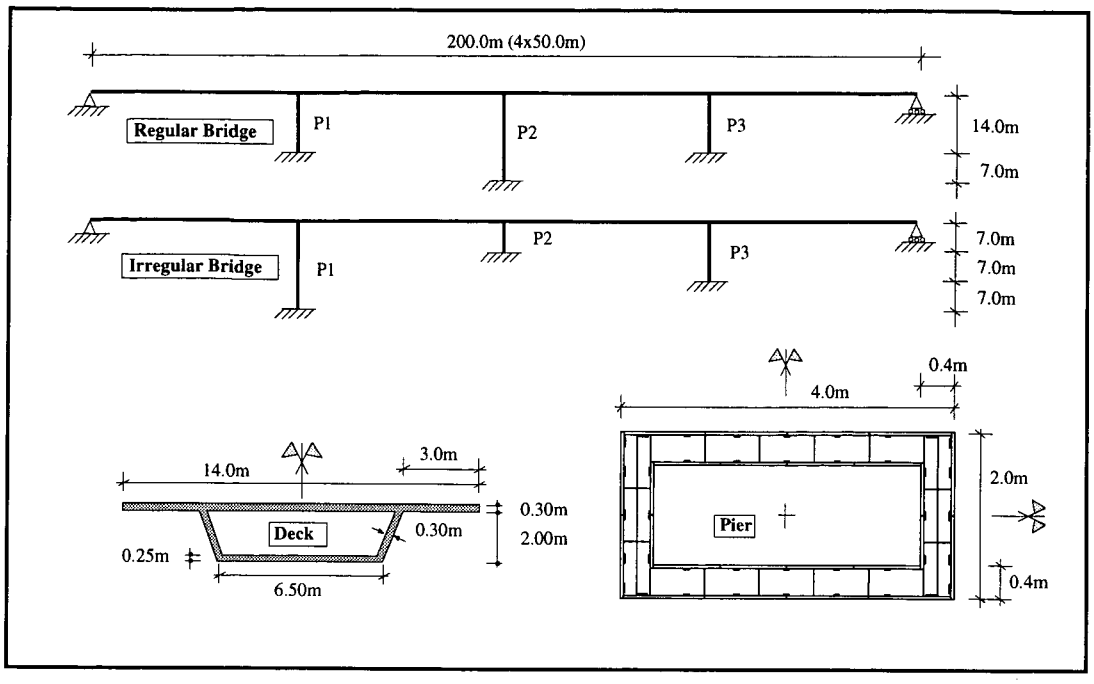

Figure 1. Full-scale scheme of the bridges being tested pseudodynamically

B213A, but were tested with seismic isolation devices and with asynchronous base motion respectively.

The bridge corresponding to the standard application of the design code was also tested with the view of including non-synchronous base-motions and seismic isolation devices. No special provisions have, however, been included in the design.

3. PSEUDODYNAMIC TESTS ON THE RC BRIDGES

3.1. Pseudodynamic testing

A pseudodynamic test is one which, although carried out quasi-statically, uses on-line computer calculation and control together with experimental measurement of the actual properties of the structure to provide a realistic simulation of the dynamic response. The equations of motion for a discrete parameter model of the test structure are solved on-line using a step-by-step numerical time integration method. Inertial and viscous damping forces are modelled analytically - a relatively straightforward matter compared to the nonlinear structural restoring forces, which are measured experimentally because of the practical impossibility of modelling them accurately. The process automatically accounts for the hysteretic damping due to inelastic deformation and damage of the structural materials which is the major source of energy dissipation.

To simulate the earthquake response of a structure, a record of an actual or artificially generated earthquake ground acceleration history is given as input data to the computer running the pseudodynamic algorithm. The horizontal displacements of the controlled degrees of freedom (where the mass of the structure can be considered to be concentrated) are calculated for a small time step using a suitable time integration algorithm. These displacements are then applied to the test structure by servo-controlled hydraulic actuators fixed to the reaction wall. Load cells on the actuators measure the forces necessary to achieve the required displacements

and these structural restoring forces are returned to the computer for use in the next time-step calculation. Details of the capabilities of the ELSA Laboratory and of the pseudodynamic implementation are given elsewhere [2].

The pseudodynamic test method is a hybrid technique which combines the numerical integration of equations of motion of complex structures condensed on a reduced number of degrees-of-freedom (d.o.f.), with the experimental measurement of the reaction forces resulting from this motion. Despite the potential of the pseudodynamic technique, direct testing of very large civil engineering structures like bridges would require a number of controlled d.o.f. that could exceed the experimental capabilities. It is, however, possible to extend the field of application of the method, at least when the behaviour of a part of the structure is well known, by introducing a substructuring technique [6]. This technique takes advantage of the hybrid character of the pseudodynamic test method by combining the numerical simulation of the known part of the structure, the substructure, with the physical testing of the remaining structural part, the tested structure. The method is well suited for bridges since their largest part, the deck, can be assumed to be linear elastic and therefore modelled by any finite-element software: only the piers, whose dimensions remain reasonably small, and where damage is expected, are tested in the laboratory.

A further advantage, which is again well suited for bridges, is the possibility of dealing with situations where the seismic excitation is asynchronous or presents different amplitudes along the foundation.

Details of the ELSA implementation of pseudodynamic testing with substructuring are given in [2].

3.2. Test setup

The piers were aligned in front of the reaction wall, with the shorter one in the middle, as can be seen in Figure 2.. The plinths of the piers were rigidly attached to the strong floor by means of steel bars passing through the floor itself. A stiff steel cap was connected with bolts and epoxy resin to the tip of the piers. The cap was used to apply the vertical load corresponding to the weight of the deck as well as to apply the horizontal loads required to impose the computed displacements.

The axial force (1700 kN) was applied by means of four actuators, placed inside the hollow core pier and connected to the cap and to instrumented steel bars embedded in the pier plinth. The vertical force was imposed at the beginning of the test and remained practically constant, thanks to the hydraulic accumulators placed to compensate the effects of the horizontal displacement.

Two double-acting servo-hydraulic actuators (three for the central pier in the test B213B), capable of a load of 1.0 MN each were used to apply the horizontal displacements. They were connected by spherical joints to the steel cap at one side and to a steel plate attached to the reaction wall at the opposite side. The imposed displacements were measured with respect to two independent steel frames using digital optical transducers.

On-line numerical simulation of the substructured part was performed using a fibre Timoshenko beam element described in [10]. Furthermore, the 'required' pre and post-test simulations were also carried out [11].

3.3. Instrumentation

The instrumentation of the piers included both active measurements -those which are related to the pseudodynamic control algorithm-, and passive instruments. Passive instruments can be grouped in the following sets: *Rotations*: Pairs of displacement transducers have been placed at different levels on the two external opposite faces of the specimens to measure the local rota-

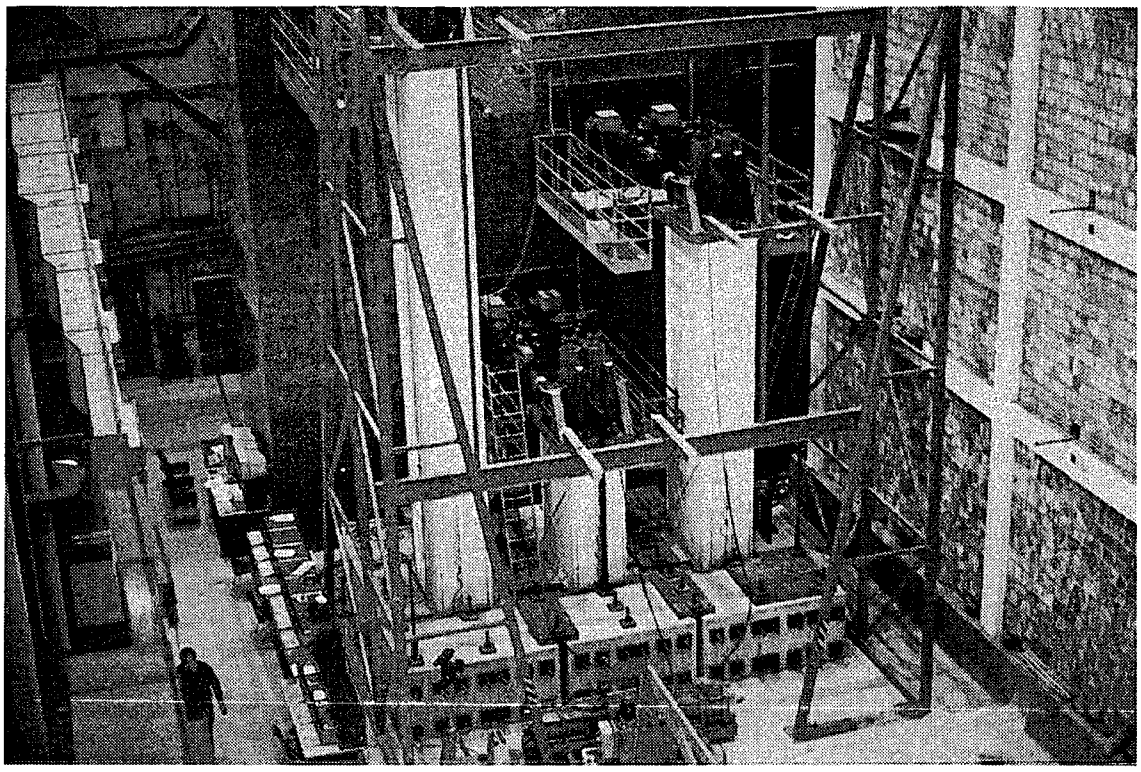

Figure 2. Test setup - General view

tion. Additional pairs of transducers were placed to monitor unexpected orthogonal rotations. Another set of transducers is used to measure both the total rotation of the pier and its elongation; *Diagonal deformations:* The two diagonals were instrumented to measure the shear deformation; *Horizontal Displacements*: Another set of transducers were placed at different levels between the side of the pier and a steel bar connected with swivel joints to the base and to the cap. This allows to monitor the deflected shape.; *Section Warping: A* set of transducers were placed on the same horizontal basis to follow the in-plane deformation of the cross-section enabling to measure the section warping due to shear.

3.4. Input Motion and Testing Procedure

The tests used one of the artificial accelerograms used in the analysis, with a nominal peak acceleration of 0.35 g. The accelerogram is depicted in Figure 3., together with the corresponding elastic response spectrum. The accelerogram was intended to fit the response spectrum specified in EC8 for peak ground acceleration 0.35 g and medium soil conditions.

The mass matrix to be used in the substructured part was scaled by λ^3, λ=2.5 being the geometrical scale factor, consequently the ordinates of the accelerogram were multiplied by λ, and the time scale was accordingly reduced. The original accelerogram of ten seconds became 4 seconds long. The axial load applied by the vertical actuators was independent from the mass values. A constant value of 1700 kN was applied, to keep the normalized axial load the same as in the real structure (ν=0.1).

No specific testing procedure (type of loading and corresponding intensity) is presently available for dynamic tests of earthquake resistant structures. In principle, this testing procedure is tailored to the general objectives of the tests that must be well clarified.

Concerning the PSD testing of the bridges the main objectives are recalled: Evaluation of the

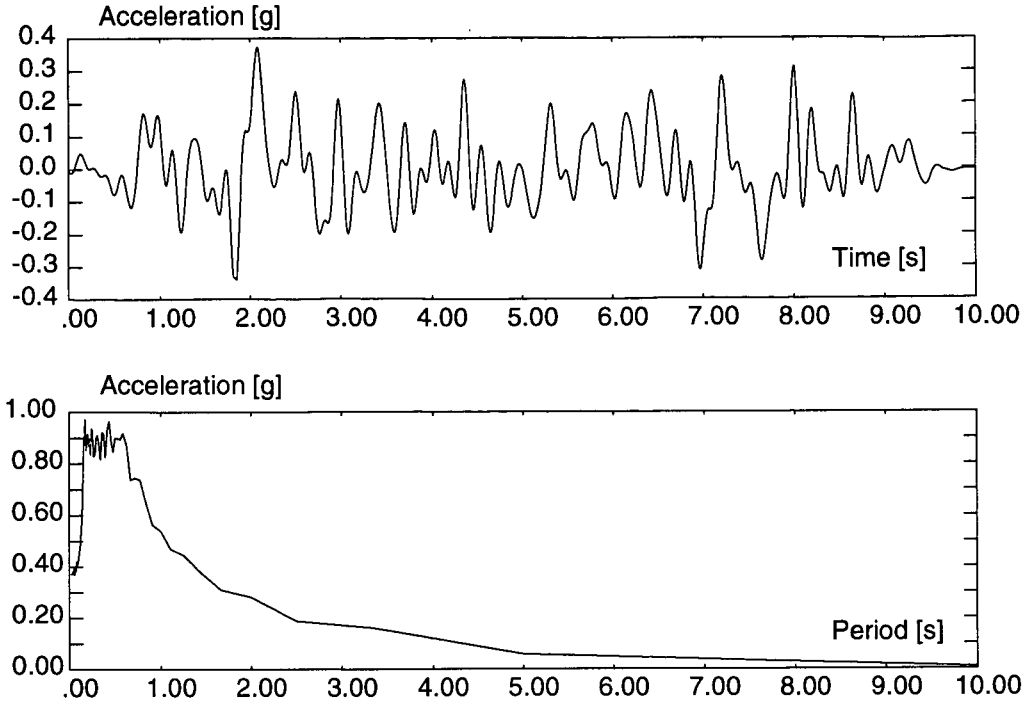

Figure 3. Artificial accelerogram and corresponding response spectrum (5% damping)

seismic performance of bridges designed in accordance with the present version of EC8; Comparison of three design solutions for irregular bridges; Evaluation of safety margins for each design solution.

Thus, it was decided to test the bridges using first the 'design earthquake' as input motion and then an intensity of the input motion as close as possible to the one causing failure (high level earthquake). Additionally, for the set of irregular bridges the intensity of the high level earthquake has been tailored to the weak design solution (bridge B213C).

Accordingly and based on the numerical predictions, the scaling factors adopted for the high level earthquake were 1.2 and 2.0 respectively for the irregular bridges and for the regular one. A smaller value would not have caused major damage to the regular bridge.

The external piers in bridge B213A did not suffer significant damage during the test with the reference accelerogram at the nominal intensity, as expected. Therefore, they have been used again in the bridge B213B, and will also be used in the tests with seismic isolation and asynchronous base motion. The tests with the accelerogram multiplied by 1.2 have been physically performed on the short pier only, by providing a numerical model for the other piers. This has been done by using the substructuring capabilities of the pseudodynamic implementation. A nonlinear elastic model, calibrated with the results of the 1.0 test has been used.

3.5. Results from the tests on conventional bridges

Representative results of the tests are given in Figures 4, in terms of global hysteresis loops. In Table 2, the extreme values of displacement, ductility and damage are given. The damage index was computed from the Park and Ang model [14]. Displacement profiles of the three irregular bridges are shown in Figure 5 for the two earthquake levels.

The results of the test on bridge B232 comply with the regularity issue, as mentioned in EC8, part 2. Dissipation of energy takes place in all piers, and a ductile behaviour could have been

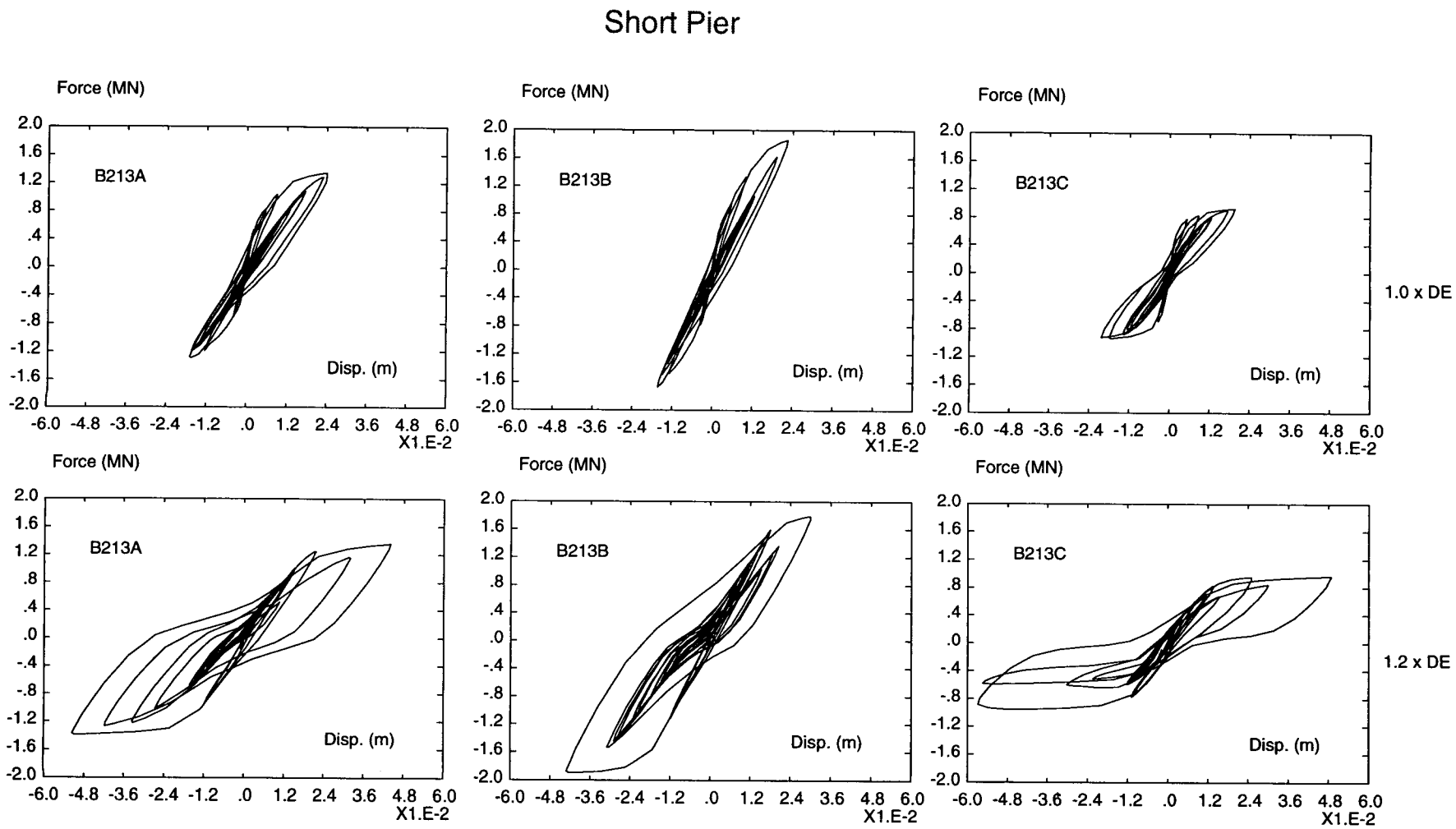

Figure 4. Force-displacement diagrams of the short piers of the irregular bridges for the two earthquake levels

Table 2: Seismic response of the bridges for the two earthquake levels

BRIDGE	Pier	Design Earthquake			High-Level Earthquake[a]		
		Top. Disp. [m]	Ductility	Damage Index	Top. Disp. [m]	Ductility	Damage Index
B232	1	.044	1.4	.22	.089	2.8	.47
	2	.062	1.9	.34	.132	4.1	.79
B213A	1	.022	<1	---	(.029)[b]	---	---
	2	.024	2.0	.30	.052	4.0	.70
	3	.028	<1	---	(.050)	---	---
B213B	1	.025	<1	---	(.028)	---	---
	2	.023	1.5	.25	.043	2.5	.50
	3	.028	<1	---	(.048)	---	---
B213C	1	.017	<1	.09	.041	1.3	.22
	2	.020	4.2	.35	.057	11.9	1.03
	3	.026	<1	.09	.049	<1	.16

a. 1.2 and 2.0 times the design earthquake respectively for bridge B232 and for the irregular bridges (B213A, B213B and B213C).

b. (.) Values obtained from the numerical model (pier substructured)

assumed. The dissipative mechanism turned out to be stable and efficient, with demands roughly proportional to capacities, and an input signal 2 times larger than the design signal was applied without loss of capacity.

In the case of test B213A the dissipation of energy was limited to the short pier. This corresponds to the situation for which a warning is issued in EC8, part 2: Behaviour factors > 1.2 should not be used without special consideration, if the development of plastic hinges in the piers is not probable, because the piers do not reach yielding under the design seismic action. The ductility demand on the short pier was, however, reasonably small.

In the test B213B the short pier, which was stronger than in the previous bridge, attracted much larger forces, but experienced considerably lower ductility demands. Again, energy dissipation took place in the short pier only. The crack pattern was found to be much more spread than in the previous test.

In test B213C, the goal to obtain a more regular force distribution was achieved. The distribution of the maximum bending moment among the piers was, in fact, fairly constant. Ductility demands in the short pier were, however, much larger than in test B213A. The advantages of the corresponding design approach are, therefore, debatable.

It should be underlined that the maximum values of ductility demand and damage index for the Design Earthquake are quite similar for all bridges (except for the Bridge B213C). However, the irregular bridges, tested with an input motion slightly higher than the design earthquake (1.2 times) and much lower than the intensity used for the regular bridge (2.0 times), have been

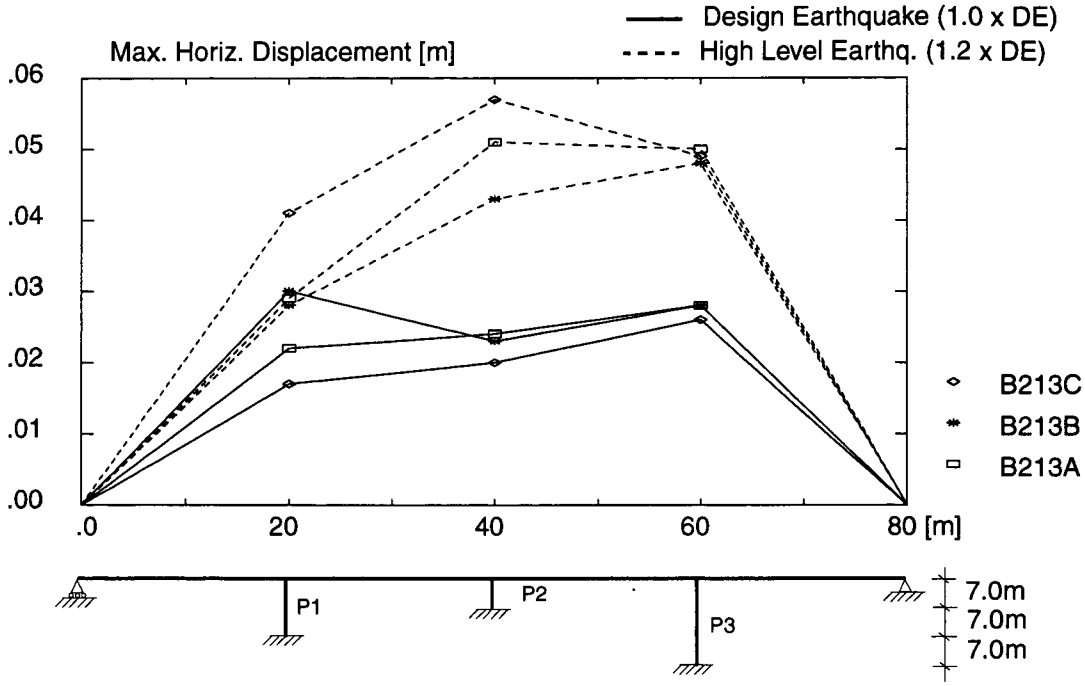

Figure 5. Displacement profiles of the irregular bridges for the two earthquake intensities

heavily damaged. The safety against collapse of the irregular bridges is quite low, compared to the safety of the regular bridge.

The test results confirm that the strategy adopted for the design of the bridge B213B, which corresponds to the use of a lower local behaviour factor, is the 'less worse' and could lead to a suitable design approach for irregular bridges. An alternative solution for these highly irregular bridges may lay on the use of Isolation/Dissipation devices, which was the object of the second part of the testing campaign in ELSA.

Finally it should be underlined that, after the pseudo-dynamic tests, the bridge piers were tested cyclically until collapse exhibiting a ductile behaviour. This confirms the adequacy of detailing provisions included in Eurocode 8 for this kind of structures.

Detailed analysis of the pseudo-dynamic test results are reported elsewhere[16], [17].

4. BRIDGES WITH ISOLATION/DISSIPATION DEVICES

The tests on the *conventionally* designed bridges concentrated on alternative design methods for irregular bridges, based on the use of non-uniform (local) behaviour factors, while the second part of the test campaign, devoted to the irregularity issue, was concerned with the use of isolation/dissipation (I/D) devices.

The scope of an isolation system is in general to reduce the force response and increase the global damping, maintaining the stiffness of the whole system within acceptable values for service loading. The isolation system designed for the bridges tested in ELSA was essentially regarded as an alternative structural solution for highly irregular bridges. In fact, the previous tests on bridges without isolation confirmed that it is quite difficult to find suitable design solutions for very irregular bridges. In spite of the improved earthquake performance of the bridges

designed with non-uniform strength reduction factors, the earthquake demands, for input accelerations higher than the design ones, were quite high compared to those of the regular structures. Therefore, the isolation appeared to be the potential and an economical solution able to satisfy the requirements for an adequate seismic performance of such an irregular structure.

4.1. The Isolation System

Two isolation solutions, shown schematically in Figure 6, were adopted for the irregular bridge. One including isolation/dissipation (I/D) devices at the abutments and over all piers - labelled Full-Isolation (FI)- and other with I/D devices only over the central short pier where demands concentrated in the conventionally designed structure. This solution was labelled Partial-Isolation (PI). Details on the design of the isolating systems can be found elsewhere [17].

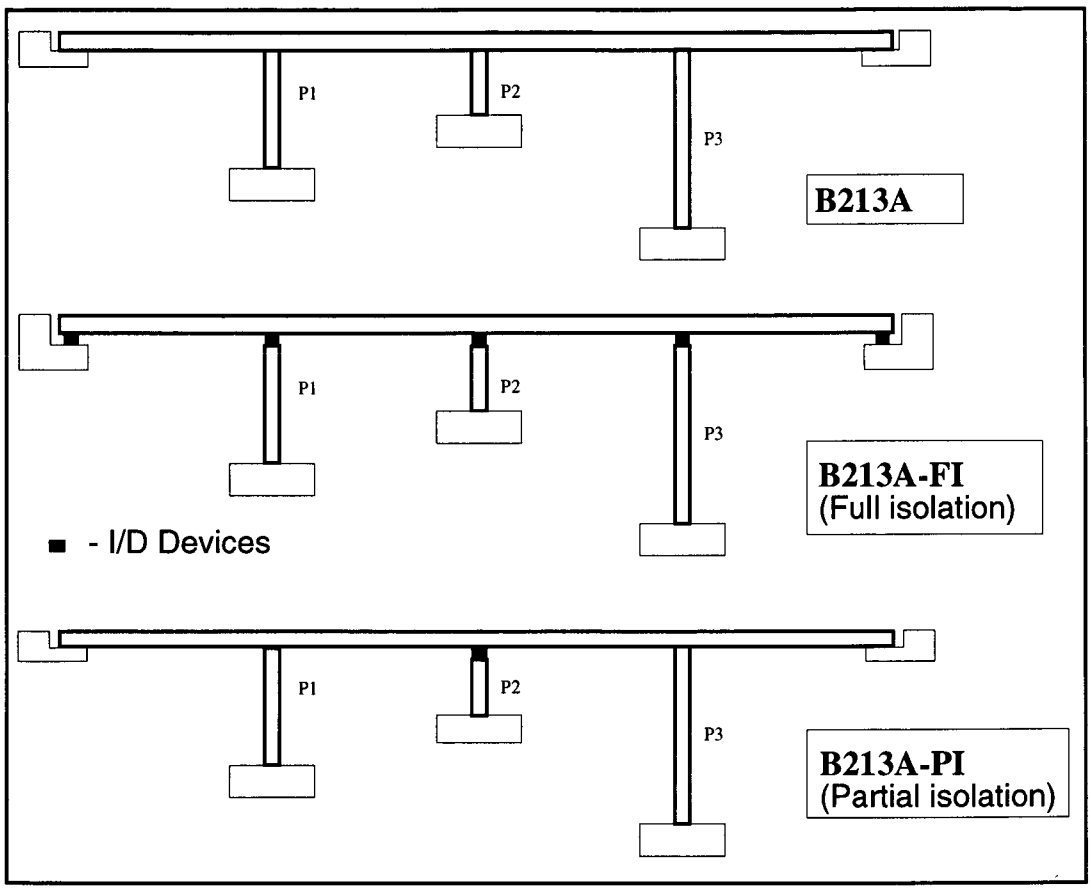

Figure 6. Schematic representation of the three test conditions: Conventionally designed bridge, fully isolated bridge and partially isolated bridges

The aim of the test campaign of the bridges with isolators was, therefore, to assess the seismic performance of two isolation schemes for irregular bridges against the behaviour of geometrically similar bridges designed following the classical behaviour factor approach.

The adopted isolation/dissipation devices are represented schematically in Figure 7 a). They are composed of two distinct mechanical parts: One, the sliding supports, designed to bear the vertical load due to self weight of the superstructure and service load and capable of sliding over the teflon pad-bearings. Another, the dissipating component (spindle), intended as the device part where the energy dissipation, through significant plastic deformations, takes place.

Furthermore, this part contributes to the lateral stiffness of the isolator.

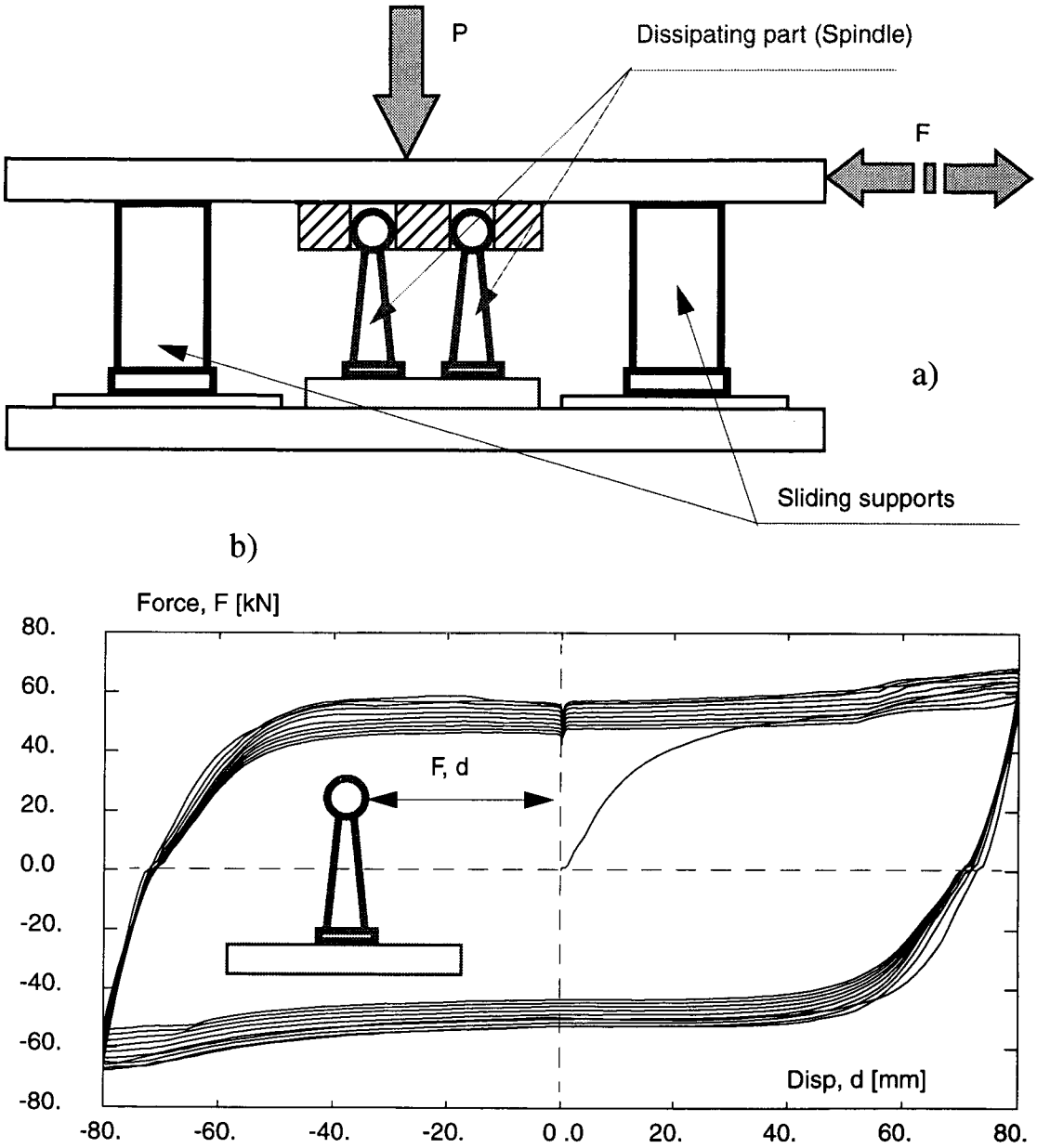

Figure 7. Isolation/Dissipation devices: a) Schematic representation and functioning b) Cyclic force displacement diagram for one dissipating element (spindle)

The dissipating part is essentially composed of vertical ductile steel spindles with a non-uniform cross section. This geometric configuration induces a spread up of plasticity exploiting so the available dissipating potential of the spindle.

Each isolation device can be composed of several dissipating elements. However, the behaviour of such a device, in terms of strength and ductility, can be characterized from test on one element. A typical curve for an element is presented in Figure 7 b). Very high ductility can be expected from these devices with a large number of quite stable dissipative loops.

It should be underlined that the use of these devices appear to be very promising for civil engineering applications. They are quite simple with well separated parts for load carrying and dissipation and they are fabricated using well-known conventional materials.

4.2. Test Set-up and Test Results

The test set-up for the bridges with I/D devices was similar to the one for the conventional bridges. However, the devices have been positioned between the top of the piers and the steel cap, which moved up the load application point. Therefore, the effective height of the isolated piers has been increased of about 340 mm. Furthermore, the test set-up for the bridge fully isolated (isolators over all deck supports) included two additional controlling actuators, one for each abutment, to impose to the isolators at the abutments the corresponding dynamic displacements.

The physical realization of this part of the test set-up was performed by fixing the base of the isolator to the reaction floor and connecting the upper part of the device to the servo-hydraulic actuator. As the vertical force, corresponding to the weight of the deck on abutment, was not required (the same did not apply to the piers because the axial force plays an important role in their non-linear behaviour), the isolation devices for the abutments only comprised the dissipating part indicated in Figure 6; the sliding supports to carry vertical loading were not included.

As discussed above, the isolation of the bridges was considered essentially as a means of designing an irregular bridge for adequate earthquake performance. Therefore, the test sequence and the earthquake intensities considered in the tests of the previous irregular bridges were assumed in the tests on the isolated ones. Thus, comparison of the seismic performance of the different design solutions is certainly easier.

Preliminary stiffness tests were performed on the bridge piers with and without earthquake isolators. From the results of these tests a decrease of the 'piers' stiffness with the application of the isolators was apparent. The earthquake tests on the isolated bridges followed the stiffness tests mentioned above. The earthquake input signal with 10 seconds duration (prototype timescale) used in the previous tests was also considered for the tests with isolation. Furthermore, the two level earthquake intensity (design earthquake (DE) and 1.2 times the design earthquake) testing strategy was also maintained.

Table 3 gives the maximum displacements measured at the top of the piers for the three bridges for the two earthquake tests. For the isolated internal deck supports (piers) the displacements were split into pier and relative device displacements. The total displacement (deck displacement) can be obtained summing the two partial displacements.

Figure 8 gives more informative results concerning the overall earthquake behaviour of the bridges. In fact, as expected, the dissipation of energy was totally concentrated in the I/D devices and the bridge piers have been completely protected. It is however important to underline that the fully isolated bridge requires quite important clearance at the abutments in order to accommodate the dynamic displacements at those zones.

From the analysis of the test results of the isolated bridges it is possible to conclude that:

- a) Seismic isolation is an effective way to protect bridge structures against the damaging effects of earthquakes;
- b) Isolation can be considered as a very good alternative solution for irregular bridges. In fact, both isolation solutions regularize the earthquake behaviour of the bridge;
- c) Furthermore, partial isolation (isolation of the critical piers) presents some advantages relatively to the full isolation. As confirmed by the test results, the full isolation leads to considerably large displacements at the abutments, which may require large clearances to accommodate those displacements. In addition to the fact that the partial isolation is more economical (one isolator instead of five in the full isolation), the partial isolation exploits in a more effective way the deformation capacity of the lateral piers.

Finally, it should be underlined that the test set-up for this test campaign with isolators was particularly designed for these tests with unidirectional loading. Therefore, practical applica-

tion of these I/D devices will require a detailed analysis considering for example the effects of the vertical components of the seismic action, in order to avoid premature malfunctioning of the mechanical devices. An up-lifting of the upper plate of the devices would lead to the loss of the horizontal stiffness of the bearing and would inhibit the required dissipation of energy.

Table 3: Maximum displacements for the isolated and non-isolated bridges for the two earthquake tests

TEST	BRIDGE	Location	Displacement x10-2 [m]				
			Left Abutm.	Medium Pier	Short Pier	Tall Pier	Right Abutm.
1.0xDE	B213A	Pier	-	2.16	2.42	2.79	-
	B213A/FI	Dev[a].	4.00	4.23	5.22	3.71	5.39
		Pier	-	0.64	0.21	1.90	-
	B213A/PI	Dev.	-	-	3.79	-	-
		Pier	-	2.50	0.28	3.68	-
1.2xDE	B213A	Pier	-	2.95	5.15	4.99	-
	B213A/FI	Dev.	4.43	4.68	6.06	4.24	6.20
		Pier	-	0.90	0.26	2.27	-
	B213A/PI	Dev.	-	-	4.55	-	-
		Pier	-	2.99	0.29	4.23	-

a. Relative displacement for the isolation/dissipation device

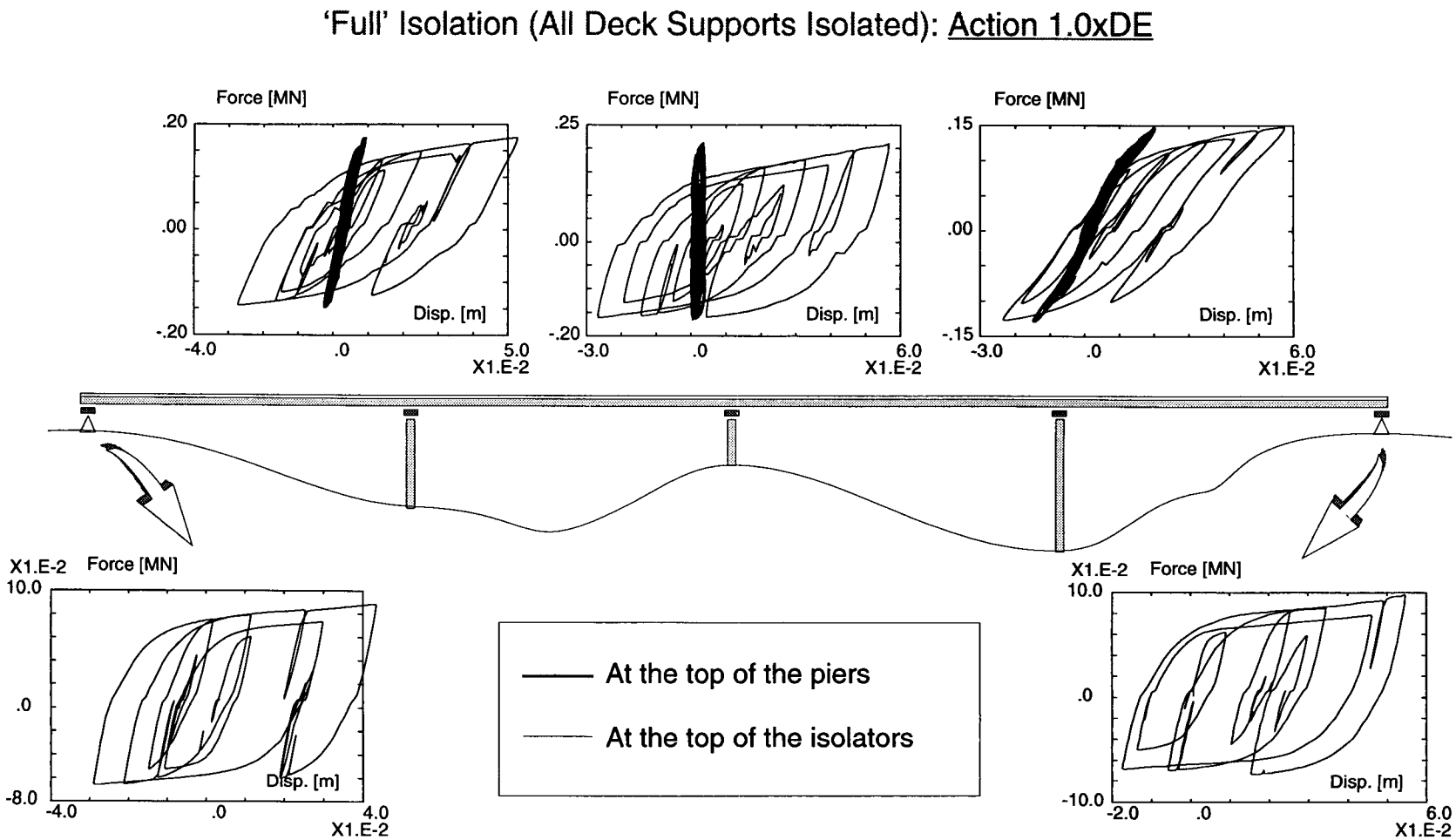

Figure 8. Bridge B213A-FI: Force-displacement diagrams for the isolator and for the bridge piers for the (1.0xDE) test

5. BRIDGES WITH ASYNCHRONOUS INPUT MOTION

From strong motion arrays installed in seismic areas (e.g. [13]) it is clearly demonstrated that the soil motion of relatively close surface points is not synchronous; even relatively close points can experience significant relative displacements, due mainly to reflection and refraction of seismic waves through underlying soil layers with different mechanical characteristics.

Recent numerical studies on the responses of R/C concrete bridges, conventional and isolated [12] [18], conclude that the traditional design under synchronous input provides a global upper bound of the response and consequently leads to a conservative design. However, the damage pattern in the bridge tends to be altered with respect to that resulting from the synchronous motion. It is therefore required to assess the effects of this asynchronous input motion, which can be partially accomplished by shaking table and/or PSD tests.

Therefore, in the Bridge research programme were included both shaking table (ST) and pseudo-dynamic (PSD) tests with asynchronous motions. The ST tests, have been carried out in the ISMES laboratories using simultaneously three independent platforms [1]. The PSD tests were performed at ELSA [16] on an irregular bridge similar to the one designed in accordance to Eurocode 8 (labelled B213A). The bridge tested with non-synchronous input motion was labelled B213A-N/S.

This section deals the pseudo-dynamic testing with asynchronous motion. The definition of the input motion for multi-support long structures is discussed below. This is followed by the description of the test set-up and procedures. Finally, the test results are presented and compared with the ones obtained from the tests with synchronous input motions.

5.1. Earthquake Input Motion for the Asynchronous Test

Earthquake ground motions produced at multiple support points of large structures, can differ considerably and induce an increase in the response demands to extents that are not covered by the traditional design methods. Therefore, it is important to consider spatial variability of ground motions in order to produce realist assessments of structural response. For that reason the recent EC8 code adopts provisions to cover the situations where spatial variability of ground motions is important (bridges, dams, pipelines, etc.).

Generally, the seismological characteristics responsible for spatial variability of ground motions are well known; important aspects associated to the source mechanism, local soil conditions and topography have been mentioned in the studies carried out with data collected by strong motions arrays [13]. However, the relative importance of each feature is very difficult to establish in a general framework. For instance, it has been referred that phenomenological features related to the source mechanism (e.g. rupture direction, velocity and stress-drop) play an important role in the study of spatial variability of ground motions in the near field, whereas, in the far field, those aspects can be almost neglected because they are masked by the reflection and the diffraction of body waves (due to local soil stratification) and also the propagation of surface waves.

Modelling of spatial variability of ground motion can be performed assuming a stochastic process characterized by a power spectral density function, $S_0(\omega)$, which can be split into a stationary power density, $S_0(\omega)$ and a coherence loss matrix, $\bar{C}(\omega)$, which terms represent the coherence loss between the support motions.

$$S(i\omega) \approx S_0(\omega) \cdot \bar{C}(\omega) \tag{1}$$

In this study no previous definition of $\bar{C}(\omega)$ was available. For this reason, it was assumed that the loss coherence terms $|\gamma_{jk}(i\omega)|$ follow the general trend found in the seismological studies referred to above. Those studies conclude that the coherence loss are decreasing functions with

increasing frequency, meaning that, cross correlation between displacements for multiple-input motions are very high (close to one), lower for velocity components and even lower for acceleration components. A frequency of 0.4 Hz was adopted to separate the correlated motions (frequency less than 0.4 Hz) from the uncorrelated ones.

Samples of the generated acceleration signals, displacements and relative displacements are given in Figure 9. More details on the generation of multi-support input motions procedure may by found in [17]

5.2. Test Set-up and Test Procedures

The test set-up for the asynchronous input motion is similar to that for the synchronous motion. However, the analytical part of the pseudo-dynamic test has been strongly modified. In fact, as stated in Section 2, the description of the motion in a unique relative reference frame is no longer valid and the description in the absolute frame is required. Due to the specific characteristics of the bridge structures, each pier can be tested in a different relative reference frame, and the difficult task to make the convenient synchronization between the various relative frames is left to the modelled structure. In short, the physical part of the test-set-up for the asynchronous motion is the same as for the synchronous tests; however the analytical part must be completely modified to take properly into account the non-synchronous input motions.

Two earthquake tests were carried out on each bridge; the first one corresponding to the design level (1.0xDE) and the second one to 1.2 times the design level (1.2xDE). The aim of this testing procedure is to assess the seismic performance of the structure with the increasing of the earthquake intensity, which corresponds to the evaluation of the vulnerability functions. As discussed in Section 4, a factor 1.2 was adopted to scale the input motion for the high level earthquake in order to make possible the comparison between different design solutions for the irregular bridge. For that very reason, the same factor was considered for the tests with asynchronous motion. A preliminary stiffness test aiming at an accurate characterization of the structure was also carried out.

5.3. Test Results

The results from the preliminary stiffness tests on the bridge piers show that the initial stuffiness of the central piers are quite similar, while the stuffiness of the two lateral piers, used in the test with asynchronous motion, are lower than the corresponding stiffness of the piers of the synchronous test. In fact, as already mentioned the two lateral piers have been used in the previous tests, which induced some damage (cracking) to those piers. The computed natural frequencies of the bridges B213A and B213A-N/S, considering the corresponding measured pier stiffness, change slightly (less than 5% for the first frequency), however the mode shapes are similar.

Test results, in terms of maximum displacement, are given in Table 4 for both the Design Earthquake (1.0xDE) and the High Level (1.2xDE) tests.

Figure 10 shows more informative data concerning the non-linear behaviour of the structure

Table 4: Maximum displacements for the two earthquake levels (1:2.5 scaled bridges)

TEST	INPUT MOTION	Displacement Type	Displacement x 10^2 [m]				
			Left Abutment	Med. Pier	Short Pier	Tall Pier	Right Abutment
1.0xDE	Synchronous	Relative	-	2.16	2.42	2.79	-
	Asynchronous	Total	6.06	8.23	8.88	9.10	6.64
		Relative	-	4.92	2.40	4.50	-
1.2xDE	Synchronous	Relative	-	2.95	5.15	4.99	-
	Asynchronous	Total	7.27	10.60	11.30	9.46	7.96
		Relative	-	7.25	3.95	5.00	-

for both synchronous and non-synchronous motions. This figure includes the force displacement diagrams for the piers for the Design earthquake test.

The results show that the maximum demands in the short pier are: a) quite similar for the synchronous and non-synchronous input motions for the design earthquake and b) lower for the asynchronous motion in the high level test. However, the ductility demand in the medium pier increased substantially.

Two aspects should be recalled: the first concerns the assumptions in the high level test with synchronous motion and the other is related to the stiffness of the medium piers in both tests. In fact, the behaviour of the medium and tall piers has been simulated analytically by a non-linear elastic relationship defined on the basis of diagram obtained for the design earthquake test. Furthermore, the stiffness of the lateral piers is lower in the asynchronous tests as discussed above.

These two facts may have some influence on the overall response of the bridge. Therefore parametric numerical analyses, with models calibrated by these test results, should be performed to quantify those effects.

Nevertheless, the tests on the irregular bridges have shown that the asynchronous earthquake input motions do not lead to higher demands compared with the synchronous motions but, as the relative displacements of the superstructure (deck) can be substantially increased. Therefore, the design of this structural part, including deck supports, must take into account the additional displacements due to the asynchronous motion in order to avoid premature collapse and/ or unseating of the superstructure.

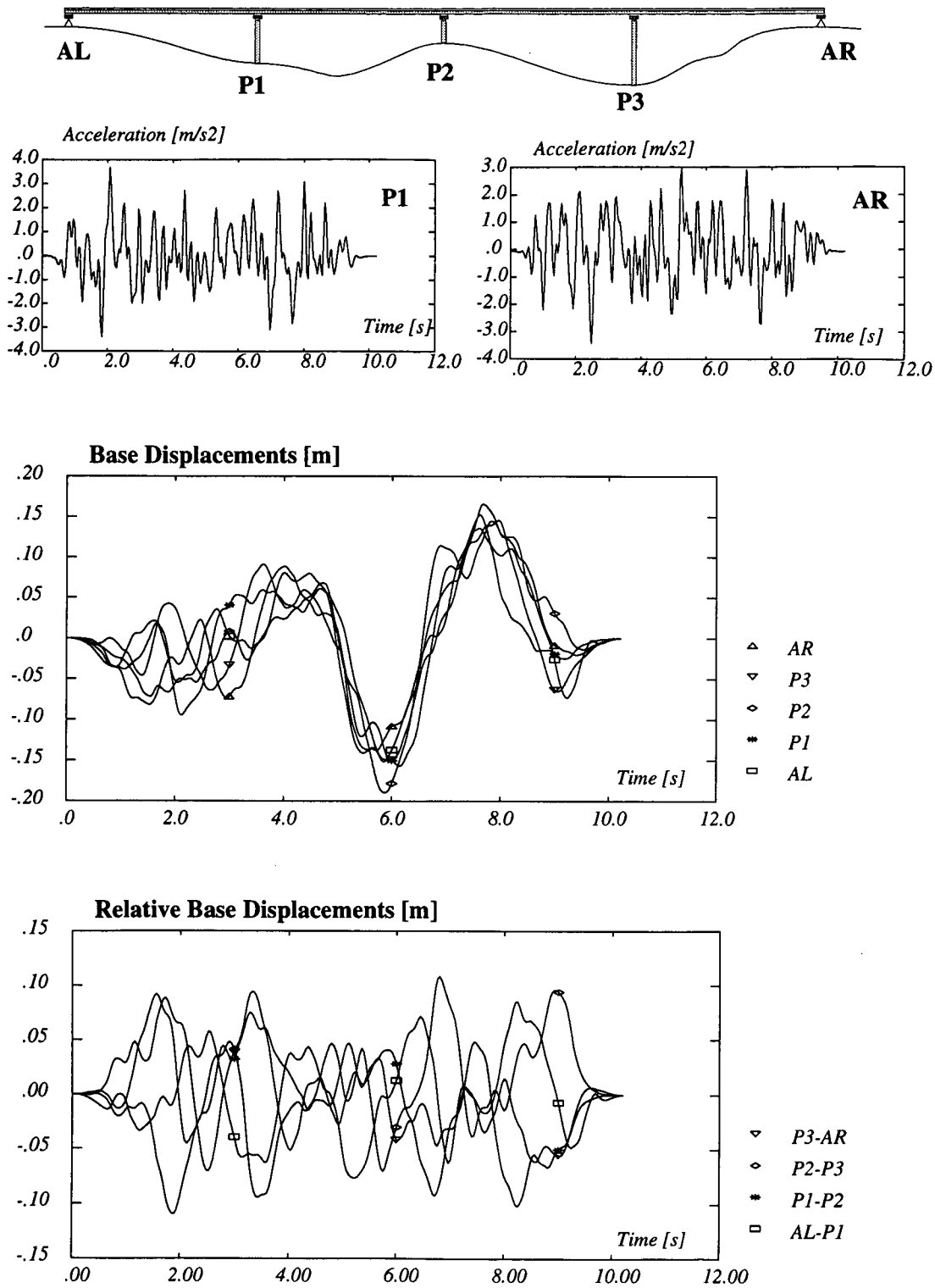

Figure 9. Input motions for the bridge asynchronous tests (values for the full-scale structure): acceleration at two base points, base displacements and relative displacements between consecutive base points

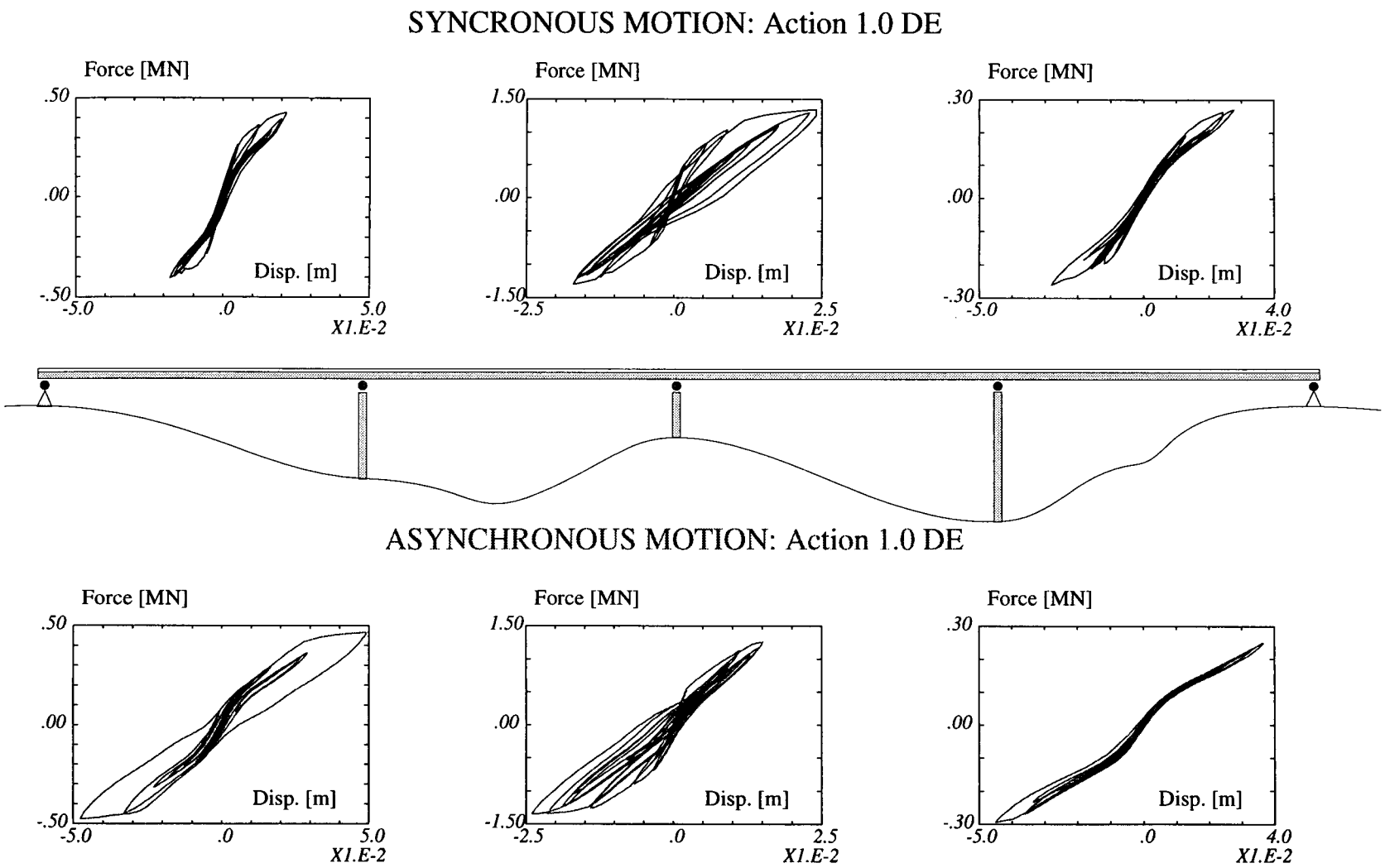

Figure 10. Force displacement diagrams for the synchronous and asynchronous input motions for the DE

6. CONCLUSIONS

A testing programme was carried out as a part of the activities of the Bridge Group of the Network for Pre-normative Research in support of EC8. The main scope of the tests was to study: (a) the implications of irregularity with the q-factor design approach, (b) the effectiveness of seismic isolation for highly irregular bridges and (c) the effects of non-synchronous input motions on the seismic performance of the structure.

Four RC bridges have been tested pseudodynamically, namely: one regular and three highly irregular bridges designed according to different design philosophies. The test results confirm that safety against collapse of the irregular bridges is quite low compared with the safety of the regular bridge designed with the same procedure. Furthermore, the comparison between the test results obtained for the three irregular bridges confirms that the strategy adopted for the design of the bridge B213B, which corresponds to the use of a lower local behaviour factor, is the 'less worse' and may lead to a suitable design approach for these bridges.

The tests on the isolated bridges confirmed that isolation is an effective approach to earthquake protection of bridges. In particular, isolation can be considered as a 'rational' alternative design solution for highly irregular bridges. Both isolation schemes have shown very good seismic performance, reducing the seismic response of the bridges to levels at which the piers remained in the elastic range for the two earthquake tests. Moreover, partial isolation (isolation of critical piers) has shown some advantages relatively to the full isolation scheme. In addition to the fact that partial isolation is more economical, this solution exploited in a better way the deformation capacity of the lateral piers and does not require considerably large clearances at the abutments.

The tests on the irregular conventionally designed bridge with asynchronous input motion (B213A-N/S) have demonstrated that the asynchronous earthquake motions do not lead to higher demands compared to the synchronous ones. However, the damage pattern in the bridge can be altered with respect to the one resulting from the synchronous motion, particularly for higher earthquake intensities. Moreover, the relative deformations of the superstructure can be substantially increased, which requires that the design of these structural part, including deck supports, must take into account the additional pseudo-static displacements due to asynchronous motion, in order to avoid premature collapse and/or unseating of the superstructure.

7. ACKNOWLEDGEMENTS

This work has been developed under the Human Capital Mobility programme of the European Commission and was part of the research programme of the Bridge Group of the PREC8 Research Network.

The participation of the members of the Bridge Group, in particular, the contributions of Professor G. M. Calvi, coordinator of PREC8 and of the Bridge Group and Professor P. E. Pinto, chairman of the technical committee for EC8 to the ELSA testing campaign is gratefully acknowledged.

It should be mentioned that the testing programme is a joint effort of the staff of the Structural Mechanics Unit, JRC. The experimental programme was directed by G. Verzeletti, Head of the Experimental Mechanics Sector. The implementation of the substructuring technique is due to P. Buchet, G. Magonette, P. Pegon and P. Tognoli.

J. Guedes provided both the numerical simulations and the preliminary interpretation of results, including most of the plots herein presented.

Finally, the support of FIP Indrustriale to the research project on seismic isolation is gratefully acknowledged.

REFERENCES

[1] Bousias. S.N.; G. Franchioni. Seismic tests with three simultaneous shaking tables on a 1:8 scaled bridge model in support of design Eurocode 8. ISMES Report. Bergamo, Italy, 1995.

[2] Buchet, P. and P. Pegon. PSD testing with substructuring - Implementation and use. *Special Publication* AMU, STI, EC, JRC, Ispra, Italy, 1994.

[3] Calvi G.M. and Pinto P.E. Seismic design of bridges: Experimental and analytical research. *Proc. of the 10th European Conference on Earthquake Engineering* Vol.4, Vienna, 1994.

[4] Calvi, G.M.; Pinto P.E (Editors). Experimental and numerical investigations on the seismic response of bridges and recommendations for code provisions. *ECOEST/PREC8 Report*, LNEC, Lisbon, 1996.

[5] Calvi, G.M. Conceptual design of isolation systems for bridge structures. *Journal of Earthquake Engineering and Engineering Seismology.* Vol.1 N.1, 1996.

[6] Dermitzakis, S.N. and S.A. Mahin. Development of substructuring techniques for on-line computer controlled seismic performance testing. *Report No. UCB/EERC-85/04.* Berkeley, California, 1985.

[7] Donea J., G. Magonette, P. Negro, P. Pegon, Pinto A. and G. Verzeletti. Pseudo-dynamic testing of large-scale models of civil engineering structures at the ELSA reaction wall. *Proc. of the 10th European Conference on Earthquake Engineering*, Vienna, 1994.

[8] Eurocode No 8, Structures in Seismic Regions - Design - Part 1 - General and Buildings - May 1988 edition, Report EUR 12266 EN, Commission of the European Communities, 1988.

[9] Eurocode No 8, Structures in Seismic Regions - Design - Part 2 - Bridges - Draft April 1993 - CEN, DOC. TC250/SC8/N76, 1993.

[10] Guedes, J., P. Pegon & A.V. Pinto. A Fibre/Timoshenko Beam Element in CASTEM 2000. *Special Publication* N. I.94.31, STI, JRC, EC, Ispra, Italy, 1994.

[11] Guedes, J. & A.V. Pinto. Numerical Predictions for the PSD testing of R/C Bridges. *Report EUR No. 16358 EN*, EC, JRC, Ispra, Italy, 1996.

[12] Monti, G., P.E. Pinto; C. Nuti. Response of conventional and isolated bridges under non-synchronous seismic motion. *European Seismic Design Practice - Research and Application*, Editor: A.S. Elnashai, A.A. Balkema/Rotterdam/Brookfield, 1995.

[13] Oliveira, C.S., Hao, H.; J. Penzien. Ground motion modelling for mutiple-input structural analysis. Structural Safety Vol. 10 N.1-3 Special Issue, 1991.

[14] Park, Y.J. & A.H-S. Ang. Mechanistic Seismic Damage Model for Reinforced Concrete, *Journal of Structural Engineering,* ASCE, Vol. 111, N. 4., 1985.

[15] Pinto A.V., G. Verzeletti, P. Negro and J. Guedes. Cyclic testing of a squat bridge-pier. *EUR Report N.16247EN* - AMU, STI, EC, JRC, Ispra, Italy, 1995

[16] Pinto A.V.; G. Verzeletti; P. Pegon; G. Magonette; P. Negro and J. Guedes. Pseudo-Dynamic Testing of Large-Scale R/C Bridges. *Report EUR 16378 EN,* EC, JRC, Ispra, Italy, 1996.

[17] Pinto, A.V. (Editor). Pseudo-dynamic and Shaking Table Tests on RC Bridges. *ECOEST/ PREC8 Report.* LNEC, Lisbon, 1997.

[18] Pinto, P.E. Research and practice on seismic design of bridges in Europe. *Proc. of the U.S. Nat. Seismic Conf. on Bridges and Highways* - San Diego, CA, December 10-13, 1995.

STRENGTH AND DUCTILITY CHARACTERISTICS OF PILE FOUNDATIONS

J. FUKUI [1], Y. KIMURA [2], M. OKOSHI [3]

1) Head, Foundation Engineering Division, Structure and Bridge Department, Public Works Research Institute, Ministry of Construction, Tsukuba City, Ibaraki-ken, Japan, 305.
2) Senior Research Engineer, Foundation Engineering Division, ditto.
3) Assistant Research Engineer, Foundation Engineering Division, ditto.

ABSTRACT

The check of ductility and dynamic strength for pile foundations has been proposed based on the results of research into the behavior of pile foundations during severe deformation. For this pile foundation analysis method, a rigid frame pile model was made accounting for the non-linear properties of the vertical resistance of piles, horizontal ground resistance, and the bending stiffness of the pile body. Horizontal loading tests of pile foundation model were performed to clarify the foundation ductility factor - degree of pile body damage relationship. These tests confirmed that at less than 4 times the yield displacement, the pile bodies are spared serious damage.

1. INTRODUCTION

The Hyogo-ken Nanbu Earthquake of January 17, 1995 caused severe damage to highway bridges, including collapsed bridge piers and bridge falls at many locations. Shortly after the earthquake, the state of this damage was surveyed by visually examining the bridge piers and other above ground structures and emergency restoration work was performed to prevent secondary damage. Because the foundations are underground, it was impossible to directly assess their damage immediately after the earthquake. Surveys of damage to the foundations conducted in conjunction with the restoration work confirmed that little damage was suffered by the foundations(1).

After the earthquake, the "Committee for Investigation on the Damage of Highway Bridges Caused by the Hyogo-ken Nanbu Earthquake" was formulated in the Ministry of Construction to survey the damage and clarify the factors which contributed to the damage. On February 27, 1995, the Committee approve the "Guide Specifications for Reconstruction and Repair of Highway Bridges Which Suffered Damage due to the Hyogo-ken Nanbu Earthquake(2)", and the Ministry of Construction noticed on the same day that the reconstruction and repair of the highway bridges which suffered damage by the Earthquake shall be made by the Guide Specifications. The design method that accounts for the non-linear behavior of pile foundations based on the results of research at the Public Works Research Institute and elsewhere was included in the Guide Specifications.

This design method, one based on the fact that a pile foundation provides greater horizontal strength than a bridge pier body, is difficult to apply in a case where the ground around the foundation will liquefy or a case where the bridge pier body has ultimate horizontal strength sufficiently great to withstand the design horizontal seismic coefficient. Thus when the Specifications for Highway Bridges were revised, a model experiment concerning the strength and ductility of pile foundations was carried out to propose an seismic design method for pile foundations.

This paper describes experiments on strength and ductility characteristics of pile foundations conducted by the Public Works Research Institute.

2. ANALYTICAL MODEL OF PILE FOUNDATIONS

In order to check of dynamic strength and ductility for pile foundations, it is necessary to calculate the horizontal strength of pile foundations and its behavior during severe deformation. The displacement method stipulated in the present Specifications handles the behavior of the foundation as linear behavior by restricting the displacement of the foundation within a range where it is assumed to be elastic behavior. It is impossible to ignore the effects of the non-linear properties of the behavior of the foundation when studying the behavior of the bridge pier during severe deformation. So when check of ductility and dynamic strength for pile foundations, it is necessary to consider the following items as non-linear properties of the behavior of a pile foundation.

[1] Vertical resistance of the piles
[2] Horizontal resistance of the piles
[3] Bending moment - curvature relation of the pile bodies

The horizontal strength of a pile foundation and its behavior during severe deformation can, as shown in Figure 1, be analyzed by replacing the pile foundation with a rigid frame structure supported by a ground spring and considering this to be non-linear.

3. VERTICAL RESISTANCE OF PILES

3.1 Vertical Load - Settlement of Piles

The vertical bearing capacity of a pile is the friction force on its skin and the bearing force of its tip. Figure 2 shows a model of these forces. Regardless of differences caused by properties of the ground, the friction resistance reaches its maximum value at a strain of about 1%, while the bearing force of the tip requires strain of a few percent or more than 10%. The vertical load - settlement curve for the pile's top is a combination of these resistance elements, but because the proportions of the vertical resistance of a pile provided by its tip and surface vary according to pile length and composition of the ground and because the state of the ground around piles fluctuates according to the execution method even in identical ground, the vertical load - settlement at the top of piles is extremely diverse.

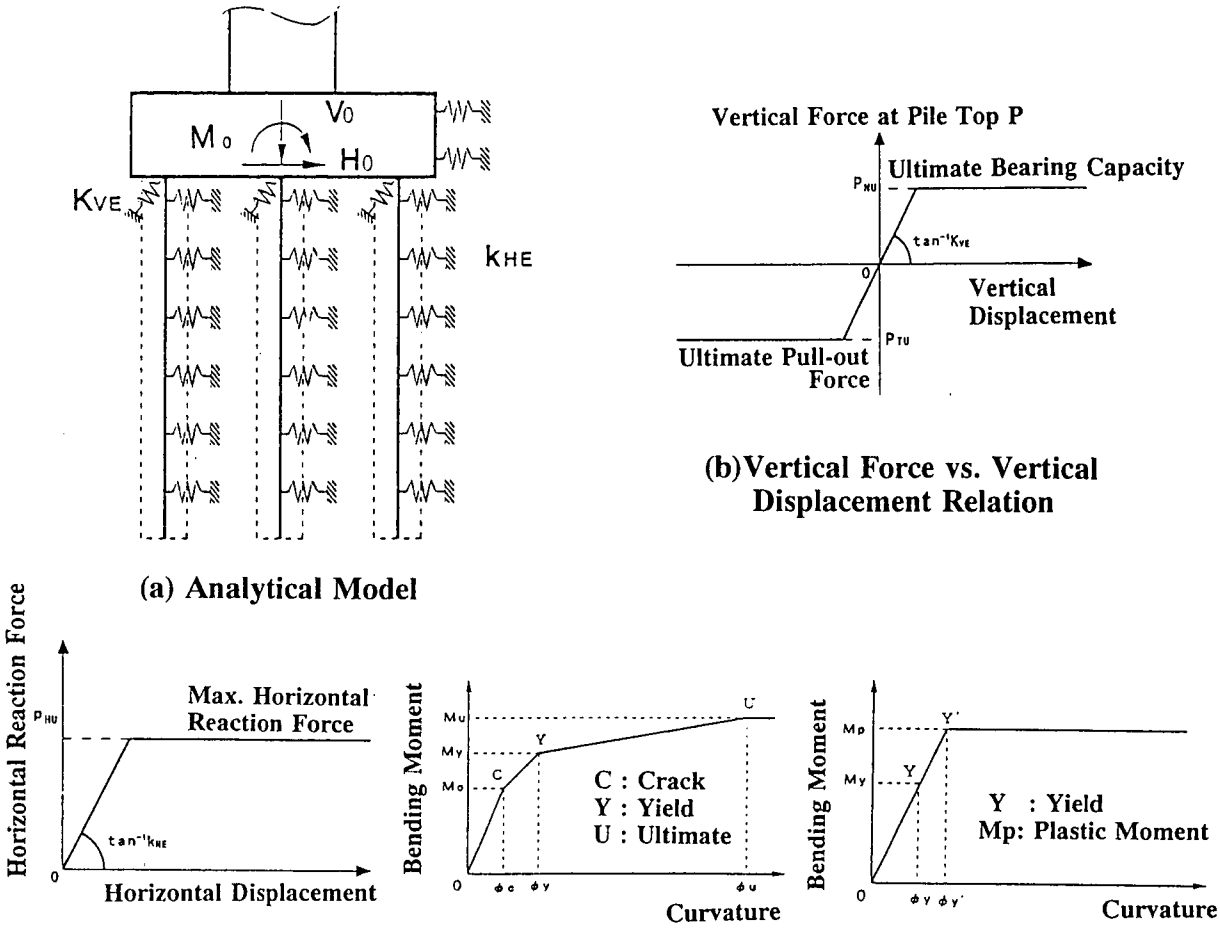

(a) Analytical Model

(b)Vertical Force vs. Vertical Displacement Relation

(c) Horizontal Force vs. Horizontal Displacement Relation

(d) Moment vs. Curvature Relation of Reinforced Concrete Piles

(e) Moment vs. Curvature Relation of Steel Pipe Piles

Figure 1. Analytical Models of Pile Foundations

3.2 Ultimate Bearing Capacity of a Pile

The ultimate bearing capacity of a pile is the load when, during a vertical loading test of the pile, the vertical load - settlement curve can be considered to be almost parallel with the amount of subsidence axis. Accordingly, it can be defined as the bearing capacity when the friction force of the pile skin and the pile tip bearing capacity have reached the ultimate state as shown in Figure 2. The friction force of the skin reaches its ultimate value at a relatively small amount of subsidence, but a large amount of subsidence is necessary for the ground reaction to the tip to reach its ultimate value. For this reason, the Specifications for Highway Bridges define the ultimate bearing capacity as the load when the amount of subsidence of the top of the pile has reached 10% of the diameter of the pile.

To design a pile, it is necessary to find the ultimate bearing capacity of the pile according to the ground conditions at the foundation location and the execution method used. Vertical loading testing is a very reliable way to estimate the ultimate bearing capacity. But many

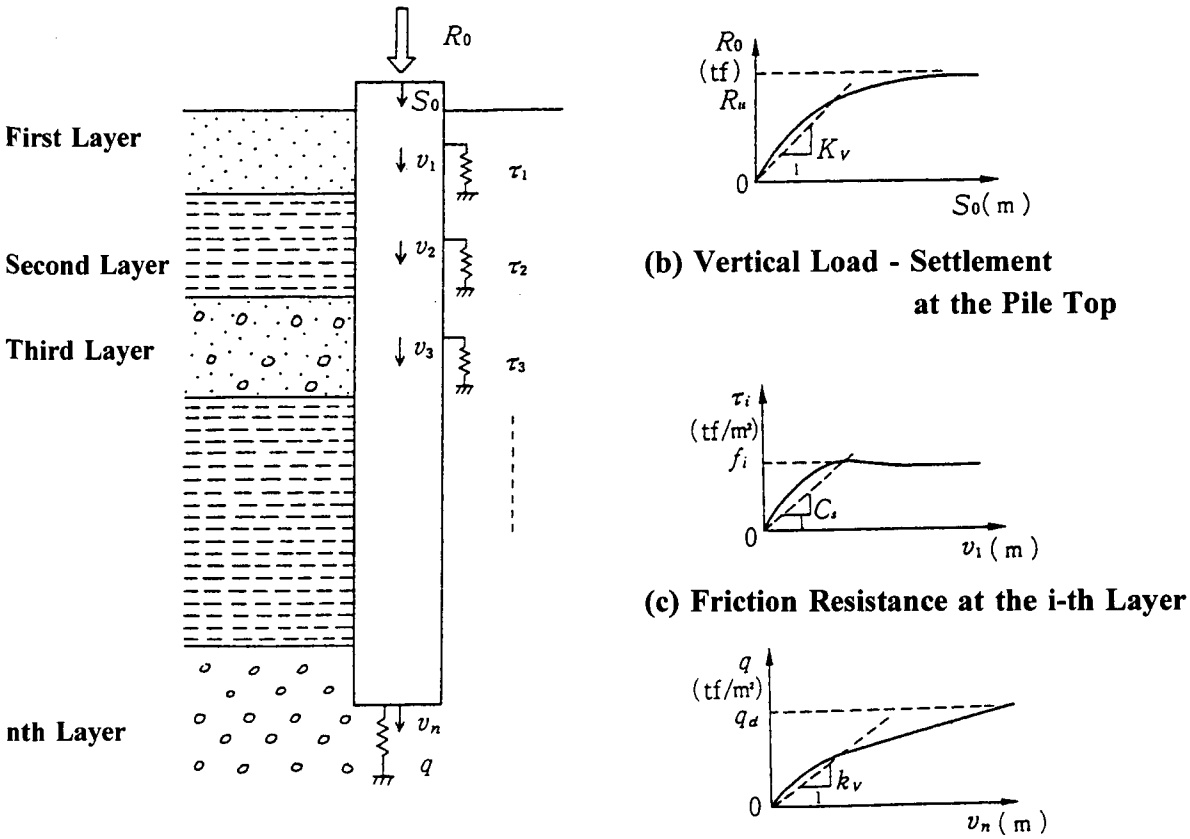

(a) Resistance Elements

(b) Vertical Load - Settlement at the Pile Top

(c) Friction Resistance at the i-th Layer

(d) Ground Reaction at Pile Tip

Figure 2. Vertical Bearing Capacity Mechanism of a Pile

problems are encountered at the design stage. For example, a test pile must be executed at great expense. So in the Specifications for Highway Bridges , the following formula is presented as a method of estimating the bearing capacity: a method created by organizing the results of past loading testing .

$$Ru = qd\ A + U\ \Sigma\ Li\ fi \qquad (1)$$

Where:

Ru: Ultimate bearing force of the pile determined from the ground (tf)

A : Area of the pile tip (m^2)

qd: Ultimate bearing capacity of the pile tip (tf/m^2)

U : Circumference of the pile (m)

Li: Thickness of the stratum assumed to be the skin friction force (m)

fi: Maximum skin friction force of the stratum (tf/m^2)

The Specifications for Highway Bridges categorize piles as driving piles, cast-in-place piles, and as inner excavated piles, and provides methods of estimating the ultimate bearing capacity at the pile tip qd and the maximum skin friction force fi for every construction method.

3.3 The Axial Spring Constant of a Pile [3)]

The axial spring constant Kv of a pile top is defined as the secant slope Ro/So of the vertical load - settlement curve of the pile top. So as Figure 1 indicates, the relationship between Ro

and So is non-linear, and Kv is seen to be dependent on the amount of subsidence. Considering the fact that the state modelled based on Kv is the elastic state, it is appropriate for the reference value to focus on the yield point on the Ro - So curve. From these facts, Kv is defined as the secant incline when the settlement is Sy, and an estimation formula is proposed based on loading testing data.

The Specifications for Highway Bridges have defined Kv as the following formula.

$$Kv = a \frac{Ap\ Ep}{L} \tag{2}$$

Where:

Ap: Net sectional area of the pile

Ep: Young's modulus of the pile body

L : Pile length

a : Coefficient

The coefficient a is converted based on the embedment depth ratio (L/D) of the pile and is customarily represented as:

$$a = \alpha\ (L/D) + \beta \tag{3}$$

Accordingly, Kv is found from loading testing of the pile, and the relational expression for a which was reverse calculated from this value using formula (2) and for the embedment depth ratio (L/D) is determined.

As an example, Figure 3 presents the results for a cast-in-place pile. This figure represents the regression formula represented by formula (3) as a solid line and the average value +/- the standard deviation as a broken line. In this way the following formulae are presented for various kinds of piles.

Driven steel pipe pile:	a = 0.014 (L/D) + 0.78	
Driven PHC pile:	a = 0.013 (L/D) + 0.61	
Cast-in-place pile:	a = 0.031 (L/D) + 0.15	(4)
Inner excavated steel pile:	a = 0.009 (L/D) + 0.39	
Inner excavated PHC pile:	a = 0.011 (L/D) + 0.36	

In cases where the embedment ratio is less than 10, an estimation formula based on the results of loading testing as described above can not be established, so it is necessary to also conduct a study based on the theoretical formula presented below.

The pile is considered to be an elastic body with spring in its skin and tip. And as shown in Figure 4, if, when axial force acts on the pile top, the spring of the pile skin is assumed to be constant at all depths, the basic equation for the stress and displacement of the pile is represented by the following formula from the balanced condition of the force and the continuous conditions of the displacement of the infinitesimal element.

$$A_p E_p \frac{d^2 v}{dx^2} - C_s U v = 0 \tag{5}$$

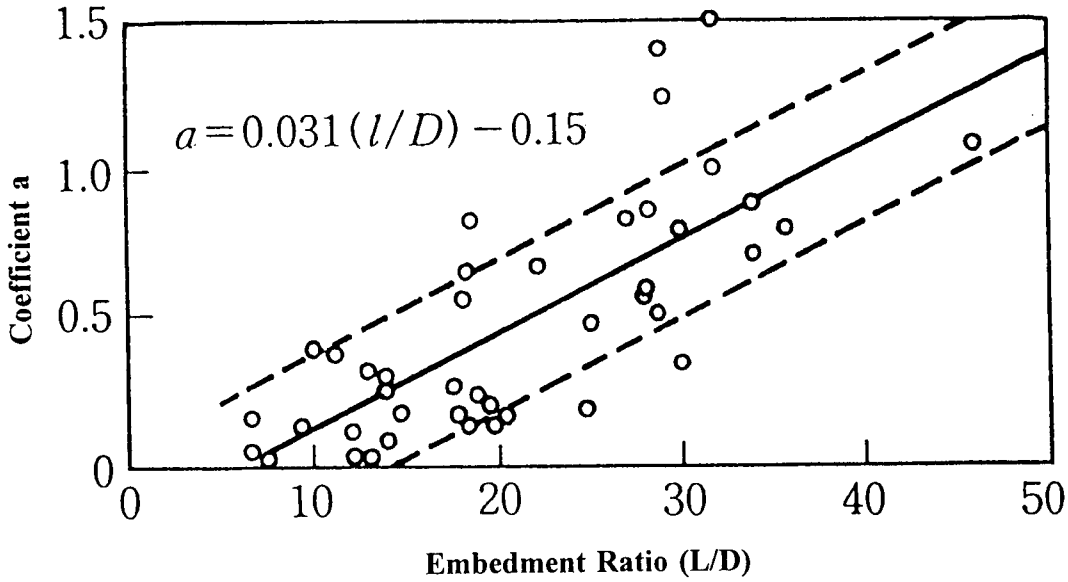

Figure 3. Coefficient a and Embedment Ratio (Cast-in-place Pile)

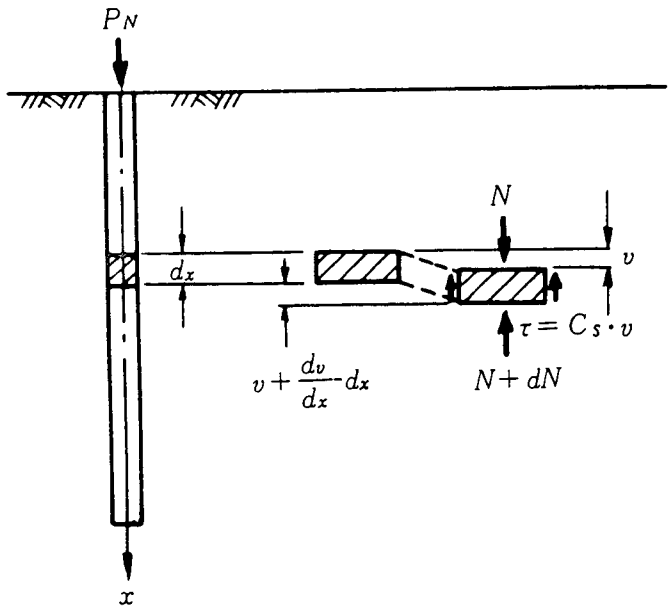

Figure 4. Stress and Displacement of a Pile Acted on by Axial Force

The spring constant Cs of the pile skin, which is called the slip coefficient, is the secant incline of the pile skin friction force - amount of subsidence curve (See Figure 2). Here, the pile skin friction force is assumed to not achieve its limit value over the entire length of the pile. And the spring of the pile tip is assumed to be the vertical ground reaction coefficient kv. If the formula is solved from the boundary conditions at the top of the pile and at the tip of the pile based on these hypotheses, the coefficient a when the axial spring constant Kv at the pile top is estimated can be estimated using the following formula.

$$a = \frac{\lambda \tanh \lambda + \gamma}{\gamma \tanh \lambda + \lambda} \lambda \qquad (6)$$

where

$$\gamma = \frac{A_i k_V L}{A_p E_p}$$

$$\lambda = L\sqrt{\frac{C_s U}{A_p E_p}}$$

Ai: enclosed area at pile tip (cm^2)
U : pile circumferential length(cm)
kv: coefficient of vertical subgrade reaction at pile tip(kfg/cm^3)
Cs: slip coefficient(kgf/cm^3)

3.4 Analytical Model

The resistance properties in the vertical direction of the pile were considered to be elasto-plastic form, with the pile axial direction spring constant K_{VE} considered to be the initial gradient, and the ultimate bearing capacity P_{NU} and the ultimate pull-out bearing capacity P_{TU} treated as the upper limit values.

In this case, the pile's axial direction spring constant K_{VE} was assumed to be the pile axial direction spring constant K_V calculated as stipulated in the Specifications.

The ultimate bearing capacity P_{NU} and the ultimate pull-out force P_{TU} were considered to be the ultimate bearing capacity of the pile R_U calculated as stipulated in the Specifications and (ultimate pull-out force of the pile P_U) + (effective weight of the pile W). These values did not exceed the ultimate bearing capacity and ultimate pull-out force determined from the stress of the pile body.

4. HORIZONTAL RESISTANCE OF A PILE

4.1 Non-linear Properties of Ground Resistance [4)]

The data selected from among the results of past horizontal loading testing for use in the analysis was data concerning cases where the displacement was 5% or more of the pile diameter. With the horizontal ground reaction coefficient k_{HS} determined using the following formula as the constant of the ground resistance and the maximum horizontal ground reaction p_{US} as the parameters, a combination where the load - displacement curve

and the pile body's bending moment distribution error was minimized was selected (Figure 5).

$$k_{HS} = \alpha_k \times (k_H \text{ based on the Specifications}) \quad (7)$$

$$p_{US} = \alpha_p \times (\text{Coulomb's passive earth pressure strength}) \quad (8)$$

Where:

α_k : Coefficient for the coefficient of horizontal ground reaction of a single pile

α_p : Coefficient for the maximum value of the horizontal ground reaction force for a single pile

As an example, a contour diagram of the analysis error in a horizontal loading test of a steel pipe pile with a length of 21 m and diameter of 61 cm driven into sandy ground is shown in Figure 6. In this example, the error is minimized when the limit value of the ground reaction is 3.5 times the passive earth pressure strength and the ground reaction coefficient is about 1.5 times the value indicated in the Specifications. While the horizontal ground reaction coefficient indicated in the Specifications is established for a case where the horizontal displacement at the pile top is 1% of the pile diameter, the horizontal ground reaction coefficient used for elasto-plastic analysis represents characteristics at a lower displacement level. Therefore α_k is 1 or greater. In the case of α_p on the other hand, it is assumed that the resistance sphere of the ground spreads three dimensionally and that the average resistance width in the sphere which has plasticized is about 3 times the pile diameter. The load - horizontal displacement curve at that time is shown in Figure 7, and the bending moment distribution of the pile body is shown in Figure 8. In both figures, the analytical values and experimentally obtained values coincide relatively closely, and even in a simplified model, it is possible to represent the behavior of the pile by appropriately assessing the constant.

α_k and α_p which obtained conformity based on various loading testing are shown in Table 1 for sandy ground and in Table 2 for cohesive ground.

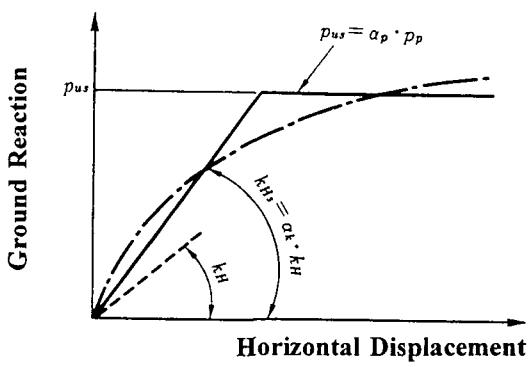

Figure 5 Modelling the Horizontal Ground Resistance

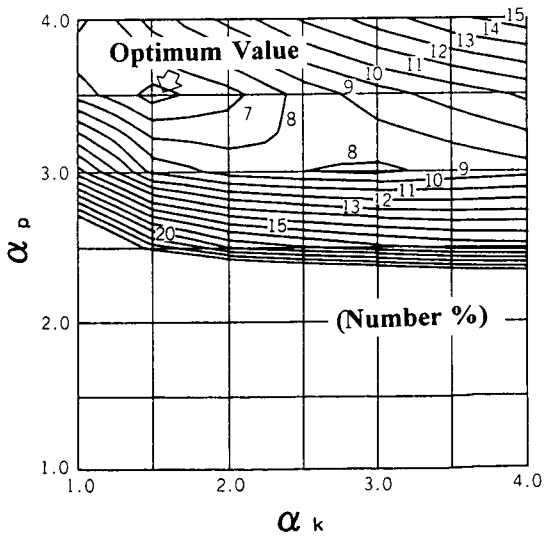

Figure 6 Contour Diagram of the Error

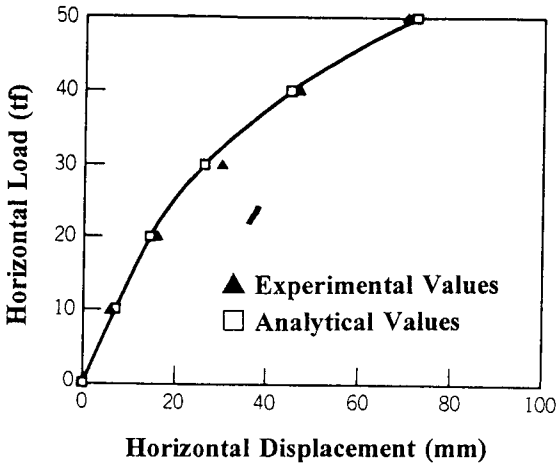

Figure 7 Horizontal Load - Horizontal Displacement Curve

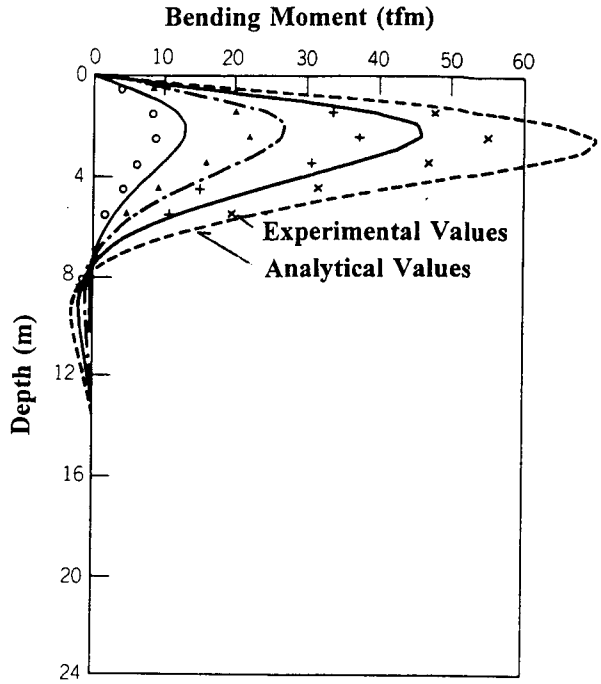

Figure 8 Bending Moment of Pile

Table 1 Loading Testing Analyzed (Sandy Ground)

No.	Pile Specifications		Max. Displacement	Max. Disp /Diameter	Optimum Values	
	Diameter × Thickness (mm)	Length (m)	(mm)	(%)	α_p	α_k
1	ϕ190.7×5.3	4.5	25.5	13.3	2.0	1.5
2	ϕ318.5×6.9	15.0	38.6	12.1	6.0	6.0
3	ϕ609.6×9.5	21.0	70.0	11.5	3.5	1.5
4	ϕ812.8×15.0	17.0	96.2	11.8	4.5	1.5
5	ϕ800.0×16.0	46.0	84.9	10.6	4.0	4.0
6	ϕ600.0×12.7	45.0	46.0	7.7	3.5	1.5
7	ϕ812.8×12.7	15.0	68.0	8.4	4.0	2.5
8	ϕ600.0×16.0	39.0	87.8	14.6	4.0	2.0
9	ϕ2 000×22	36.5	165.7	8.2	3.0	1.5

Table 2 Loading Testing Analyzed (Cohesive Ground)

No.	Pile Specifications		Max. Displacement	Max. Disp /Diameter	Optimum Values	
	Diameter × Thickness (mm)	Length (m)	(mm)	(%)	α_p	α_k
1	ϕ812.8×14.0	30.7	70.0	8.6	2.5	1.5
2	ϕ1 000×27.2	20.0	96.4	9.6	1.0	2.5
3	ϕ1 500×13.0	33.1	231.6 (96.2)	15.4 (6.4)	1.0	1.5
4	ϕ2 000×22.0	51.5	255.9 (139.0)	12.8 (7.0)	2.0	6.0
5	ϕ812.8×9.0	40.0	50.0	8.3	1.5	1.5
6	ϕ609.6×12.7	18.0	134.6	22.1	3.0	0.5
7	ϕ508.8×9.5	23.0	56.0	11.0	1.0	1.0

4.2 Effect of Pile Groups

In recent years, various organizations have studied this question by performing experiments to study the horizontal resistance of piles. One set of experiments conducted at the Public Works Research Institute of the Ministry of Construction 5) was done by installing steel pipe piles with diameters of 101.6 mm as single piles, rows of piles, side-by-side piles, and pile groups as shown in Figure 9, then loading them in test ground prepared in the soil tank shown in Figure 10. Figure 11 shows the average loaded load - footing horizontal displacement curve per pile. From this figure, it is assumed that within the range where the amount of displacement is large, load - horizontal displacement curves for multiple piles are, in all cases, below that of single piles, and that this is an effect of interference between the piles. The degree that this effect is observed is greatest for groups of 9 piles, and descends in the following order: straight line piles, and side-by-side piles, till it is close to that of single piles.

Based on experiments of this kind, an attempt was made to establish a design method by performing a simulation based on an analysis of the error in the reaction distribution of piles in a group of piles and of their behavior during large deformation. The non-linear properties of horizontal resistance of ground, which is a problem during large deformation, was handled in the bilinear form verified in 4.1. And to account for errors of the load distribution of the piles, the ground resistance properties (k_{HS}, p_{US}) which treated α_k and α_p as the parameters, were set by trial and error for each pile location, and then the values of α_k and α_p were selected so that the experimental values and analytical values for the four following items coincided most closely.

(1) Horizontal Load - Horizontal displacement curve of the foundation

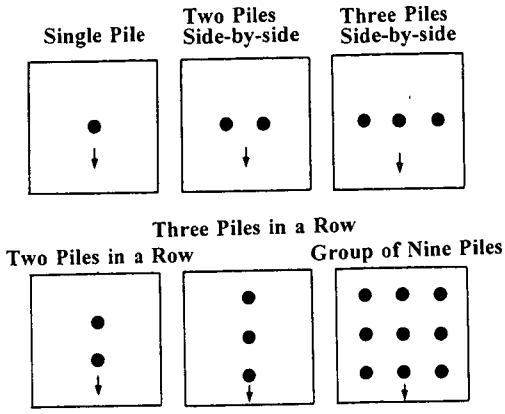

Figure 9 Experimental Cases

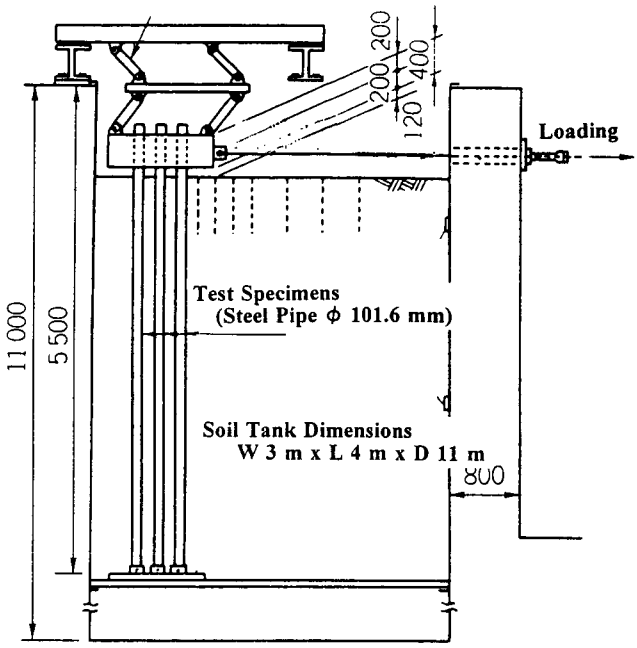

Figure 10 Outline of the Experiment

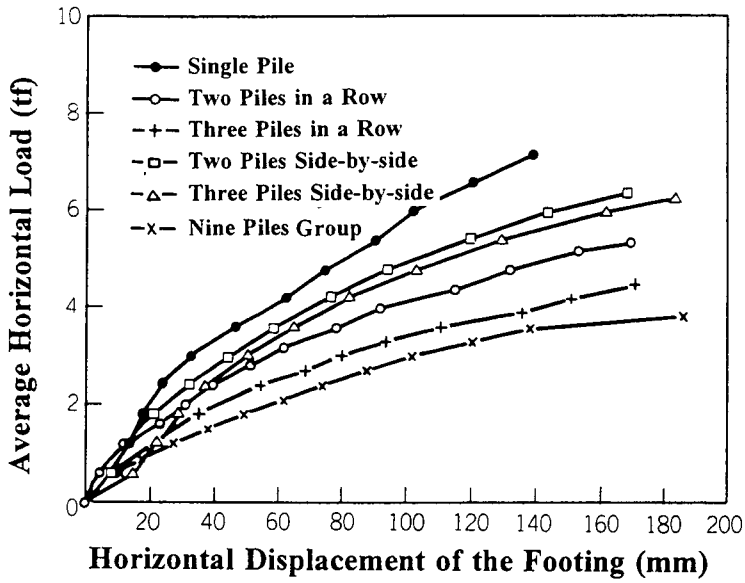

Figure 11 Average Horizontal Load - Horizontal Displacement Curve

(2) Horizontal displacement distribution of the pile
(3) Bending moment distribution of the pile
(4) Horizontal ground reaction distribution

The displacement level simulated was assumed to be that up to the point the pile body yields, and was set so it conformed up to a displacement of about 50% of the pile body diameter.

Figure 12, in which the values of α_k and α_p which conform with the actual measured values for the horizontal load - horizontal displacement curve of the footing above a group of 9 piles were selected, indicates that it is possible to perform extremely precise simulations by setting the appropriate values. Figure 13 and Figure 14 show the bending moment distribution and ground reaction distribution for the combination of α_k and α_p which conform most closely in the case of the group of 9 piles shown in Figure 12. The experimental and analytical values for these values also coincide relatively closely. In addition it was possible to obtain the same degree of conformity for the horizontal displacement of the pile body.

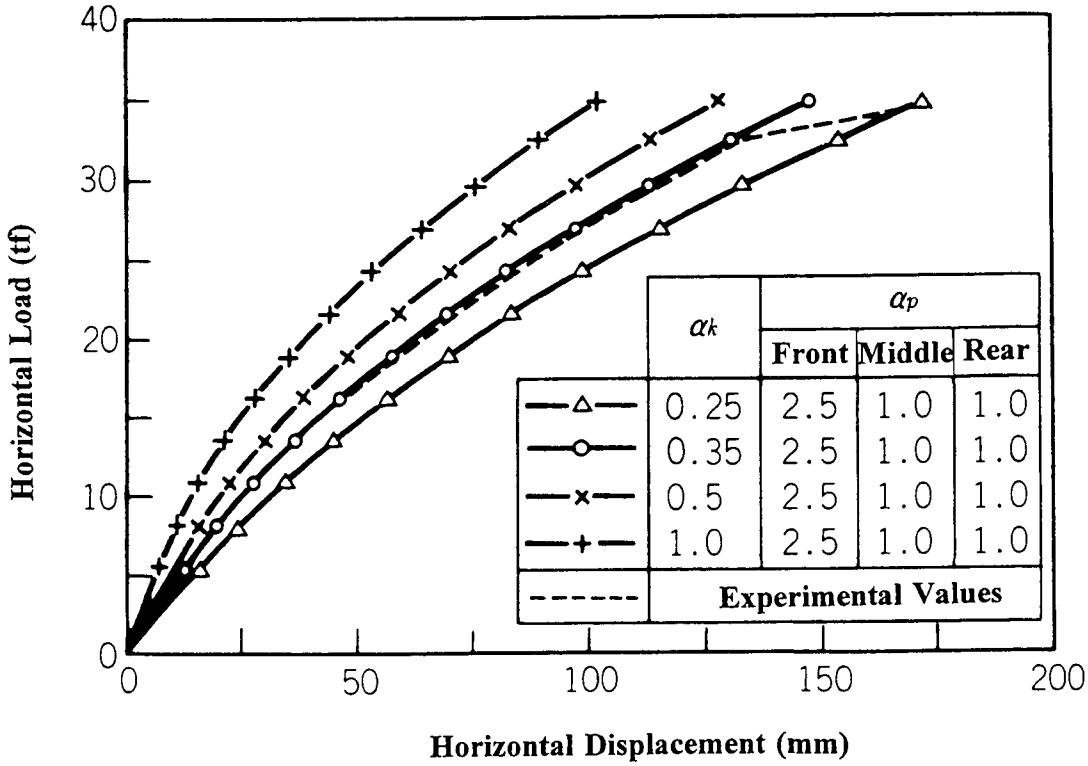

Figure 12 Horizontal Load - Horizontal Displacement Curve Analysis (Nine Piles in a Group)

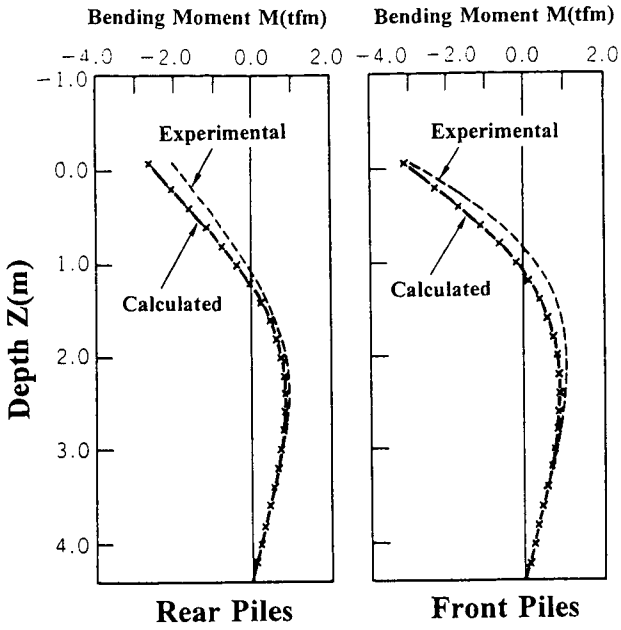

Figure 13 Analysis of Bending Moment

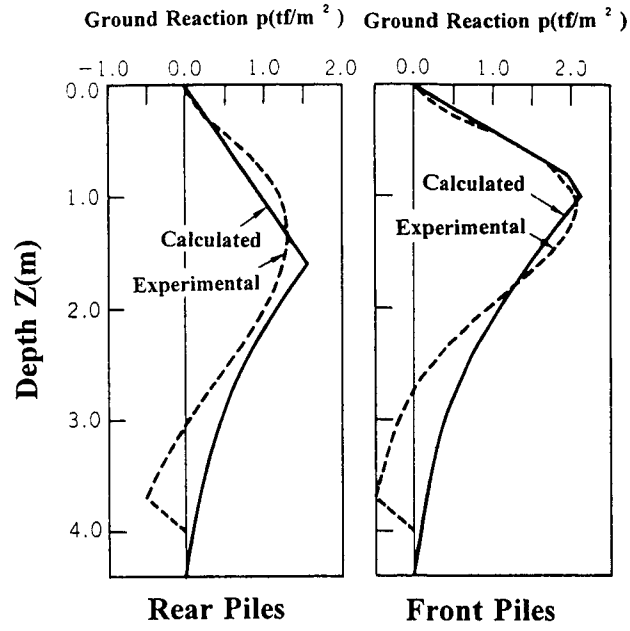

Figure 14 Analysis of the Horizontal Ground Reaction

Table 3 α_k and α_p Which Obtained Conformity with Horizontal Loading Testing of Pile Groups

Test Name	Pile Arrange	Pile Location	α_k	Ratio to Single Pile	α_k	Ratio to Single Pile
PWRI Pile (Steel pipe, sand)	Single		1.5	1.0	3.0	1.0
	9-group	Front	0.35	0.23	2.5	0.83
		Middle			1.0	0.33
		Rear			1.0	0.33
Metropolitan Exp. Public Corp. Pile (Steel pipe, sand)	Single		3.0	1.0	2.5	1.0
	9-group	Front	3.0	1.0	1.0	0.44
		Middle			0.8	0.32
		Rear			0.4	0.16
Umeda Pile (cast-in-place, sand)	Single		2.4	1.0	2.5	1.0
	2-piles	Front	2.4	1.0	2.5	1.0
		Rear			1.0	0.4
Kishiwada Pile (cast-in-place, sand)	Single		2.0	1.0	3.5	1.0
	9-group	Front	1.0	0.5	3.0	0.85
		Middle			3.0	0.85
		Rear			1.5	0.43

The results of using the same method with other loading testing to find α_k and α_p which can obtain this level of conformity are shown in Table 3. It reveals that α_k for a pile group is either equal to or lower than that of a single pile. And α_p for a pile group is, in the case of the pile toward the front, almost identical to that of a single pile, but the value declines towards the rear of the pile group. This phenomenon is believed to be caused by the decline of the ground reaction coefficient as the converted loading width increases and by the passive resistance phenomenon produced by the overlapping of the resistance ranges of each pile.

4.3 The Bending Moment - Curvature Relationship of a Pile Body

When using the displacement method, a pile body is treated as an elastic body in order to keep the stress of the reinforcing bars etc. of the pile body from exceeding the allowed stress. When calculating the horizontal strength of a pile foundation, it is important to evaluate the behavior of the pile body after yield and the ultimate strength. It is necessary to appropriately model the bending moment - curvature relationship in the pile body.

The points of inflection in the bending moment - curvature relationship when bending moment acts on a concrete pile are usually treated as the cracking time (C), the time when the reinforcing bars begin to yield (Y), and the ultimate time of the section (U). The analytical model was a trilinear model linking these points found for a circular steel reinforced concrete cross section with the axial direction N and subjected to the bending moment M (Figure 1(d)).

Because points of this sort are not clearly revealed on a steel pipe pile, it is modelled as a bilinear model with the point at which the stress of the outermost edge of the steel pipe pile reaches the yield point considered to be the initial gradient, and the plastic moment treated as the maximum value (Figure 1(e)).

4.4 Calculation Method

Based on 4.1 and 4.2, the horizontal ground resistance is found as follows.
The horizontal ground resistance properties is considered to be elasto-plastic in form with the coefficient of horizontal ground reaction K_{HE} as the initial gradient, and the maximum value of the horizontal ground reaction force P_{HU} to be the upper limit value (Figure 1 (c)). k_{HE} and p_{HU} can be found from the following formulae.

$$k_{HE} = \eta_k \alpha_k k_H \quad (9)$$

$$p_{HU} = \eta_p \alpha_p p_U \quad (10)$$

Where:

k_{HE} : Coefficient of horizontal ground reaction used for the check of ductility and dynamic strength (kgf/cm ^{3})

p_{HU} : Maximum value of the horizontal ground reaction force (kgf/cm ^{2})

k_H : Coefficient of horizontal ground reaction (kgf/cm ^{2}), found as stipulated in the Specifications.

p_U : Passive earth pressure during an earthquake (kgf/cm ^{2}), found as stipulated in the

Specifications. It can account for the weight of the soil up to the ground surface which is stable over a long period around a foundation as the overburden load.

α_k : Coefficient for the coefficient of horizontal ground reaction of a single pile.

α_p : Coefficient for the maximum value of the horizontal ground reaction force for a single pile.

η_k : Coefficient for the coefficient of horizontal ground reaction accounting for the pile group effects.

η_p : Coefficient for the maximum value of the horizontal ground reaction force accounting for the pile group effects.

Table 2 presents the values of the coefficient α_k of the coefficient of horizontal ground reaction and the coefficient α_p of the maximum value of the horizontal ground reaction force of a single pile. This was obtained based on an analysis of the results of the horizontal loading test of a single pile shown in 4.1.

Table 2 Coefficient

Type of Ground	α_k	α_p
Sandy Ground	1.5	3.0
Cohesive Ground	1.5	1.5

Note: In cohesive ground where $N \leqq 2$, α_p is assumed to equal 1.0.

The coefficient η_k for the coefficient of horizontal ground reaction accounting for the pile group effects is the following value.

$$\eta_k = 2/3 \tag{11}$$

The coefficient η_p for the maximum value of the horizontal ground reaction force accounting for the pile group effects is the following value.

Cohesive ground: $\eta_p = 1.0$ (12)

Sandy ground : $\eta_p \cdot \alpha_p$ = Interval between the centers of the piles in the direction at right angles to the loading direction / pile diameter ($\leqq \alpha_p$) (13)

In the case of piles other than those in the front pile in sandy ground, the value is 1/2 of that indicated in (13).

The values of η k, η p are found from the results of the analysis of the loading tests of group piles in 4.2.

The load - horizontal displacement curve obtained based on the horizontal loading testing of cast-in-place piles shown in Figure 17 and the results of its analysis are shown in Figure 16. Here, the ground resistance properties are treated as completely elastoplastic type. An analysis treating the pile body as linear revealed conformity in the area where the amount of

deformation is small, but as the amount of deformation rises, the values diverge. This suggests that when the non-linear properties of the bending stiffness of a pile are considered, it is possible to perform a simulation up to the large deformation stage.

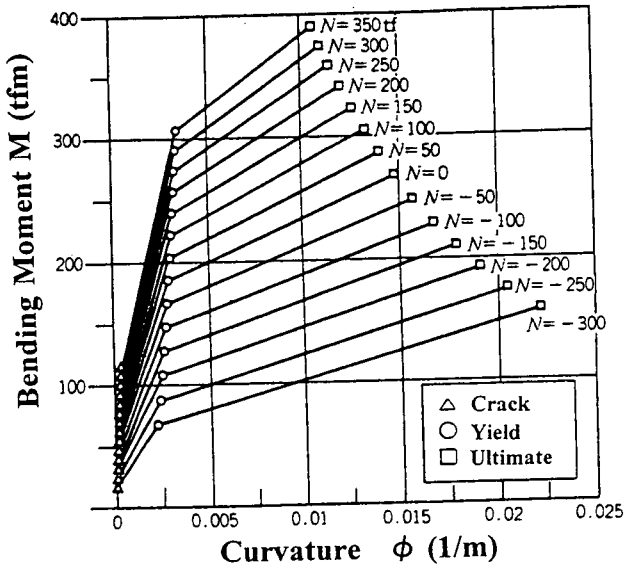

Figure 15 Bending Moment M - Curvature ϕ of a Pile

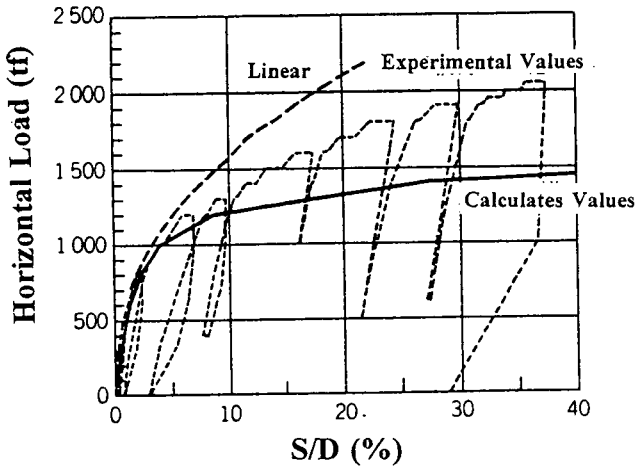

Figure 16 Analysis of the Horizontal Load Test of a Cast-in-place Piles

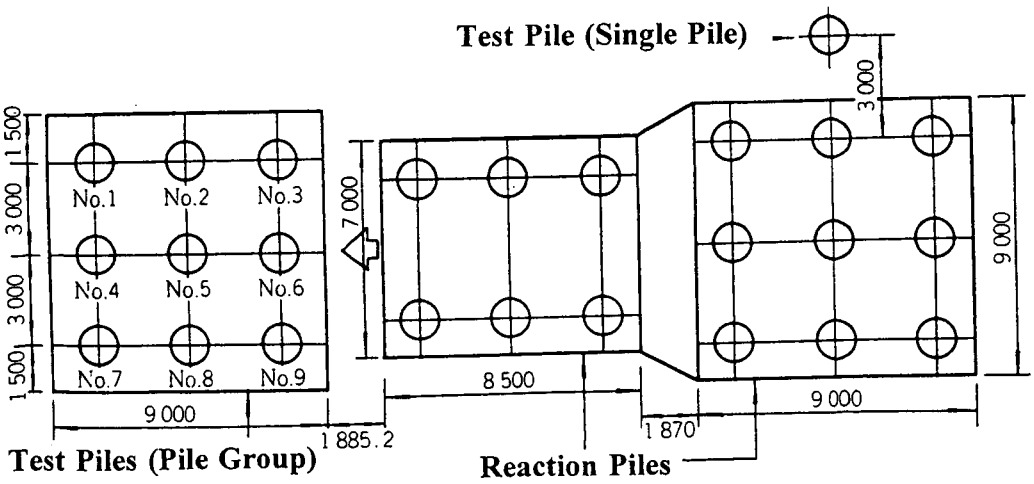

Figure 17 Loading Testing of the Kishiwada Piles

5. LOADING TESTS FOR DUCTILITY OF PILE FOUNDATIONS

5.1 Test Objectives

In the case of a wall type bridge pier at right angles to the bridge axis or a case where liquefaction will occur, it is rational to design the bridge so that the energy is absorbed by the foundation. Even in these cases, it is necessary to design the bridge so that the response ductility factor of the foundation is within a certain value in order to prevent excessive damage to the foundation body.

As a limiting value for this ductility factor, the safety coefficient for the ultimate was used to determine the allowed ductility factor for a reinforced concrete bridge pier. Even when a member which is part of the pile body of a pile foundation reaches the ultimate state, this does not result in an immediate conspicuous horizontal strength decline in the overall foundation system. It is difficult to define the ultimate for an entire pile foundation system. For this reason, loading tests of a model pile foundation is done to clarify the ductility factor of the foundation and the state of damage to the pile body. This information is used as reference data when determining the limiting value of the ductility factor.

Loading tests were performed using PHC, cast-in-place piles, and steel pipe piles which are used for pile foundations of highway bridges. The following section refers to the tests of cast-in-place and PHC piles.

5.2 Test Method

Figure 18 shows an overview of the loading method. This testing, which is done to clarify the state of damage to a pile body when horizontal force acts upon pile groups, requires that moment and horizontal force act on the model simultaneously. The loading was performed by simultaneously controlling three jacks to hold the vertical load at a constant level and performing alternating positive and negative loading of a horizontal force with the horizontal force H/moment M ratio constant at M/H = 2.5 m.

The pile foundation models used were six reinforced concrete piles with a diameter of 30 cm and a length of 180 cm; three set in the loading direction and two at right angles to the loading direction. The interval between their centers was 75 cm, which was 2.5 times their diameters.

The displacement of the horizontal loading position at the level where the axial direction reinforcing bars at the outer edge of the pile bodies of all piles yielded in the previous analysis was set at 1 δ_y, and positive - negative alternating loading was performed while increasing the displacement in increments of 1 δ_y. Three cycles of loading were done for each δ_y. The vertical load was 84 tf.

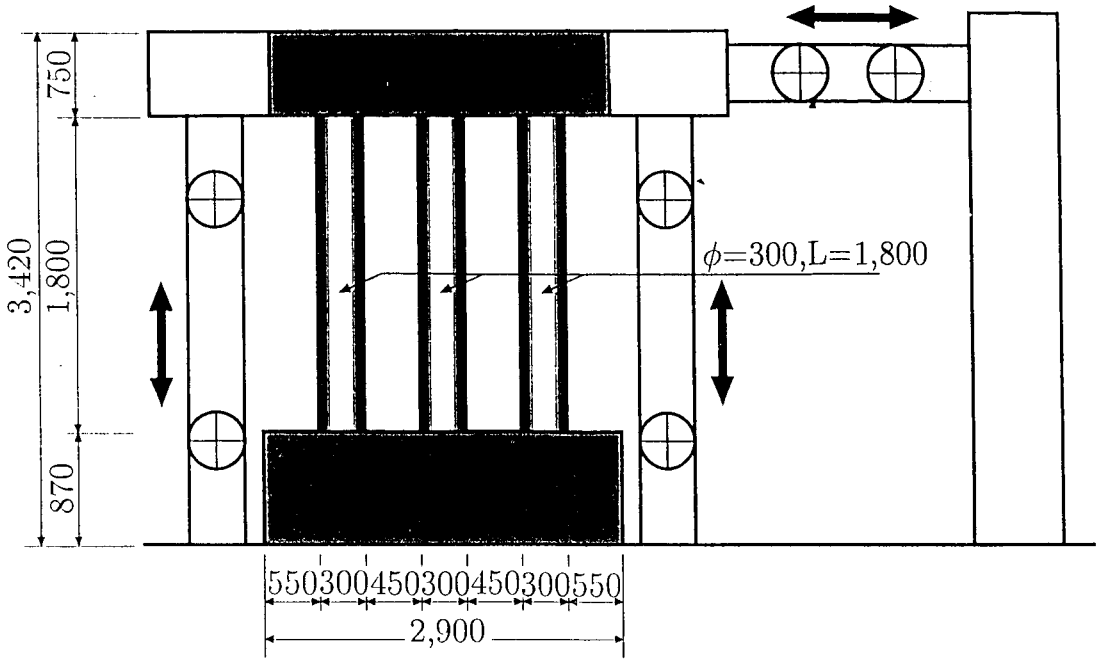

Figure 18. Loading Test

5.3 Test Results

The models of cast-in-place piles were made using 16 reinforcing bars of type SD295A, D10 as the axial direction reinforcement. The hoop ties were made of SD295A, D4 installed at 4 cm intervals. The distance from the outer surfaces of the piles to the centers of their axial direction reinforcement was 5 cm. The results of material testing show that the compressive strength of the concrete was 323 kgf/cm ^{2} while the yield point of the steel reinforcing bars was 3,757 kgf/cm ^{2} .

Figure 19 shows the hysteresis curve of the horizontal force and the horizontal displacement of the cast-in-place piles. A description of the state of damage to the piles follows.

At 2 δ_y , signs that the covering concrete would soon collapse appeared at the top and bottom bases of the piles at the ends and in the bottom of the piles in the middle, and maximum load was reached at 3 δ_y . At that time, some of the covering concrete at the bottom of pile 1 separated. At 4 δ_y , covering concrete at the top of pile 1, the top and bottom of pile 3, and the bottom of pile 2 separated, but this did not expose any of the reinforcing steel rods (Photograph 1). At 6 δ_y , steel reinforcing rods were exposed and buckled at the bottom of pile 1 and at the top and bottom of pile 3, and at 7 δ_y , steel reinforcing rods were exposed and buckled even at the top of pile 1. As the cyclic loading continued, the hoop ties and axial direction reinforcement failed reducing the horizontal strength.

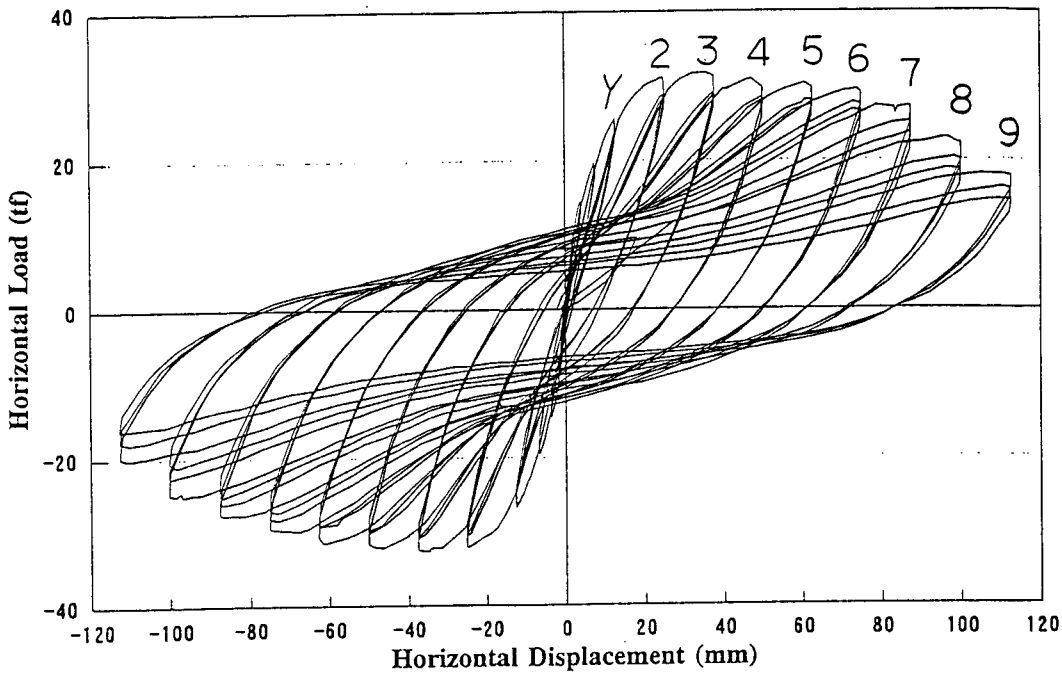

Figure 19 horizontal Load - horizontal Displacement Hysteresis Curve (Cast- in-Place Piles)

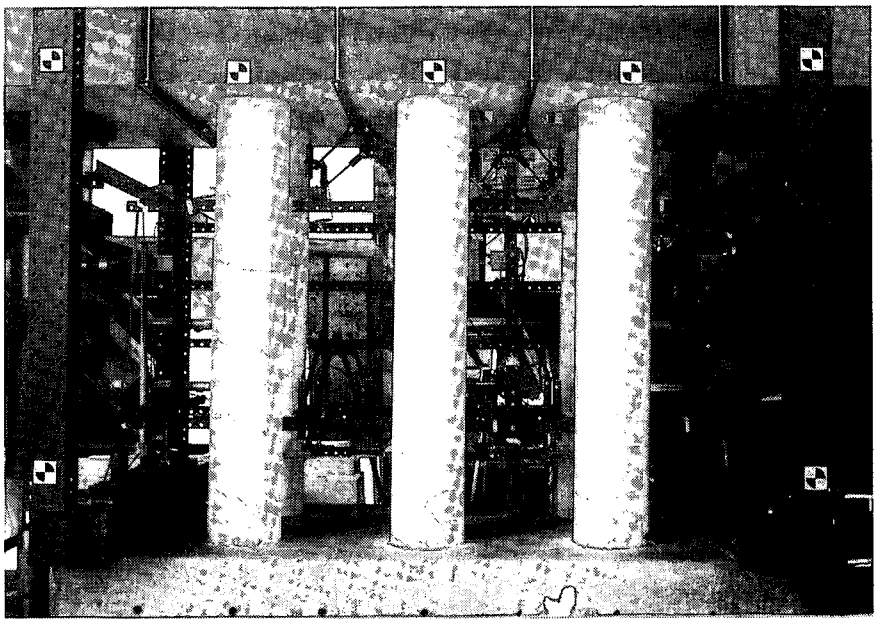

Photograph 1. State of Damage to Pile Bodies (Cast-in-place Piles, + 4 δ_y)

6. CONCLUSION

The check of dynamic strength and ductility for pile foundations has been proposed based on the results of research into the behavior of pile foundations during severe deformation. For this pile foundation analysis method, a rigid frame pile model was made accounting for the non-linear properties of the vertical resistance of piles, horizontal ground resistance, and the bending stiffness of the pile body. Horizontal loading testing of models of pile foundations was performed to clarify the foundation ductility factor - degree of pile body damage relationship. This test confirmed that at less than 4 times the yield displacement, the pile bodies are spared serious damage.

REFERENCES

1) Ministry of Construction : Report on the Damage of Highway Bridges by the Hyogo-ken Nanbu Earthquake, Committee for Investigation on the Damage of Highway Bridges caused by the Hyogo-ken Nanbu Earthquake, 1995.
2) Ministry of Construction : Guide Specifications for Reconsturuction and Repair of Highway Bridges Which Suffered Damage due to the Hyogo-ken Nanbu Earthquake, 1995.
3) Okahara et. al.: Research on the Bearing Capacity of Single Piles and Design Methods for Column-shaped Foundations, Technical Memorandum of Public Works Research Institute No. 2919, 1991.
4) Kimura, Tatsuta, Kasuga: Evaluation of the Non-linear Properties of horizontal Resistance of Piles During Severe Deformation, Papers Presented at the Symposium on Limit State Design Methods for Foundation Structures, 1995.
5) Fujiwara, Okahara, Nakatani, Kimura and TAKAGI: Horizontal Bearing Capacity of Pile Foundations Based on Horizontal Loading Tests, 24th UJNR Joint Panel Meeting,1992.

NON LINEAR SEISMIC ANALYSIS OF RAILWAY BRIDGES

M. Dolce **D. Liberatore**

Department of Structures, Soil Mechanics, Applied Geology, University of Basilicata
Via della Tecnica 3, 85100-Potenza

G. Traini

ITALFERR SYS-TAV S.p.A.
Via Marsala 53, 00100 - Roma

ABSTRACT

The most peculiar problems of railway bridges subjected to seismic actions are discussed and the computer program BRIE (Bridge-Railway Interaction due to Earthquakes) is presented. BRIE is a three-dimensional non linear finite element program. It is purposely made to model some peculiar aspects of railway bridges, such as the non linear behaviour of track-bridge connection (ballast), the dynamic behaviour of train vehicles, the unilateral contact constrain between wheel and rail. Moreover, it has the capability of modelling the most usual passive control devices, such as elasto-plastic isolators and dampers. The seismic action can be modelled with either syncronous or non-syncronous motions. With the above features, the program is able to evaluate the seismic effects not only on the structure, but also on the track and on the vehicles, making it possible to assess the seismic safety with respect to ultimate as well as service conditions.

1. INTRODUCTION

The importance of the seismic safety of railway bridges was especially highlighted by the recent January 95 Kobe Earthquake. Heavy structural damage and collapse as well as large permanent displacements of track and tilting up of train vehicles occurred, causing the complete interruption of the railway service for a long period. Railway serviceability, in fact, is conditioned not only by structural damage or collapse, but even by permanent track displacements due to vibrations and relative displacements in dynamically excited bridges. Moreover structural vibrations induce tilting moment in train vehicles, either still or moving, possibly causing their tilting up and compromising the runnability of bridges during earthquakes.

The computer programs for the non linear analyses of bridges do not normally address this type of problems, as they cannot account for the interaction between train, track and bridge. Peculiar problems that are not normally dealt with are the modelling of:

- track-bridge connection (ballast),

- train vehicles,
- unilateral contact between vehicle, wheel and rail.

For the above reasons, the new software package BRIE (Bridge-Railway Interactions under Earhquakes) has been devised and implemented.

BRIE is a three-dimensional non linear finite element program, which models accurately R/C structural elements (piers and abutments), track, track-deck connection (ballast or direct fastening), train vehicles, wheel-rail unilateral contact constraint. It can also model accurately the characteristics of bearings, taking into account friction and unilateral restrain, and of passive control devices, such as elasto-plastic or visco-elastic isolators and dampers. Finally synchronous or non-synchronous seismic motions can be considered. The analysis is carried out by applying the static actions first (vertical dead and live loads, temperature variations) and then the earthquake.

The program has been recently set up and a parametric analysis is being started, to study the seismic behaviour of the most common types of bridges of the Italian new high speed lines.

In this paper the most peculiar features of BRIE are described, the results of a typical railway bridge are illustrated and the future development of the study are outlined.

2. BRIE

BRIE has been conceived to evaluate the response of railway bridges, taking into account the important interactions between bridge, track and train. Bridge-track and bridge-train interactions have already been studied in the past for the static or quasi-static actions due to temperature variations, braking forces and vertical loads, and for the dynamic vertical actions due to the train transit along the bridge. Two finite element computer programs were purposely implemented to analyse these two problem: ISTBS and IDTBS.

ISTBS is a non linear finite element static analysis program [1], which is now equipped with a powerful graphic pre-post- processor (PRIS). It is able to evaluate the three-dimensional quasi-static response of a track-bridge system, under temperature variations of track and bridge, moving vertical loads and braking forces of train. An accurate non linear modelling of the track-bridge connection, the consideration of large displacements of track and the ability of monitoring the non-linear response of the track-bridge system, while the train is moving along the bridge, are the peculiar features of PRIS-ISTBS.

IDTBS is a linear dynamic finite element program [2], which is now equipped with a powerful alphanumeric pre-processor. It is able to analyse the three-dimensional dynamic response of a train-bridge system when the train is moving, for any type of bridge. An accurate modelling of the train vehicles and of the track irregularities, as well as the ability of monitoring the linear response of the bridge system while the train is moving along the bridge, are the peculiar features of IDTBS.

BRIE extends the capabilities of these two programs to evaluate the dynamic non linear response of train-track-bridge systems subjected to earthquakes. It exploits some features of the two above programs, such as the accuracy of ISTBS in modelling the track-bridge connection medium and the accuracy of IDTBS in modelling the train vehicles. However it also adds many other important new features, that allows the program to obtain a very accurate simulation of the complicated non linear phenomena caused by seismic actions.

BRIE is made up of four modules:

- BRIE-Pre, the alphanumeric Pre-processor, that produces complicated non linear models from a reduced set of data;
- BRIE-Sol, the finite element Solver;
- BRIE-Post, the Post-processor which summarises the results and provides graphic capabilities plot the structural model and make the diagrams of time histories of the most significan quantities;
- BRIE-Winter, the friendly interface for the management of input and output data; it operates in the Microsoft Windows© environment, making use of most of its features.

In the following paragraphs a detailed description of BRIE-Sol will be provided, with an insight to the characteristics of the finite elements and of the analysis procedures. The main features of the other modules will also be shortly described.

2.1 Library elements

The modelling capabilities of BRIE depends mainly on its library of finite elements. In the following paragraphs a description of their main features is given.

2.1.1 Fibre beam-column element

This is a 2-nodes 12-degrees-of-freedom beam-column elements, with inelastic material characteristics. It is especially conceived to simulate accurately the flexural behaviour of reinforced concrete members. The element is transversely discretised into concrete and steel fibres and longitudinally into sub-elements of different lengths, as shown in fig. 1.

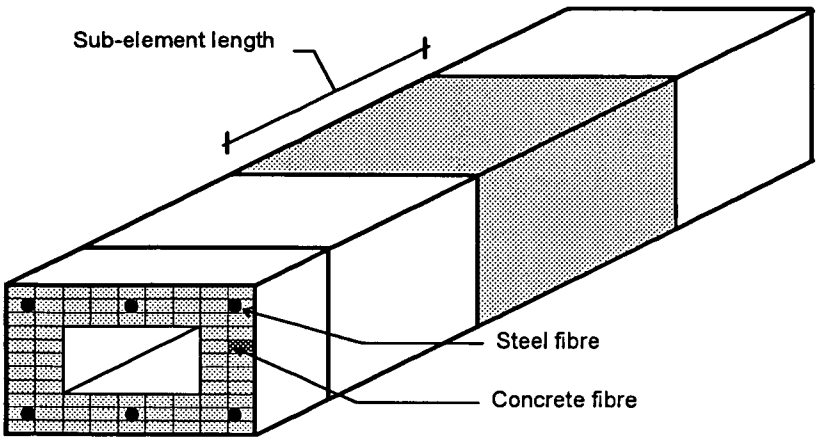

Fig. 1 - Typical fibre beam-column element.

The stress-strain constitutive laws are multi-linear hysteretic for both materials, giving great flexibility in modelling the usual cyclic behaviours of steel and concrete. The stress state is evaluated at the mid-length of each sub-element. The cross sections of the element are assumed to remain plane, according to the Navier hypothesis. The element is assumed to be elastic in shear and torsion.

The calculation of the stiffness matrix and force vector of the element is carried out through a mixed stiffness/flexibility method. It is assumed that the element end nodes are subjected to prescribed incremental displacements, according to the classical equilibrium iteration method. For each loop of the equilibrium iteration, the stiffness matrix and the force vector of the element are calculated through an inner iteration, which consists of the following steps.

1. For the incremental displacements prescribed at the end nodes, the incremental forces are calculated through the element stiffness matrix and added to the element total forces.

2. The incremental forces of each sub-element are calculated. Since it is assumed that no intermediate load is applied to the element, the axial force is constant along the element length, and the two principal bending moments exhibit linear variations.
3. The incremental axial strain and curvatures of each sub-element are evaluated, the state variables of fibres are updated, the stress and tangent elastic moduli of fibres are found.
4. The sub-element flexibility matrix is calculated through the assemblage and inversion of the sub-element stiffness matrix. The sub-element flexibility matrices are assembled over all sub-elements, producing the element flexibility matrix. Finally, this is inverted, giving the element stiffness matrix.
5. The axial force and the two principal bending moments of the sub-element are calculated. Since in general these are not in equilibrium with the axial force and bending moments at the element end nodes, incremental deformations should be applied to the sub-element in order to re-establish equilibrium. These deformations are assembled over all sub-elements, yielding the element deformations. They are "incompatible", in the sense that they violate the displacements prescribed at the element end nodes.
6. The incremental forces corresponding to the element incompatible incremental deformations are calculated and subtracted to the element total forces.
7. The element incremental forces calculated at step 6 are checked for convergence. If the check is satisfied, the loop is terminated, otherwise the procedure returns to step 2.

The procedure is very efficient from the computational point of view, as convergence is usually attained within 2 or 3 iterations.

2.1.2 Elastic large-displacement beam element

This is a 2-nodes 12-degrees-of-freedom beam elements, with elastic material characteristics, which simulates the behaviour of Timoshenko beams.

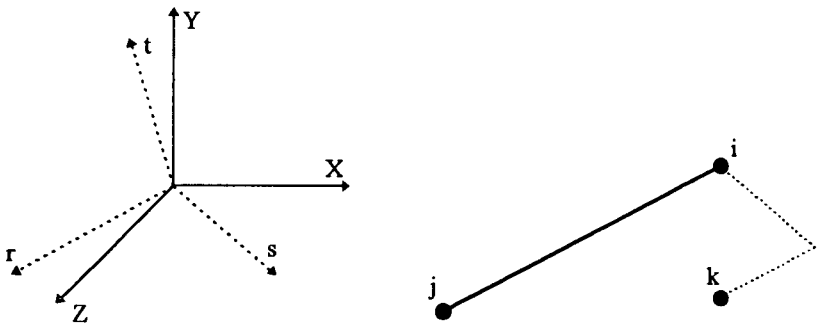

Fig. 2 - Local system of the elastic beam element.

The main feature of this element for track modelling is its capability of including the geometrical stiffness and of accounting for large displacements through an Updated-Lagrangian approach.

End-release codes can be assigned, to release the end constraint conditions. Temperature variations can be considered for each element. The local system is defined by the end nodes *i* and *j*, and by a third *k* node, as shown in fig. 2.

2.1.3 Ballast spring element

According to its name, this element has been especially conceived to model the behaviour of the ballast. For its features, however, it can be used in a wider range of situations, to get a more or less refined simulation of different behaviours. For example it can simulate unilateral contacts, elastic spring constraints, fixed bearings, sliders, elasto-plastic isolators, soil springs.

The ballast spring element is a 2-nodes 12 degrees-of-freedom element. It is made of three translational and three rotational springs, with different elastic or non linear characteristics. The springs are connected to the two nodes through rigid arms. The directions of the springs and of the rigid arms are parallel to the axes of the local reference system *r-s-t*, as shown in fig. 3.

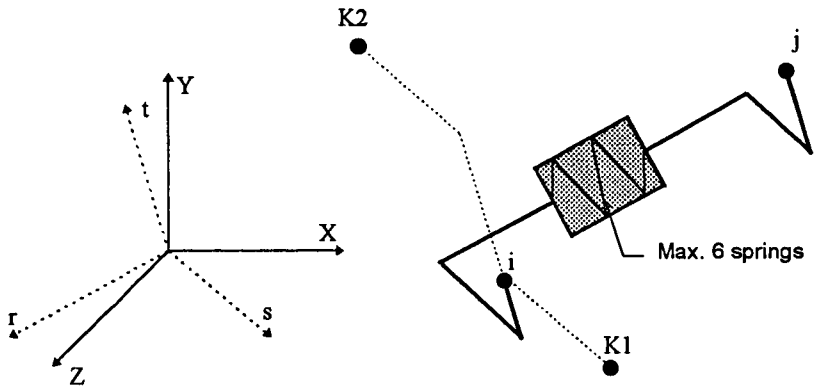

Fig. 3 - Ballast spring element.

The springs can be either linear or non linear. Linear springs are defined by their elastic stiffness. Two different behaviours of non linear springs are defined, according to their direction. The spring acting in the r-direction has a non-linear behaviour, such as that shown in fig. 4, where the initial stiffness in tension and in compression are different. It permits to simulate a unilateral constraint. The other two translational and all the three rotational springs follow an elastic perfectly plastic hysteretic law, whose elastic stiffness and plastic force depend, at any moment, on the stress state of the first spring, according to fig. 4. Different elasto-plastic characteristics can be assigned to the various springs of a same element. An initial different cohesive resistance can be assigned to each spring, which is annihilated as soon as one of the springs reach the failure value.

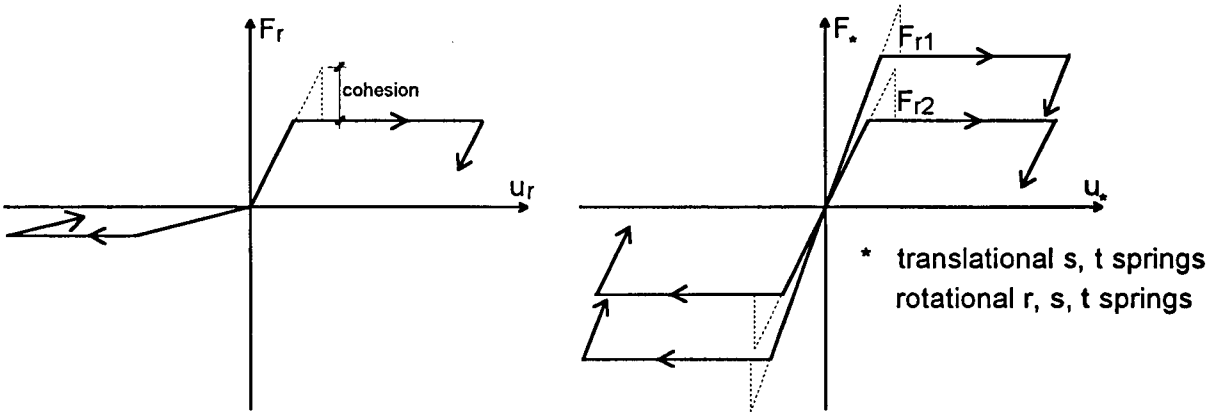

Fig. 4 - Force - displacement characteristics of the springs of the ballast element.

2.1.4 Elasto-plastic truss element

This is a classical 2-nodes 6-degrees-of-freedom truss elements, with a linear or hysteretic bilinear behaviour. It can be used for a wide range of situations, particularly for special antiseismic devices.

2.1.5 Viscous truss element

This is a 2-nodes 6-degrees-of-freedom truss element, with a viscous behaviour. A linear viscosity law is assumed, so that its force is proportional to the relative velocity of the two

nodes. It is purposely made to model the damping system of the train vehicles, some special seismic devices (dampers, couplers), as well as the hysteretic and radiation damping in the foundations.

2.2 Analysis procedures

The dynamic equations of motion are solved in the time domain through step-by-step time integration, making use of the Newmark method.

The classical Newton-Raphson equilibrium iteration procedure has been implemented, with the aim to improve numerical accuracy. It usually converges within 2 iterations. The use of equilibrium iterations permits to adopt a relatively large time step (typically 0.01 s), thus saving computer time.

In typical situations, the number of unknowns can reach several thousands. In order to save computer time, as well as computer storage, the sky-line representation of the stiffness matrix has been implemented, together with an efficient bandwidth optimizer. This has been purposely conceived to exploit the usual layout of track-bridge models, which are strongly developed along the longitudinal direction. Bandwith optimization is achieved by sorting the degrees of freedom of the system according to the longitudinal co-ordinate of the nodes. In typical situations, the mean bandwith after optimization does not exceed 30.

2.3 BRIE-Winter, BRIE-Pre and BRIE-Post

BRIE-Winter (Windows interface) is the friendly graphic interface for input and output data management, which exploits the features of the Microsoft Windows© environment. It allows the user to input interactively a reduced set of data, concerning the geometry of the bridge and of the track, the mechanical characteristics of the materials, etc., from which the program creates the model. For the train and the seismic actions, which represent the most complicated items to be inputted, BRIE-Winter makes use of a library from which the user can select the type of interest among the most commonly used ones. An easy and continuous control of most of the input data is made possible by an extensive use of graphic representations. BRIE-Winter is also connected to BRIE-Post, thus permitting to select interactively the quantities to be extracted from the results and put into diagrams.

BRIE-Pre is the alpha-numeric pre-processor, which creates the model and the relevant input file for BRIE-Sol, from the reduced set of data required by BRIE-Winter. The main tasks of BRIE-Pre are:

- Creation of the models of the vehicles;
- Discretisation of the track and of the deck into beam elements, as well as of their connection medium into ballast elements;
- Discretisation of the piers and of the abutments into fibre elements, starting from the description of the section geometry and of its steel reinforcements;
- Modelling of bearings, links and other seismic devices;
- Application of the vertical loads according to a suitable sequence consistent with the construction phases;
- Application of the time-history displacements at every soil-structure nodes.

BRIE-Post is a post processor written in FORTRAN, which summarises the huge amount of output data and prepare the files to be converted into diagrams. The typical quantities that are dealt with by BRIE-Post are:

- displacements and acceleration of train vehicles;
- relative wheel-rail displacements and forces;
- absolute and relative (with respect to the deck) displacements of track in the longitudinal and transverse direction, in critical points (i.e. near the deck joints);
- displacements and accelerations of decks;
- relative displacements and reactions in the bearings;
- rail stresses;
- displacements, curvature and damage indices of piers and abutments;

For most of these quantities in selected points, the time history are plotted and the maximum and residual values are extracted, for a fast examination of the performances of the train-track-bridge system.

3. TRAIN-TRACK-BRIDGE AND EARTHQUAKE MODELLING

Making use of the finite element types described in the previous chapter, any train-track-bridge system can be accurately modelled for seismic analysis. Though BRIE-Sol has as many modelling possibilities as a finite element code would permit, BRIE-Pre and BRIE-Winter normally operate by using the modelling rules shortly described in the following paragraphs, thus finalising the capabilities of BRIE-Sol to the most usual railway bridge configurations.

3.1 Track

Although the track is made of two rails connected by sleepers, BRIE models the track as a unique elastic beam, in which its stiffness properties are concentrated, Thus saving computing time and memory. The stiffening effect of the sleeper is taken into account by suitably calibrating the stiffness of the ballast rotational springs. The elastic large displacement beam elements are used, so that buckling is taken into account.

The ballast spring elements simulate the track-deck and track-soil connection medium, considering the three transla-

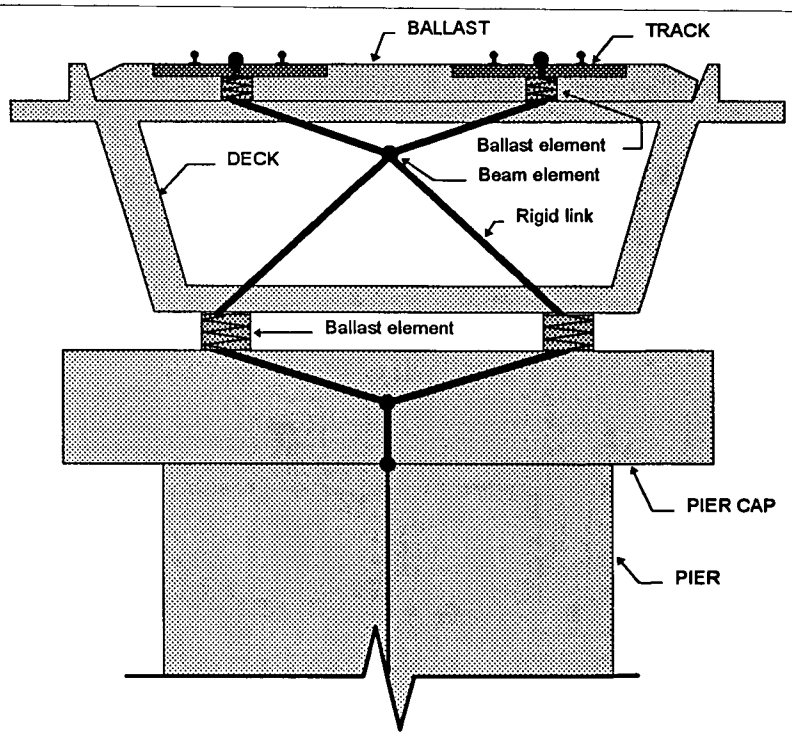

Fig. 5 - Trasverse view of the modelled track-bridge system.

tional springs and the three rotational springs. The r-axis of the first translational spring is vertically directed, while the horizontal s-axis and t-axis are longitudinally and transversely directed respectively, so that the stiffness and strength of these two latter depend on the force of the former one, i.e. on the load acting on the track.

The beam elements which model tracks are aligned along the track axis line. The springs of the ballast element are located in correspondence of the ballast or of the direct fastening connection. They are joined to the track axis and to the deck axis through the rigid arms of the ballast element, as shown in figs. 5 and 6.

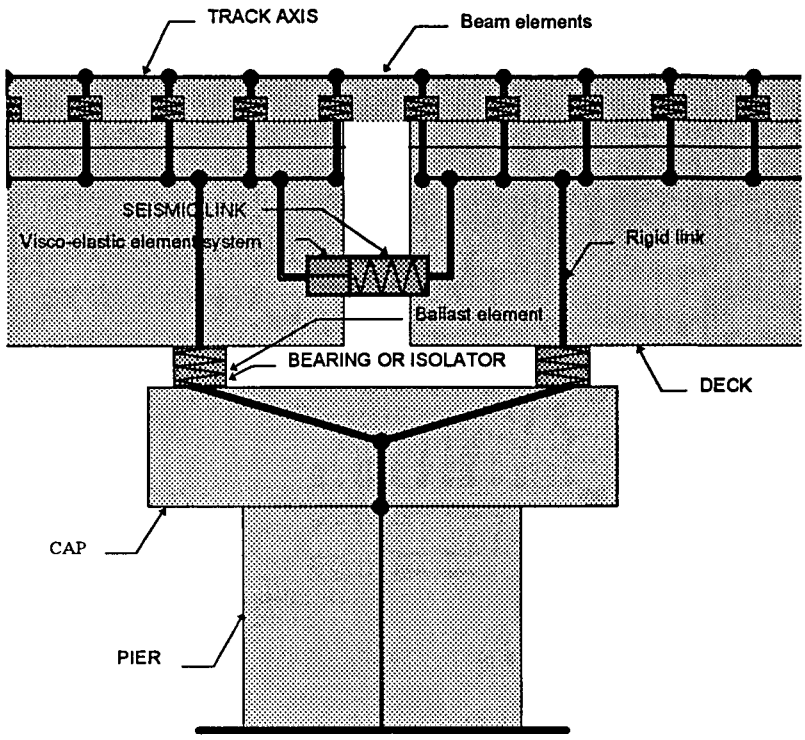

Fig. 6 - Longitudinal view of the track-bridge system.

3.2 Deck

The deck is normally modelled with elastic beam elements, as non linear effects are not expected, especially for the simply supported deck bridges used in the Italian railways. Beam elements are aligned along the centroidal axis of the deck, as shown in figs. 5, 6.

3.3 Bearings

Bearings are modelled with ballast elements, in different ways.

Elastic springs are used for conventional fixed and movable bearings. High stiffness and low or zero stiffness elastic springs can be used to model "fixed" and "movable" conditions respectively, in the various directions.

Non linear springs are used to model more sophisticated behaviours, such as the unilateral constraint in the vertical direction, the friction in the horizontal directions of the movable bearings, the yielding of an elasto-plastic isolator.

In figs. 5 and 6 there is shown the typical modelling of the track-deck-bearing ensemble, where the role played by the rigid arms of the ballast elements is evident.

3.4 Seismic devices

Special anti-seismic deck-deck or deck-pier links are modelled by using elastic, elasto-plastic and/or viscous truss elements, according to their behaviour. A typical arrangement of a deck-deck link is shown in fig. 6

3.5 Piers

R/C piers are modelled with non linear fibre beam elements. They make it possible to model accurately the flexural behaviour of R/C columns, taking into account any axial force variation. Although this element can model columns with any section shape, BRIE-Pre refers to four fundamental shapes (rectangular or circular, full or hollow) for which it automatically discretises the section into fibres, according to the directions of the user.

Both single bent and framed piers can be modelled. BRIE-Pre considers any number of columns connected at the top of the pier through a rigid cap.

Any number of elements and sub-elements can be used to model the pier columns. Since the fibre element is very time consuming, it is normally used to model the plastic hinge parts only, while the parts that are envisaged to remain elastic are simulated by elastic beam elements. A typical discretisation of a pier is shown in fig. 7.

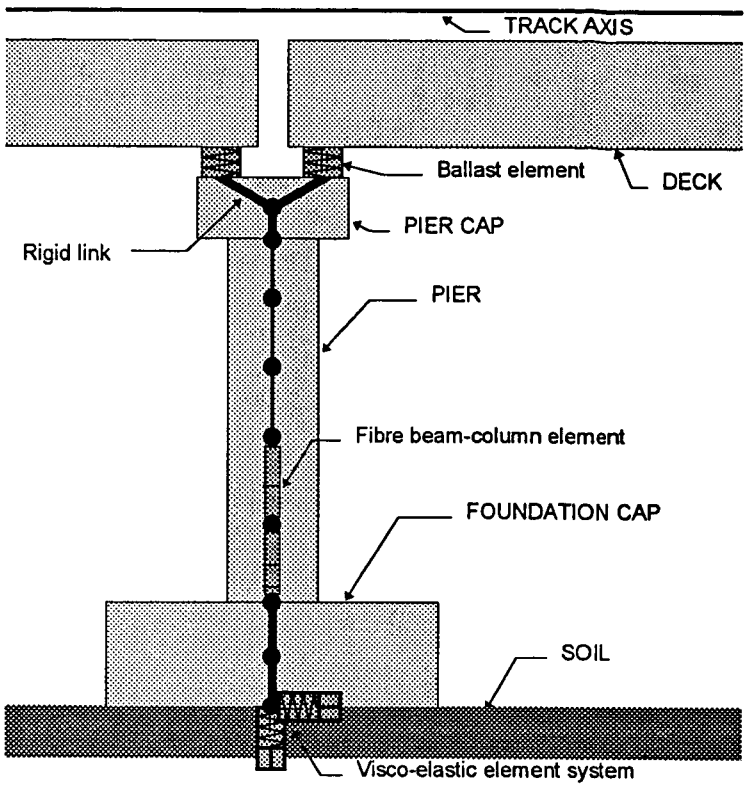

Fig. 7 - Typical discretisation of a cap-pier-foundation system.

3.6 Abutments

Like piers, abutments are modelled with non linear fibre beam elements. Regularly spaced non linear springs (ballast elements) simulate the behaviour of the soil behind the abutment. Their characteristics are calibrated taking into account the stiffness of the soil as well as the static interaction forces between soil and abutment.

Any number of elements and sub-elements can be used to model the abutments. A typical discretisation is shown in fig. 8

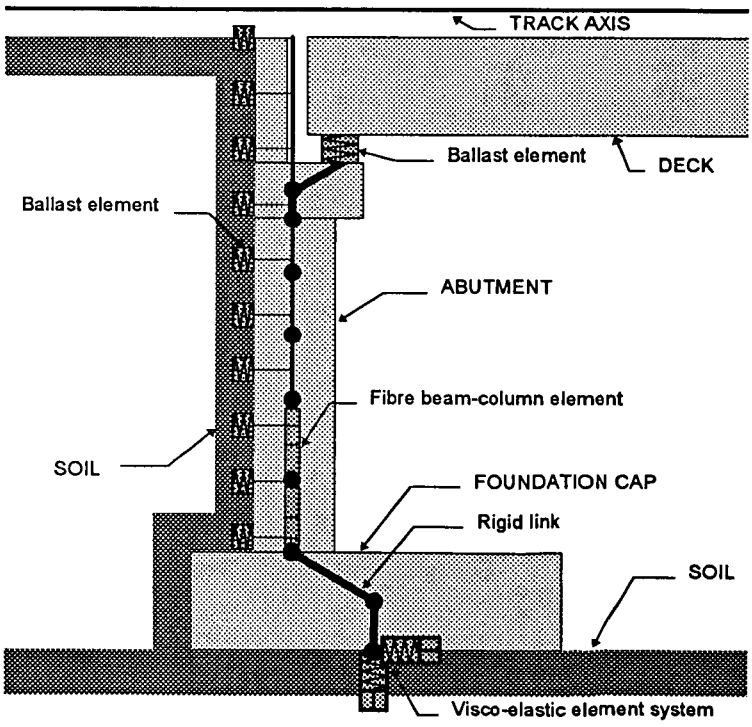

Fig. 8 - Typical discretisation of an abutment-foundation system.

3.7 Foundations

The foundations of piers and abutments are modelled with a system

of elastic and viscous trusses in the three translational and rotational degrees of freedom (see figs. 7 and 8). By calibrating these elements it is possible to account for the soil-structure interaction.

3.8 Train

The train vehicles are normally represented as systems of masses (car-body, bogies) connected through elastic and viscous truss elements and rigid links, which reproduce in detail the secondary suspension system of the vehicle. A typical vehicle model is shown in figs. 9 and 10.

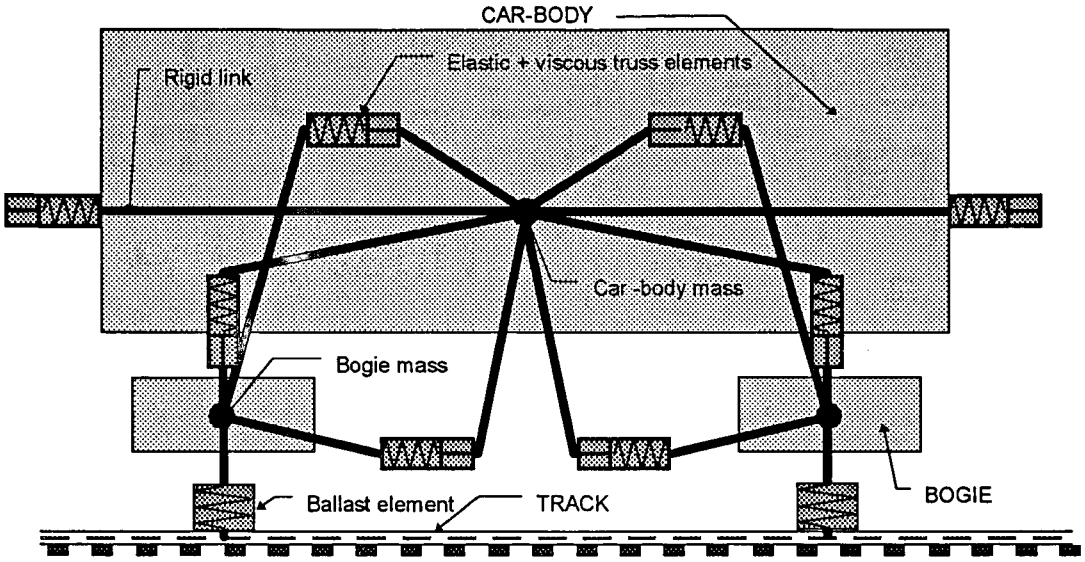

Fig. 9 - Lateral view of a typical vehicle model.

The wheel-rail contact is modelled by the ballast spring element, exploiting the non linear characteristics of the first spring.

Besides the unilateral constraint in the vertical direction, they are able to reproduce the frictional behaviour of the rail-wheel contact in the horizontal directions. In the ballast element there are also concentrated the elastic characteristics of the primary suspension system, whose very low damping can be neglected.

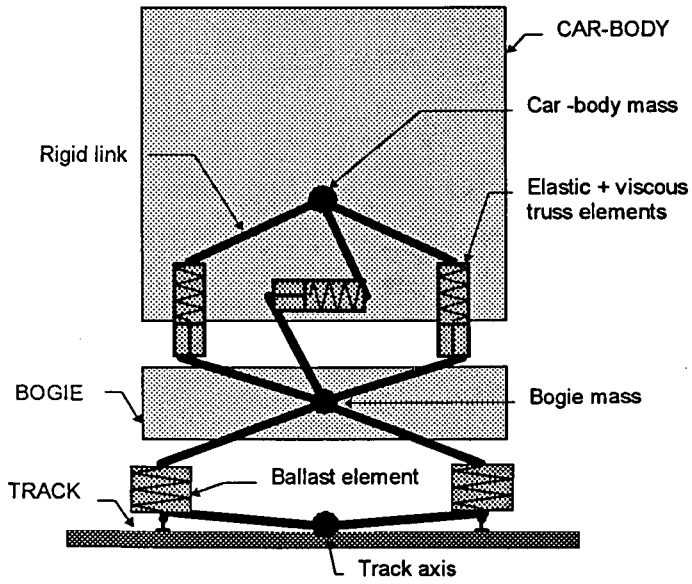

Fig. 10 - Frontal view of typical vehicle model.

As can be seen in fig. 10, two rigid links from the axis of the track reproduce the actual position of the rails upon which the wheels rely. All the wheelsets of a bogie are idealised in only one wheelset model, to simplify the model while keeping good accuracy. Bogie masses are connected to car-body mass through a complicated system of rigid links and visco-elastic systems (which are made of an elastic truss and a viscous

truss working in parallel), which reproduce the secondary suspension system of the vehicle.

3.9 Actions

The vertical loads due to the dead and live (train) loads are applied before starting the seismic dynamic analysis, to initialise the stress state of the various elements when the earthquake occurs. A particular care is devoted to the construction phases of a railway bridge, in order to avoid fictitious stress states. Therefore dead loads are applied to the structure without track, while only train loads and thermal actions are applied to the complete track-structure system.

The seismic action is given by the three displacement history components along the three reference axes. Equal, syncronous or delayed, or different time histories can be applied at the foundation of each pier and abutment, so that any type of syncronous or non-syncronous motion can be modelled. The delay of the ground motion arrival times at the various pier foundations are automatically calculated, according to the direction and the propagation velocity of seismic waves.

4. EXAMPLE OF APPLICATION

To show the capability of BRIE to detect some peculiarities of the seismic response of a railway bridge, the results relevant to the analysis of a typical railway bridge of the new Italian high speed lines are described in this chapter.

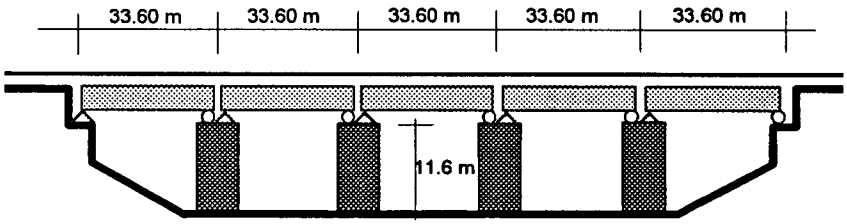

Fig. 11 - Scheme of the 5 span railway bridge.

In fig. 11 there is reported a lateral view of the scheme of the bridge. Figs. 12, 13, 14 show its main structural characteristics. It is a double track simply supported deck bridge, with five 33.60 m long spans and 11.6 m tall piers. The bridge is designed for the 2nd Italian Seismic Category, for which a reduced spectrum with 0.07g maximum acceleration and about 1.7 safety coefficient on steel strength is prescribed. However minimum reinforcement code requirements produce a considerable overstrength.

This bridge was subjected to a synchronous 3D action, whose horizontal components and vertical component have 0.28g and 0.187g PGA respectively. The three components are independent and were generated to fit the EC8 type B spectrum, having 10 secs. duration.

A simplified model has been used, with respect to the full capabilities of BRIE. No train is considered. The motion is assumed synchronous and the abutments are very stiff. 4 fibre elements and 4 beam elastic elements are used to model each pier. The fibre elements have 28 concrete fibres and 32 steel fibres. The strength of concrete and steel are assumed to be 35 and 430 MPa respectively. Very stiff foundations are assumed for piers, thus neglecting any soil-structure interaction.

The discretisation length of the tracks and the deck is 1.00 m, resulting in about 290 beam elements to model each track and 170 to model the deck. The total number of degrees of freedom is about 5000 with 21 bandwidth. The integration time step is 0.01 sec., resulting in 1000 total number of steps. The execution time is about 2 hours on a 166MHz Pentium machine.

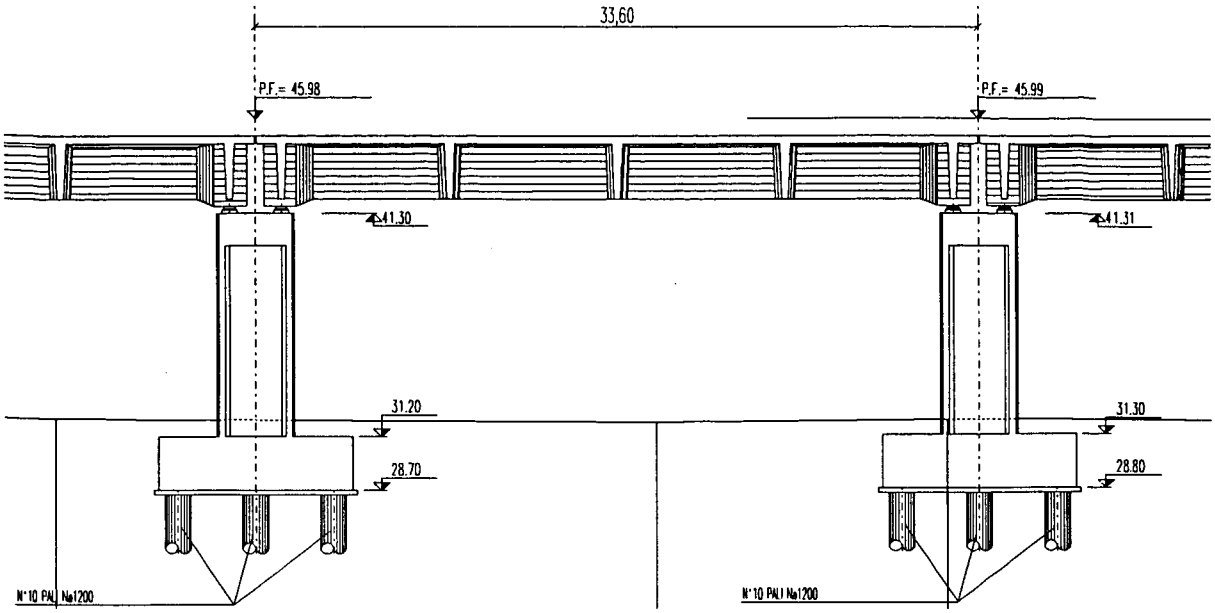

Fig. 12 - Typical span configuration.

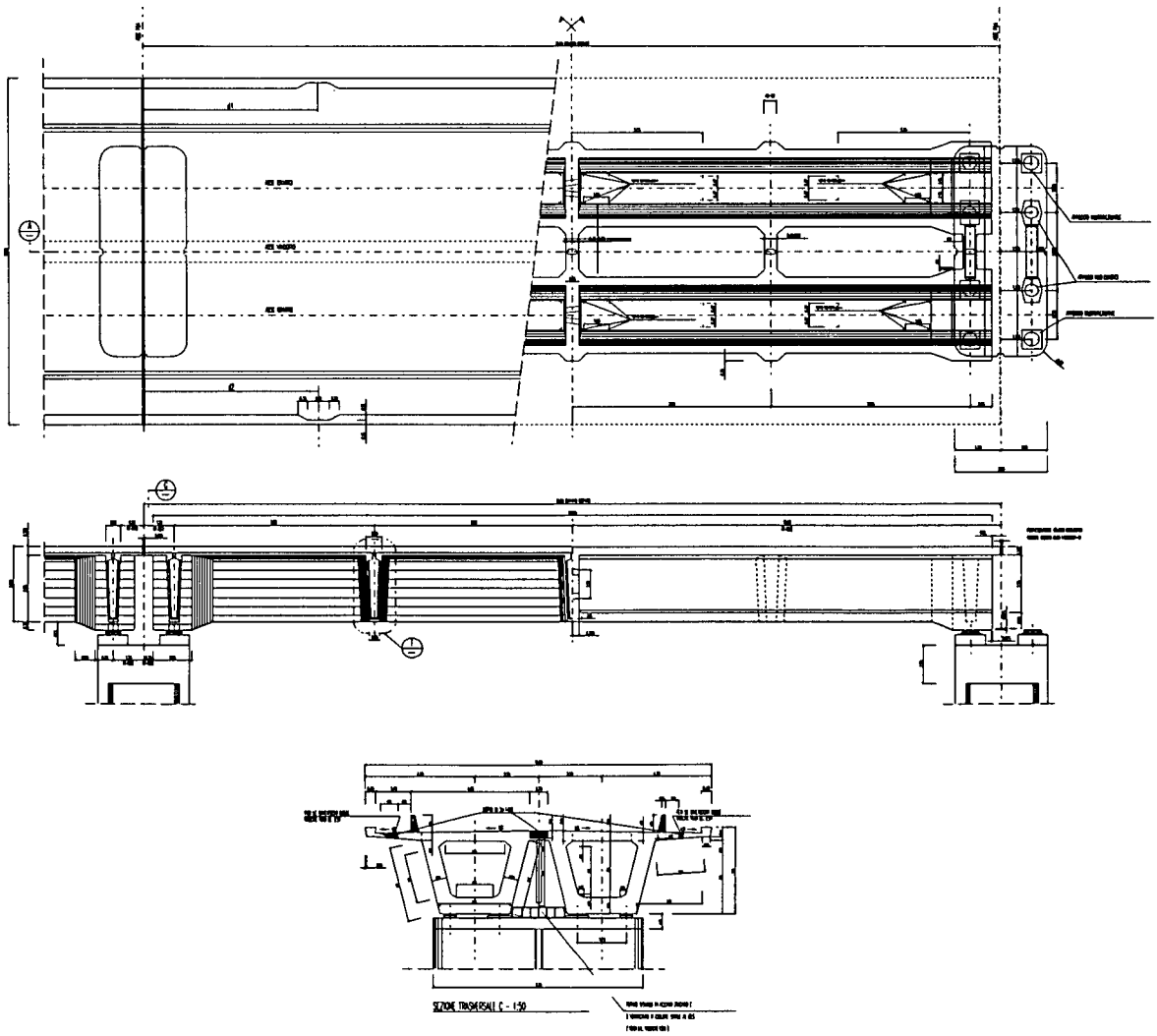

Fig. 13 - Geometrical characteristics of the deck.

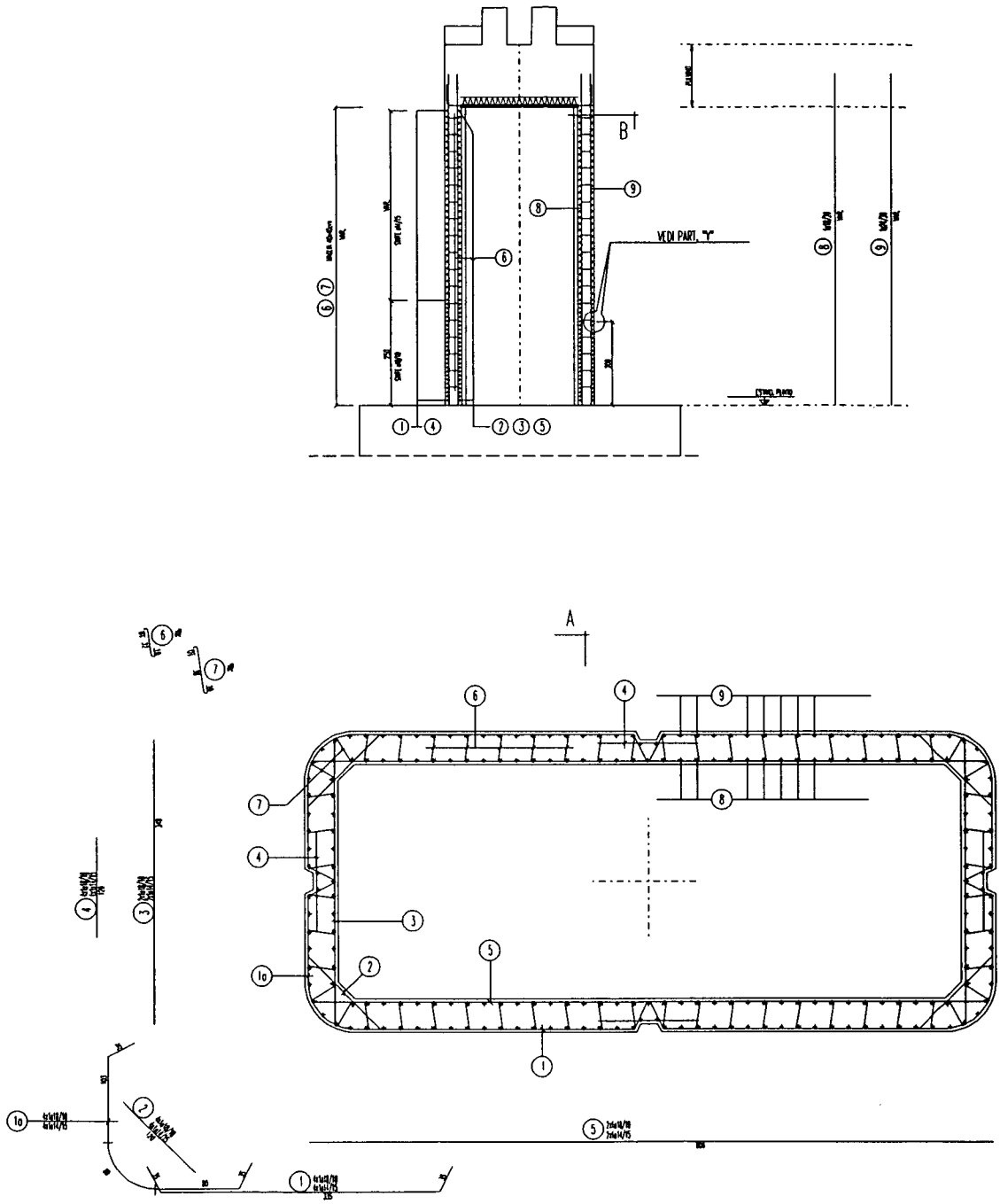

Fig. 14 - Details of the pier reinforcements.

In fig. 15 there are shown the moment-curvature cycles at the base of piers 1 and 2. Piers 3 and 4 behave similarly to piers 2 and 1 respectively, and the relevant diagrams are not reported. As can be seen, in all the piers only cracking occurs. Greater curvatures and moments, resulting in incipent yielding, can be noticed in the internal pier (2) with respect to the external one. This difference accounts for different effects in the two directions. In the longitudinal direction the track, playing the role of a link between bridge and embankment, is particularly effective in reducing strains and stresses, as well as displacements, in the first and last piers. In the transverse direction the participating mass of deck is practically halved for the first and last deck, thus reducing the dynamic forces on piers 1 and 4.

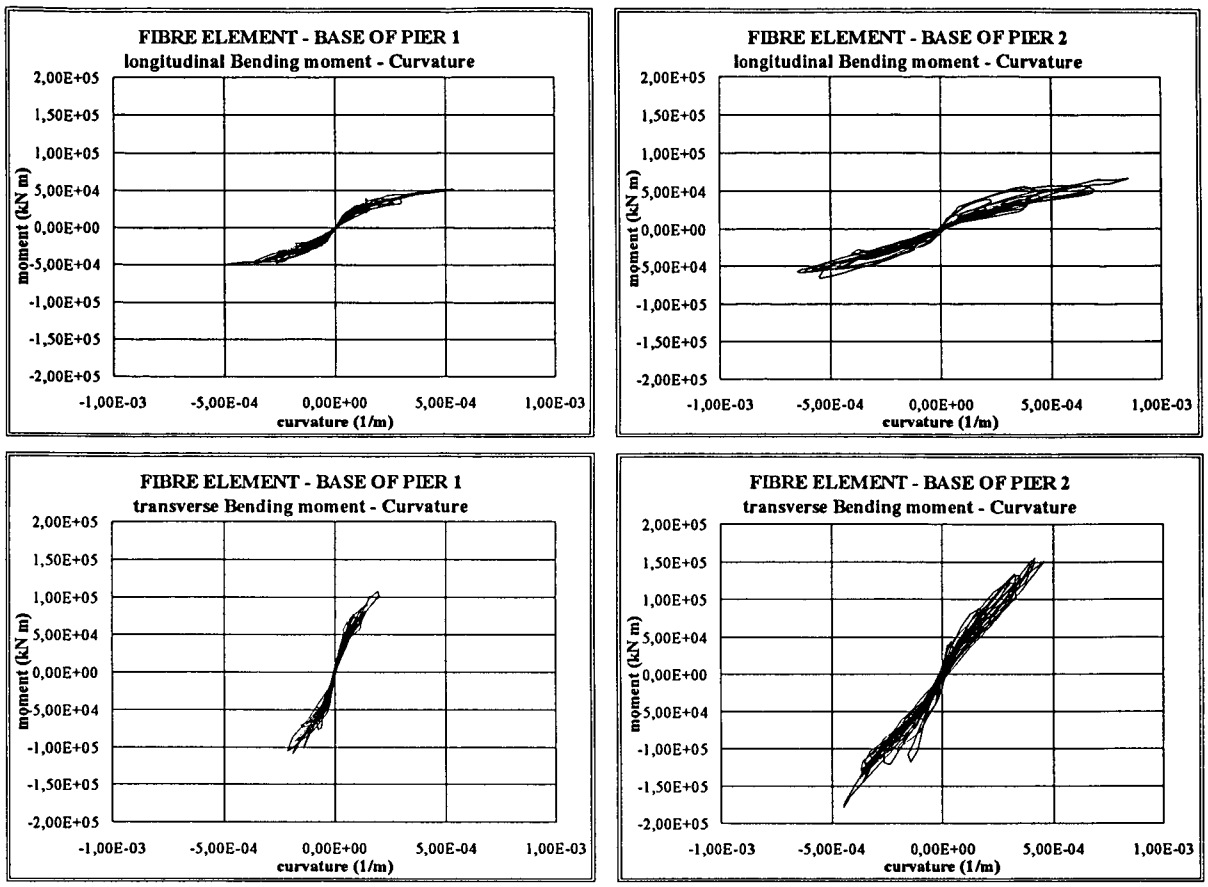

Fig. 15 - Moment-curvature cycles at the base of piers 1 and 2.

The transverse moment is much larger than the longitudinal moment and the axial force variability (see fig. 16) affects them markedly. Moreover the stiffness ratio between the two direction, even accounting for cracking is of the order of three.

In fig. 16 there are reported the time histories of the top displacements relative to the ground of piers 1 (thin line) and 2 (thick line) along the three main directions and, correspondingly, the longitudinal and transverse base shears and the axial force. The responses of piers 3 and 4 are very similar to that of piers 2 and 1 respectively and are not reported. The response values of pier 1 are lower than the corresponding values of piers 2, for the above explained reasons. However the two piers move well in phase, because of their equal characteristics and the perfect motion synchronism.

The initial axial forces due to static loading is 15700 KN, while the maximum shear is 6793 KN in the longitudinal direction and 14440 KN in the transverse direction. It is evident the important contribution of the track in reducing the pier response in the longitudinal direction. This is also confirmed by the maximum values of horizontal displacements, 28 and 17 mm in the longitudinal and transverse directions respectively, which appear to be quite close if compared to the stiffness ratio.

Looking at both displacements and forces, the average vibration frequencies are about 2-2.5 Hz and 3-3.3 Hz in the longitudinal and transverse directions respectively. They results from the flexibility of both the pier, taking account of cracking, and of the bearing devices. This latter is not negligible especially in the transverse direction, owing to the high stiffness of piers.

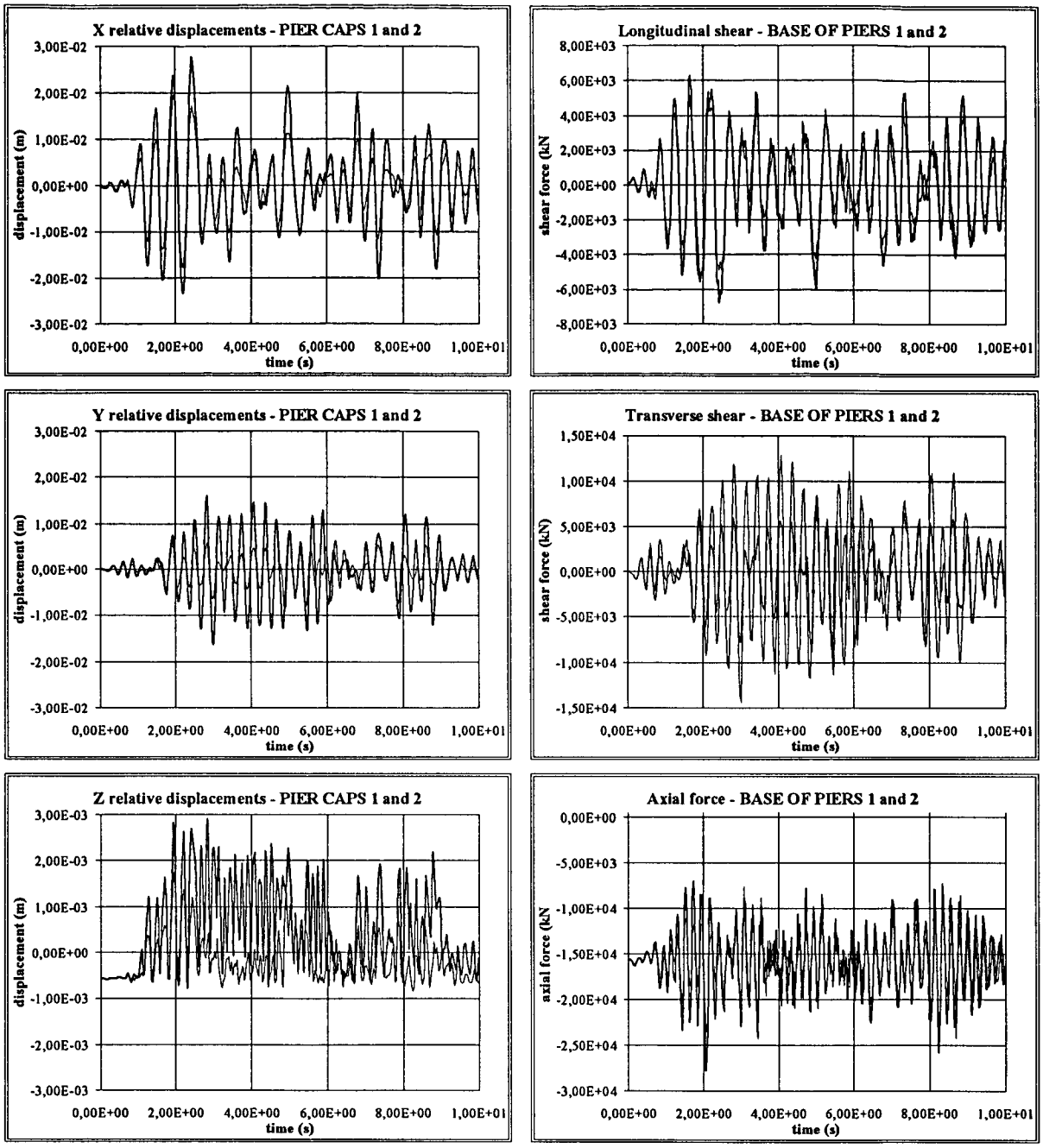

Fig. 16 - Ground relative top displacement and base forces of piers 1 and 2.

The axial force shows variations of the order of 12000 KN from its initial static value, being the maximum value in pier 2 equal to 27720 KN. These large variations, occurring at 4.5 Hz frequency, cannot be ascribed solely to the vertical component of the ground shaking, whose PGA is only 0.187g. To understand this phenomenon, it is necessary to look at the time history of the vertical displacements (fig.16), showing 3 mm maximum value and about 5.5 Hz frequency, and at the time history of the vertical acceleration at the deck midspan (fig. 17), showing 1.2g maximum value and 4.5÷5.5 Hz frequency range. This latter clearly shows a dynamic resonance at the fundamental frequency of the deck (4.5 Hz) whose excitation is given by the vertical displacement at the top of the pier (5.5 Hz). The vertical displacements of the piers must be ascribed to the cracking in bending which elongates the centroidal pier axis.

In fact the frequency of this cyclic elongation is 5.5 Hz, i.e. the double of the average frequencies of the longitudinal and transverse bending moments at the pier base. This elongation has been also observed in experimental tests on large scale piers in [4] with much higher values, because of the large yielding occurring during test. In the present case the effects on the structure are more evident because the vertical vibrations of the deck are taken into account and its fundamental frequency is close to the pier elongation frequency.

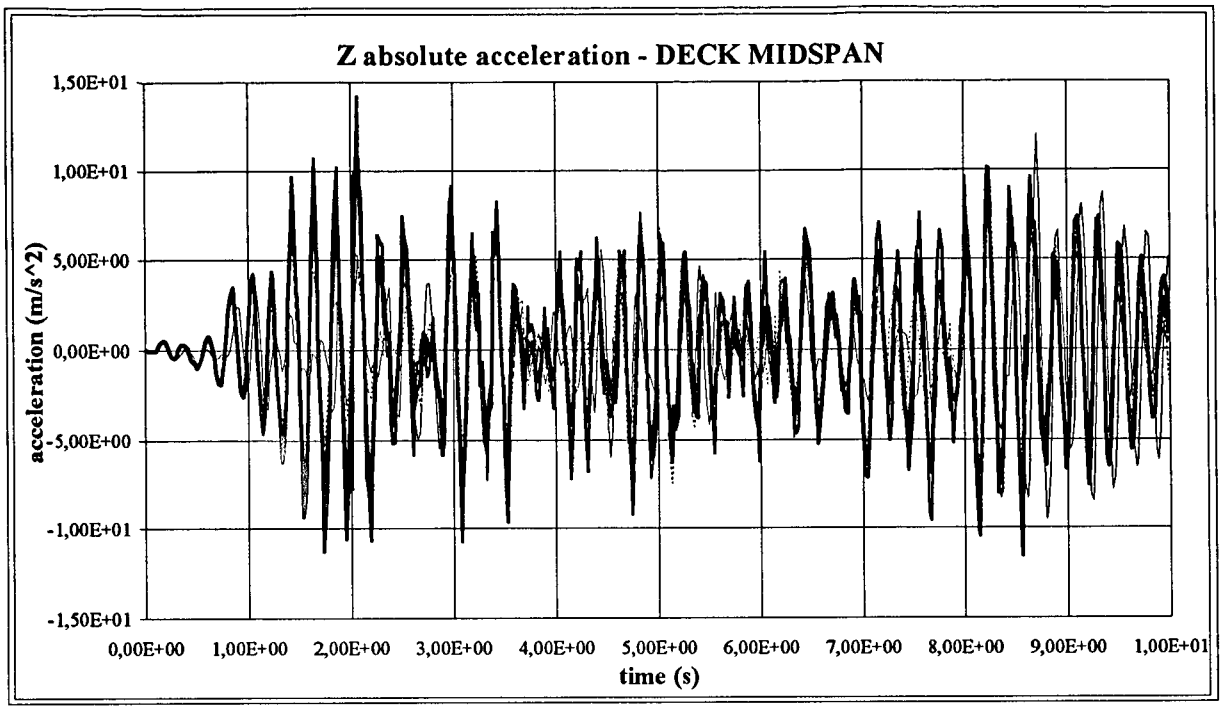

Fig. 17 - Vertical absolute acceleration at midspan of decks.

In fig. 18 there are plotted, as an example, the time histories of the reaction forces in the two fixed bearings at the left deck end of span 3. The maximum values of the reaction forces in the three directions, however, occur in different bearings, being equal to 4380 KN longitudinal in span 1, 3894 KN transverse in span 3, -4369 KN vertical in span 3.

The time history features of the longitudinal reactions in the two fixed bearings result from two concurrent effects: the longitudinal translational vibrations and the rotational movement of the deck around a vertical axis, due to the differential transverse displacements of the top of consecutive piers (see fig. 15). The latter effect causes some differences in the longitudinal reactions of the two fixed bearings and is more evident in span 1 and 2 than in span 3, due to the different lateral displacements of the abutment, pier 1 and pier 2. However the prevailing effect, i.e. the longitudinal movement, can be recognised to have 2.5 Hz average frequency.

In the transverse direction the reactions of the two fixed bearings are obviously equal. The average frequency is, again, about 3.3 Hz and the maximum total reaction is about 1.2 times the half weight of the deck, resulting in an amplification coefficient about 4.

The time histories of the vertical reactions show a considerable increase in compression and a total decompression (actually a lifting) in the external bearings. Starting from 1590 KN initial static value, the force raises up to 4369 KN during the earthquake, owing to both the above described vertical dynamic amplification of deck vibrations and the roll of deck due to the transverse bending of piers. This latter effect is evident in fig. 18, where the maximum reaction in one external bearing occurs when the minimum reaction, or zero, occur in the opposite one.

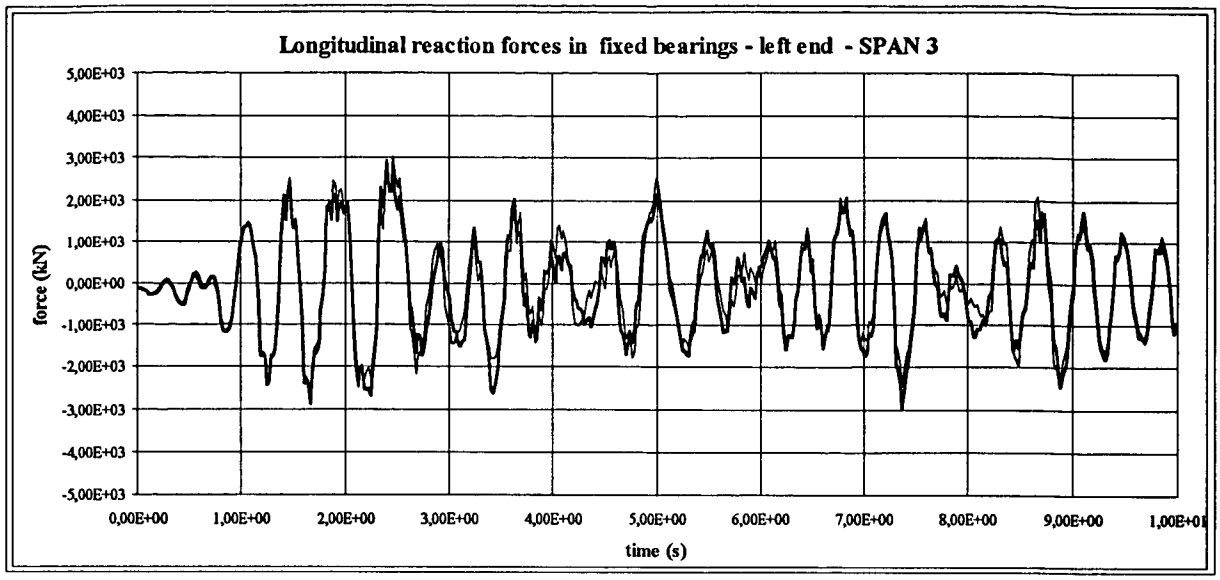

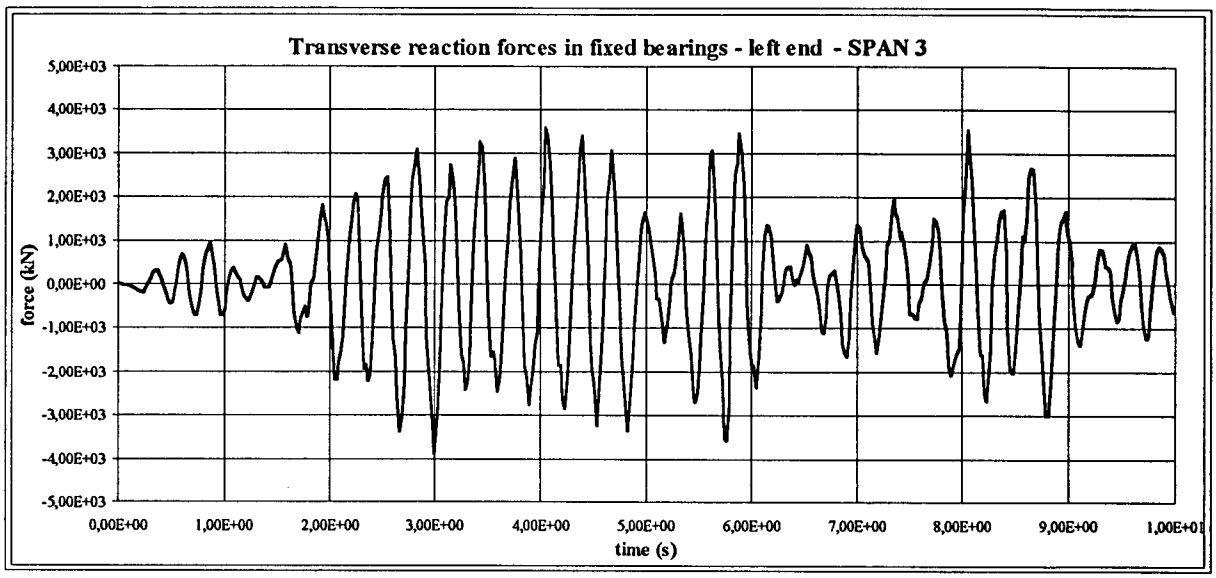

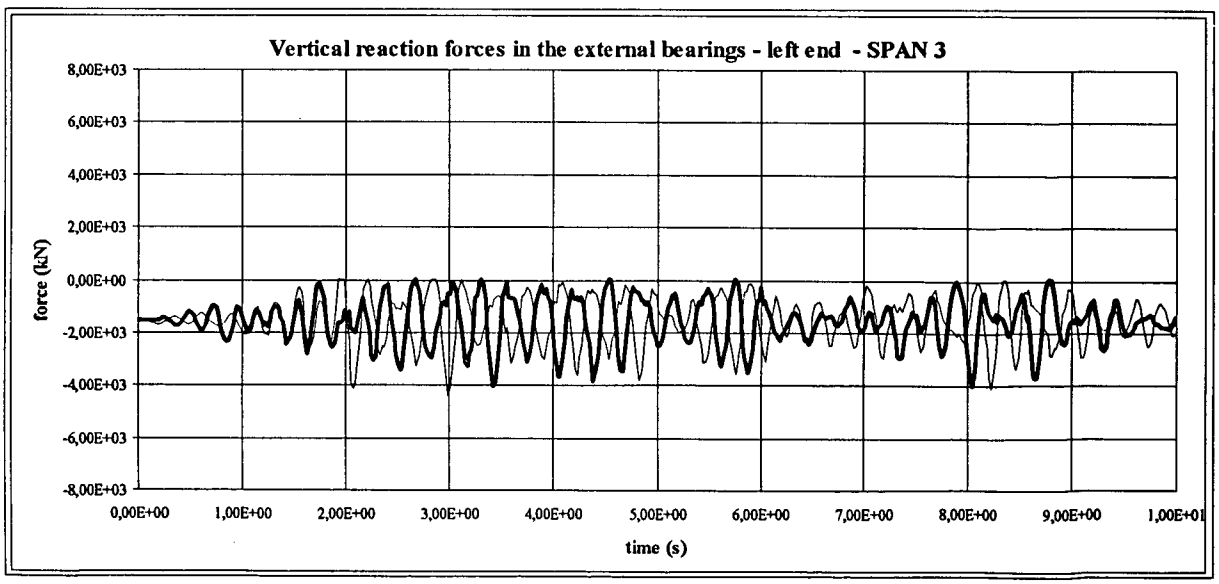

Fig. 18 - Reaction force time histories in the bearing devices at the left end of span 3.

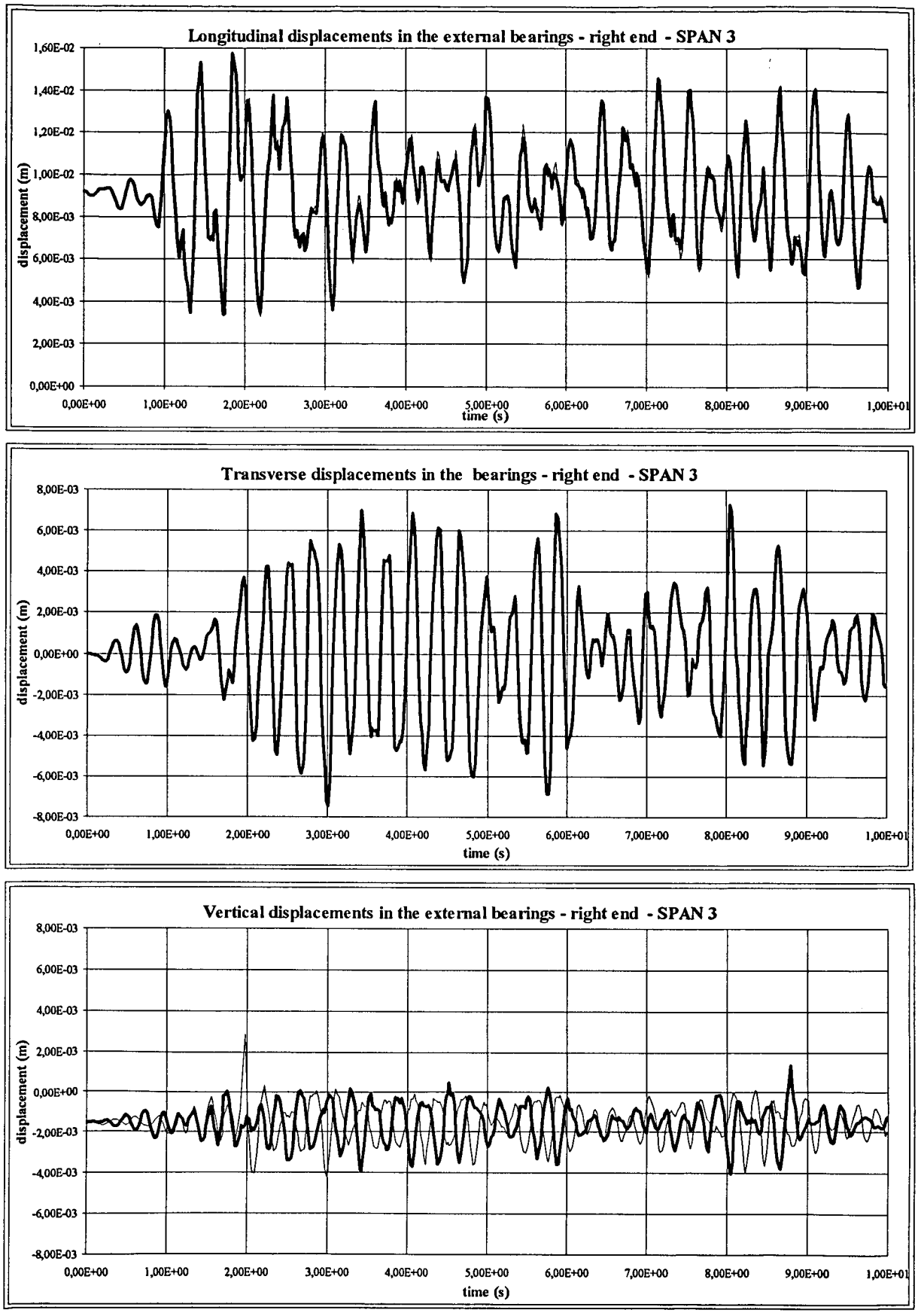

Fig. 19 - Displacement time history in the external bearing devices at the right end of span 3.

In fig. 19 there are reported the time histories of the relative displacements in the external bearings at the right deck end of span 3. The maximum values of the displacements are 29 mm longitudinal on the right abutment, 7.5 mm transverse on pier 3 (span 3), and 4.2 mm vertical(lifting) on pier 3 (span 3).

The longitudinal displacements in the movable bearings in span 3 start from about 9 mm, resulting from thermal effects and vertical loads, raising up to 16 mm during the earthquake. Some differences in the time histories of the different bearings confirm the effect of the rotation around a vertical axis of the deck.

The maximum transverse displacement of the bearing is limited, as this displacement is controlled by the laterally fixed bearing.

The time histories of the vertical displacements confirm the remarkable effect of the roll of deck, which is evident when looking at the simultaneous values in the four bearings. A lifting of the bearing as high as 4.2 mm is certainly something that must be carefully considered when designing bearings which resist horizontal forces. This effect can be much more important if yielding in piers occurs, resulting in greater rotations of their pier caps.

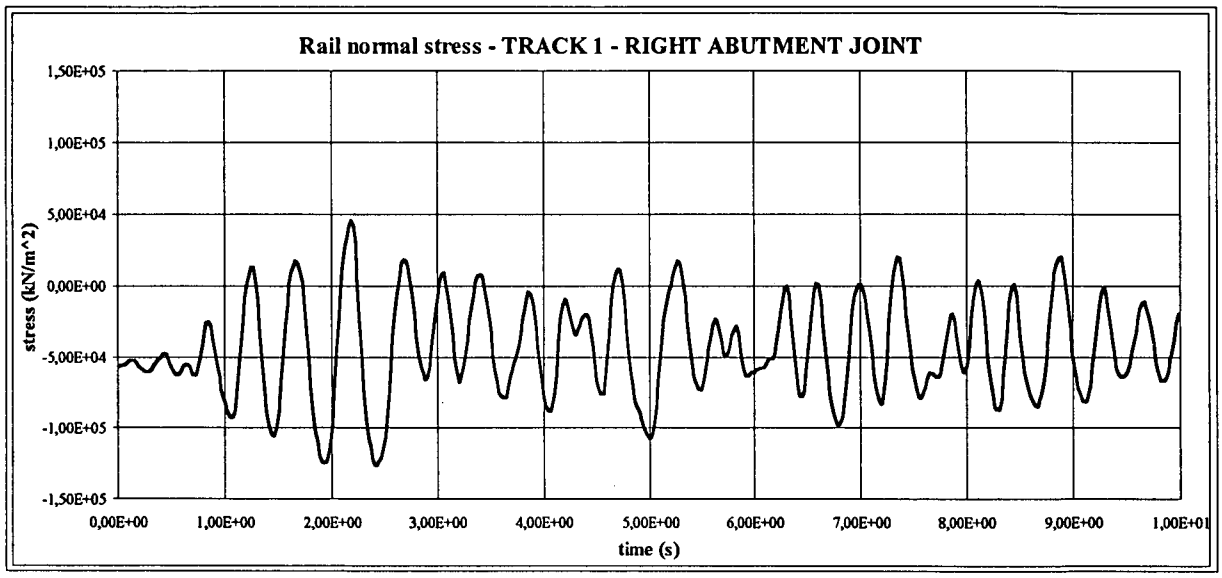

Fig. 20 - Rail normal stress time history in the point where the maximum value occurs.

In fig. 20 there is shown the time history of the normal stress in the rails of the 1st track. This is very similar to that of the 2nd track, which is not reported. The initial static value is almost –58000 KN/m^2 = -58 MPa, which results from both the continuous welded rail (CWR) stress for a 20°C thermal variation (=205000*0.00001*20° = 41MPa) and the track-bridge interaction for 15°C thermal variation of deck. The maximum and minimum values during the earthquake are 47 and -128 MPa, resulting in about ±88 MPa increase due to earthquake with respect to the CWR stress. This value is beyond or close the acceptable additional compressive and tensile values for bridge-deck interaction, which are of the order of -72 and 92 MPa respectively. As expected, the residual stress at the end of the action can be deduced to be approximately equal to the CWR stress, meaning that the interaction stresses are relaxed by the earthquake vibrations.

In fig. 21 there are reported the relative displacements between track and deck. They give important information about the possible deterioration of the ballast and the residual displacement in the track, that can compromise the service conditions.

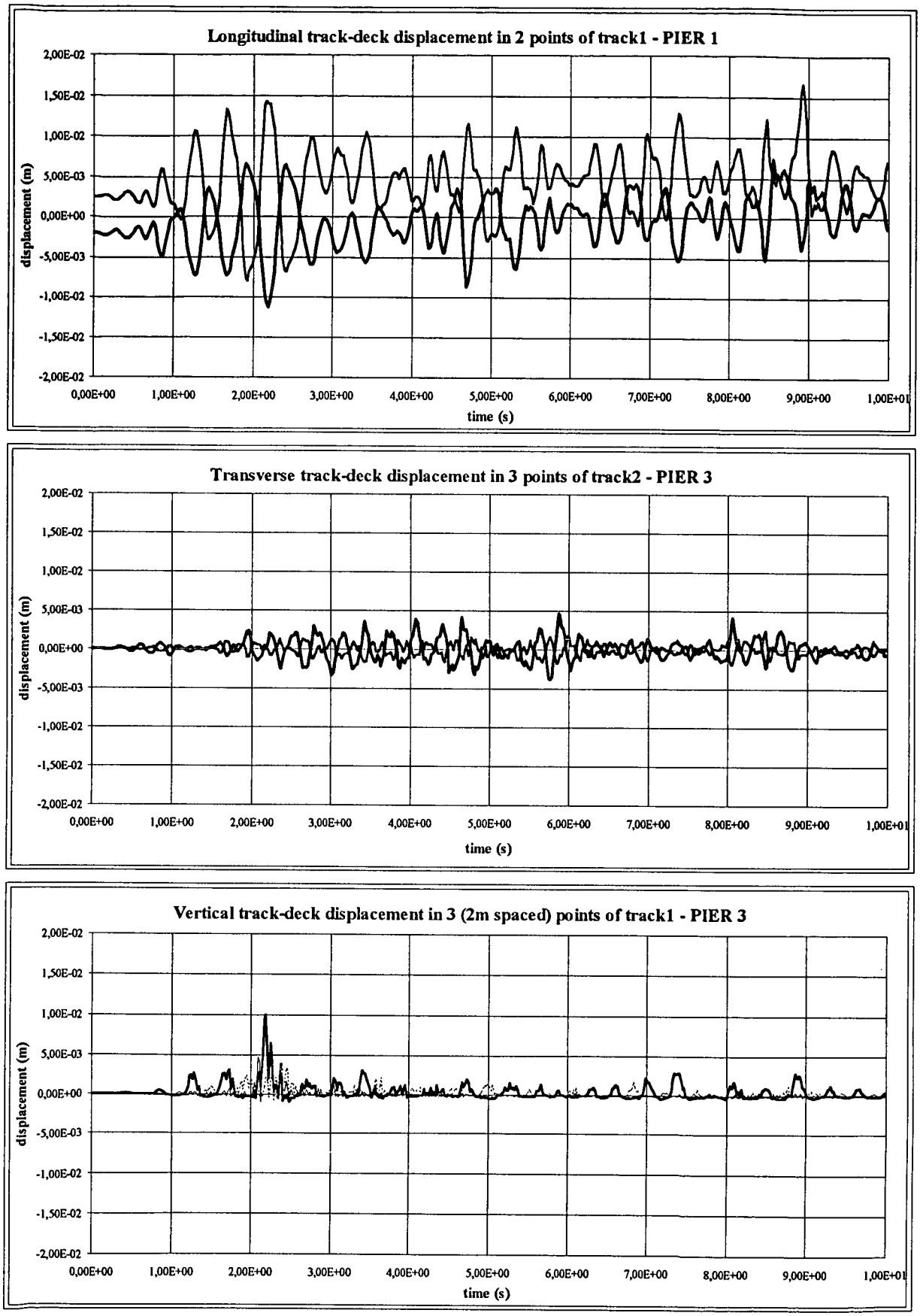

Fig. 21 - Track-deck relative displacement time history where maximum values occur.

The maximum longitudinal displacement is 16.5 mm, and the total excursion is 24 mm. Longitudinal cyclic displacements of this order, combined with the vertical ones below described, can result in a ballast deconsolidation, which can compromise the serviceability condition of the track at the end of the earthquake.

The maximum transverse displacements is 5 mm, a small value which means the negligibility of any buckling or second order effect in the track. In fact the residual lateral displacement is also negligible.

The maximum vertical displacement of the track results in a lifting of 10 mm. This occurs in a single points and reduces rapidly in the nearby points.

Although the results reported in this paragraph were mainly aimed at showing the characteristics of BRIE, they have clearly demonstrated that some peculiar aspects of railway bridges, especially concerning the serviceability conditions, are to be considered carefully and deserve specific studies.

5. CONCLUSION

The software package BRIE for the seismic analyses of railway bridges has been presented. Its peculiar features permit to take account of the train-track-bridge interactions in a full three-dimensional model and, then, to evaluate the seismic safety also with respect to the serviceability conditions of railways.

An example of application has been illustrated. It shows some peculiar aspects of the general behaviour of bridges that only a full three-dimensional analysis can detect. One of them is the influence of the elongation of pier due to concrete cracking and, eventually, steel yielding on the vertical vibration of deck. Very important vertical inertia forces occur due to this phenomenon. Another important phenomenon is the roll of the deck, due to the pier cap transverse rotations, which produces important overstresses and lifting in the bearing devices.

In the example it was also demonstrated that important track-deck interaction effects influence both the response of the bridge and the stresses in the rails, as well as the conditions of ballast. The bridge response, in terms of pier displacements, curvatures and moments, can considerably benefit from the presence of the track, especially in the longitudinal direction. On the other hand important stresses in the rail and displacements in the ballast can seriously compromise the service conditions.

Obviously this single example can not give definite answer to the complex problem of railway bridge seismic design and safety, since many parameters not here considered can significantly affect their seismic response

In Italy railway bridges and viaducts typically have simply supported beam schemes. This is because such schemes reduce the track-bridge interactions due to temperature and braking, when the continuous welded rail is used, and are economically convenient for pre-casting. At present the only provision which is taken with respect to large displacements [3] is the separation of adjacent decks with an adequately wide gap, in order to allow them to move freely without impacts. This gap is normally very large, as it is calculated without taking into account the effect of the track as a longitudinal link, thus resulting in an important overcost for the structure. On the other hand, this is an effective provision to protect the structure against deck damage, but it cannot be for the continuous welded rail, which is subjected to important

compressive and tensile stresses and to lateral movements. Dangerous effects on the track can be caused not only by destructive earthquakes, but even by medium intensity frequent earthquakes, which do not damage the structure. The railway service would therefore be conditioned by the damage to the track rather than by the damage to the structural elements.

It is expected that extensive parametric analyses, to be made by using BRIE, will help significantly to understand the behaviour of railway bridges and to improve their design. A first investigation is being completed with reference to the usual structural layout. Due to the great number of parameters governing the response and the need of understanding many phenomena occurring during an earthquake, the attention has been focused on a reduced set of parameters:

- intensity (medium/high) of the action
- height variability of piers
- presence/absence of train
- syncronous/non-syncronous motion

After this study, it is envisaged that a more extensive investigation is carried out to improve the understanding of the seismic behaviour of normal railway bridges as well as of continuous beam schemes. Moreover the attention will be focused on the effectiveness of different types of antiseismic devices and passive control systems, such as seismic isolators, dampers, etc., with respect to both the safety of track and vehicles and to the structural collapse.

REFERENCES

[1] Dolce, M., Static Interaction Train-Track-Structure: the program ISTBS (*Interazione Statica Treno-Binario-Struttura: Il programma ISTBS),* INGEGNERIA FERROVIARIA, September 1992, Roma (in Italian).

[2] Liberatore, D., Dynamic Interaction Train-Track-Structure: the Program IDTBS (Interazione Dinamica Treno-Binario-Struttura: il programma IDTBS), INGEGNERIA FERROVIARIA, December 1992, Roma (in Italian).

[3] FS - ASA Servizi di Ingegneria, Guidelines FS 44b: Technical Guidelines for Railway Manufacts in Seismic Area (Istruzione FS 44b: Istruzioni tecniche per manufatti sotto binario da costruire in zona sismica), January 1996, Roma (in Italian).

[4] Pinto, A.V., Verzelletti, G., Pegon, P., Magonette, G., Negro, P., Guedes, J., Pseudo-Dynamic Testing of Large-Scale R/C Bridges, Joint Research Centre - European Commission, Report EUR 16378 EN.

Session 6

Topic 5 Foundations and Soil Stability
Topic 6 Isolation and Retrofit (1)

DESIGN METHODS OF BRIDGE FOUNDATIONS AGAINST SOIL LIQUEFACTION AND LIQUEFACTION-INDUCED GROUND FLOW

Koichi Yokoyama [1], Keiichi Tamura [2] and Osamu Matsuo [3]

1 Director, Earthquake Disaster Prevention Research Center, Public Works Research Institute, Ministry of Construction, 1 Asahi, Tsukuba-shi, Ibaraki-ken 305 Japan
2 Head, Ground Vibration Division, Earthquake Disaster Prevention Research Center, ditto
3 Head, Soil Dynamics Division, Earthquake Disaster Prevention Research Center, ditto

ABSTRACT

In this paper, a revised method to assess liquefaction potential of soils and a seismic design treatment of soil liquefaction for highway bridges are presented. The presented liquefaction potential assessment depends simply on the blow counts of a standard penetration test and soil gradation parameters. The design treatment of liquefaction for bridges verifies the ductility of foundation by the principle of conservation of energy. Also presented in this paper are the influence of liquefaction-induced ground flow on highway bridge foundations and its treatment in seismic design, in which the effect of ground flow is considered as static force acting to a bridge foundation.

INTRODUCTION

The Hyogo-ken Nanbu Earthquake of 1995 caused extensive soil liquefaction over a wide area of offshore reclaimed lands and natural deposits [1),2)]. Besides that, near the water's edge, liquefaction induced ground flow with the movement of sea walls. Liquefaction and its associated ground flow exerted serious influence on various engineering structures. Although highway bridges did not suffer destructive damage due to liquefaction, liquefaction-induced ground flow caused large deformation of highway bridge foundations.

In the former "Specifications for Highway Bridges" [3)], the assessment of liquefaction was made mainly for loose sand against moderate ground motions, and a seismic design treatment of liquefaction was prescribed. However, the strong ground motions such as generated by the Hyogo-ken Nanbu Earthquake were not considered, and no concrete provision regarding the liquefaction-induced ground flow was given in the Specifications.

This paper first summarizes the newly proposed method to estimate liquefaction potential considering the feature of soil liquefaction caused by the Hyogo-ken Nanbu Earthquake [4]. This method was calibrated by comparing with field performance data. The design treatment of liquefaction for bridge foundations that aims to ensure sufficient deformation capacity is also described.

Then, this paper presents a feature of the liquefaction-induced ground flow due to the Hyogo-ken Nanbu Earthquake, its influence on highway bridges which includes an estimation of ground flow force acting on a bridge foundation and an outline of seismic design treatment of the liquefaction-induced ground flow.

ESTIMATION OF LIQUEFACTION POTENTIAL

Soil Layers to Be Assessed

The Hyogo-ken Nanbu Earthquake of 1995 caused liquefaction even at coarse sand or gravel layers that had been regarded invulnerable to liquefy, and the design practice has been changed to include a gravel layer in the soil layers that require liquefaction potential estimation. Based on field performance data, the upper limit of mean grain size D_{50}, for which liquefaction potential estimation is necessary, has been changed from 2mm to 10mm.

Estimation of Liquefaction Potential

Liquefaction potential is estimated by the safety factor against liquefaction F_L as follows: [3]

$$F_L = R/L \tag{1}$$

where

F_L : liquefaction resistant ratio,
R : dynamic shear strength ratio,
L : shear stress ratio during an earthquake.

The dynamic shear strength ratio R may be expressed as

$$R = c_w R_L \tag{2}$$

where

c_w : corrective coefficient for ground motion characteristics,

R_L : cyclic triaxial strength ratio; a ratio of cyclic shear stress required to cause 5% double amplitude axial strain in 20 cycles of loading to the confining pressure.

The cyclic triaxial strength ratio was estimated by laboratory tests with undisturbed samples by in situ freezing method. The samples were formed into cylindrical specimens 10cm long and 5cm in diameter for sand, and 60cm long and 30cm in diameter for gravel, respectively. It should be noted that in this paper "sand" and "gravel" are defined as materials with a mean grain size D_{50} <2mm and $D_{50} \geqq$ 2mm, respectively. The specimens were set in a triaxial cell and undrained cyclic triaxial tests were performed. Isotropic consolidation were performed under the effective overburden pressure in situ. Sinusoidal load with a frequency of 0.1 Hz was applied to the specimens.

The undrained cyclic triaxial strength ratio R_L obtained from the laboratory tests is hereafter presented in correlation with the blow count per foot, N-value of a standard penetration test. This N-value is corrected by the overburden pressure as follows:

$$N_1 = 1.7N/(\sigma_v' + 0.7) \tag{3}$$

where

N_1 : corrected N-value to an effective overburden pressure of 1 kgf/cm^2,

σ_v': effective overburden stress, in kgf/cm^2.

Sands

Figure 1 presents test results for clean sands i.e., sands with less than 10 % fine particles passing a 0.075mm sieve. The figure clearly demonstrates that for alluvial sands the cyclic triaxial strength ratio R_L increases significantly as N_1 exceeds 20 to 25, and the sand with N_1 greater than 30 is unlikely to liquefy even under very strong cyclic stresses. For diluvial sands, R_L is larger than that of alluvial sands and increases more rapidly with the increase of N_1. Although the data for reclaimed soils are limited in number and are scattering, it seems that R_L is smaller than that of natural deposits. For alluvial clean sands, the relationship between R_L and N_1 may be expressed as

$$R_L = \begin{cases} 0.0882\sqrt{N_1/1.7} & (N_1 < 14) \\ 0.0882\sqrt{N_1/1.7} + 1.6 \times 10^{-6} \cdot (N_1 - 14)^{4.5} & (N_1 \geqq 14) \end{cases} \tag{4}$$

Eq.(4) is also demonstrated in Figure 1.

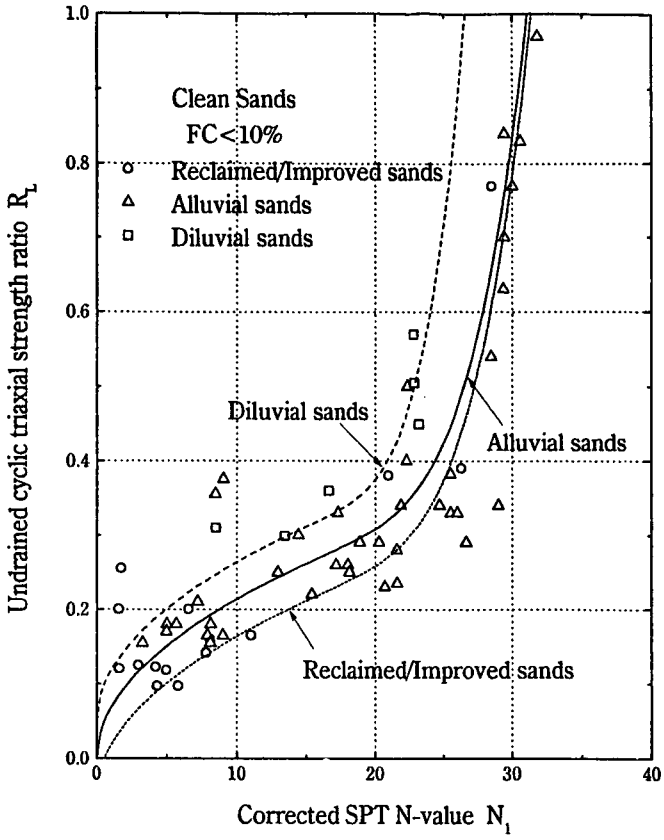

Figure 1 Relationship between R_L and N_1 for Clean Sands (FC<10%)

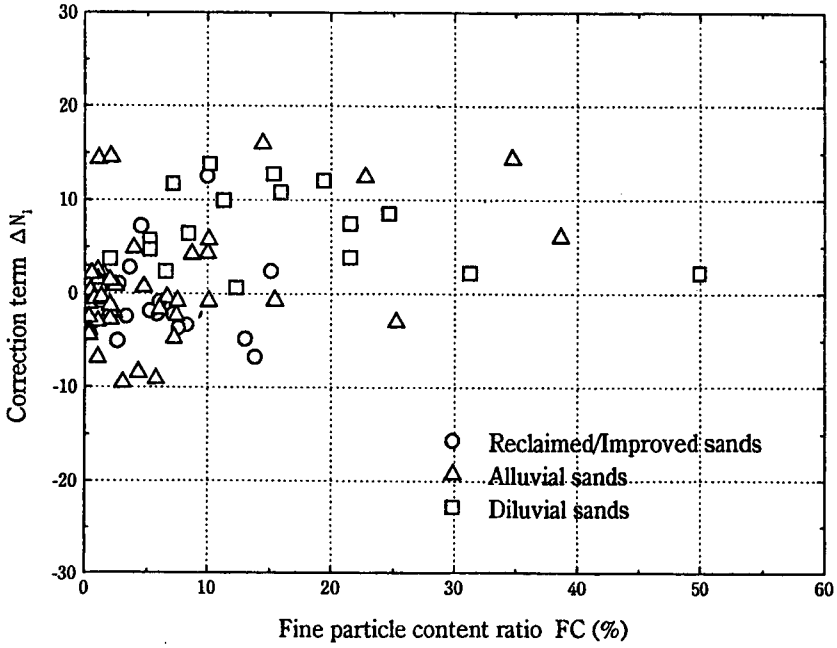

Figure 2 Relationship between ΔN_1 and FC(%)

The effect of soil gradation on the cyclic triaxial strength ratio R_L is studied by the following form

$$R_L = R_{L1}(N_1 + \Delta N_1 \text{ (soil gradation parameters)})$$
$$= R_{L1}(Na) \qquad (5)$$

where

R_{L1} : cyclic triaxial strength ratio of clean sand,

Na : corrected N−value considering the effects of fine particles.

Figure 2 shows the relationship between the correction term ΔN_1 and fine particle content ratio FC, i.e., weight percentage of particles less than 0.074mm in diameter. It can be seen from Figure 2 that ΔN_1 increases with FC. In this study, Na is estimated as

$$Na = c_1 N_1 + c_2 \qquad (6)$$

where c_1 and c_2 are parameters expressed by functions of FC as follows:

$$c_1 = \begin{cases} 1 & (0\% \leqq FC < 10\%) \\ (FC+40)/50 & (10\% \leqq FC < 60\%) \\ FC/20-1 & (60\% \leqq FC) \end{cases} \qquad (7)$$

$$c_2 = \begin{cases} 0 & (0\% \leqq FC < 10\%) \\ (FC-10)/18 & (10\% \leqq FC) \end{cases} \qquad (8)$$

Gravels

Figure 3 plots test results for gravels on the relationship between the cyclic strength ratio R_L and the corrected N−value N_1. In this figure, results for various blow count measurements other than N_1 are also presented. $N_{1(10)}$ represents the three times the minimum blow count among three of 10cm penetration. $N_{1(min)}$ represents the minimum value of (blow count)/(penetration length) and extrapolate this to 30cm. It is obvious that there is very weak correlation between R_L and N_1 or other N−values.

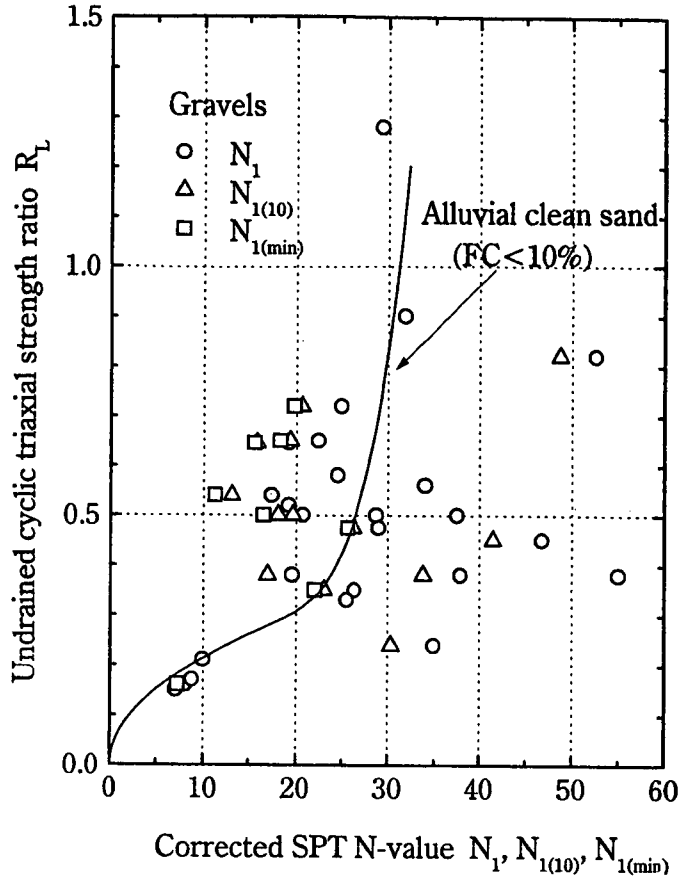

Figure 3 Relationship between R_L and Corrected N−values for Gravels

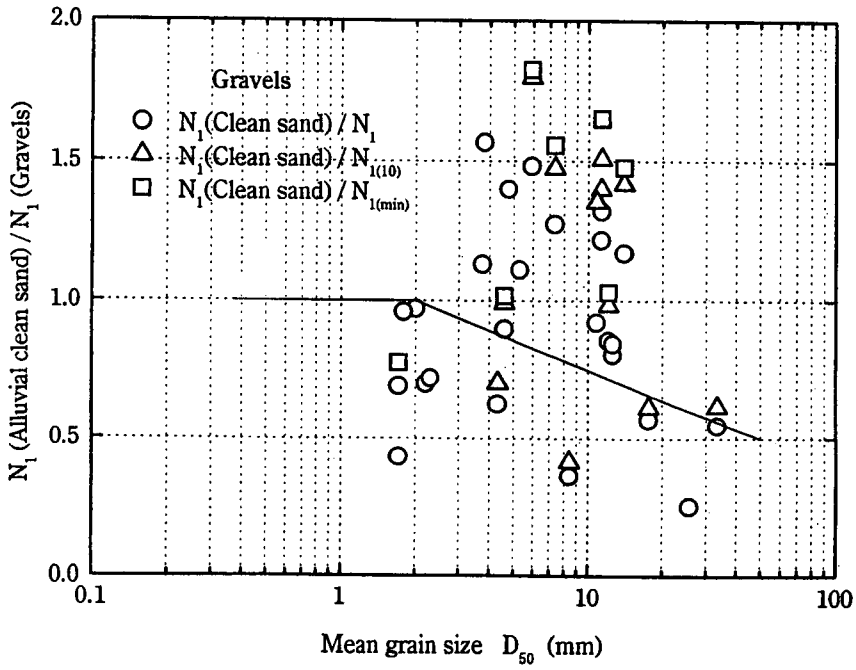

Figure 4 Relationship between the Ratio of Blow Count for Gravels to that for Clean Sand and the Mean Grain Size

Figure 4 shows the relationship between the ratio of blow count for gravels to that for clean sand with the same cyclic triaxial strength ratio and the mean grain size. Although considerable scattering exists, the ratio decreases as the mean grain size becomes large. The average relationship may be estimated as

$$N_1 \text{ (alluvial clean sand)}/N_1 \text{ (gravels)} = 1 - 0.36\log_{10}(D_{50}/2) \quad (D_{50} \geqq 2) \qquad (9)$$

in which the mean grain size D_{50} is measured in mm. Combining Eqs.(4) and (9), R_L for gravels can be estimated from blow counts of a standard penetration test.

Corrective Coefficient for Ground Motion Characteristics

When cyclic shear strength of a soil is compared with seismic shear stress induced by an irregular ground motion, it is necessary to convert the seismic shear stress time history to an equivalent cyclic shear stress time history. In this context, "equivalent" means that the both shear stress time histories yield the same degree of damage or degree of liquefaction. The modified accumulative damage concept developed by Tatsuoka et al. [5] was employed to estimate the corrective coefficient for ground motion characteristics c_w in Eq.(2).

The cyclic triaxial strength ratio curve was obtained by performing undrained cyclic triaxial tests for Toyoura sand over a wide density range. A total of 130 ground motion records from eight earthquakes were analyzed. The results on c_w obtained from records of each earthquake are finally averaged, and shown in Figure 5. As seen from this figure, the results for c_w seem to be divided into two groups. One is for the ground motions generated by interplate earthquakes (Type I), the other is for those generated by inland intraplate earthquakes (Type II). c_w may be expressed as

for Type I ground motions:

$$c_w = 1.0 \qquad (10)$$

for Type II ground motions:

$$c_w = \begin{cases} 1.0 & (R_L \leqq 0.1) \\ 3.3R_L + 0.67 & (0.1 < R_L \leqq 0.4) \\ 2.0 & (0.4 < R_L) \end{cases} \qquad (11)$$

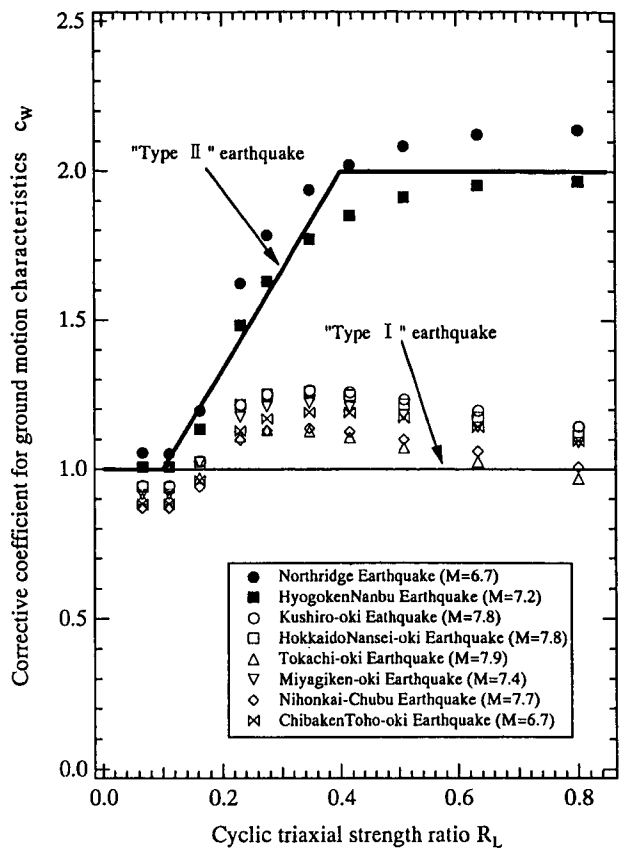

Figure 5 Corrective Coefficient for Ground Motion Characteristics c_w

Calibration with Field Performance Data

The newly developed method for estimating the in situ liquefaction potential as presented in the above was examined by comparing with field performance data during past eight earthquakes [4]. A total of 216 data include 145 of liquefied sites and 71 of non-liquefied sites. Judgement of liquefaction occurrence at a site was made primarily based on visual inspection of surface evidences such as sand boils, cracking or settlement.

Figure 6 shows an example of relationships between the corrected N-value N_1 and shear stress ratio during an earthquake L inferred from field performance data, where the dynamic shear strength ratio R estimated from the proposed method is superimposed. This figure indicates that the proposed dynamic shear strength ratio line classifies liquefied and non-liquefied data fairly well.

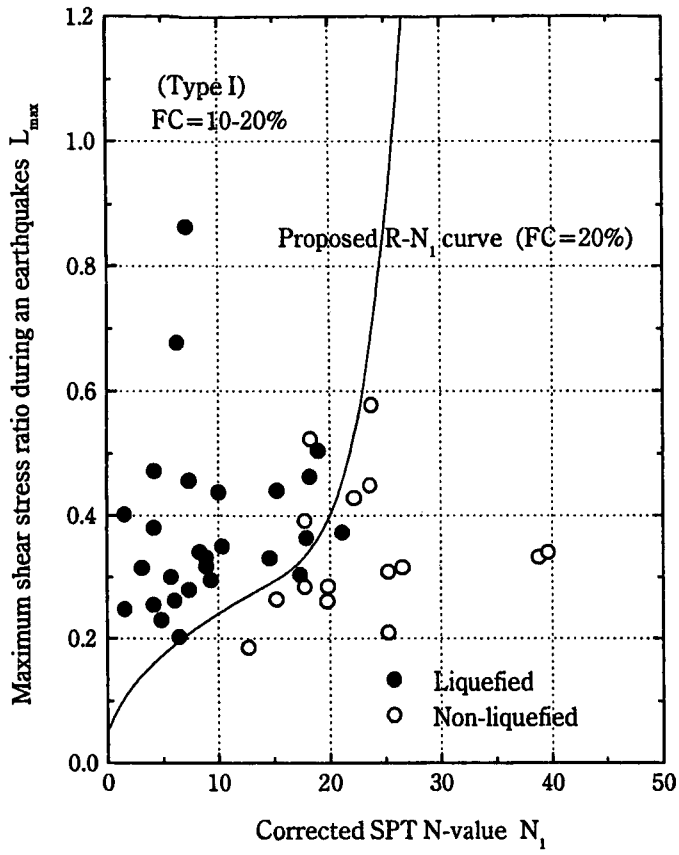

(a) 10% ≦ FC<20%, Type I Ground Motion

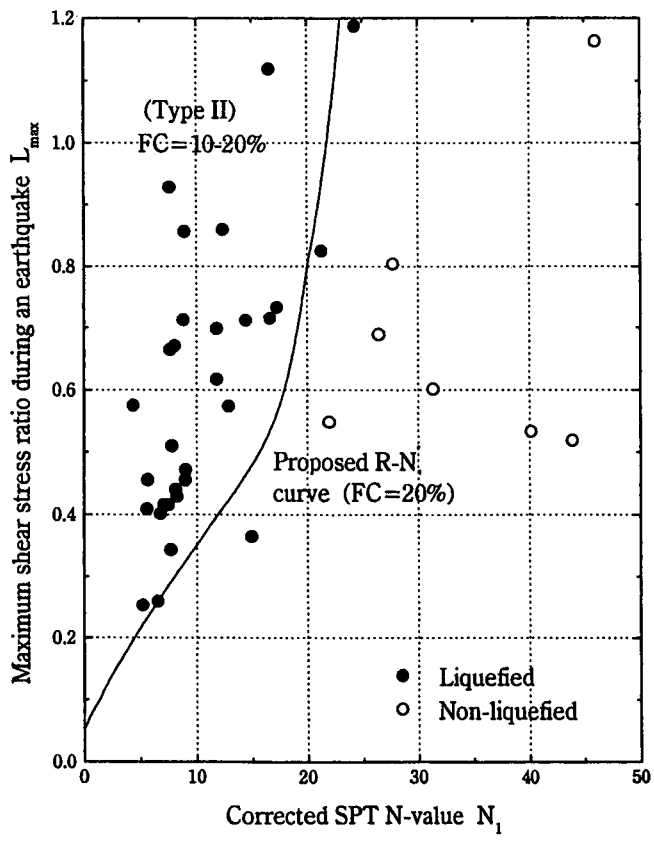

(b) 10% ≦ FC<20%, Type II Ground Motion

Figure 6 Comparison of Field Performance Data and the Proposed Method

SEISMIC DESIGN TREATMENT OF LIQUEFACTION FOR BRIDGE FOUNDATIONS

Soil Constants of Liquefiable Layer

The strength and the bearing capacity of a soil decreases when it liquefies. Based on this, for seismic design of highway bridges, soil constants of a sandy soil layer which is judged liable to liquefy are reduced according to the value of F_L, the liquefaction resistant ratio [3]. The reduced constants are calculated by multiplying the coefficient D_E in Table 1 to the soil constants estimated on an assumption that the soil layer does not liquefy [3].

Table 1 Coefficient D_E to be Multiplied to Soil Constants

Range of F_L	Depth from the Present Ground Surface x(m)	Dynamic Shear Strength Ratio R	
		$R \leqq 0.3$	$0.3 < R$
$F_L \leqq 1/3$	$0 \leqq x \leqq 10$	0	1/6
	$10 < x \leqq 20$	1/3	1/3
$1/3 < F_L \leqq 2/3$	$0 \leqq x \leqq 10$	1/3	2/3
	$10 < x \leqq 20$	2/3	2/3
$2/3 < F_L \leqq 1$	$0 \leqq x \leqq 10$	2/3	1
	$10 < x \leqq 20$	1	1

The coefficient D_E is based on the results of shaking table tests and analyses of bridge foundations damaged by earthquakes. The values of D_E are prescribed to be different for above and below the depth of 10m, because the ground vibration decreases as the depth increases and the cases in which soil layers totally liquefied below the depth of 10m are limited. The values of D_E are also different according to the dynamic shear strength ratio R of soil. This is because that the greater strength can be expected when R is large even if F_L is same.

Seismic Design of Bridge Foundations against Liquefaction

Since a bridge foundation is built in the ground, it is more difficult to identify damage to it than to a bridge pier and it is also difficult to repair a foundation. For these reasons, a

bridge foundation is to be designed so that it has greater dynamic strength than a bridge pier or that it has sufficient deformation capacity [6]. When a sandy layer liquefies, the strength of foundation decreases with the decrease of strength and bearing capacity of the ground, it is not rational to ensure the strength of a foundation greater than that of a pier by excessively strengthening the foundation. For such a case, it may be rational to allow a foundation to go into a plastic zone whereby preventing to yield excessive damage to the foundation and absorbing earthquake motion energy at a foundation.

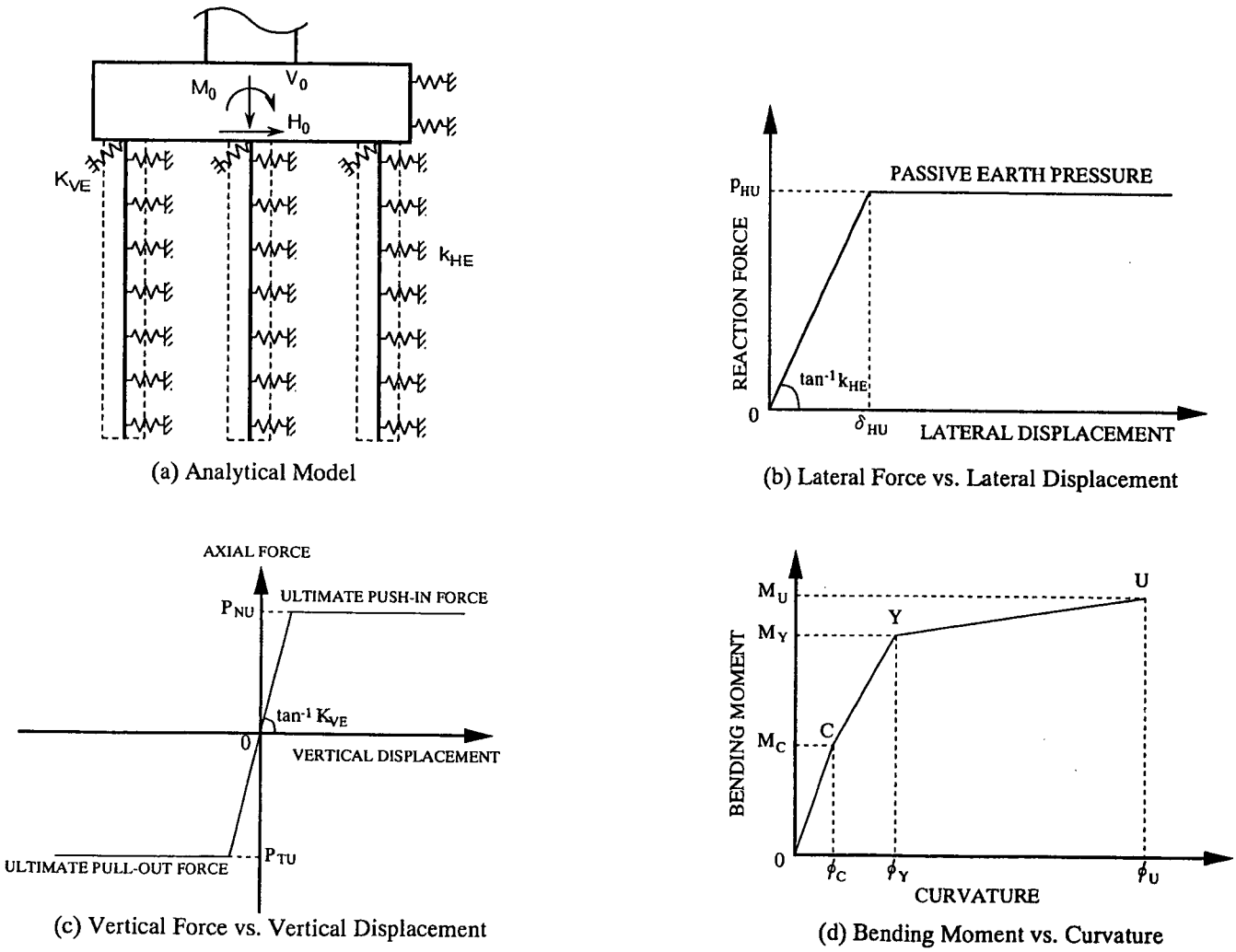

Figure 7 Idealization of Pile Foundation for Analysis

For seismic design of highway bridges, the deformation capacity of a foundation is checked by confirming that the response ductility factor of a foundation is equal to or less than the allowable value [6], using the principle of conservation of energy by N. M. Newmark et al. [7]. This principal assumes that the input energy of elasto–plastic response and elastic response is same when structure is subjected to an earthquake

motion. The allowable ductility factor for a pile foundation may be taken as 4 from model experiments [6]. To check the ductility of a bridge foundation, it is so idealized that a rigid footing is supported by piles that are supported by soils, considering nonlinear properties of pile bodies and the ground as shown in Figure 7 [8].

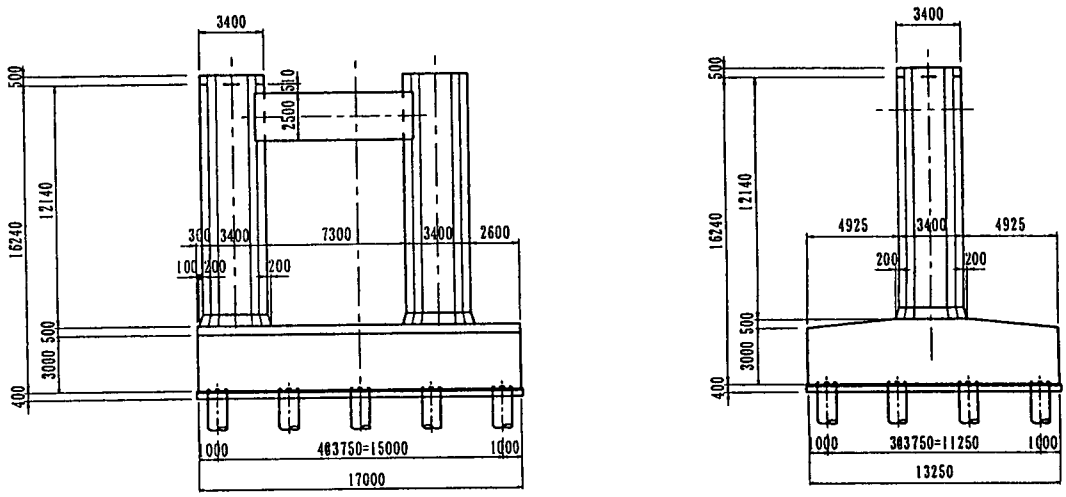

(a) Transverse Direction (b) Longitudinal Direction

Figure 8 General View of the Analyzed Pier

An example of checking the ductility of a foundation is presented in Figure 8 through Figure 10. Figure 8 shows a general view of the pier analyzed. The superstructure for this pier is a 9-span continuous PC box girder. The girder is supported by movable bearings at this pier. Figure 9 shows a schematic view of the foundation and soil condition. The footing is supported by cast-in-place concrete piles 1.5m in diameter and 32.5 m long. The soil is alternation of sand and clay. A sandy soil layer beneath the footing is judged to liquefy, and soil constants of this layer are regarded to be 0 for seismic design. The relationship between lateral force and displacement for the foundation is presented in Figure 10. From this figure, the response ductility factor is calculated as 2.9, which means that this foundation is judged to have sufficient deformation capacity.

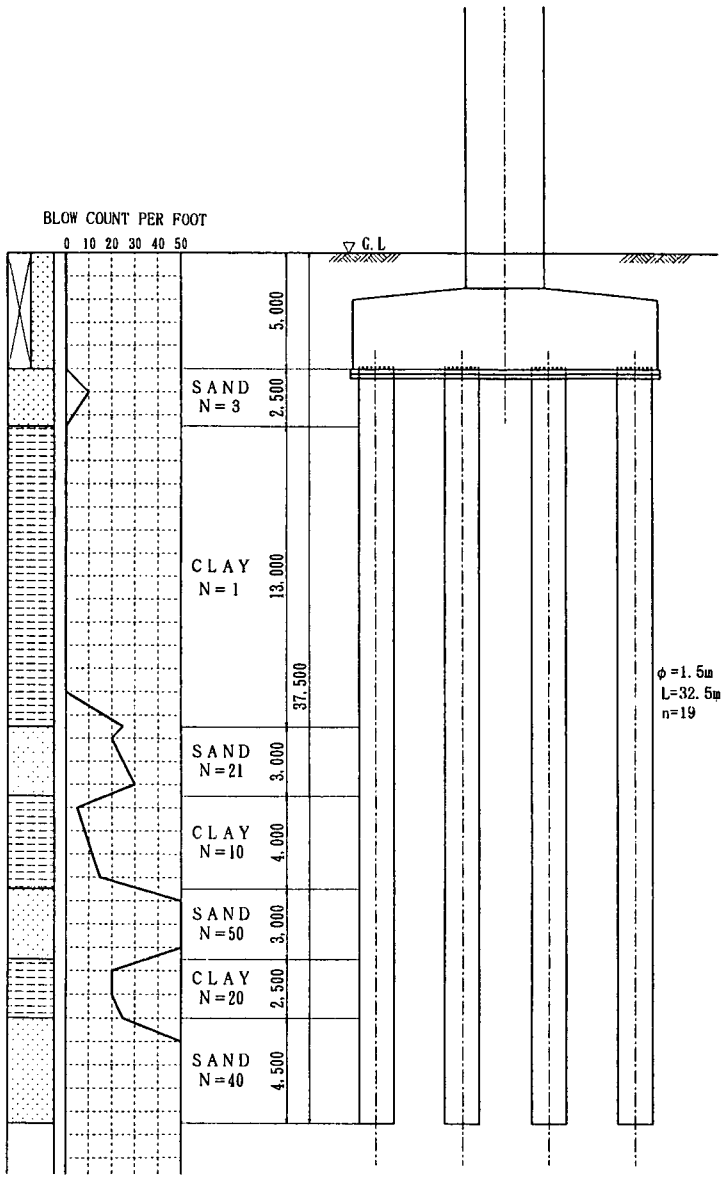

Figure 9 Schematic View of the Foundation

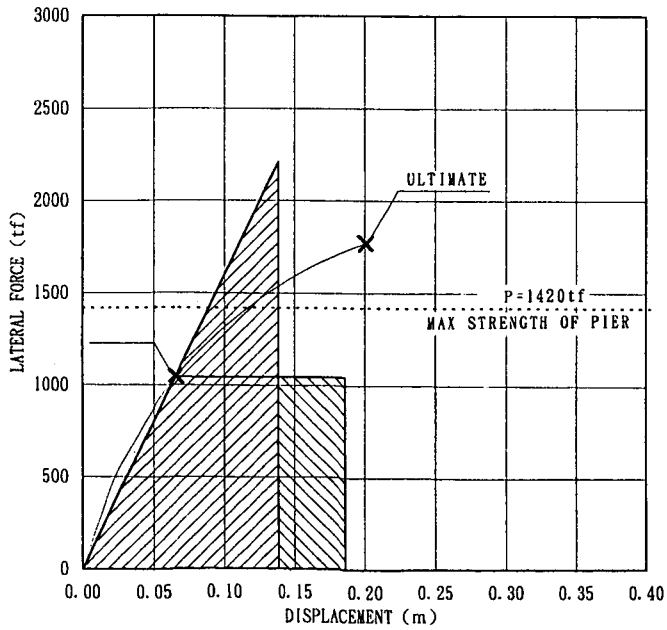

Figure 10 Relationship between Lateral Force and Displacement at Pile Top

INFLUENCE OF LIQUEFACTION-INDUCED GROUND FLOW ON HIGHWAY BRIDGES

Damage to Highway Bridges due to Liquefaction-Induced Ground Flow

No highway bridge suffered serious damage such as collapse of a superstructure directly due to the liquefaction-induced ground flow in the 1995 Hyogo-ken Nanbu Earthquake, however, the ground flow yielded large deformation of bridge foundations and related damage. As an example of damage to a highway bridge, the case of Shin- Shukugawa Bridge on Route 5, Bay Shore Line of the Hanshin Expressway is here presented [9].

The Shin-Shukugawa Bridge completed in 1993 is a 3-span cantilever box girder bridge which crosses a watercourse between reclaimed lands, i.e., Nishinomiya-hama and Minami Ashiya-hama. An overview of the damage to this bridge is shown in Figure 11. Since a toll gate is located on the P-134 pier on Minami Ashiya-hama, the width of the bridge varies from 28m to 69m. The bridge is supported by movable supports at its both ends on reclaimed lands, and by fixed supports on intermediate piers.

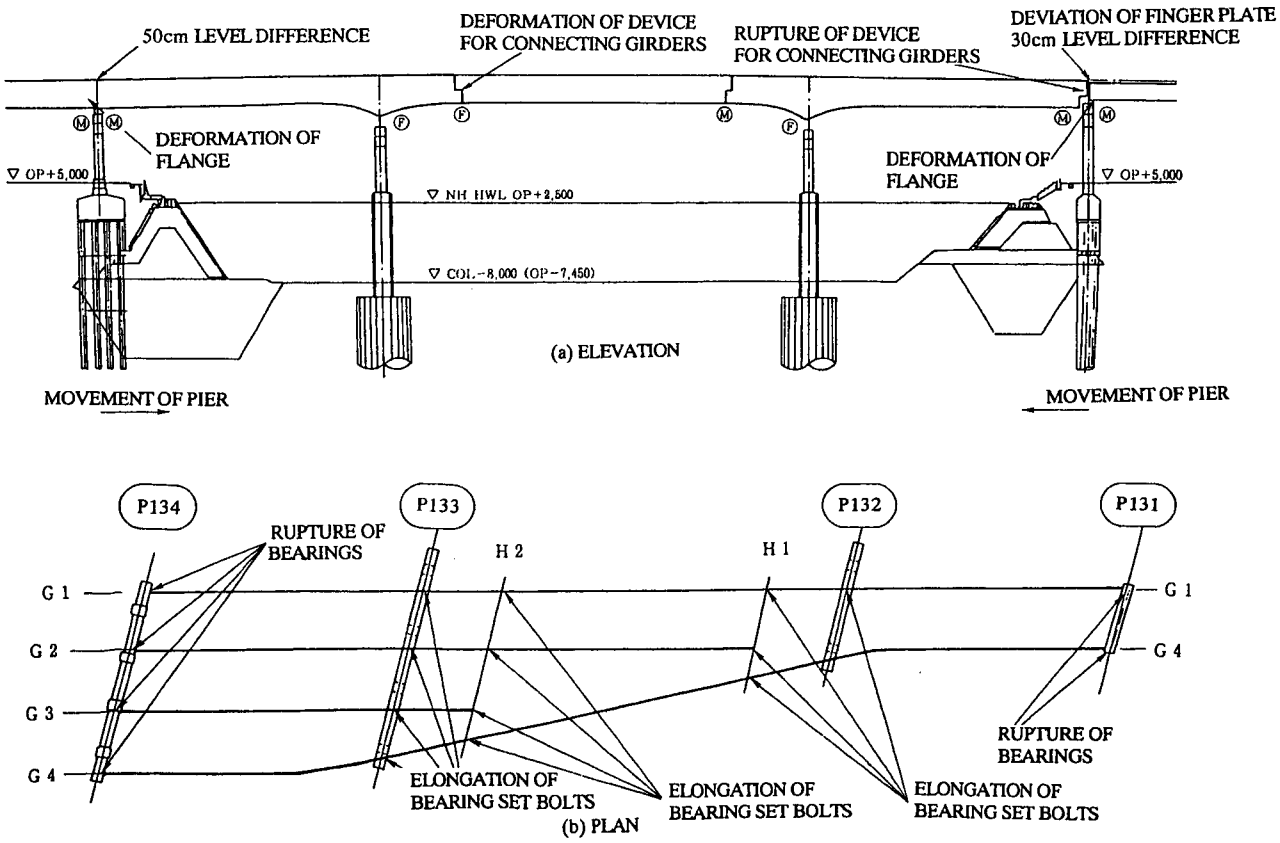

Figure 11 Overview of Damage to the Shin-Shukugawa Bridge

The P−131 pier on Nishinomiya−hama was a 2−column RC rigid frame pier with two caisson foundations, 6m in diameter. The P−134 pier on Minami Ashiya−hama was a 4−column steel rigid frame pier and was supported by cast−in−place concrete piles, 1.5m in diameter. The foundations were constructed in the reclaimed soil and supported by a diluvial sandy layer.

Photo 1 Ground Failure near the Shin−Shukugawa Bridge

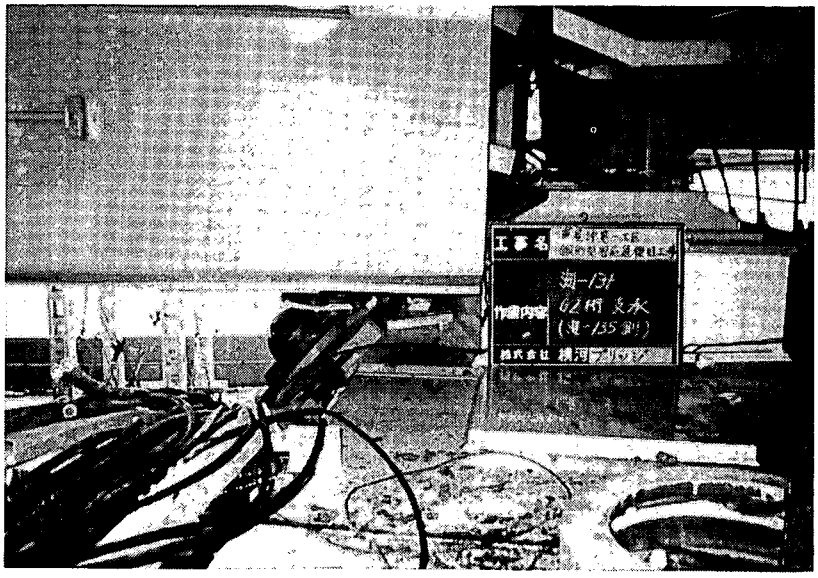

Photo 2 Damage to Bearing Support of the Shin−Shukugawa Bridge

Extensive liquefaction occurred around the bridge as shown in Photo 1, and both P−131 and P−134 piers moved toward the watercourse with the movement of sea walls. The damage was concentrated to the end piers on reclaimed lands. The piers were installed

with pivot roller supports, whose upper and lower shoes diverged as shown in Photo 2, which caused the difference in level between adjacent girders. A device for connecting girders on the P−131 pier was ruptured. A device for connecting girders was deformed at a cantilever hinge.

Ground Movement due to Ground Flow

The aerial photogrammetry was employed to estimate the ground movement vectors by comparing aerial photos taken before and after the earthquake [10]. The result of aerial photogrammetry conducted by Hamada et al. [11] was referred in this study. The main modifications from their study are as follows:

1) Hamada et al. used three survey points on Rokko Island as reference points for aerial photogrammetry, while six points established for surveying the bridge pier locations of the Route 5, Bay Shore Line of the Hanshin Expressway were used as reference points in this study.
2) Hamada et al. found displacement vectors of fixed objects on the ground surface such as manhole covers. In the present study, displacement vectors at intersection points of 20m interval grids were inferred from the movement of fixed objects. The residual horizontal displacements of bridge piers at the height of 1m above the ground level were also estimated in this study by another survey conducted after the earthquake.

The horizontal displacement vectors of the ground and bridge piers were found to include uniformly about 20cm component for the south−west direction. In addition to this, triangulation points near the Route 5 of the Hanshin Expressway shifted the same amount for the south−west direction. This displacement may be attributed to the base ground movement caused by fault movement or wide area ground movement. In the present study, this displacement is excluded from the result of aerial photogrammetry of the ground displacement and the residual displacement of bridge piers. The displacement vectors found may include a certain degree of error because of the errors associated with aerial survey and photographic interpretation. The accuracy of measurement is estimated as ± 30cm for the ground displacement and ± 10cm for residual displacement of bridge piers, respectively [10].

Figure 12 shows the vectors of the ground displacement and residual displacement of bridge piers near the north shore of Rokko Island. The sea walls moved toward the watercourse and the ground flow occurred, which caused the movement of the ground and bridge piers behind the walls. At the edge of the water, the ground moved more than 2m, and a bridge pier moved approximately 0.9m. The movements of the ground and bridge piers generally decrease as the distance from the watercourse increases.

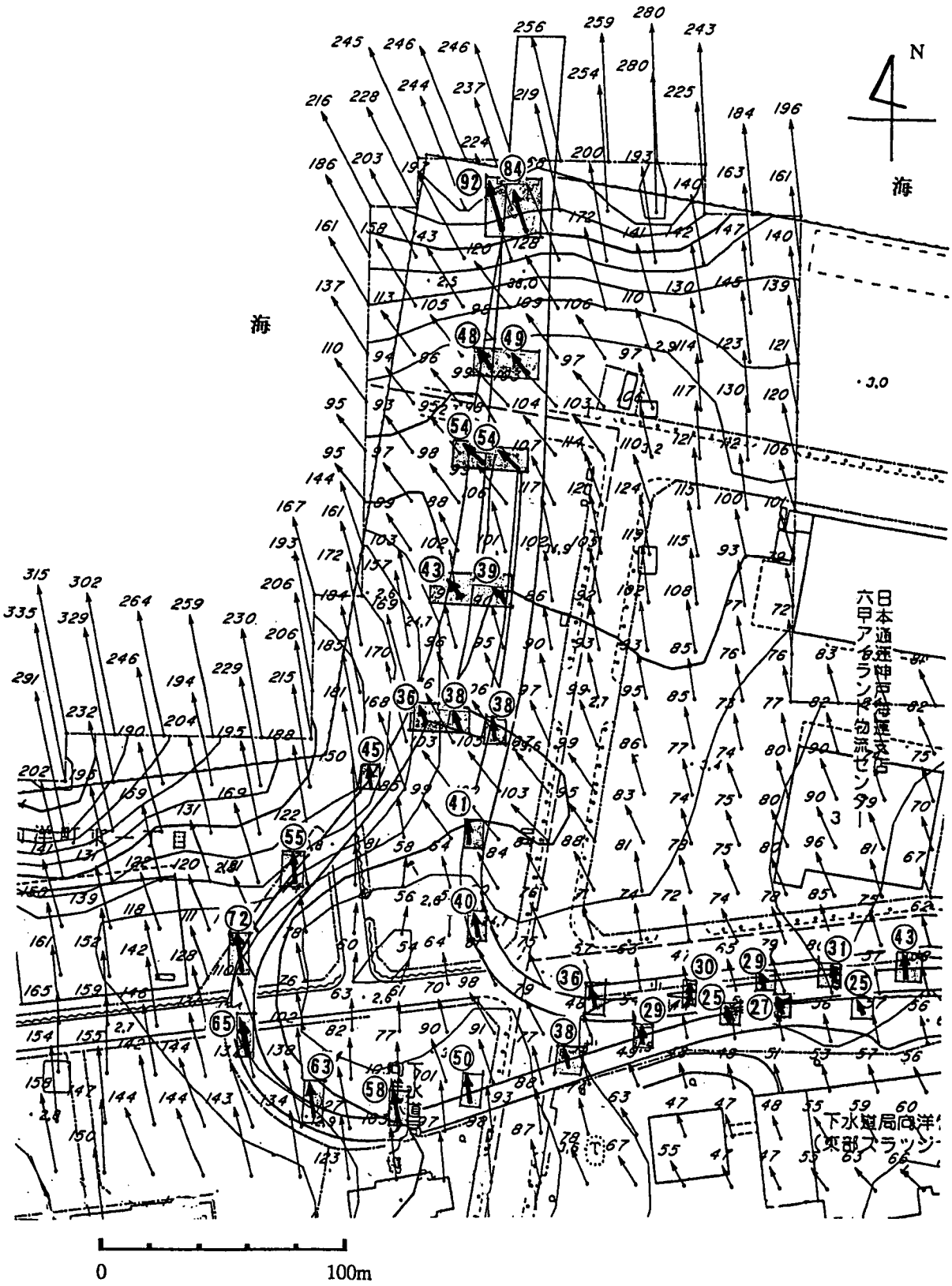

NOTE : Number at arrows and in circles represent horizontal displacements of the ground and residual horizontal displacements of bridge piers, respectively. (Unit : cm)

Figure 12 Horizontal Displacements of the Ground and Residual Displacements of Bridge Piers at Rokko Island

Figure 13 shows the relationship between the residual horizontal displacements of bridge piers and the horizontal displacements of the ground on the Route 5 of the Hanshin Expressway. Although the considerable scatters exist, the residual displacements of bridge piers tend to increase as the ground displacements increase, in general. The residual displacements of piers with rigid foundations, i.e., caisson and diaphragm wall foundations, are smaller than those with pile foundations for a certain amount of ground displacement.

The relationship between the residual horizontal displacements of bridge piers and the distance from the water's edge is shown in Figure 14. The residual displacement rapidly decreases with the increase of distance from the edge of the water. The range in which prominent residual displacement occurred is limited to approximately 100m from the water's edge.

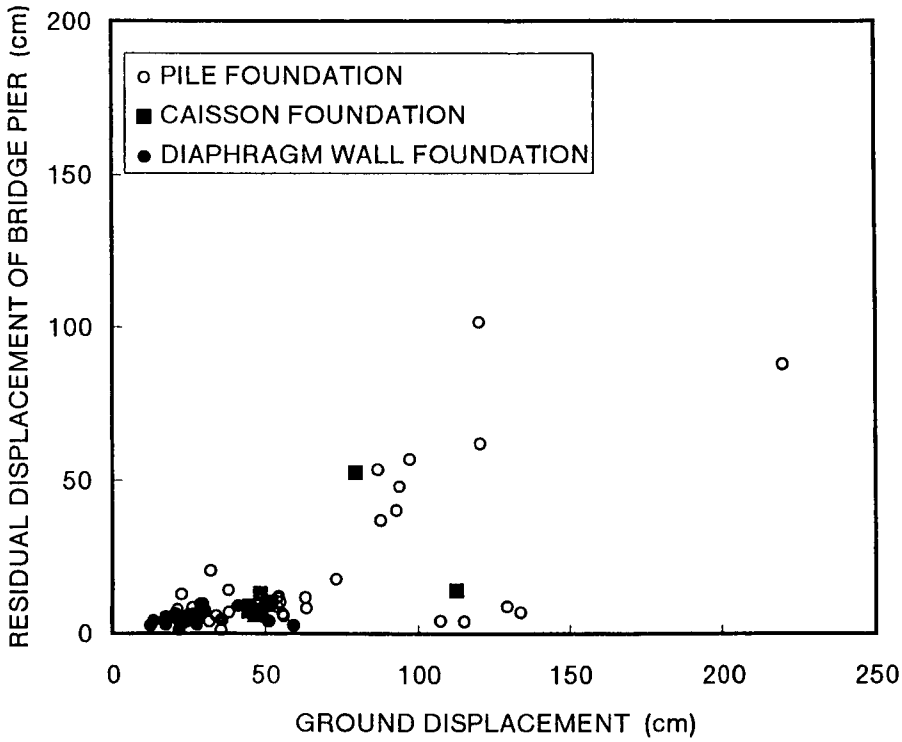

Figure 13 Relationship between Residual Horizontal Displacements of Bridge Piers and Horizontal Displacements of the Ground

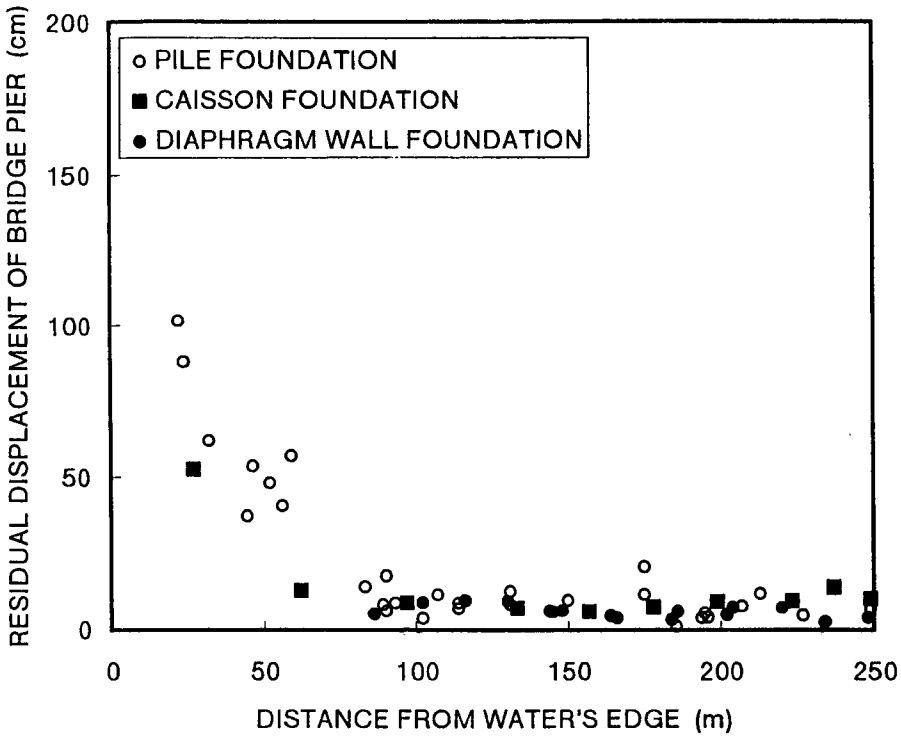

Figure 14 Relationship between Residual Horizontal Displacements of Bridge Piers and Distance from Water's Edge

Estimation of Ground Flow Force by Back Analysis

The force acted on a bridge foundation due to the liquefaction-induced ground flow was estimated by back analysis of bridges which suffered residual horizontal displacements. The result for P-216 pier, which is located at the north edge of Rokko Island, is here presented. The P-216 pier was a 2-story steel rigid frame pier and was supported by cast-in-place concrete piles, 1.5m in diameter. The bearings on this pier are fixed for the watercourse-side girder and movable for the inland-side girder. The soils are composed of sandy artificial fill, alluvial clay and alternation of diluvial sand and clay. The residual horizontal displacement of this pier was 0.9m, as shown in Figure 12. The ground water level of the site was 3.3m below the ground surface, and the liquefaction was judged to occur in the sandy artificial fill below the ground water level.

In the estimation of the force acted on a bridge foundation due to the ground flow, it was assumed that the layer near the ground surface which did not liquefy (non-liquefied layer) moved with the layer which liquefied (liquefied layer), and both layers caused force to a bridge foundation [12]. Since the non-liquefied layer was considered to move toward the structure and exert force on it, the force equivalent to the passive earth pressure was assumed to act on a bridge foundation in the non-liquefied layer. The

liquefied layer was considered to move fluidly around the structure, and the force corresponding to a certain portion of overburden pressure was assumed to act on a bridge foundation in the liquefied layer. This portion was estimated by back analysis of bridge piers with residual displacements.

An idealization of bridge foundation presented in Figure 7 was also employed in this analysis, except that the soil resistance were ignored for the non-liquefied and liquefied layers which were considered to move when the ground flow occurred. The width for which the ground flow force applied was set as the width of structure for a pier and footing, and the projected width between the end piles for pile bodies. Figure 15 shows an overview of the analyzed foundation and the applied force.

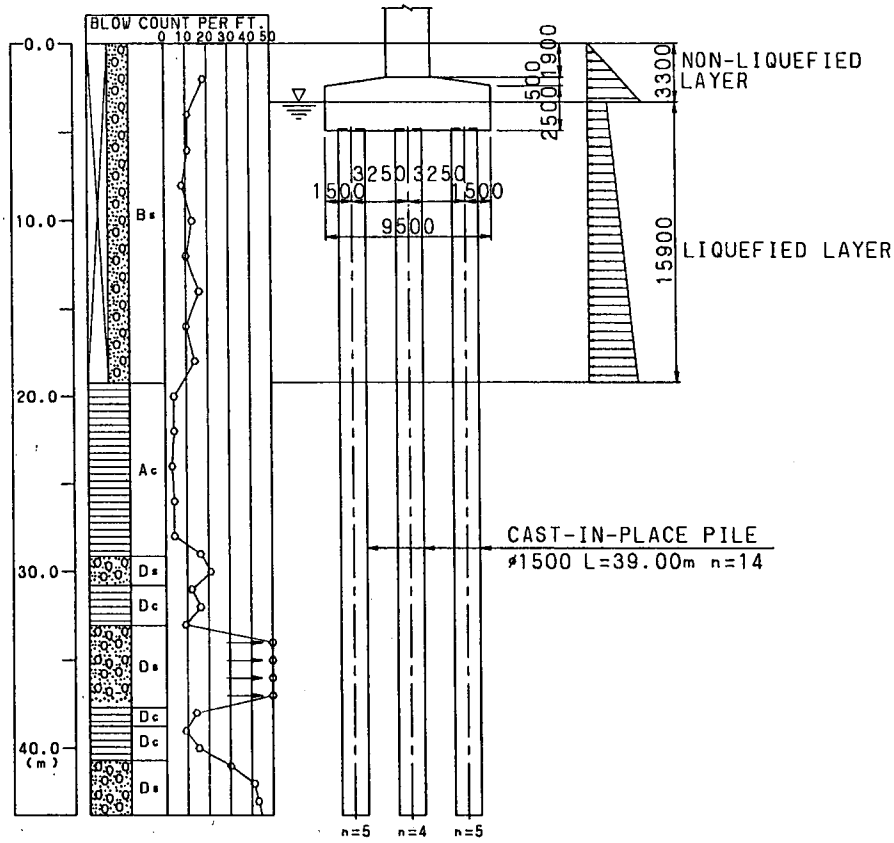

Figure 15 Overview of Analyzed Foundation and Applied Force

Since how much portion of the overburden pressure of the liquefied layer acted on a bridge foundation was unknown, varying this portion parametrically and calculating the relationship between lateral force and displacement, the amount of force that was consistent with the residual displacement was estimated. The result is shown in Figure 16. The total force which caused the residual displacement of 0.9m to the P-216 pier was estimated as 2,256tf; 578tf for non-liquefied layer and 1,678tf for liquefied layer.

The ratio of the force applied in the liquefied layer to the overburden pressure was calculated as 0.32 for this pier. Similar analysis was conducted for the four bridge piers on the Route 5 of the Hanshin Expressway, and the contribution factor of overburden pressure was estimated approximately as 0.3.

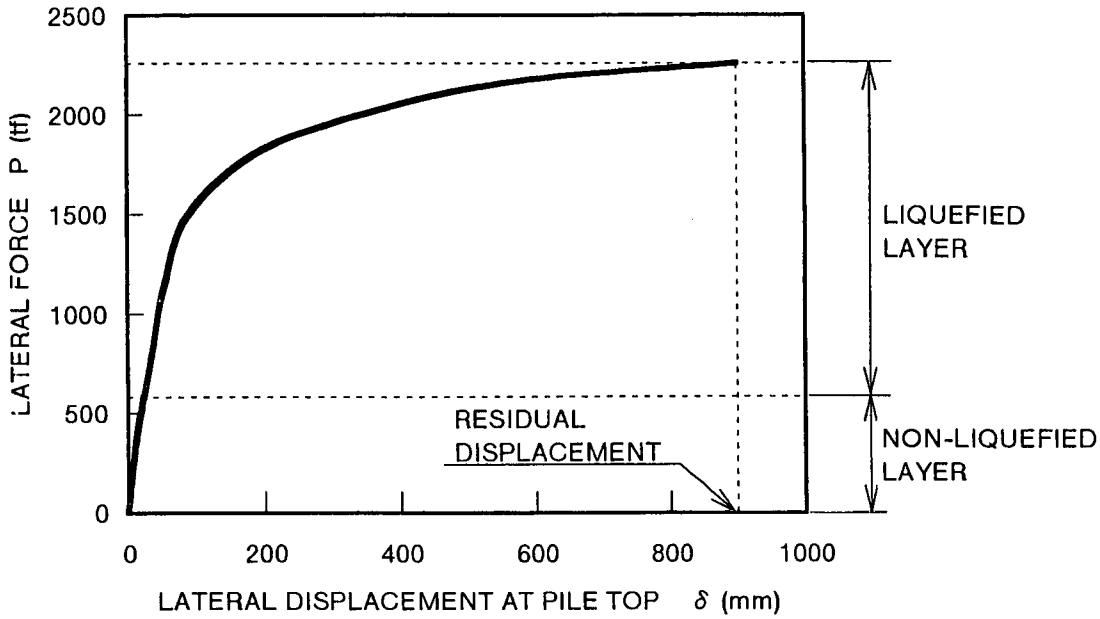

Figure 16 Relationship between Lateral Force and Displacement at Pile Top

SEISMIC DESIGN TREATMENT OF GROUND FLOW FOR BRIDGE FOUNDATIONS

When the liquefaction–induced ground flow that may affect bridge seismicity is likely to occur, this influence has become to be considered in the newly revised "Specifications for Highway Bridges" [6] . An outline of the seismic design treatment of liquefaction–induced ground flow is hereinafter introduced.

The case in which the ground flow that may affect bridge seismicity is likely to occur is generally that the ground is judged to be liquefiable and is exposed to biased earth pressure, e.g., the ground behind a sea wall. The effect of liquefaction–induced ground flow is considered as the static force acting on structure. This method premises that the surface soil is of the non–liquefiable and liquefiable layers, and the forces equivalent to the passive earth pressure and 30% of the overburden pressure are applied to the structure in the non–liquefiable layer and liquefiable layer, respectively. As seen from Figure 14, since the magnitude of ground flow decreases as the distance from the water's edge increases, modification by distance is incorporated in the estimation of the ground flow force. Modification by the degree of liquefaction is also established.

The seismic safety of a foundation is checked by confirming the displacement at the top of foundation caused by ground flow does not exceed an allowable value, in which a foundation and the ground are idealized as shown in Figure 7. The allowable displacement of foundation may be taken as two times the yield displacement of foundation. In this process, the inertia force of structure is not necessary to be considered simultaneously, because the liquefaction–induced ground flow may take place after the principal ground motion ends.

CONCLUSIONS

The following conclusions may be deduced from the present study.

1) A simple procedure to assess liquefaction potential of soils has been developed, in which the effects of soil gradation and ground motion irregularity are incorporated. This procedure is applicable up to gravelly soils.

2) A seismic design procedure of bridge foundations is demonstrated in which the effect of soil liquefaction is taken into account by reducing the soil constants and the deformation capacity of a foundation is checked by the principle of conservation of energy.

3) A simple design treatment of liquefaction–induced ground flow for bridge foundations is introduced, in which the ground flow force may be estimated as the sum of the passive earth pressure of the non–liquefied layer and 30% of the overburden pressure of the liquefied layer.

REFERENCES

1) Japanese Geotechnical Society: Special Issue on Geotechnical Aspects of the January 17 1995 Hyogoken–Nambu Earthquake, 1996

2) Japan Society of Civil Engineers: The 1995 Hyogoken–Nanbu Earthquake – Investigation into Damage to Civil Engineering Structures –, 1996

3) Japan Road Association: Specifications for Highway Bridges, Part V Seismic Design, 1990

4) Matsuo, O. et al.: Revised Liquefaction Potential Procedure and Seismic Design Treatment of Liquefaction for Bridge Foundations, Proc. of Twelfth U.S.–Japan

Bridge Engineering Workshop, U.S.–Japan Panel on Wind and Seismic Effects, UJNR, 1996

5) Tatsuoka, F., Maeda, S., Ochi, K. and Fujii, S.: Prediction of Cyclic Undrained Strength of Sand Subjected to Irregular Loading, Soils and Foundations, Vol.26, No.2, 1986

6) Japan Road Association: Specifications for Highway Bridges, Part V Seismic Design, 1996 (in Japanese)

7) Veletsos, A. S. and Newmark, N. M.: Effect of Inelastic Behavior on the Response of Simple Systems to Earthquake Motion, Proc. of Second World Conference on Earthquake Engineering, 1960

8) Japan Road Association: Reference for Applying the Guide Specifications for Reconstruction and Repair of Highway Bridges which Suffered Damage due to the Hyogo–ken Nanbu Earthquake of 1995, 1995 (in Japanese)

9) Otsuka, H. et al.: Report on the Disaster Caused by the 1995 Hyogoken Nanbu Earthquake, Chapter 5, Damage to Highway Bridges, Report of PWRI, No.196, 1996

10) Committee for Investigation on the Damage of Highway Bridges by the Hyogo–ken Nanbu Earthquake, 1995: Report on the Damage of Highway Bridges by the Hyogo–ken Nanbu Earthquake, 1995 (in Japanese)

11) Hamada, M., Isoyama, R. and Wakamatsu, K.: The 1995 Hyogoken–Nanbu (Kobe) Earthquake, Liquefaction, Ground Displacement and Soil condition in Hanshin Area, Association for Development of Earthquake Prediction, 1995

12) Tamura, K., Hamada, T. and Azuma, T.: Seismic Design Treatment of Liquefaction –Induced Ground Flow, Proc. of Third U.S.–Japan Workshop on Seismic Retrofit of Bridges, U.S.–Japan Panel on Wind and Seismic Effects, UJNR, 1996

A Study on Measures Against Ground Flow Using The Finite Element Method

By M. Ogasawara,[1] H. Tsunoda,[1] and T.Makita [1]

1) Engineer, Metropolitan Expressway Public Corp., Tokyo, Japan

Abstract

It is assumed that ground flow accompanying liquefaction occurs when the ground becomes unbalanced under the effects of deformation of a revetment. This paper reports on the use of FEM analysis to estimate the state of imbalance of ground caused by liquefaction, and describes ground flow protection measures which treat the ground displacement estimated in this way as an external force. The FEM analysis of the imbalanced state includes an assessment performed by varying the stiffness of the ground before and after liquefaction. A study was performed to develop a method of protecting structures from this problem by installing steel pipe sheet-piles between revetments and the structures. When considering measures for dealing with ground flow, it is necessary to understand its mechanism. Consequently, ground flow mechanism was considered, and based on this mechanism, two evaluation methods were studied. One assesses ground displacement as an external force as described above and another treats the ground flow as shearing deformation. Finally the ways the two methods handle a sample
disaster were studied.

Introduction

During the Hyogo-ken Nanbu Earthquake (January 17, 1995), liquefaction in landfill near revetments along the harbor shoreline caused ground flow (movement) accompanied by the movement of structures. A report from the Hyogo-ken Nanbu Earthquake Road Bridge Earthquake Damage Counter-measures Committee (1995) reports bridge pier movement as great as about 1.0 m.

This ground flow did not occur only as a result of liquefaction in horizontal ground. It is induced by plastic flow occured in the surrounding ground after that nearby revetments subside and move as result of liquefaction. Consequently, ground deformation was greatest near the revetments, but declined as the distance from the revetments increased. In other words, the ground flow force declined as the distance rose. For this reason, it has been concluded that one effective way to prevent ground flow would be to locate ground flow protection work between the revetment and the structure to be protected, and as far as possible from the revetment (close to the structure).

The horizontal motion of ground accompanying the deformation of a revetment is assumed to be the sum of the motion during and after the earthquake. Little is known about the percentage accounted for by the two motions, it is difficult to analytically clarify this factor, and it is difficult to believe that doing so would provide practical benefits. So the method employed involved varying the stiffness of the liquefied stratum before and after liquefaction and treating the resulting difference between the ground displacements calculated from the dead weight analyses performed with the FEM method as the total horizontal motion of the ground. The revised Specification for Highway Bridges state that it is appropriate to apply this method when the ground condition is complex.

Two methods of assessing the external force acting on a structure from the ground displacement have been considered. One is the response displacement method which applies ground displacement to a structure. The other method assumes that the deformation of the ground is shear deformation and treats the shear force which causes this shear deformation as an external force. Based on the results of analyses of a sample disaster using these two methods, the response displacement method has been judged to be effective and was used as the external force for the counter-measure work.

The results of a study of measures to protect bridge piers in the area under the jurisdiction of the Metropolitan Expressway Public Corporation performed using the above method show that the installation of steel pipe sheet-piles with a diameter of 1.2 m and a sheet thickness of 19 mm in front of a line of piers can be counted on to provide a certain level of effectiveness.

Mechanism of Ground Flow Induced by Liquefaction

Figure 1 is a schematic diagram of the effect of ground flow on bridge piers. In this figure, it is hypothesized that there is no liquefaction from the ground surface to the bottom of the footing (non-liquefied stratum), but that liquefaction occurs deeper than the bottom of the footing (liquefied stratum). The numbers inside the circles signify the sequence of phenomena up to the point that horizontal displacement of the

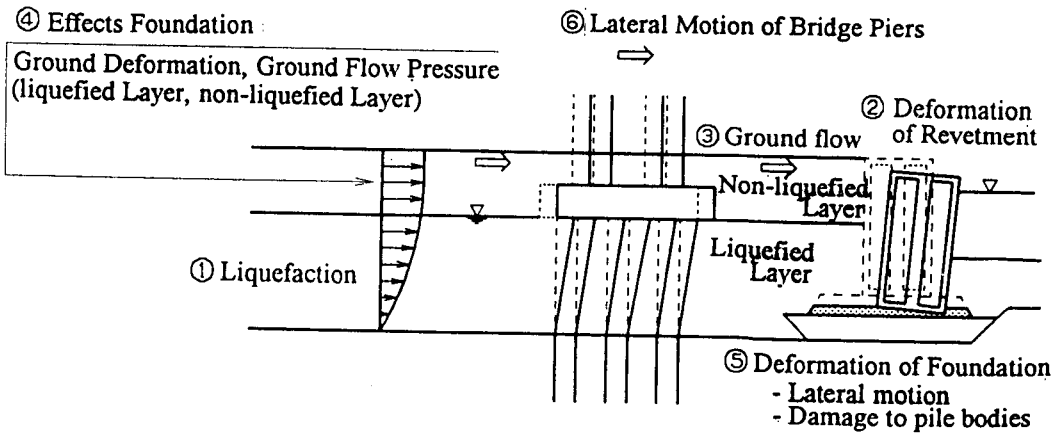

Figure 1.Concept on the Mechanism of the Effect of Ground flow on Bridge Pier Foundations

bridge piers occurs.① Liquefaction: The liquified stratum in the diagram is liquefied by the earthquake.

② Deformation of the revetment: The revetment inclines towards the ocean, subsides, and moves horizontally under the effects of increasing soil pressure and a decline in the bearing force of the foundation ground caused by the liquefaction.③ Ground flow: As the revetment is deformed, the ground behind it moves a long distance horizontally towards the ocean as it subsides.④ Effect on the foundation: The horizontal motion of the ground applies flow pressure on the structure.⑤ & ⑥: Deformation of the foundation and lateral motion of the bridge piers: The bridge piers are moved horizontally by the flow pressure.

This mechanism shows that the deformation of the revetment is transmitted to the bridge piers through the ground. As a result, it has been concluded that the implementation of measures to block this transmission process will be effective (a measure taken between the revetment and structure).

Estimation of Ground Flow Displacement

The amount of ground flow is estimated based on a static elastic FEM analysis. To find the amount of ground flow, the stiffness of the liquefied stratum is reduced from the stiffness prior to liquefaction and the amount of ground flow is found by means of dead weight analyses. This method provides the following benefits.

① It is easy to handle.

② The effectiveness of counter-measure work can be assessed as the difference between the amount of ground flow before and after its execution.

③ It is possible to assess the flow pressure in accordance with the amount of ground flow.

④ The effects of the thickness of the flow stratum, the distance from the revetment, the inclination of the ground, etc. can be reflected in the amount of ground flow.

Figure 2 is a flow chart of this study process. The non-liquefied stratum above the liquefied stratum is reduced in order to mitigate resistance caused by cracking of the ground surface during liquefaction and tensile force generated analytically.

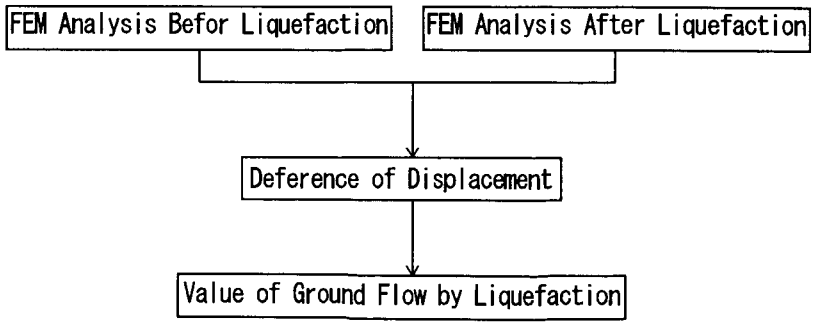

Fig.2 Estimation on Displacement of Ground Flow

The amount of ground flow was calculated for a case where there are neither bridge piers nor protective work, in order to account for the joint element with an upper limit value for tension and slippage between the revetment and the ground.

Ground Flow Force Estimation Procedure

Procedure Considering Ground Flow Force as Displacement

A method of providing the displacement of the ground at the location of the structure, the flow pressure P is assessed using formula (1).

$$p = k \times \left(\delta_g - \delta_f\right) \leq p_p \quad \cdots\cdots\cdots\cdots \quad (1)$$

Where, p : Flow pressure (tf/m^2), δ_g: Ground displacement (m), δ_f: Foundation displacement (m), k : Ground spring constant of the flow stratum $\left(tf/m^3\right)$, Pp: Passive soil pressure $\left(tf/m^2\right)$. Figure 3 is a schematic diagram illustrating this concept. k_H in the figure is the resistance spring constant of the ground in which the piles are placed, and the passive soil pressure is treated as the upper limit. The spring constant of the liquefied stratum is the value obtained by multiplying the coefficient of subgrade reaction used for the design by the reduction rate of the ground stiffness after liquefaction obtained when calculating the ground flow. The ground depth direction displacement distribution treats the displacement at the ground surface as the maximum value and assumes that it is a cosine distribution with the displacement at the bottom surface of the liquefaction stratum equal to zero. The structure is assumed to be non-linear material using M (bending moment) ~ ϕ (curvature).

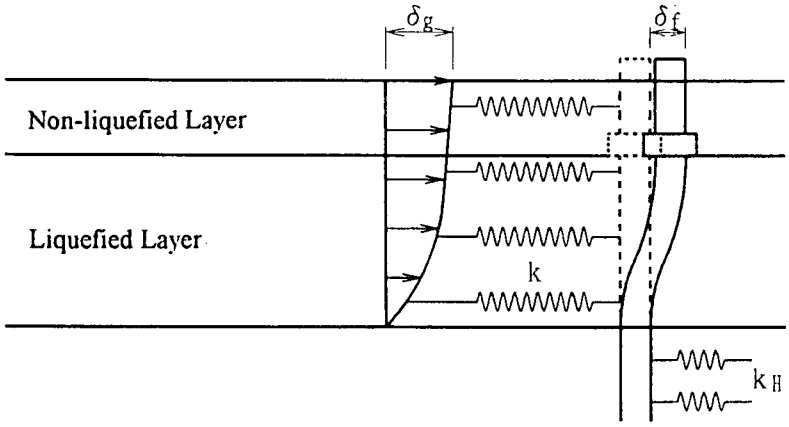

Figure 3.Concept of Ground Displacement as the Flow Pressure

Procedure Considering Ground Flow Force as Shearing Deformation

Using this method, it is assumed that the horizontal direction displacement accompanying the ground flow is an inverted triangular shear deformation as shown in Figure 4, the shear strain is found by reducing the ground surface displacement (δ_g) by the flow stratum thickness (H), and the assessment is performed treating the shear force equivalent to shear deformation within a certain range as the flow pressure.

The amount of deformation of the ground is greatest at the location of the revetment, declining with increasing distance from the revetment. If this is thought of as the change in the shear

strain, it can be approximated by the curve shown in Figure 5 with reference to an example of past deformation. In this figure, the vertical axis is the shear strain while the horizontal axis is the distance from the revetment. γ_0 is the shear strain at the center of the bridge pier, and it is hypothesized that the shear force which corresponds to the shear deformation of the ground behind this location is the flow pressure. In this study, it is assumed that there is action by a shear force (S) generated in an imaginary soil column in a range α times the liquefied stratum thickness (H) as shown in Figure 5. This shear force acts on the structure as a uniform load in the stratum thickness direction. Consequently, the size of the flow pressure (p) is found from formula (2).

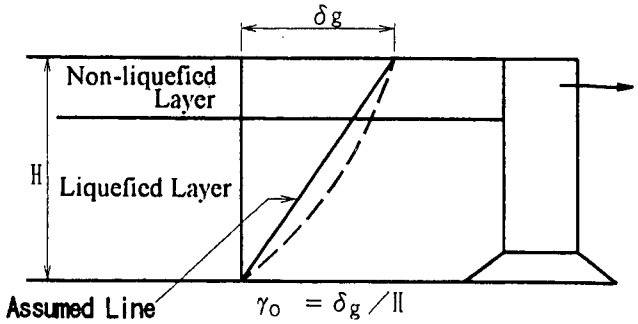

Figure 4.Shear Deformation Concept

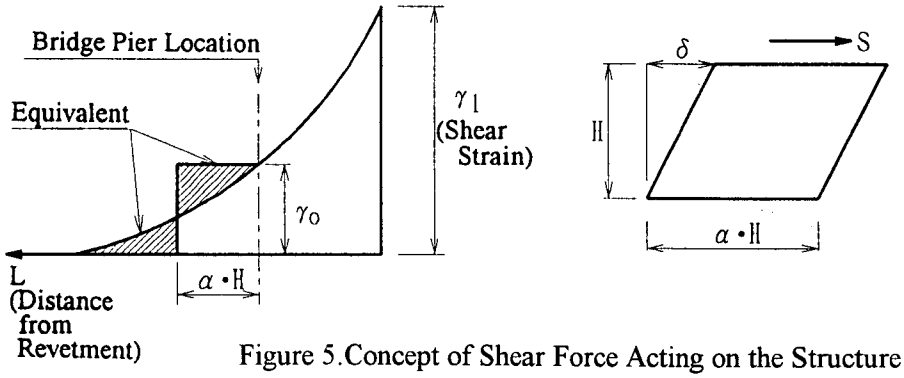

Figure 5.Concept of Shear Force Acting on the Structure

$$p=S/H=G\cdot\gamma_0\cdot\alpha\cdot H/H=G\cdot\gamma_0\cdot\alpha \quad \cdots\cdots\cdots \quad (2)$$

Where G is the shear stiffness of the flow stratum, and the value after liquefaction obtained through FEM analysis is used. Figure 6 shows an analytical model.

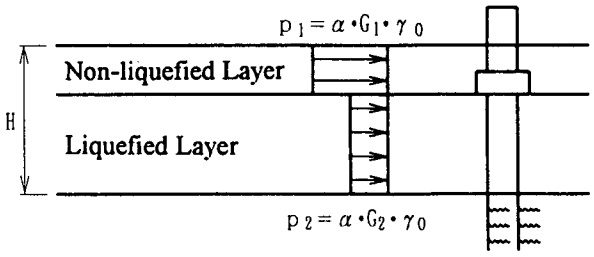

Figure 6.Calculation Model for the Method Which Treats Shear Force as Flow Pressure

Test of the Procedures Based on an Example of Past Deformation

Estimation of Ground Flow Displacement

Using measured amounts of movement of the ground surface caused by liquefaction observed after the Hyogo-ken Nanbu Earthquake, the methods were verified by varying the ground stiffness before and after liquefaction. Because there is no detailed data concerning the physical properties of the ground, the following hypotheses were established. Because with this method, the difference between the relative displacements is assumed to be the amount of

ground flow, the important points are the hypothetical stiffness reduction rate and Poisson's ratio of the liquefied stratum after liquefaction. The modulus of deformation of the ground before liquefaction (Eo) was 28 • N (N: standard penetration test value), while Poisson's ratio (ν) was 0.33. The unit weight used was the weight in water. The modulus of deformation of the liquified stratum after liquefaction was 1/100 of that before liquefaction. This reduction rate was set based on parametric analysis for an actual example with reference to the results of research by Yasuda et al (1994). The modulus of deformation of the non-liquefied stratum above the liquefied stratum was set at about 1/10 of that before liquefaction. This was done to mitigate the resistance caused by the tensile stress, which is a shortcoming of elastic analysis. And the boundaries of the ground were set 500 m inland from the back of the revetment and 100 m on the ocean side. The horizontal displacement was fixed and the vertical displacement was free.

Figures 7 to 9 show comparisons of the observed values and analytic values of the horizontal displacement of the ground surface. These are examples of Minami Ashiya Beach, Uozaki Beach (See the model in Figure 10), and Port Island. These figures demonstrate that it is possible to estimate the approximate amount of displacement of ground using this method.

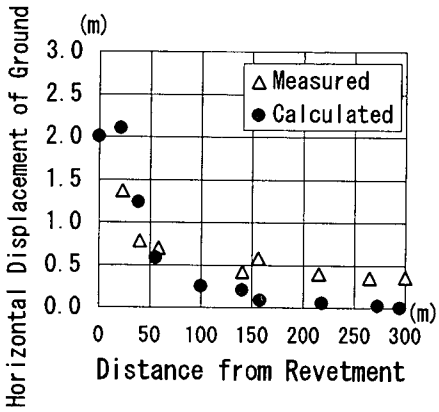

Fig.7 Distance from Revetment-Displacement Relationship(Minami Asiya Beach)

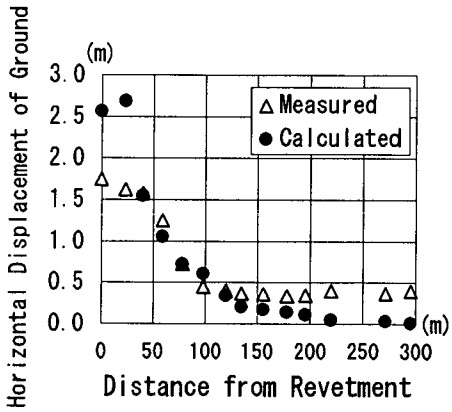

Fig.8 Distance from Revetment-Displacement Relationship(UOSAKI Beach)

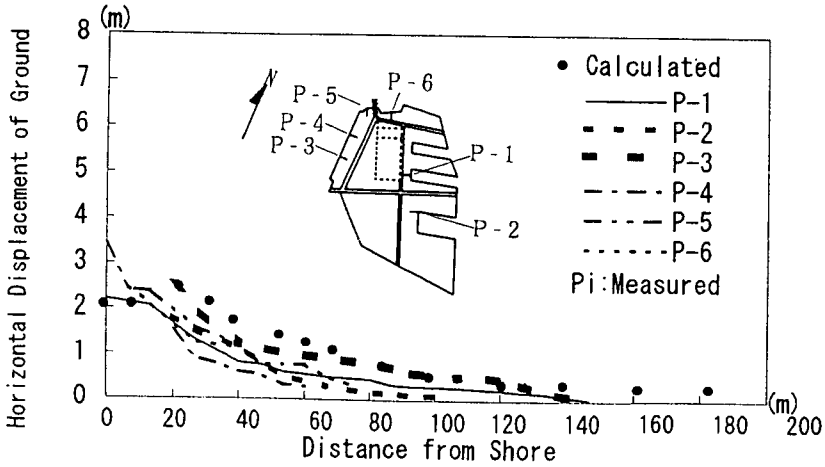

Fig.9 Distance From Revetment-Displacement Relationship (Port Island:Measured Displacement Based on Reference Source No.2)

Ground Flow Force Estimation Procedure

The ground flow force is estimated based on the ground displacement found as described above. It is found for deformed bridge piers at Minami Ashiya Beach, Uozaki Beach, and near Rokko Island. In all cases, they were cast-in-place concrete piles with a diameter of 1.5 m. Figure 10 presents the ground model for Uozaki Beach and the arrangement of its bridge pier foundations as an example. Figure 11, an example of calculation results, reveals that the flow pressure in the non-liquefied stratum was passive soil pressure in all cases, but the flow pressure in the liquefied stratum was found to be 2,296 tf using the method which considers the displacement

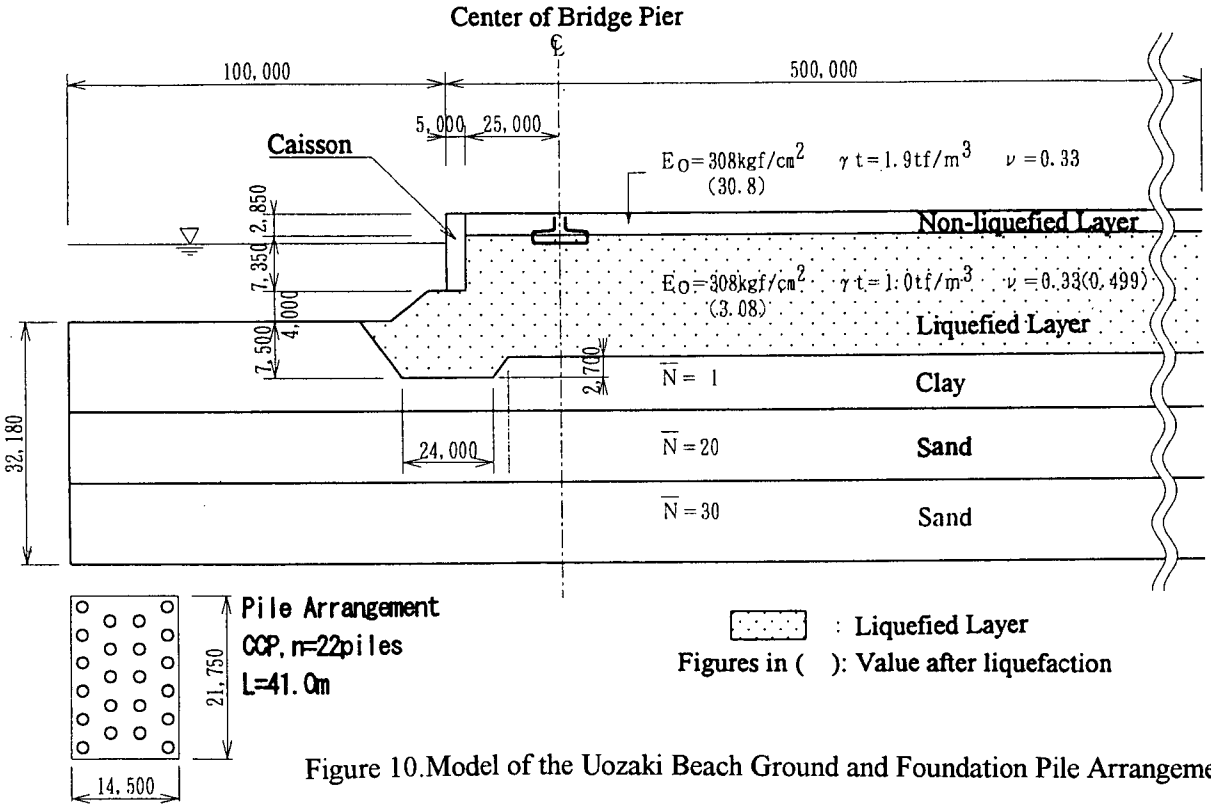

Figure 10.Model of the Uozaki Beach Ground and Foundation Pile Arrangement

of the ground, and it was found to be 1,502 tf using the method which assesses this force based on shear deformation; the flow pressure is smaller in the latter case. The size of the flow pressure in the liquefied stratum varies by about 35%, but the amount of displacement of the foundation varies by more than three times. This difference is a result of the

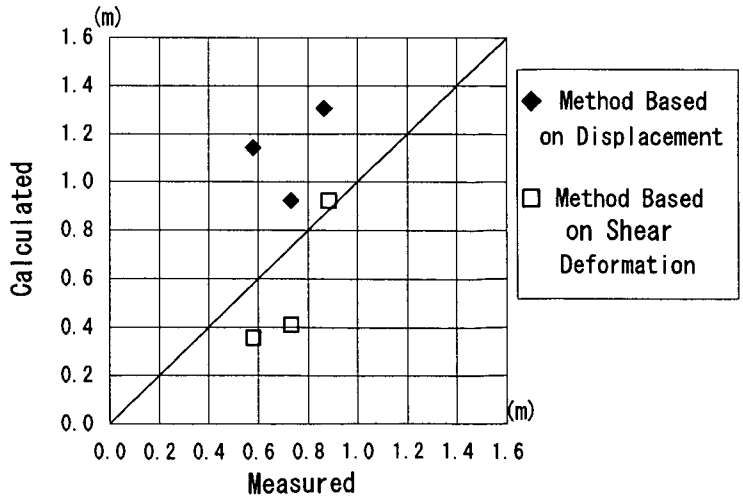

Fig.12 Measured and Calculated Horizontal Displacement Relation of the Foundation

non-linear properties of the foundation.

Figure 12 summarizes a comparison of the measured and calculated values for the displacement of the structure. This reveals that the method of assessing the displacement of the ground as the flow pressure is on the safe side. Consequently, this method is used to study counter measures.

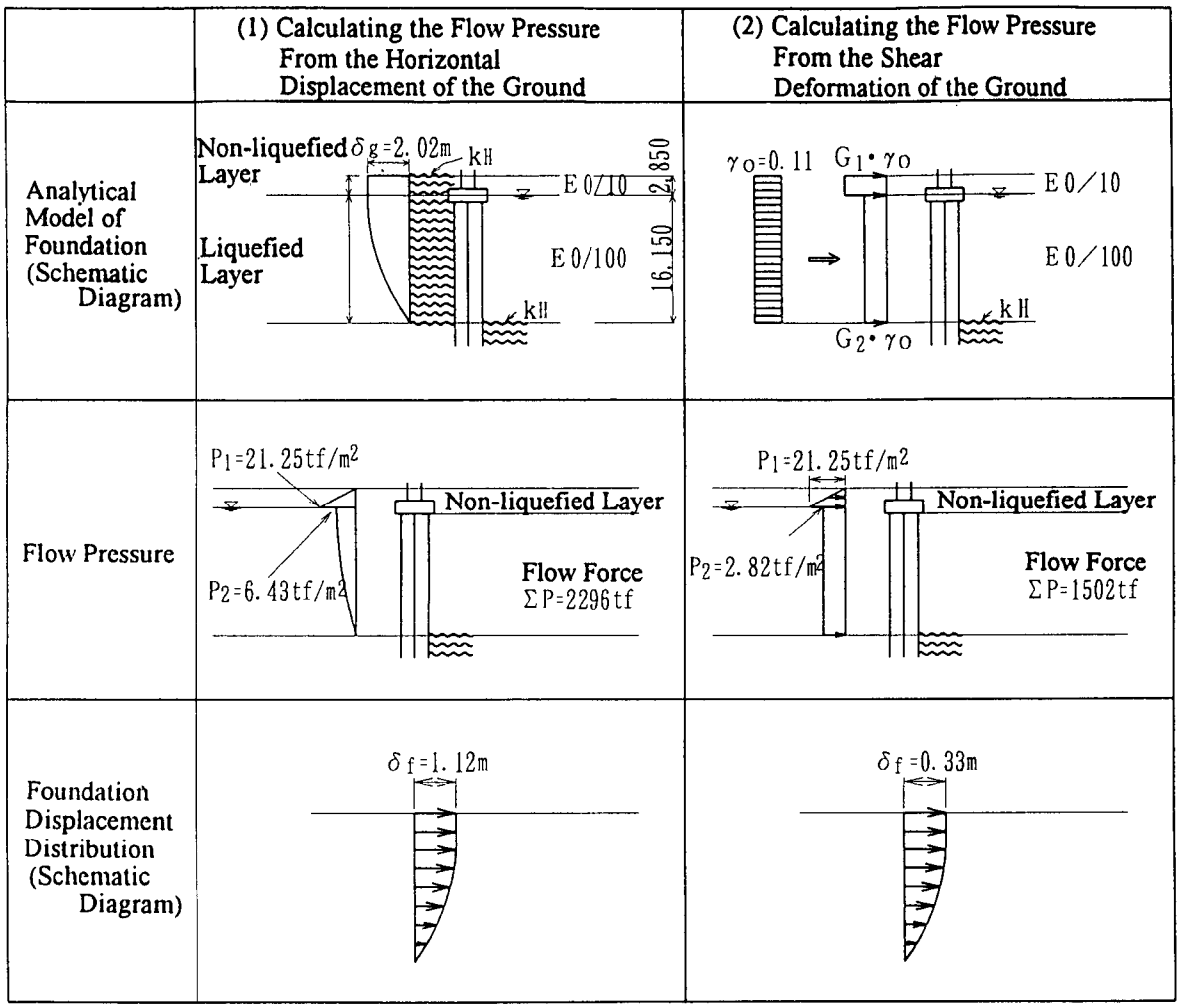

Figure 11.Comparison of Calculated Values(Uozaki Beach)

Measures to Protect Metropolitan Expressway Bridge Foundations From Ground Flow Damage

Estimation of Ground Flow Displacement Using FEM Analysis

Figure 13 is a general drawing of the structure of the bridge piers studied. Their foundations are cast-in-place concrete piles with a diameter of 1.5 m. The amount of flow of the foundation is analyzed without a structure. The revetment, which is a steel sheet-pile Type III (length: 15 m), is linked by tie rods to and supported by a steel sheet-pile Type II with a length of 5.5 m. The liquefied stratum is assumed to extend from the top surface of the footing to a depth of about 12.4 m. The modulus of deformation prior to liquefaction is shown in the

same figure. The modulus of deformation was 84 kgf/cm2 for both the non-liquefied stratum above the liquefied stratum and for the liquefied stratum, but after liquefaction, these fell to 1/10 and 1/100 respectively and FEM analysis was used to perform dead weight analysis. Figure 14 shows the depth direction distribution of the ground displacement in the mesh diagram and at various locations. At the revetment location, it is inclined towards the sea and the ground is deformed in the shape of an inverted triangle, but as the distance from the revetment increases, the deformation comes to resemble cosin distribution. At the foundation location, ground displacement of 1.69 m is forecast.

Check on the Safety of Pile Foundations

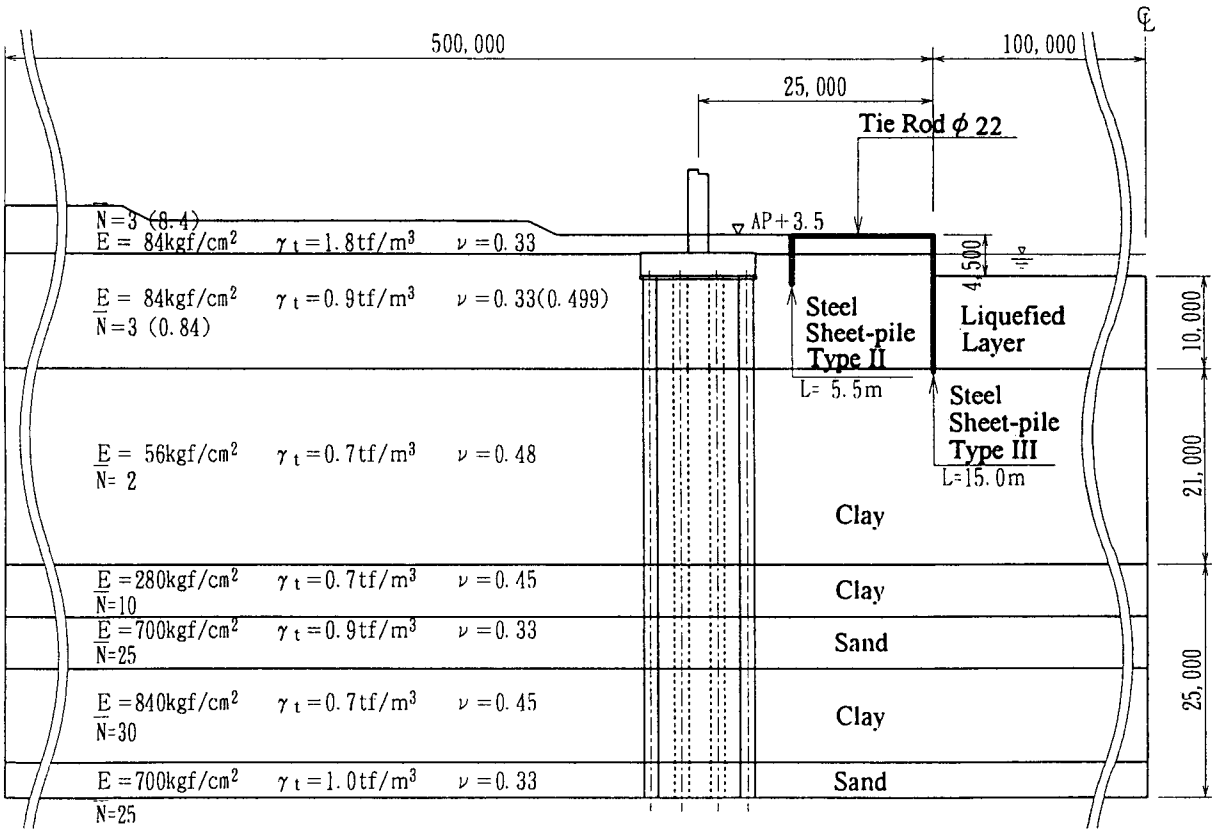

Figure 13.Model of the Ground at the Shoreline Canal

Figure 15 shows the bending moment distribution obtained by allowing the ground displacement found by means of FEM analysis to act on the structure. Based on this, it is forecast that the horizontal displacement of the foundation will be 83.1 cm and the maximum bending moment will exceed the failure moment for all piles.

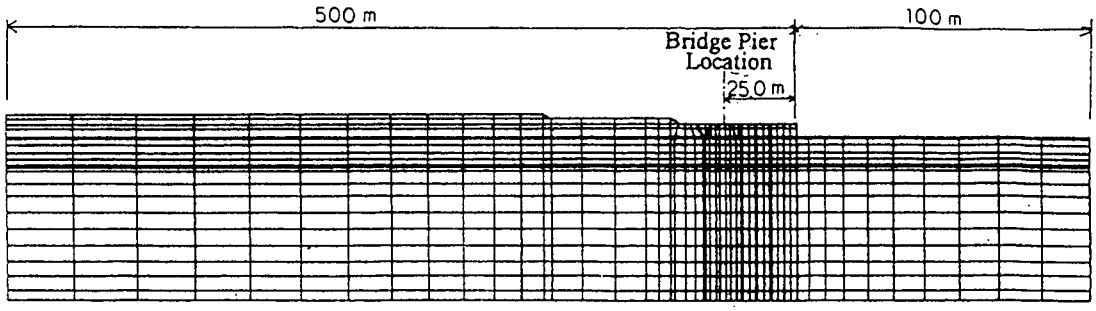

(a) Mesh Diagram

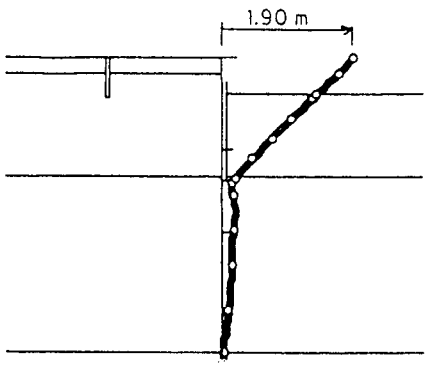

(b) Revetment Location

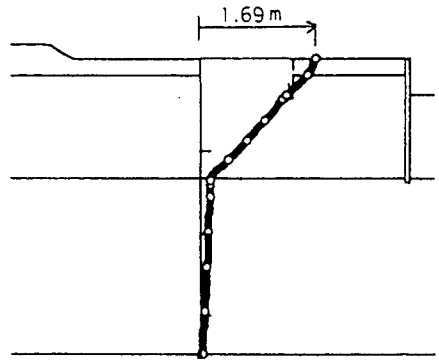

(c) Foundation Location + (25 m from Revetment)

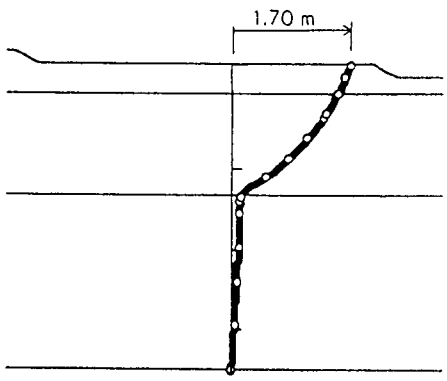

(d) Location 60 m from Revetment

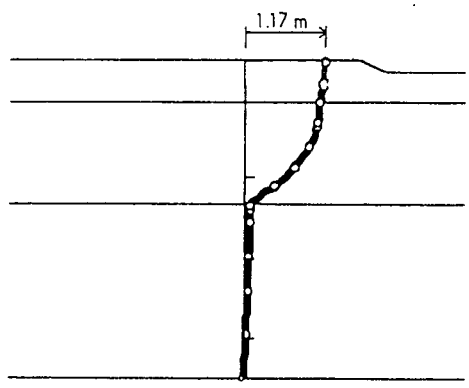

(e) Location 100 m from Revetment

Figure 14.Analytical Processing of Ground Displacement

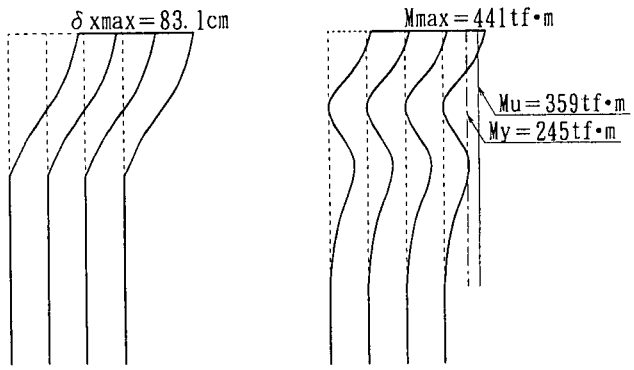

Displacement

Bending Moment

Figure 15.Results of Non-linear Analysis of Piles
(Method Considering Ground Displacement)

Design of Ground Flow Damage Protection Measures

A study was performed to propose a measure involving the installation of steel pipe sheet-piles in front of the bridge piers. Figure 16 shows the calculation model. It shows a proposed case in which the tops of the steel pipe sheet-piles are installed close to the boundary between the liquefied and non-liquefied strata. This approach was proposed because it is believed that it will permit a big reduction of the ground displacement by restricting the displacement of the liquefied stratum, and that by preventing large flow pressure in the non-liquefied stratum, it will be possible to design economic protection work. The displacement as external force which was used was the ground displacement at the foundation location. As a result, it was possible to reduce the steel pipe sheet-pile's maximum bending moment (214.8 tf-m/m) to a level below the yield bending moment (355.2 tf-m/m) by installing a row of steel pipe sheet-piles with a diameter of 1.2 m and a sheet thickness of 19 mm. In cases where it is not possible to execute the large diameter steel pipe sheet-piles adopted in this case, multiple rows of steel pipe sheet-piles which can be placed will be installed to control the deformation of the ground.

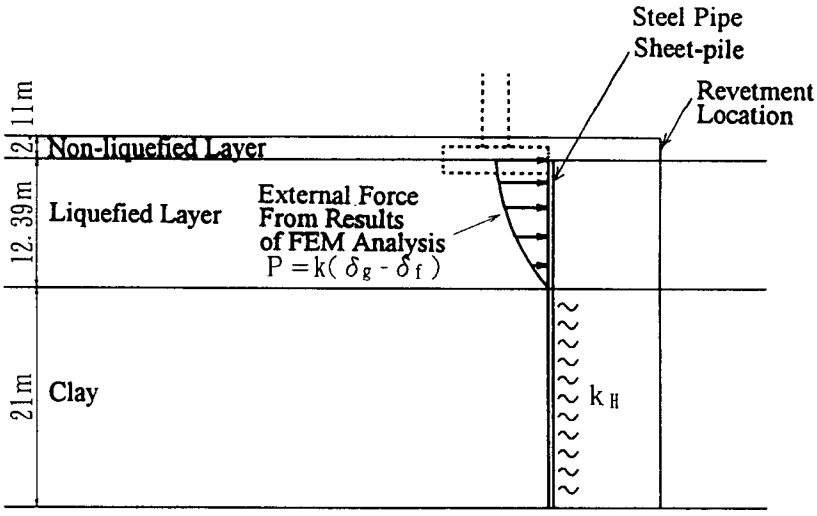

Figure 16.Effects of Sheet-pile Based on the Method Accounting for Ground Displacement(Calculation Model)

Figure 17 shows the results of FEM analysis of the displacement of the ground at the revetment location and at the foundation locations when the above steel pipe sheet-piles have been installed. The foundation location sharply to 0.34 m. Figure 18 shows the results of an analysis of the action of this displacement on a bridge pier foundation as an external force. As this figure shows, the displacement of the foundation is cut from 83.1 cm to 3.8 cm and the maximum bending moment is lower than the yield bending moment, confirming that the safety of the structure is guaranteed by this measure.

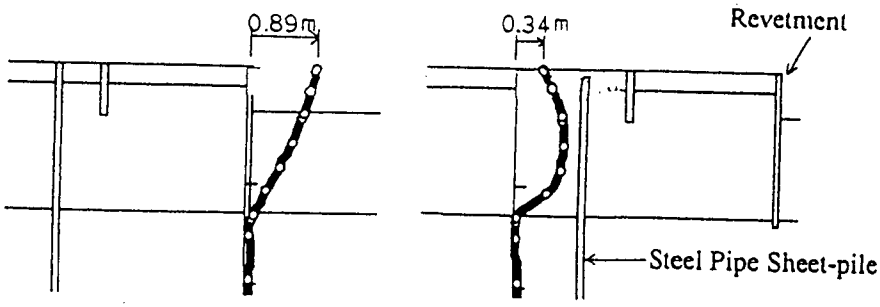

(a) Revetment Location (b) Foundation Location

Figure 17.Displacement of the Ground After Installation of yhe Protective Work

Acknowledgements

This report is a summary of details of deliberations now being conducted by the Survey and Research Committee On the Effect of Ground Flow on Viaducts (Committee Chairman: Shioi Yukitaka, Professor at Hachinohe Institute of Technology) at the Technology Research Center for National Land Development. The authors wish to express their gratitude to all the members of the committee for their work.

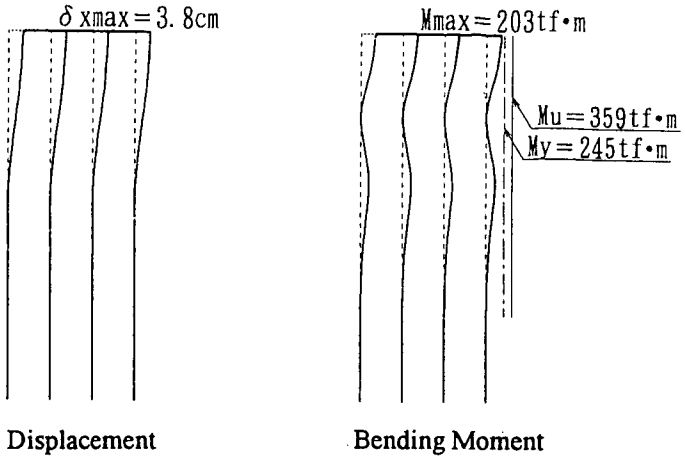

Figure 18.Results of Non-linear Analysis of Piles (After Protective Work)

References

1) Hyogo-ken Nanbu Earthquake Road Bridge Earthquake Damage Counter-measures Committee (1995): Report on a Survey of Damage to Road Bridges by the Hyogo-ken Nanbu Earthquake, pp 55.

2) Ishihara,K.(1995): Soil Properties and Ground Deformation, Report on Hanshin Earthquake, The Japanease Geotechnical Society.

3) Yasuda,S. Masuda,S. Nagase,H. Oda,S. (1994): Dynamic Modulus of Deformation in Undisturbed Material Taken Continuously in the Depth Direction, 9th Japan Earthquake Engineering Symposium, pp. 835 - 840.

4) Kiku,H. Yasuda,S. Masuda,T. Itafuji,S. Mine,K. (1994): Torsional Shear Testing of the Strength and Deformation of Liquefied Sand, 9th Japan Earthquake Engineering Symposium, pp. 871 - 876.

MENSHIN DESIGN FOR HIGHWAY BRIDGES

Kazuhiko KAWASHIMA[1] and Shigeki UNJOH[2]

1) Professor, Department of Civil Engineering Tokyo Institute of Technology, O-okayama, Meguroku, Tokyo, 152, Japan
2) Head, Earthquake Engineering Division, Public Works Research Institute, Ministry of Construction, Tsukuba Science City, Ibaraki-ken, 305, Japan

ABSTRACT

This paper describes the Menshin design (seismic isolation) of highway bridges in Japan. The Menshin design has been extensively used in design of highway bridges since the 1995 Hyogo-ken Nanbu earthquake. It was included in the new "Part V Seismic Design" of the "Design Specifications of Highway Bridges" in 1996. This paper describes the outline of the Menshin design method as well as a background of the introduction of the Menshin design into the new design specifications.
KEY WORDS : Seismic Isolation, Menshin Design, Highway Bridges, Seismic Design

INTRODUCTION

Various technical developments have been conducted for long time to reduce bridge response during an earthquake[1)2)10)12)23)25)]. A first attempt in Japan was the use of viscous dampers which were installed between a deck and piers. Viscous dampers were often adopted in 1970s, but because temperature effect was predominant at those days, they were used as the damper stoppers. Other type of devices such as SU-damper, PC cable spring tapered plate-spring and link have been effectively adopted for bridges from short and medium span to long span bridges [10)].

The seismic isolation has been incorporated since late 1980s in highway bridges in Japan. Various analyses have been conducted for the effectiveness of the seismic isolation. The first design manual was issued in a form of the "Guidelines for Base Isolation Design of Highway Bridges" in 1989 as a final accomplishment of a 3-year research program[10)]. It has been recognized through such studies that the elongation of natural period causes various disadvantage in an application to the highway bridges.

One of the most significant problems is the large clearance required between a deck and an abutment or between two adjacent decks so that the deck can move with an amount of design displacement of isolators and dampers. This could be in the range of 300- 600 mm during the Hyogo-ken Nanbu type earthquakes, whereas the clearance is generally about 50 - 100 mm in the conventional design. The large clearance at expansion join[s increases noise and

vibration pollution, and increases maintenance due to heavy traffic. Although the knock-off abutment was studied through experiments and analysis, it was found not easy to shear-off the upper part of an abutment in the back-fill side because of a resistance of pavement and back-fills[4]. Anchor bolts required, against heavy traffic load, to tie down the upper part of the knock-off abutment to the lower part is also problem for smooth shear-off.

From such reasons, it is preferable not to increase natural period for aiming to decrease the seismic force, but to put an emphasis on an increase of energy dissipation and a distribution of lateral force of a deck to as many substructures as possible. It may be effective to adjust natural period of a bridge so as to avoid the resonance with ground motion.

Such design concept was more clearly formulated as "Menshin design" in a 3-year joint research program between the Public Works Research Institute and 28 companies from 1989 to 1992. From a study for favorable application of the seismic isolation, it was found that the menshin design is effective to construct super-multi-span continuous bridges with deck length over 1 km[3]. Also studied was an application of the menshin design for the seismic retrofit of existing bridges. Use of isolators and dampers was found effective to connect existing simply supported bridges so that they behave as a continuous bridge against traffic loads[28]. In the program, not only the menshin design method but also various devices such as high damping laminated rubber bearings[26], sliding friction bearings[6], unseating prevention devices[22], and a finger expansion joint movable not only in longitudinal direction but in transverse direction[22] were developed. Requirements for menshin devices in static and dynamic behavior and approving test procedures were also proposed[13][14]. Including those technical developments, the "Manual for Menshin Design of Highway Bridges" was issued by the Public Works Research Institute in 1992[11][24].

Based on the Guidelines and the Menshin Manual, a pilot program to construct several Menshin bridges was initiated in 1989 in the Ministry of Construction. A working group was formulated in the Ministry of Construction to supervise the design and construction. Miyagawa bridge, three-span continuos plate girder bridge with a deck length of 105 m, was completed in 1992 as the first Menshin bridge in the program[19].

During the ready increase of implementation of the Menshin design, Hyogo-ken Nanbu earthquake occurred in January 1995 to cause destructive damage to various structures. Highway bridges also suffered destructive damage. Importance to increase ductility of structural components and redundancy of bridges was strongly recognized from the damage[16][20]. When the "Guide Specifications for Reconstruction and Repair of Highway Bridges which Suffered Damage due to the Hyogo-ken Nanbu Earthquake" was issued by the Ministry of Construction on February 27, 1995[21], it was described in the Guide Specifications that the Menshin design should be more actively used to mitigate shocks and reduce lateral force by increasing energy dissipation. It was suggested in the Guide Specifications that the Menshin Manual should be referred to in design of the Menshin

bridges. It was also recommended in the Guide Specifications that the laminated rubber bearings, in particular Menshin bearings should be more used in stead of steel bearing vulnerable to seismic disturbance. It had been recognized for long time that laminated rubber bearings are superior to steel bearings from maintenance and corrosion point of view. Lead rubber bearings (LRBs) and high damping rubber bearings (HDRs) were suggested in the Guide Specifications.

Subsequently in May 1995, it was decided by the Ministry of Construction that the Guide Specifications should be referred to in seismic design of all new bridges and seismic retrofit of existing bridges in the country as an emergency measure until the Design Specifications of Highway Bridges was revised. Based on such a background, LRB and HDR have been increasingly used since the Hyogo-ken Nanbu earthquake. Not only in the Menshin bridges but also in the bridges where tall laminated rubber bearings are required to distribute the lateral force of a superstructure to substructures, LRB and HDR have been used Although statistical data are not available at this moment, majority of highway bridges use the laminated rubber bearings, LRB and HDR.

The "Design Specifications of Highway Bridges" was revised in November 1996[7]. There were various major revisions. The first was the introduction of thorough check of lateral capacity for all structural components in which seismic effect is predominant. Although the lateral capacity had teen checked since 1990 (1990 Design Specifications), it was not mandatory, and had been used only for reinforced concrete piers. Furthermore, because it was not a design method but a "check", it had been effective only to increase the sections and reinforcements, if required, which were designed by the Seismic Coefficient Method. In the 1996 Specifications, the "check of lateral capacity" was upgraded to a seismic design method called as "Lateral Capacity Method" which has the equal importance with the Seismic Coefficient Method. It has been used for not only reinforced concrete piers but all structural components where seismic effect is predominant. The second was the introduction of the ground motions induced during the Hyogo-ken Nanbu earthquake as a Type-II design force. The third was the introduction of menshin design. Main part of the Menshin Manual was included in the 1996 Specifications as Chapter 8 in the "Part V Seismic Design."

This paper introduces the Menshin design which was included in the new "Part V Seismic Design" of the "1996 Design Specifications of Highway Bridges."

SEISMIC PERFORMANCE LEVEL

Table 1 shows a classification of the seismic performance levels and design methods The badges are categorized into two groups depending on their importance; standard bridges (Type-A bridges) and important bridges (Type-B bridges). Seismic performance levels depends on the importance of bridges. For moderate ground motions induced by earthquakes with high probability to occur, both A and B bridges should behave in an elastic manner

without any essential structural damage. For extreme ground motions induced by earthquakes with low probability to occur, the Type-A bridges should prevent critical failure, while the Type-B bridges should perform with limited damage .

In the Lateral Capacity Method, two types of ground motions most be considered. The first is the ground motions which could be induced by plate boundary earthquakes with magnitude of about 8 at a distance of about 50 km from the faults. Ground motions which developed at Tokyo during the 1923 Kanto earthquake are a typical of this type of ground motions. The second is the ground motions developed by earthquakes with magnitude of about 7-7.2 at very short distances. Obviously the ground motions developed at Kobe during the Hyogo-ken Nanbu earthquake are typical target of this type of ground motions. The first and the second ground motions are caned as Type-I and Type-II ground motions, respectively. The recurrence time of the Type-II ground motion is much longer that that of the Type-I ground motion.

Table 1 Seismic Performance Levels

<table>
<tr><td colspan="2" rowspan="2">Type of Design Ground Motions</td><td colspan="2">Importance of Bridges</td><td colspan="2">Design Methods</td></tr>
<tr><td>Type-A (Standard Bridges)</td><td>Type-B (Important Bridges)</td><td>Equivalent Static Lateral Force Methods</td><td>Dynamic Analysis</td></tr>
<tr><td colspan="2">Ground Motions with High Probability to Occur</td><td colspan="2">Prevent Damage</td><td>Seismic Coefficient Method</td><td rowspan="3">Step by Step Analysis or Response Spectrum Analysis</td></tr>
<tr><td rowspan="2">Ground Motions with Low Probability to Occur</td><td>Type-I (Plate Boundary Earthquakes)</td><td rowspan="2">Prevent Critical Damage</td><td rowspan="2">Limited Damage</td><td rowspan="2">Lateral Capacity Method</td></tr>
<tr><td>Type-II (Inland Earthquakes)</td></tr>
</table>

Lateral force coefficient k_{hc} in the Lateral Capacity Method is given as

$$k_{hc} = c_z \cdot k_{hc0} \tag{1}$$

in which c_z = modification coefficient for zone, and is 0.7, 0.85 and 1.0 depending on zone, and k_{hc0} = standard modification coefficient. **Table 2** and **Fig.1** show the standard lateral force coefficients k_{hc0} for the Type-I and the Type-II ground motions. The Type-I ground motions have been used since 1990 (1990 Specifications), while the Type-II ground motions were newly introduced in the 1996 Specifications. It should be noted here that the k_{hc0} at stiff site (Group I) has been always assumed smaller than the k_{hc0} at moderate (Group II) and soft soil (Group III) sites in the Type-I ground motions as well as the seismic coefficients used for the Seismic Coefficient Method. The Type-I ground motions were essentially estimated from an attenuation equation for response spectra [8]. Although the response spectral accelerations at short natural period are generally larger at stiff sites that at soft soil sites, the

tendency has not been explicitly included in the past. This is because damage has been more developed at soft sites than at stiff sites. To consider this fact, the design force at stiff sites has been always assumed smaller than that at soft sites even at short natural period. However without such a traditional consideration, the Type-II ground motions were determined by simply taking envelops of response accelerations of major strong motions recorded at Kobe during the Hyogo-ken Nanbu earthquake. It was considered appropriate to set realistic ground motions.

The acceleration response spectral intensity at short natural period is higher in the Type-II ground motions than in the Type-I ground motions. However, the duration of extreme accelerations is much longer in the Type-I ground motions than the Type-n ground motions. The duration was only 8-10 seconds in the strong motions recorded at Kobe during the Hyogo-ken Nanbu earthquake. As Will be described later, such a difference of the duration is taken into account to evaluate the ductility factor of a pier.

Table 2 Lateral Force Coefficient k_{hco} in the Lateral Capacity Method

(a) Type-I Ground Motions

Soil Condition	Lateral Force Coefficient k_{hc0}		
Group I (stiff)	$k_{hc0}=0.7$ for $T \leqq 1.4$		$k_{hc0}=0.876T^{-2/3}$ for $T > 1.4$
Group II (moderate)	$k_{hc0}=1.51T^{1/3}$ ($k_{hc0} \geqq 0.7$) for $T < 0.18$	$k_{hc0}=0.85$ for $0.18 \leqq T \leqq 1.6$	$k_{hc0}=1.16T^{-2/3}$ for $T > 1.6$
Group III (soft)	$k_{hc0}=1.51T^{1/3}$ ($k_{hc0} \geqq 0.7$) for $T < 0.29$	$k_{hc0}=1.0$ for $0.29 \leqq T \leqq 2.0$	$k_{hc0}=1.59T^{-2/3}$ for $T > 2.0$

(b) Type-II Ground Motions

Soil Condition	Lateral Force Coefficient k_{hc0}		
Group I (stiff)	$k_{hc0}=4.46T^{2/3}$ for $T \leqq 0.3$	$k_{hc0}=2.00$ for $0.3 \leqq T \leqq 0.7$	$k_{hc0}=1.24T^{-4/3}$ for $T > 0.7$
Group II (moderate)	$k_{hc0}=3.22T^{2/3}$ for $T < 0.4$	$k_{hc0}=1.75$ for $0.4 \leqq T \leqq 1.2$	$k_{hc0}=2.23T^{-4/3}$ for $T > 1.2$
Group III (soft)	$k_{hc0}=2.38T^{2/3}$ for $T < 0.5$	$k_{hc0}=1.50$ for $0.5 \leqq T \leqq 1.5$	$k_{hc0}=2.57T^{-4/3}$ for $T > 1.5$

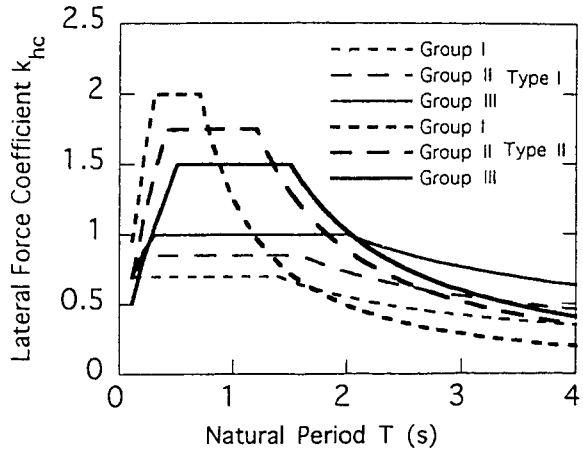

Fig.1 Type I and Type II Ground Motions for the Lateral Capacity Method

BASIC PRINCIPLE OF MENSHIN DESIGN

Implementation of the Menshin bridges should be carefully decided from not only seismic performance but function for traffic and maintenance point of view, based on the advantage and disadvantage of increasing natural period The Menshin design should not be adopted at the following conditions;

(a) sites vulnerable to lose bearing capacity due to the soil liquefaction and the lateral spreading
(b) bridges supported by flexible columns
(c) soft soil sites where potential resonance with surrounding soils could be developed by increasing the fundamental natural period
(d) bridges with uplift force at bearings

It is suggested that the design should be made with an emphasis on an increase of energy dissipating capability and a distribution of lateral force to as many substructures as possible. To concentrate the hysteretic deformation at not piers but bearings, the fundamental natural period of a Menshin bridge should be about 2 times or longer than the fundamental natural period of the same bridge supported by the conventional bearings. It should be noted that an elongation of natural period aiming to decrease the lateral force should not be attempted.

Simple devices stable against extreme earthquakes have to be used. The bearings have to be anchored to a deck and substructures with bolts, and should be replaceable. The clearance has to be provided between a deck and substructures or between two adjacent decks.

MENSHIN DESIGN AND DESIGN FORCE

IDEALIZATION

In the Menshin design, the bridges are first designed by the standard equivalent linear static

design method. Then seismic safety of the static design is precisely evaluated by a dynamic response analysis. Menshin devices are generally idealized by a set of equivalent linear springs in the equivalent static analyses while they are idealized by either the equivalent linear springs or nonlinear hysteretic springs in the dynamic response analysis. Equivalent stiffness and equivalent damping ratio of isolator and dampers are the key parameters in the equivalent linear analysis.

In the equivalent static analysis, natural period T of a menshin bridge is evaluated following the standard procedure as

$$T = 2.01\sqrt{\delta} \tag{2}$$

$$\delta = \frac{\Sigma\, w_i \cdot u_i^2}{\Sigma\, w_i \cdot u_i} \tag{3}$$

in which w_i = dead weight per unit length of a bridge at i-th point and u_i = lateral displacement developed at i-th point by subjecting to a lateral force equivalent to the dead weight in a desired direction.

Modal damping ratio of a menshin bridge h for the fundamental mode is computed as[15)]

$$h = \frac{\Sigma\, K_{Bi} \cdot u_{Bi}^2 \left(h_{Bi} + \frac{h_{Pi} \cdot K_{Bi}}{K_{Pi}} + \frac{h_{Fui} \cdot K_{Bi}}{K_{Fui}} + \frac{h_{F\theta i} \cdot K_{Bi} \cdot H^2}{K_{F\theta i}}\right)}{\Sigma\, K_{Bi} \cdot u_{Bi}^2 \left(1 + \frac{K_{Bi}}{K_{Pi}} + \frac{K_{Bi}}{K_{Fui}} + \frac{K_{Bi} \cdot H^2}{K_{F\theta i}}\right)} \tag{4}$$

in which h_{Bi} = damping ratio of i-th damper, h_{Pi} = damping ratio of i-th pier or abutment, h_{Fui} = damping ratio of i-th foundation associated with translational displacement, $h_{\theta i}$ = damping ratio of i-th foundation associated with rotational displacement, K_{Pi} = equivalent stiffness of i-th pier or abutment, K_{Fui} = translational stiffness of i-th foundation, $K_{F\theta i}$ = rotational stiffness of i-th foundation, u_{Bi} = design displacement of i-th Menshin device, and H = distance from a bottom of pier to a gravity center of a deck.

A bridge may be divided into several sub-structures in which energy. dissipating mechanism can be assumed essentially the same. If one can specify a damping ratio of each sub-structure for a given mode shape, the modal damping ratio for i-th mode may be evaluated as

$$h_i = \frac{\sum_{j=1}^{n} h_j \{\phi_{ij}\}^T [K_j] \{\phi_{ij}\}}{\{\Phi_i\}^T [K] \{\Phi_i\}} \tag{5}$$

in which h_i = damping ratio of j-th substructure in i-th mode, ϕ_{ij} = mode vector of j-th substructure in i-th mode, k_j = stiffness matrix of j-th substructure, K= stiffness matrix of a bridge, and Φ_i = mode vector of a bridge in i-th mode, and is given as

$$\Phi_i^T = \{\phi_{i1}^T, \phi_{i2}^T, \cdots\cdots\cdots, \phi_{in}^T\} \tag{6}$$

Table 3 shows recommended damping ratios for major structural components.

Table 3 Recommended Damping Ratios for Major Structural Components in a Menshin Bridge

Structural Components	Elastic Response		Nonlinear Response	
	Steel	Concrete	Steel	Concrete
Superstructure	0.02 ~ 0.03	0.03 ~ 0.05	0.02 ~ 0.03	0.03 ~ 0.05
Rubber Bearings	0.02		0.02	
Menshin Bearings	Equivalent Damping Ratio by Eq.(26)		Equivalent Damping Ratio by Eq.(26)	
Substructures	0.03 ~ 0.05	0.05 ~ 0.1	0.1 ~ 0.2	0.12 ~ 0.2
Foundations	0.1 ~ 0.3		0.2 ~ 0.4	

DESIGN FORCE

Menshin bridges are designed by both the Seismic Coefficient Method and the Lateral Capacity Method. In the Seismic Coefficient Method, a lateral force coefficient ranging from 0.2 to 0.3 has been used based on the allowable stress design approach.

In the Lateral Capacity Method the equivalent lateral force coefficient k_{hem} in the Menshin design is evaluated as

$$k_{hem} = \frac{k_{hcm}}{\sqrt{2\mu_m - 1}} \tag{7}$$

$$k_{hcm} = c_E \cdot k_{hc} \tag{8}$$

in which k_{hcm} = lateral force coefficient in menshin design, μ_m = allowable ductility factor of a pier, c_E = modification coefficient for energy dissipating capability (refer to **Table 4**), and k_{hc} = lateral force coefficient by Eq.(1).

Because the k_{hc} is the lateral force coefficient for a bridge supported by the conventional bearings, Eq.(8) means that the lateral force in the Menshin design can be reduced, as large as 30 %, by the modification coefficient c_E depending on the modal damping ratio of a bridge.

Table 4 Modification Coefficient for Energy Dissipation Capability

Damping Ratio for 1st Mode h	Coefficient c_E
$h < 0.1$	1.0
$0.1 \leqq h < 0.12$	0.9
$0.12 \leqq h < 0.15$	0.8
$h \geqq 0.15$	0.7

It is important to note here that the allowable ductility factor μ_m in Eh. (7) depends on the type of ground motions and that μ_m is smaller than the allowable ductility factor μ_a in the conventional design evaluated as[1]

$$\mu_a = 1 + \frac{\delta_u - \delta_y}{\alpha \delta_y} \tag{9}$$

in which α = safety factor, δ_y = yield displacement of a pier, and δ_u = ultimate displacement of a pier. In Eq.(9), the ultimate displacement δ_u is evaluated as

$$\delta_u = \delta_y + (\phi_u - \phi_y) L_p(h - L_p/2) \tag{10}$$

in which ϕ_y = yield curvature of a pier at bottom, ϕ_u = ultimate curvature of a pier at bottom, h = height of a pier, and L_p = plastic hinge length of a pier. The plastic hinge length is given as

$$L_p = 0.2h - 0.1D \quad (0.1D \leqq L_p \leqq 0.5D) \tag{11}$$

in which D is a width or a diameter of a pier.

The yield curvature ϕ_y and ultimate curvature ϕ_u in Eq.(10) are evaluated assuming a stress-strain relation of reinforcements and concrete as shown in **Fig.2**. The stress σ_c - strain ε_c relation of concrete is assumed as[5]

$$\sigma_c = \begin{cases} E_c \varepsilon_c \{1 - \frac{1}{n} (\frac{\varepsilon_c}{\varepsilon_{cc}})^{n-1}\} & (0 \leqq \varepsilon_c \leqq \varepsilon_{cc}) \\ \sigma_{cc} - E_{des}(\varepsilon_c - \varepsilon_{cc}) & (\varepsilon_{cc} < \varepsilon_c \leqq \varepsilon_{cu}) \end{cases} \tag{12}$$

$$n = \frac{E_c \varepsilon_{cc}}{E_c \varepsilon_{cc} - \sigma_{cc}} \tag{13}$$

in which σ_{cc} = strength of confined concrete, E_c = elastic modules of concrete, ε_{cc} = strain at maximum strength, and E_{des} = gradient at descending branch. In Eq.(12), σ_{cc}, ε_{cc} and E_{des} are determined as

$$\sigma_{cc} = \sigma_{ck} + 3.8 \alpha \rho_s \sigma_{sy} \tag{14}$$

$$\varepsilon_{cc} = 0.002 + 0.033 \beta \frac{\rho_s \sigma_{sy}}{\sigma_{ck}} \tag{15}$$

$$E_{des} = 11.2 \frac{\sigma_{ck}^2}{\rho_s \sigma_{sy}} \tag{16}$$

in which σ_{ck} = design strength of concrete, σ_{sy} = yield strength of reinforcements, α and β = coefficients depending on shape of pier (α =1.0 and β =1.0 for a circular pier, and α = 0.2 and β = 0.4 for a rectangular pier), and ρ_s = tie reinforcement ratio defined as

$$\rho_s = \frac{4A_h}{sd} \leqq 0.018 \tag{17}$$

in which A_h = area of tie reinforcements, s = space of tie reinforcements, and d = effective with of tie reinforcements.

The ultimate curvature ϕ_u is defined as a curvature when concrete strain at longitudinal reinforcing bars in compression reaches an ultimate strain ε_{cu} defined as

$$\varepsilon_{cu} = \begin{cases} \varepsilon_{cc} & \text{for Type I ground motions} \\ \varepsilon_{cc} + \frac{0.2 \sigma_{cc}}{E_{des}} & \text{for Type II ground motions} \end{cases} \tag{18}$$

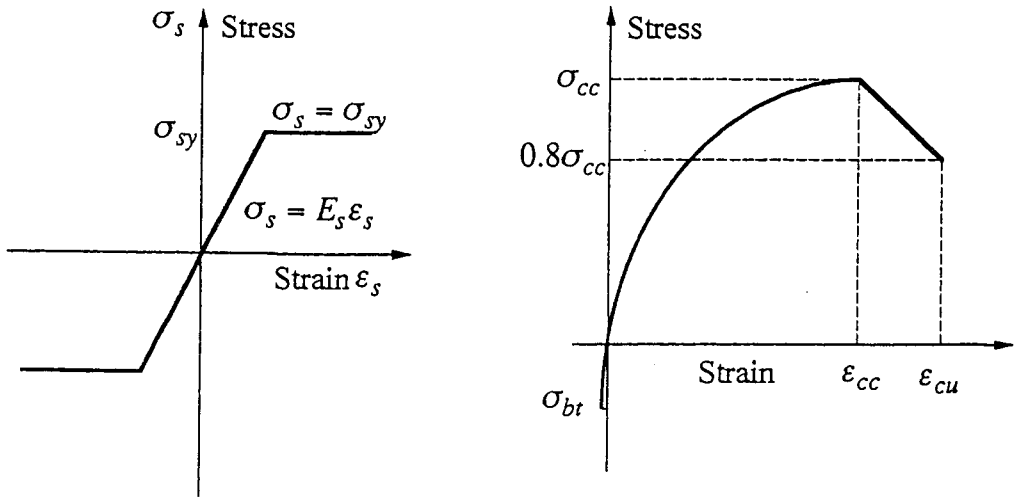

(a) Steel (b) Concrete

Fig.2 Stress and Strain Relation of Confined Concrete and Reinforcing Bars

It is important to note here that the ultimate strain ε_{cu} depends on the types of ground motions; the ε_{cu} for the Type-II ground motions is larger than that for the Type-I ground motions. Based on a loading test, it is known that a certain level of failure in a pier such as a sudden decrease of lateral capacity occurs at smaller lateral displacement in a pier subjected to a loading hysteresis with more number of load reversals[9)27)]. To reflect such a fact, it was decided that the ultimate strain ε_{cu} should be evaluated by Eq.(18), depending on the type of ground motions. Thus, the allowable ductility factor μ_a depends on the type of ground motions; the μ_a is larger in a pier subjected to the Type-II ground motions than a pier subjected to the Type-I ground motions.

It should be noted that the safety factor α in Eq.(9) also depends on the type of bridges as well as the type of ground motions as shown in **Table 5**. This is to preserve higher seismic safety in the important bridges, and to take account of the difference of recurrent time between the Type-I and the Type-II ground motions.

Table 5 Safety Factor α in Eq.(9)

Type of Bridges	Type-I Ground Motions	Type-II Ground Motions
Type-B	3.0	1.5
Type-A	2.4	1.2

On the other hand, in the Menshin design, the allowable ductility factor of a pier μ_m in Eq. (7) is evaluated b y

$$\mu_m = 1 + \frac{\delta_u - \delta_y}{\alpha_m \delta_y} \tag{19}$$

in which α_m is a safety factor used in Menshin design, and is given as

$$\mu_m = 2\alpha \tag{20}$$

Eq.(20) means that the allowable ductility factor in the Menshin design μ_m should be smaller than the allowable ductility factor μ_a by Eq.(9) in the conventional design. The purpose to use smaller allowable ductility factor in the Menshin design is to make the nonlinear hysteretic behavior of a pier at the plastic hinge zone as small as possible.

DYNAMIC RESPONSE ANALYSIS

Dynamic response analysis is required in the Menshin design to verify seismic safety of the static design. In dynamic response analysis, ground motions which are spectral fitted to the following response spectra are used;

$$S_I = c_Z \cdot c_D \cdot S_{I0} \tag{21}$$

$$S_{II} = c_Z \cdot c_D \cdot S_{II0} \tag{22}$$

in which S_I = acceleration response spectrum for Type-I ground motions, S_{II} = acceleration response spectrum for Type-II ground motions, S_{I0} = standard acceleration response spectrum for Type-I ground motions, S_{II0} = standard acceleration response spectrum for Type-II ground motions, c_Z = modification coefficient for zone (refer to Eq.(1)), and c_D = modification coefficient for damping ratio given as

$$c_D = \frac{1.5}{40h_i + 1} + 0.5 \tag{23}$$

Table 6 and **Fig.3** show the standard acceleration response spectra (damping ratio h=0.05) for the Type-I and Type-II ground motions.

It is recommended to use at least three ground motions per analysis, and take an average, considering the validity of the analysis, to evaluate the response.

DESIGN OF MENSHIN DEVICES

The bearings are classified into two groups. The first is the bearings which resist the seismic force of Eq.(7). The second is the bearings which resist the seismic force considered in the Seismic Coefficient Method. The first and the second bearings are called as the Type-B bearings and the Type-A bearings, respectively. Seismic performance of the Type-B bearings is, of course, much higher than the Type-A bearings. In the Type-A bearings, a displacement limiting device, which will be described later, has to be co-installed in both longitudinal and transverse directions, while it is not required in the Type-B bearings. Because of the importance of bearings as one of the main structural components, the Type-B bearings should be used in the Menshin bridges.

Isolators and dampers must be designed for a desired design displacement u_B. The design displacement u_B is evaluated as

Table 6 Standard Acceleration Response Spectra

(a) Type-I Response Spectra S_{I0}

Soil Condition	Response Acceleration S_{I0} (gal=cm/sec^2)		
Group I	$S_{I0}=700$ for $T_i \leqq 1.4$	$S_{I0}=980/T_i$ for $T_i > 1.4$	
Group II	$S_{I0}=1{,}505T_i^{1/3}$ ($S_{I0} \geqq 700$) for $T_i < 0.18$	$S_{I0}=850$ for $0.18 \leqq T_i \leqq 1.6$	$S_{I0}=1{,}360/T_i$ for $T_i > 1.6$
Group III	$S_{I0}=1{,}511T_i^{1/3}$ ($S_{I0} \geqq 700$) for $T_i < 0.29$	$S_{I0}=1{,}000$ for $0.29 \leqq T_i \leqq 2.0$	$S_{I0}=2{,}000/T_i$ for $T_i > 2.0$

(b) Type-II Response Spectra S_{II0}

Soil Condition	Response Acceleration S_{II0} (gal=cm/sec^2)		
Group I	$S_{II0}=4{,}463T_i^{2/3}$ for $T_i \leqq 0.3$	$S_{II0}=2{,}000$ for $0.3 \leqq T_i \leqq 0.7$	$S_{II0}=1{,}104/T_i^{5/3}$ for $T_i > 0.7$
Group II	$S_{II0}=3{,}224T_i^{2/3}$ for $T_i < 0.4$	$S_{II0}=1{,}750$ for $0.4 \leqq T_i \leqq 1.2$	$S_{II0}=2{,}371/T_i^{5/3}$ for $T_i > 1.2$
Group III	$S_{II0}=2{,}381T_i^{2/3}$ for $T_i < 0.5$	$S_{II0}=1{,}500$ for $0.5 \leqq T_i \leqq 1.5$	$S_{II0}=2{,}948/T_i^{5/3}$ for $T_i > 1.5$

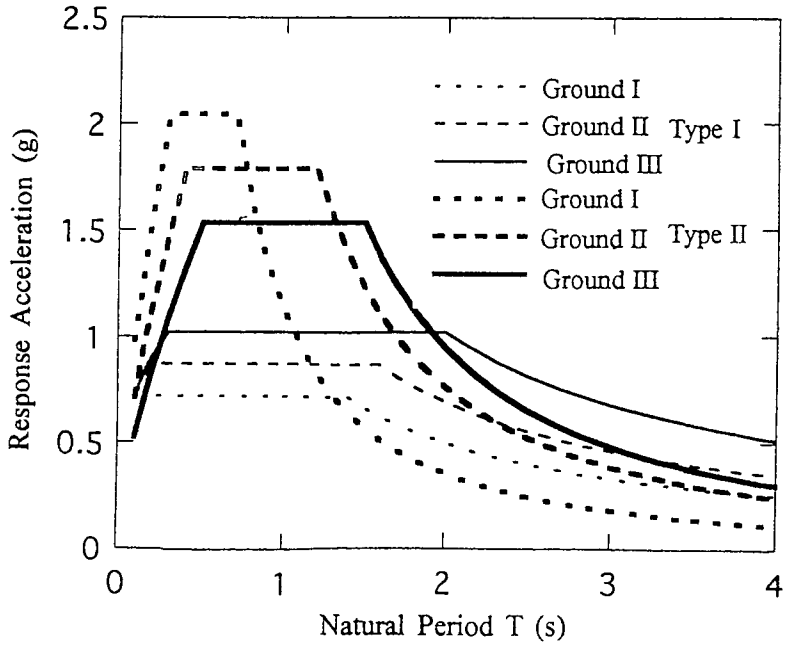

Fig.3 Response Acceleration Spectra (h=0.05) for Type I and Type II Ground Motions

$$u_B = \frac{k_{hem} \cdot W_u}{K_B} \tag{24}$$

in which k_{hem} = equivalent lateral force coefficient by Eq.(7), K_B = equivalent stiffness, and W_u = dead weight of a superstructure. It should be noted that because the equivalent lateral force coefficient k_{hem} depends on the type of ground motions, the design displacement u_B also depends on it.

The equivalent stiffness K_B and equivalent damping ratio h_B of a Menshin device are evaluated as

$$K_B = \frac{F(u_{Be}) - F(-u_{Be})}{2u_{Be}} \tag{25}$$

$$h_B = \frac{\Delta W}{2\pi W} \tag{26}$$

$$u_{Be} = c_B \cdot u_B \tag{27}$$

in which F(u) = restoring force of a device at a displacement u , u_{Be} = effective design displacement, ΔW = energy dissipated per cycle, W = elastic strain energy, and c_B = coefficient to evaluate effective displacement (=0.7).

In design of devices, the following requirements have to be satisfied:

1) The displacement computed by Eq.(24) should be within ± 10% from the assumed design displacement us, and the equivalent damping ratio evaluated by Eq.(26) should not be less that the equivalent damping ratio assumed in design.
2) Shear strain induced in a laminated rubber bearing γ subjected to a lateral force equivalent the equivalent lateral force coefficient k_{hem} by Eq.(7) are evaluated as

$$\gamma = \frac{u_B}{\sum_{i=1}^{n} t_{ei}} \tag{28}$$

in which u_B = design displacement of a rubber bearing by Eq.(24), t_{ei} = thickness of i-th rubber, and n = number of layers of rubber. The shear strain by Eq.(28) should be less than 250 %.

3) Local shear strain should be less than the rupture strain divided by a safety factor of 1.2. Recommended rupture strains are presented in **Table 7**.

Table 7 Recommended Rupture Strain of Rubber

Type of Rubbers	Shear Modulus G (N/mm^2)	Rupture Strain (%)
Natural Rubbers	80	500
	100	
	120	400
Chloroplane Rubbers	80	
	100	

4) The devices have to be designed and fabricated so that scatter of the equivalent stiffness K_B and the equivalent damping ratio h_B be within $\pm$ 10% of the design values.
5) The devices have to be stable against at least 50 and 15 load reversals, for the Type-I and Type-II ground motions, respectively, with the design displacement by Eq.(24) under a vertical force equivalent to the dead weight of a superstructure.
6) Tangential stiffness of a device should be positive at any displacement within the design displacement. This is to prevent a possible shake-down of the devices in one side, when they are subjected to large cyclic load reversals.
7) A deck should return to the rest position even after it is subjected to an large earthquake. The residual displacement u_{BR} developed in a device after it is smoothly released from a deformed displacement equivalent to the design displacement by Eq.(24) should be less than 10% of the design displacement.
8) The equivalent stiffness and the equivalent damping ratio of a device shall be stable against a change of load condition and natural environment such as the temperature change.

UNSEATING PREVENTION SYSTEMS

Unseating prevention measures are required for the highway. bridges. Because of the unique structural response of the Menshin bridges, some additional measures are required. The measures required for the highway bridges are as:

1) The unseating prevention systems have to be so designed that unseating of a superstructure from their supports can be prevented even if unpredictable failures of the structural members occur.
2) The unseating prevention systems are consisted of providing enough seat length, a falling-down prevention device, a displacement limiting device, and a settlement prevention device.
3) Against longitudinal response, enough seat length must be provided and a falling-down prevention device must be installed at the ends of a superstructures, if the Type-B bearings are used. On the other hand, if the Type-A bearings are used, a displacement limiting device has to be further installed at not only the ends of a superstructure but each intermediate support in a continuous bridge.
4) Against transverse response, a displacement limiting device is requested at each support, if the Type-A bearings are used, while it is not required in the Type-B bearings, except in skewed bridges, curved bridges, bridges supported by columns with narrow crest, bridges supported by few bearings per piers, and bridges constructed at the sites vulnerable to lateral spreading associated with soil liquefaction.

The seat length S_E is evaluated as

$$S_E = u_R + u_G \geqq S_{EM} \tag{29}$$

$$S_{EM} = 70 + 0.5l \tag{30}$$

$$u_G = 100 \cdot \varepsilon_G \cdot L \tag{31}$$

in which u_R = relative displacement (cm) developed between a superstructure and a substructure subjected to a seismic force equivalent to the equivalent lateral force coefficient k_{hc} by Eq.(7), u_G = relative displacement of ground along the bridge axis, S_{EM} = minimum seat length (cm), ε_G = ground strain induced during an earthquake along the bridge axis, and is 0.0025, 0.00375, and 0.005 for Group-I, II and III sites, respectively, L= distance which contributes to the relative displacement of ground (m), and 1 = span length (m). If two adjacent deck are supported by a pier, the lager span length should be l in evaluating the seat length.

In addition to the above requirements, the following measures should be adopted in the menshin design.

To prevent collisions between a deck and an abutment or between two adjacent decks, enough clearance must be provided. The clearance between those structural components S_B shall be evaluated as

$$S_B = \begin{cases} u_B + L_A & \text{between a deck and an abutment} \\ c_B \cdot u_B + L_A & \text{between two adjacent decks} \end{cases} \tag{32}$$

in which u_B = design displacement of menshin devices (cm) by Eq.(24), L_A = redundancy of a clearance (generally $\pm$ 1.5cm), and c_B = modification coefficient for clearance (refer to **Table 8**). The modification coefficient cs was determined based on an analysis of the relative displacement response spectra[17]. It depends on a difference of natural periods $\triangle T = T_1 - T_2$ ($T_1 > T_2$), in which T_1 and T_2 represent the natural period of the two adjacent bridge systems.

Table 8 Modification Coefficient for Clearance c_B

$\triangle T/T_1$	c_B
$0 \leqq \triangle T/T_1 < 0.1$	1
$0.1 \leqq \triangle T/T_1 < 0.8$	$\sqrt{2}$
$0.8 \leqq \triangle T/T_1 \leqq 1.0$	1

The clearance at an expansion joint L_E is evaluated as

$$L_E = u_B + L_A \tag{33}$$

in which u_B = design displacement of menshin devices (cm) by Eq.(24), and L_A = redundancy of a clearance (generally $\pm$ 1.5cm).

CONCLUDING REMARKS

The menshin design has been adopted extensively throughout the country since the Hyogo-ken Nanbu earthquake. It obviously extended the freedom of design and construction of the bridges, in particular the bridges with multiple-span continuous bridges with a deck length over 0.5km. However, it should be noted that seismic performance of the menshin

bridges against an extreme earthquake has not yet fully verified. For example, what is the most appropriate clearance between a deck and an abutment or between two adjacent decks, and what is the effect of hysteretic behavior of piers at the plastic hinge on the total response of bridges requires more analysis. More accumulation of analysis and experience is a key for future technical development of the menshin design and seismic isolation.

ACKNOWLEDGMENTS

Drafting of the revised version of the "Part V Seismic Design" of the "Design Specifications of Highway Bridges" was conducted at the "Special Sub-committee for Seismic Countermeasures for Highway Bridges" and was approved by the Bridge Committee, Japan Road Association. The first and second authors of this paper served as chairman and an executive member in the Special Sub-committee. The authors thank all members of the Special Sub-Committee and the Bridge Committee.

REFERENCES

1) Billings, I.J. and Kirkcaldie, D.K.: Base Isolation of Bridges in New Zealand, Proc. New Zealand-Japan Workshop on Base Isolation of Highway Bridges, Wellington, New Zealand 1987.
2) Buckle, I. G. and Mayes, R. L.: Seismic Isolation - History, Application and Performance- A World View, Earthquake Spectra, Vol.6, No.2, 1990
3) Goto, Y., Tokunaga, M., Yoshimura, T. and Shintaku M.: Seismic Response of Multi-span Continuous Bridge with Length of 1 km, Proc. 1st US-Japan Workshop on Earthquake Protective Systems of Bridges, February 1992, Buffalo, NY, USA, Technical Report NCEER 92-0004, National Center for Earthquake Engineering Research, State University of New York at Buffalo
4) Goto, Y., Kikuchi,T., Kimishima, T., Matsuo, F., Ozaki, D. and Tsukamoto, A.: Development of Expansion Joint, Stoppers and Knock-off Abutment for Menshin Design, Proc. 2nd US-Japan Workshop on Earthquake Protective Systems of Bridges, Technical Memorandum, No.3196, Public Works Research Institute, 1992
5) Hoshikuma, J., Kawashima, K., and Nagaya, K.: A Stress-Strain Model for Reinforced Concrete Bridge Piers Confined by Hoop Reinforcement, Proc. Japan Society of Civil Engineers, No.520/V-28, pp. 1-11, 1995
6) Iguchi, T.: Development of Sliding Friction Damper, Proc. 1st US-Japan Workshop on Earthquake Protective Systems of Bridges, February 1992, Buffalo, NY, USA, Technical Report NCEER 92-0004, National Center for Earthquake Engineering Research, State University of New York at Buffalo
7) Japan Road Association : Design Specifications of Highway Bridges, Part I Common Part, Part II Steel Bridges, Part III Concrete Bridges, Part IV Foundations, and Part V Seismic Design, 1996
8) Kawashima, K., Aizawa, K. and Takahashi, K.: Attenuation of Peak Ground Motions

and Absolute Acceleration Response Spectra, Report of f PWRI, Vol.166, Public Works Research Institute, 1985

9) Kawashima, K. and Koyama, T.: Effect of Number of Loading Cycles on Dynamic Characteristics of Reinforced Concrete Bridge Pier Columns, Structural Engineering/Earthquake Engineering, Vol.5, No. 1, pp.183-191, Japan Society of Civil Engineers, 1988

10) Kawashima, K. , Hasegawa, K. and Nagashima, H. : A Perspective of Menshin Design for Highway Bridges in Japan, Proc. 1st US-Japan Workshop on Earthquake Protective Systems of Bridges, February 1992, Buffalo, NY, USA, Technical Report NCEER 92-0004, pp.3-26, National Center for Earthquake Engineering Research, State University of New York at Buffalo

11) Kawashima, K. : Manual for Menshin Design of Highway Bridges, Proc. 2nd US-Japan Workshop on Earthquake Protective Systems of Bridges, Tsukuba Japan, PWRI Technical Memorandum No.3196, pp.195-219, Public Works Research Institute, Japan

12) Kawashima, K. : Menshin Design of Highway Bridges in Japan, Proc. 3rd US-Japan Workshop on Earthquake Protective Systems of Bridges, January 1994, Berkeley, CA, USA, Technical Report NCEER 94-0009, pp.1.3-1.31, National Center for Earthquake Engineering Research, State University of New York at Buffalo

13) Kawashima, K., Hasegawa K., Nagashima, H., Makiguchi, Y. and Suizu Y. : Certificate Test of Menshin Devices, Proc. 1st US-Japan Workshop on Earthquake Protective Systems of Bridges, February 1992, Buffalo, NY, USA, Technical Report NCEER 92-0004, pp.205-212, National Center for Earthquake Engineering Research, State University of New York at Buffalo

14) Kawashima, K., Makiguchi, Y., Suizu Y. and Endo, K. : Approving Test Procedure for Menshin Devices, Proc. 2nd US-Japan Workshop on Earthquake Protective Systems of Bridges, Tsukuba, Japan, PWRI Technical Memorandum No.3196, pp.3-20, Public Works Research Institute, Japan

15) Kawashima, K., Nagashima, H. and Iwasaki, H.: Evaluation of Modal Damping Ratio of Bridges Based on Strain Energy Proportional Method, Proc. 9th US-Japan Bridge Workshop, Technical Memorandum, Public Works Research Institute, Tsukuba, Japan, 1993

16) Kawashima, K.: Impact of Hanshin/Awaji Earthquake on Seismic Design and Seismic Strengthening of Highway Bridges, Report No. TIT/EERG 95-2, Tokyo Institute of Technology., 1995

17) Kawashima, K. and Sato H.: Relative Displacement Response Spectrum and Its Application, Proc. 11th World Conference on Earthquake Engineering, Acapulco, Mexico, 1996

18) Kawashima, T., Harada, H. and Ozaki, D.: Development of a Finger Joint Movable in Horizontal Directions for Menshin Bridges, Proc. 1st US-Japan Workshop on Earthquake Protective Systems of Bridges, February 1992, Buffalo, NY, USA, Technical Report NCEER 92-0004, National Center for Earthquake Engineering Research, State University of New York at Buffalo

19) Matsuo, Y. and Hara, K.: Design and Construction of Miyagawa Bridge, Proc. 1st US-Japan Workshop on Earthquake Protective Systems of Bridges, February 1992, Buffalo, NY, USA, Technical Report NCEER 92-0004. National Center for Earthquake Engineering Research, State University of New York at Buffalo
20) Ministry of Construction: Report on the Damage of Highway Bridges by the Hyogo-ken Nanbu Earthquake, Committee for Investigation on the Damage of Highway Bridges Caused by the Hyogo-ken Nanbu Earthquake, 1995
21) Ministry of Construction: Guide Specifications for Reconstruction and Repair of Highway Bridges Which Suffered Damage due to the Hyogo-ken Nanbu Earthquake, 1995
22) Ozaki, D. and Matsumoto, F.: Development of Falling-off Prevention Devices for Menshin Bridges, Proc. 1st US-Japan Workshop on Earthquake Protective Systems of Bridges, February 1992, Buffalo, NY, USA, Technical Report NCEER 92-0004, National Center for Earthquake Engineering Research, State University of New York at Buffalo
23) Priestley, N., Seible, F. and Calvi, M.: Seismic Design and Seismic Retrofit of Bridges, John Wiley and Sons, 1996
24) Public Works Research Center: Menshin Manual of Highway Bridges, English version is available by Sugita H. and Mahin, S.: Manual for Menshin Design of Highway Bridges: Ministry of Construction, Japan, Report No. UCB/EERC 94-10, Earthquake Engineering Research Center, University of California, Berkeley, 1994
25) Skinner, Robinson, McVerry: Introduction to Seismic Isolation, John Wiley and Sons, 1993
26) Suizu Y. and Sudo, C. (Part 1), Kawashima, K., Koshitoge, M., Endo, K., Yamada, C., and Nishimoto, T. (Part 2), and Nishikawa, I., Kato, M., Ito, M., and Muramatsu Y. (Part 3): Development of High Damping Rubber Bearings for Menshin Design, Proc. 1st US-Japan Workshop on Earthquake Protective Systems of Bridges, February 1992, Bufallo, NY, USA, Technical Report NCEER 92-0004, National Center for Earthquake Engineering Research, State University of New York at Buffalo
27) Takemura, H. and Kawashima, K.: Effect of Number of Load Reversal on Ductility and Dynamic Strength of Reinforced Concrete Piers, Report No.TIT/EERG 96-5, Tokyo Institute of Technology, 1996
28) Yamaguchi, M., Makiguchi, Y. and Kawasaki, I.: Application of Menshin Design to Seismic Retrofit of Bridges by Connecting Slabs of Adjacent Girders, Proc. 1st US-Japan Workshop on Earthquake Protective Systems of Bridges, February 1992, Buffalo, NY, USA, Technical Report NCEER 92-0004, National Center for Earthquake Engineering Research, State University of New York at Buffalo

CONCEPTUAL DESIGN OF ISOLATION SYSTEMS FOR BRIDGE STRUCTURES

G. M. Calvi A. Pavese

Università degli Studi di Pavia, Dipartimento di Meccanica Strutturale
via Ferrata 1, Pavia, 27100, Italy

ASTRACT

In the first part of the paper the objectives of an isolation system for a bridge structure are discussed, in relation to modelling options and modification of the traditional capacity design principles. A displacement based design approach is then presented, using a linear equivalent single degree-of-freedom model.
The preliminary design of an isolation system for existing bridges is based on the definition of a "structure regularity" which allows to estimate whether the response of the real structure will be similar to the response predicted in the preliminary design phase.The efficiency of the approach is shown designing the isolation system for a highly irregular bridge.

1. INTRODUCTION

It is believed that several hundreds of isolated bridges exist in the world, but very few codes of practice and design documents have been published on the topic [1, 2, 3]. Several kinds of devices have been designed and successfully tested, but effective design methods have still to be developed and a sound base to relate safety level and devices features needs further studies. It is therefore true that in this field practice and technology went farther than research and codes. The limited experience on response during severe earthquakes is certainly contributing to this dichotomy, even if there is a good capacity of simulating the non-linear response of isolated structures and a high and reliable technological production level. On the other hand broad probabilistic studies to estimate the safety level associated with different protection factors and response parameters have not yet been completed and are an important future research field.
The problem of designing an isolating system is particularly difficult, and interesting, when dealing with an existing bridge, in which case strength and stiffness of each pier is given and it is not possible to tailor them to the global desired response.
This paper focuses on the conceptual, preliminary design of an isolation system, and therefore on the capacity of predicting the expected response of an isolated bridge on the base of relatively simple models. The paper is largely based on the research work done for the preparation of the book [4], but relevant novel material is presented, particularly on the

design of isolating system for existing bridges based on the evaluation of a measure of the "regularity" of the structure.

2. OBJECTIVES OF AN ISOLATING/DISSIPATING (I/D) SYSTEM

There are several conditions that, alone or together, may support the idea of isolating a bridge:

- there is a need to avoid brittle failure modes in some pier, and it is difficult or expensive to strengthen a specific failure mode;
- the bridge has stiff piers, with low period of vibration;
- the bridge is highly non regular, for example with piers of significantly different height and it has therefore a high potential for concentration of ductility demands;
- the nature of the expected motion is very well characterised for the given site, with high dominant frequencies and low energy at large periods of vibration: in most case this means shallow earthquake, near fault and foundation on rock.

Similarly, different objectives may coexist and have different relevance when conceiving an isolation system:

- The capacity design protection of undesired collapse modes has a fundamental importance when dealing with existing bridges. Limiting the shear force passing through the isolator at the top of the pier at a level lower than the weakest assessed failure mode, the whole soil-foundation-pier system is protected.
- A proper selection of the stiffness, and particularly of the strength, of each isolator allows a regularization of the response, with a consequent decrease of the sensitivity to the motion characteristics and a protection of the deck against cracking and possible yielding.
- The increase of the energy dissipation capacity, obtained through a stable hysteretic response of the isolators, reduces both shear forces and horizontal displacements increasing the effective equivalent damping.
- Since the only elements where a non-linear response is expected are the isolators, an increased reparability and a better damage control normally results, particularly if repositioning and substitution of the isolating devices is conceived in the design phase.
- A period elongation and a consequent decrease in the effective accelerations results automatically due to the insertion of additional deformable elements. This effect should not be pursued per-se, because of the potential implication of increased displacements.

3. DESIGN AND MODELLING PRINCIPLES FOR ISOLATED BRIDGES

The design of a bridge provided with I/D devices can be simpler than the design of a standard bridge, since elastic response of all members (with the obvious exclusion of the isolators) can be assured, while, on the contrary, it is usually more demanding in the analysis phase, since a non-linear analysis is in most cases to be recommended. When designing an isolated bridge the bridge geometry and the pier and deck sections have usually already been defined, resulting from functional and aesthetic requirements and non-seismic load conditions. The piers reinforcement and the characteristics of the isolating system are therefore the unknown design. When dealing with the problem of retrofitting an existent

bridge the pier reinforcement is also known, and the isolating system becomes the only unknown.
It is easy to recognise that the "force reduction factor approach" (q-factor approach in Europe) commonly applied to design ordinary bridges becomes quite unsatisfactory for the case of isolated bridges. Unfortunately little effort has been devoted to develop an alternative design procedure and it is common to design isolating system without any rational basis, simply analysing a tentative isolated bridge and accepting it when the results are satisfactory. Obviously in this way there is no guarantee of an efficient design. Attempts of developing simple models for designing [5] have been based on the concept of "equivalent structure" [6], where a linear model representing the real structure is characterised by equivalent stiffness and damping. To this end a secant stiffness to an equivalent displacement is adopted, together with a viscous damping equivalent to the damping due to the energy dissipated by the hysteretic response (see figure 1).

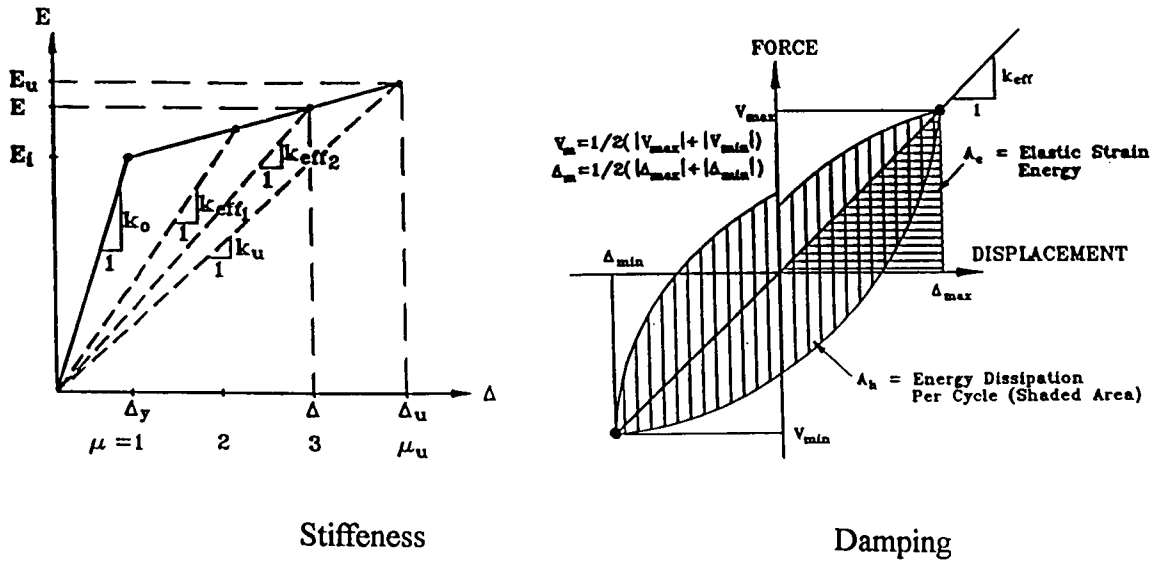

figure 1: substitute structure model [4]

The response of the real structure and of the substitute model should in principle be characterised by the same maximum displacement, which is considered to be a sufficiently accurate measure of the structural damage and therefore of the target limit state.
The substitute model will be used to enter acceleration and displacement response spectra, using the equivalent period of vibration and the appropriate level of equivalent viscous damping (figure 2 and figure 3).

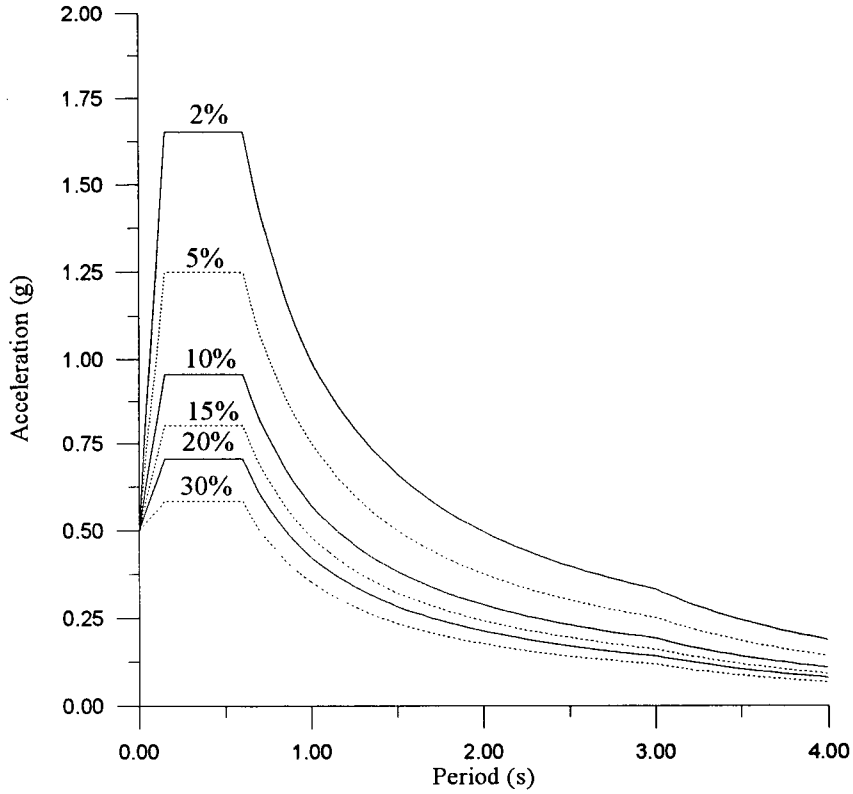

figure 2: acceleration response spectra, with period and damping variations (EC8 [3], soil type B, ground acceleration 0.5 g)

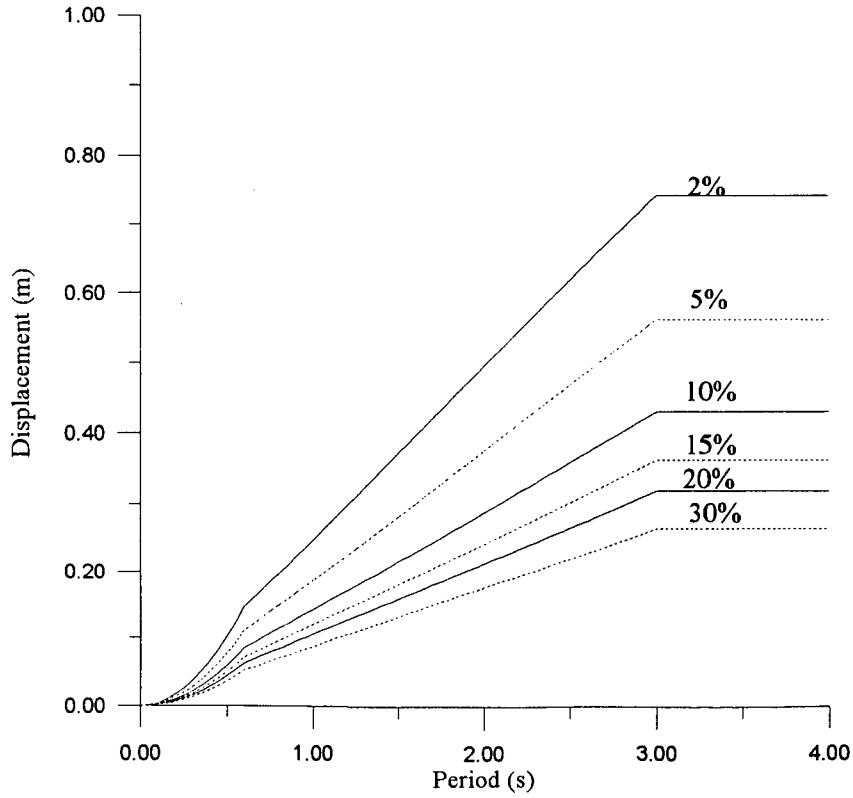

figure 3: displacement response spectra, with period and damping variations (EC8 [3], soil type B, ground acceleration 0.5 g)

4. CAPACITY DESIGN PRINCIPLES

To design an isolated bridge one fundamental capacity design principle will be applied, i.e. the isolating system will be the only element where a non linear response will be permitted. This means to set the yielding strength of each isolator at a strength not greater than a fraction of the lowest strength (flexure, shear, footing, etc.) of the corresponding pier.
More appropriately, it may be assumed that the greater part of the energy dissipation takes place in the isolating system, and only in extreme cases some ductility is induced into the piers. When the response of the isolating system shows some strain hardening, the force corresponding to the expected displacement, rather than the yielding force should be considered in setting the pier design force levels.
The protection factor to be applied depends obviously on the reliability of the mechanical characteristics of the isolating system; in most cases it is required that the actual strength of an I/D device does not differ of more than 10 % from its ideal strength and it is therefore felt appropriate to require that the strength of the device at the expected displacement be equal to 85 % of the design nominal strength of the pier. The protection factors applied to calculate the design strength will therefore protect the pier against yielding. Some initial yielding could still take place in the most external reinforcement because of the bi-linear idealisation of the actual force-displacement curve, which implies that yielding starts at a significantly lower force.
When designing a new bridge the capacity design principles usually applied to avoid undesired failure modes in the pier and in the foundation system may still be applied, but considering the force level assured by the isolation system, therefore it will no longer be necessary to ensure column shear strength (for example) exceeds column flexural strength. Capacity protection factors have obviously to be applied also to the strength of supports, connections and abutments.
The ultimate displacement capacity to be required of each device will be calculated applying a safety factor to the expected maximum displacement obtained from a preliminary analysis. The value of the safety factor will depend on the reliability of the expected displacement (i.e. on the reliability of the input motion and of the method of analysis) and on the consequences of larger than expected displacement demand (i.e. on the properties of the pier and of the isolating system). For example if the device shows an increasing strain hardening at large deformation, as in the case of some steel damper, a larger than expected displacement demand will result in some ductility demand in the piers. This should not be considered an undesirable event in case of an extremely large earthquake, and a significant safety margin in the ultimate displacement may not be necessary. On the other hand, for other kinds of devices a larger displacement demand could result in a local failure that will completely change the response of the bridge to the remaining part of the seismic excitation. This is obviously not acceptable and will require larger safety margins.
It is therefore important to underline that a significant, and possibly increasing with deformation, strain hardening is a desirable property of I/D devices, that will favour the exploitation of the structural resources when needed. Unfortunately the contribution of the eventual pier ductility to the global ductility of the system could be significant only if the pier was rather flexible with respect to the isolating system, and will be negligible for very stiff piers, as shown in figure 4, for the case of a pier 4 times stiffer than the isolator, a pier ductility equal to 4 and an isolator ductility equal to 6.

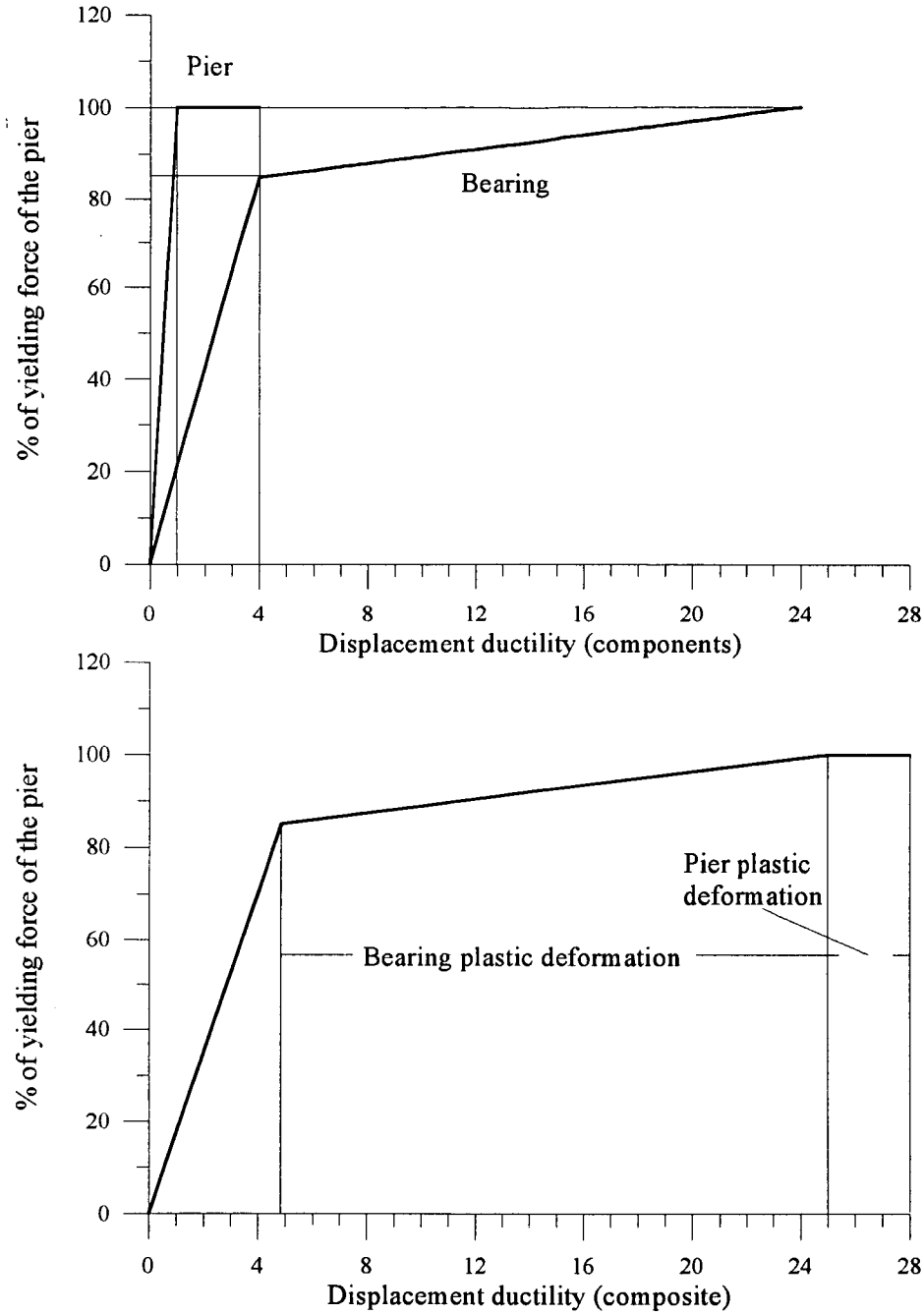

figure 4: pier response, isolator response and combined response [4]

5. APPLICATION OF DISPLACEMENT-BASED DESIGN APPROACHES

There has been growing interest recently in the development of displacement based seismic design (DBD) procedures for bridges. Displacement-based design offers the ability to control explicitly the displacement demand in each member rather than assigning a single, force-based behaviour factor to the entire structure.

The fundamental conceptual shift required in switching from a force-based to a displacement-based design approach has been presented by Kowalski and Priestley [6] for the case of a single degree-of-freedom (SDOF) bridge pier structure. In summary, the

required design displacement demand for the structure can be specified, and the displacement response spectra consulted to determine the required period of vibration (stiffness) necessary to achieve it, provided that the structure has been modelled assuming a linear behaviour and a viscous damping equivalent to the actual non-linear response. In this manner, strength and stiffness become end-products of the design rather than primary design goals. For simple SDOF structures, the process outlined has been applied successfully to bridge piers over a range of possible design parameters. The application of the method to more complex MDOF structural systems is not necessarily straightforward, and requires some additional steps [5]. The development of an equivalent SDOF representation of a MDOF structure has been suggested, to allow SDOF design spectra to be used. This is achieved by imposing a pre-defined displaced shape on the structure, and establishing the other properties of the equivalent SDOF structure accordingly.

When designing a new isolated bridge the best choice is to set all the isolator at the same strength, and to compensate the stiffness of each pier with the stiffness of the corresponding isolator, to obtain a perfectly regular system, where the deck should remain almost undeformed during the earthquake. This philosophy will be applicable to existing bridges as well, but it may imply a significant loss in strength, since the weakest pier will govern the strength of all piers. A better exploitation of the piers strength will require more refined non linear analyses and possible iterations of the final analysis process. In general it will be attempted to obtain a regular structure with a single dominating mode, where the energy dissipation capacity of the isolation system will dominate the global equivalent damping of the structure.

The application of a displacement based approach to isolated bridges allows the definition of a set of displacements, one for each foundation-pier-isolation system, setting aside the problem of defining a single force reduction factor. The criteria to define the appropriate set of displacements constitute the essence of the design approach presented in this paper. It is also recognised that the yield strength of each isolator can be treated as an independent variable, with the only requirement of being lower than 85 % of the critical strength of the corresponding pier.

6. MODELLING AND ANALYSIS OF ISOLATED BRIDGES

Modelling and analysing an isolated bridge requires a somewhat different attitude in comparison to that for a non-isolated structure. In particular a number of connection elements need to be more carefully considered because of their increased influence on the structural response. These comprise not only the isolating devices, but the bearing support (if existent) with the appropriate friction forces, any displacement limiting device to protect possible failure due to I/D displacement limitation, and any connection element between different adjacent decks at movement joints. On the other hand if the structure is assumed to be protected through the isolating system there is no need for taking into account a non-linear response of the pier elements, where the reinforcement should not yield (and of course this has to be checked at the end of the analysis). It can be more important, however, to take into account the pier masses and their own modes of vibration, since the isolation of the lower frequency modes involving the deck mass may increase the importance of higher frequency modes due to the response of the piers alone, fixed at the base and restrained at the top. The deck can obviously be simulated with linear elements, but again a more detailed mass distribution and a more careful consideration of higher modes of vibration could be appropriate.

The appropriate selection of model and analysis tool has to be based on the earthquake level, or on the limit state, considered. As an example consider that at the design earthquake level only a moderate penetration into the non-linear range of the isolation system is likely to be required, while at the extreme earthquake level the large displacement demand may imply hardening of the isolation system, or operating of the stopping system, with a consequent exploitation of the ductility capacity of the structure [4].
Two specific topics deserve special attention: the known sensitivity of isolated structures to the characteristics of soil motion, and their potentially high sensitivity to non-synchronous input. The first problem addresses to the recourse to site-specific studies rather than using standard spectral shapes. On the second topic a pioneering work [8] seems to indicate that the variability of the motion does not alter the order of magnitude of the displacements, which however seem to increase systematically particularly at the piers closer to the bridge ends. The combination of spatial variability and input frequency content different from that assumed in the design phase may well result in displacement increase on the order of 50 %.
The focus of this paper is on the definition of a simple equivalent structure, there is therefore a need to define an appropriate model for each foundation-pier-isolator system and then of the bridge as a whole. The first step is the definition of equivalent stiffness and damping.

6.1. Stiffness evaluation

The purpose of this section is to define a stiffness value globally equivalent to the variable stiffness of the pier-isolator system. The interaction with soil will be here neglected for simplicity, but the extension to this case is rather obvious.
The effective stiffness of each pier can be taken as equal to the secant stiffness to yielding (K_{Py}), the effective stiffness of the isolating system located at its top as the secant stiffness to the expected maximum displacement (K_{DE}). The global effective stiffness of the system is therefore:

$$K_G = 1/\left(1/K_{Py} + 1/K_{DE}\right) \qquad (6.1)$$

In some design, as discussed subsequently, the global pier-bearing stiffness will be established to optimise response. The effective stiffness of the damper can be then computed, as a function of global stiffness and pier stiffness, by inverting Eq (6.1), obtaining:

$$K_{DE} = K_{Py}K_G/\left(K_{Py} - K_G\right) \qquad (6.2)$$

It should be noted that the effective stiffness of the isolator is not taken at the maximum displacement capacity of the isolator, but at the expected displacement demand. The ratio between the two values, to be assumed in the design phase, will depend on the type of response of the isolator and on the desired protection.

6.2. Damping evaluation

The soil-foundation-pier system is assumed to have a linear elastic response, with a standard viscous damping (ξ_P) equal to, say, 5%. The isolating system could be characterised by a high viscous damping (ξ_{DV}) and by an essentially linear response, or by an effective

damping (ξ_{DE}) equivalent to the dissipated hysteretic energy. In the first case the global damping (ξ_G) of the pier-isolator system can be calculated according to the following relation, which assumes a stiffness proportional damping [4]:

$$\xi_G = \left(\Delta_P \xi_P + \Delta_D \xi_{DV}\right) / \left(\Delta_P + \Delta_D\right) \quad (6.3)$$

In the second case, the effective damping of the isolator should be evaluated as a function of its hysteretic response and of the expected ductility demand at the equivalent displacement. For example in the case of a response essentially elastic-perfectly-plastic, the following relation applies:

$$\xi_{DE} = 2\,(1 - 1/\mu_D) / \pi \qquad (6.4)$$

while a smaller damping corresponds to thinner cycles or more complex non-linear response [11]. It is often convenient to express the hysteretic dissipation capacity of a damper giving the ratio of the area of its typical cycle to the area of a corresponding elastic-perfectly-plastic cycle, in which case Eq. (6.4) can be simply factorized with the given value.
The effective global ductility of the pier-isolator system is related to the damper ductility by the expression (see figure 4 and the qualitative response shown in figure 5):

$$\mu_G = 1 + \left(\mu_D - 1\right) \frac{\Delta_{DE}}{\Delta_S + \Delta_{DE}} \quad (6.5)$$

A flexible pier therefore reduces the equivalent global ductility, and consequently the global equivalent damping, since the pier displacement does not increase after yielding of the isolator as shown in figure 6.
Possible relations between equivalent damping and structure displacement ductility are shown in figure 7. It is worth noticing that for large value of ductility there is little variation on the damping value.

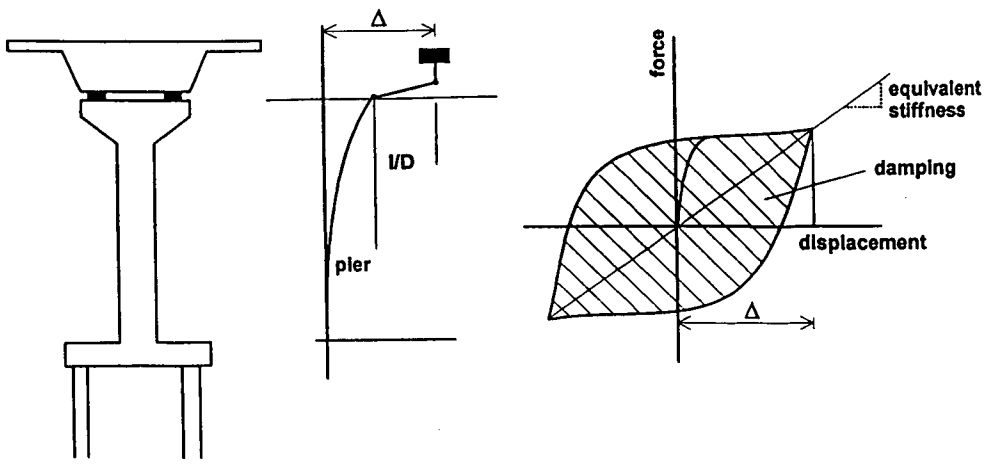

figure 5: Qualitative response of the pier-isolator system

7. DESIGN OF NEW BRIDGES USING ISOLATION SYSTEMS

A procedure to design new bridges using isolation systems has been described in [4] and is summarised in the following. It is important to observe that the philosophy of this procedure is such that a very different design of the pier reinforcement will result, if compared with the case of standard non-isolated bridge. Actually the fundamental assumption consists in imposing a rigid deformation of the deck, obtained by forcing each pier-isolator system to respond with the same peak force. This implies that taller piers should be capable to resist higher bending moments, and therefore they will require larger reinforcement percentage than shorter piers. Clearly this is exactly the opposite of what usually happens for non-isolated bridges, where shorter piers are stiffer, tend to attract larger forces and therefore require larger reinforcement percentages. On the contrary this is consistent with the standard requirement of a gravity (non-seismic) design, in which case higher piers normally require larger strength, and therefore larger reinforcement for the case of similar sections.

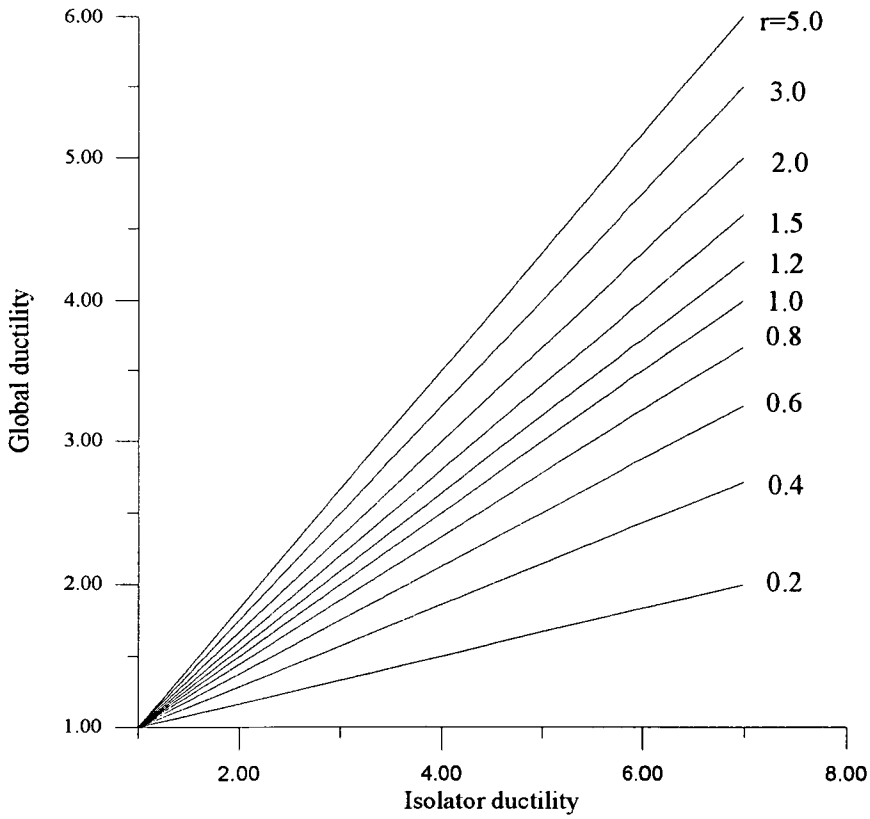

figure 6: Global ductility as a function of isolator ductility and ratio (r) between ultimate isolator displacement and elastic structure displacement

The assumption of having a rigid deformation of the deck allows a very good estimation of the expected response, since a SDOF model will be accurate in describing the structure response.

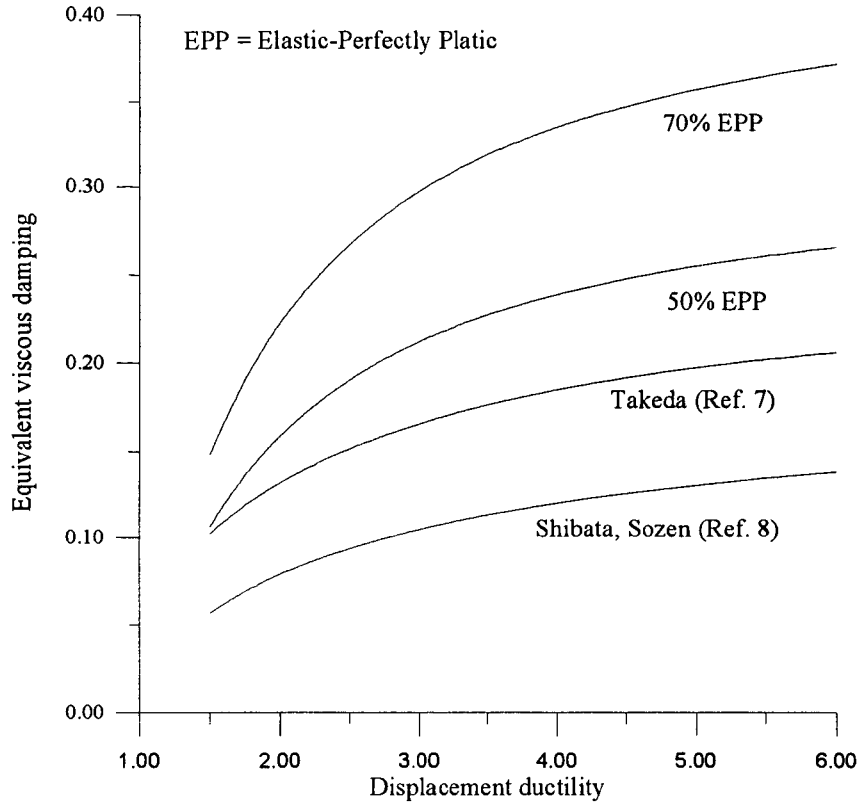

figure 7: equivalent viscous damping according to different kinds of non linear response

The design procedure can be described in the following steps.

(i) The accepted maximum displacement (Δ_e) to be expected during the design earthquake will be decided. This maximum displacement will in principle apply to all piers and abutments, because a theoretically perfectly regular structure will be designed.

(ii) The yielding displacement of each pier (Δ_{Py}) will be calculated from the following relation, i.e. integrating the curvature along column height and assuming proportionality between moment and curvature:

$$\Delta_{Py,i} = \phi_{Py,i} H_i^2/3 \qquad (7.1)$$

where $\phi_{Py,i}$ is the yield rotation and H_i is the height of the ith pier.
This relation assumes a single bending moment condition along the height, and can be easily modified to consider different restraints at the top or the influence of soil-foundation deformation. The yield rotation may be estimated from the following approximate relations [4]:

$$\phi_{Py,i} D = \zeta \varepsilon_y \qquad (7.2)$$

with ζ= 2.45 and 15% is the maximum estimated error for circular sections and with ζ= 2.14 and 10% maximum error for rectangular sections. These equations have been essentially derived from experimental results and take into account the global pier response, including the effect of the steel deformation outside the critical sections.

(iii) The effective displacement of each isolator will be obtained from the following equation, which assumes that the force in each isolator at the expected displacement will be 85 % of the yield force of each pier, as previously discussed:

$$\Delta_{DE,i=} = \Delta_e - 0.85\Delta_{Py,i} \qquad (7.3)$$

(iv) The ductility demand desired for the isolators at the effective displacement (μ_{DE}) will be decided, applying an appropriate factor to the isolator ductility capacity, to avoid collapse in case of an extreme seismic event. The yield displacement of each device ($\Delta_{Dy,i}$) will be calculated dividing the effective displacement by the ductility:

$$\Delta_{Dy,i} = \frac{\Delta_{DE}}{\mu_{DE}} \quad (7.4)$$

The yield displacement of the isolator is often difficult to be imposed to the manufacturer, who tends to design the devices for a yield strength and a maximum displacement capacity. It has to be noted, however, that the structural response is not very sensitive to a variation of the yield displacement (i. e. the initial stiffness of the isolator) provided that the required displacement capacity is available. Also, for large values of ductility the equivalent viscous damping does not vary significantly, as mentioned in relation to figure 7.

(v) The effective ductility demand of each (foundation)-pier-isolator system will be calculated as:

$$\mu_{E,i} = \frac{\Delta_e}{\Delta_{Dy,i} + \Delta_{Py,i}} \quad (7.5)$$

(vi) and the corresponding effective damping (ξ_i) will be calculated from the appropriate form of Eq. (6.4), i. e. considering the appropriate equivalent viscous damping, either using a more accurate expression or at least factorizing the equation valid for an elastic-perfectly-plastic response, or alternatively from the appropriate curve in figure 7. In addition to the reduced dissipation with respect to an elastic-perfectly-plastic response, the probability of several reduced amplitude cycles during the seismic response should be considered. This means that extensive parametric studies will be needed to calibrate the equivalent damping to be used in the preliminary design phase.

(vii) The global effective damping of the structure can be approximately computed from the following equation, which expresses a weighted average of the different damping ratios (M_i is the tributary mass of pier i and M_d is the total mass of the deck). This equation takes empirically into account that the equivalent yield displacement is shifted from the first yield displacement according to the ratio of the last yield force to the first yield force, but the area of the hysteresis loop is also progressively reduced. Better expression could be easily derived using the appropriate force-displacement curves for each foundation-pier-isolator system coupled in parallel.

$$\xi_b = \frac{\sum \xi_i M_i}{M_d} \quad (7.6)$$

(viii) Entering the spectra of figure 3 with displacement and damping, period of vibration (T_b) and effective acceleration (S_a) of the first mode of vibration of the bridge will be computed.

(ix) The equivalent stiffness of the bridge (K_b) will then result from the following equation, where M_d is the total mass of the deck:

$$K_b = 4\pi^2 M_d / T_b^2 \quad (7.7)$$

and the stiffness of each (foundation)-pier-isolator system can be calculated assuming proportionality between stiffness and tributary mass:

$$K_i = M_i K_b / M_d \quad (7.8)$$

(x) In accordance with the previous discussion of capacity design principles, it will also be assumed that the yielding force of the damper is equal to 85 % of the pier strength. The proportionality between displacement and stiffness, used in conjunction with Eq. (6.1) will then imply the following relations:

$$K_{DE,i} = K_i\left(1 + 0.85\left(\Delta_{PY,i}/\Delta_{DE,i}\right)\right) \qquad (7.9)$$

$$K_{P,i} = K_{DE,i}\,\Delta_{DE,i}/0.85\Delta_{PY,i} \qquad (7.10)$$

(xi) The design forces for each pier can be obtained multiplying stiffness by displacement, and the pier reinforcement will finally be designed in the usual way.

As already mentioned the above procedure does not assure that a consistent and effective design will result. For example the stiffness and strength obtained for the piers could be incompatible with a reasonable reinforcement ratio, or the effective coupling of the deck could cause a response significantly different from the expected one. A more refined analysis should therefore be always performed to check the response of the bridge and some iteration may be necessary. The outlined design procedure is intended to serve essentially as a guidance to the way of reasoning and it is aimed to obtaining a regular structure, where all the (foundation)-pier-isolator systems should vibrate in phase, with similar periods of vibration and amplitudes, and stiffness proportional to the tributary masses.

8. RETROFIT OF EXISTING BRIDGES USING ISOLATION SYSTEMS

When the reinforcement of the piers of a bridge is already given, for example when it is required to design the retrofit a of bridge, or when it is desired to keep the reinforcement obtained from non-seismic constraints, only the I/D system has really to be designed, but it will be difficult to obtain a regular response in the sense used in the previous design approach. Since the strength of the piers will be known, the strength of the isolators at design response could be set at 85 % the strength of the corresponding pier. In this case it will be impossible to have both similar stiffness and similar expected displacement for different piers, if the strengths are different. A time history analysis to check the design is in this case fundamental, since the real response could be significantly different from that obtained with a simplified model, because the coupling effect of the deck could have important effects. Another possible choice is to design the isolators using as a reference the strength of the weakest pier. In this case the design process becomes easier, and the bridge response more regular, but the global low strength could imply the necessity of very large damping and low stiffness. In general a compromise should be pursued, iterating the design process and verifying the effectiveness of the solution using a time history analysis.

8.1. Equal (minimum) strength approach

This approach is likely to provide a structure whose actual non-linear response will be similar to the response predicted in the preliminary design phase. This is not considered important to simplify the design, but rather to obtain a reliable response and therefore a good estimation of the safety of the structure. The cost to be paid is to provide larger dissipation capacity and/or larger displacement capacity, since the global strength of the structure will be lower. The procedure can be summarised in the following steps.

(i) All the yield forces of the isolators will be set at the strength level of the weakest pier, factorizing the forces according to the tributary masses. At the abutments there is often a certain freedom, because they may have been designed more conservatively and because different forces will not imply a deformation of the deck. It could be convenient to have higher yield strength in the devices used at the abutments, to reduce the importance of the torsional mode in the horizontal plane. For the same reason it is appropriate to try to have a rotationally equilibrated system of forces, when all the isolators have yielded.
(ii) Entering the design spectra with the total force, a reasonable couple of damping and period of vibration will be selected, obtaining a value for the effective displacement of the equivalent system, which should be kept in a range of 1 to 5 % of the height of all piers, if possible.
(iii) The pier yield displacement and the pier displacement corresponding to yield in the isolators will be computed.
(iv) The effective displacement required from each isolator will be obtained as the difference between global displacement and pier displacement.
(v) The accepted maximum ductility for the isolators will be decided, and the global ductility of each foundation-pier-isolator system will be computed. The equivalent damping of the bridge will be then computed.
(vi) If the value of the global damping is not compatible with that assumed in step 2, some iteration is needed, either accepting different ductility demands in the isolators, or accepting a different displacement (i.e. a different period of vibration) at step 2.

Since all the foundation-pier-isolator systems have similar effective force, displacement and stiffness, it is very likely that the time history analysis will confirm the expected response, which assumed that the total force was shared according to a tributary mass principle. The higher frequency response modes of the piers itself will also be checked at the end of the design process, since it is very likely that they will be uncoupled from the global response modes of the bridge.

8.2. Maximum strength approach

The assumption of equal forces in the piers allows a regular response with negligible deformation of the deck, but forcing to have all strengths cut at the level of the weakest pier leads to potential needs of large period of vibration and large equivalent viscous damping, i.e. of large displacement and large energy dissipation demand (see figure 8).

It is therefore worthwhile to explore the possibility of designing an isolating system with yield forces of the isolators as close as possible to the pier shear strength. The starting point is in this case the obvious choice of adopting the factorized pier strengths. Doing so an unacceptable design may result, with extremely different displacement and ductility demand to the isolators (see the appropriate example given in the next section). To improve the design of the isolating system a "regularity index" to be maximised is proposed.

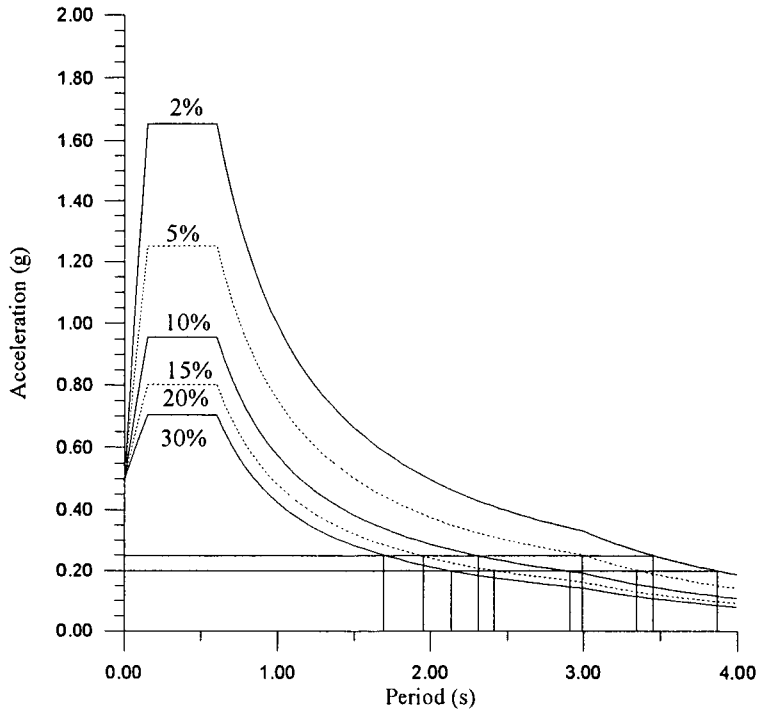

figure 8: Possible couples period-damping as a function of the global equivalent strength

8.2.1 Definition of regularity

The problem of regularity has been the object of previous studies [7] where the objective was to be able to predict whether a bridge will respond as expected in the preliminary design phase. To this end an index was defined as follows:

$$R_1 = 1 - \frac{\sum_{i=1}^{n}\sum_{j=1}^{n}\left[\left(1-\delta_{ij}\right)\left|\underline{\Phi}_i^B\,\underline{M}\,\underline{\Phi}_j^D\right|\right]}{n} \qquad (8.1)$$

where $\underline{\Phi}_j^B, \underline{\Phi}_j^D\,\underline{M}$ are the modal shapes of the bridge and the modal shapes and the mass matrix of the deck alone (i.e. considered as a beam supported at the abutments).
This index is therefore based on the geometry only, and is a measure of the difference of the modal shape of the bridge and of the deck alone. The reason why it appeared to work is that at increasing damage, and therefore of non linearity, in the pier response, the deck tends to drive the response and when it tends to keep the same deformed shape of the whole structure the ductility demand in the piers tends to be the same.
An improvement of this index should consider the higher response modes and the expected frequency content of the input.
An alternative, and more efficient, definition of regularity has been attempted starting from the assumption of knowing a desired displacement shape of the bridge. This is the case when a displacement based approach is adopted, and a target deformed shape has been defined. In this case a measure of regularity may be based on the measure of a difference between a vector containing the product of modal mass and spectral amplification, which defines the algebraic combination of the modal displacements produced by the input motion, and a vector containing the coefficients producing the target deformed shape, when applied to the modes. This is expressed in the following relationships:

$$R_2 = 1 - \frac{|\underline{y} - \underline{z}|}{|\underline{y}| + |\underline{z}|} = 1 - \frac{\sqrt{\sum_{i=1}^{m}(y_i - z_i)^2}}{\sqrt{\sum_{i=1}^{m}(y_i)^2} + \sqrt{\sum_{i=1}^{m}(z_i)^2}} \quad (8.2)$$

where

$$y_i = \frac{\underline{\Phi}_i^t \underline{M}\underline{v}}{\underline{\Phi}_i^t \underline{M}\underline{\Phi}_i} \quad (8.3)$$

so that

$$\underline{v} = y_1 \underline{\Phi}_{1+} + y_2 \underline{\Phi}_2 + y_3 \underline{\Phi}_3 + \ldots\ldots (8.4)$$

and

$$\underline{z}_i = \beta_i S_{di} \quad (8.5)$$

where β_i is the modal participating factor, $\underline{v}$ is the vector of the imposed displacements, $\underline{\Phi}_i$ are the eigenvectors of the whole bridge, and S_{di} are the spectral displacements.
In case of a linear response, it is immediate to realise that the factor R_2 will assume a value equal to one for a perfectly "regular" structure, i.e. for a structure which is likely to behave as expected, and it would tend to zero in the opposite case.
Unfortunately the non-linear response of the structure will impair this index to work properly, since the strengths of the piers have not been considered and it is well possible that a pier will still be elastic when another has penetrated significantly into the non-linear range. It has to be kept in mind that in a preliminary design phase an "equivalent linear structure" is being used and therefore a different displacement implies a different force, while in a non-linear simulation the forces will remain constant after yielding.
To overcome the problem it is necessary to include a measure of the difference between the yield strength of each pier and the force that would be reached with an hypothetical elastic response in the index. Eq. (8.2) is therefore modified, adding a second term as shown below:

$$R_3 = 1 - \frac{1}{2}\left(\frac{\sqrt{\sum_{i=1}^{m}(y_i - z_i)^2}}{\sqrt{\sum_{i=1}^{m}(y_i)^2 + \sum_{i=1}^{m}(z_i)^2}} + \frac{\left(\sqrt{\sum_{i=1}^{n}(V_i - k_{ei}\Delta_{ei})}\right)}{\sqrt{\sum_{j=1}^{n} V_j^2}} \right) \quad (8.6)$$

where the first part of the equation is the same as Eq. (8.2), V_i are the yield strengths of the piers (or of the isolators, if present, i.e. 85 % of the critical strength of the corresponding pier), k_{ei} are the elastic stiffness of the isolators and Δ_{ei} are the yielding displacements of the isolators (both values are proportional to the correspondent values for the substitute structure).

8.2.2 Use of a regularity index to design an isolating system

The design of the isolating system can be based on the definition of a regular structure, in which case the prediction of the preliminary design is more likely to be confirmed by a non-linear analysis. A possible approach can be summarised in the following steps:

(i) Choice of a deformed shape, based on maximum and minimum drifts, on symmetry considerations, on the first mode of vibration of the deck.
(ii) Computation of the contribution of each pier displacement to the corresponding deck displacement, assuming in the first trial a complete exploitation of the pier strength (with an appropriate safety factor, here taken as 0.85).
(iii) Computation of the global ductility from Eq. (6.5) and consequent equivalent viscous damping of each pier-isolator system (modified form of Eq. (6.4)).
(iv) Computation of eigenvalues and eigenvectors of the linear equivalent structure (using the secant stiffness to the target displacement of each pier-isolator system).
(v) Computation of the coefficients y_i from Eq. (8.3) and of the coefficients z_i from the design spectrum according to Eq. (8.5).
(vi) Computation of the regularity index. If R_3 is close to 1 the bridge will be able to produce the deformed shape assumed, the displacement demand of each pier-isolator system will be therefore similar to the displacement assumed in the preliminary design phase. In case of a low value of R_3 the procedure will be repeated selecting a different displacement shape. If it should result impossible to obtain an acceptable value of R_3, the strengths of the isolators will be modified (obviously reducing them, since the first iteration loop is tempted with all the forces at 85 % of the critical values) and the iterative procedure on the deformed shape will be repeated. Several algorithms are available to optimize the choice of new deformed shapes and isolators strengths, for the present case the algorithm presented in [11] has been implemented in the procedure.

Clearly there is in principle no guarantee that the global resulting strength will be significantly larger than the "minimum strength" discussed in the previous section, but the difference could be significant, with a consequent reduction in the displacement and energy dissipation capacity to be provided to the isolators. This approach will be defined "optimal strength approach".

To clarify the concepts expressed in the above discussion a sample bridge is considered in the following, showing the results obtained applying different design approaches.

9. DESIGN EXAMPLES

(i) A bridge without isolators, designed according to EC8/2 [3], is shown in figure 9. It can be noted that the bridge geometry is highly irregular, with piers of very different heights. The reinforcement percentages are 0.5, 0.92, 0.5 %, where 0.5 % has been assumed as minimum reinforcement. The results obtained from a non-linear analysis with peak ground acceleration equal to 1.2 times the design ground acceleration (0.35 g was assumed in the design phase, the peak acceleration resulting in the non-linear analysis was 0.446 g) are shown in Table 1 and in figure 10. The regularity index of this bridge is $R_1 = 0.7564$.

It has to be noted that the displacement ductility demand of the three piers is significantly different, even if assumed constantly equal to 3 in the preliminary design phase.

Pier height	Ultimate displacement [mm]	C.O.V.	Yielding displacement [mm]	Ductility demand	Yield strength [kN]
14 m	64	13 %	65	-	2920
7 m	68	14 %	17	4.1	7791
21 m	80	6 %	147	-	1945

Table 1: results of the non-linear analyses performed on the non-isolated bridge shown in figure 9 using 7 accelerograms generated from the EC8 response spectrum, soil type 'B', peak ground acceleration 0.446 g

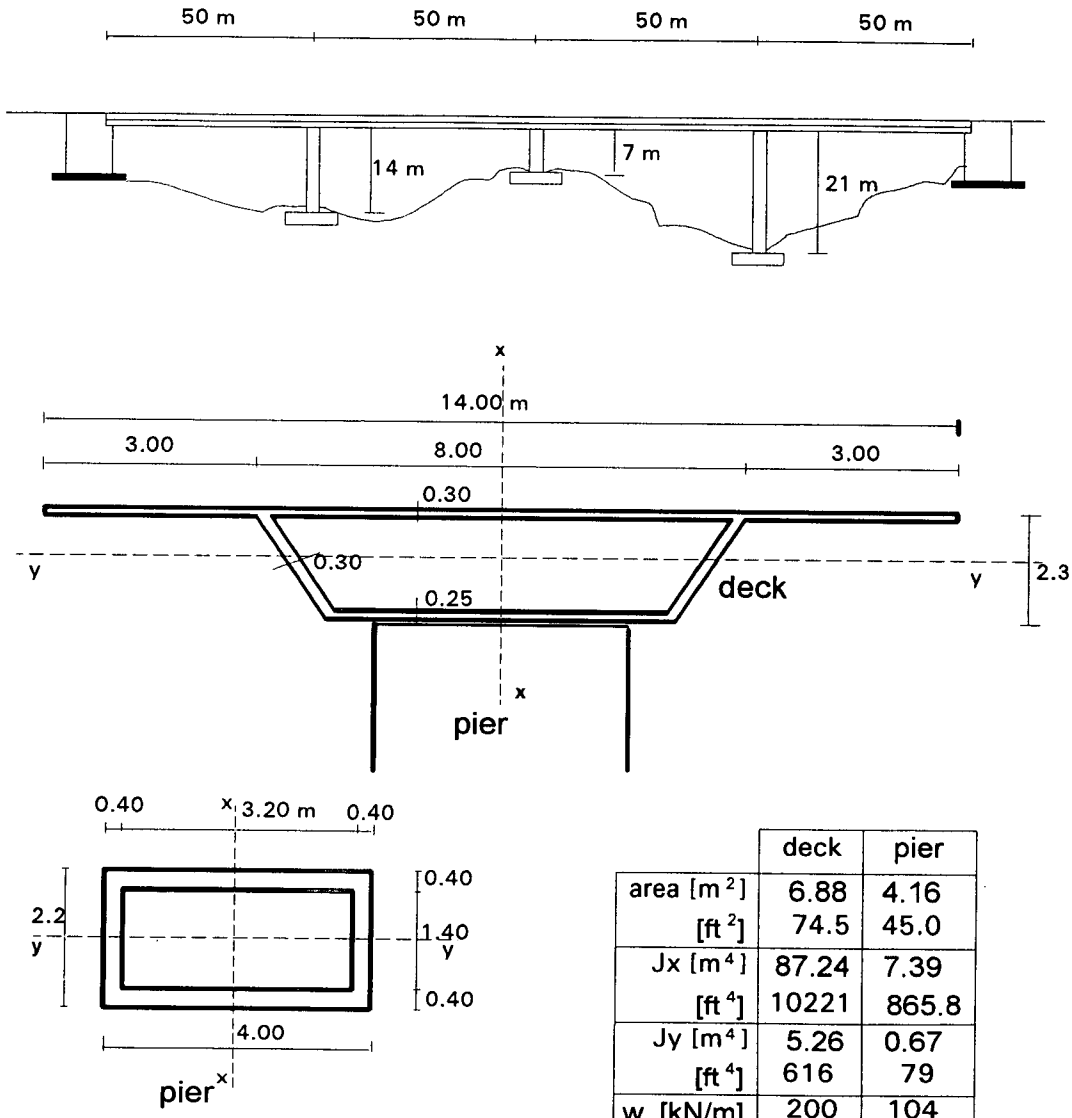

	deck	pier
area [m²]	6.88	4.16
[ft²]	74.5	45.0
Jx [m⁴]	87.24	7.39
[ft⁴]	10221	865.8
Jy [m⁴]	5.26	0.67
[ft⁴]	616	79
w [kN/m]	200	104
[k/ft]	13.7	7.1

figure 9: The bridge used for the examples

(ii) An isolation system has been designed according to the "minimum strength" design approach presented in the previous section, i.e. setting all the isolator strengths to 85 % of the critical strength of the weakest pier. It has been assumed a constant ductility capacity for all the isolators, equal to 4.
The main results of both preliminary design and non-linear analysis are shown in table 2. It can be immediately recognised that the bridge responds essentially as predicted in the design phase, with errors in a range of 15 % ("error" is defined as the perceptual difference between the displacement predicted in the preliminary design phase and the displacement obtained from the non linear analysis). This value is significantly lower than the dispersion of the results due to different input motions. The dispersion of the displacements obtained by the non-linear analysis is significantly increased as a consequence of the period elongation. It has to be noted that the low strength of the isolators (the global strength of the bridge is equal to 16.5 % of the total weight of the deck) is paid in terms of much larger displacement demands.
The regularity indices of this bridge have the following values: R_2 = 0.9996, R_3 = 0.9560

Abutments /piers	Design			Non-linear analysis					
	Average Displacement [mm]		Isolators strength [kN]	Average Displacement [mm]		C.O.V. over 7 accelerograms		Average error	
	Deck	Isolat.		Deck	Isolat.	Deck	Isolat.	Deck	Isolat.
Abutment	210	210	825	183	183	29 %	29 %	-13 %	-13 %
14 m pier	210	145	1650	178	141	21 %	26 %	-15 %	-3 %
7 m pier	210	193	1650	173	169	18 %	18 %	-18 %	-12 %
21 m pier	210	63	1650	188	71	22 %	38 %	-10 %	13 %
Abutment	210	210	825	242	242	27 %	27 %	15 %	15 %

table 2: "Minimum strength" design approach (isolator strengths equal to 85% of the weakest pier): comparison of the results of preliminary design and non-linear analysis.

(iii) A second isolation system has been designed according to the "maximum strength" design approach, setting all the isolator strengths to 85 % of the critical strength of the corresponding pier and assuming a constant ductility capacity for all the isolators equal to 4. The displacement shape of the bridge has been defined according to the R_2 factor presented in the previous section, i.e. without considering any possible correction of the isolator strength, nor any influence of the strength on the regularity factor. The regularity indices of this bridge have the following values: R_2 = 0.9999, R_3 = 0.8811
The main results of both preliminary design and non-linear analysis are shown in table 3. In this case the results of the non-linear analysis are completely different from the prediction of the preliminary design. The errors are in the range of 50 %, i.e. much larger than the dispersion of the results due to different input motions.
The increased strength of the system with respect to the minimum strength approach (actual strength equal to 36 % of the total weight of the deck), does not result in significantly lower displacements, which are in the same range of the previous case.

Abutments /piers	Design			Non-linear analysis					
	Average Displacement [mm]		Isolators strength [kN]	Average Displacement [mm]		C.O.V. over 7 accelerograms		Average error	
	Deck	Isolat.		Deck	Isolat.	Deck	Isolat.	Deck	Isolat.
Abutment	71	71	1793	111	111	16 %	16 %	56 %	56 %
14 m pier	178	113	2482	98	47	14 %	25 %	-45 %	-58 %
7 m pier	146	129	6623	100	85	8 %	9 %	-32 %	-34 %
21 m pier	281	135	1654	129	26	7 %	13 %	-54 %	-81 %
Abutment	105	105	1793	161	161	12 %	12 %	53 %	53 %

table 3: "Maximum strength" design approach (isolator strengths equal to 85% of the corresponding pier): comparison of the results of preliminary design and non-linear analysis.

A third isolation system has been designed according to the "optimal strength" design approach, assuming variable strength for the isolators, with an upper limit equal to 85 % of the critical strength of the corresponding pier. A constant ductility capacity for all the isolators equal to 4 has been still assumed, consistently with the previous examples. The displacement shape of the bridge has been defined according to the R_3 factor presented in the previous section, i.e. optimising the displaced shape as a function of both displacement shape and isolators strength. The regularity indices of this bridge have the following values: R_2 =0.9891, R_3 = 0.9650. The global strength of the system is now equal to 38 % of the total weight of the deck. The main results of both preliminary design and non-linear analysis are shown in table 3. The results of the non-linear analysis are similar to the prediction of the preliminary design, with errors smaller than 20 %, i.e. within the dispersion due to different input motions. The higher global strength of the bridge, combined with the optimal design of the displaced shape allows a significant reduction of the displacement demand, for deck and isolators.

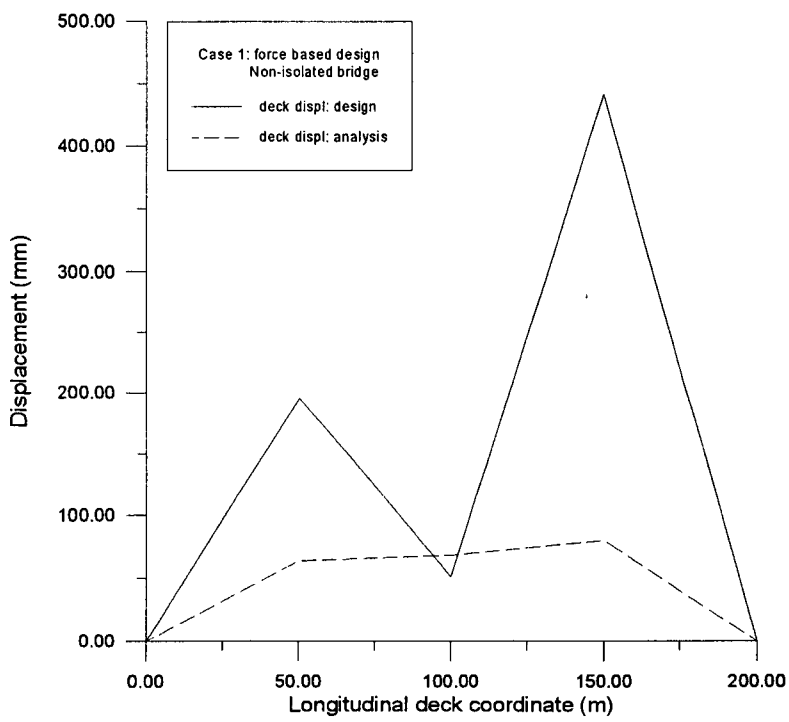

figure 10a: ultimate displacement shapes obtained using different design methods

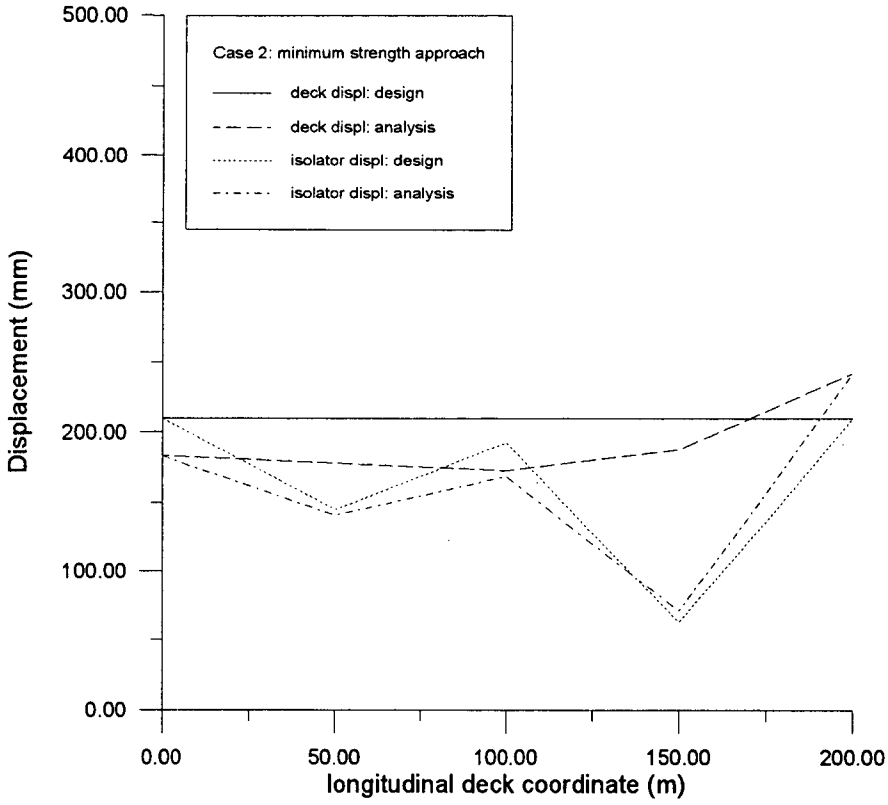

figure 10b: ultimate displacement shapes obtained using different design methods

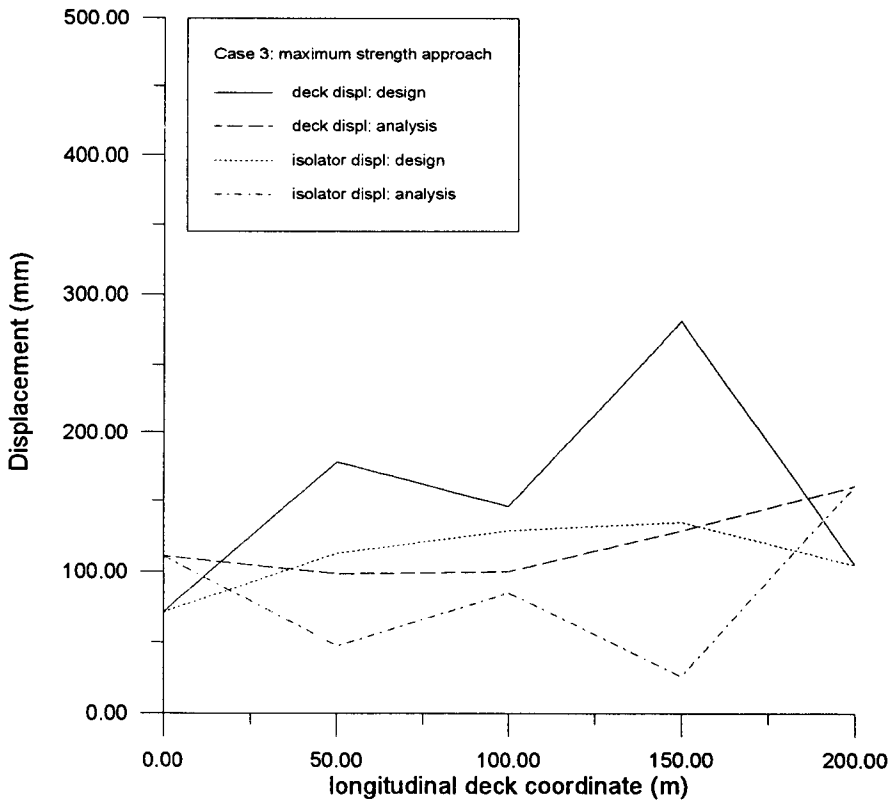

figure 10c: ultimate displacement shapes obtained using different design methods

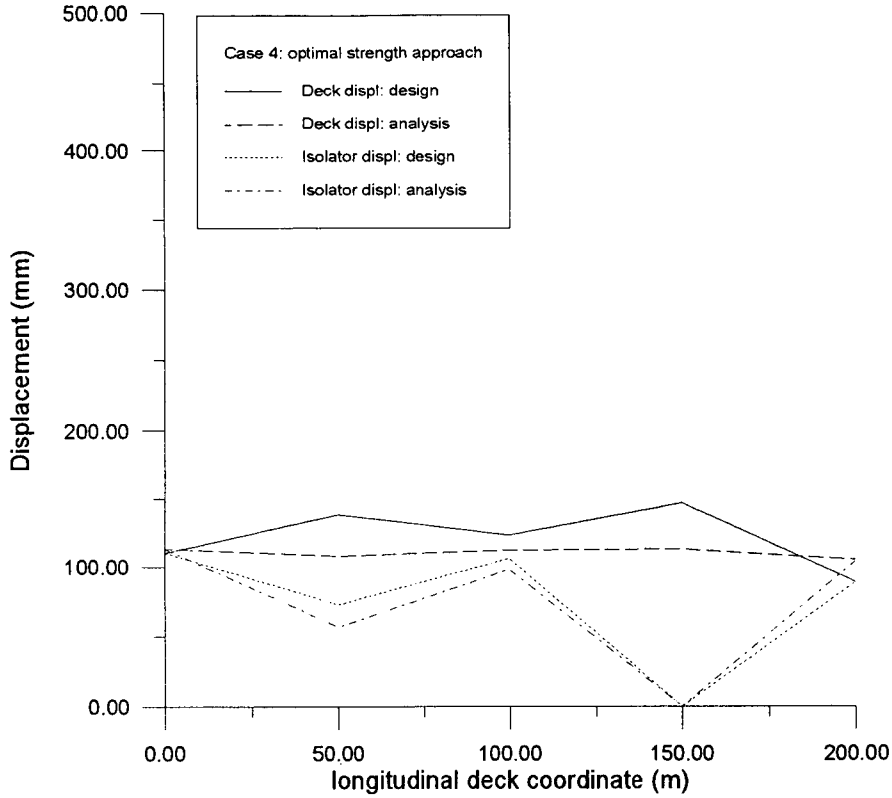

figure 10d: ultimate displacement shapes obtained using different design methods

Abutments /piers	Design			Non-linear analysis					
	Average Displacement [mm]		Isolators strength [kN]	Average Displacement [mm]		C.O.V. over 7 accelerograms		Average error	
	Deck	Isolat.		Deck	Isolat.	Deck	Isolat.	Deck	Isolat.
Abutment	110	110	2219	113	113	22 %	22 %	3 %	3 %
14 m pier	138	73	2317	108	57	17 %	32 %	-22 %	-22 %
7 m pier	123	106	6344	112	98	8 %	9 %	-9 %	-8 %
21 m pier	147	0	1630	113	0	11 %	-	23 %	-
Abutment	89	89	2572	105	104	22 %	22 %	18 %	17 %

table 4: "Optimal strength" design approach (isolator strengths optimised to obtain a target displaced shape consistent with the expected response): comparison of the results of preliminary design and non-linear analysis.

It is also interesting to observe that the application of the "optimal strength" approach results in the elimination of the isolator on the taller pier, which is not required. Obviously the pier can be still protected designing a shear key with the appropriate strength level.

10. CONCLUSIONS

In this paper a bridge structure protected by an isolation system is modelled with a single degree-of-freedom linear equivalent model, according to approaches already presented in previous works [4, 5, 6].
Using this model a procedure for the design of an "optimal" isolation system is presented, for the case of a new or an existing bridge. The approach adopted for this last case is particularly interesting, because of the difficulty of the problem, of the large number of existing bridges which may need to be retrofitted and because of the novelty of the approach.
Two different "coefficients of regularity" are discussed in this paper. The first one (Eq. (8.1)) was proposed in a former paper, and is based on purely geometric concepts. It can therefore be applied to bridges for which the piers reinforcement (and therefore the piers strength) is not known. The second coefficient (Eq. (8.6)) takes into account also the input characteristics and the piers strength, therefore it can be applied only to existing bridges or after having completed the design.
This second coefficient is particularly valuable when used to design an isolation system for an existing bridge, with the purpose of protecting all the undesired failure mode. An algorithm based on the index allows to select isolators strength and stiffness in such a way that the isolated bridge will respond as predicted in the preliminary design phase.
This result is clearly shown in figure 10, where the deformed shapes of the four bridges considered are depicted, considering the results of the preliminary design phase and the response obtained from a series of non-linear dynamic analysis. The superiority of the bridge designed using the approach proposed in this paper (number 4) is evident, both considering the similarity of the results and considering the limitation of the displacement values.
The sound definition of the regularity index and the results obtained in these first cases considered, particularly difficult because of the irregularity of the original bridge, allow some optimism in an extensive applicability for design. Extensive parametric analyses and consideration of more realistic cases are needed before a practical use of the design approach.

ACKNOWLEDGEMENTS

The research presented in this paper has been partially funded by the Italian "Gruppo Nazionale per la Difesa dai Terremoti" (GNDT).

REFERENCES

[1] "*Guidelines for seismic design of bridges with isolator/dissipator devices*" (1991), Autostrade S.p.a., Roma

[2] Ministry of Construction, Japan (1994), "*Manual for menshin design of bridges*", (translated by H. Sugita and S. A. Mahin), Report No. UCB/EERC-94/10, Berkeley

[3] "*Eurocode 8 - Design provisions for earthquake resistance of structures - Part 2: Bridges*" (1994), ENV 1998-2, CEN, Brussels

[4] Priestley M.J.N., F. Seible and G.M. Calvi (1996), "*Seismic design and retrofit of bridges*", John Wiley, New York

[5] Calvi G. M. and G. R. Kingsley (1995), "Displacement based design of multi-degree-of-freedom bridge structures", *Earthquake Engineering and Structural Dynamics*, Vol. 24, pp. 1247-1266

[6] Kowalski M. J., M. J. N. Priestley and G.A. MacRae (1995), "Displacement-Based Design of RC Bridge Columns in Seismic Regions", *Earthquake Engineering and Structural Dynamics*, pp. 1623-1643

[7] Takeda T. and al. (1970). R/C response to simulated earthquakes. *J. Struct. Div. ASCE*, 96. ST12, pp. 2557-2573.

[8] Shibata A. and M. Sozen (1976), "Substitute-Structure Method for Seismic Dsign in R/C", *J. Str. Div. ASCE*, 102

[9] Calvi G.M., A. Elnashai and A. Pavese (1994), "Analytical Behaviour Factor of Irregular RC Bridges for Seismic Design", 2nd international Workshop on Seismic Design and Retrofitting of RC Bridges, Queenstown

[10] Monti G., C. Nuti and P. E. Pinto (1995), "Response of conventional and isolated bridges under non-synchronous seismic motion", Proc. of the 5th SECED Conf., Chester, pp. 117-124

[11] Fardis M.N. and T.B. Panagiotakos (1996), "Histeretic damping of R.C. Elements", 11 World Conference on Earthquake Engineering, Acapulco, June 23-28

[12] Gagliardo E. and G. Sacchi (1978), "An operator improving the efficiency of minimization algorithms", *Rivista di Informatica*, III:51-59

Session 7

Topic 6 Isolation and Retrofit (2)

DESIGN OF THE 19-SPAN CONTINUOUS RIGID FRAME BRIDGE WITH SEISMIC ISOLATOR

Hidenao HAYASHI[1], Shiro KAWAKITA[2], Yoshihei HORIE[3]

1) Head, Research and Design Section, Kobe Route Reconstruction Division, Hanshin Expressway Public Corporation, Kobe, Japan

2) Chief Engineer, Research and Design Section, Kobe Route Reconstruction Division, Hanshin Expressway Public Corporation, Kobe, Japan

3) Chief Engineer, Design Section, Engineering Division, Head Office, Hanshin Expressway Public Corporation, Osaka, Japan

SUMMARY

The Hanshin Awaji Earthquake occurred on January 17, 1995, caused tremendous damages among the rest on the Hanshin Expressway Kobe Route. Especially at Benten section (referred in Figure 1) 3 bridges out of 8 completely fell down, subjecting all bridge structures except foundations removed after the earthquake. This paper reports the outline of the seismic isolation design of 19-span continuous rigid frame bridge with seismic isolator, which was installed between RC supports and bottoms of steel pier. Results of vibration experiment applied onto the structure are also reported.

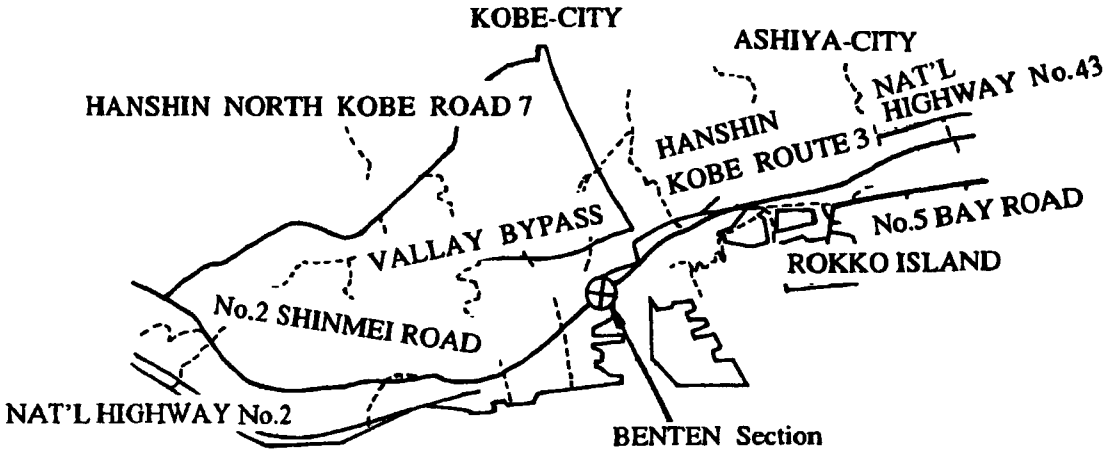

Figure 1. Location

1. INTRODUCTION

After the scrutiny of suffered condition caused by the earthquake the Benten bridge was determined to be the 19-span continuous rigid frame with steel deck along with the installation of seismic isolator underneath the piers. The general view of design is shown in Figure 2.

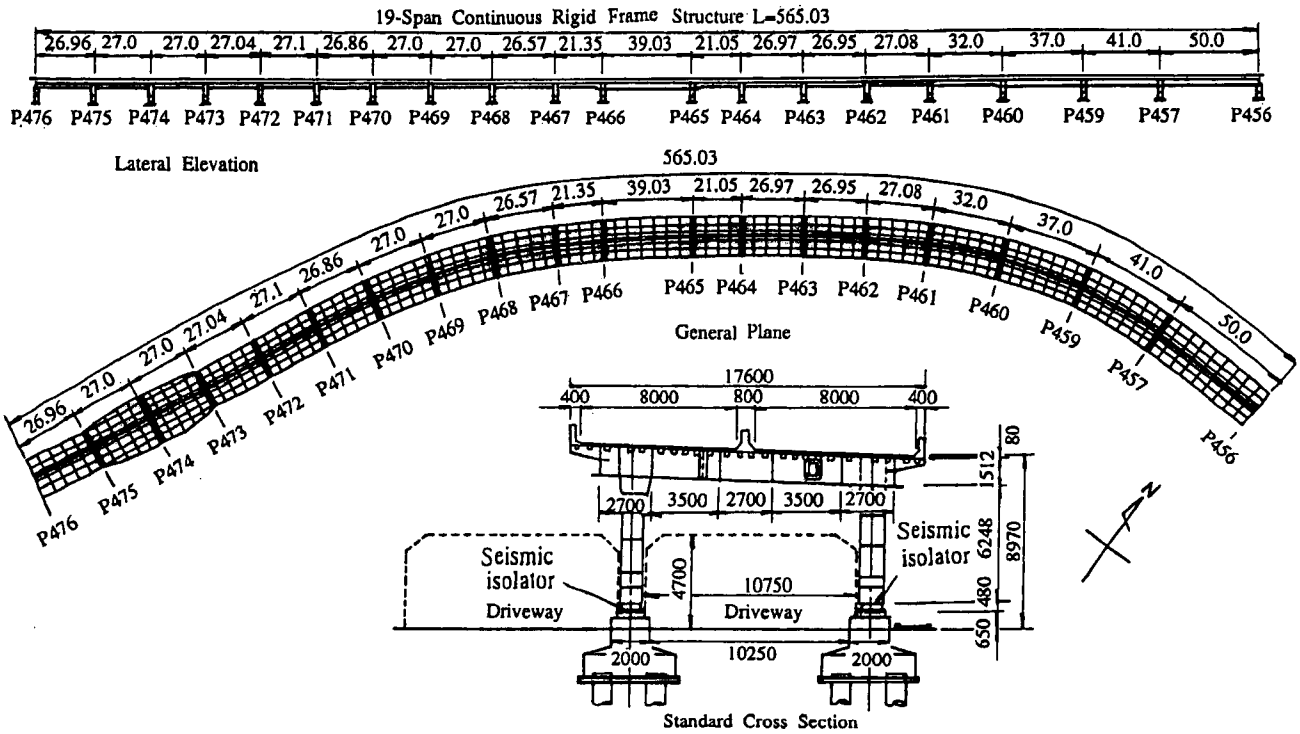

Figure 2. General View of Benten Bridge

Such a bridge structure that provides seismic isolation underneath the bridge supporting piers had theoretically been studied in the past [1], however, virtual application is almost none in practical use and it was indeed a first example to be introduced on the highway bridge.

The experiment of vibration was carried out with the use of Rapid Release Jack System and large vehicles to inspect and to ascertain various hypothetical constant figures. This paper describes the outline of seismic isolation design on the 19-span continuous rigid frame with the seismic isolator and experiment of applied vibration.

2. OUTLINE OF DESIGN

2.1 Design Scheme

Before the earthquake one each of lower piers stood on the middle of separating zone and on the pedestrian lane, and they were of single RC pier (1.0m by 1.7m). These piers were connected with the upper structure by means of steel bearings that were placed on top of the pier head. The cause of bridge fall or girder buckling were all taken into considerations such as shearing breakage of the RC pier during the earthquake and the breakage of steel bearing at the connecting points to determine the basic scheme of construction. These elements were settled as follows ;

1) It was found that there has been no damage on the piled foundation so that it could be utilized as they are.
2) Deck of the expressway could become light weighted by using steel deck and design to decrease seismic force by using isolation bearing.
3) In order to prevent bridges falling down each bridge pier and the beam of upper structure would be tied rigidly and to maintain continuous girder forms as much longer as can be.

Above basic conditions were studied and it was decided to adopt a continuous rigid frame. It was supposed that the additional piling reinforcement is needed for rigid connection or hinge connection and finally concluded to adopt the structure of installing seismic isolation bearing on the foundation. Since the Benten bridge is warped to the seaside and the overhang length of beams differs slightly, analysis was made on the whole structural model of the two types shown on Figure 3.

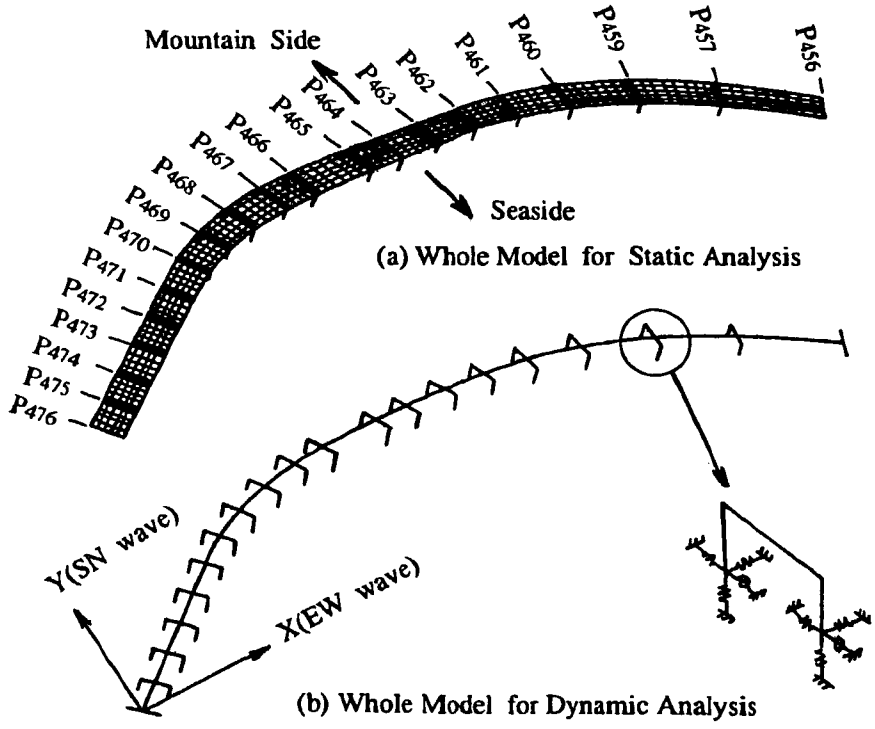

Figure 3. Whole Model for Analysis

In static analysis model (a) in the Figure 3 was used. The upper structure consists of main girders, beams, and piers which is supported by the two way horizontal spring as well as perpendicular and rotating with springs in the model.

In dynamic analysis model the number of lattice was decreased in a manner that main girders and deck plates were assembled together to a piece of beam form so that they would make a whole simple model. Adequacy of analysis results had been inspected and proved to be appropriate by using two dimensional model.

2.2 Seismic Isolation Design of Bearing

A study was made regarding the seismic isolation characteristic on whether the structure as a whole can anticipate vibration isolate effect based on the "Manual of Seismic Isolation Design for Highway Bridge" [2].

In seismic isolation design the characteristic of structure is expressed in the value of natural period (T) and the ratio of yield point load Qd/Wu (where, Qd is yield strength of lead plug. Wu is weight of a upperstructure portion supported by the Seismic isolator.). In order to work out an appropriate value, were designed the period and the ratio of yield point load by applying a representative bridge pier that support the upper structure that would satisfy the following 3 design objectives;

1) In the designed vibration from the horizontal bearing capacity piers would not excessively be plastic during the earthquake. (Khe<0.68)
2) In seismic coefficient method, a designed vibration can at least be decreased by the damping effect. (Damping ratio by seismic coefficient at the vibration h>10%)
3) Seismic Isolator will not be deformed extremely. (Horizontal bearing capacity during earthquake was investigated referring to the upper structure that deflects<250%)

Specific figure to satisfy the above condition, a combination of T=1.4 sec Qd/Wu=12.6% has been adopted. One of the model of bearing is shown in Figure 4.

2.3 Dynamic Analysis

In the dynamic analysis two types of plane model shown on the Figure 5 was introduced and following points were inspected by comparing two models and ascertained the adequacy of simplified model.

1) A degree of influence whether the non linear characteristic of Seismic isolator and material characteristic of steel bridge pier reflects to the responding results.
2) In inspecting 3-Dimensional model, adequacy of replacing girders to one piece beam.

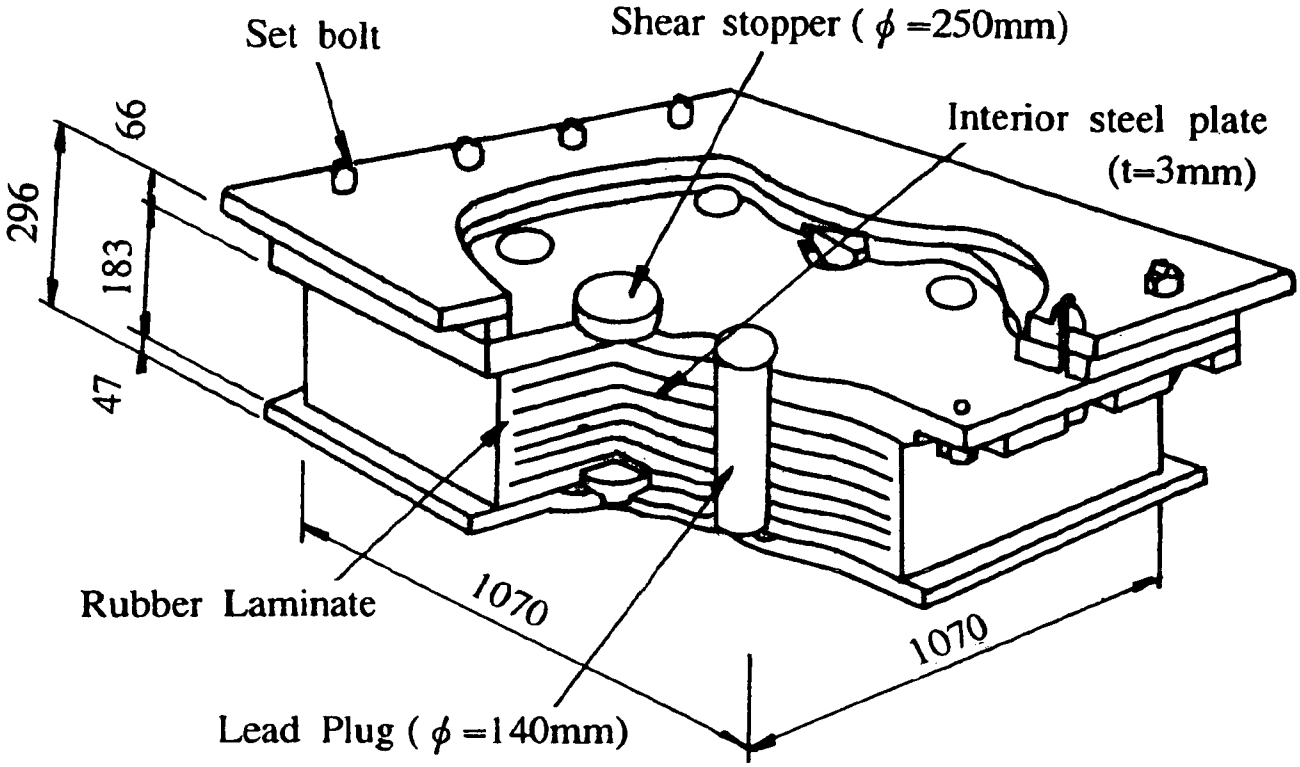

Specification for Seismic Isolator (P457-P461)

Applied Reaction Force		R	987.6tf
Dead Lord Reaction Force		Rd	627.3tf
Vibration At dedign	Design Horizontal Vibration	Kh	0.23
	Allowable Shear deflection	γ_1	150%
Retained horizontal force durig Earthquake at design point	Design Horizontal Vibration	Khc	0.68
	allowable shear deflection	γ_2	250%
Reaction force by Wind load		F	85.5tf
Bearing height (Rubber thickness)		297(168)mm	
Lead plug : pieces × diameter		4pcs × 140mm	

Figure 4. General View of Seismic Isolator

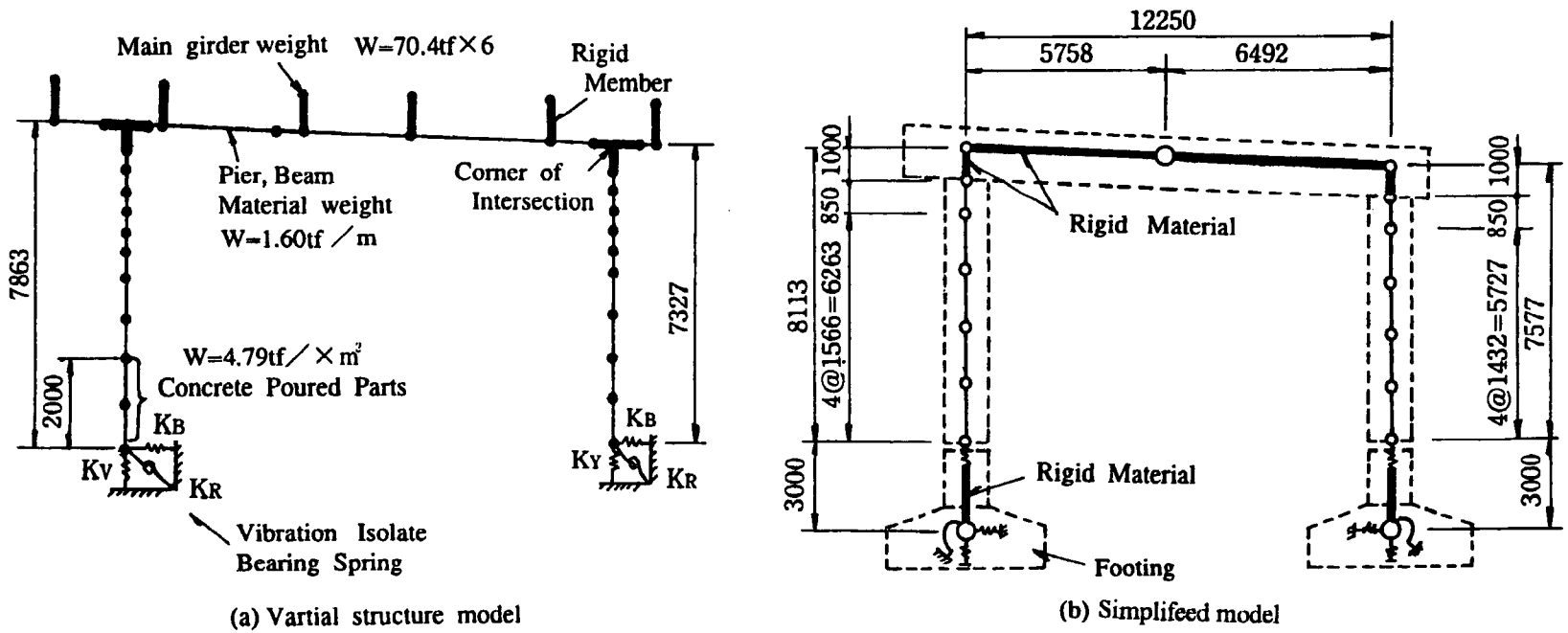

Figure 5. Plane Model for Earthquake Responding Analysis

The seismic wave taken at the JR Takatori Station was applied [2] for the input of seismic vibration. Seismic force of EW wave was put into from chord direction of warped bridge and SN wave to the lateral direction simultaneously.
In comparing the responding values of each model it became apparent that there was least influence due to the non-linear characteristic of bearing and that the deflection at the most part of steel pier was within the elastic deformation.

A comparison of the test results of simplified model that treats bearing and steel pier in a linear form to that of actual structure model, is shown on Table 1. The values for a simplified model are larger but being within safe side it was judged to present no problem to carry out dynamic analysis by applying whole model shown in Figure 3(b).

Table 1. Comparison Between Virtual Model and Simplified Model

			Virtual Structural Model	Simplified Model	Ratio
Position of main girder	Accelerated speed (gal)		1280	1313	1.03
	Horizontal defomation (cm)		660	70.1	1.06
Position of Bearing	Horizontal deformation	seaside (cm)	59.6	67.0	1.12
		mountain side (cm)	60.5	67.2	1.11

2.4 Result of Analysis

From the static analysis, deflections were calculated for each bearing and for the girders at the edge. Girder's deflection reached ±84mm maximum depending on the varied temperature range. Expansion joints was designed based on this deflection.

The results of natural vibration analysis on the whole model is shown on Figure 6 and all up to 5th modes shows inherent mode of horizontal direction. From the result of natural vibration analysis applied on a plane model, the mode for horizontal move at the bearing position is so remarkable that the similar tendency may be seen in a 3-Dimenmsional model.

The time histories were exemplified in the Figure 7 for the response in the horizontal deflection of the seismic isolator and the bending moment at the beam joint at P470. Maximum deflections were 428mm in the longitudinal direction of bridge and 568mm in the lateral direction, which were

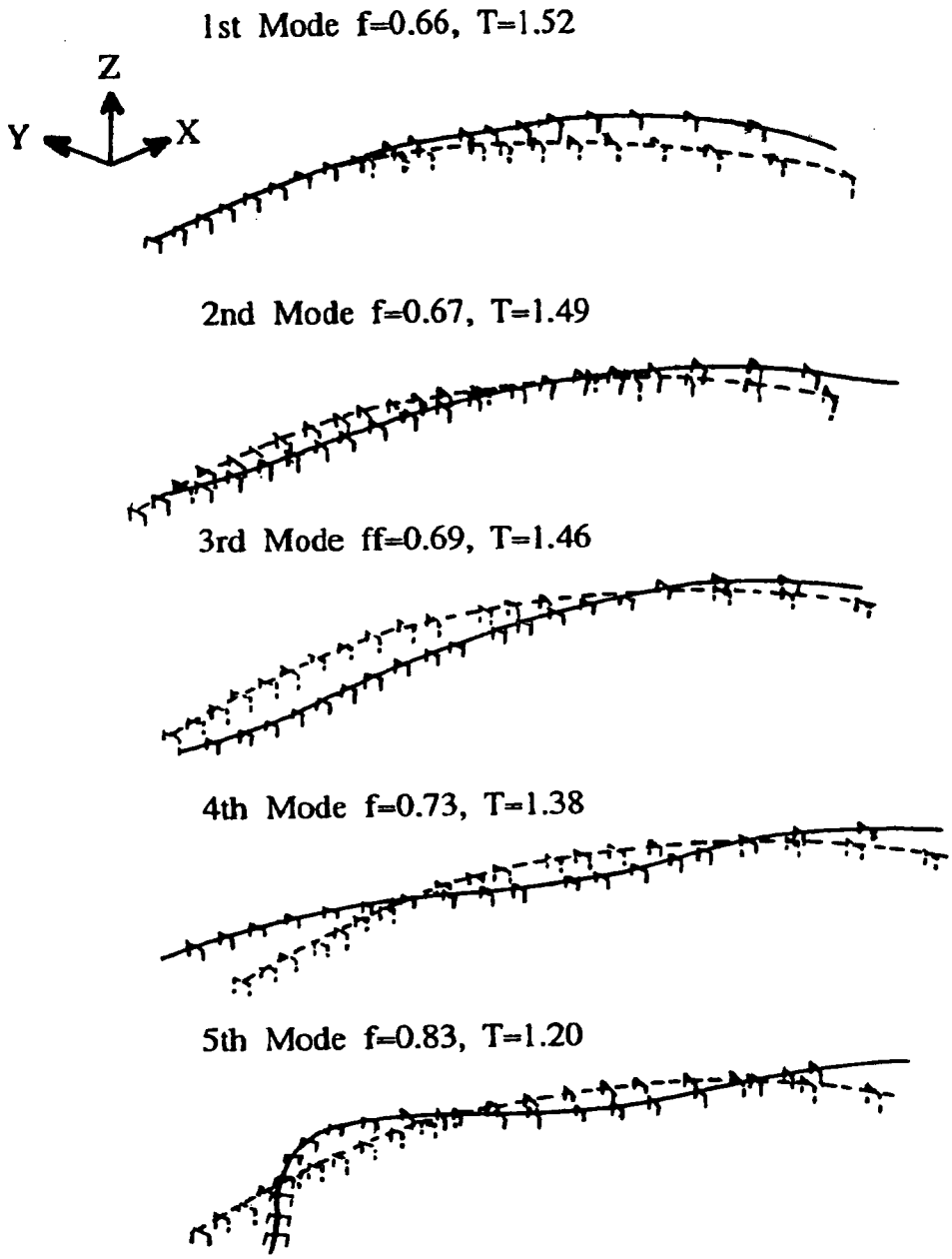

Figure 6. Result of Natural Vibration Analysis

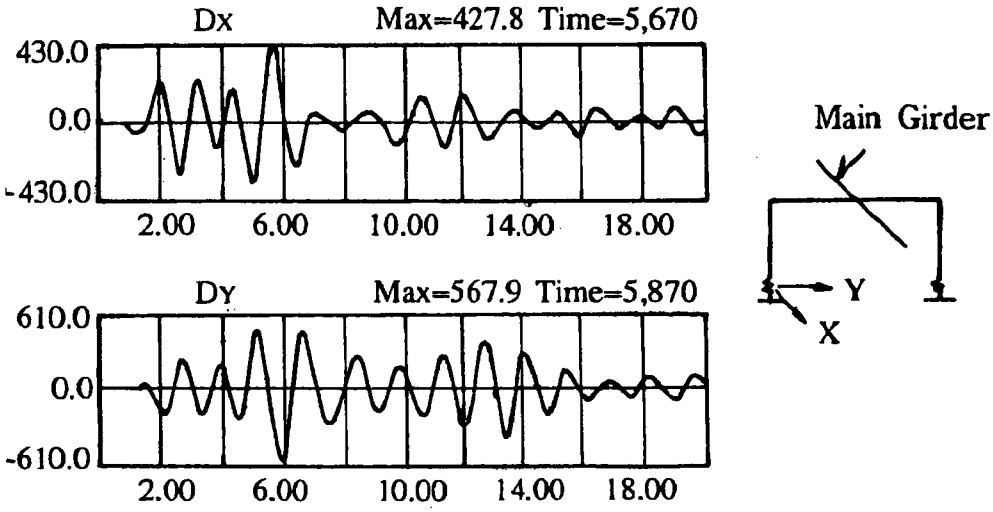

(a) Horizontal deflection of Lead Rubber Bearing at P470 (Seaside)
(X, EW wave Y, NS wave)

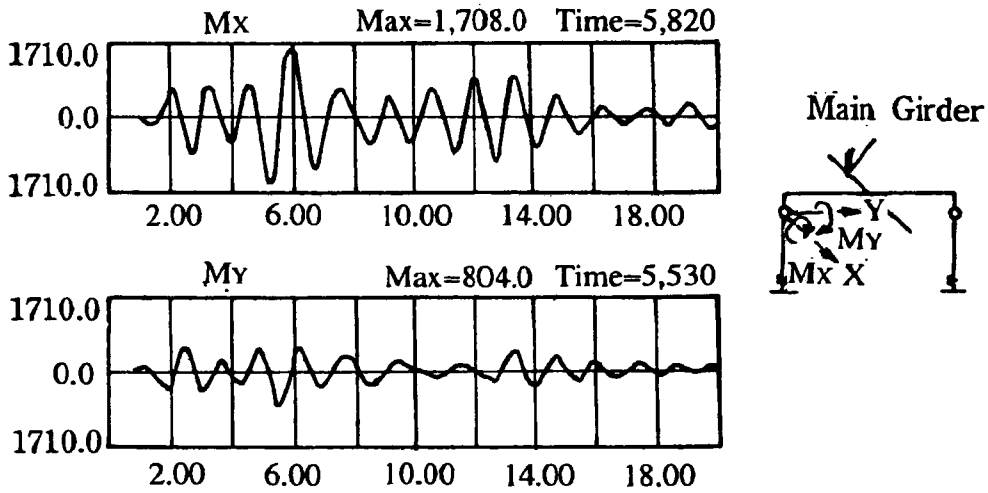

(b) Bending moment at the Corner of Bridge Pier P470 (Seaside) (tf -m)
(X : EW wave Y : NS wave corrected rigidity)

Figure 7. An Example of Response Analysis on Time History

observed after 6 seconds from the beginning of earthquake.

Also the response analysis on time history is confirmed in the rotating deflection of seismic isolator and axial force of pier, which led to carry the test confirming the effectiveness of bearing by using the response value for the 1/3 scale model bearing.

Again the stresses of intersection at the beam and the pier were investigated as the parts that receive axial compressive force and bi-axial bending moment by applying maximum response values.

3. VIBRATION TEST

3.1 Outline of Experiment

In order to ascertain dynamic characteristic of the bridge, it was planned to carry out experiment using the actual bridge. (As shown as Table 2) Since that the bridge has 19-spans which is so much longer and heavier that the vibration experiment by using vibratory equipment, a rapid force release test was brought and the free damping vibration was measured after the release of force. Jointly with this horizontal reaction force and deflection was measured in the static load condition. In grasping vibratory behavior of girders and vibration transmittance through seismic isolation four axis wrecker vehicles of gross weight 47tf (Maximum 4 vehicles simultaneously) was used to run on the bridge and responding figure was measured.

Table 2. Detail and Purpose of Experiment

Detail of Experiment	Purpose
Static load experiment	Confirmation of horizontal spring force equivalent damping constant value
Rapid force release Experiment	Confirmation of vibration mode in the rapid force release. No. of Cycle and damping constant value
Running Experiment of test vehicle	Confirmation of vibrating character of main girders and beams, and rigidity of upper structure Vibration transmittance mechanism to the sorrounding soil

Reaction force support was installed on the bridge foundation and horizontal force was loaded to the lateral direction of the bridge, as shown on Figure 8. Six units of rapid release system were applied

for loading. After studying the effective loading points it was determined to place them at both mountain and sea side piers betweenP462 and P464. Loaded position and measured item as well as position of measure is also shown on Figure 9.

3.2 Static Loading Experiment

Static loading experiment was carried out for the piers of both mountain and sea side individually, or altogether between P462 to P464 and further carried simultaneous load test onto 3 bridge piers. The load was gradually incremented in the order of 50, 100, 150, and 180tf. As an example of experimental result of static loading, deformation of pier P463 is shown on Figure 10(a) and 10(b) when piers between P462 to P464 were loaded on mountain side only and simultaneously from both sea and mountain sides.

As has been studied from this drawing, the loading on one pier represents bigger deflection of loaded pier while the other members shows practically less deflection. Also the case of simultaneous loading from sea and mountain side piers confirm the move to lateral direction but even in this case the deflection value of upper part is smaller than the lower one. Deflection form of whole bridge in lateral direction at this time is shown on Figure 11.

The maximum deflection is 110mm at the pier P463 with the load of 180tf while there was little deflection on the piers with no loads. Figure 12 shows relationship in the horizontal spring rigidity to deflection figure obtained in the laboratory test as well as actual test on bridges. There is a slight difference in a small deflection but the actual data of the horizontal spring rigidity remains as same as done in the laboratory in the range above 80mm.

3.3 Rapid Release Test

Rapid release test was carried out in the loaded condition to reach up to 180tf when the load was abruptly released. Deflection and acceleration were exemplified in Figure 13 in an example of mountain side P463. Deflection went back near to the original position when load was discharged and the vibration component is damped to die. Thereafter the deflection had slowly decreased and in a few minutes after the release went back to the original position completely.

In a response of acceleration, while the free damping vibration is confirmed to remain as in the case of deflection, its vibrated element shows high spectrum at the point of 2Hz. By measuring rotating deflection of bearing and pursuing the vibrating mode of gate bridge pier it became apparent that horizontal vibration at the pier foundation had been damped immediately after the release and thereafter rocking vibration was seen at the center of each bearing .From such observation in the response to the acceleration, higher frequency of vibration is considered to be due to the rocking effect and it correspond with the result of inherent value analysis of hinge reaction which substitute bearing applied to the plane model.

In the response analysis on the time history applied on the cubic model that evaluates the rigidity, it

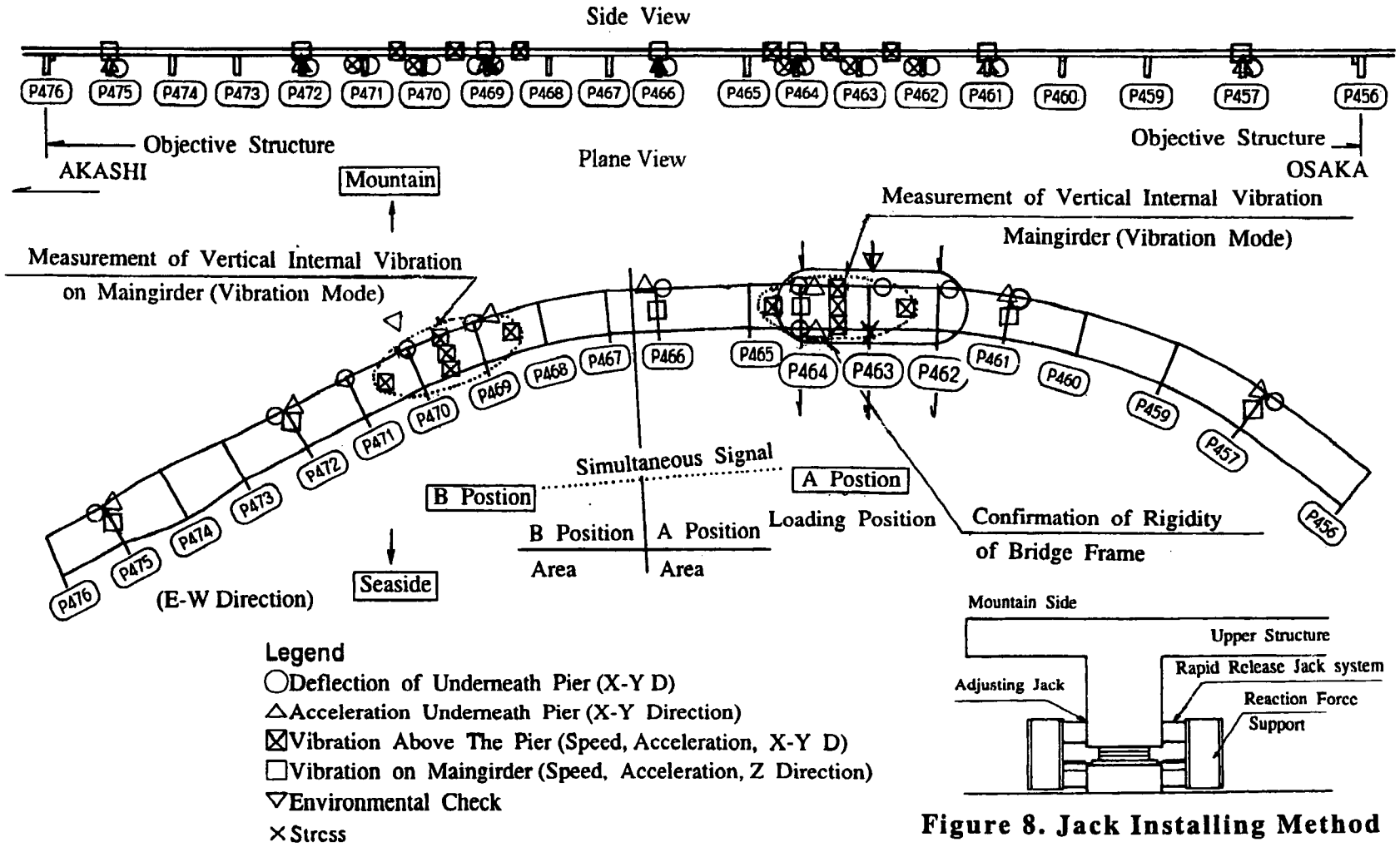

Figure 8. Jack Installing Method

Figure 9. Loading Position and Measured Position

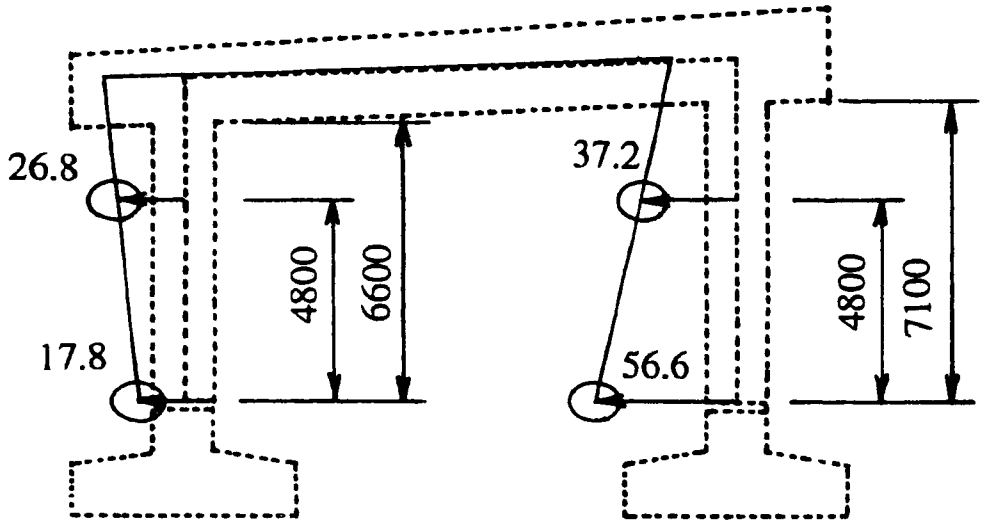

(a) Loading on Mountain Side

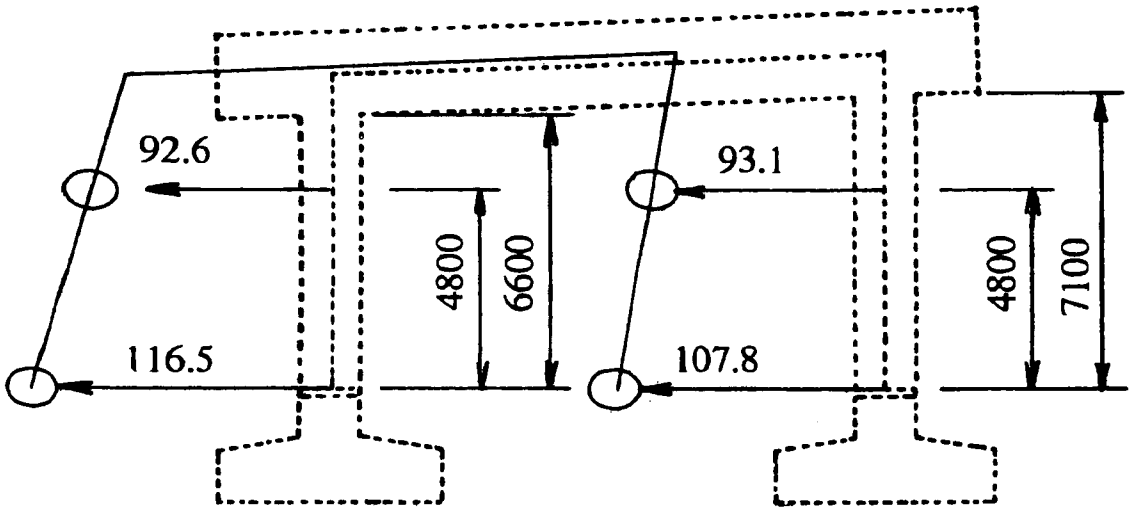

Seaside Pier Mountain Side Pier

(b)Loading on both Mountain and Sea Sides

Figure 10. Deformation of Piers

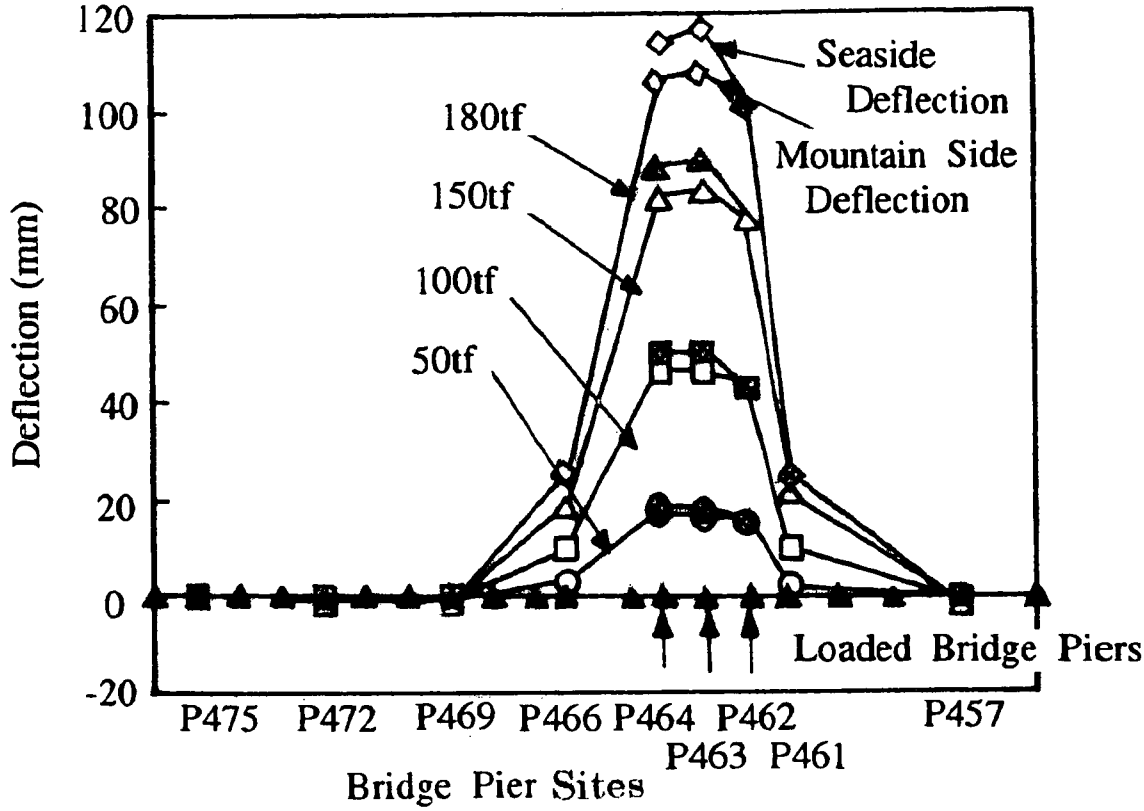

Figure 11. Deflection of Pier Loaded on Downside

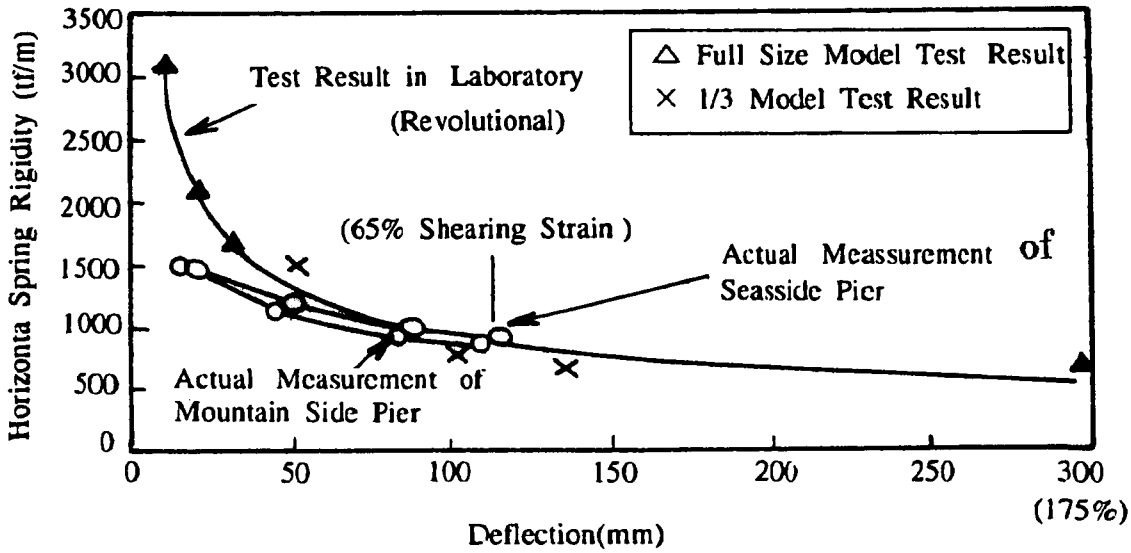

Figure 12. Design and Measurement of Spring Rigidity

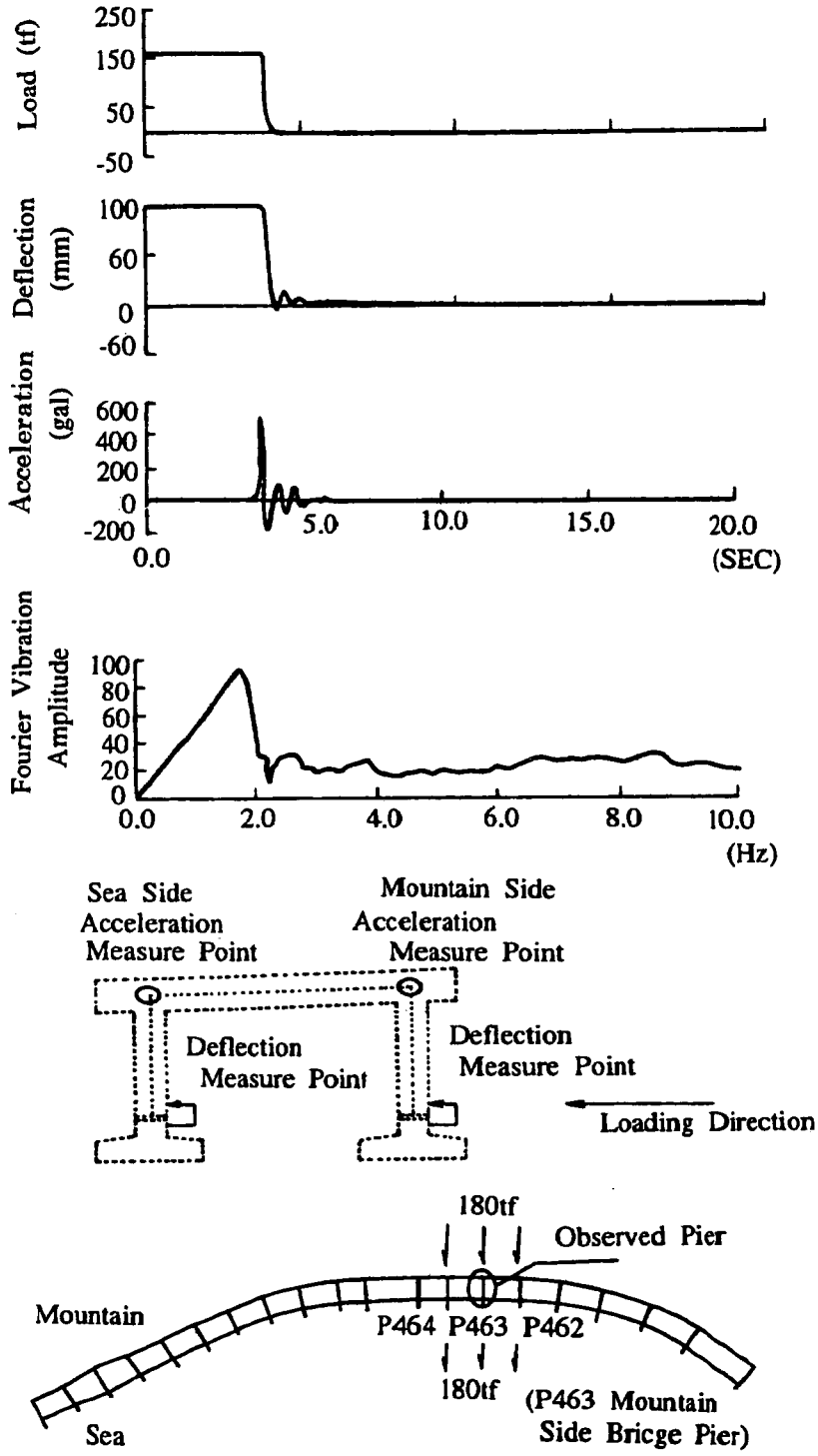

Figure 13. Response Wave Mode at Rapid Release Test

is confirmed that vibration modes of 1st through 3rd are all located under the 0.7Hz, while all present experiments under partial vibrating condition shows a different vibrating element from the designed vibrating characteristics.

Secondly, vibration mode on the whole bridge at the release of load is like Figure 14 and ballooned vibration mode in the vicinity of bridge pier having two nodes prevails immediately after the release of road, however, the position of node moves near around the center of pier P466 and the ballooned mode had been changed to show different vibrating character. Also while the horizontal vibration of whole gate bridge pier has shown the damping effect at the first wave, it was the result to show the case that the vibration at the bearing showed over damping and the deformation figure at the experiment is greater than designed figure.

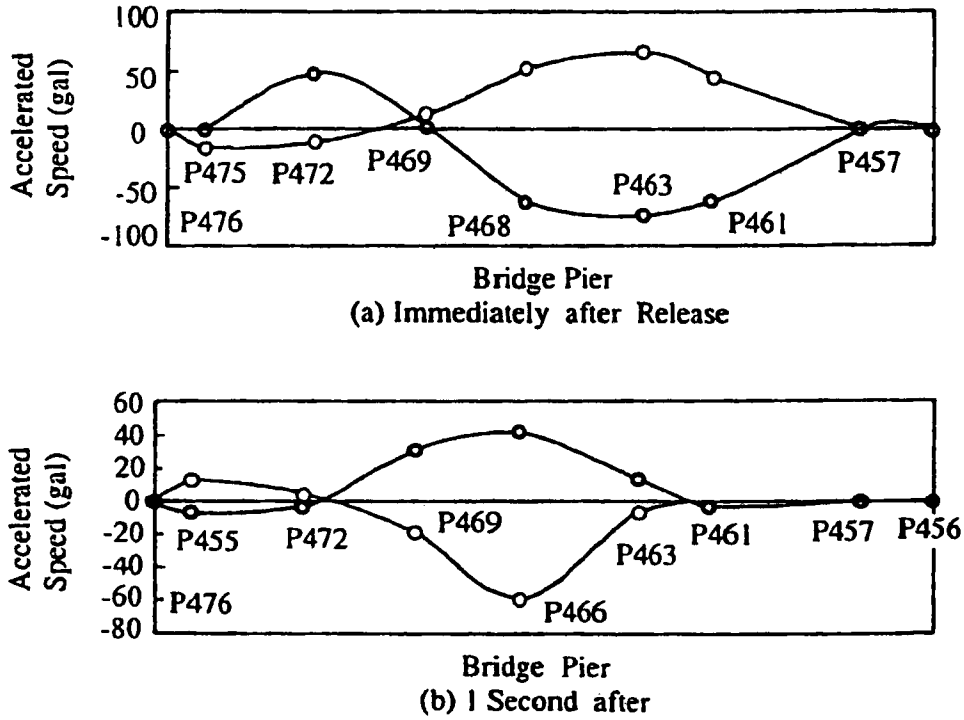

Figure 14. Vibration Mode after Release of Force

In the design of upper part, 2% damping was anticipated, however, calculated damping coefficient from the logarithmic decrement of actual damping wave in a vertical direction had dispersed in the 4~5% area.

At the time of rapid release the representing vibration mode of main girder and its vibrating frequency values between 5.3Hz and 6.3Hz in torsional mode, and between 9.0Hz and 10.0Hz in bending mode, shown in Figure 15.

Vibration Mode	Vibration Frequency	Vibration Mode Figure
Tortional Mode	5.3~6.3 Hz	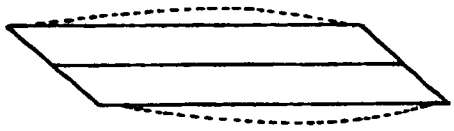
Bend Mode	9.0~10.0 Hz	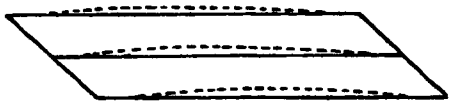

Figure 15. Vibration Mode and Frequency on Main Girder

3.4 Test Vehicle Running Experiment

Vehicle Load running experiment had been carried out at the speed of 20,40,60 km/hr with one vehicle and parallel drive of 2 or 4 vehicles at 20km/hr speed and the effect of each running pattern was studied. As an example of the result, the pattern for the damping effect taken from the longitudinal direction of bridge with one vehicle at the speed of 60km/hr is shown on Figure 16.
Both underneath and upper bridge pier vibration had prevailed to show 2.32, 2.47, and 2.66, however, the above frequency zone did not prevail at the foundation. Similar tendency was observed in the lateral direction.

4. CONCLUDING REMARKS

Here it was reported of the new trial 19-span continuous rigid frame bridge with seismic isolator at the bridge piers and outline of design as well as contents of vibration experiment carried on actual bridge. Although the loading condition is limited to a partial experiment, the vibration character of seismic isolator, bridge pier and upper structure was confirmed. However, the present experiment could not verify the vibration obtained in the dynamic analysis. This is due to the fact that the loading was done only 3 sets of bridge pier out of 18 and that the rigidity of bearing had a bigger value than what was presumed to be.

5. ACKNOWLEDGMENTS

We are greatly indebted to the courtesy of Technical Committee For The Restoration From The Earthquake(Chairman, Dr. Yoshikazu YAMADA) and especially to the Benten Bridge Structure Study Sub-committee (Chairman Dr. Yuhshi FUKUMOTO) for their valued suggestions and

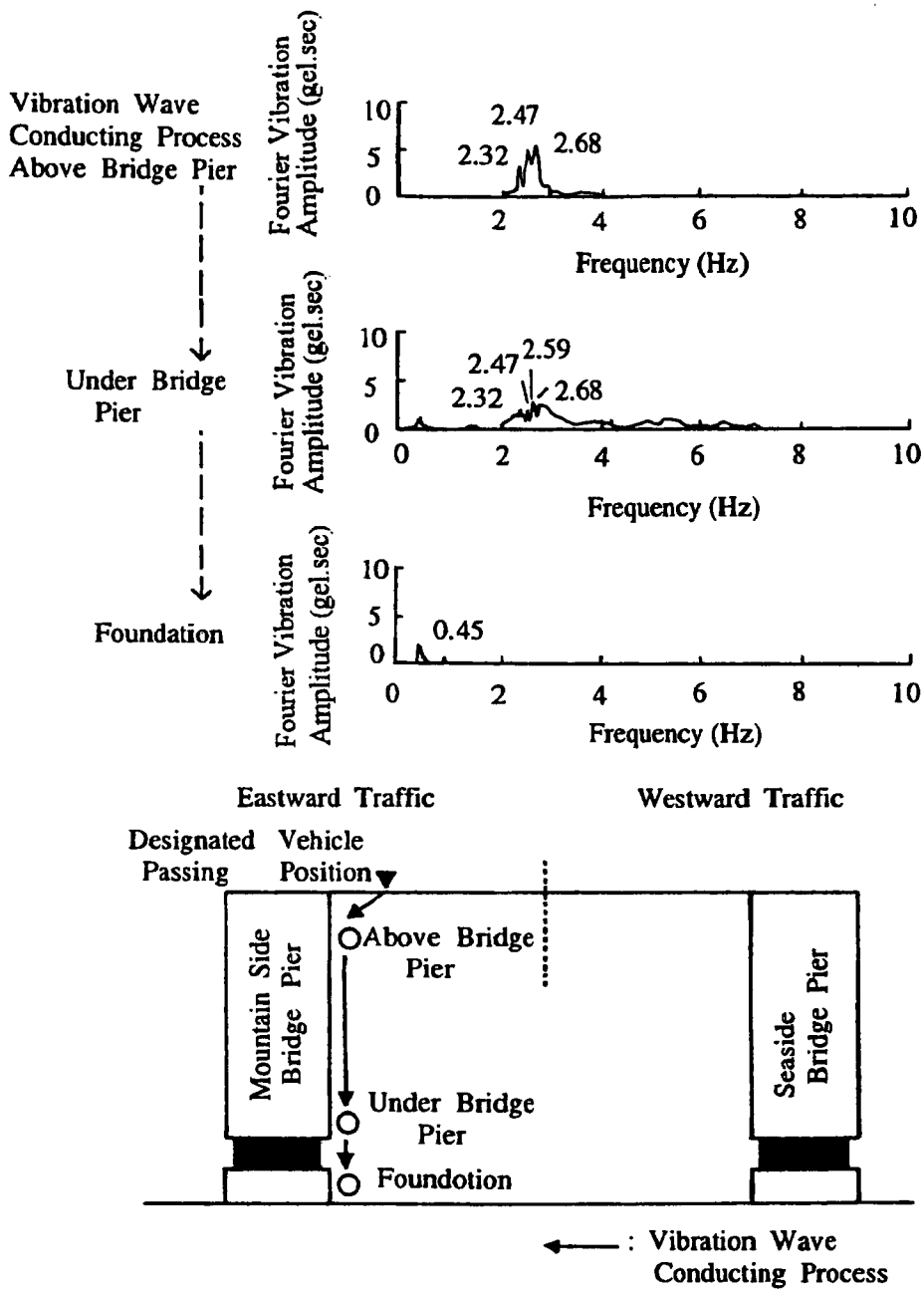

Figure 16. Damping Effect of Wave Frequency Zone at the Time of Test Vehicle Running Experiment (Bridge Axial Direction)

comments. Our appreciation also goes to the courtesy of the Institute Of Laboratory, in The Japan Highway Public Corp. for providing equipment for Rapid Release Jack System, together with the collaboration extended from Fuji Engineering Co., Ltd. to achieve actual experiment on the aforementioned bridges.

REFERENCES

[1] Japan Institute of Construction Engineering : Report on the Anti-seismic Design for High way Bridge with Seismic Isolator

[2] Railway Technical Research institute, Mr. Yutaka NAKAMURA : Seismic Vibration Report on The Hanshin Awaji Earthquake, 1995 and Its analysis, JRVI,I Earthquake Report No.23c, 1995

SEISMIC RETROFITTING OF A HIGHWAY BRIDGE THROUGH SLAB JOINING AND ISOLATION

G. Monti [1] R. Marnetto [2]

[1] Dipartimento di Ingegneria Strutturale e Geotecnica – Università La Sapienza, Roma

[2] T.I.S. S.p.A., Roma

ABSTRACT

A retrofitting intervention is presented of a bridge located on a highway of central Italy, in a highly seismic area. The bridge is made of a series of simply supported decks. In order to avoid slab joints between adjacent spans, it was required to join the deck slab, thus modifying the mechanical configuration of the bridge and its seismic response. An isolation intervention was therefore deemed necessary, in order to avoid the high ductility demands on the shorter piers induced by the new configuration. The isolation was obtained through a new type of isolating device, which was extensively tested and showed a stable hysteretic behavior. A series of dynamic analyses, both at the ultimate and the damage limit state, are here presented, carried out to verify the effectiveness of the intervention. The analyses also account for the effects of temperature variation with respect to the time of installation of the isolation devices.

1. INTRODUCTION

In Italy, seismic isolation techniques are widely adopted for retrofitting highway bridges. A large amount of bridges of the Italian highway system have been built in the sixties with a structural scheme of cantilever piers and a deck made from simply supported beams. A typical retrofitting technique is the joining of the deck slab which is therefore transformed into a continuous beam. This solution is generally adopted to redistribute the seismic forces among the piers in the transverse direction or to concentrate the longitudinal ones on elements (piers or abutments) whose seismic resistance can be improved to a satisfactory level. In the case of long decks, where significant forces are mobilized by the seismic action, it is possible that this improvement cannot be obtained, and therefore the solution of isolating the piers is adopted.

Such an intervention has been recently proposed on the S. Angelo bridge, located along the Roma–L'Aquila highway in a zone of high seismic risk. The intervention will be executed in the coming spring and in this paper a series of analyses, performed to verify the effectiveness of the retrofitting intervention, are presented.

The paper is divided into two parts. In the first part, the essential features of the adopted isolating devices are presented, along with some experimental results attesting for their satisfactory performance under seismic action. In the second part, the results of numerical step-by-step dynamic analyses on the bridge are presented, both before and after the intervention, where problems related to both the ultimate and the damage limit state are addressed. As a final investigation, the changes introduced in the isolators performance by a temperature variation are studied.

2. DESCRIPTION OF THE ISOLATING DEVICE

At the design stage, different solutions were investigated regarding the type of device to be adopted for the isolation of the S. Angelo bridge. As a first attempt, elastomeric bearings were considered, because of their widely known features, such as: isotropic horizontal mechanical properties, high number of large cyclic deformations, and the ability to carry also vertical loads as well as to absorb all service load deformations. However, this option was soon discarded because it was also recognized that, beyond the positive aspects described above, some substantial drawbacks exist, such as: sensitivity to aging effects, durability problems if used in aggressive environment, additional $P-\Delta$ effect brought in by the isolator deformation. All of these drawbacks contrasted with the requirements deemed as fundamental by the client of a reliable and durable retrofitting intervention.

On the basis of the above considerations, it was decided to adopt a new type of elasto-plastic device, internationally patented by T.I.S. S.p.A. (Italy). The technology is based on the use of metallic strips, cold bended to obtain U-shaped elements. The mechanics of such an element is depicted in Figure 1 where a single U-element is shown. Under relative longitudinal movements of the opposite ends, the element behaves like a track: sections belonging to the straight legs enter the rounded portion, where they are imposed a yielding curvature, while sections belonging to the rounded portion are transfered to the legs, where they are straightened. The yielded sections keep moving along the rounded portion, with constant curvature, and therefore maintain their yield stress, without undergoing any hardening. As a consequence, the resisting force of the isolator has no further increase, which is a desirable feature for a force-cutting device.

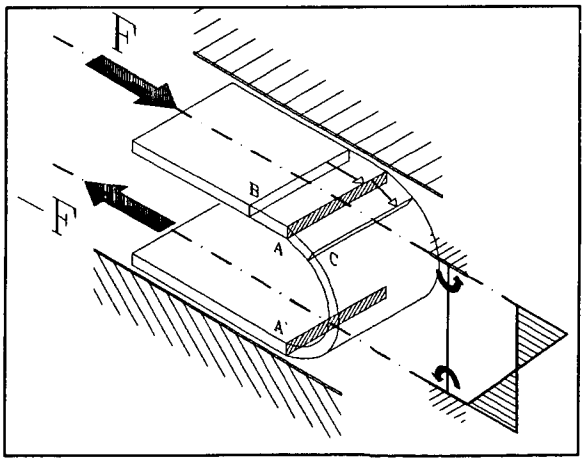

Figure 1. Mechanics of a single U-shaped element.

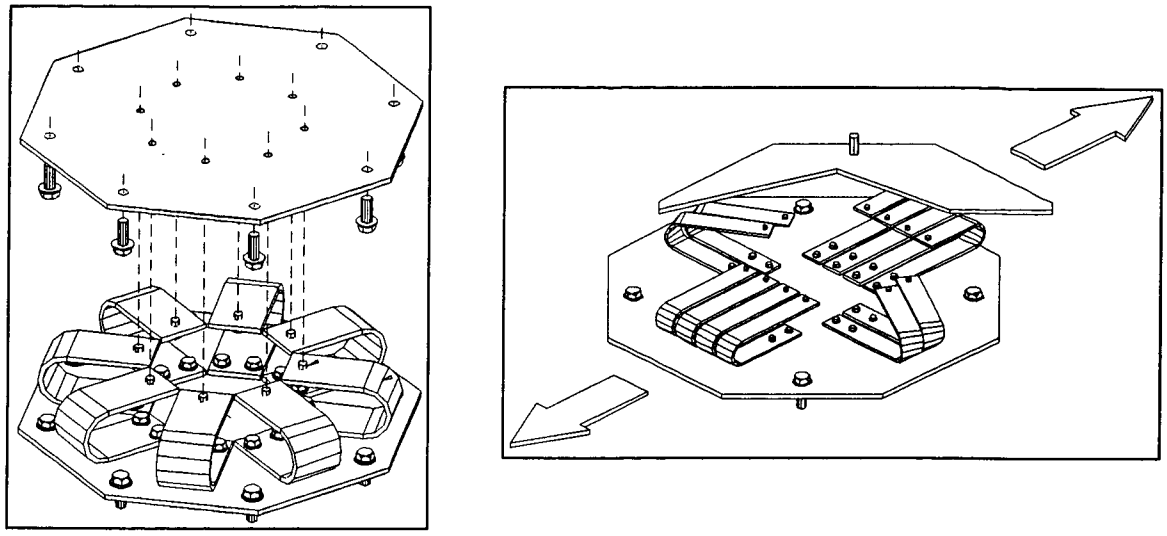

Figure 2. Bi-axial devices: plane-isotropic (left) and plane-orthotropic (right).

The dimensions of the U-shaped steel elements can be easily and independently calibrated to obtain the desired values of initial stiffness, yield threshold, and maximum displacement. In particular, it should be noted that the initial stiffness and the yield threshold depend only on thickness and radius of the rounded portion, while the maximum displacement depends only on the length of the straight legs, being almost double of it.

Bi-axial devices can be realized by simply combining U-elements in a radial pattern. Through this arrangement, it is possible to obtain devices with plane-isotropic response or plane-orthotropic response (Figure 2). A practical implementation is achieved by connecting the legs of each U-element to two external plates. The connections are realized by two bolts on one plate, to obtain a torsional constraint, and by a single bolt on the other plate, to obtain a cylindrical hinge (Figure 3).

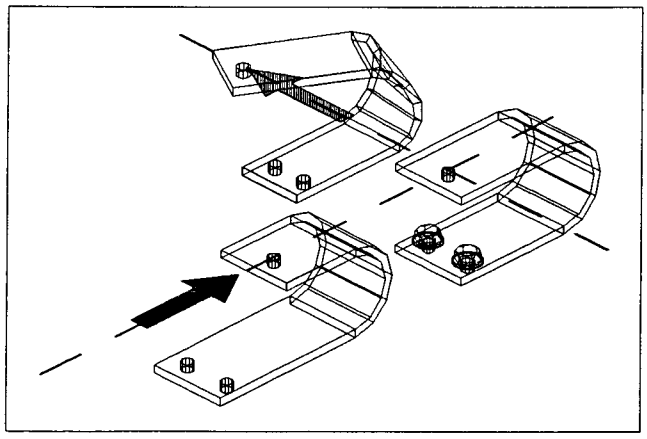

Figure 3. Bolted connections arrangement for transverse deformation mode.

Within the assembled device, each U-element undergoes deformations on any direction of the horizontal plane. It is expedient to consider the device response as resulting from the superposition of different deformation modes, two of which are represented in Figure 4. However, while the U-element response can be easily predicted under longitudinal deformations (mode A), it becomes significantly more complex under transverse deformations

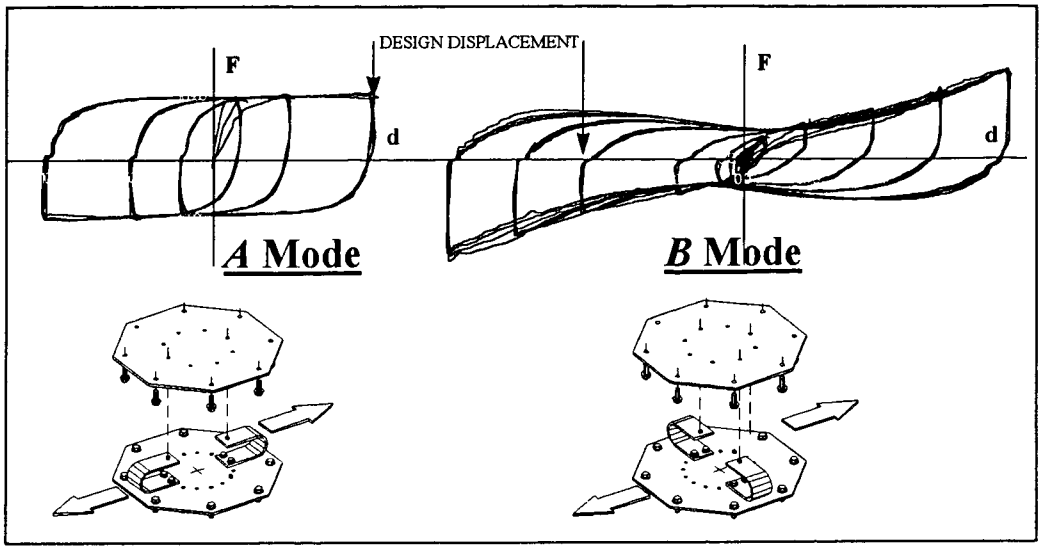

Figure 4. Deformation modes and relative force-displacement diagrams.

(mode B), due to the interaction of flexure with torsion, shear and tension/compression at various sections of the strip. Consequently, the actual overall nonlinear behavior due to the composite action of the various modes is more difficult to predict.

Experimental tests as well as numerical simulations have been performed (Dolce *et al.* 1996) to study the actual load-displacement relationships. The examination of the diagrams in Figure 4 allows a better understanding of the U-element behavior, especially for as regards the influence of the deformation angle with respect to the element axis.

It can be observed that, for mode A, a very stable hysteretic response is obtained and that the plastic branch practically shows no hardening, as mentioned above. Mode B is also stable, but the post-elastic stiffness increases as the displacement increases, and becomes very steep for high displacements. This stiffening effect is due by the tensile action of the strips that mobilizes as they deform transversely, and is proportional to the "transverse-displacement/leg-length" ratio. However, it should be remarked that the stiffening effect starts becoming significant at transverse displacement levels comparable to the leg length. Therefore, since the length of the U-element legs is usually designed as equal to (or slightly lower than) the maximum design displacement in longitudinal direction, this means that in the composite action the transverse displacement cannot exceed the leg length, and then this phenomenon can be disregarded from the practical standpoint.

3. RETROFITTING OF THE S. ANGELO BRIDGE

3.1 Description of the bridge

The S. Angelo bridge is located along the Roma–L'Aquila highway, in a highly seismic area, classified as first category in the Italian Seismic Code, with an (elastic) peak response acceleration (seismic coefficient) equal to 0.1g. The longitudinal profile of the bridge is shown in Figure 5, where it can be observed that the deck is supported by 18 piers of different height.

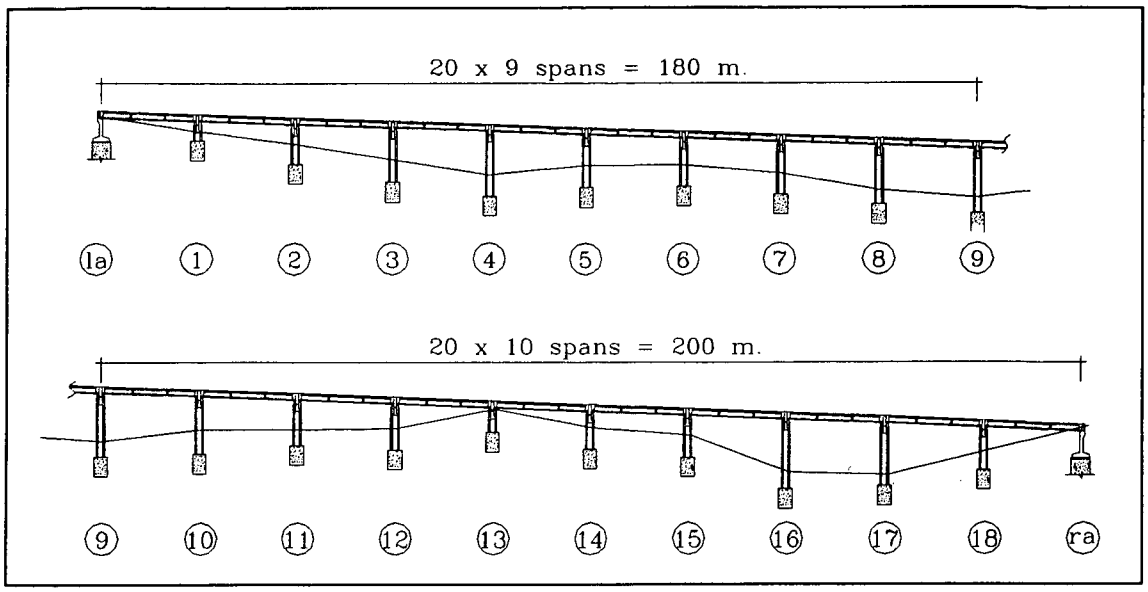

Figure 5. Longitudinal profile of the S. Angelo bridge, from left abutment to pier 9 (above) and from pier 9 to right abutment (below).

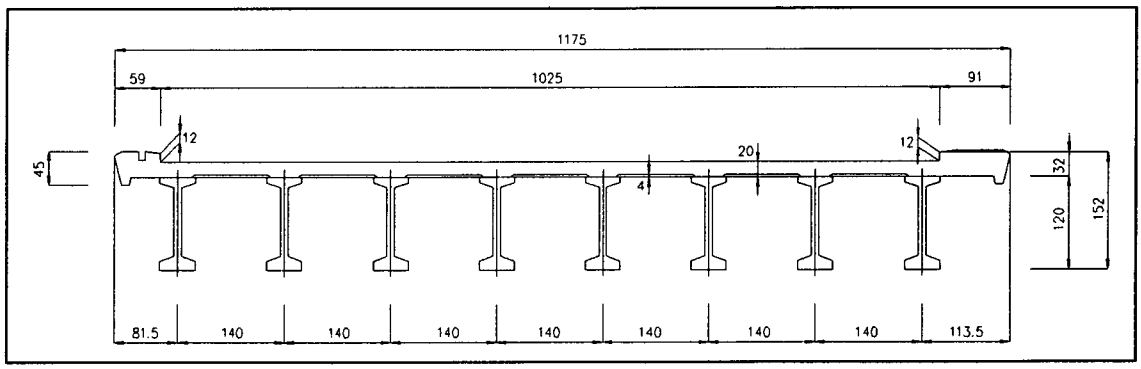

Figure 6. Transverse section of the deck.

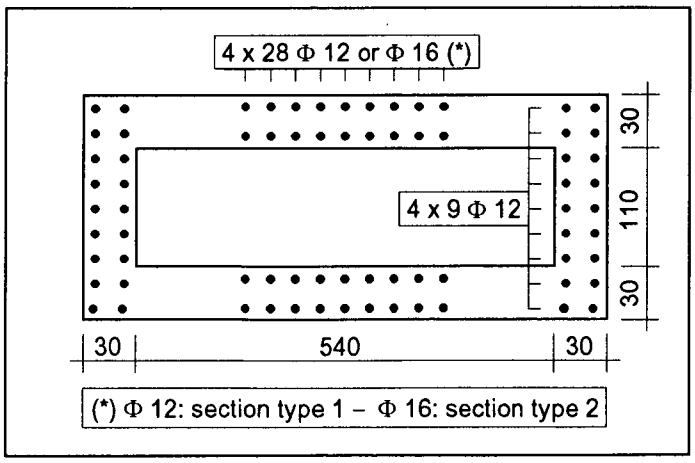

Figure 7. Dimensions and reinforcement of section types 1 and 2.

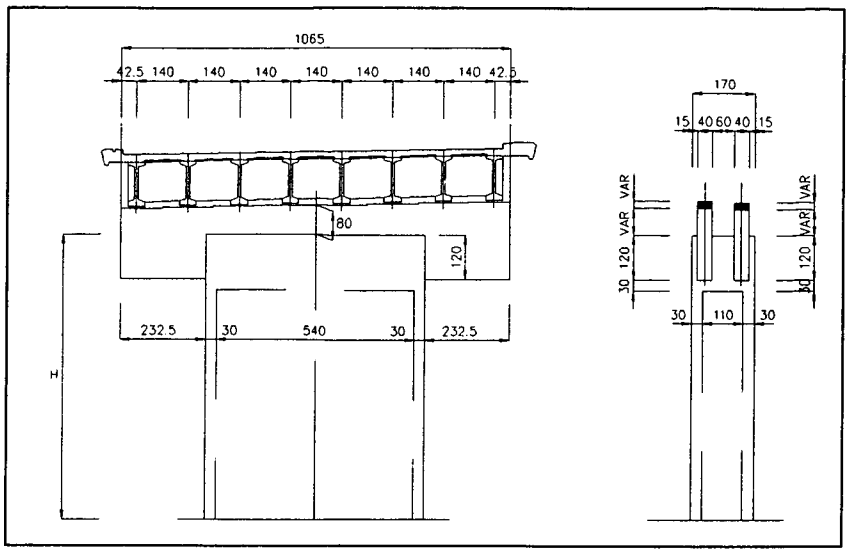

Figure 8. Transverse (left) and longitudinal (right) view of the standard pier and the pier cap.

The deck is constituted by eight simply supported prestressed beams, topped by a concrete slab jointed at each pier support (Figure 6).

The piers have a hollow rectangular section, and are all of the same dimensions, with two different types of reinforcement configuration (Figure 7). The pier cap is made from a full concrete topping and from two walls supporting the deck beams (Figure 8).

In Table 1 the height and section type of each pier are listed.

Table 1. Characteristics of the piers (H = height (in m), Sec = section type).

Pier	1	2	3	4	5	6	7	8	9	10	11	12	13	14	15	16	17	18
H	4.0	8.0	11.0	13.0	10.6	9.6	10.6	11.9	12.9	11.7	9.1	9.2	4.8	7.5	8.4	14.1	12.6	8.6
Sec	1	1	2	2	2	1	2	2	2	2	1	1	1	1	1	2	2	1

3.2 Description of the intervention

The S.A.R.A. (Roma–L'Aquila Highway Department) required that the bridge be retrofitted, by giving as primary design input the possibility of having a continuous slab, in order to reduce the cost of joints maintenance. For reasons related to temperature variation, it was necessary to foresee a joint at center bridge over pier 9, thus dividing the whole bridge into two independent bridges (denoted as bridge 1 and bridge 2, from now on) with continuous deck slab: bridge 1, spanning from the left abutment to pier 9, for a total length of 180 m, and bridge 2, spanning from pier 9 to the right abutment, for a total length of 200 m.

The joining of the deck slab is performed by first demolishing part of the existing slab on each side of the deck on all the piers, and then by constructing a reinforced concrete slab with the bars well anchored in the existing slab (Figure 9).

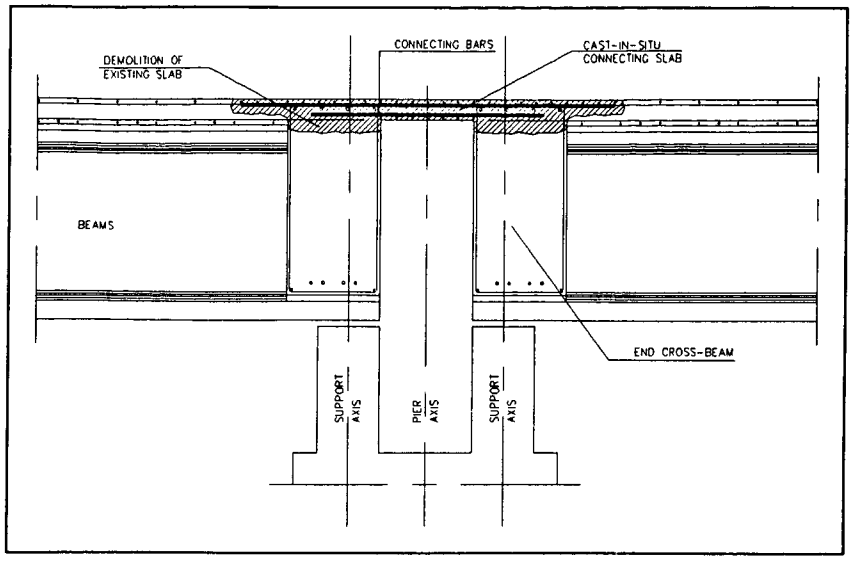

Figure 9. Slab joining intervention.

The isolation is achieved by means of the dissipative devices presented in the previous section. In Figure 10 and Figure 11 a detail of the intervention is depicted, where it can be seen that one single isolator is installed on top of each pier at the middle of the end cross-beam. The isolator is connected at the top to the two facing end cross-beams by a steel flange, while at the base it is anchored to a cast-in-situ support slab. In Figure 10 it is also shown that a replacement of the pier cap concrete cover was done. The particular configuration of the isolating devices (Figure 12) was imposed by the limited space available between the deck and the piers cap. The isolating devices in Figure 12 have an in-plane ortho-isotropic type of behavior. The analyses to be presented in the following section, however, refer to the longitudinal direction only, which is by far the most unfavorable one for the piers.

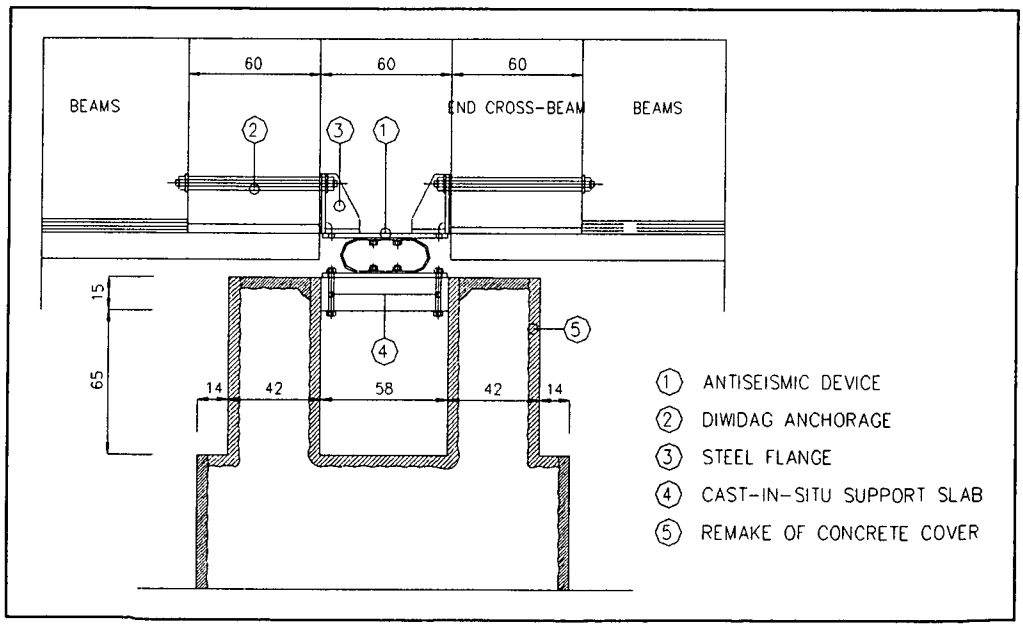

Figure 10. Isolating device arrangement on standard piers (longitudinal section).

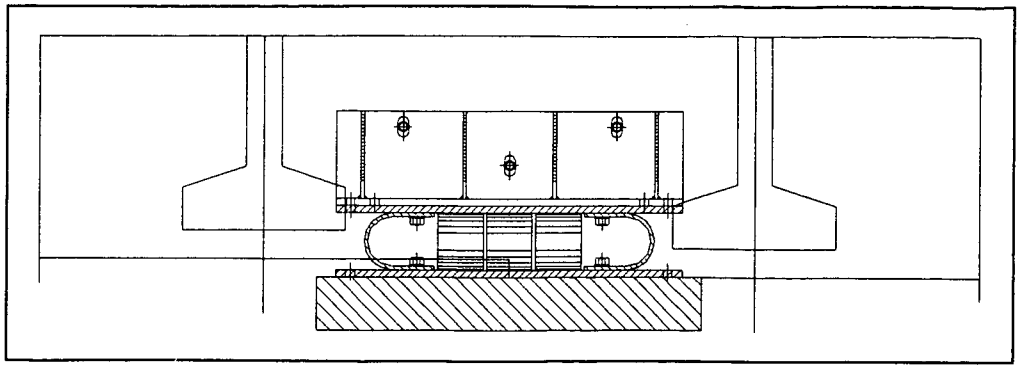

Figure 11. Isolating device arrangement on standard piers (transverse section).

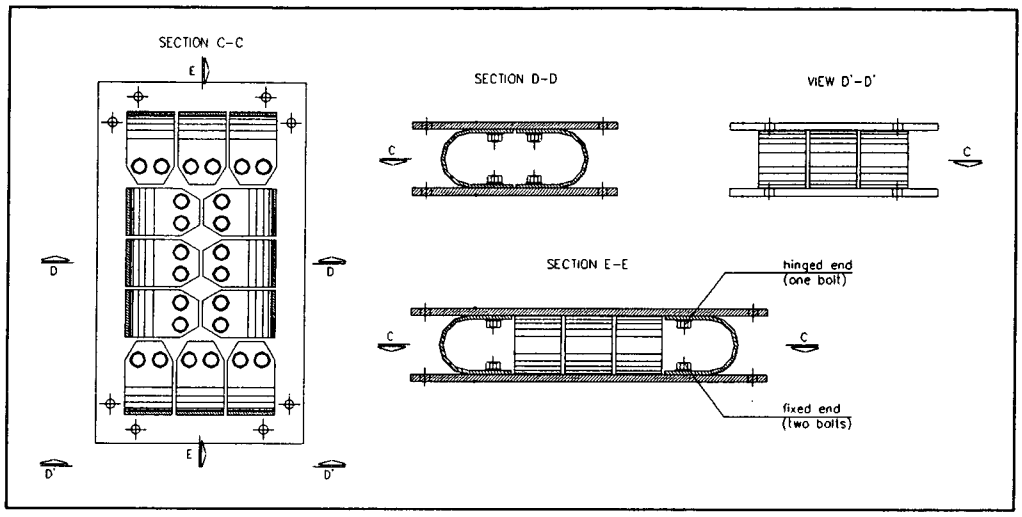

Figure 12. Isolating device.

4. NUMERICAL VERIFICATION OF THE INTERVENTION

4.1 Nonlinear model of the bridge

The seismic performance of the bridge, both before and after the retrofitting intervention, was numerically simulated by means of a modified version of the program ASPIDEA (Giannini *et al.* 1992), which performs a direct step-by-step analysis of bridges subjected to earthquake. In the model, dissipation devices can be inserted between deck and piers or abutments. The deck is considered as elastic, which is a reasonable assumption for the case at hand where the deck is made from prestressed beams. Piers and isolators have a nonlinear behavior. The piers are cantilevers with a plastic hinge of finite length at the base. The base section has a nonlinear Takeda model. In the analyses, $P-\Delta$ effect due to the pier deflection is included. Note that, in the bridge examined, $P-\Delta$ effects come from the piers top deflection, but no additional $P-\Delta$ effect is brought in by the isolator displacement with respect to the pier top, because the deck weight is transferred to the pier through teflon bearings at fixed positions. The program was modified to account also for temperature effects.

All analyses were conducted by sequentially imposing 5 different synchronous acceleration histories at the piers base. The artificially generated histories all have a duration of 20 sec with

a central stationary part of 12 sec and have been obtained from the EC8 response spectrum on firm soil.

The moment-curvature relationship of the base sections of the piers was evaluated with the program CYRUS (Monti *et al.* 1996), in which the section is discretized into concrete and steel fibers. The mean values of concrete and steel strength were considered, equal to 35 MPa and 500 MPa, respectively. The two section types identified in the previous section are subjected to constant axial load equal to 4083 kN and 4560 kN, respectively, determined as the average of the different axial loads (coefficient of variation 8% and 3%, respectively) on the piers with the same section type. The sections, under monotonically increasing curvatures, are then driven to collapse, identified either when the uppermost confined concrete fiber reaches the strain of 0.005 or when (which was always the case) the lowermost steel bar reaches the strain of 0.1.

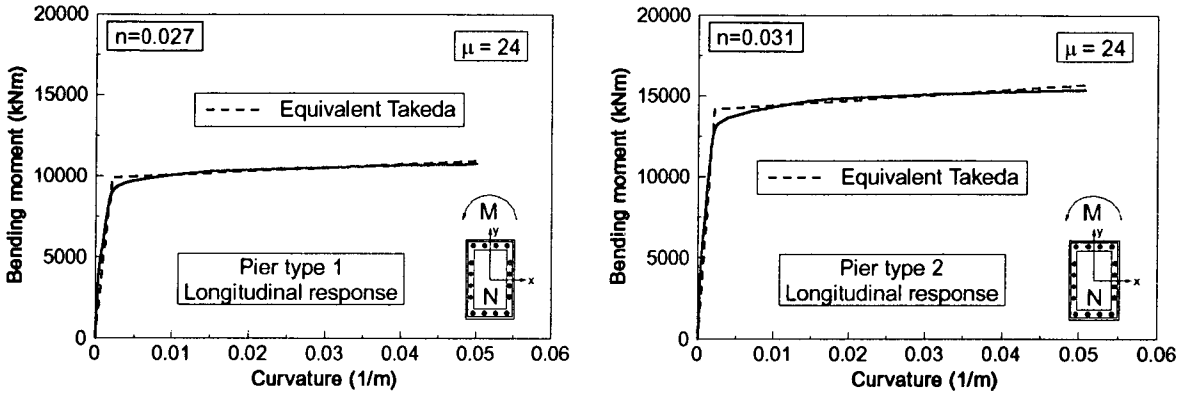

Figure 13. Response of section types 1 and 2.

The sections responses are depicted in Figure 13. The high available ductility of $\mu = 24$ is due to the reduced axial load n, which is extremely low in both cases. The so-determined section behaviors are then represented through two simplified models of the Takeda type, whose parameters have been identified as indicated in Table 2:

Table 2. Takeda-parameters of section types 1 and 2
(Note: curvatures in 1/m, moments in kNm, stiffnesses in kNm^2).

Section Type	Yield Curvature	Yield Moment	Yield Stiffness	Ultimate Curvature	Ultimate Moment	Hardening Ratio
1	.002059	9916	4,815,000	.0501	10940	.004
2	.002082	14139	6,792,000	.0507	15678	.005

Table 3. Characteristics of the isolating devices.

Isolator Type	Yield Force (kN)	Stiffness (kPa)	Hardening	Friction
1 (standard piers)	550	22000	0.03	0.01
2 (pier 9)	275	11000	0.03	0.01

In Table 3 the characteristics of the two adopted types of isolating device are listed. Isolator type 1 is used on all the piers, while isolator type 2 (with halved strength and stiffness) represents the twin isolators that are installed on pier 9 under the two jointed deck ends. Note

that the values listed in Table 3 represent the effective upper bound values (a variation of ±7% with respect to the design value is suggested by the producer).

A pragmatic design constraint imposed that all the isolators have the same characteristics. Therefore, the yield force of the isolators was designed according to the following criterion: the force on top of each pier producing the allowable stress state at the base section was calculated (this force amounts to almost half of the force producing yield at the base section) and the lowest among these values was adopted as the yield force of all the isolators.

The isolators stiffness was chosen in order to have a yield displacement of 25 mm. This value was meant to be at least 50% larger than the maximum displacement imposed on the isolators by the deck under a temperature variation of $\Delta T = \pm 15°$. Since the deck is supported by rollers at the abutments, the elongation due to temperature variation takes place symmetrically with respect to the deck center: therefore the isolators will undergo imposed displacements proportional to their distance from the deck center. The maximum displacement amounts to 14 mm ($\alpha \, \Delta T \, L_{TOT}/2 = 10^{-5} \cdot 15 \cdot 180/2$) for the isolators on the farthest piers of bridge 1 (piers 1 and 9) and 15 mm ($\alpha \, \Delta T \, L_{TOT}/2 = 10^{-5} \cdot 15 \cdot 200/2$) for the isolators on the farthest piers of bridge 2 (piers 9 and 18).

The hardening adopted in the calculations is that obtained from experimental tests on the isolator device.

The friction coefficient of 0.01 is that typical of teflon bearings, even though experimental evidence shows that lower values can be attained. Analyses with a friction coefficient of 0.03, as suggested by the Italian Seismic Code, were also performed, where it resulted that in this case, as expected, a lower ductility was required in the isolators and that the elastic behavior of the piers was not significantly affected. Being closer to the actual one, the coefficient 0.01 was adopted for all the calculations.

In the following, the verification analyses performed on the bridge are presented. As already indicated, longitudinal analyses only have been performed, after having checked that the bridge transverse behavior does not present particular problems, thanks to the high transverse strength of the piers. The analyses are divided into two groups: those meant to ascertain the ultimate limit state of the bridge under a peak ground acceleration (PGA) of 0.35g, and those assessing the damage limit state under a PGA of 0.12g. To complete the study, additional analyses have been performed to assess the effects of temperature variation on the isolators.

4.2 Ultimate limit state analyses

The bridge response was analyzed under PGA=0.35g. The following situations were studied:

- bridge response before the intervention,
- bridge response with only the slab joining intervention,
- bridge response with both the slab joining and the isolation intervention.

The bridge response is presented in the following Figures. The responses of the two parts of the bridge, 1 and 2, are depicted in the left and the right Figures, respectively. The pier in common between the two bridges is pier 9, where the expansion joint is located. The bridge

response in each one of the above-described situations was obtained from 5 analyses performed under 5 different spectrum-compatible acceleration histories. The response is evaluated in terms of the maximum request of curvature ductility at the piers base and the maximum request of ductility in the isolators. For each pier and isolator, the mean value and the high/low range are represented.

In Figure 14 the bridge performance before the intervention is depicted. All the piers act as free cantilevers, since the deck spans are simply supported on adjacent piers. It is seen that the required curvature ductilities are well below the available one ($\mu = 24$), but their values are high enough to produce significant damage at the plastic hinges and to justify a retrofitting.

It should however be recalled that the basic requirement, imposed by the Highway Department, was to obtain a continuous deck. The bridge performance under this new static scheme is presented in Figure 15 (above), where it can be observed that in this case the shortest piers (1 and 13) attract a significant portion of the seismic force, and are therefore required an amount of ductility closer or higher than the available one. In order to avoid such an undesired behavior, an alternative scheme with rollers on the shortest piers was examined (Figure 15, below). Piers 1 and 13 remain obviously in the elastic range, but the request of ductility in the others results nonetheless so high that it was decided to resort to isolation anyway.

The response of the isolated bridge is presented in Figure 16, where the beneficial effects of isolation can be appreciated on all the piers, that remain elastic also for the upper bounds. As regards the ductility extracted from the isolators (Figure 16, below), most of them have an average value around 4.5, with upper bound around 7, while those on the taller piers have ductility requests of around 2. Referring to the average values, and considering the value of 2 as the isolators damage threshold, in view of a post-quake intervention, it can be estimated that 13 out 18 isolators need to be replaced. The maximum deck displacement was found to be around 0.10 m (not shown here) which is exactly the width of the seismic joint foreseen at the two deck-abutment interfaces.

As regards the seismic joint on pier 9, which divides the bridge into two parts, analyses indicated that the two independent bridges oscillate synchronously, thus leaving theoretically the joint width constant during the earthquake. Without giving full credit to the results of the analyses, it was estimated that pounding should actually not take place between the two decks. Additional analyses accounting for possible nonsynchronism of the seismic action along the bridge length were deemed unessential.

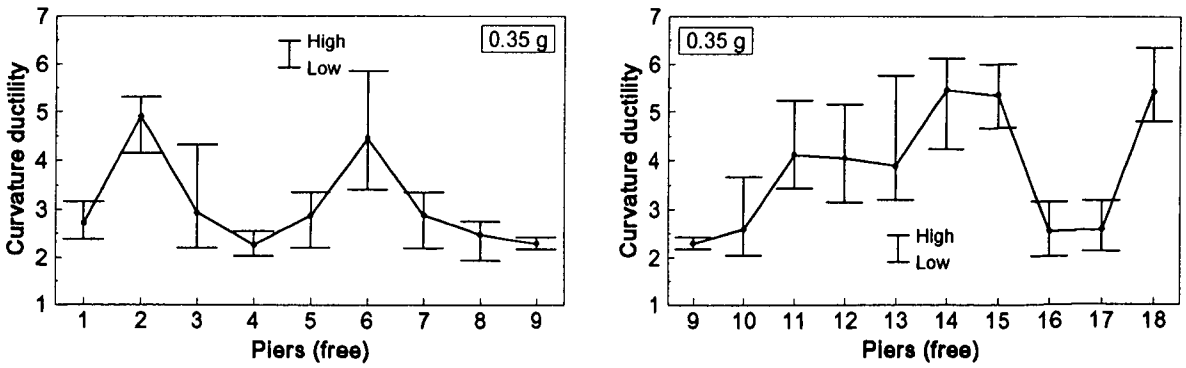

Figure 14. Curvature ductility request at piers base before the intervention.

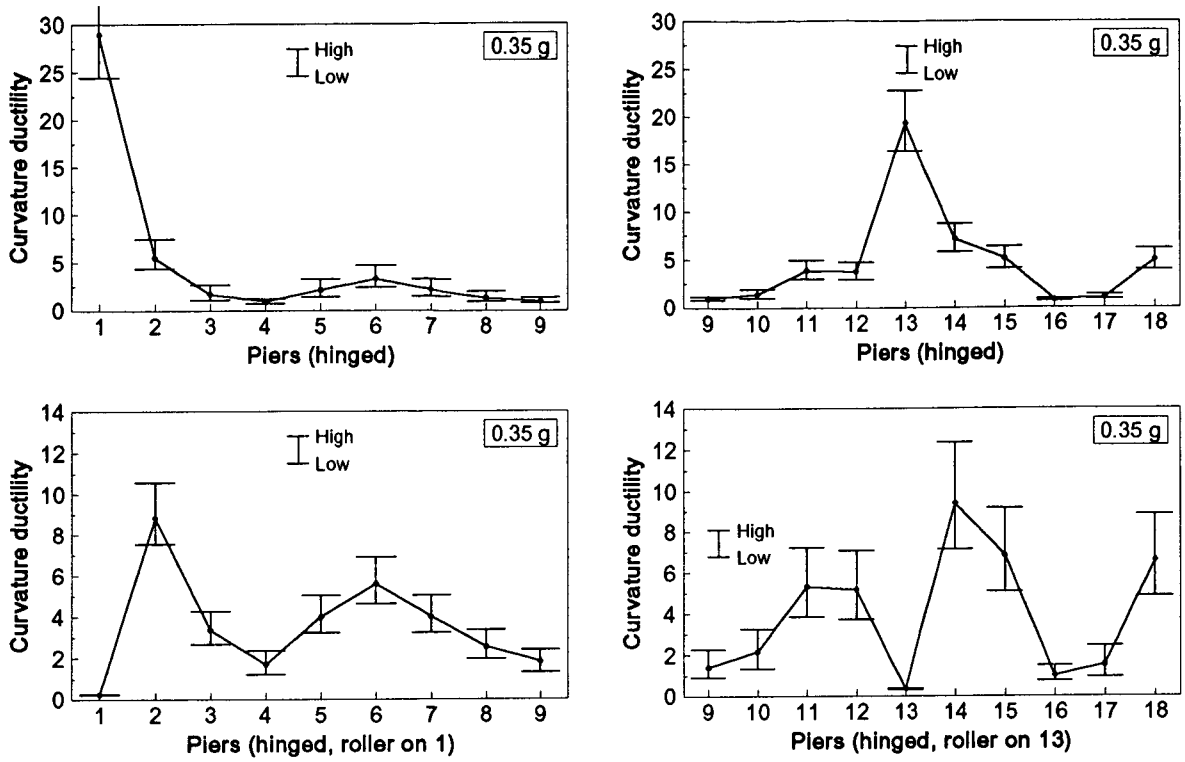

Figure 15. Curvature ductility request at piers base with only the slab joining intervention: all piers hinged (above), roller on the shortest piers (below).

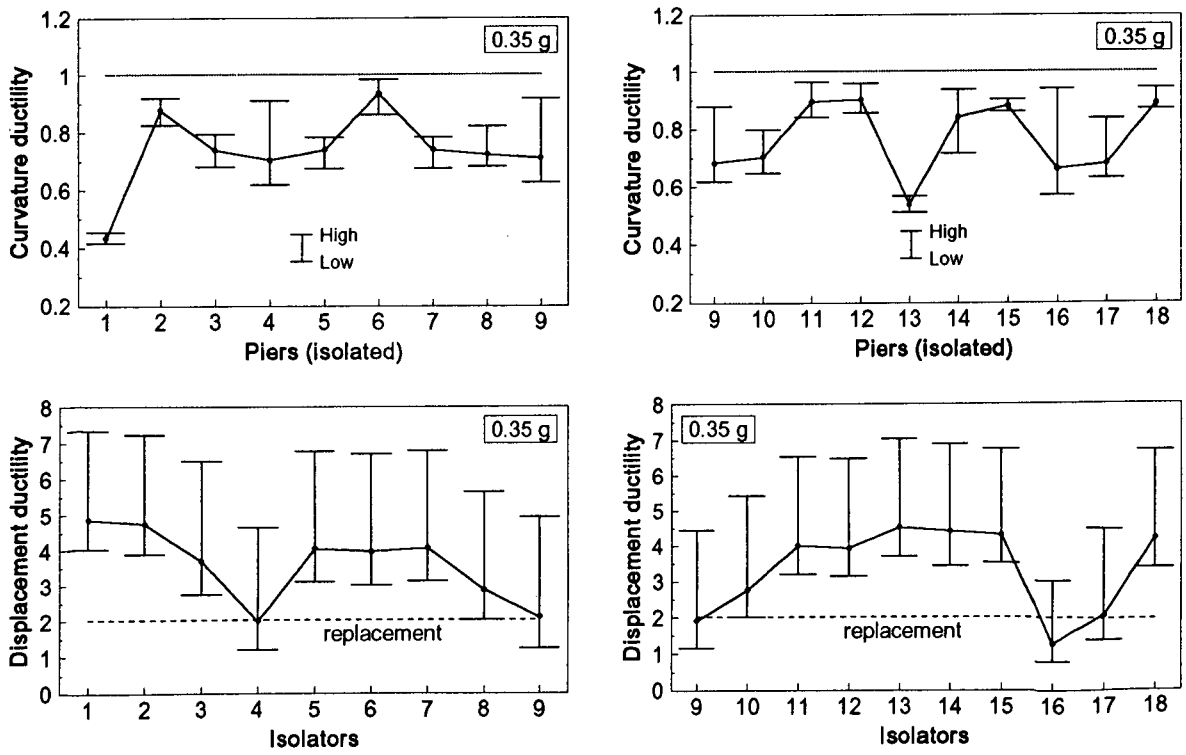

Figure 16. Ductility request at piers base (above) and in the isolators (below) after the complete intervention.

4.3 Damage limit state analyses

The bridge response was analyzed under PGA=0.12g. The bridge response is presented with the same organization as in the previous section, with the same cases analyzed.

In Figure 17 the state of the bridge before the retrofitting intervention shows that, based on the average values, only 2 piers in bridge 1 and 5 piers in bridge 2, enter the inelastic range, even though with low values of required ductility. The situation changes when, as shown in Figure 18 (above), the continuous slab bridge is studied. In this case, all the piers remain elastic and the shortest piers 1 and 13 are required rather high values of ductility. The picture dramatically changes when rollers are inserted on top of these two piers (Figure 18, below): the ductility request shifts to the adjacent piers 2 and 14. These are required lower values of ductility than in the previous case, which, however, are incompatible with damage limit state requirements, where all the structural elements are supposed to remain elastic.

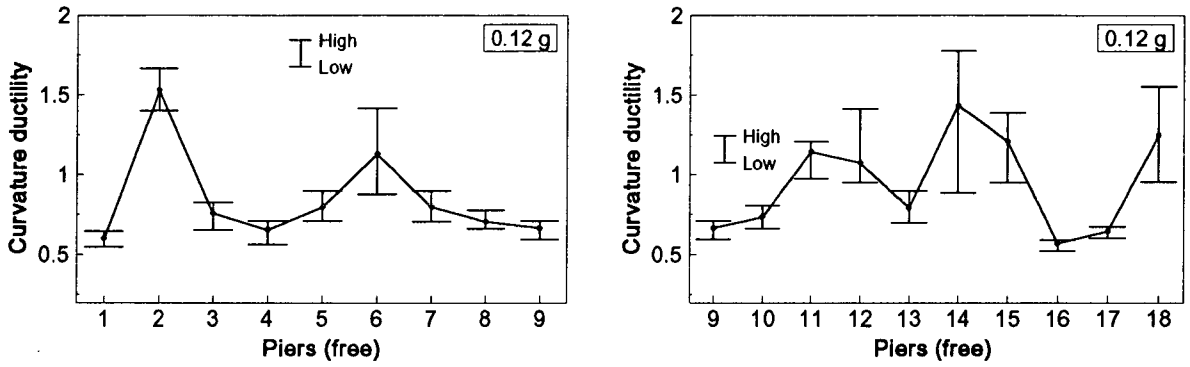

Figure 17. Curvature ductility request at piers base before the intervention.

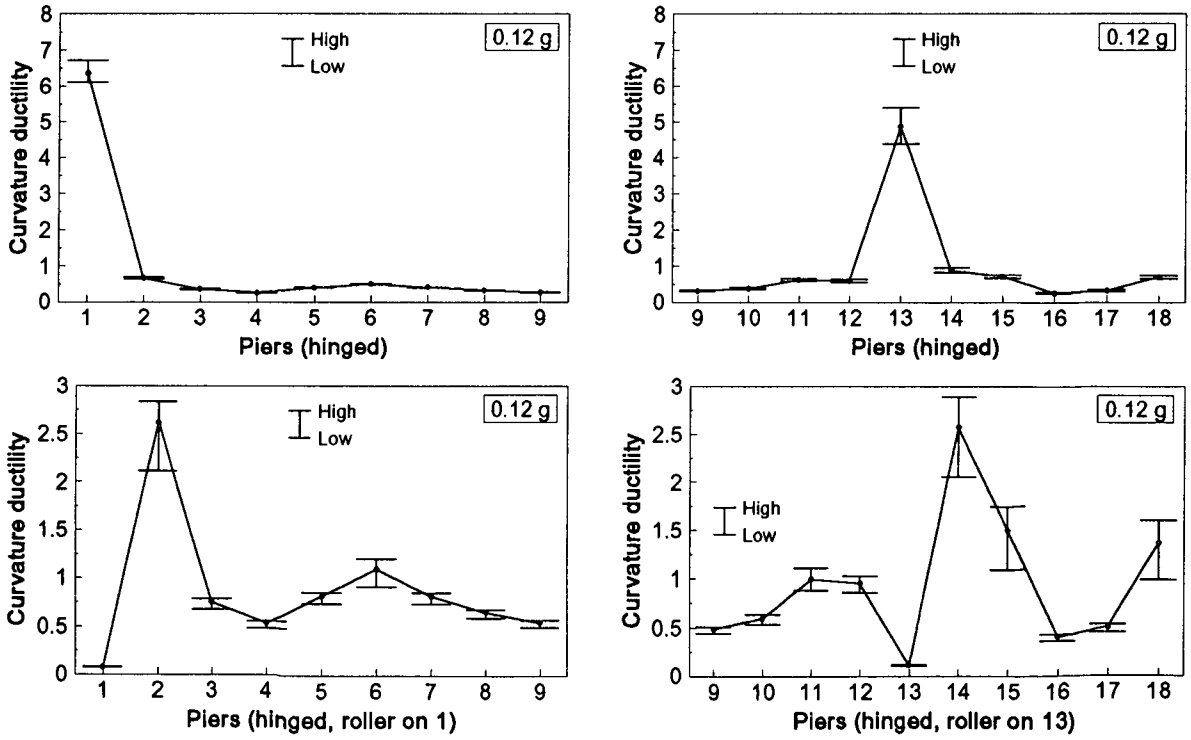

Figure 18. Curvature ductility request at piers base with only the slab joining intervention: all piers hinged (above), roller on the shortest piers (below).

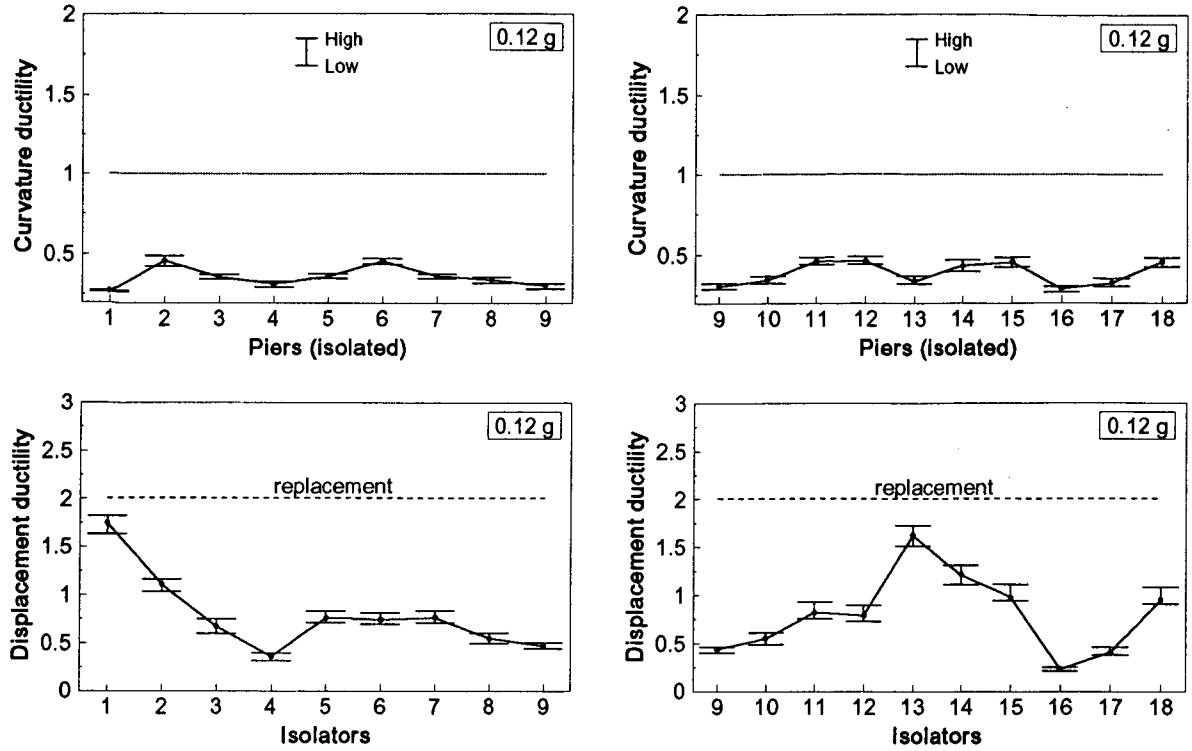

Figure 19. Ductility request at piers base (above) and in the isolators (below) after the complete intervention.

The isolated bridge shows, in this respect, a satisfactory behavior, both in terms of the piers remaining well below the yield threshold (Figure 19, above) and of the isolators, only 4 of which (isolator no. 1, 2, 13 and 14) enter the plastic range (Figure 19, below). From the maintenance standpoint, on account of what already observed at the end of the previous section, it can be considered that none of the isolators need to be replaced after a moderate earthquake.

4.4 Temperature effects

Since the deck is now made from two continuous slabs, with length equal to 180 and 200 m for the two halves, respectively, it was deemed necessary to study the effects of a temperature variation on the deck itself. In this case, the deck (either shrinking or dilating) imposes different displacements to the isolators, the larger the farther the isolators are located from the deck center. As already mentioned, at the design stage the isolators stiffness was calibrated so that they remain elastic under a temperature variation. It was considered, however, that when an earthquake strikes, not all of the isolators are in an undeformed position, and that this may result in an undesired ductility request in the isolators, even for the damage limit state earthquake. In this case maintenance problems arise, since the isolation intervention is actually meant to obtain an elastic response, or at most a low ductility request, in all the isolators under low-level PGAs. To try to solve the problem, the isolator yield displacement has been increased by 50% with respect to the maximum temperature-imposed displacement. Analyses were then performed to check the effectiveness of this provision. No analyses were carried out under ultimate limit state conditions, because it was ascertained that in that case the ductility

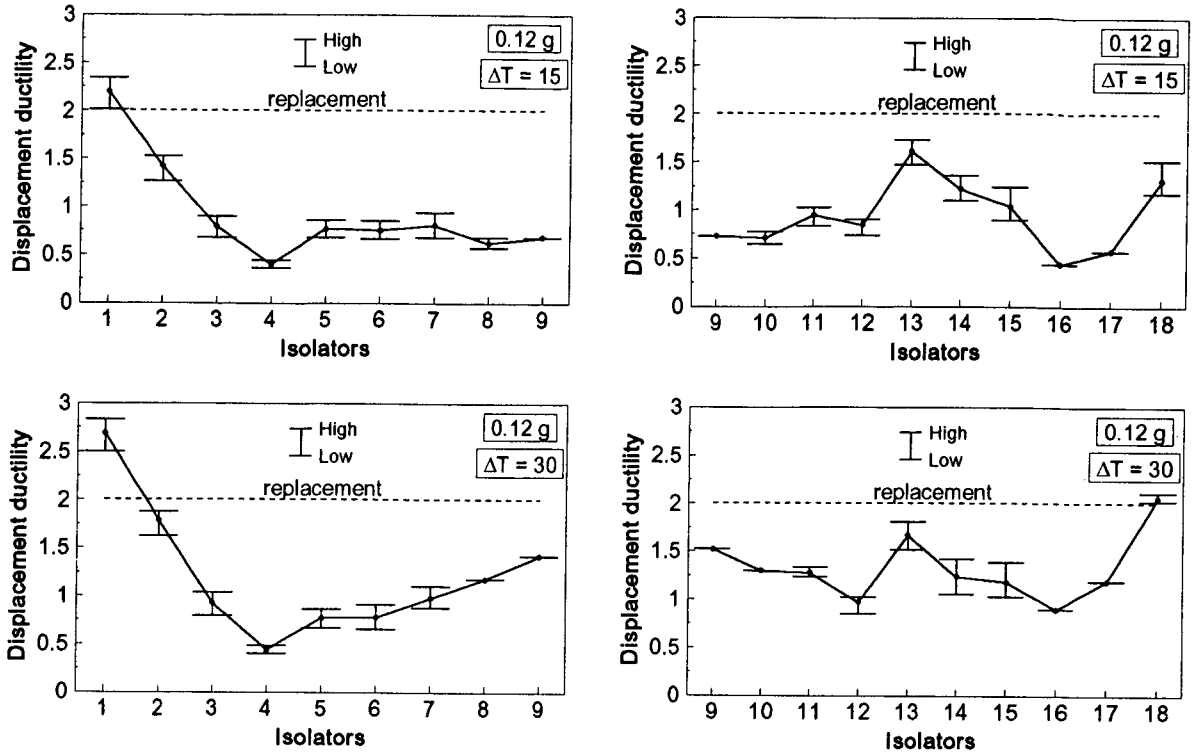

Figure 20. Ductility request in the isolators for temperature variation of 15° (above) and 30° (below).

requested to the isolators by the seismic action was much larger than that requested by a temperature variation.

In the following, the temperature variation ΔT represents the difference in temperature between the time of installation of the isolating devices and the time of occurrence of the seismic event. In case of a summertime occurrence of the seismic event, two different values are considered: $\Delta T = 15°$, representative of a variation with respect to a springtime installation, and $\Delta T = 30°$, representative of a variation with respect to a wintertime installation.

In Figure 20 the isolators request of ductility are depicted for the two temperature variations considered. It is observed that, with respect to the case of no temperature variation in Figure 19 (below), the number of isolators that enter the inelastic range increases from 4 to 6 ($\Delta T = 15°$) and to 12 ($\Delta T = 30°$). In Figure 21 the change in ductility request in the isolators is represented for the two cases. As expected, the higher changes occur in the isolators closer to the deck ends, while the central isolators do not experience any significant change. Assuming, as above, that a value of 2 for the ductility request can be considered as a threshold beyond which replacement cannot be avoided, it should be noted that, for the case $\Delta T = 15°$, the requests of ductility are such as not require a replacement, except for the isolator on pier 1. In the case $\Delta T = 30°$ there is undoubtedly a more spread damage in the isolators, but most of them are below the chosen threshold, with the exceptions of isolators 1 and 18. Thus, if one accounts for temperature variation effects, replacement of at least two isolators has to be anticipated after a low-intensity earthquake, as opposed to the case of no temperature variation, where no replacement was foreseen.

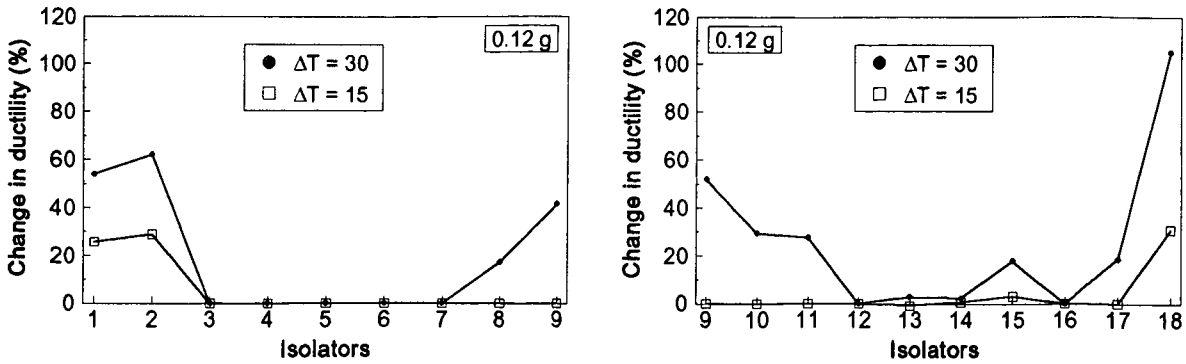

Figure 21. Change in the isolators ductility request for temperature variation of 15° and 30°.

A possible alternative which would avoid any maintenance of the isolators after moderate earthquakes, would be to couple each isolating device in series with a shock-transmitter: in case of slow (temperature-induced) displacement variations, the latter would absorb the displacement and leave the isolator in its at-rest position, whereas in case of fast (earthquake-induced) displacement variations, it would become stiff thus letting the isolator undergo the imposed displacement. A less expensive solution would be to pre-deform the isolators with a displacement contrasting that corresponding to the temperature variation between the installation time and a reference temperature (for example, a springtime temperature). In this case, particular care should be devoted to the evaluation of the pre-deformation value to be assigned to each isolator, proportionally to its distance from the deck's thermal centroid.

5. CONCLUSIONS

A retrofitting intervention on a highway bridge is presented. The intervention consists in the joining of the deck slab and in the installation of a new type of isolating device between the piers cap and the deck. The device has proven to be well suited for the seismic retrofitting of existing structures, because of its high versatility that allows the designer to select the seismic force cut at any desired level, while easily controlling the device's plastic displacements.

The effectiveness of the retrofitting intervention was extensively tested in this paper, by carrying out a series of dynamic step-by-step numerical analyses, aimed at assessing the longitudinal bridge performance at both the ultimate and the damage limit state. For this latter case, the effect of a temperature variation was considered to assess its impact on the seismic performance of the isolating devices. From the analyses it resulted that the retrofitting intervention was well designed and that, under the high-intensity earthquake, all the piers remain in the elastic range, while the isolators are required ductility levels which are perfectly compatible with the adopted isolator performance. Also under the low-intensity earthquake, no problem was observed in the bridge behavior, in the sense that no isolator needs to be replaced after the seismic event. Additional analyses were carried out to assess the effects on the isolators of a temperature variation, which was actually accounted for at the design stage when calibrating the isolators stiffness. These analyses have shown that the isolators that are closer to the deck's ends actually experience a higher request of ductility than in the case where no temperature variation is accounted for.

ACKNOWLEDGMENTS

The authors wish to thank Ing. Marco Temussi of STE, Roma, who designed the retrofitting intervention, for his precious availability in providing all the necessary material and information.

REFERENCES

Dolce, M., Filardi, B., Marnetto, R., Nigro, D.: Experimental tests and applications of a new biaxial elasto-plastic device for the passive control of structures. *Fourth World Congress on Joint Sealants and Bearing Systems for Concrete Structures*, Ed. B. Atkinson, Sacramento, USA, September 29 - October 3, 1996.

Giannini R., Monti G., Nuti C., Pagnoni T.: ASPIDEA - A program for nonlinear analysis of isolated bridges under nonsynchronous seismic action. *Report 5/92, Dipartimento di Ingegneria delle Strutture delle acque e del terreno, Università degli Studi dell'Aquila*, October, 1992.

Monti G., Nuti C., Santini S.: CYRUS: CYclic Response of Upgraded Sections. A program for the analysis of retrofitted or repaired sections under biaxial cyclic loading including buckling of rebars. *Report DSSAR 2/96 Materiali, Università degli Studi G. D'Annunzio, Chieti*, May, 1996.

SEISMIC RETROFIT OF EXISTING REINFORCED CONCRETE COLUMNS BY STEEL JACKETING

Jun-ichi Hoshikuma
Research Engineer, Earthquake Engineering Division, Public Works Research Institute
Ministry of Construction

Sigeki Unjoh
Head, Earthquake Engineering Division, Public Works Research Institute
Ministry of Construction

ABSTRACT

A new steel-jacketing strengthening method for enhanced flexural response of existing reinforce concrete bridge columns with square section was proposed in this paper. A series of large-scale specimens were cyclic-loaded, to examine the strengthening effect. Test results showed that the strengthening method was effective in enhancing both the flexural strength and the ductility. Also, effects of steel-jacket details were studied based on the loading tests. Furthermore, an analytical model for the steel-jacketing reinforced concrete columns was proposed. The flexural strength and the ductility analyzed by the model showed good agreements with the test results.

INTRODUCTION

When the Hyogo-ken Nambu Earthquake hit the Hanshin and Awaji districts in the early morning of January 17, 1995, civil engineering structures, including highway bridges, were severely damaged that had never been seen in past earthquakes. As noted to damage to highway bridges, reinforced concrete bridge columns that had been designed in accordance with the 1964 or 1971 seismic specifications suffered severe damage(1). The reason for the damage was officially concluded that the ground motion had properties that produced greater effects on highway bridges than had ever been observed. It has been estimated that severely damaged bridges received seismic forces larger than had been assumed in their design (1).

To make a bridge sufficiently resistant to earthquakes such as the Hyogo-ken Nanbu Earthquake, structures have to be designed tougher by increasing the strength and ductility of the bridge as a total system (2). The philosophy of seismic design for a bridge also applies to the seismic retrofitting of existing bridges, so that it is necessary to adopt a retrofitting method that can be expected to enhance both the flexural strength and the ductility of the columns. However, when the flexural strength of columns is enhanced, the seismic forces propagated into the foundation are increased all the more. Therefore, if the estimated lateral strength of the foundation of a bridge is smaller than that of retrofitted columns, it would be necessary to do more wide-ranging retrofitting of the bridge by strengthening foundation as well. On the other hand, if the columns were retrofitted by only ductility enhancement, while their flexural strength is left as it is, this may lead to substantial plastic deformation during a

major earthquake, which would cause a residual deformation that could not be repaired after the earthquake (3). It is therefore important to develop a philosophy of seismic retrofit design that is capable of enhancing the flexural strength of the piers as required, within the range that can be supported by existing foundation, and to make this enhancement match the improvement in the ductility.

There are several kinds of seismic retrofit method which are based on above design philosophy. Figure 1 illustrates typical retrofit methods for existing single reinforced concrete bridge columns. In the Public Works Research Institute, the seismic retrofit research projects have been conducted for steel jacketing, reinforced concrete jacketing and carbon fiber jacketing. In this paper, the seismic retrofit by steel jacket are discussed.

This paper proposes the steel jacketing method, with a controlled increase in flexural strength so that enhancement of both the flexural strength and the ductility of reinforced concrete column be well-balanced. It also describes the results of a cyclic loading test using large-scale models constructed in order to examine the effects of enhancing the strength and ductility of bridge piers using this retrofitting method. Furthermore, the analytical method considering the confinement effect is checked the validness by comparing the test results.

SEISMIC RETROFITTING OF REINFORCED CONCRETE PIERS BY STEEL JACKET WITH ANCHOR BARS

The steel jacket method, providing a controlled increase in flexural strength, involves steel plates around the reinforced concrete bridge piers, and bonding the steel jacket to the pier with epoxy resin or non-shrinkage mortar, while anchoring the jacket to the footing with anchor bars, as shown in Figure 1. This retrofitting method mainly aims to compensate for the inadequate cut-off of the longitudinal reinforcement and, at the same time, to enhance the flexural strength and ductility of the pier. The structure has several important characteristics, including the anchoring of the steel jacket to the footing with anchor bars, the vertical gap between the lower end of steel jacket and the top of the footing, and the use of H-beams fastened at the lower end of the jacket. These characteristics are described below.

First, the anchor bars play a part in enhancing the flexural strength of the pier, as well as in controlling the seismic forces propagated into the footing. This is because the increase in the flexural strength of the pier resulting from the retrofitting method can be controlled by adjusting the number and diameter of the anchor bars installed. The vertical gap between the lower end of the steel jacket and the top of the footing is provided because it is expected that, when it receives a large seismic force, the steel jacket may come into contact with the footing, which may then buckle under the unexpectedly large compressive force and receive damage. However, when the length of the vertical gap is too large, the confining effect of the jacket at the bottom of pier is reduced. The length should therefore be as small as possible.

Piers with a rectangular section also have H-beams installed around them at the lower end of the jacket. The reason for this is that, when the base of the pier suffers from a deformation with a large curvature, the jacket at the plastic hinge zone swells out, and the confining effect of the jacket is liable to be lost. When the lower end of the jacket is attached with the H-beams, however, then even under large deformations it still functions as a lateral reinforcement.

CYCLIC LOADING TEST FOR MODELS OF RETROFITTED REINFORCED CONCRETE PIERS

Specimens

The specimens used are shown in Figure 2. Their section was a square of 60 cm x 60 cm. The height from the base to the loading point was 3.01 m. The shear span ratio was 5.0. As longitudinal reinforcements, SD295/D10 bars were arranged, and the ratio of longitudinal reinforcement was 1.58% (the ratio of tensile reinforcement was 0.55%). As hoop reinforcements, SD295/D6 hoops were arranged at intervals of 20 cm. In the specimens used in the test, the longitudinal reinforcement was not cut off at mid-height. This was because previous studies (4) had found that the steel jacket method can prevent damage to the cut-off sections of longitudinal reinforcement, thus it was decided that effect of this method in retrofitting the cut-off sections was not to be examined in this test.

When the steel jacket was applied to the specimen to be retrofitted, two steel plates with a thickness of 1.6 mm (SS400) were each bent into a channel -shape, and then welded into a jacket. Finally, the jacket was slipped from above over the specimen. As described above, however, a vertical gap of 5-15 cm was set between the lower end of steel jacket and the top of the footing (see Photo 1). In addition, H-beams (100 x 100 x 6 x 8, SS400) were used to strengthen the lower end of the jacket. Epoxy resin was poured in between the reinforced concrete pier and the steel jacket, with a thickness of 4 mm, to bond them.

The numbers and diameters of the anchor bars were set in such a way that the flexural strength of the specimen could increase by approximately 30%. As described above, with this retrofitting method, any increase in the strength of the pier has to be set so that its resulting strength will not exceed that of the foundation. In this test, it was arbitrarily decided that the pier strength should be increased by about 30%. It was found that, using the calculation method described later, when anchor bars equivalent to about 60% of the total strength of the steel jacket were used, the pier strength increased by approximately 30%. Consequently, it was decided that twenty anchor bars, made by processing SD345 /D13 reinforcements into an M12 screw bolt (effective section area: 0.843 cm^2), should be arranged at intervals of 12 cm. The bars were anchored with resin anchors 55.6 mm outside the external edge of the concrete. The upper ends of the anchor bars were fastened to the webs of the H-beams by double nuts, as shown in Photo 2. In this structure, the axial force produced in the anchor bars must be propagated smoothly via the H-beams to the steel jacket. In the specimens for the test, therefore, the H-beams and the steel jacket were joined with six rib plates (thickness: 6 mm) per side, as shown in Figure 2b and Photo 1. The anchor bars were anchored to the footing for a length of 65 cm.

In order to examine the retrofitting effect produced by the steel jacket, and the effect of vertical gaps of varying length between the lower end of jacket and the top of the footing, one as-built specimen (P-1) and three retrofitted specimens (P-2 - P-4) were used in this test. The vertical gap length in specimen P-2 was 10 cm, while those of specimens P-3 and P-4 were 5 cm and 15 cm, respectively.

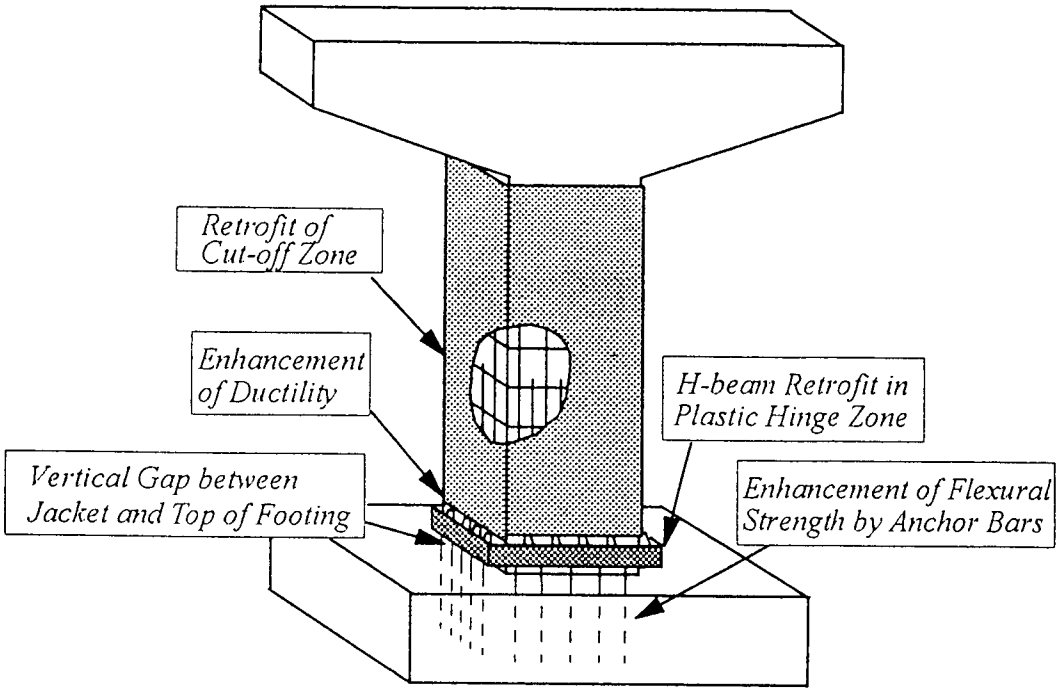

Fig. 1 Illustraion of Retrofit by Steel-Jacketing with Anchor Bars

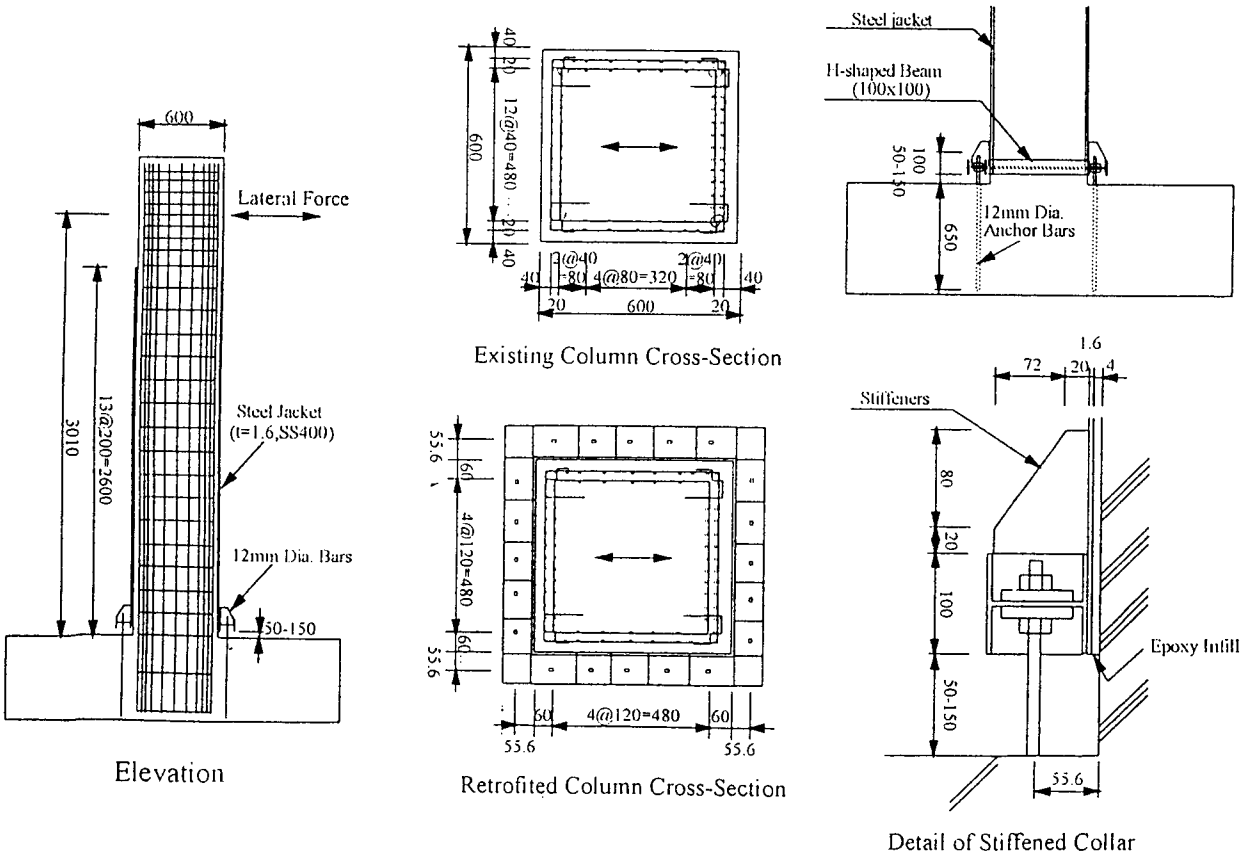

Fig. 2 Details of Test Specimens (unit: mm)

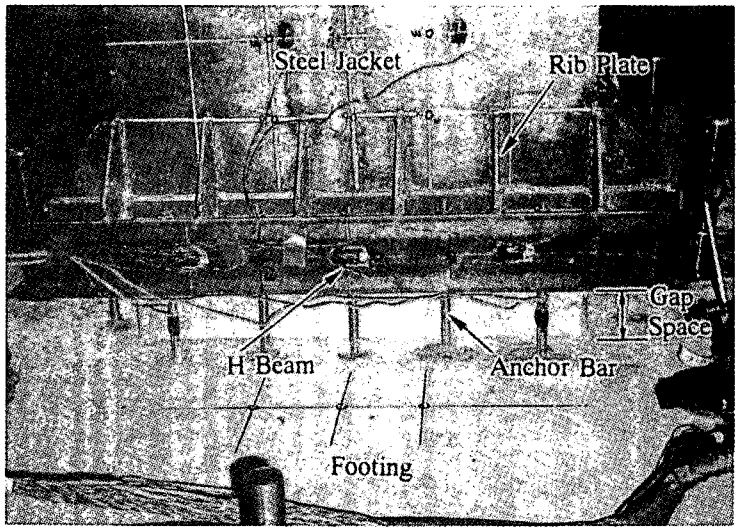

Photo 1 Detail around Base

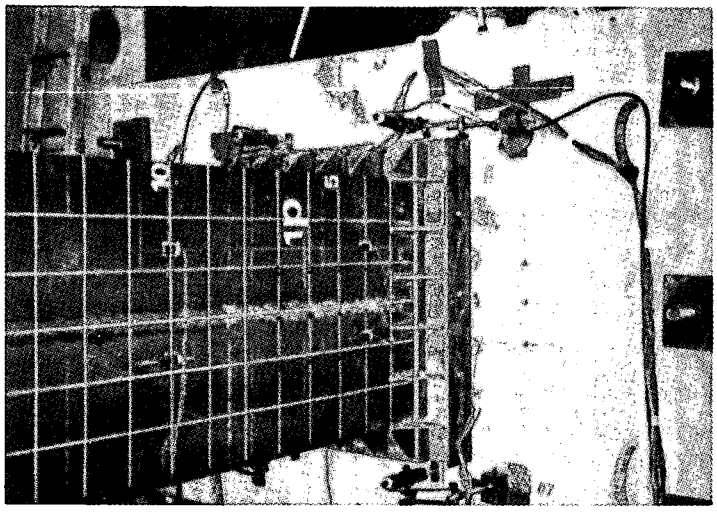

Photo 2 Steel Jacket and Anchor

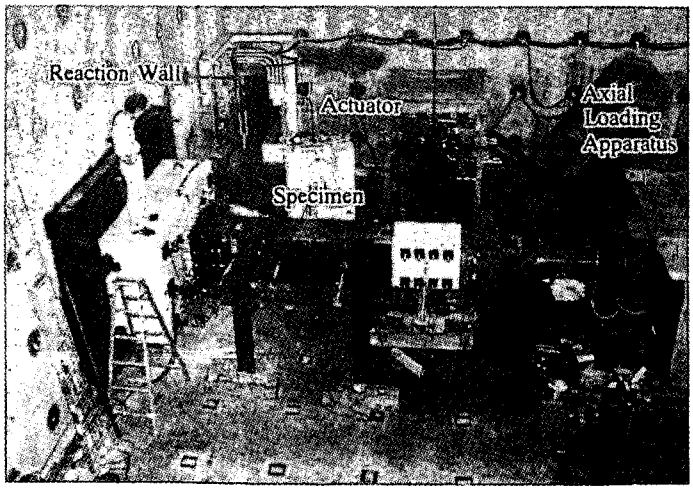

Photo 3 Set-up of Cyclic Loading Test

Loading Procedure

Photo 3 shows the way in which each specimen was loaded. While an axial force equivalent to a dead-load reaction was applied to each specimen laid down, a level load was applied to it by an actuator installed on a reaction wall. An axial force of 55 tf was used in this test. This is equivalent to a compressive stress of 15.3 kgf/cm ^{2}.

The yield displacement at the loading point was determined here when the longitudinal reinforcement of the base of the as-built specimen yielded, or the anchor bars of each retrofitted specimen yielded. Alternative displacements were given to the specimens by the displacement control. The loading displacement was made by a sine wave; the loading speed 3 cm/sec; and the number of loading cycles per loading step was to be three. The ultimate displacement during the test was defined here as the displacement when the strength was deteriorated to the yield strength.

RETROFITTING EFFECT OF STEEL JACKET WITH ANCHOR BARS

Hysteresis loop and aggravation of damage

Figure 3 shows the hysteresis loops of the relationships between lateral load and the displacement at the loading points of all the specimens. Figure 4 illustrates the damage to specimens P-1 and P-2 was aggravated.

In the case of P-1, the as-built specimen, based on the value for the longitudinal reinforcement strain at the base, the yield displacement was measured to be 16.0 mm. Its peak strength was 23.1 tf. This was maintained until 4 δ y was loaded, when its cover concrete started to spall off. In the stage of 5 δ y loading, the core concrete started to suffer damage, and the hysteresis loop began to become unstable. When even greater loads continued to be applied, damage to the core concrete was aggravated, with the level strength gradually reduced.

In the case of P-2, a retrofitted specimen, based on the yield strain of its anchor bars, the yield displacement was measured at 12.7 mm. In comparison with P-1, its yield displacement was smaller, because the flexural stiffness was increased by the steel jacket. Its peak strength was 31.8 tf. This was maintained until 6 δ y was loaded. Its anchor bars started to buckle under the load of 4 δ y. In the stage of the 6 δ y loading, seven anchor bars were broken. At the same time, the external edge of the concrete pier, in the 10cm vertical gap provided at the base, began to fail due to the cyclic pressure, with the lateral strength reduced. Under the 7 δ y loading, a total of ten anchor bars broke, and two longitudinal reinforcements of the pier were also broken, with the lateral strength reduced below the yield strength. Even under the final 8 δ y loading, the steel jacket did not suffer from deformations such as buckling or swelling out.

Strength and ductility

Figure 5 compares the envelope curves of the hysteresis loops in the four specimens. Table 1 compares their strength and ductility. The comparison between P-1 and P-2 shows that the

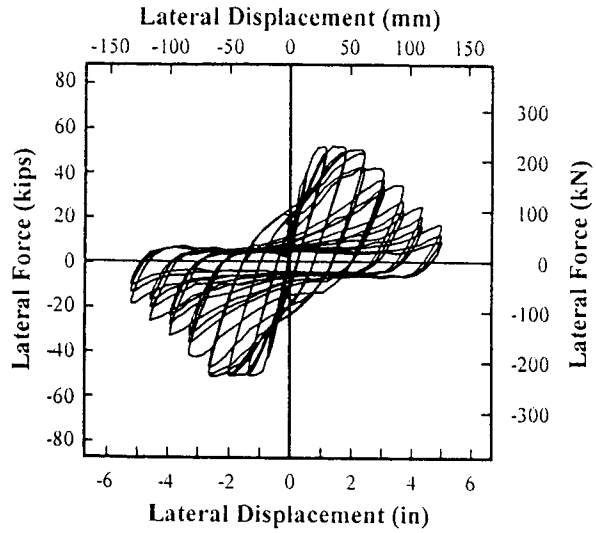

(a) P-1 Specimen

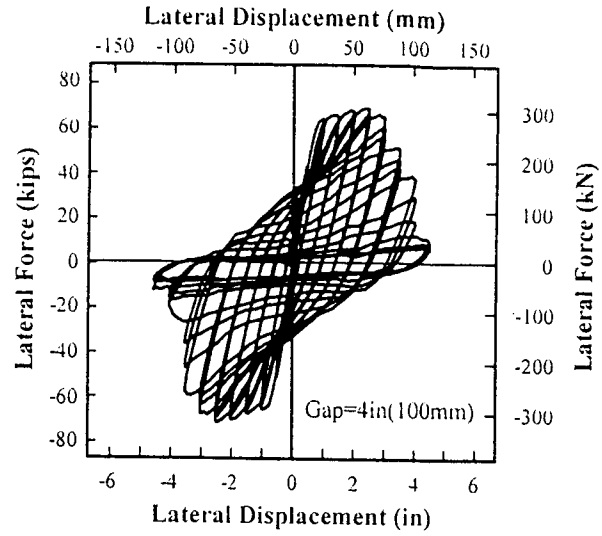

(b) P-2 Specimen

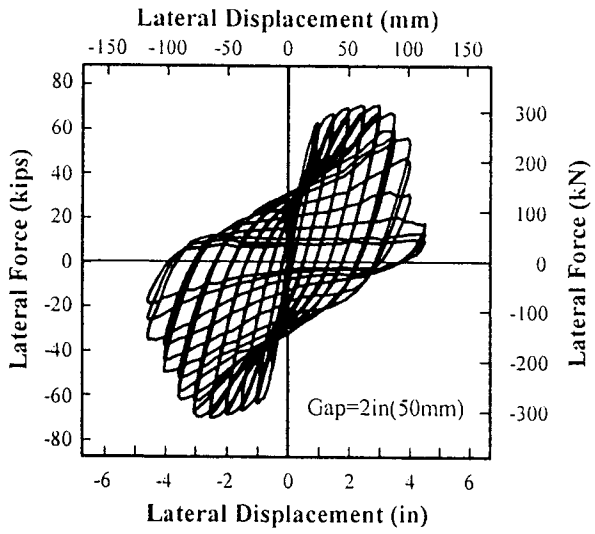

(c) P-1 Specimen

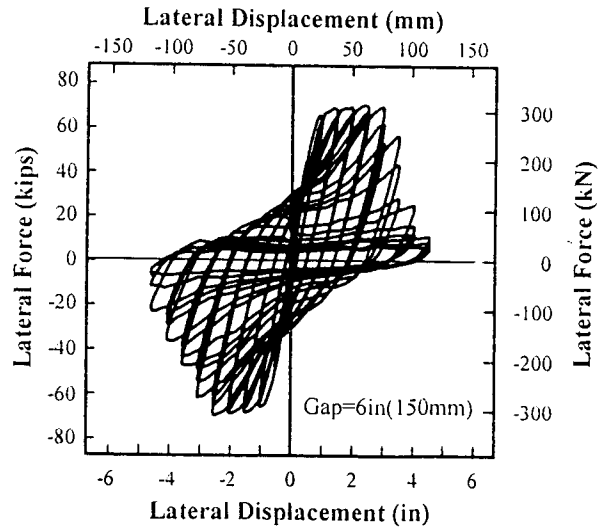

(d) P-2 Specimen

Fig. 3 Hysteresis Roop of Lateral Load and Displacement Relation

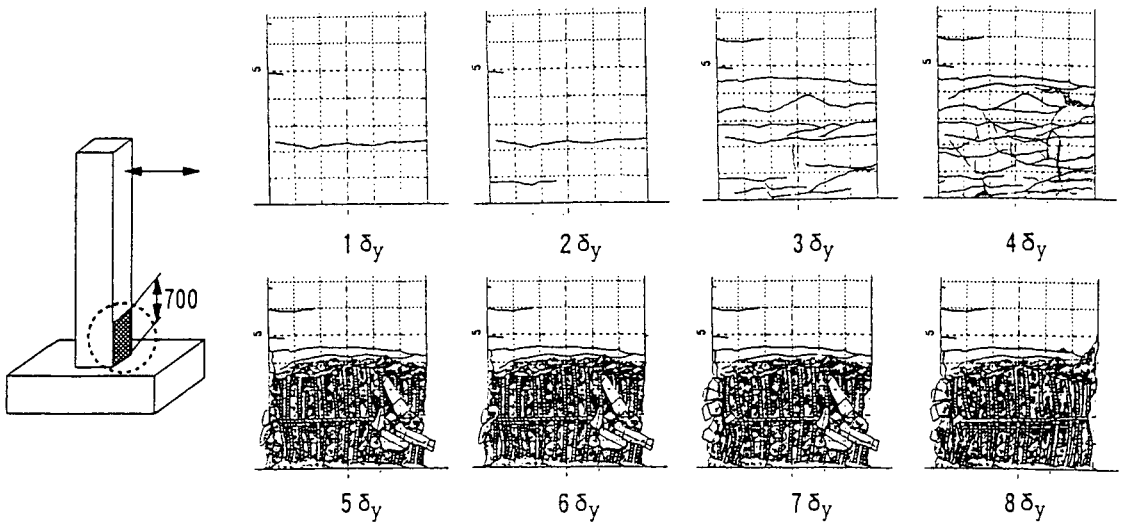

(a) P-1 Specimen

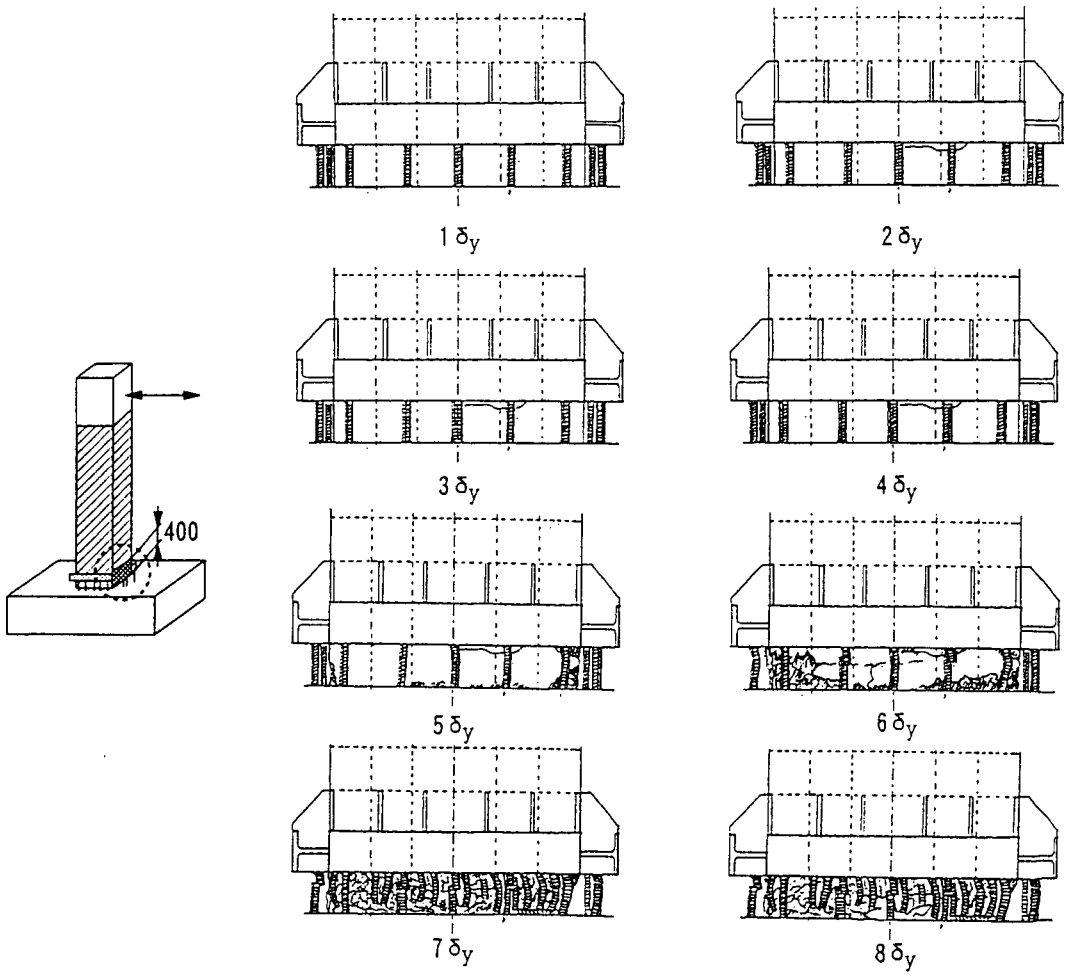

(b) P-2 Specimen

Fig.4 Damage Process Observed in Specimens

peak strength and the ductility factor of the pier were enhanced by the steel jacket, with a controlled increase in flexural strength. Also, while the effect of the vertical gap length on the peak strength was only slight, the smaller the length, the larger was the ductility ratio. Based on the result of this test, it is recommended to make the vertical gap length small, at least about 5 cm, in the case of piers with dimensions similar to these specimens.

Figure 6 shows the relationship between equivalent stiffness and lateral displacement. Equivalent stiffness was defined here as being the gradient of the straight line connecting the points of the maximum and minimum displacements in the first loading loop in each loading step. The figure shows that the equivalent stiffnesses of P-2 to P-4 under the 1 δ y loading were about 1.5 times greater than that of P-1. The reason for this will be that the flexural stiffnesses of the retrofitted specimens were greater than that of the as-built one, because of their increased stiffness due to the anchor bars, and because the steel jackets covering the whole height of the piers also functioned as a longitudinal reinforcement. However, the effect of the difference in the vertical gap length was not noticeable over the range of 5 to 15 cm.

Energy absorption

Figure 7 compares the specimens with regard to accumulated energy absorption. Energy absorption in each loading step was computed here by integrating the hysteresis loop concerned. The figure shows that in the case of P-1, the as-built specimen, from around the time of 5 δ y, when the core concrete started to suffer damage, the energy absorption in each loading step began to decrease. In the case of P-2 to P-4, on the other hand, energy absorption was stable even after 5 δ y. It was also found that the smaller the vertical gap length, the greater was the energy absorption under loads above 7 δ y loading step.

Figure 8 shows effect of the retrofitting on the equivalent damping ratio. The ratio computed was based here on the hysteresis loop in the first loading in each loading step. While the ratio of P-1 was greater in the range of lateral displacement below 5 δ y, it began to decrease when the displacement increased beyond that. On the other hand, the equivalent damping ratios of P-2 to P-4 rose constantly as the lateral displacement increased, indicating that stable damping performance was obtained with the retrofitting method. It can also be seen that the damping performance of P-4, with a vertical gap length of 15 cm, was slightly poorer than those of P-2 and P-3 after 7 δ y loading step.

Strain Performance

Figure 9 compares the reinforcement and the steel jacket of P-2 with regard to the peak axial strain on the tensile side of the section at a height of 20 cm from the base at each loading step. Under the load for 1 δ y, the axial strain of the jacket was 0.0838%, and it had not yet yielded. Since the design had foreseen that five anchor bars on the tensile side would yield under this load, it is estimated from the yield strength (observed value: 3,916 kgf/cm ^{2}) and section area of the anchor bars that an axial strength, Na, of the value obtained by the following formula was at work:

$$N_a = 3{,}916 \times (0.843 \times 5) = 1.65 \times 10^4 \text{ kgf} \qquad (1)$$

Assuming this axial strength to be the tensile strength propagated to the tensile side of the steel jacket, the strain produced in the jacket is computed as follows:

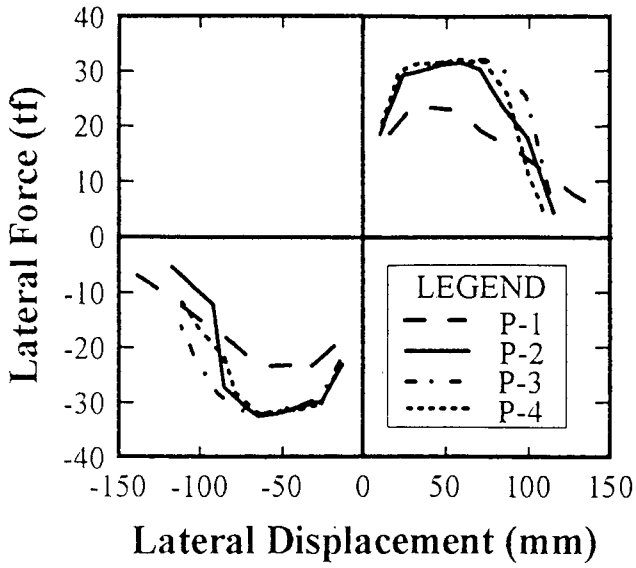

Fig. 5 Comparison of Envelope of Hysteresis Roop

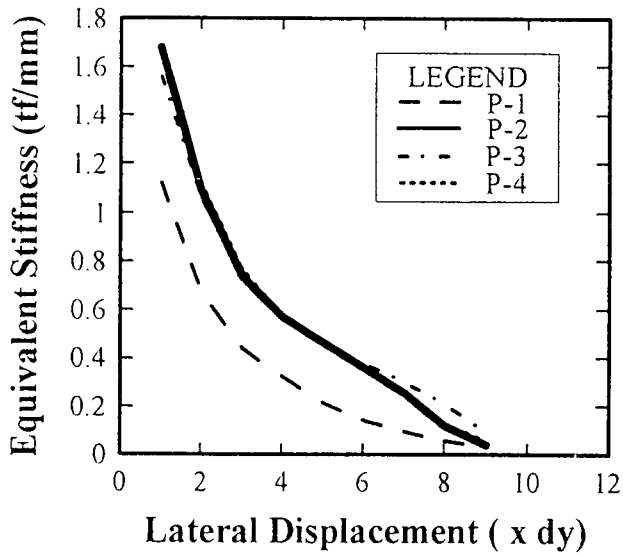

Fig. 6 Effect of Retrofit on Equivalent Stiffness

Table 1 Observed Strength and Ductility

Specimen		P-1	P-2	P-3	P-4
Strength	Yield Strength (tf)	18.8	21.3	20.2	21.5
	Peak Strength (tf)	23.1	31.8	31.7	31.9
	P_M/P_y	1.23	1.49	1.57	1.48
Ductility	Yield Displacement (mm)	16.0	12.7	12.7	12.7
	Ultimate Displacement (mm)	87.0	96.5	110.9	96.0
	Ductility Factor	5.4	7.6	8.7	7.6

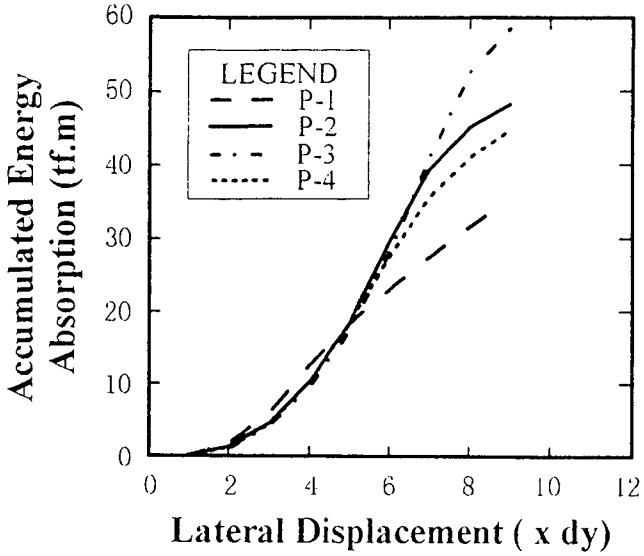

Fig. 7 Effect of Retrofit on Accumulated Energy Absorption

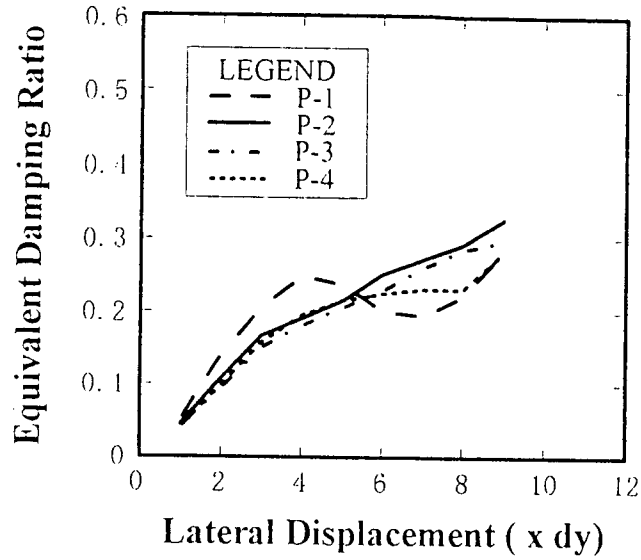

Fig. 8 Effect of Retrofit on Equivalent Damping Ratio

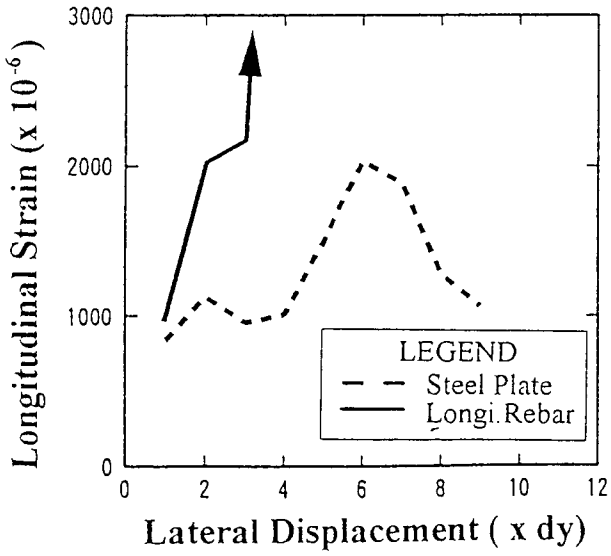

Fig. 9 Axial Strain of Longitudinal Reinforcement and Steel Plate in Specime P-2

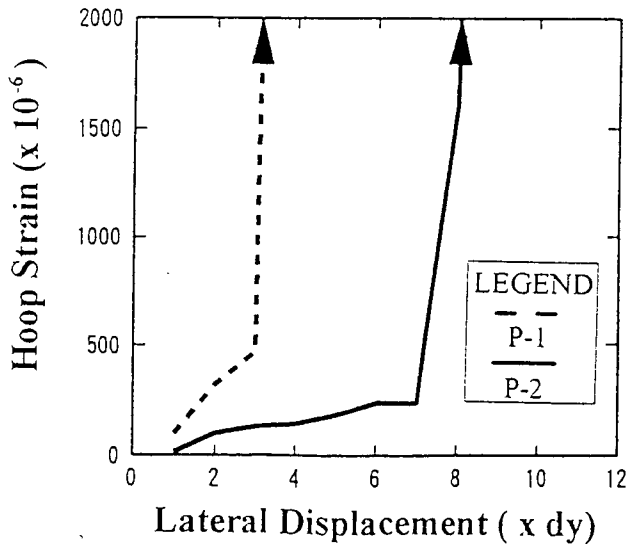

Fig. 10 Comparison of Strain of Hoop

$$\varepsilon_j = 1.65 \times 10^4 / (0.16 \times 60) \times 2.1 \times 10^6$$
$$\fallingdotseq 818 \times 10^{-6} \quad (2)$$

As can be seen, the strain on the jacket thus obtained agrees well with the observed value mentioned above. Consequently, judging from the strains on the anchor bars and the steel jacket under the elastic loading, it can be said that the jacket functioned effectively as a longitudinal reinforcement of a strength equivalent to that of the anchor bars. Also, because the jacket did not suffer from any visible plastic deformation, such as swelling out under the loads for 1 δ y or more displacements, it can be expected that the jacket will produce the proper effect of confining the concrete. The axial strain on the jacket peaked under the load for 6 δ y. The displacement was equivalent to the one immediately before the anchor bars were broken, and the strength began to decrease after remaining stable near its maximum. On the other hand, Figure 10 compares P-1 and P-2 with regard to the strain of the hoop reinforcement positioned at the section at a height of 40 cm from the base. It can be seen from the figure that the strain produced in the hoop reinforcement of P-2 was smaller at every loading step, indicating that the jacket functioned effectively as a hoop reinforcement confining the lateral deformation of the concrete pier.

ANALYSIS OF STRENGTH AND DUCTILITY OF REINFORCED CONCRETE PIERS RETROFITTED BY STEEL JACKET WITH ANCHOR BARS

Analysis Procedure

To make a seismic design procedure, it is necessary to estimate the lateral load and displacement relation of the retrofitted pier adequately. The relation between lateral load and displacement is calculated by a method based on the moment-curvature relation described in the seismic design for reinforced concrete piers (5). In this paper, a model of analysis of the retrofitting effect based on this method is therefore used.

The test results mentioned above show that the strength and ductility of the pier are enhanced by the steel jacket with anchor bars. Specifically, the anchor bars and the jacket function as longitudinal reinforcements. Only forces equivalent to the strength of the anchor bars act on the jacket, and the jacket also functions as a hoop reinforcement to confine the concrete. On the basis of these test results, the following assumptions will be made in analyzing the strength and ductility of retrofitted reinforced concrete piers.

(1) Only the strength of the anchor bars can be counted as a effective longitudinal reinforcement by the steel jacket. Reinforcement bars are assumed to be positioned at the external edge of the concrete, as shown in Figure 11.
(2) The whole sectional area of the jacket works as a hoop reinforcement. This effect, combined with that of the existing hoop reinforcement, can be taken into account the stress-strain curve.
(3) The vertical gap length is understood to be better as small as possible, and the steel jacket and the footing will not expected to come into contact if the pier becomes deformed, the confining strength of the jacket can be considered to be propagated into the concrete in this section. The confining effect on the gap section should be the same as that on the section covered by the jacket.

With regard to the modeling of the position of the anchor bars, there are two potential

approaches. One is to assume that the anchor bars are positioned where they are actually anchored in the base (55.6 mm outside the external edge of the concrete pier, in the case of P-2); and the other is to assume that they are positioned on the external edge of the concrete pier, where the steel jacket is placed. In the former case, while the conditions in the actual structure and the analysis model correspond to one other in relation to the vertical gap section with a length from the pier base of 5 to 15 cm, in the section covered by the jacket the flexural stiffness tends to be overestimated, because the effective height of the anchor bars is greater than it actually is. It was therefore decided that, in the design model, the anchor bars should be arranged on the external edge of the concrete pier.

In this analysis, the model of the stress-strain curve in concrete proposed by Hoshikuma et al. (6) was used, since it allows the confining effect of the hoop reinforcement to be taken into consideration. However, the strain produced when compressive stress is reduced to 80% of its peak is considered as the ultimate strain (2). This is equivalent to the strain produced when the concrete starts to spall off due to the compression.

Analyzing retrofitting effect upon specimens

To verify the method of analysis, the strength and ductility of P-2 were analyzed, and a comparison between these results and the test results is carried out. Values obtained from a materials test were used in the analysis.

The volumetric ratio of lateral reinforcement of the reinforced concrete pier, ρ_s, was computed by the following equation, converting the steel jacket into hoop reinforcement:

$$\rho_s = \frac{4A_h}{s \cdot d_h} + \frac{4t}{d_j} \cdot \frac{f_{yj}}{f_{yh}} \qquad (3)$$

where:

A_h: section area of a hoop reinforcement (cm^2)
s: spacing between hoop reinforcements (cm)
d_h: effective length of hoop reinforcement (2) (cm)
d_j: effective length of steel jacket (cm)
t: thickness of steel jacket (cm)
f_{yh}: yield strength of hoop reinforcement (kgf/cm^2)
f_{yj}: yield strength of steel jacket (kgf/cm^2)

In Eq. (3), the first term is the volumetric ratio of the lateral reinforcement of the pier, while the second term gives the volumetric ratio of the steel jacket as converted into hoop reinforcement. The effective length of the jacket, dj, can be assumed here as the side length of the section of the concrete pier, in the case of structures like this, in which steel plates are placed like a jacket. Consequently, in the case of the specimens for this test, the effective length of the jacket, d_j, was 60 cm. Hence, the volumetric ratio of lateral reinforcement of P-1, ρ_s, was computed to be 0.00253. The ratio of P-2, ρ_s, was 0.0115. Figure 12 shows the stress-strain curve for the concrete pier obtained by using these values.
Using this stress-strain curve for the concrete, an analysis was made of the moment-curvature relation of the section, and the lateral load and displacement relation at the loading point was computed. Figure 13 compares the analysis results and the envelope curve of the loading

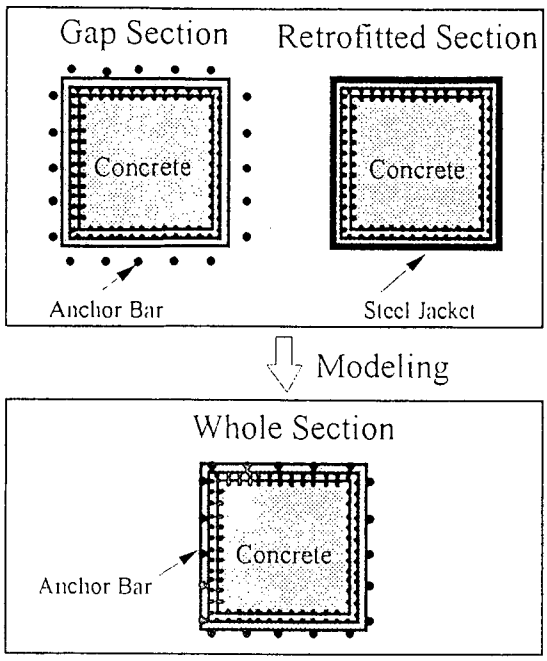

Fig. 11 Analyzing Model of Steel Jacketing with Anchor Bars

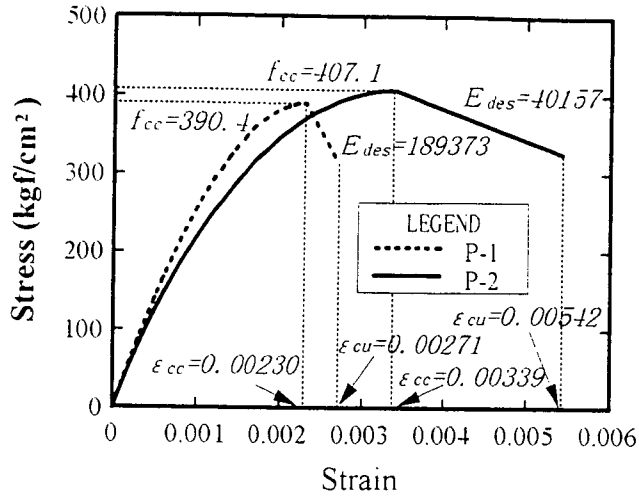

Fig. 12 Stress-strain Curve Used in Analysis

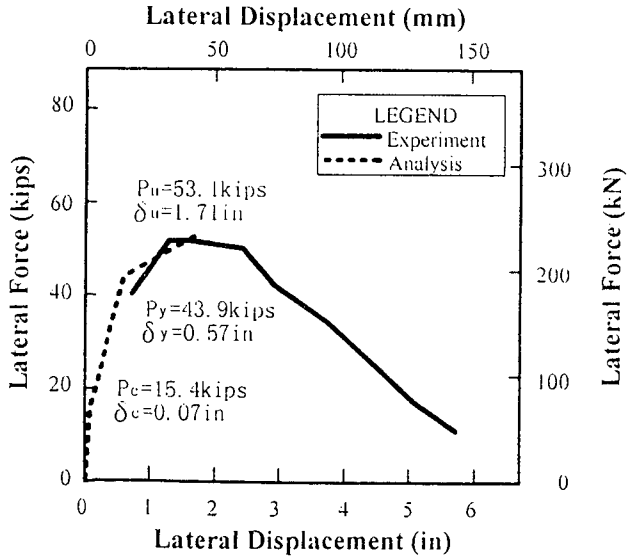

(a) P-1 Specimen

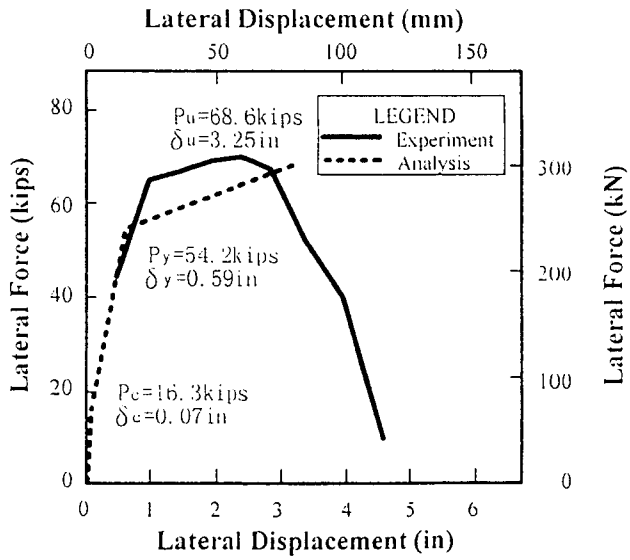

(b) P-2 Specimen

Fig. 13 Comparison of Lateral Load and Displacemetn Relation

hysteresis loop for P-1 and P-2. In the analysis, the peak strengths of P-1 and P-2 were computed to be 24.1 tf and 31.1 tf, respectively. These figures both agreed well with the test results. It was concluded, therefore, that the method of analysis was able to estimate the strength of the retrofitted piers with sufficient precision.

On the other hand, the ductility factors of P-1 and P-2 calculated in this analysis were 3.0 and 5.3, respectively. The corresponding test results were both higher than these analysis values. This is due to a difference in definition of ultimate stage. In the loading test, on the one hand, ultimate displacement was defined as the lateral displacement recorded when the strength was reduced to the yield strength. In the analysis, on the other hand, ultimate displacement was defined as the lateral displacement recorded when the strain of the most external edge of the concrete pier reached its ultimate strain. The ultimate displacement of P-2 obtained by the analysis method was 82.5 mm. To compare this with the damage caused in the test when a lateral displacement of this extent was effected, the anchor bars began to buckle, reaching the stage of damage immediately before breaking, and the concrete started to spall off, with the peak strength starting to fall after having remained stable. This damage degree corresponds to the state defined as "ultimate" in the analysis. On the other hand, when P-2 was so deformed that its strength had been reduced to yield strength, the anchor bars had already broken, and the longitudinal reinforcement was also about to break. Based on these considerations, the ultimate displacement obtained by the method had a value suitable for the design, from the points of view of residual strength, degree of difficulty of restoration, etc. It should be noted that the plastic hinge length would be different between P-1 and P-2, as shown in Figure 4. In above analysis, the ductility is calculated without taking account of the effect of the plastic hinge length, which may cause the under- or overestimate of the ultimate displacement.

CONCLUSIONS

We have proposed here a method of designing a steel jacket with anchor bars as a method of enhancing the ductility of reinforced concrete piers while controlling the increase in its strength. We carried out a lateral loading test using large models, including models retrofitted with this method. We also examined a way of analyzing the retrofitting effect, i.e., the effect of enhancing the strength and ductility with this method. The following is the summary of results of the study:

(1) The test clearly showed that the ductility of a pier can be enhanced while controlling the increase in its strength using a steel jacket with anchor bars. The pier's energy absorption and damping performance were also enhanced.

(2) It was confirmed that the jacket and hoop reinforcement were strained in such a way that the steel jacket functions effectively as a longitudinal and hoop reinforcement, with a strength equivalent to that of the anchor bars.

(3) A comparison of the three cases with a vertical gap between the lower end of jacket and the top of the base -5cm, 10cm and 15cm- showed that, while the peak strengths were all equal, the smaller the vertical gap length, the larger the ductility factor.

(4) A method of analyzing the retrofitting effect of this type of steel jacket with a controlled increase in flexural strength was described. It was confirmed that the strength calculated according to this method of analysis corresponded well with the observed test results. On the basis of the results of the test (number of cycles of loading: 3), the ultimate

displacement obtained by this analysis is equivalent to the stage in which the anchor bars buckle, having reached the stage of damage that immediately precedes breaking. At this stage, concrete starts to spall off, and the peak strength begins to deteriorate after having remained stable for a time.

REFERENCES

1) Ministry of Construction: Report on the Damage of Highway Bridges by the Hyogo-ken Nanbu Earthquake, Committee for Investigation on the Damage of Highway Bridges Caused by the Hyogo-ken Nanbu Earthquake, 1995
2) Ministry of Construction: Guide Specifications for Reconstruction and Repair of Highway Bridges Which Suffered Damage due to the Hyogo-ken Nambu Earthquake, Feb. 1995
3) Kazuhiko Kawashima, G.A. MacRae, Jun-ichi Hoshikuma and Kazuhiro Nagaya: Residual Displacement Response Spectrum and its Application to Evaluate Residual Displacement Developed in Reinforced Concrete Bridge Columns, 28th Joint Meeting of U.S.-Japan Panel on Wind and Seismic Effects, UJNR, May 1996
4) Kazuhiko Kawashima, Shigeki Unjo and Hiroyuki Iida: Seismic Inspection and Seismic Strengthening of Reinforced Concrete Piers at Mid-height Where Main Reinforcement is Terminated, First U.S.-Japan Workshop on Seismic Retrofit of Bridges, UJNR, Tsukuba, Dec. 1990
5) Design Specifications for Highway Bridges, V Seismic Design, Japan Road Association, Feb. 1990
6) Jun-ichi Hoshikuma, Kazuhiko Kawashima and Kazuhiro Nagaya: A Stress-Strain Model for Reinforced Concrete Bridge Piers Confined by Hoop Reinforcement, Proceedings of the Second International Workshop, Seismic Design and Retrofitting of Reinforced Concrete Bridges, New Zealand, Aug. 1994

ANALYSIS OF RC BRIDGE PIERS EXTERNALLY REINFORCED WITH FIBER-REINFORCED PLASTICS

G. Monti [1] M.R. Spoelstra [2]

[1] Dipartimento di Ingegneria Strutturale e Geotecnica – Università La Sapienza, Roma, Italy

[2] Department of Civil Engineering – University of Technology, Delft, the Netherlands

ABSTRACT

Results of analyses on circular reinforced concrete bridge piers retrofitted with fiber-reinforced plastics (FRP) jackets are presented. In order to model the interaction between concrete and jacket, a uniaxial model for concrete confined with fiber-reinforced plastics (FRP), under monotonic and cyclic loading is developed. This model explicitly accounts for the lateral dilation of concrete and its interaction with the confining device and can also be used for concrete confined with steel jackets or conventional transverse reinforcement. The model is based on an incremental-iterative approach, which uses a relation between axial and lateral strains, from which the confined concrete properties are calculated starting from an unconfined state. This relation is the main feature of the model. Comparisons with a set of experimental data show very good agreement. Furthermore, a simplified moment-curvature analysis on retrofitted circular reinforced concrete bridge columns is carried out, based on the new model, and a parametric study is carried out on the influence of fiber-reinforced plastic (FRP) external reinforcement on flexural strength, ductility and failure mechnism of full circular reinforced concrete piers, with or without full composite action between jacket and pier.

1. INTRODUCTION

Recent destructive earthquakes have indicated that old reinforced concrete bridges, designed according to inadequate seismic codes, are highly vulnerable to seismic attack, and that in most cases collapse results from failures in the piers. Therefore, there is an urgent need to upgrade these bridges to current seismic design standards in regions with high seismicity.

Two typical causes of potential failure are: inadequate lateral reinforcement, resulting in both insufficient ductility and buckling of longitudinal reinforcement, and poor detailing of lap-splices, resulting in too low flexural capacity. It is already well known that concrete strength and ductility can be enhanced by increasing the confinement action, which, in addition, prevents also debonding of longitudinal reinforcement. For these reasons, existing retrofitting

techniques are typically based on increasing the confinement pressure in either the potential plastic hinge region or over the entire pier (see, among others, Chai *et al.* 1991). Sometimes, enhancement of the flexural strength is also required, especially in the presence of lap-splices.

Steel jacketing has proved to be an effective measure for retrofitting. Although this has been widely used in practice in California and elsewhere, the engineering community is also looking for alternatives, particularly with improved easiness of construction. The problem of corrosion of steel jackets also remains unsolved.

Recently, advanced composite materials have been recognized to represent a valuable retrofit technique for bridge piers. Composite materials have some advantageous properties over other materials:

- high stiffness (for some materials), high strength (up to four times steel's),
- properties can be designed and optimised depending on the structural application,
- low thickness and weight, with significant advantages for transportation and assemblage,
- reduction of waste material, through easier dismantling for reuse or demolition,
- resistance to corrosion, so that less maintenance is required.

Although several experimental studies on columns confined with fiber-reinforced plastics (FRP) have been carried out (Saadatmanesh *et al.* 1994, Seible *et al.* 1995, Xiao *et al.* 1995), studies aiming at obtaining reliable and accurate numerical models of their behavior are still unsatisfactory.

A major obstacle to such developments is the lack of a concrete model explicitly accounting for the interaction with the confining device. An FRP jacket, as opposed to a steel one that applies a constant confining pressure after yield, has an elastic behavior up to failure and therefore exerts a continuously increasing confining action. The amount of this action depends on the lateral dilation of concrete, which in turn is affected by the confining pressure. The modeling of such an interaction is the scope of the following section.

2. DEVELOPMENT OF A CONTINUOUS CONFINEMENT MODEL

2.1 A uniaxial models for unconfined concrete accounting for lateral expansion

Pantazopoulou and Mills (1995) developed a general but simple constitutive model for concrete under uniaxial compressive loading where the volume strain ε_V is taken as a measure for the internal damage from cracking. The uniaxial behavior of plain concrete is described as follows:

$$f_c' = E_{curr} \cdot \varepsilon_1 \qquad E_{curr} = E_0 \frac{1}{1+\varepsilon_A/\beta} \tag{1a,b}$$

with: E_{curr} = current secant modulus; ε_1 = axial strain; E_0 = initial elastic modulus; ε_A = area strain. The constant β is evaluated as follows

$$\beta = \frac{V_p^3 \nu_{pc}}{3} \tag{2}$$

where V_p = volume fraction of paste in concrete, and

$$\nu_{pc} = 3.22 \frac{w_0 - 0.3064\alpha_\infty}{1 + 3.22 w_0} \qquad \alpha_\infty = \frac{1.031 w_0}{0.194 + w_0} \tag{3}$$

where w_0 = water/cement ratio.

In order to effectively use this model, a relationship between the area-strain ε_A and the axial strain ε_1 is necessary. Experimental uniaxial tests on unconfined concrete specimens show that (Figure 1): the initial slope of the $\varepsilon_V - \varepsilon_1$ curve (1-2ν), where ν is the Poisson's ratio of the undamaged material. At a certain value $\varepsilon_{\lim}$, deviation from this linear behavior occurs. This is due to micro-cracking, so that the transverse (lateral) strain ε_{lat} increases at a faster rate than the theory of elasticity would predict. The deviation of the $\varepsilon_V - \varepsilon_1$ curve from the linear behavior increases with increasing axial strain, so that, at a value ε_1^*, the volume strain reverts to zero. Beyond ε_1^*, the volume strain increases continuously. Noticing that the area strain ε_A is given by the difference between the $\varepsilon_V - \varepsilon_1$ curve and the line $\varepsilon_V = \varepsilon_1$ and that the lateral strain ε_{lat} is half the area strain, Pantazopoulou and Mills (1995) derived the following direct relation between lateral and axial strain:

$$\varepsilon_{lat} = 0.5\,\varepsilon_A = -\nu\,\varepsilon_1 - \left(\frac{1-2\nu}{2}\right)\varepsilon_1^* \left(\frac{\langle \varepsilon_1 - \varepsilon_{\lim} \rangle}{\varepsilon_1^* - \varepsilon_{\lim}}\right)^c \tag{4}$$

where the McAuley brackets $\langle \cdot \rangle$ indicate that the non-linear term is only considered when $\varepsilon_1 > \varepsilon_{\lim}$, and

$$\varepsilon_1^* = \alpha\,\varepsilon_{co} \qquad \varepsilon_V = \varepsilon_A + \varepsilon_1 \qquad \varepsilon_A = 2\,\varepsilon_{lat} \tag{5a,b,c}$$

where ε_1^* is the axial strain at $\varepsilon_V = 0$, ε_{co} is the strain at peak stress, $\varepsilon_{\lim}$ is the limit axial strain beyond which microcracking starts to occur, which can be evaluated as

$$\varepsilon_{\lim} = \frac{-\varepsilon_{cr}}{\nu} = \frac{0.10 f'_{co}}{\nu E_0} \tag{6}$$

For unconfined concrete one usually has: $\alpha \approx 0.9 \div 1.0$, c= 2 and $\varepsilon_{\lim} \approx 0.001$.

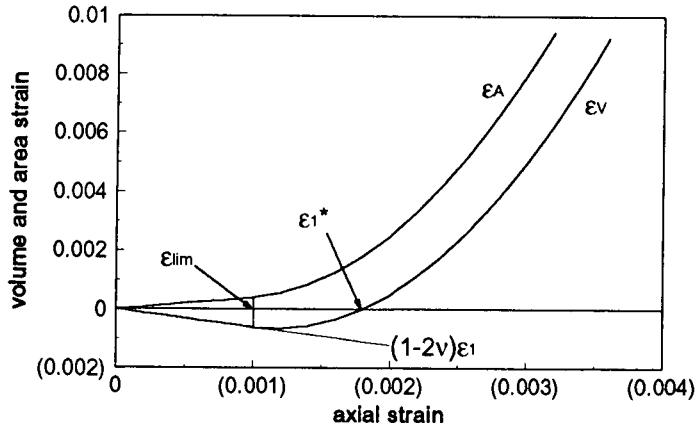

Figure 1. Volume and area strain according to Pantazopoulou and Mills (1995).

2.2 A modification proposed for the constant β

The value of β (2) is evaluated from the volume fraction of paste and the water-cement ratio. However, it would be more convenient to have a relation that yields β as a function of readily available unconfined concrete properties such as peak strength f'_{co}, strain at peak strength ε_{co} and initial elastic modulus E_0. By rewriting (1b), we obtain:

$$\beta = \frac{\varepsilon_A}{\left(\frac{E_0}{E_{curr}}\right) - 1} \tag{7}$$

Since β is a constant, the above expression can be evaluated at a convenient point, such as $\varepsilon_1 = \varepsilon_{co}$. There, the secant-modulus is:

$$E_{curr} = \frac{f'_{co}}{\varepsilon_{co}} \tag{8}$$

The axial strain ε_1^* at which $\varepsilon_V = 0$ is taken as $\varepsilon_1^* = \varepsilon_{co}$ (that is, α=1). In the expression of ε_A (4), the term containing $\varepsilon_{\lim}$ becomes unity, because $\varepsilon_1 = \varepsilon_{co} = \varepsilon_1^*$. The area strain is then given by: $\varepsilon_A = -\varepsilon_{co}$. Then, from (7), the value of β can be finally expressed as:

$$\beta = \frac{f'_{co}\,\varepsilon_{co}}{f'_{co} - E_0\,\varepsilon_{co}} \tag{9}$$

Now β only depends on the unconfined concrete properties f'_{co}, ε_{co} and E_0. With equations (1), (4), (6) and (9), the monotonic stress-strain curve for unconfined concrete is obtained.

To check the accuracy of the proposed expression of β, the model of Pantazopoulou and Mills with (9) is compared to the equation of Popovic (1973), which is widely recognized as an accurate model of the unconfined concrete behavior, and shows excellent correlation to experimental testing, as shown by Mander *et al.* (1988b). The equation is given by:

$$f'_c = \frac{f'_{co} \cdot x \cdot r}{r - 1 + x^r} \tag{10}$$

$$x = \frac{\varepsilon_c}{\varepsilon_{co}} \qquad r = \frac{E_0}{E_0 - E_{\sec}} \qquad E_{\sec} = \frac{f'_{co}}{\varepsilon_{co}} \tag{11}$$

with the meaning of the symbols as above.

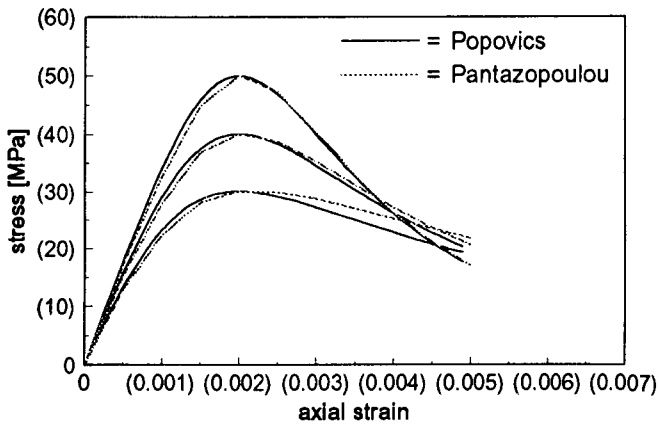

Figure 2. Consistency between Popovics (1973) and Pantazopoulou and Mills (1995) with proposed β.

The comparison between the two models is depicted in Figure 2. The following values are used: $\varepsilon_1^* = \varepsilon_{co} = 0.002$, $\nu = 0.20$. Three different concrete types are compared, f'_{co} = 30, 40, 50 MPa. As it can be seen from Figure 2, the two models show excellent correlation, therefore it can be concluded that the proposed espression (9) gives a good estimate of β for a wide range of different concrete types.

2.3 A new model for concrete confined with Fiber-Reinforced Plastics (FRP)

The relation between lateral and axial strain (4) was developed to model the lateral expansion of unconfined concrete. In order to use it for confined concrete, the effect of confinement on the lateral expansion should be accounted for. Unfortunately, no relation exists in the literature that expresses the lateral expansion of concrete for triaxial stress states, nor experimental data are available. Such a relation should describe the lateral strain as a function of the axial strain, for different levels of confining pressure, so that, with (1) and (9), a stress-strain curve for (actively) confined concrete would be obtained. Since such relation does not exist, a heuristic approach is followed: starting from a stress-strain model for confined concrete, which has been extensively tested against experimental data, the variation of the lateral strain in the presence of a confining pressure is derived. The chosen model is that of Mander *et al.* (1988a).

The model offers a simple equivalent uniaxial stress-strain curve for confined concrete, based on the formula by Popovics (1973), and shows excellent correlation to experimental testing, as shown by Mander *et al.* (1988b). The model is given by

$$f'_c = \frac{f'_{cc} \cdot x \cdot r}{r - 1 + x^r} \tag{12}$$

where

$$\frac{f'_{cc}}{f'_{co}} = 2.254\sqrt{1 + 7.94\frac{f_l'}{f_{co}'}} - 2\frac{f_l'}{f_{co}'} - 1.254 \tag{13}$$

$$\varepsilon_{cc} = \varepsilon_{co}\left[1 + 5\left(\frac{f'_{cc}}{f'_{co}} - 1\right)\right] \qquad E_{\sec} = \frac{f'_{cc}}{\varepsilon_{cc}} \qquad r = \frac{E_c}{E_c - E_{\sec}} \qquad x = \frac{\varepsilon_c}{\varepsilon_{cc}} \tag{14}$$

where f'_{cc} and f'_{co} are the compressive strengths of confined and unconfined concrete respectively, and ε_{cc} and ε_{co} are the compressive strains at peak strength of confined and unconfined concrete, respectively, and f_l is the effective confining pressure, calculated as:

$$f_l = \frac{1}{2} k_e \, \rho_s f_s \tag{15}$$

$$\rho_s = \frac{4 A_s}{s \, d_s} \text{ (hoops or spirals)} \quad or \quad \rho_s = \frac{4 t}{d_s} \text{ (jackets)} \tag{16}$$

where k_e is a coefficient accounting for the arching-effect (k_e=1 for jackets), ρ_s is the volumetric ratio of the confining steel, s and d_s are the spacing between and the diameter of the hoops or spirals, respectively, and f_s is the yield stress of the confining steel.

In recent years, researchers have attempted to extend Mander's model to predict the level of confinement provided by fiber-reinforced plastics. However, there are some potential problems that make its use in the present form unsuitable for fiber-composite jackets.

For example, the maximum peak strength is obtained when the confining pressure is about 2.4 times the unconfined concrete strength, after which, for any further increase of the confining pressure, the model yields the erroneous results that the confined concrete peak strength decreases (Mirmiran *et al.* 1996). However, in the case of FRP-confined concrete, such high confining pressures can only be attained by means of high-strength carbon-fibers jackets of very large thickness, which is quite impractical. Thus, in this study this problem is neglected.

A major drawback, instead, is that Mander's model is based on a constant value of the confining pressure throughout the loading history. In reality, passive confinement increases as concrete expands laterally, and its amount depends on the stress-strain law of the confining device. Mander's model has been developed for transverse steel reinforcement with elasto-plastic behavior, so that, except for the initial phase before steel yields, the constant confining pressure assumption is realistic, because when steel yields the confining pressure it exerts remains constant. Conversely, fiber-reinforced plastics behave elastically until failure, an the inward pressure they apply increases continuously. Therefore, in this case, this simplification is not appropriate, and a new confinement model is needed for use with fiber-reinforced plastics.

From (1) and (4) it is possible to express the lateral expansion as a function of the axial strain and the confinement pressure. In this study, it is assumed that the Mander's model gives an accurate description of the behavior of confined concrete. Thus, considering that each Mander curve describes the behavior of concrete under a *constant value* of active confining pressure, the sought relation can be derived as explained hereafter.

By rewriting (1a) and (1b), with $\varepsilon_{lat} = 0.5 \cdot \varepsilon_A$, it is obtained:

$$E_{curr}(\varepsilon_1, f_l) = \frac{f_c'(\varepsilon_1, f_l)}{\varepsilon_1} \tag{17}$$

$$\varepsilon_{lat}(\varepsilon_1, f_l) = 0.5\beta \cdot \frac{E_0 - E_{curr}(\varepsilon_1, f_l)}{E_{curr}(\varepsilon_1, f_l)} \tag{18}$$

where β is the constant before developed in (9), depending on the concrete type. The lateral expansion ε_{lat} can be calculated with (17) and (18) as function of the axial strain ε_1 and of an estimate of the confining pressure f_l. From ε_{lat}, it is possible to calculate the strain and stress in the jacket (for the simplest case of axial load on a circular section: $\varepsilon_j = \varepsilon_{lat}$), and therefore the corresponding confining pressure f_l. This updated value is used for a new estimate of ε_{lat}. The whole procedure is repeated until f_l converges to a stable value.

The iterative procedure can be summarized as in Figure 3, where: f_l is the confining stress, f_{cc}' and ε_{cc} are the ultimate compressive stress and strain at peak stress of confined concrete according to Mander's model, ρ is the jacket volumetric ratio, E_j is the modulus of elasticity of the jacket material, f_{lA} is the active confinement pressure, and f_y and f_u are the yield and ultimate stress of the jacket material.

The whole procedure is repeated for every value of axial strain ε_1, over the complete stress-strain curve. In all numerical tests it has been observed that convergence at each step is very fast.

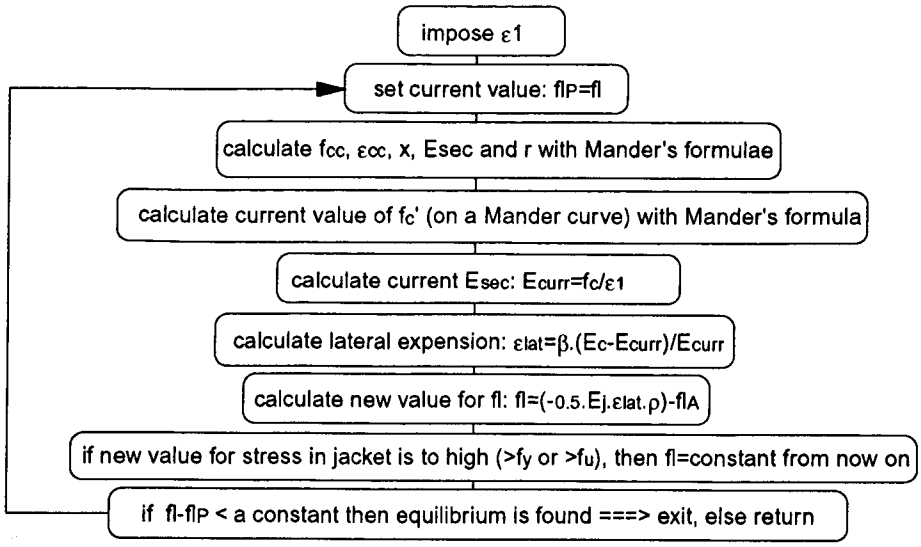

Figure 3. Iterative procedure.

2.4 FRP-confinement effect on ultimate compressive strain

The ultimate compressive strain of confined concrete is defined by Mander *et al.* (1988a) as the longitudinal strain corresponding to the failure of the transverse reinforcement. That event results in an abrupt reduction of the concrete compressive strength. An energy-balance method is used to predict the maximum compressive axial strain:

$$U_j = U_{cc} - U_{co} + U_{sc} \tag{19}$$

where: U_j = total strain energy in confining device; U_{cc} = area under confined concrete curve; U_{co} = area under unconfined concrete curve; U_{sc} = energy needed to maintain yield in longitudinal reinforcing steel.

It is assumed that the increase in strain energy capacity of compressed concrete due to confinement be provided by the confining device strain energy capacity. The ultimate strain energy capacity of the confining device is given by the area under the stress-strain curve times the volumetric ratio. If the accumulated strain energy reaches this ultimate value, the confining device collapses. Priestley and Seible (1992) derived an equation, based on the energy-balance method, for steel transverse reinforcement:

$$\varepsilon_{cu} = 0.004 + \frac{1.4\,\rho_s f_{yh}\,\varepsilon_{sm}}{f'_{cc}} \geq 0.005 \tag{20}$$

where ρ_s = steel volumetric ratio, f_{yh} = steel yield strength, ε_{sm} = strain at peak stress, and f'_{cc} = confined strength of concrete, calculated with (13). The complete stress-strain curve for concrete confined with steel hoops, spirals or steel jackets is shown in Figure 4.

Alike in Mander's model, in this study the ultimate compressive axial strain of confined concrete is defined as the axial strain at which the FRP jacket reaches its ultimate tensile strain. That event results in a sudden reduction of the concrete compressive strength. For FRP-confined concrete, Priestley *et al.* (1995) experimentally derived the following formula:

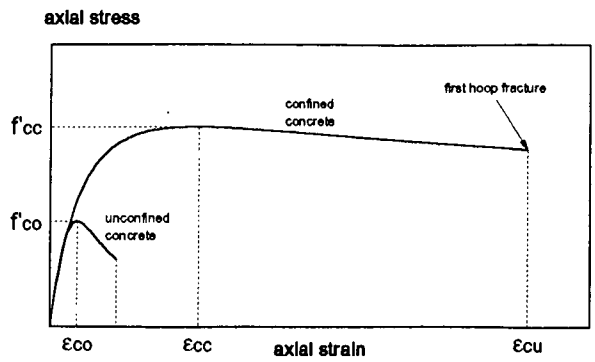

Figure 4. Stress-strain curve for steel-confined concrete according to Mander *et al.* (1988a).

$$\varepsilon_{cu} = 0.004 + \frac{2.5\,\rho_j f_u\,\varepsilon_u}{f'_{cc}} \tag{21}$$

where f_u, ε_u = ultimate or allowable strength and strain, respectively, of the jacket material. This equation predicts a higher ultimate compressive strain than the energy-balance method. In Mirmiran *et al.* (1996) it is also mentioned that the failure point determined by the energy balance method always occurs before the peak stress f'_{cc} is reached. Therefore, it is recognized that the energy-balance method is not satisfactory for FRP materials.

Because of the above-described problems with the energy-balance method for concrete confined with FRP, in this study it is assumed that the ultimate compressive axial strain of concrete corresponds to the event:

$$\varepsilon_{lat} = \varepsilon_{j,u} \tag{22}$$

where ε_{lat} = lateral strain of concrete, and $\varepsilon_{j,u}$ = ultimate tensile strain of the jacket. This means that when the lateral strain of concrete reaches the ultimate or allowable strain of the FRP material, the jacket fails. Because in the incremental-iterative approach of the proposed model, the relation between lateral and axial strain is known, the ultimate axial strain is also known. When a circular concrete section is subjected to constant axial strain over the entire cross-section, the lateral (radial) strain is constant along a radius of the section, and therefore the strain in the jacket is constant along the circumference. This assumption is close to the actual behavior because FRP behaves elastically up to failure, whereas, in case of concrete confined with steel, the circumferential strain varies because of yield localization.

2.5 The complete monotonic stress-strain curve for confined concrete

The proposed model can be used for circular concrete sections confined with either steel or FRP, and subjected to either monotonic or cyclic loading. When a steel jacket is used (Figure 5), the resulting stress-strain curve is the same as calculated with the model of Mander *et al.* (1988a), except for the initial branch, where the proposed model gives slightly lower stresses, in compliance with the fact that steel is still elastic. When the jacket yields, the same behavior is obtained. When an FRP jacket is used (Figure 6 and Figure 7), the stress-strain curves show a gradually growing behavior, until the jacket ruptures. The strength never decreases during the loading history, except when very thin and low-stiffness materials are used. The curves also

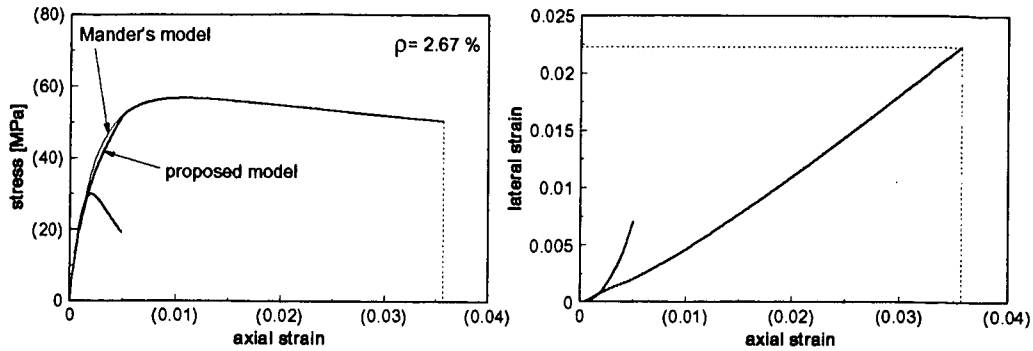

Figure 5. Stress-strain curve for concrete confined with steel jacket.

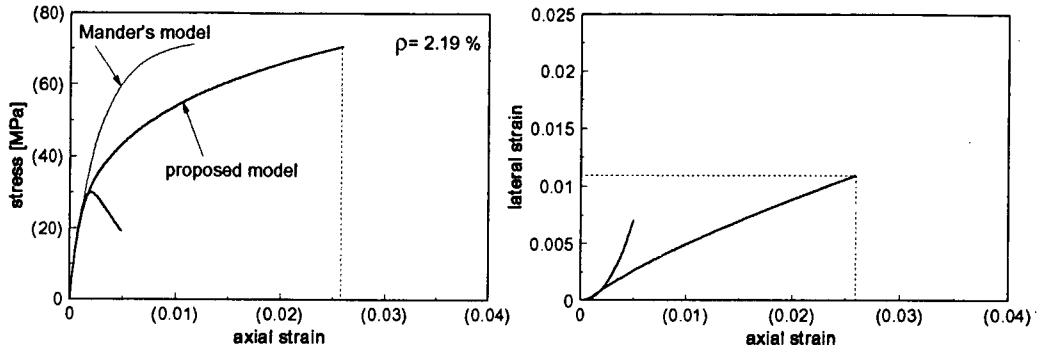

Figure 6. Stress-strain curve for concrete confined with carbonfiber/epoxy jacket.

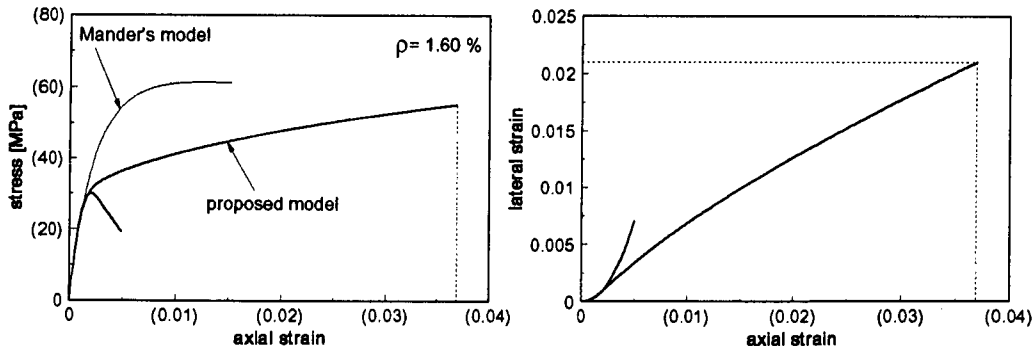

Figure 7. Stress-strain curve for concrete confined with fiberglass/epoxy jacket.

show a much more ductile and less strong behavior compared to the model of Mander. It should be mentioned here that the ultimate concrete compressive strain was derived with the theoretical value of the FRP tensile strain. Normally the jacket will fail earlier, due to the biaxial stress state that it undergoes, but this only influences the ductility, not the stress-strain curve. The main feature of the proposed model is that the stress-strain characteristics, and therefore the stiffness, of the confining mechanism are explicitly accounted for.

2.6 Remarks on the rules for cyclic loading

At load reversals, concrete confined with steel unloads and recovers the elastic deformation. The confinement effect of the jacketing steel depends on the steel status: if it is elastic, it follows the concrete in this deformation and applies on it an active confining pressure; whereas, if it has yielded, it only recovers the elastic deformation and concrete is not under any hydrostatic pressure. For this case Chang and Mander (1994) proposed reversal rules with degrading unloading and reloading stiffness, which are believed to give excellent prediction of experimental results.

The cyclic behaviour of concrete confined with FRP is not the same as with steel. Because of its elastic behaviour, the FRP jacket tends to shrink back to its undeformed original position and follows the concrete deformations. Thus, concrete is always under a state of active hydrostatic pressure. Both the elastic and some plastic deformation will be recovered, except for a residual lateral plastic strain, which causes the jacket to be under some residual stress.

To the authors' knowledge there is not any experimental data available in the literature about cyclic loading of FRP-confined concrete cylinders. The only conclusion that can be drawn is that the un- and reloading stiffness will be lower than when confined with steel (the strain at which the strength reaches zero is less). Therefore, in this study, the following reversal rules are adopted, which are a simplification of Chang and Mander (1994) rules. The point $(\varepsilon_{un}, f_{un})$ denotes a reversal point on a specific Mander-curve, whose peak stress f'_{cc} and strain at peak stress ε_{cc}, calculated through the above described iterative procedure, are known. From those, the axial strain where concrete reaches zero stress is calculated as

$$\varepsilon_{pl} = \varepsilon_{un} - \frac{f_{un}}{E_{\sec}} \tag{23}$$

where

$$E_{\sec} = E_c \left(\frac{\left| \dfrac{f_{un}}{E_c\, \varepsilon_{cc}} \right| + 0.57}{\left| \dfrac{\varepsilon_{un}}{\varepsilon_{cc}} \right| + 0.57} \right) \tag{24}$$

The un- and reloading paths between points $(\varepsilon_{un}, f_{un})$ and $(\varepsilon_{pl}, 0)$ are considered as linear (Figure 8):

$$f_{un}(\varepsilon_1) = E_{\sec}(\varepsilon_1 - \varepsilon_{pl}) \tag{25}$$

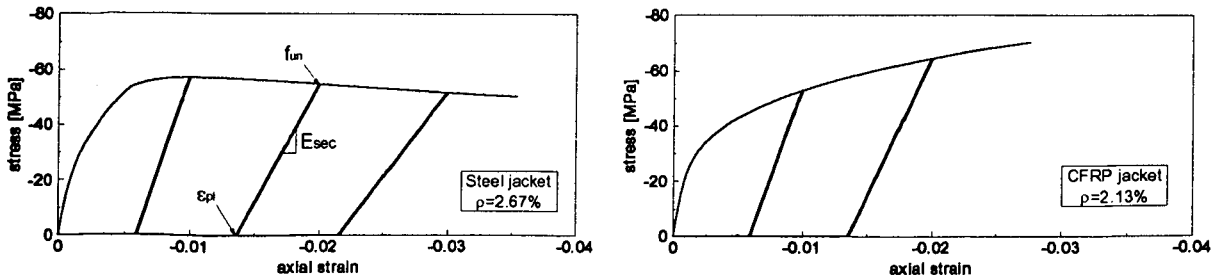

Figure 8. Cyclic stress-strain curves for confined concrete confined with steel (left) and CFRP (right) jacket.

3. COMPARISON WITH EXPERIMENTAL DATA

3.1 Definition of composite action

In experimental tests performed on axially loaded cylindrical concrete specimens wrapped with FRP sheets, the measured quantities are: axial stress, axial strain and radial strain. The latter is equal to the transverse strain in the jacket. As a consequence, one can expect failure of the wrapped specimen when the radial strain equals the ultimate strain in the jacket $\varepsilon_{j,u}$. However, experimental evidence shows that failure of the cylinders occurs at lower radial strains.

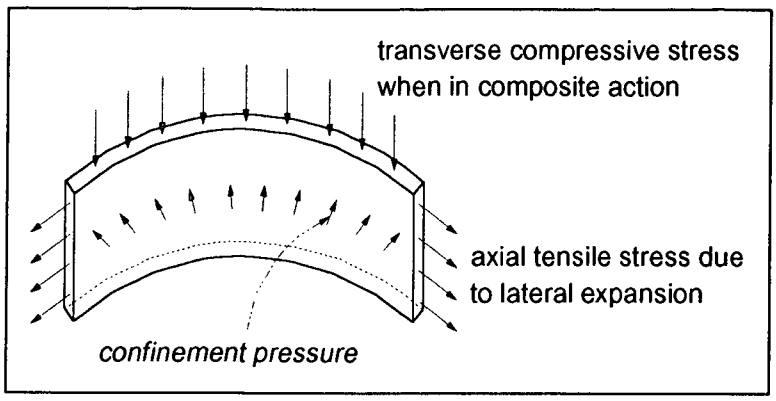

Figure 9. Biaxial state of stress in FRP sheets.

This reduction is due to the fact that the FRP jacket is subjected to a biaxial stress state, as shown in Figure 9. Here, the concept of *composite action* of the jacket is introduced, which essentially denotes the ability of the jacket of providing transverse confinement and, at the same time, longitudinal load-carrying capacity.

The amount of this action depends on the stiffness of the glue layer between the jacket and the concrete specimen, and on the roughness of the jacket and concrete surface. For an infinitely flexible glue (*no composite action*), concrete slips within the jacket, therefore no longitudinal stress transfer takes place and the jacket does not contribute to the axial strength. For an infinitely stiff glue (*full composite action*), the jacket deforms longitudinally together with concrete, thus contributing with a load-carrying action. In both cases, the confinement action is present.

In case of no composite action, the jacket only undergoes transverse strains and therefore can only fail in axial mode, due to either fiber collapse or delamination between layers. Thus, failure of the specimen occurs when the radial strain of concrete reaches the value of $\varepsilon_{j,u}$.

In case of composite action, the jacket undergoes both transverse and longitudinal strains, which affect the axial failure mode. The ultimate stress and strain in the axial direction of the sheets are then reduced. Thus, failure of the specimen occurs at lower radial strain than $\varepsilon_{j,u}$.

In view of future developments where the composite action is directly accounted for, in what follows the ultimate strain of the jacket is taken equal to the concrete lateral strain $\varepsilon_{lat,u}$ measured in the tests at failure.

3.2 The experimental tests by Picher *et al.* (1996)

The experimental results obtained from one set of FRP-confined concrete specimens (Picher *et al.* 1996) are considered. The experiments were carried out on sets of five concrete cylinders: one unconfined and four confined with carbonfiber/epoxy (CFRP) sheets, at different winding angles: 0°, 6°, 12° and 18° with the transverse direction. The ultimate strain of the CFRP sheets was provided by the manufacturer as $\varepsilon_{j,u}$=1.5%, for 0° winding angle, that is, in a uniaxial stress state. In Table 1, where each cylinder specimen is identified via a 'C' followed by a number denoting the sheet winding angle, the experimental results are compared with the numerical ones, in terms of: the ratio $\sigma_{1,u}/f'_{co}$ between the failure stress and the unconfined strength, the ultimate axial and lateral strains in concrete $\varepsilon_{1,u}$ and $\varepsilon_{lat,u}$. The effective confinement stiffness E_j is here calculated with the Classical Lamination Theory (see, for example, Kim 1995). The value of the constant β in the proposed model is estimated with (9).

In Figure 10 the results relative to cylinders C0 and C18 are shown. It can be observed that the numerical results are in good agreement with the experimental values.

Table 1. Experimental results (Picher *et al.* 1996) and results with new model.

Cylinder	E_j (GPa)	$\sigma_{1,u}/f'_{co}$ (exper.)	$\varepsilon_{1,u}$ (exper.)	$\varepsilon_{lat,u}$ (exper.)	$\sigma_{1,u}/f'_{co}$ *(analysis)*	$\varepsilon_{1,u}$ *(analysis)*	$\varepsilon_{lat,u}$ *(analysis)*
unconf.	0.0	1.00	0.20	--	*1.00*	*0.22*	*0.13*
C18	70.2	1.16	0.66	0.50	*1.20*	*0.59*	*0.50*
C12	77.4	1.37	1.03	0.64	*1.28*	*0.76*	*0.64*
C6	81.9	1.32	0.88	0.72	*1.33*	*0.87*	*0.72*
C0	83.0	1.41	1.07	0.84	*1.37*	*1.02*	*0.84*

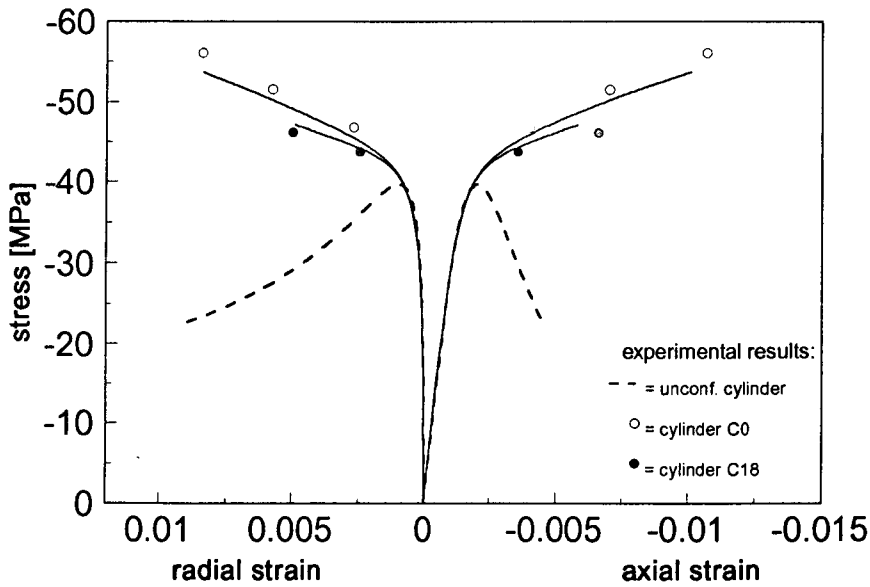

Figure 10. Comparison between experiment (Picher *et al.* 1996) and analysis with new model for unconfined cylinder, cylinder C0 and C18.

4. MONOTONIC AND CYCLIC MOMENT-CURVATURE ANALYSIS

4.1 Evaluation of confinement in eccentrically loaded sections

Let us consider a circular section with a linearly distributed axial strain field imposed on it. It is assumed that, at a given distance from the section's centroid, the lateral strain can be calculated, by means of the proposed model, from the corresponding axial strain. On the circumference, this allows to calculate the transverse strain in the jacket from the corresponding radial strain, and therefore the stress in the jacket and the induced confining pressure. This amounts to assume that the confining pressure only depends on the distance from the neutral axis (Figure 11).

This assumption has been verified in numerical analyses conducted in the linear range (Monti and Spoelstra 1997) giving results that corroborate the chosen simplified approach. More refined analysis are being carried out with advanced nonlinear FE codes to account for the nonlinear behavior of concrete under triaxial stress states.

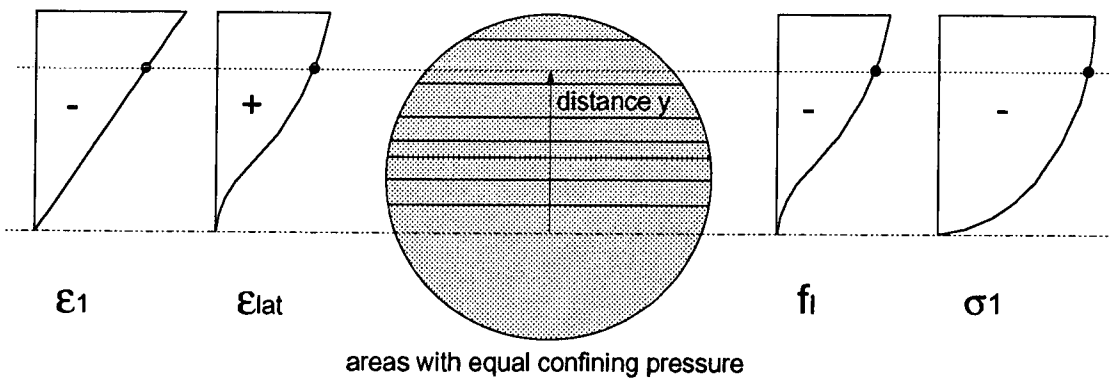

Figure 11. Calculation method for confining pressure f_l and concrete strength σ_1.

4.2 Moment-curvature and load-displacement analysis

In most case, retrofitting of existing bridge piers only concerns enhancement of ductility, while normally flexural strength is adequate. It is believed that composite action between jacket and pier should be avoided as much as possible, since it generally enhances flexural strength to a larger extent than ductility. Also, a study by Orito *et al.* (1987) reported that unbonded concrete-filled steel tubes would perform better than bonded tubes, because in the former case the jacket does not undergo longitudinal stresses. Therefore, the jacket will not buckle, and will continue confining the pier up to its maximum strength.

These considerations imply that a fiber winding-angle of 0° is the most effective, when no composite action is foreseen. In reality, a certain degree of composite action between pier and FRP jacket cannot be excluded *a priori*. Therefore, with 0° winding-angle the jacket will fail under longitudinal tensile strains, due to separation of parallel fibers. A jacket made of several plies with different winding-angles would be a more practical option. The possibility of using a

material with a lower stiffness and higher deformability, applied in the longitudinal direction, can also be considered.

Special care should be devoted to the shear capacity of a retrofitted pier. Because there will always be some degree of composite action, the flexural strength will increase. Since the shear capacity should always exceed the flexural capacity, in order to avoid brittle shear collapse, it should be checked that the shear capacity is still adequate after retrofitting.

As an example of retrofitting a pier with an FRP jacket, a moment-curvature and a load-displacement analysis have been carried out with the programs CYRUS (Monti *et al.* 1996) and CYBERPIE (CYclic BEhavior of Retrofitted PIErs), respectively.

The cross-section of the selected pier, which was already used in another parametric study (Mirmiran *et al.* 1996), is shown in Figure 12.

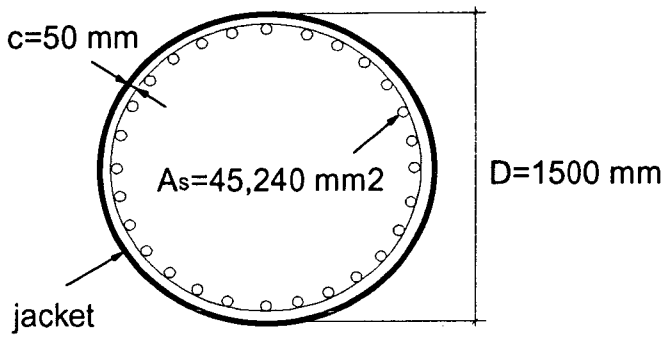

Figure 12. Typical reinforced concrete pier section.

The pier is 1500 mm in diameter and has 36ø40 mm rebars (total area: 45,240 mm², with ρ_s = 2.94%) having yield strength 440 MPa and ultimate strain 12%. The unconfined concrete properties are: f'_{co} = 35 MPa and E_0 = 29,580 MPa. The transverse reinforcement consists of ø16mm ties at a spacing of 80 mm (ρ_t= 0.72%). The length of the pier is 6,000 mm, and it is subjected to single bending. The foundation is assumed infinitely stiff. According to Priestley and Seible (1992), the plastic hinge length L_p is calculated as:

$$\begin{aligned} L_p &= 0.08\,L + \chi \cdot d_b \qquad \text{(without jacket)} \\ L_p &= g + 2\chi \cdot d_b \qquad \text{(with jacket)} \end{aligned} \tag{26}$$

in which L is the pier hight, $\chi = 9$, d_b is the bars diameter, and g is the gap between jacket and footing, here taken as 50 mm.

The pier is confined with layers of carbonfiber/epoxy material, with fiber winding-angle of ±15°, and with layers of fiberglass/epoxy, with fiber winding-angle of ±75°. The mechanical properties of the materials are listed in Table 2, where the indices 1 and 2 denote the directions parallel and orthogonal to the fibers, respectively, while the apices + and - denote tension and compression, respectively. With a total thickness of the jacket of 9 mm and using the CLT relations, the mechanical properties of the jacket result as in Table 3, where the indices x and y denote the directions orthogonal and parallel to the pier longitudinal axis, respectively. In Table 3, the corresponding ultimate strain for concrete, as evaluated with the proposed model, is shown.

Table 2. Mechanical on-axis properties of CFRP (1st row) and GFRP (2nd row) material.

E_1 (GPa)	E_2 (GPa)	G_{12} (Gpa)	σ_1^+ (Mpa)	ε_1^+ (%)	σ_1^- (MPa)	ε_1^- (%)	σ_2^+ (MPa)	ε_2^+ (%)	σ_2^- (MPa)	ε_2^- (%)	ν_{12}
134	8.90	51	2130	1.59	1100	0.82	80	0.90	200	2.25	0.28
38.6	8.27	4.14	1062	2.75	610	1.58	31	0.38	118	1.43	0.26

Table 3. Equivalent mechanical properties of CFRP/GFRP jacket, with corresponding ultimate axial strain of concrete.

θ (degree)	E_x (MPa)	σ_x^+ (Mpa)	ε_x^+ (%)	E_y (MPa)	σ_y^+ (MPa)	ε_y^+ (%)	ε_{cu} (t=9 mm) (%)
[75, 15]	61760	953	1.54	21971	570	2.59	3.10

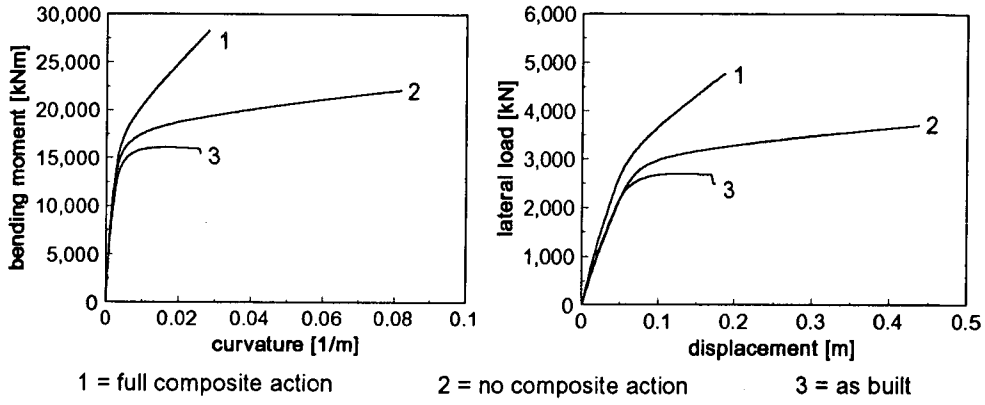

Figure 13. Numerical monotonic analyses.

The results of the monotonic analyses are shown in Figure 13, from which the following ductility factors were calculated.

Table 4. Curvature ductility factors for the retrofitted pier.

Pier	M_y [kNm]	ϕ_y [1/m]	M_u [kNm]	ϕ_u [1/m]	μ_ϕ
As-built	12848	0.0031	17418	0.0320	10.3
Full comp.	14589	0.0030	28254	0.0283	9.4
No comp.	13753	0.0030	22072	0.0820	27.3

Table 5. Displacement ductility factors for the retrofitted pier.

Pier	H_y [kN]	d_y [m]	H_u [kN]	d_u [m]	μ_Δ
As-built	2135	0.048	2343	0.192	4.0
Full comp.	2421	0.044	4765	0.186	4.2
No comp.	2257	0.052	3691	0.438	8.4

In Figure 14, the cyclic behavior of the as-built pier and of the retrofitted pier without composite action is shown. It can be seen that the retrofitted pier shows very stable hysteresis loops, until failure occurs at a curvature ductility factor of about 27, which results in a displacement ductility factor larger than 8.

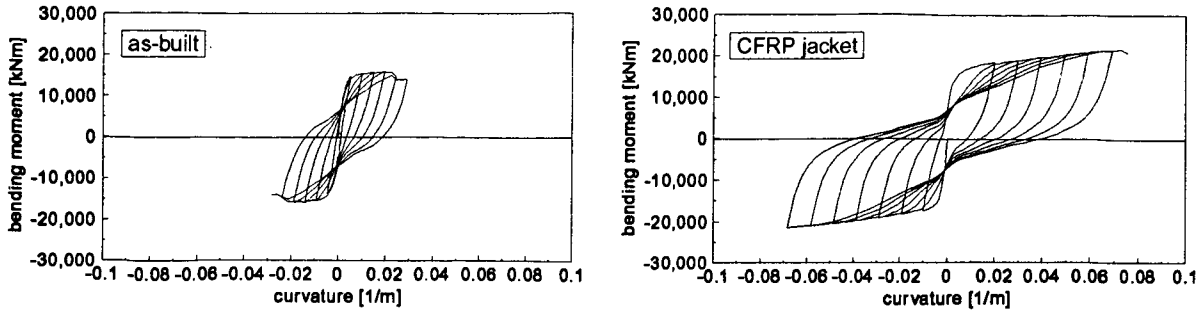

Figure 14. Numerical cyclic tests on as-built (left) and CFRP-jacketed (right) piers.

5. PARAMETRIC STUDY ON FRP-CONFINED SECTIONS

A parametric study has been carried out with the program CYRUS (Monti *et al.* 1996), on the same section considered above, to examine the influence of different configurations of the FRP external reinforcement on relevant response quantities, such as: flexural strength, ductility and failure mechanism.

The proposed confinement model was used to determine the response of the concrete fibers. The Classical Lamination Theory (CLT) was used to evaluate the equivalent stiffness and ultimate strain and strength of the jackets for both the longitudinal and the transverse directions.

Two limit situations were studied, among other factors depending on the stiffness of the glue layer between jacket and pier:

- full composite action between jacket and pier. This situation corresponds to perfect bond provided by the glue layer,
- no composite action between jacket and pier. This situation corresponds to a glue layer that only provides transverse bond, so the jacket exerts only a confining action.

It should be noted that, as opposed to the former case where an infinitely stiff glue layer in both directions is considered, the latter situation corresponds to having a glue layer that is infinitely stiff in the transverse direction and infinitely flexible in the longitudinal direction. This is of course a speculative case, that has the purpose of defining a lower bound for the composite action, since the former one defines an upper bound. The real response should be in between these two bounds. Further studies are necessary to include the effect of the stiffness of the glue layer in the model. However, for practical purposes, since it is recognized that the commercially available epoxy resins provide quasi-perfect bond in both directions, the former case can actually be considered as a satisfactory representation of a real behavior.

The following assumptions were made:

1. The jacket exerts its action until the maximum theoretical strength and strain,
2. The compressive elastic moduli of the FRP materials are equal to the tensile ones,
3. The failure criteria of the jackets are based on the ultimate strain theory. In the analyses without composite action, the jackets fail when the equivalent transverse ultimate strain is

reached. In the anallyses with full composite action, the jackets fail when either the ultimate transverse strain or the ultimate longitudinal compressive/tensile strain is reached.

4. The failure point of the pier was determined by first ply-failure of the jackets. That is, no subsequent stress redistribution among the remaining plyes is considered.
5. The contribution from concrete tensile strength is ignored, as well as shear stresses on the section and possible bond-slip of the rebars.

The parameters considered in this study were the jacket thickness and the fibers winding-angle.

Confinement was provided by an external FRP jacket made of several plies with ±θ fiber winding-angle. Four different jacket thicknesses (t_j = 0, 6, 9 and 12 mm) and seven winding angles (θ = 0, 15, 30, 45, 60 and 90°) were analyzed. For the jacket material carbonfiber/epoxy was selected. Using the CLT relations, the mechanical properties of the confining mechanisms are shown in Table 6 only for the thickness of 9 mm (the corresponding values for the ultimate concrete compressive stress ε_{cu} were calculated with the proposed concrete model).

Table 6. Equivalent mechanical properties of CFRP jacket for different winding angles with corresponding ultimate axial strain of concrete (jacket thickness = 9 mm).

θ (degree)	E_x (MPa)	σ_x^+ (Mpa)	ε_x^+ (%)	E_y (MPa)	σ_y^+ (MPa)	ε_y^+ (%)	$\varepsilon_{cu\,(t=9\,mm)}$ (%)
0	134000	2130	1.59	8900	80	0.90	4.35
15	109080	1684	1.54	9160	87	0.95	3.89
30	47670	676	1.42	10710	115	1.07	2.53
45	17940	223	1.25	17940	223	1.25	1.49
60	10710	115	1.07	47670	667	1.42	1.06
75	9160	87	0.95	109080	1684	1.54	0.90
90	8900	80	0.90	134000	2130	1.59	0.85

Table 7. Failure mechanisms.

Full composite action	Without composite action
1. Crushing of concrete (transverse tensile failure of jacket)	1. Crushing of concrete (transverse tensile failure of jacket)
2. Longitudinal tensile failure of jacket	2. Tensile failure of reinforcing steel
3. Longitudinal compressive failure of jacket	

As regards the failure criteria, the envisaged mechanisms are in Table 7:

The results are presented in terms of normalized interaction diagrams with respect to the unconfined properties: the ratio of confined to unconfined axial force (P/P_{co}) is plotted versus the ratio of confined to unconfined flexural strength (M_{cu}/M_{co}) and versus the ratio of confined to unconfined ultimate curvature (κ_{cu}/κ_{co}). The unconfined pier properties are: $P_{co} = f_{co} A_{gr}$ = 61,850 kN, M_{co} = 10,454 kN and κ_{co} = 0.0194 1/m.

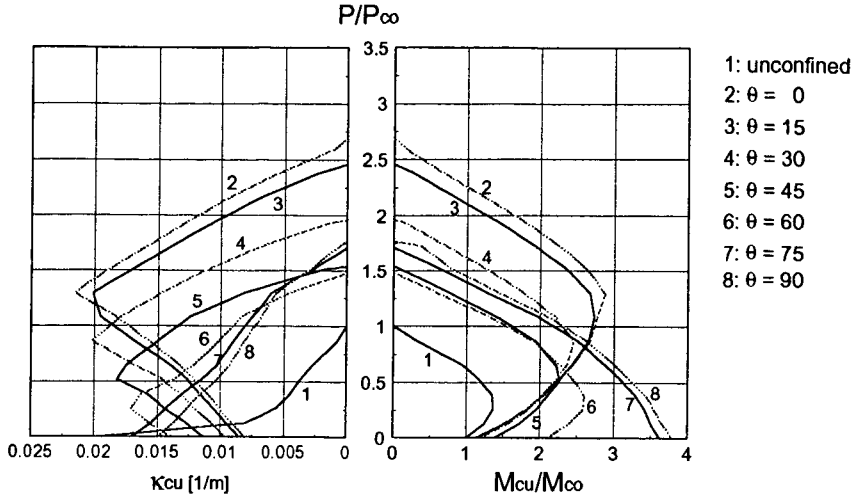

Figure 15 Interaction diagrams with full composite action. Effect of winding angle θ variation for thickness 9 mm.

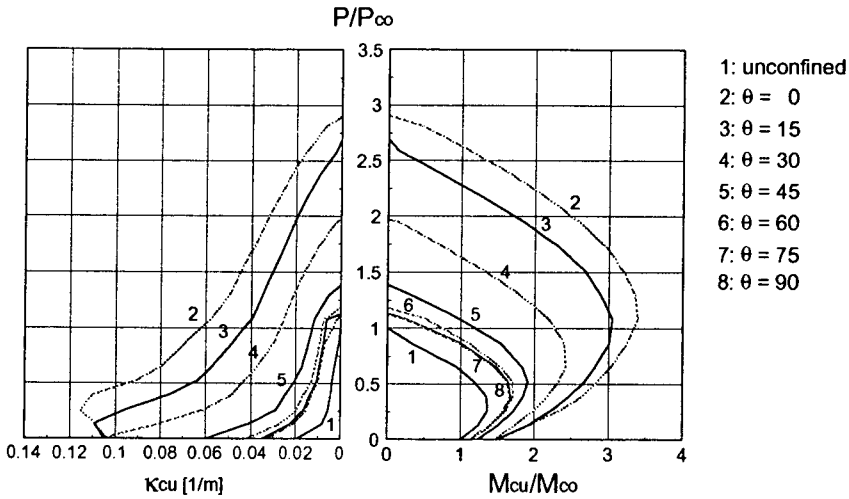

Figure 16. Interaction diagrams without composite action. Effect of winding angle θ variation for thickness 9 mm.

Figure 15 and Figure 16 show the axial load/flexural strength and axial load/ultimate curvature interaction diagrams for a jacket thickness of 9 mm and various winding-angles, with and without composite action. In Figure 15, it is noticed that under pure bending (P/P_{co}=0), an enhancement of the flexural strength is obtained for all winding angles, with a maximum of almost four times when the fiber winding angle is 90°. Also for as regards the ultimate curvature, there is an increase which is more significant for higher axial load (for example, for P/P_{co}=0.5, the ultimate curvature is increased by a factor that varies from 3 to 4). On the other hand, looking at the case of pure axial load, it is observed that the sectional axial strength increases by reducing the winding angle: with θ=0° the increase is more than three times. In the cases where both the axial load and the bending moment are acting on the section, the shape of the interaction diagrams changes according to the dominant failure mechanism. In the range of low axial loads (say, P/P_{co}<0.75), which is more interesting from the practical standpoint, it should be observed that for the cases with θ=75°, 90°, the flexural strength decreases for increasing axial load, as opposed to the other cases where the behavior is like

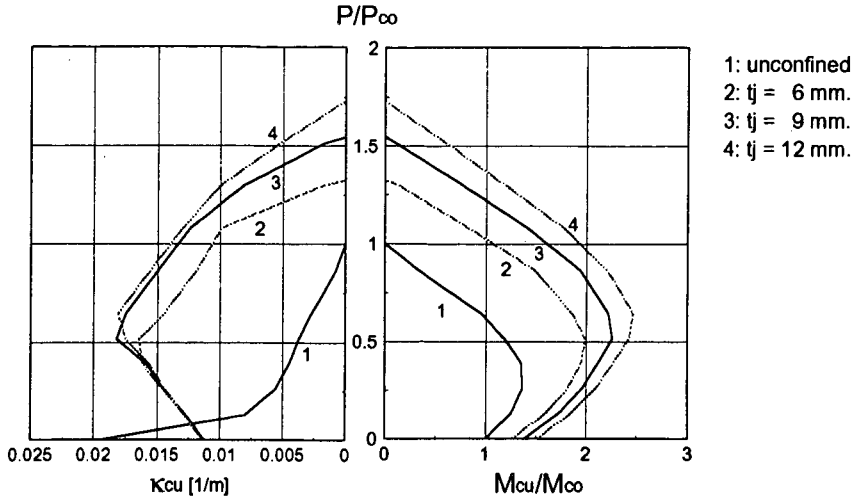

Figure 17. Interaction diagrams with full composite action. Effect of thickness t variation for winding angle of 45°.

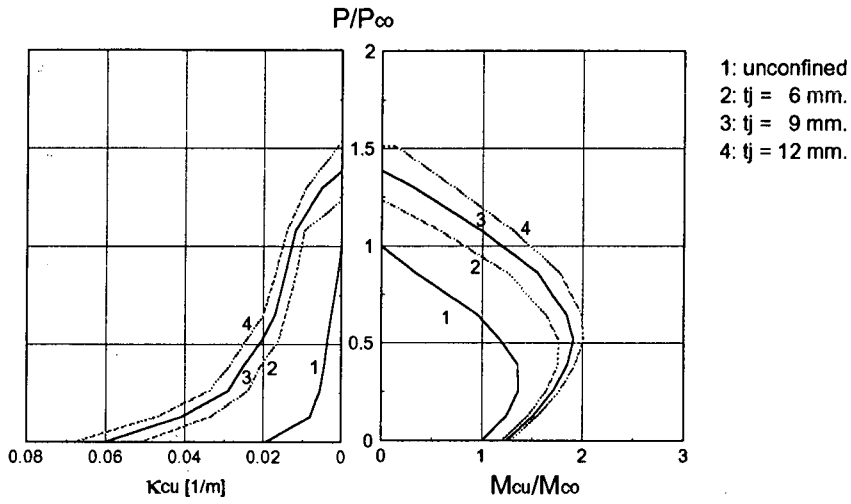

Figure 18. Interaction diagrams without composite action. Effect of thickness t variation for winding angle of 45°.

one would expect. This is essentially due to the fact that collapse of the section occurs due to longitudinal tensile failure of the jacket, before the reinforcing bars have completely exerted their ductility. It can be concluded, therefore, that jackets under full composite action are better suited for flexural strength increase instead of ductility enhancement.

In Figure 16, under pure bending (P/P_{co}=0), there is no significant increase of flexural strength (at most 1.5 times the unconfined one), but the available ductility sensibly increases as the winding angle decreases (up to 5.5 times when θ=0°, 15°, 30°), attaining much higher values than the previous case where full composite action is considered. Note that in this case the shape of the interaction diagrams does not change with the wrapping configuration: they are simply scaled up. This reflects the fact that the failure mechanism is always due to concrete crushing, as opposed to the previous case where the jacket can also fail due to longitudinal strain. As expected, it is observed that significant improvements are obtained only for winding angles less than 45°. In this case, the conclusive remarks is opposite than that of the previous case: jackets without composite action are better suited for ductility enhancement instead of

flexural strength increase. As already observed, the actual behavior of a jacketed section is in between the two cases analyzed above.

In Figure 17 and Figure 18, the effect of the jacket thickness is studied for a winding-angle of 45°, with and without composite action. For the former case, it is seen that significant ductility increase is obtained above values of P/P_{co}=0.2, while for lower values, the ductility is essentially the same as that of the unconfined section. It is important to notice that for low values of the axial load, any increase in thickness brings no significant improvement to the response. In Figure 18, the observed failure mechanism was always crushing of concrete. From comparison of Figure 18 and Figure 17, it can be observed that the difference between full and no composite action, for all thicknesses, in ultimate flexural strength is about 20%, in pure axial capacity about 15%, but available ductility is much larger without composite action. In pure flexural strength the difference is very small. Also in this case, for the practical values of the axial load, no significant improvement is brought in by increasing the jacket thickness.

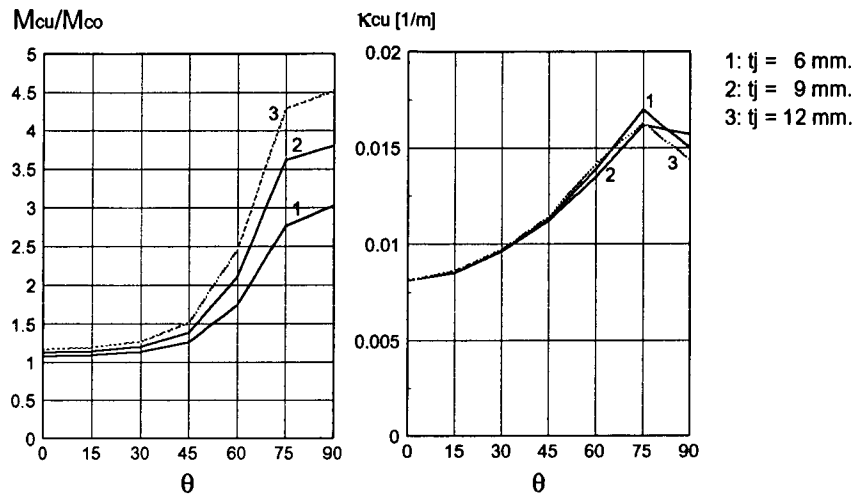

Figure 19. Effect of winding angle θ on pure flexural strength and ultimate curvature, for full composite action.

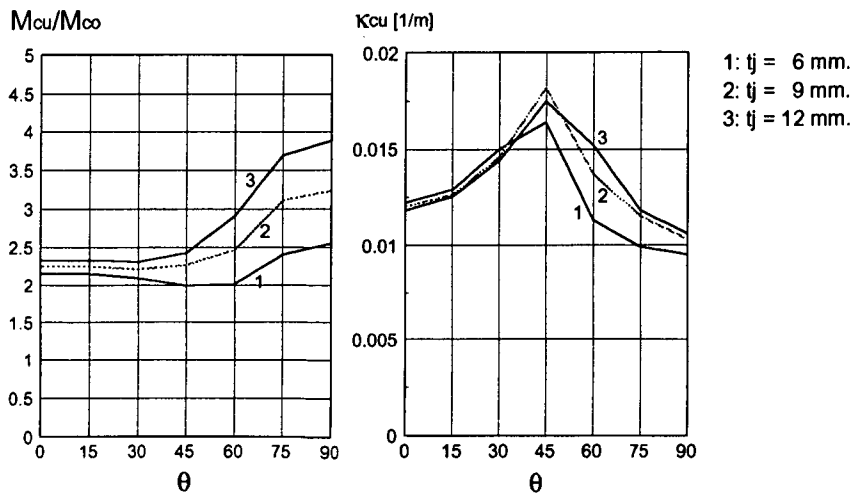

Figure 20. Effect of winding angle θ on flexural strength and ultimate curvature, for full composite action and P/P_{co}= 0.52.

Figure 19 to Figure 23 show the effect of winding-angle and jacket thickness on flexural strength and ultimate curvature at two levels of axial load, and on the pure axial capacity.

Figure 19 shows a steadily increasing pure flexural strength with increasing winding-angle and jacket thickness. But the rate of increase suddenly drops between 75° and 90° winding angle, while the ultimate curvature shows a maximum for 75°. This is the result of a different failure mechanism: for 90° the jackets fails in longitudinal compression, while with the other winding angles it fails in longitudinal tension. Furthermore, the increase in pure flexural strength with increasing jacket thickness is much larger for larger winding angles, and the increase in ultimate curvature is almost zero. In Figure 20, the same two diagrams are represented, relative to P/P_{co}=0.52, the maximum curvature occurs at 45° winding-angle for every thickness, because for larger winding-angles the jackets failed in compression. This is also the reason why the flexural strength for larger winding-angles is less than in Figure 19 with P/P_{co}=0. Because of the axial load, the jackets failed sooner. For the lower winding-angles the flexural strength is larger than in Figure 19, due to extra confinement effects.

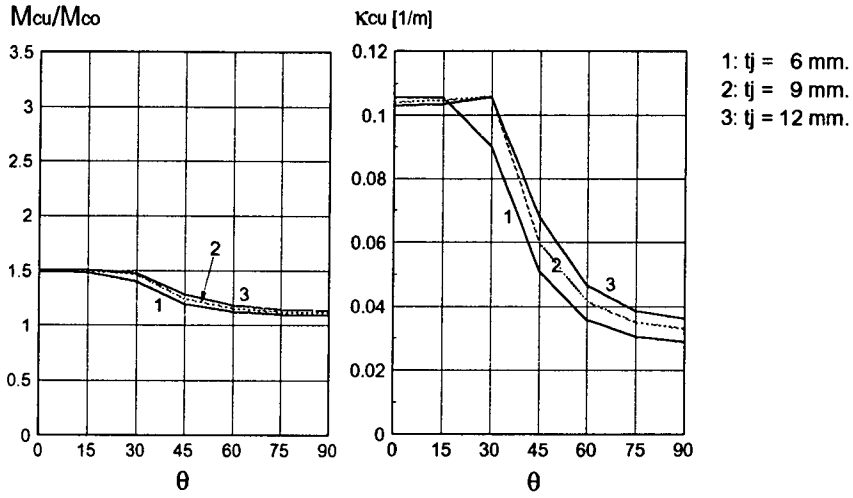

Figure 21. Effect of winding angle θ on pure flexural strength and ultimate curvature, without composite action.

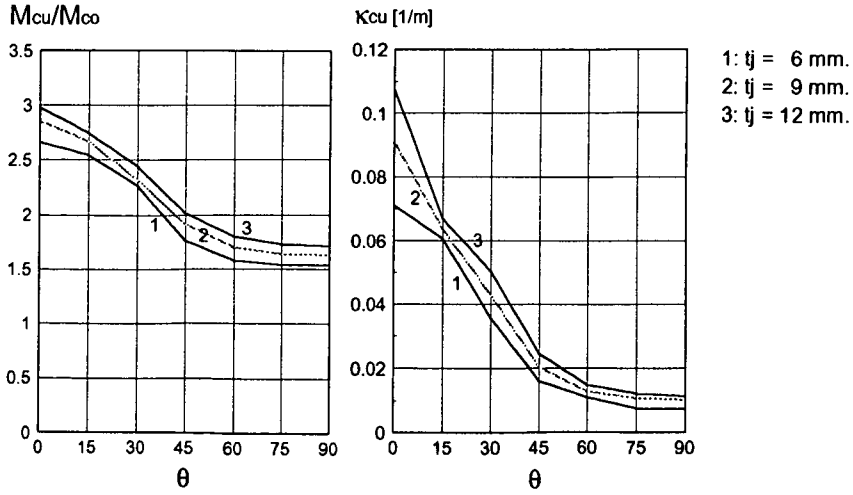

Figure 22. Effect of winding angle θ on flexural strength and ultimate curvature, without composite action and P/P_{co}= 0.52.

In case of no composite action, comparison of Figure 21 and Figure 22 shows clearly the effect of confinement on the flexural strength. The higher the axial load level, the higher the confinement effect, and therefore the ultimate flexural strength. The decrease of flexural strength and ultimate curvature with increasing winding-angle is expected, since the transverse stiffness and ultimate strain of the jackets decrease rapidly. The rate of decrease is larger at higher axial load levels.

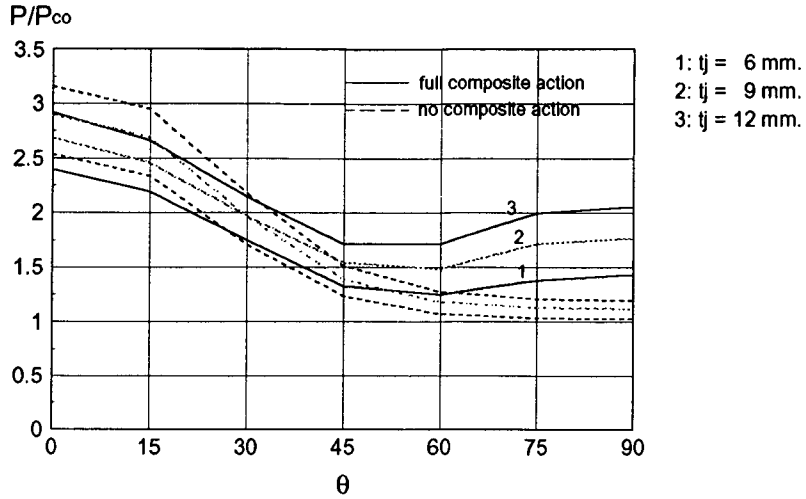

Figure 23. Effect of winding angle θ on pure axial capacity.

Figure 23 shows the influence of the presence or absence of composite action on pure axial capacity. Without composite action, the only influencing factor is the confined concrete strength. Therefore the axial capacity decreases with increasing winding-angle, and the decrease is more pronounced for thicker jackets. With full composite action, there are two influencing factors: ultimate confined concrete strain and jacket longitudinal compressive strain. When the latter is smaller than the confined concrete strain, the jacket is the main factor. For winding-angles smaller than 30° this is the case for every thickness, explaining the lower axial capacity than without composite action. For the larger winding-angles the influence of concrete strength becomes more apparent, and a minimum can be observed for a winding-angle of about 60°.

From the analyses performed, the following conclusions can be drawn:

1. The failure mechanism is the most important concern in the evaluation of flexural strength and ductility. The observed failure mechanism is strongly dependent on jacket thickness, winding angle and axial load level.

2. Composite action does not significantly improve the pure axial capacity; it can even impart a decrease, due to the relative poor compressive behavior of the jackets.

3. Composite action improves flexural strength for the larger (>45°) winding-angles. The source of increase is the direct load-carrying capacity of the jacket, rather than its confining action. This further explains why larger winding-angles result in higher flexural capacity. For (very) high levels of axial load and small winding angles, flexural strength is decreased.

4. Composite action strongly decreases the available ductility for smaller (<45°) winding-angles, for the larger winding-angles and high axial load levels (P/P_{co}>1.0) the decrease is less apparent or even can revert to an increase.
5. As the thickness of the jacket increases, the axial and flexural capacity and the available ductility all increase, but the rate of increase depends on axial load and the presence or absence of composite action.
6. The winding-angle has no significant impact on pure flexural capacity of the pier without composite action, but a large decrease in pure ductility is occuring for increasing winding-angles. With composite action, an increased winding-angle strongly increases both pure flexural strength and pure ductility.

6. CONCLUSIONS

The proposed confinement model is useful in numerical analysis to predict the increase in strength and ductility of concrete confined with fiber-reinforced plastics (FRP). It predicts the behavior of FRP-confined concrete as being relatively ductile and less strong than the existing confinement models do. However, further research is needed to account for several factors (*e.g.*, progressive ply-failure, delamination, biaxial stress state, local buckling) that affect the behavior of FRP materials and reduce the ultimate concrete compression strain, and therefore the ductility of a jacketed bridge pier.

When more data become available on monotonic and cyclic testing of concrete specimens confined with composite materials, further verifications are needed to confirm the good correlation between analysis and experiments. Moreover, additional research is needed to improve the un- and re-loading rules.

From the analyses performed, it is concluded that fiber-reinforced plastic jackets can improve the behavior of existing concrete bridge piers significantly. The choice of the material and of the layout should be chosen based on the specific requirements in each separate case.

It is recognized that an important goal for the future should be a re-examination of the existing (and possibly the development of new simple and rational) design rules for FRP jackets in plastic hinge regions, for flexural and ductility enhancement, and increase in shear capacity.

ACKNOWLEDGMENTS

The study presented in this paper was carried out at the University of Rome, Department of Structural Engineering and Geotechnics, in Italy, and at the Delft University of Technology, Department of Civil Engineering, in The Netherlands The authors especially express their gratitude to Prof. P.E. Pinto and Prof. J.C. Walraven.

REFERENCES

Chai, Y.H., Priestley, M.J.N. and Seible, F. (1991). Seismic retrofit of circular bridge columns for enhanced flexural performance, *ACI Structural Journal*, Vol. 88, September-October, 572-584.

Chang, G.A. and Mander, J.B. (1994). Seismic energy based fatigue damage analysis of bridge columns: Part 1 - Evaluation of seismic capacity, *Report No. NCEER-94-0006*, National Center for Earthquake Engineering Research, State University of New York at Buffalo, New York, USA.

Kim, D.H. (1995). **Composite structures for civil and architectural engineering**, E&FN Spon Eds., New York, USA.

Mander, J.B., Priestley, M.J.N. and Park, R. (1988a). Theoretical stress-strain model for confined concrete, *Journal of Structural Engineering*, ASCE, Vol. 114(8), 1804-1826.

Mander, J.B., Priestley, M.J.N. and Park, R. (1988b). Observed stress-strain behavior of confined concrete, *Journal of Structural Engineering*, ASCE, Vol. 114(8), 1827-1849.

Mirmiran, A., Kargahi, M., Samaan, M. and Shahawy, M. (1996). Composite FRP-concrete column with bi-directional external reinforcement, *Proc. 1st International Conference on Composites in Infrastructure*, Tucson, Arizona, USA, 888-902.

Monti, G., Nuti, C. and Santini, S. (1996). CYRUS – CYclic Response of Upgraded Sections – A program for the analysis of retrofitted or repaired r.c. sections under biaxial cyclic loading including buckling of rebars, *Rep. DSSAR 2/96 MATERIALI*, Dip. Scienze, Storia dell'Architettura e Restauro, Università G. D'Annunzio, Chieti, Italy.

Monti, G. and Spoelstra, M.R. (1997). Fiber-section analysis of rc bridge piers retrofitted with FRP jackets. *ASCE Structures Congress, Portland, Oregon, USA*.

Orito, Y., Sato, T., Tanaka, N. and Watanabe, Y. (1987). Study on the unbounded steel tube structure, *Proc. International Conference on Composite Construction in Steel and Concrete*, ASCE, 786-804.

Pantazopoulou, S.J. and Mills, R.H. (1995). Microstructural Aspects of the mechanical response of plain concrete, *ACI Materials Journal*, Vol. 92, November-December, 605-616.

Picher, F., Rochette, P. and Labossière, P. (1996). Confinement of concrete cylinders with CFRP, *Proc. First International Conference on Composite Infrastructures*, Tucson, Arizona, USA, 829-841.

Popovics, S. (1973). Numerical approach to the complete stress-strain relation for concrete, *Cement and Concrete Res.*, Vol. 3(5), 583-599.

Priestley, M.J.N. and Seible, F. (1992). Design guidelines for assessment, retrofit and repair of bridges for seismic performance, *Report No. SSRP-92/01*, Department of Applied Mechanics and Engineering Sciences, University of California, San Diego, La Jolla, California 92093.

Priestley, M.J.N., Seible, F. and Calvi, M. (1995). **Seismic design and retrofit of bridges**, John Wiley & Sons, New York.

Saadatmanesh, H., Ehsani, M.R. and Li, M.W. (1994). Strength and ductility of concrete columns externally reinforced with fiber composite straps, *ACI Structural Journal*, Vol. 91, July-August, 434-447.

Seible, F., Burgueño, R., Abdallah, M.G. and Nuismer, R. (1995). Advanced composite carbon shell systems for bridge columns under seismic loads, *Progress in research and practice, Proc. of the National seismic conference on bridges and highways*, San Diego, California, USA, December.

Seible, F., Hegemier, G.A., Priestley, M.J.N. and Innamorato, D. (1995). Developments in bridge column jacketing using advanced composites, *Progress in research and practice, Proc. of the National seismic conference on bridges and highways*, San Diego, California, USA, December.

Watson, S., Zahn, F.A. and Park, R. (1994). Confining reinforcement for concrete columns, *Journal of Structural Engineering*, ASCE, Vol. 120(6), 1798-1824.

Xiao, Y., Martin, G.R., Yin, Z. and Ma, R. (1995). Retrofit design of existing reinforced concrete bridge columns using prefabricated composite jacketing, *Progress in research and practice, Proc. of the National seismic conference on bridges and highways*, San Diego, California, USA, December.

CARBON FIBER STRENGTHENING OF EXISTING HIGH BRIDGE PIERS

Y. Yasukawa[1], M. Nakasu[2], Y. Tamura[3]

1)Bridge Structural Engineering Division, Japan Highway Public Corporation

2)Research Institute, Japan Highway Public Corporation

3)Research Institute, Japan Highway Public Corporation

ABSTRACT

Usually, for economic reasons, in the design of RC bridge piers the steel ratio of the main reinforcement is reduced from a section in the middle portion of the pier. However, in some older designs, the development length of this longitudinal reinforcement is inadequate, or there is a lack of lateral hoop. In the case of an extreme earthquake, there is a danger of damage occurring in this steel ratio reduction region in these bridge piers. Generally, methods of overcoming this problem such as the "RC Covering Method" or the "Steel Plate Covering Method" are adopted, but due to various restrictions in their use, there are cases where these methods are difficult to apply. Especially in the case of high piers. Therefore, as a simply applied alternative method for such cases, "Method of Improving Earthquake Resistance using Carbon Fiber" was conceived and experiments carried out for its development into a practically usable method.

INTRODUCTION

Usually, for economic reasons, in the design of RC bridge piers the steel ratio of the main reinforcement is reduced from a section in the middle portion of the pier. However, in cases of bridge piers designed before the 1980 amendments to the Specifications for Highway Bridges, in comparison with the current specifications, there are cases where the development length of the longitudinal reinforcement is inadequate, or there is a lack of lateral hoop. In the case of an extreme earthquake there is a danger of damage occurring in the region of steel ratio reduction in these bridge piers. Generally, methods of overcoming this problem such as the "RC Covering Method" or the "Steel Plate Covering Method" are adopted. However, in the former of these methods there are environmental problems such as the noise

produced during chipping of the old concrete surface that will form the joint where the new concrete is to be placed, and there are cases where the building foundation has to be modified to compensate for the additional weight of the building frame. In the case of the latter method, the work involves difficult operations such as the welding of steel plate or the injection of resin, and there is also the need for workspace for the manufacture of falsework. In order to overcome these various problems the "Method of Improving Earthquake Resistance using Carbon Fiber" was conceived that offers light weight with high tensile strength, is easily carried out, and does not require a large workspace. This report describes the experimental investigation carried out to develop the concept into a practically usable method, presents a guide to its design and use, and also briefly introduces the planning of high bridge pier.

MAIN BODY OF TEXT

Method of improving earthquake resistance using carbon fiber

The carbon fiber used for the method of earthquake resistance upgrading of bridge piers in the region of the reduction in reinforcement using carbon fiber (referred to below as carbon fiber strengthening method), is continuous fiber having a diameter of 7-14 μ m having high strength and elasticity. **Fig. 1** shows an example of the stress-strain relationship of the carbon fiber used. The strength of the fiber is extremely high in comparison to steel, and it has approximately the same value of elastic modulus. Other properties include light weight compared to steel, high durability as it does not corrode, and high flexibility.

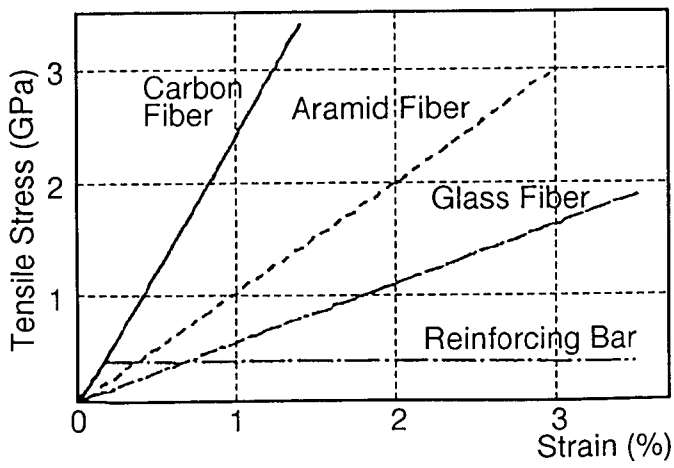

Fig.1 Comparison of Stress - strain Relationship of Various Materials

A schematic of the application of the method is shown in **Fig.2**. The two basic methods of strengthening using the carbon fiber sheet are:

i) Flexural Strengthening: The sheet is applied to the surface of the concrete in the axial direction and provides additional strength in the direction of the longitudinal reinforcement therefore increasing the flexural rigidity.

ii) Shear Strengthening: The sheet is applied to the surface of the concrete at right angles to the axial direction and provides additional strength in the direction of the hoop reinforcement therefore increasing the shear strength of the member.

The carbon fiber strengthening method is achieved by combining the two basic methods described above. The result is to prevent failure in the region of the reduction in reinforcement and cause a change in the failure mode to antecedent bending failure at the base of the pier. The method makes full use of the ductility of the pier. If the base of the pier is considered to be lacking in shear strength, strengthening in accordance with method ii) above is carried out.

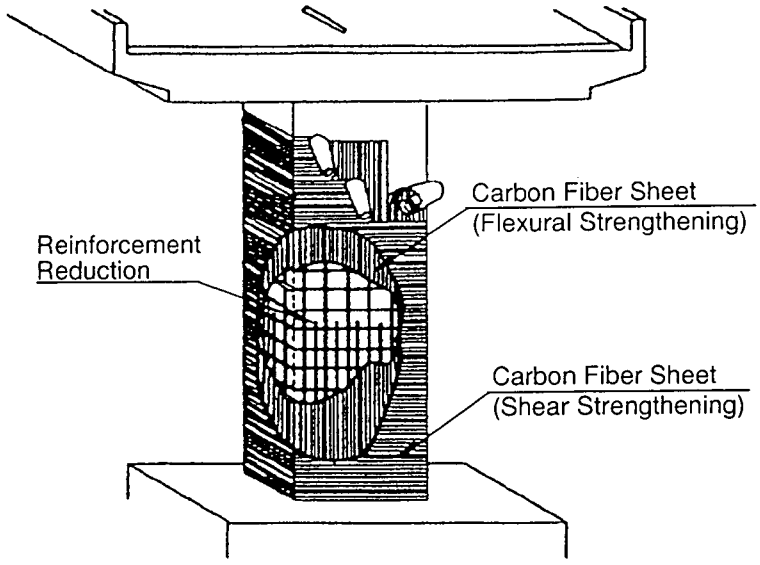

Fig.2 Carbon Fiber Strengthening Method Schematic

The carbon fiber strengthening method is normally carried out using the following procedure :

i) Surface Preparation: The weathered layer of the concrete surface and unevenness are removed to provide a smooth flat surface on which the carbon fiber sheet will be bonded.

ii) Chamfering: In the case of piers having a rectangular section, chamfering with a radius of at least 5 cm is carried out.

iii) Priming: To enhance the bonding of the carbon fiber sheet, the concrete is coated with resin.
iv) Flexural Strengthening: The required number of carbon fiber sheets are bonded to the surface in the axial direction using epoxy resin as the impregnant adhesive.
v) Shear Strengthening: Using the same epoxy resin as for the flexural strengthening, the required number of carbon fiber sheets are bonded around the pier at right angles to the axial direction.
vi) Finishing: To protect the carbon fiber sheet, the surface is finished by coating with mortar or paint.

Outline of the experiment and results

In applying the carbon fiber strengthening method there are cases where many layers of carbon fiber sheet have to be applied to achieve the required strength or resist external forces. Therefore, in order to determine the effects of applying successive layers on the tensile strength and modulus of elasticity, tensile tests were performed varying the number of layers from 1 to 10. The cross section of the carbon fiber strengthening is composed of carbon fibers in a resin matrix (referred to below as CFRP) that resist the externally applied forces; however, for the purposes of the experiments, the tests were evaluated with regard to the carbon fiber cross section alone. The results of the tests are indicated in **Fig.3**. From these results it was found that there was no significant difference in the tensile strength for different numbers of layers. Furthermore, it can be assumed that tests with one layer can be considered representative for the purposes of evaluation. Also, it was found that similar results were achieved for the modulus of elasticity of the carbon fiber sheet.

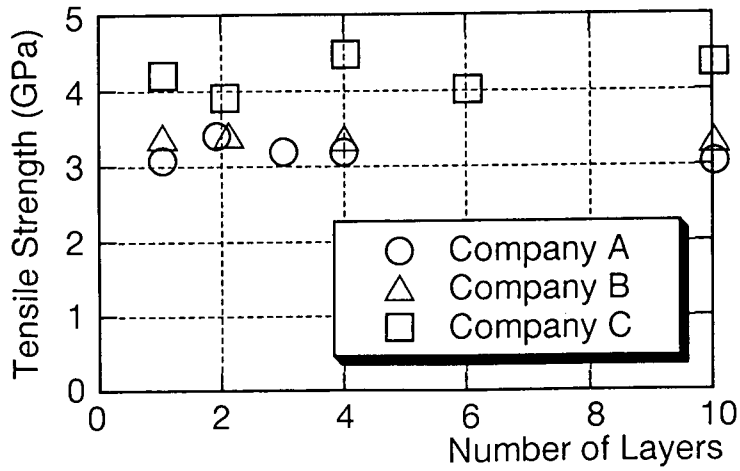

Fig.3 Relationship between Number of Layers and Tensile Strength

To achieve the full effectiveness of the flexural strengthening that was mentioned before, adequate bonding between the CFRP sheet and the concrete is essential. Therefore, in order to determine the bond strength and failure mechanism of the bond between the CFRP sheet and the concrete, CFRP sheet was applied to the bottom of a column and the test cases shown in **Table 1** were carried out in the same way as the flexural strength test that will be described later. To determine the necessary adhesive strength from these experiments, attention was paid to the anchorage length from the point of maximum moment of the flexurally strengthened member to the end of the CFRP sheet and a design method using the average bond stress obtained from the total bond area was investigated. **Fig.4** shows the results obtained in this way. From these results it was found that rupture and bond failure of the CFRP sheet separated at an average bond stress of around 0.45 MPa. Therefore, this value was used for the average bond stress for the calculation of the anchorage length for flexural strengthening.

Table.1 Test Specimens

Specimen Symbol	Steel Distribution of RC Portion		Method of CFRP Strengthening	
	Main Reinforcement	Shear Reinforcement	Flexural Strengthening	Bond Strengthening
F1	4 · D25 for both tension and compression sides Steel Ratio for Main Reinforcement 0.70%	D10 @100mm Steel Ratio for Hoop Reinforcement 0.64%	Unstrengthened	Unstrengthened
F2			4 Layers	
F3			6 Layers	3 Layers
F4			10 Layers	3 Layers

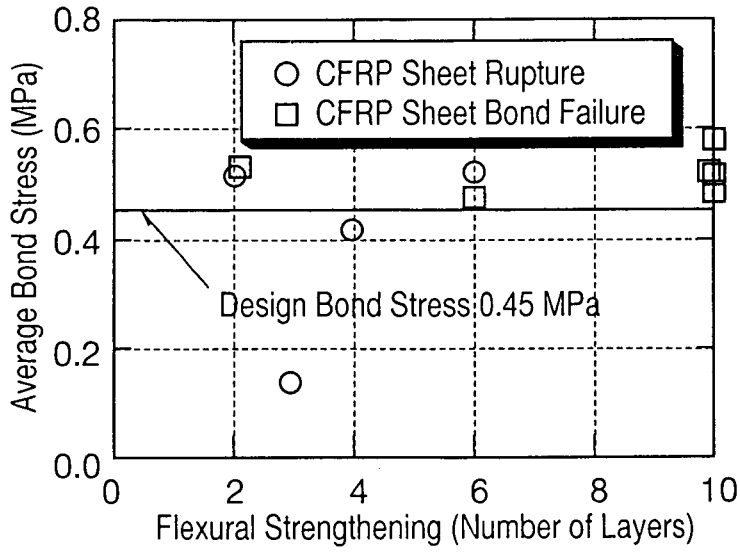

Fig.4 Relationship between Flexural strengthening and Average Bond Stress

The tests shown in **Fig.5** were performed for the cases shown in **Table.2** to determine the method of calculating the flexural strength of the CFRP sheet strengthened member. The relationship between the experimental and calculated values of the ultimate resisting moment resulting from the tests is shown in **Fig.6**. The values were calculated on the assumption that the strain is proportional to the distance from the neutral axis using the material characteristics shown in **Fig.7**. On comparison of the experimental and calculated values of **Fig.6**, it can be seen that the experimental values are slightly lower. This is thought to be the effect of stress concentrations at the surfaces of cracks in the concrete. For this reason, the tensile strength of the CFRP cannot be fully achieved during the material tests. Values calculated with the value of tensile stress that can be resisted by the CFRP sheet reduced to 3/4 are indicated by the solded line in Fig. 6. In this way calculated values that err on the safe side with regard to the experimental values can be obtained.

Table.2 Test Specimens

Specimen Symbol	Main Tensile Reinforcement	Strengthening Method Using CFRP Sheet
B1	2–D13	Unstrengthened
B2	None	Flexural Strengthening 1 Layer
B3	2–D13	Flexural Strengthening 1 Layer
B4	2–D13	Flexural Strengthening 1 Layer and Shear Strengthening 1 Layer

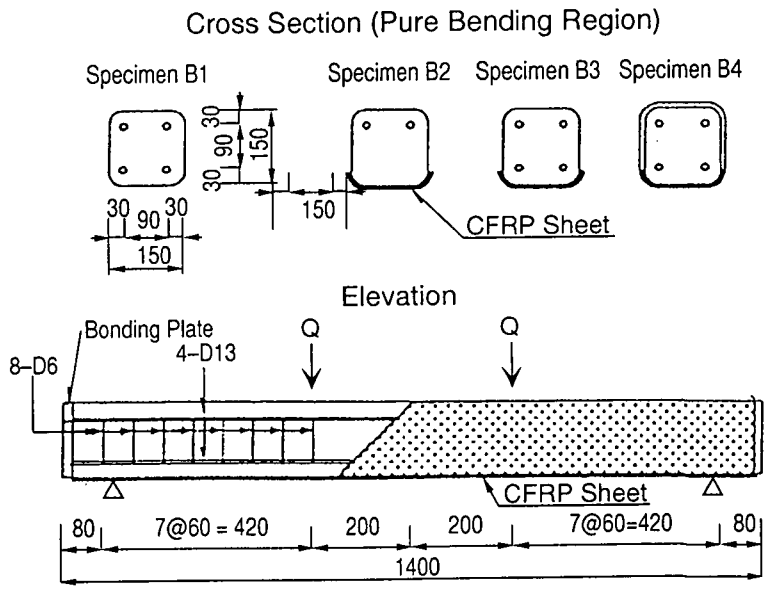

Fig.5 Specimen Dimensions and Distribution of Reinforcement

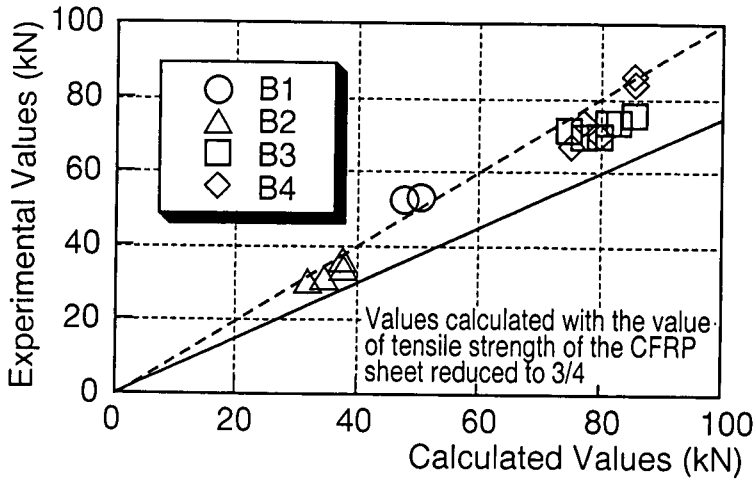

Fig.6 Comparison of Experimental and Calculated Bending Strength Values

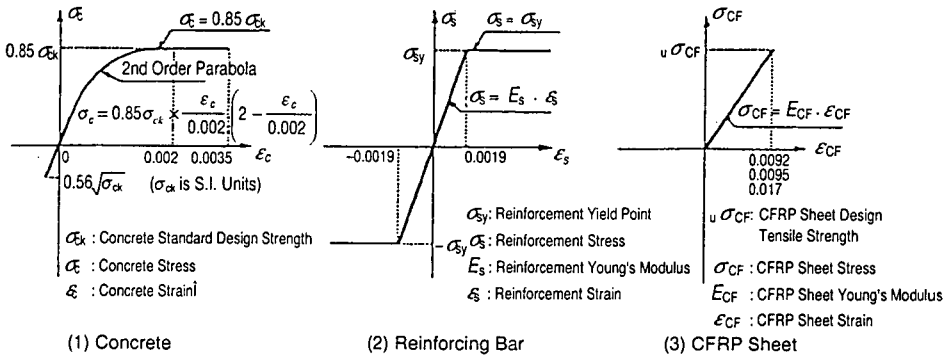

Fig.7 Material Stress - strain Curves

To determine the shear strength of members strengthened using CFRP sheet, the tests shown in **Fig.8** were carried out for the cases shown in **Table 3**. The relationship between load and displacement obtained from these tests is shown in **Fig.9**. From this it can be seen that the shear strength increases with increasing CFRP sheet in the same way as if the reinforcing steel had been increased. From this it can be seen that the CFRP sheet is acting in combination with the hoop reinforcement to provide shear strength .

Table.3 Test Specimens

Specimen Symbol	Hoop Reinforcement	CFRP Strengthening
S1	D6 @150 mm	Unstrengthened
S2	D6 @150 mm	0.5 Layers
S3	D6 @150 mm	1 Layer
S4	D10 @150 mm	Unstrengthened
S5	D10 @100 mm	Unstrengthened

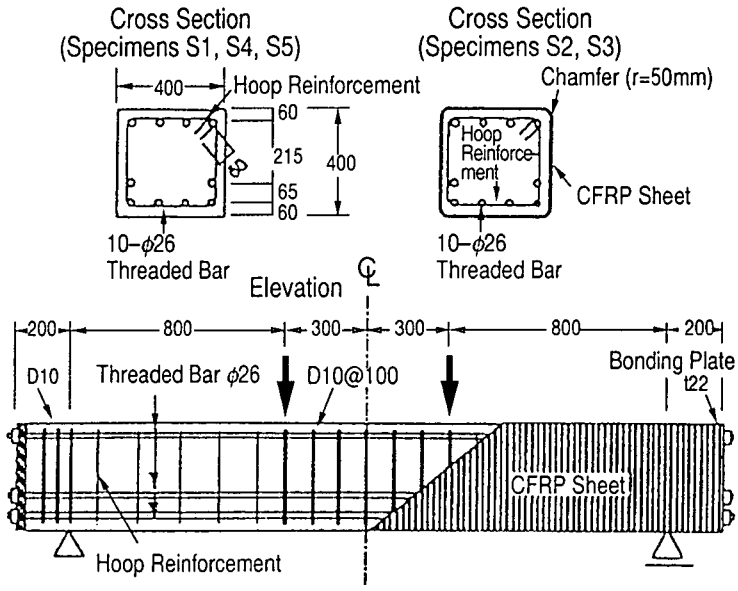

Fig.8 Specimen Dimensions and Distribution of Reinforcement

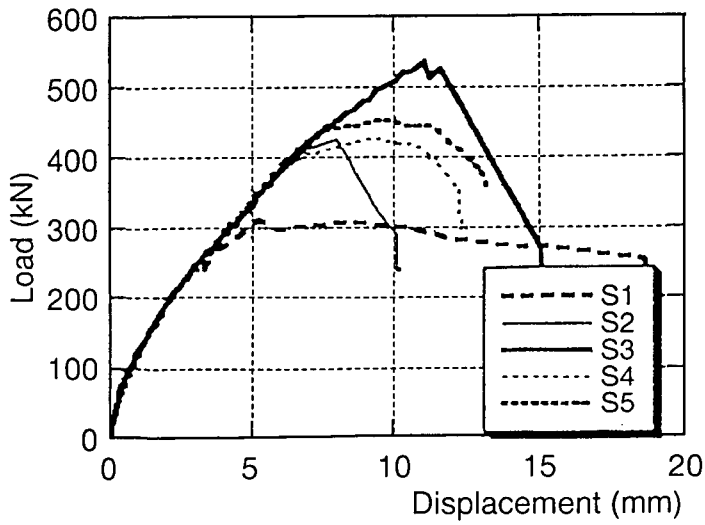

Fig.9 Shear Displacement Curve

Alternating horizontal loading tests were performed using the model shown in **Fig. 10** with the loading cases indicated in **Table.4** in order to determine the seismic strengthening effect of the CFRP sheet on bridge piers in which the reinforcement has been reduced. The tests were carried out taking the yield displacement (1 δ y) as the displacement in the reinforcement in the tensile side of the test specimen at the time of yield, and applying alternate loading three times at amplitudes of integer multiples of the yield displacement. In **Fig.11** is shown the relationship between the horizontal loading and horizontal displacement of the top of the bridge pier. At failure, crushing of the concrete in the region of the reinforcement reduction occurred in the case of specimen C1 ; and in the case of specimen C2, rupture of the CFRP sheet occurred. As a result of the tests, it was found that strengthening using the CFRP sheet improved the ductility of the bridge piers.

Table.4 Test Specimens

Specimen Symbol	Reinforcement Reduction	Range of Strengthening by CFRP Sheet (mm)			CFRP Sheet Strengthening		
		Above Reduction	Below Reduction	Base	At Reduction		At Base
					Flexural Strengthening	Shear Strengthening	Shear Strengthening
C1	Exists	Unstrengthened			—	—	—
C2		530	400	500	2 Layers	2 Layers	2 Layers

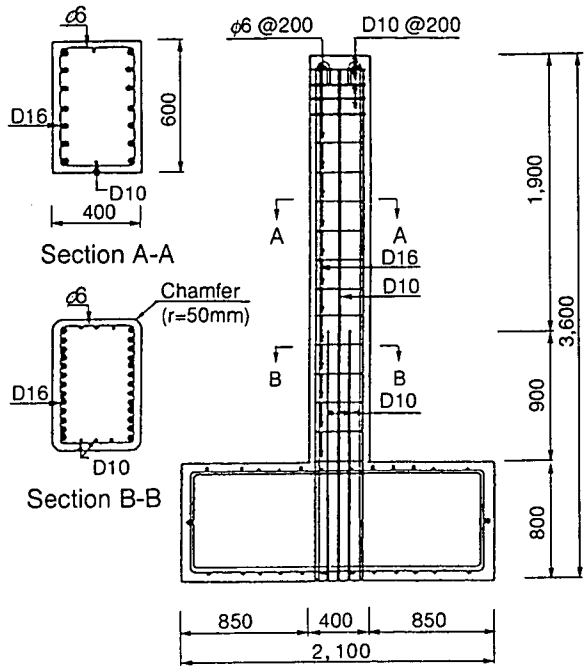

Fig.10 Specimen Dimensions and Distribution of Reinforcement

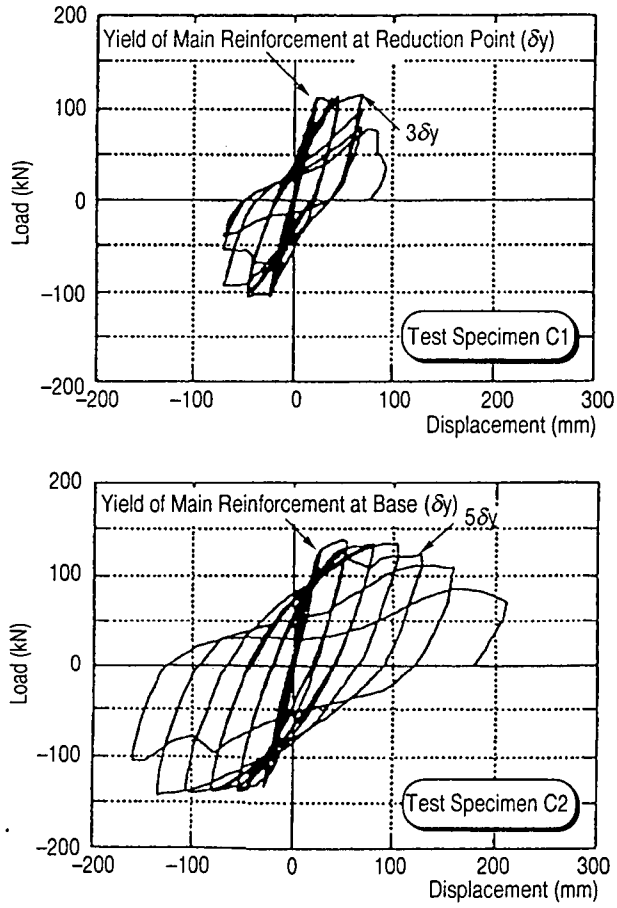

Fig.11 Horizontal Load- Displacement at Top of Pier

Carbon fiber strengthening design method

The result of the carbon fiber strengthening method is to prevent failure in the region of the reduction in reinforcement and cause a change in the failure mode to antecedent bending failure at the base of the pier. A schematic of the strengthening design is shown in **Fig. 12**.

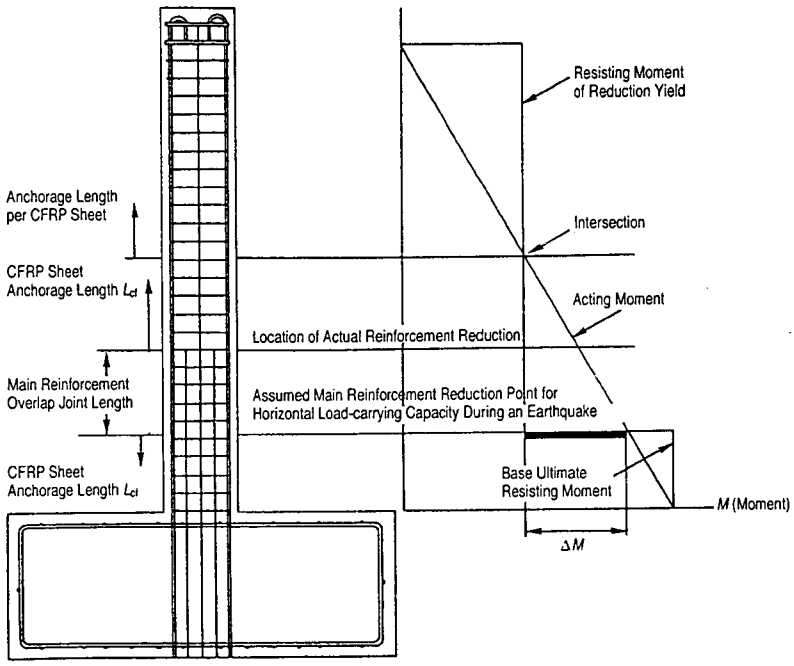

Fig. 12 Strengthening Design Model

For bridge piers in which the reinforcement is reduced, damage will progress rapidly from the base of the pier to the point of reduction when reinforcement in the axial direction at the reduction yields due to the effect of an earthquake, and the resulting failure is brittle failure. Therefore, it is necessary to strengthen the reduction region so that no appreciable damage will occur before the maximum strength of the base is reached. In order to achieve this, strengthening sufficient to ensure that the moment occurring at the point of reduction after the strengthening is less than the ultimate

resisting moment at the base of the pier. Therefore, the bending moment deficiency that must be supplemented by the CFRP strengthening is given by the following equation:

$$\Delta M = Mul - My \qquad (1)$$

where,

ΔM : bending moment deficiency at the assumed point of reduction

Mul:bending moment occurring at the assumed point of reduction when the moment reaches the ultimate resisting moment of the base of the pier

My:yield bending moment at the assumed point of reduction before strengthening

The basic principle behind the shear strengthening involves not the pier shear. but , making the mode of failure antecedent bending failure at the base of the pier. Therefore, the requisite shear strengthening for the pier will be given by the following equation:

$$\Delta P = Pu - Ps \qquad (2)$$

Where,

ΔP : shear force deficiency

Pu : horizontal force when the ultimate bending moment is reached at the base of the pier

Ps : shear strength before strengthening

The range of strengthening of the CFRP sheet is taken to be from the assumed point of reduction to the point of intersection of the yield resisting bending moment of the assumed point of reduction and the moment acting when the ultimate resisting moment is reached at the base.

The anchorage length to be achieved from the actual point of reinforcement reduction is taken to be that given by the following equation :

$$Lcf = \sigma f \times n \times tcf / \tau cf \qquad (3)$$

where,

Lcf: CFRP sheet anchorage length

σ f: CFRP sheet standard design stress

n : required number of CFRP sheets

tcf: flexural strengthening CFRP sheet thickness

τ cf : flexural strengthening CFRP sheet design strength

However, if the anchorage length mentioned above is shorter than the bonding length per CFRP sheet (Lcf l), the value of Lcf is to be extended to L cf l .

When applying flexural strengthening CFRP sheet, even if not indicated necessary by

calculation, one layer of CFRP sheet should be applied externally at right angles to the axial direction.

Application of high bridge pier

This bridge which now we focus on is one of the biggest bridges in Tomei expressway and it was built in 1967(**Figure.13**). In those days, to confirm the calculated values, vibrating tests were done with using rocket force on the top of the pier. Now from the point of aseismicity, the pier needs reinforcement. This pier is very high and not filled with concrete from the reason of weight. So we decided to choose the method of using carbon fiber. The schematic of strengthening pier is shown in **Figure.14**. The present step is that we do more experiments and confirm the ultimate state and the failure mechanism of reinforcement pier in case of an extreme earthquake.

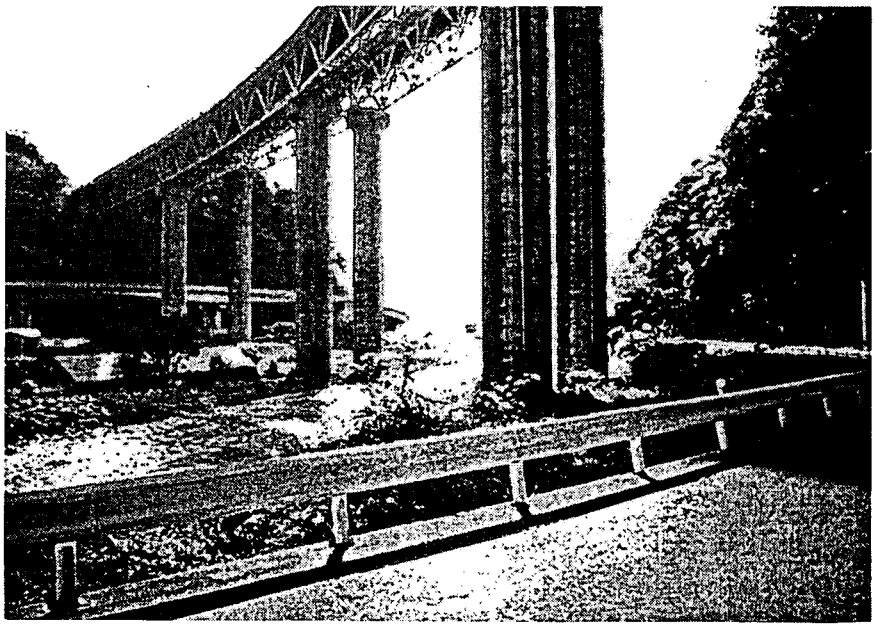

Fig.13 The Overall View of Sakawagawa Bridge

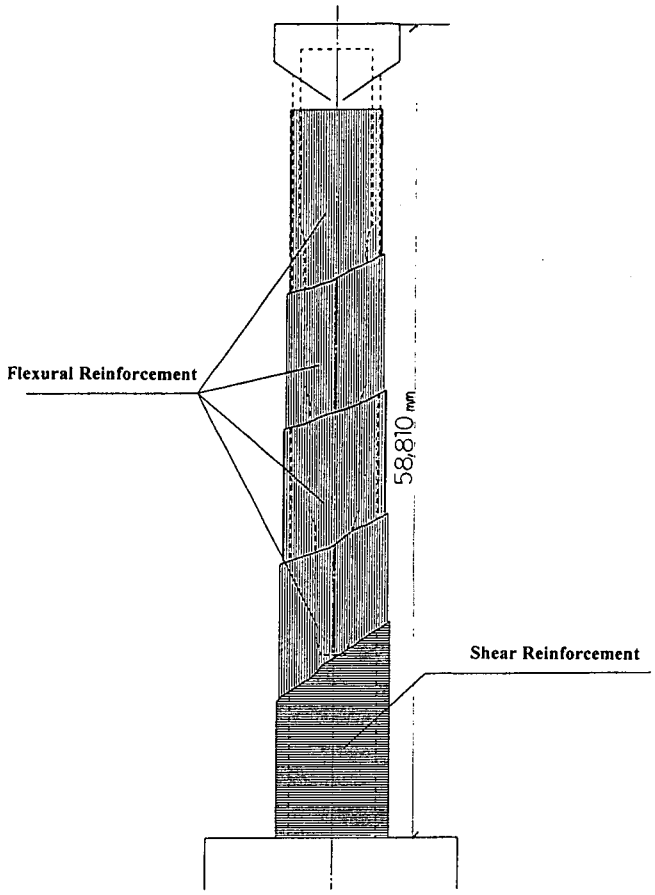

Fig.14 Schematic of Carbon Fiber Strengthening Pier

CONCLUSIONS

The carbon fiber strengthening method was developed for the strengthening of the reduction of reinforcement region of RC bridge piers, and is at present being used for the strengthening of existing bridge piers in the region affected by the Hanshin Awaji Earthquake. Furthermore, the use of carbon fiber in the strengthening of existing structures is receiving more and more attention due to the properties of carbon fiber and its ease of use as a repair material. Research and development into such things as the constraining effect of wrapping layers of carbon fiber sheet around members of existing structures for the improvement of earthquake resistance are being pursued, and the range of application should broaden in the future.

ACKNOWLEDGMENT

Finally, the authors would like to acknowledge the fact that this research was carried out jointly with Obayashi Corporation, and with the additional cooperation of the Carbon Fiber Retrofitting System Study Group.

REFERENCES

Japan Highway Public Corporation (JH), Research Institute. (1995) Carbon fiber strengthening for RC structures methods, *Design and Work Guidelines.*

Ogata, N., et al. (1995) Improving the Earthquake Resistance of Existing RC Bridge Piers Having Reduction in Reinforcement Using Carbon Fiber, *Proceedings of the Japan Society of Civil Engineers.*

Japan Road Association. (1990) *Specifications for Highway Bridges Appendix V Aseismic Design.*

Japan Highway Public Corporation (JH), Research Institute. (1996) *Experimental Research into Improving Earthquake Resistance of Wall-type Bridge Piers.*

RESOLUTION

THE SECOND ITALY-JAPAN WORKSHOP ON SEISMIC DESIGN AND RETROFIT OF BRIDGES

Rome, February 27-28, 1997

RESOLUTIONS

The workshop was participated by 15 Italian and 18 Japanese researchers and engineers. Twelve presentations from the Italian side and 14 presentations from the Japan side and active discussions were made during the two days workshop.

The participants agreed that the workshop was successful and that it led to a deeper understanding of many technical issues in seismic design and retrofit of bridges. While much information has already been developed on these important issues, the participants agreed that many problems remain unsolved and that additional research and studies are still needed.

The participants recommended that increased cooperation between Italy and Japan would be beneficial to both countries for improving the technology and the state-of-practice for seismic design and retrofit of bridges.

As a result, three resolutions were developed and approved during the workshop :

1. There are several topics of common interest related to the development of seismic design and retrofit of bridges.
   Exchange of technical information will promote a greater understanding of seismic behavior of bridge structures, and facilitate the development of countermeasures for reliable performance of bridges in the future. It is therefore resolved that continued cooperation between researchers and bridge engineers in both countries be actively encouraged.
2. In view of the success of this workshop, and the rapidly advancing state-of-the-art, it is resolved that a third Japan-Italy Workshop on Seismic Design and Retrofit of Bridges be held in Japan. The date of the workshop will be based on the agreement of the two countries.
3. It is resolved that the third workshop be oriented towards state-of-the-art reviews, research and application.
   Topics to be covered should include : (1) review and analysis of the earthquake damage ; (2) characteristics of earthquake ground motion; (3) seismic design and retrofit methods for bridges; (4) innovative protective systems; and (5) experimental verification of performance.

APPENDICES

1. Schedule of the Workshop

1997

February 25 (Tue)	10:50	Lv. Narita, TOKYO (by LH711,3566)
	18:05	Ar. Rome
		Stay at Grand Hotel Plaza
February 26 (Wed)		Preparation for Workshop
		Stay at Grand Hotel Plaza
February 27 (Thu)	9:00	Workshop (1st Day)
		Stay at Grand Hotel Plaza
February 28 (Fri)	9:30	Workshop (2nd Day)
		Stay at Grand Hotel Plaza
March 1 (Sat)		Technical Study Tour (Ancient Bridges)
		Stay at Grand Hotel Plaza
March 2 (Sun)	11:50	Lv. Rome (by AZ788)
	12:55	Ar. Milan
		Stay at Ibis Ca'granda Hotel
March 3 (Mon)		Technical Study Tour (Visit to EC-JRC, ISPRA)
		Stay at Ibis Ca'granda Hotel
March 4 (Tue)		Technical Study Tour (Visit to ISMES, Bergamo)
		Stay at Ibis Ca'granda Hotel
March 5 (Wed)	13:35	Lv. Milan (by JAL410)
March 6 (Thu)	9:30	Ar. Narita, TOKYO

2. Program of the Workshop

Thursday, 27 February 1997

9:00 - 9:30 Opening Addresses : Prof. Paolo E. PINTO
Mr. Toshinori MIZUTANI

9:30 - 11:10 Session 1 : Topic 1 General Presentations
Chair : S. Unjoh P. E. Pinto

1) New Seismic Design Specifications for Highway Bridges
(K.Kawashima, M. Nakano, S. Unjoh)
2) An Automatic Procedure for Quantitative Evaluation of Seismic Reliability of Highway Networks
(P. E. Pinto, R. Giannini)

11:10 - 11:30 Coffee Break

11:30 - 13:00 Session 2 : Topic 2 Seismic Input for Bridges
Topic 3 Modelling and Analysis (1)
Chair : G. Mancini K. Yokoyama

3) Ground Motion Characteristics for Seismic Design of Highway Bridges
(K. Tamura, R. Honda)
4) Italian Research Activity for the Definition of the Design Seismic Input
(T. Sano, A. Pugliese)
5) Ductility Evaluation of Reinforced Concrete Bridge Columns
(J. Hoshikuma, K. Kawashima, S. Unjoh)
6) Combined Flexural and Shear Effects on Bridge Piers
(G. Mancini, A. Recupero)

13:00 - 14:30 Lunch Break

14:30 - 16:00 Session 3 : Topic 3 Modelling and Analysis (2)
Chair : G. M. Calvi K. Kawashima

7) Strength and Ductility Characteristics of Two Column–Bents
(T. Terayama, H. Otsuka)
8) A Numerical Model for Shear–Dominated Bridge Piers
(J. Guedes, A. V. Pinto)

9) Shear Strength of Reinforced Concrete Columns – Effect of Specimen Size and Load Reversal –
(H. Kawano, H. Watanabe)

10) Seismic Response by Pseudodynamic Tests of RC Bridges Designed to Eurocode 8
(C. Nuti, A. De Sortis)

16:00 - 16:20 Coffee Break

16:20 - 17:50 Session 4 : Topic 4 Design and Case Studies
Chair : C. Nuti J. Hoshikuma

11) New Approach on Bearings and Falling–off Prevention Systems of Highway Bridges after Hyogo–ken–Nanbu Earthquake
(M. Kanda, K. Nishikawa)

12) Finite Element Modelling of the Hanshin Viaducts Failure in Kobe
(M. Petrangeli, P. E. Pinto)

13) Effect of the Hyogo–ken–nanbu Earthquake on Akashi Kaikyo Bridge
(S. Saeki, T. Kurihara, R. Toriumi, M. Nishitani)

14) Seismic Aspects of the Wadi Dib Cable–Stayed Bridge
(M. P. Petrangeli, M. Petrangeli)

Thursday, 27 February 1997

9:30 - 10:40 Session 5 : Topic 3 Modelling and Analysis (3)
Chair : M. P. Petrangeli K. Tamura

15) Experimental Assessment of Bridges with Isolation and Nonsynchronous Input Motion
(A. V. Pinto, N. Negro)

16) Strength and Ductility Characteristics of Pile Foundations
(J. Fukui, Y. Kimura)

17) Nonlinear Seismic Analysis of Railway Bridges
(M. Dolce)

10:40 - 11:00 Coffee Break

11:00 - 12:30 Session 6 : Topic 5 Foundations and Soil Stability
Topic 6 Isolation and Retrofit (1)
Chair : T. Sano' M. Kanda

18) Design Methods of Bridge Foundations against Soil Liquefaction and Liquefaction–Induced Ground Flow
(K. Yokoyama, K. Tamura, O. Matsuo)

19) A Study on Measures against Ground Flow Using the Finite Element Method
(M. Ogasawara, H. Tsunoda, T. Makita, S. Gose)

20) Menshin Design for Highway Bridges
(K. Kawashima, S. Unjoh)

21) Conceptual Design of Isolation Systems for Bridge Structures
(G. M. Calvi, A. Pavese)

12:30 - 14:00 Lunch Break

14:00 - 16:00 Session 7 : Topic 6 Isolation and Retrofit (2)
Chair : M. Dolce T. Terayama

22) Design of the 19–Span Continuous Rigid Frame Bridge with Seismic Isolator
(H. Hayashi, S. Kawakita, Y. Horie)

23) Seismic Retrofitting of Highway Bridges through Slab Joining and Isolation
(R. Marnetto, G. Monti)

24) Seismic Retrofit of Existing Reinforced Concrete Columns by Steel Jacketing
(J. Hoshikuma, S. Unjoh)

25) Analysis of RC Bridge Columns externally Reinforced with Fiber-reinforced Plastics
(G. Monti, M. R. Spoelstra)

26) Carbon Fiber Strengthening of Existing High Bridge Piers
(Y. Yasukawa, M. Nakasu, Y. Tamura)

16:00 - 16:15 Closure of the Workshop

3. List of Participants

PARTICIPANTS FROM THE JAPAN SIDE

Mr. Toshinori MIZUTANI
Leader of the Japan Side
Assistant Director–General
Public Works Research Institute
Ministry of Construction
1, Asahi, Tsukuba–shi
Ibaraki–ken, 305 Japan

Dr. Koichi YOKOYAMA
Director
Earthquake Disaster Prevention
Research Center
Public Works Research Institute

Dr. Kazuhiko KAWASHIMA
Professor
Civil Engineering Department
Tokyo Institute of Technology
O–Okayama, Meguro–ku
Tokyo, 152, Japan

Mr. Masaji SAITO
Manager
Research Information and Library Division
Planning and Research
Administration Department
Public Works Research Institute

Mr. Takashi NISHIO
International Research Cooperation Section
Planning Division
Planning and Research
Administration Department
Public Works Research Institute

Dr. Shigeki UNJOH
Head
Earthquake Engineering Division
Earthquake Disaster Prevention
Research Center
Public Works Research Institute

Mr. Toru TERAYAMA
Senior Research Engineer
Earthquake Engineering Division
Earthquake Disaster Prevention
Research Center
Public Works Research Institute

Mr. Jun–ichi HOSHIKUMA
Research Engineer
Earthquake Engineering Division
Earthquake Disaster Prevention
Research Center
Public Works Research Institute

Dr. Kei–ichi TAMURA
Head
Ground Vibration Division
Earthquake Disaster Prevention
Research Center
Public Works Research Institute

Dr. Hideki SUGITA
Head
Earthquake Disaster Prevention Division

Earthquake Disaster Prevention
Research Center
Public Works Research Institute

Mr. Yoshitomi KIMURA
Senior Research Engineer
Foundation Engineering Division
Structure and Bridge Department
Public Works Research Institute

Mr. Masayuki KANDA
Senior Research Engineer
Bridge Division
Structure and Bridge Department
Public Works Research Institute

Mr. Hiroshi WATANABE
Senior Research Engineer
Concrete Division
Material and Construction
Method Department
Public Works Research Institute

Mr. Yoshiyuki YASUKAWA
Senior Engineer
Structural Engineering Division
Engineering Department
Japan Highway Public Corporation
3-2-3, Kasumigaseki, Chiyoda-ku
Tokyo, 100, Japan

Mr. Hiroshi TSUNODA
Engineer
Design and Research Division
Engineering Department
Metropolitan Expressway Public
Corporation
1-4-1, Kasumigaseki, Chiyoda-ku
Tokyo, 100, Japan

Mr. Yoshihei HORIE
Chief Engineer
Design Division
Engineering Department
Hanshin Expressway Public Corporation
4-1-3, Kyutaro-cho, Chuo-ku,
Osaka, 541, Japan

Mr. Toshihiro KURIHARA
Deputy Manager
Third Design Division
Design Department
Honshu-Shikoku Bridge Authority
5-1-5, Toranomon, Minato-ku
Tokyo, 105, Japan

Mr. Ryoji IKEDA
Senior Manager
Japan International Science and
Technology Center
2-12-6, Kouji-machi, Chiyoda-ku
Tokyo, 102, Japan

PARTICIPANTS FROM THE ITALIAN SIDE

Dr. Paolo Emilio PINTO
Dipartimento di Ingegneria Strutturale e Geotechnica
Universita di Roma "La Sapienza"

Dr. Camillo NUTI
Dipartimento di Scienza e Storia dell'Architettura
Universita "G.D'Annunzio" di Pescara

Dr. Gian Michele CALVI
Dipartimento di Meccanica Strutturale
Universita di Pavia

Dr. Mauro DOLCE
Dipartimento di Strutture, Geotecnica, Geologia applicata all'Ingegneria
Universita della Basilicata – Potenza

Dr. Mario Paolo PETRANGELI
Dipartimento di Ingegneria Strutturale e Geotechnica
Universita di Roma "La Sapienza"

Dr. Marco PETRANGELI
Dipartimento di Ingegneria Strutturale e Geotechnica
Universita di Roma "La Sapienza"

Dr. Giuseppe MANCINI
Dipartimento di Ingegneria Strutturale
Politecnico di Torino

Dr. Paolo NEGRO
ELSA Laboratory
Joint Research Centre
European Commission
Ispra

Dr. Artur V. Pinto
ELSA Laboratory
Joint Research Centre
European Commission
Ispra

Dr. Giorgio MONTI
Dipartimento di Ingegneria Strutturale e Geotechnica
Universita di Roma "La Sapienza"

DR. Fadriano DE SORTIS
Presidenza del Consiglio Ministri
Servizio Sismico Nazionale
Roma

Dr. Tito SANO
Agenzia Nazionale Protezione Ambiente
Roma

Dr. Antonio PUGLIESE
Presidenza del Consiglio Ministri
Servizio Sismico Nazionale
Roma

Dr. Franco BRAGA
Dipartimento di Strutture, Geotecnica, Geologia applicata all'Ingegneria
Universita della Basilicata – Potenza

Dr. Roberto MARNETTO
TIS
Roma

PROCEEDINGS OF THE SECOND ITALY-JAPAN WORKSHOP ON SEISMIC DESIGN AND RETROFIT OF BRIDGES

ISSN 0386-5878
Technical Memorandum
of PWRI No. 3503
May, 1997

This proceedings include the results of the Second Italy-Japan Workshop on Seismic Design and Retrofit of Bridges. The Workshop was held at Rome University in Rome, Italy, on February 27 and 28, 1997.

Key words: Highway Bridge, Seismic Desgin, Retrofit, Design Specifications, Analysis and Modeling

郵 便 は が き

Postage stamp

3 0 5 - □□

建設省土木研究所耐震技術研究センター耐震研究室
〒305 茨 城 県 つ く ば 市 大 字 旭 1 番 地

Earthquake Engineering Division,
Public Works Research Institute
Tsukuba Science City
Japan 305

No. _____

No. _____

配 布 先 氏 名

配 布 先 住 所

Receipt of

Technical Memorandum of PWRI No. 3503

Name _____

Address _____

_____

_____